plants

Special Issue Reprint

Responses of Crops to Abiotic Stress

Edited by
Georgios Koubouris and Giora Ben-Ari

mdpi.com/journal/plants

MDPI

Responses of Crops to Abiotic Stress

Responses of Crops to Abiotic Stress

Guest Editors

Georgios Koubouris
Giora Ben-Ari

MDPI

Basel • Beijing • Wuhan • Barcelona • Belgrade • Novi Sad • Cluj • Manchester

Guest Editors

Georgios Koubouris
Hellenic Agricultural
Organization ELGO
DIMITRA
Chania
Greece

Giora Ben-Ari
Volcani Center
Institute of Plant Sciences
Rishon LeZion
Israel

Editorial Office
MDPI AG
Grosspeteranlage 5
4052 Basel, Switzerland

This is a reprint of the Special Issue, published open access by the journal *Plants* (ISSN 2223-7747), freely accessible at: https://www.mdpi.com/journal/plants/special_issues/OD3HF9V54T.

For citation purposes, cite each article independently as indicated on the article page online and as indicated below:

Lastname, A.A.; Lastname, B.B. Article Title. *Journal Name* **Year**, *Volume Number*, Page Range.

ISBN 978-3-7258-9291-4 (Hbk)
ISBN 978-3-7258-9292-1 (PDF)
https://doi.org/10.3390/books978-3-7258-9292-1

© 2026 by the authors. Articles in this reprint are Open Access and distributed under the Creative Commons Attribution (CC BY) license. The reprint as a whole is distributed by MDPI under the terms and conditions of the Creative Commons Attribution-NonCommercial-NoDerivs (CC BY-NC-ND) license (https://creativecommons.org/licenses/by-nc-nd/4.0/).

Contents

About the Editors . . . . . **vii**

Giora Ben-Ari and Georgios Koubouris
Responses of Crops to Abiotic Stress
Reprinted from: *Plants* **2025**, *14*, 1927, https://doi.org/10.3390/plants14131927 . . . . . **1**

Zhonghui Feng, Yang Xu, Zhiming Xie, Yaqiong Yang, Guanru Lu, Yangyang Jin, et al.
Overexpression of Abscisic Acid Biosynthesis Gene *OsNCED3* Enhances Survival Rate and Tolerance to Alkaline Stress in Rice Seedlings
Reprinted from: *Plants* **2024**, *13*, 1713, https://doi.org/10.3390/plants13121713 . . . . . **5**

Guijie Luo, Weijia Cai, Hao Wang, Wei Liu, Xu Liu, Shizheng Shi and Lei Wang
Overexpression of a '*Paulownia fortunei*' MYB Factor Gene, *PfMYB44*, Increases Salt and Drought Tolerance in *Arabidopsis thaliana*
Reprinted from: *Plants* **2024**, *13*, 2264, https://doi.org/10.3390/plants13162264 . . . . . **22**

Gang Li, Ziqiang Chen, Xinrui Guo, Dagang Tian, Chenchen Li, Min Lin, et al.
Genome-Wide Identification and Analysis of Maize *DnaJ* Family Genes in Response to Salt, Heat, and Cold at the Seedling Stage
Reprinted from: *Plants* **2024**, *13*, 2488, https://doi.org/10.3390/plants13172488 . . . . . **37**

Tatiana Rondon, Manuel Guzmán-Hernández, Maria C. Torres-Madronero, Maria Casamitjana, Lucas Cano, July Galeano and Manuel Goez
Comparative Analysis of Water Stress Regimes in Avocado Plants during the Early Development Stage
Reprinted from: *Plants* **2024**, *13*, 2660, https://doi.org/10.3390/plants13182660 . . . . . **54**

Dekun Yang, Hongli Chen, Yu Zhang, Yan Wang, Yongqi Zhai, Gang Xu, et al.
Genome-Wide Identification and Expression Analysis of the Melon Aldehyde Dehydrogenase (ALDH) Gene Family in Response to Abiotic and Biotic Stresses
Reprinted from: *Plants* **2024**, *13*, 2939, https://doi.org/10.3390/plants13202939 . . . . . **71**

Wang Yu, Xiangru Zhou, Jinhao Meng, Xiaofu Zhou and Hongwei Xu
Multi-Omics Research Reveals the Effects of the ABA-Regulated Phenylpropanoid Biosynthesis Pathway on the UV-B Response in *Rhododendron chrysanthum* Pall.
Reprinted from: *Plants* **2025**, *14*, 101, https://doi.org/10.3390/plants14010101 . . . . . **92**

Wang Yu, Xiangru Zhou, Jinhao Meng, Hongwei Xu and Xiaofu Zhou
WRKY Transcription Factors Modulate the Flavonoid Pathway of *Rhododendron chrysanthum* Pall. Under UV-B Stress
Reprinted from: *Plants* **2025**, *14*, 133, https://doi.org/10.3390/plants14010133 . . . . . **116**

Xinqiao Zhan, Zhangqun Li, Minxia Pang, Guoxiang Yao and Bizeng Mao
Comprehensive Omics Analysis Reveals Cold-Induced Metabolic Reprogramming and Alternative Splicing in *Dendrobium officinale*
Reprinted from: *Plants* **2025**, *14*, 412, https://doi.org/10.3390/plants14030412 . . . . . **139**

Yanzi Zhang, Yanlin Zhang, Zhicheng Yang, Qingyan Li, Weixiang Chen, Xinyan Wen, et al.
Genome-Wide Identification, Characterization, and Expression Analysis of *BES1* Family Genes in '*Tieguanyin*' Tea Under Abiotic Stress
Reprinted from: *Plants* **2025**, *14*, 473, https://doi.org/10.3390/plants14030473 . . . . . **158**

Nikolaos Tzortzakis, Giannis Neofytou and Antonios Chrysargyris
Nitrogen Fertilization Coupled with Zinc Foliar Applications Modulate the Production, Quality, and Stress Response of *Sideritis cypria* Plants Grown Hydroponically Under Excess Copper Concentrations
Reprinted from: *Plants* **2025**, *14*, 691, https://doi.org/10.3390/plants14050691 . . . . . **182**

Guimin Li, Xinying Shi, Qinmin Lin, Mengmeng Lv, Jing Chen, Yingxin Wen, et al.
Genome-Wide Identification and Expression Analysis of Heat Shock Transcription Factors in *Camellia sinensis* Under Abiotic Stress
Reprinted from: *Plants* **2025**, *14*, 697, https://doi.org/10.3390/plants14050697 . . . . . **201**

Younghwan Ju, Juyoung Choi, Sungho Yun and Jun Ichi Sakagami
Heat Priming and Heat Stress Enhance Transgenerational Heat Tolerance in the Early Growth Stages of *Oryza sativa* L. Progeny
Reprinted from: *Plants* **2025**, *14*, 1593, https://doi.org/10.3390/plants14111593 . . . . . **218**

About the Editors

Georgios Koubouris

Georgios Koubouris is a Senior Researcher at the Institute of Olive Tree, Subtropical Plants and Viticulture of the Hellenic Agricultural Organization – DIMITRA, based in Chania, Crete, Greece. He holds a Ph.D. in Plant Physiology and his research employs cutting-edge plant phenotyping technologies and focuses on the impact of abiotic stresses—such as drought, salinity, and high temperatures—on Mediterranean crops, particularly olives, grapevines, and avocados. Over the past two decades, he has coordinated and participated in several national and European research projects aimed at improving crop resilience, optimizing water use, and promoting sustainable agricultural practices under climate change conditions. His work combines field trials with physiological and biochemical analyses to better understand plant stress responses and develop practical mitigation strategies. He has published more than 90 peer-reviewed articles and he contributes regularly as a reviewer and collaborator in international research networks.

Giora Ben-Ari

Giora Ben-Ari is a Senior Researcher at the Volcani Institute. Upon receiving his position there in 2009, he began work on the response mechanisms of plants to drought, concentrating particularly on those of grapes. When the researcher directing the Israeli olive breeding program retired, he was asked to take over this program and shift his research efforts to issues concerning olive culture and genetics. He used his early experience in molecular biology, mainly with DNA markers and high-throughput data analysis, to join the small community of researchers using molecular biology to study various facets of olive oil production. He established the first phylogenetic analysis of a germplasm collection based on SNP markers and used transcriptomic analyses to clarify the mechanisms of fruit abscission, flower and fruit development, and olive oil biosynthesis. In recent years, he has studied the effects of high temperatures on fruit set, fruit development, oil synthesis, and oil quality

plants

MDPI

Editorial

Responses of Crops to Abiotic Stress

Giora Ben-Ari [1,*] and Georgios Koubouris [2,*]

[1] Institute of Plant Sciences, ARO, The Volcani Institute, Rishon LeZion 7528809, Israel
[2] Hellenic Agricultural Organization (ELGO) DIMITRA, Institute of Olive Tree, Subtropical Crops and Viticulture, 73134 Chania, Greece
* Correspondence: giora@agri.gov.il (G.B.-A.); koubouris@elgo.gr (G.K.)

1. Introduction

During recent years, agriculture has been undergoing a significant transformation in response to contemporary economic pressures and the escalating impact of climate change. Global climate change is recognized as a critical threat to the stability and sustainability of natural ecosystems. It represents a complex and multifactorial process involving shifts in key environmental parameters, including elevated atmospheric CO_2 concentrations, temperature fluctuations, intensified heat waves, and changes in precipitation patterns. These alterations contribute to the emergence and proliferation of novel pests, weeds, and pathogens, thereby exerting additional stress on agricultural systems.

Climate change exerts profound effects on plant physiology, particularly through abiotic stressors that often interact synergistically to induce morphological, physiological, biochemical, and molecular alterations. These stress-induced changes inhibit plant growth, development, and productivity, ultimately leading to yield reductions. Among the various growth stages, the sexual reproductive phase is especially susceptible to the deleterious effects of abiotic stress, thus severely limiting reproductive success and crop yield. This Special Issue will bring together recent advancements in understanding the impacts of climate change on crop yield and quality.

2. Overview of the Published Manuscripts

The responses of crops to abiotic stresses involve many transcription factor families, which induce varied responses in different plants. This Special Issue presents studies of six gene families involved in these responses.

Heat shock factors (*Hsfs*) are a group of transcription factors that regulate the expression of heat shock proteins (HSPs) in response to stress. The regulatory capacity of *Hsfs* is largely due to their ability to preserve protein stability under stressful conditions. The first study presented in this Special Issue found 22 Hsf genes in the tea plant *Camellia sinensis*. These genes were classified as belonging in three major subfamilies: CsHsfA, CsHsfB, and CsHsfC. The expression of many *CsHsf* genes was found to be affected by abiotic stresses such as low temperature and excess light. These results lay a solid groundwork for further investigations into *CsHsf* involvement in the responses of the tea plant *Camellia sinensis* to abiotic stresses [1].

In response to abiotic stresses, plants produce heat shock proteins (Hsps), which are essential for cell survival during periods of stress. Hsps are classified as Hsp100, Hsp90, Hsp70, Hsp60, Hsp40, and Hsp20 based on their molecular weight. Hsp40 proteins are the most prevalent in eukaryotic organisms. *ZmDnaJ* (HSP40s) genes from maize were analyzed and classified into three types. Analysis of cis-regulatory elements in *ZmDnaJ* promoters suggested their involvement in stress responses, growth and development, and

phytohormone sensitivity in maize. RNA-seq analysis showed the constitutive expression of most *ZmDnaJ* genes, some specifically in pollen and endosperm. Various genes of this gene family responded to salinity, heat, and cold stresses, indicating potential interaction between stress regulatory networks [2].

Another gene family that was investigated in the tea plant is the *BES1* gene family. A total of 10 *BES1* genes were identified in the tea genome. Analysis of the promoter regions in these genes revealed two types of light-responsive cis-elements. An expression analysis showed that some of these genes are significantly upregulated under light exposure. The study has provided insights into the functional roles of the BES1 gene family in response to abiotic stresses such as exposure to high-intensity light [3].

The depletion of the ozone layer has resulted in elevated ultraviolet-B (UV-B) radiation levels, posing a significant risk to terrestrial plant growth. The responses of WRKY transcription factors in *Rhododendron chrysanthum* Pall. (*R. chrysanthum*) to UV-B stress and their regulation of flavonoid synthesis were studied. The study revealed changes in the expression of 113 flavonoid-related metabolites and 42 associated genes, with WRKY transcription factors showing significant correlation with these alterations. It should be noted that WRKY transcription factors can influence the expression of key enzyme genes in the flavonoid metabolic pathway, thereby affecting metabolite production [4].

Aldehyde dehydrogenase (ALDH) is effective at eliminating active aldehyde molecules in plants. The study presented in this Special Issue explores the impact of the ALDH gene family on melon growth, their development, and their expression patterns in various tissues and under different stress conditions. The expression patterns of various genes in this family were regulated under all six tested biotic and abiotic stress parameters, namely salinity, frost, waterlogging, powdery mildew, *Fusarium* wilt, and gummy stem blight. The study paves the way for future genetic improvements in melon molecular breeding [5].

An investigation of the MYB transcription factors in *Paulownia fortunei*, used cloning of the *PfMYB44* gene from *Paulownia fortunei*. Overexpression-*PfMYB44* plants were constructed, and physiological and molecular analysis showed that *PfMYB44* could positively regulate salt and drought stresses in Arabidopsis. Under conditions of drought stress, AtP5CS, AtCAT1, AtNCED3 and AtSnRK2.4 expression levels in transgenic lines were also significantly induced. Salt stress induced the expression of *AtNHX1*, *AtSOS1*, *AtSOS2* and *AtSOS3* genes. In conclusion, the functional study of *PfMYB44* laid the foundation for the study of *Paulownia* stress resistance and delved into its stress resistance mechanism and the cultivation of new stress-resistant varieties [6].

One of the plant hormones involved in the responses of plants to abiotic stress is abscisic acid (ABA). Two studies published in this Special Issue explore the role of the ABA plant hormone in the responses of rice and *R. chrysanthum*.

Abscisic acid (ABA) influences *R. chrysanthum*'s metabolic responses under UV-B stress. It was observed that UV-B stress negatively impacts the plant's photosynthetic machinery, disrupting multiple metabolic processes. Multi-omics analysis revealed that applying ABA mitigates the detrimental effects of UV-B on photosynthesis and bolsters the plant's antioxidant defenses. These findings underscore ABA's crucial function in improving plant resistance to UV-B stress and offer novel insights into plant stress biology [7].

In rice, *OsNCED3*-overexpressing lines have increased ABA content by up to 50.90% and improved the transcription levels of numerous genes involved in stress responses, thus significantly enhancing seedling survival rates. They also increased the dry weight contents of the total chlorophyll, proline, soluble sugar, and starch, in addition to increasing the activity of antioxidant enzymes of rice seedlings and reducing the contents of O_2^-, H_2O_2, and malondialdehyde under hydroponic alkaline stress conditions. The results of these findings suggest that inducing *OsNCED3* upregulates endogenous ABA levels and

the expression of additional stress response genes. This represents an innovative molecular approach for enhancing the alkaline tolerance of rice seedlings [8].

Other interesting studies published in this Special Issue investigate various aspects of plant responses to abiotic stress.

One study examined the effects of heat priming and heat stress on delayed germination, shoot length, and shoot fresh and dry weight under elevated-temperature conditions. The results demonstrate that while heat stress delayed germination in progeny, heat priming significantly accelerated germination rates. Furthermore, heat priming helped to maintain low levels of reactive oxygen species (ROS) and malondialdehyde (MDA), contributing to greater biomass accumulation. These findings suggest that heat priming enhances heat tolerance in rice [9].

Sideritis cypria Post is a promising medicinal and aromatic plant. Another study published in this Special Issue described the cultivation of *S. cypria* plants hydroponically, using nutrient solutions (NSs) with different N and Cu levels, combined with the foliar spraying of Zn. Excess Cu increased lipid peroxidation (MDA) at low and moderate N levels in the NS, while foliar Zn reduced both MDA and hydrogen peroxide contents, contingent upon Cu and N levels. These results may be utilized to aid in optimizing nutrient management strategies for cultivating *S. cypria*, considering the potential benefits of Zn foliar applications under conditions of Cu contamination [10].

The cold stress response of the *D. officinale* plant is the subject of another article that we have included. The results suggest that the glycine metabolism-related genes *Dca003913* and *Dca022726* play pivotal roles in both cold and drought stress adaptation. Carbohydrate metabolism showed specific changes in reaction to freezing conditions. These involved a variety of hormonal responses. The study highlights the roles of metabolic reprogramming and RNA splicing in responses to cold [11].

The final study evaluated the performance of two avocado rootstocks under four conditions of water stress during the nursery stage. Plant height, leaf area (LA), dry matter (DM), and carbon (OC) contents in the roots, stems, and leaves were measured. One rootstock of the four measured aspects was found to have higher sensitivity to extreme changes in water availability. These insights are crucial for selecting rootstocks that ensure optimal performance under varying conditions of water availability, enhancing productivity and sustainability [12].

3. Concluding Remarks

The manuscripts featured in this Special Issue encompass studies covering varied plant responses to abiotic stress. As Guest Editors of this Special Issue, titled "Responses of Crops to Abiotic Stress", we would like to thank all the authors for submitting such interesting manuscripts. The studies reported in this collection will help farmers to mitigate the negative effects of abiotic stresses that have increased dramatically in recent years, which are likely to increase in intensity in the future. It has been a pleasure to read and learn from their works. We would also like to thank the reviewers for their valuable comments on the manuscripts, as well as the Editorial Office for their support.

Author Contributions: Conceptualization, writing, review and editing, G.B.-A. and G.K. All authors have read and agreed to the published version of the manuscript.

Conflicts of Interest: The authors declare no conflict of interest.

References

1. Li, G.; Shi, X.; Lin, Q.; Lv, M.; Chen, J.; Wen, Y.; Feng, Z.; Azam, S.M.; Cheng, Y.; Wang, S.; et al. Genome-Wide Identification and Expression Analysis of Heat Shock Transcription Factors in Camellia sinensis Under Abiotic Stress. *Plants* **2025**, *14*, 697. [CrossRef] [PubMed]
2. Li, G.; Chen, Z.; Guo, X.; Tian, D.; Li, C.; Lin, M.; Hu, C.; Yan, J. Genome-Wide Identification and Analysis of Maize DnaJ Family Genes in Response to Salt, Heat, and Cold at the Seedling Stage. *Plants* **2024**, *13*, 2488. [CrossRef] [PubMed]
3. Zhang, Y.; Zhang, Y.; Yang, Z.; Li, Q.; Chen, W.; Wen, X.; Chen, H.; Cao, S. Genome-Wide Identification, Characterization, and Expression Analysis of BES1 Family Genes in 'Tieguanyin' Tea Under Abiotic Stress. *Plants* **2025**, *14*, 473. [CrossRef] [PubMed]
4. Yu, W.; Zhou, X.; Meng, J.; Xu, H.; Zhou, X. WRKY Transcription Factors Modulate the Flavonoid Pathway of Rhododendron chrysanthum Pall. Under UV-B Stress. *Plants* **2025**, *14*, 133. [CrossRef] [PubMed]
5. Yang, D.; Chen, H.; Zhang, Y.; Wang, Y.; Zhai, Y.; Xu, G.; Ding, Q.; Wang, M.; Zhang, Q.-a.; Lu, X.; et al. Genome-Wide Identification and Expression Analysis of the Melon Aldehyde Dehydrogenase (ALDH) Gene Family in Response to Abiotic and Biotic Stresses. *Plants* **2024**, *13*, 2939. [CrossRef] [PubMed]
6. Luo, G.; Cai, W.; Wang, H.; Liu, W.; Liu, X.; Shi, S.; Wang, L. Overexpression of a 'Paulownia fortunei' MYB Factor Gene, PfMYB44, Increases Salt and Drought Tolerance in Arabidopsis thaliana. *Plants* **2024**, *13*, 2264. [CrossRef] [PubMed]
7. Yu, W.; Zhou, X.; Meng, J.; Zhou, X.; Xu, H. Multi-Omics Research Reveals the Effects of the ABA-Regulated Phenylpropanoid Biosynthesis Pathway on the UV-B Response in *Rhododendron chrysanthum* Pall. *Plants* **2025**, *14*, 101. [CrossRef] [PubMed]
8. Feng, Z.; Xu, Y.; Xie, Z.; Yang, Y.; Lu, G.; Jin, Y.; Wang, M.; Liu, M.; Yang, H.; Li, W.; et al. Overexpression of Abscisic Acid Biosynthesis Gene OsNCED3 Enhances Survival Rate and Tolerance to Alkaline Stress in Rice Seedlings. *Plants* **2024**, *13*, 1713. [CrossRef] [PubMed]
9. Ju, Y.; Choi, J.; Yun, S.; Sakagami, J.I. Heat Priming and Heat Stress Enhance Transgenerational Heat Tolerance in the Early Growth Stages of *Oryza sativa* L. Progeny. *Plants* **2025**, *14*, 1593. [CrossRef] [PubMed]
10. Tzortzakis, N.; Neofytou, G.; Chrysargyris, A. Nitrogen Fertilization Coupled with Zinc Foliar Applications Modulate the Production, Quality, and Stress Response of *Sideritis cypria* Plants Grown Hydroponically Under Excess Copper Concentrations. *Plants* **2025**, *14*, 691. [CrossRef] [PubMed]
11. Zhan, X.; Li, Z.; Pang, M.; Yao, G.; Mao, B. Comprehensive Omics Analysis Reveals Cold-Induced Metabolic Reprogramming and Alternative Splicing in *Dendrobium officinale*. *Plants* **2025**, *14*, 412. [CrossRef] [PubMed]
12. Rondon, T.; Guzmán-Hernández, M.; Torres-Madronero, M.C.; Casamitjana, M.; Cano, L.; Galeano, J.; Goez, M. Comparative Analysis of Water Stress Regimes in *Avocado* Plants during the Early Development Stage. *Plants* **2024**, *13*, 2660. [CrossRef] [PubMed]

Disclaimer/Publisher's Note: The statements, opinions and data contained in all publications are solely those of the individual author(s) and contributor(s) and not of MDPI and/or the editor(s). MDPI and/or the editor(s) disclaim responsibility for any injury to people or property resulting from any ideas, methods, instructions or products referred to in the content.

plants

MDPI

Article

Overexpression of Abscisic Acid Biosynthesis Gene *OsNCED3* Enhances Survival Rate and Tolerance to Alkaline Stress in Rice Seedlings

Zhonghui Feng [1,2,†], Yang Xu [2,†], Zhiming Xie [1], Yaqiong Yang [1], Guanru Lu [2], Yangyang Jin [2], Mingming Wang [2,3], Miao Liu [2,3], Haoyu Yang [2,3], Weiqiang Li [2,3,*] and Zhengwei Liang [2,3,*]

[1] College of Life Science, Baicheng Normal University, Baicheng 137000, China; fengzhonghui@bcnu.edu.cn (Z.F.); xiezhiming@bcnu.edu.cn (Z.X.); yangyaqiong2004@163.com (Y.Y.)
[2] State Key Laboratory of Black Soils Conservation and Utilization, Northeast Institute of Geography and Agroecology, Chinese Academy of Sciences, Changchun 130102, China; xuyang@iga.ac.cn (Y.X.); luguanru@iga.ac.cn (G.L.); jinyangyang@iga.ac.cn (Y.J.); wangmingming@iga.ac.cn (M.W.); liumiao@iga.ac.cn (M.L.); yanghaoyu@iga.ac.cn (H.Y.)
[3] Jilin Da'an Farmland Ecosystem National Observation and Research Station, Da'an 131317, China
* Correspondence: liweiqiang@iga.ac.cn (W.L.); liangzw@iga.ac.cn (Z.L.); Tel.: +86-431-8554-2347 (Z.L.)
† These authors contributed equally to this work.

Abstract: Alkaline stress with high pH levels could significantly influence plant growth and survival. The enzyme 9-cis-epoxycarotenoid dioxygenase (NCED) serves as a critical bottleneck in the biosynthesis of abscisic acid (ABA), making it essential for regulating stress tolerance. Here, we show that *OsNCED3*-overexpressing rice lines have increased ABA content by up to 50.90% and improved transcription levels of numerous genes involved in stress responses that significantly enhance seedling survival rates. Overexpression of *OsNCED3* increased the dry weight contents of the total chlorophyll, proline, soluble sugar, starch, and the activities of antioxidant enzymes of rice seedlings, while reducing the contents of $O_2 \cdot^-$, H_2O_2, and malondialdehyde under hydroponic alkaline stress conditions simulated by 10, 15, and 20 mmol L^{-1} of Na_2CO_3. Additionally, the *OsNCED3*-overexpressing rice lines exhibited a notable increase in the expression of *OsNCED3*; ABA response-related genes *OsSalT* and *OsWsi18*; ion homeostasis-related genes *OsAKT1*, *OsHKT1;5*, *OsSOS1*, and *OsNHX5*; and ROS scavenging-related genes *OsCu/Zn-SOD*, *OsFe-SOD*, *OsPOX1*, *OsCATA*, *OsCATB*, and *OsAPX1* in rice seedling leaves. The results of these findings suggest that overexpression of *OsNCED3* upregulates endogenous ABA levels and the expression of stress response genes, which represents an innovative molecular approach for enhancing the alkaline tolerance of rice seedlings.

Keywords: abscisic acid (ABA) content; alkaline tolerance; *OsNCED3*; rice (*Oryza sativa* L.)

1. Introduction

Based on statistics released by the Food and Agriculture Organization of the United Nations (FAO), approximately 950 million hectares of land across the globe are impacted by soil salinization and alkalization [1]. Saline–alkaline soils can be categorized as either saline or alkaline soils. Saline soil, primarily composed of neutral salts (NaCl or Na_2SO_4), typically has a pH level of approximately 7–8. In contrast, alkaline soil, primarily composed of carbonates or bicarbonates (Na_2CO_3, $NaHCO_3$, or mixtures of Na_2CO_3 + $NaHCO_3$), usually has a pH value higher than 8.5. Although both saline and alkaline stresses fall under the category of salinization stress, alkaline stress possesses unique characteristics compared with neutral saline stress [2]. The most distinct feature that distinguishes alkaline stress from saline stress is high pH, which causes severe damage to plant growth [3–5]. Development of paddy fields for rice (*Oryza sativa* L.) cultivation is an effective method for comprehensive improvement and utilization of soda saline–alkaline soils, which has been jointly discovered through practical experience and scientific exploration [6,7]. Rice production is intricately

tied to economic growth. Advancements in rice varieties, cultivation methods, and post-harvest management have led to higher yields and lower costs, making rice more available and affordable for consumers. However, rice is regarded as a crop that is susceptible to the adverse effects of saline–alkaline stress [8,9]. Compared to saline stress, alkaline stress exhibits a more significant inhibitory effect on rice [3], which inhibits plant growth via osmotic stress [10,11], ion toxicity [12–14], oxidative damage [14–16], and disrupts physiological metabolism [15–17]. The seedling stage of rice is the most sensitive to saline–alkaline stress, resulting in a severe decrease in survival rates, leading to seedling death and ultimately affecting crop yield [5,18]. Enhancing the survival rate of rice seedlings is essential in improving the tolerance to alkaline stress.

Abscisic acid (ABA) is a crucial plant hormone that not only regulates plant growth and development but also serves as a stress signal factor mediating plant responses to abiotic stresses [19–22]. By activating various defense mechanisms, ABA significantly regulates plant responses to adversity, helping plants adapt to potential challenges [23,24]. ABA improves the stability of the cell membrane by elevating the intracellular concentration of Ca^{2+} [25]. Additionally, ABA regulates the expression of stress-responsive genes encoding functionally specific proteins, including enzymes responsible for detoxifying reactive oxygen species (ROS) and enzymes involved in phospholipid-mediated signaling pathways [26]. ABA triggers adaptive responses in plants exposed to saline and alkaline conditions [27]. However, subtle differences might potentially exist in the regulatory mechanisms underlying saline tolerance and alkaline tolerance.

In the majority of higher plants, ABA is produced from carotenoids via the indirect C40 pathway. The catalytic reaction catalyzed by 9-cis-epoxycarotenoid dioxygenase (NCED) serves as a critical rate-limiting step in the biosynthetic pathway of ABA, with the NCED enzyme playing a pivotal role in regulating the overall biosynthetic reaction [28–30]. Prior research has demonstrated that the biosynthesis of ABA is modulated by distinct *NCED* genes at various stages of plant tissue growth [31]. In rice, there are five *NCED* genes, namely *OsNCED1–OsNCED5*, and different *OsNCED* genes play roles in different biological processes [32,33]. *OsNCED1* and *OsNCED3* are the principal genes regulating ABA biosynthesis in rice, whereas *OsNCED4* does not contribute to this regulatory mechanism [34]. Conversely, *OsNCED5* is involved in the expression of ABA-dependent genes linked to non-biotic stress and senescence, thereby regulating plant development and stress resistance [35]. *OsNCED2* is primarily expressed in seeds and regulates seed germination [33,36]. Furthermore, ectopic overexpression of *OsNCED3* leads to elevated endogenous ABA levels in transgenic lines and enhanced drought tolerance in *Arabidopsis* [37]. Using CRISPR/Cas9 technology, mutant lines of the *OsNCED3* gene, *nced 3-1* and *nced 3-2*, exhibited significantly reduced ABA content and early germination characteristics compared to the wild type (WT) under drought stress [38]. There appears to be a strong correlation between the *NCED* gene family and abiotic stress tolerance in plants. However, reports on the regulation of tolerance to high pH stress in rice by genes associated with ABA biosynthesis remain scarce.

Previous research has revealed that ABA serves as a key factor in improving the tolerance of rice seedlings to saline–alkaline stress, showing broad application prospects in agricultural practices and production [39,40]. However, issues such as high cost and photodecomposition limit the application. Rapid stress-induced increases in endogenous ABA levels and enhancement of ABA signaling are closely related to ABA biosynthesis and metabolism in plants [41]. Therefore, the molecular method of regulating endogenous ABA levels in rice may represent a feasible and effective approach for improving alkaline tolerance. In this study, we overexpressed the critical gene *OsNCED3* involved in the ABA biosynthesis pathway to investigate its function in ABA-mediated alkaline tolerance. As a result, the survival rates and tolerance of rice seedlings towards alkaline stress conditions were significantly improved. This constituted a significant and innovative approach towards enhancing the alkaline tolerance of rice seedlings through the utilization of molecular techniques.

2. Results

2.1. Overexpression of OsNCED3 Mitigated the Inhibitory Effects of Na_2CO_3 Stress Conditions on Plant Growth

To determine the role of *OsNCED3* in alkaline stress tolerance in rice, we constructed *OsNCED3* transgenic lines (OE-1 to OE-3). With an increase in Na_2CO_3 stress concentration and duration, the phenotypic differences between the overexpressing *OsNCED3*-transgenic lines and wild-type (WT) plants became more apparent (Figure 1). The transgenic lines demonstrated significantly superior growth compared to the WT plants when subjected to alkaline stress conditions, with OE-2 showing the best growth phenotype. After 7 d of 20 mM Na_2CO_3 stress, the leaves of the WT plants wilted and curled severely, nearly approaching death, while the transgenic lines exhibited significantly less wilting.

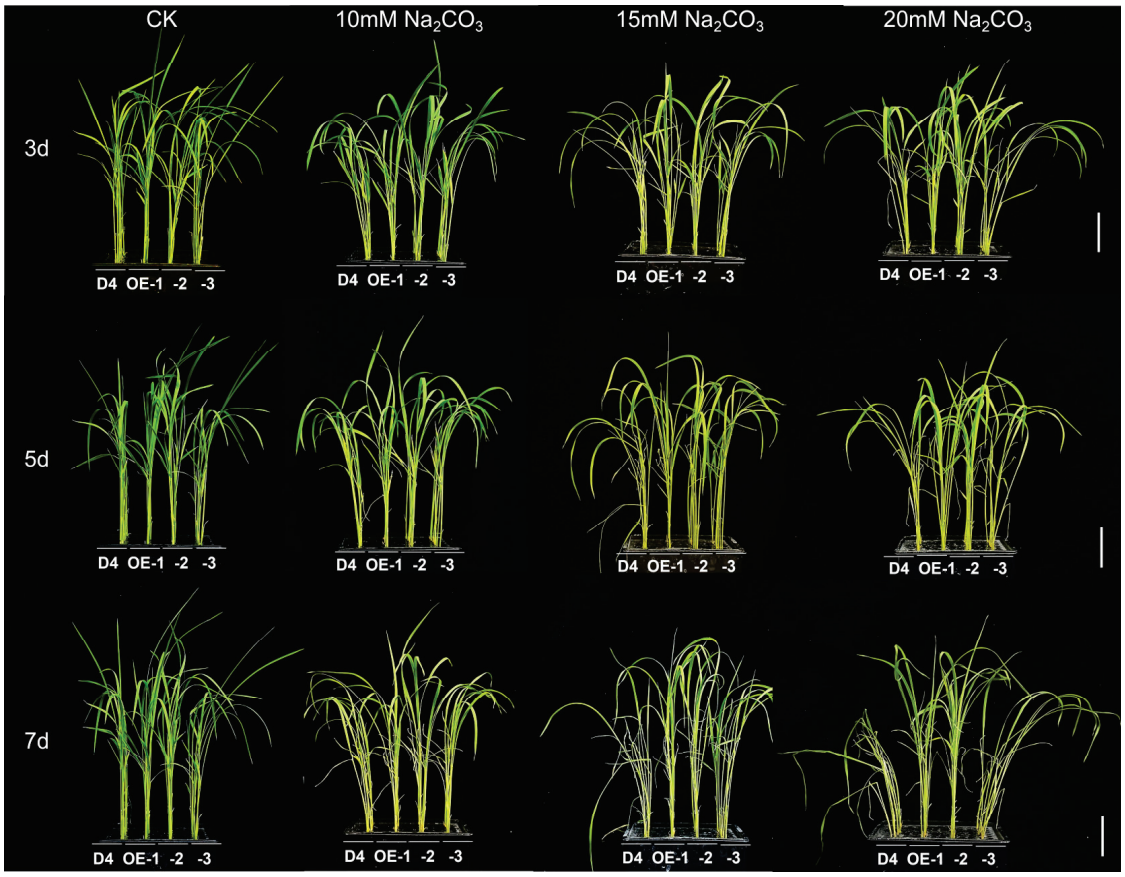


Figure 1. Plant growth of different rice seedling lines under alkaline stress conditions. The growth of D4 (WT) and transgenic line (OE-1, OE-2, and OE-3) rice seedlings at three leaf stages under 10, 15, and 20 mM Na_2CO_3 and non-stress conditions (CK, pure nutrient solution) for 3, 5, and 7 d. The scale bar represents 5 cm.

2.2. Overexpression of OsNCED3 Enhanced the Survival Rates, Dry Weights, and Chlorophyll Contents of Rice Seedlings under Na_2CO_3 Stress Conditions

No statistically significant difference was noted in the survival rates across various lines when the Na_2CO_3 stress duration was less than 3 d ($p < 0.05$). However, when the Na_2CO_3 stress concentration was higher than 10 mM and the stress duration was longer than 3 days, the survival rates of the transgenic lines were higher than those of the WT plants (Figure 2A). The survival rates of OE-1, OE-2, and OE-3 increased by 5.0-, 5.5, and 4.5 times, respectively, compared to the WT plants under 20 mM Na_2CO_3 stress for 7 d, reaching a significant difference ($p < 0.05$).

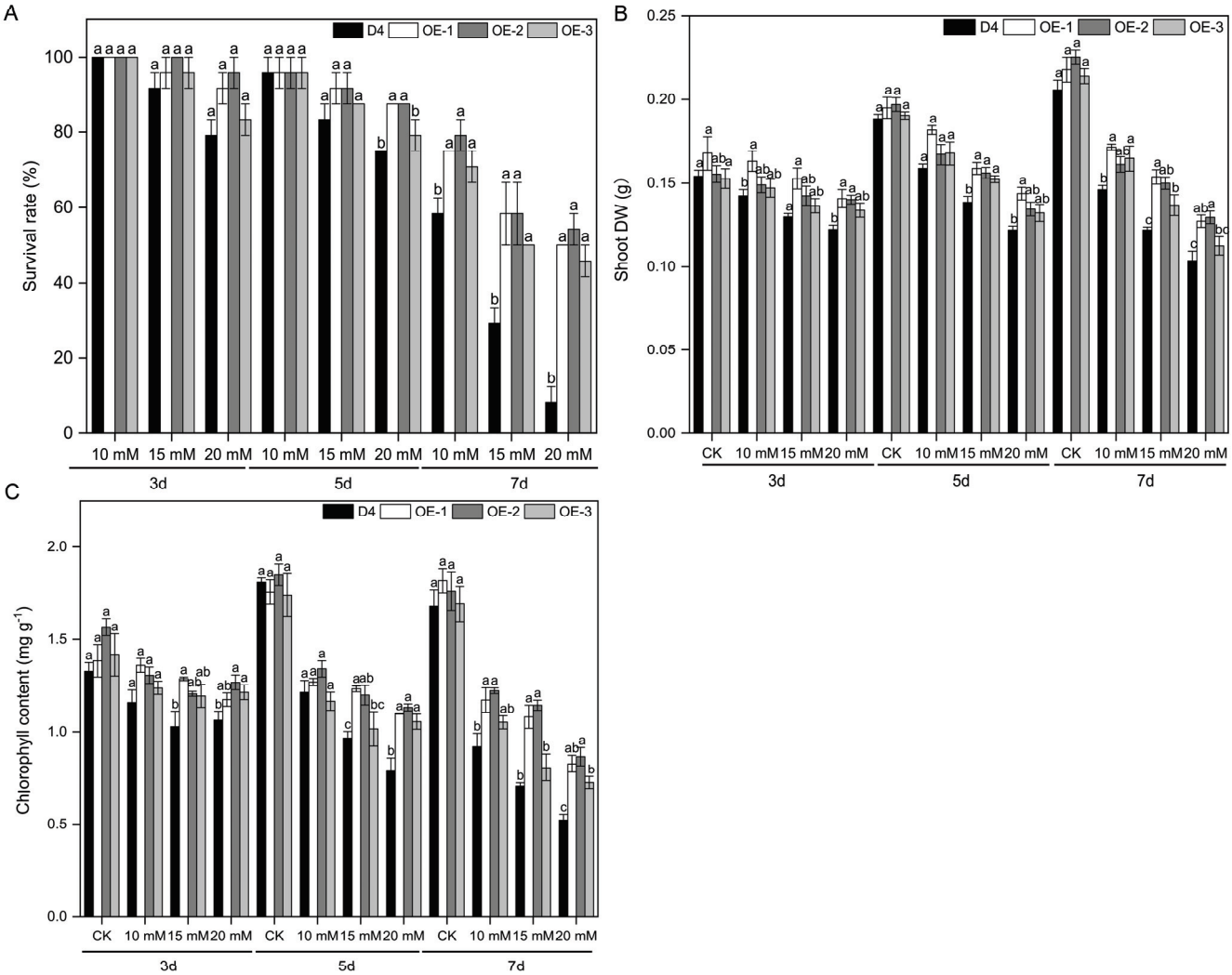


Figure 2. Survival rates, dry weights, and chlorophyll contents of different rice seedling lines under alkaline stress conditions. The survival rates (**A**), dry weights (DWs) (**B**), and chlorophyll contents (**C**) of D4 and transgenic line (OE-1, OE-2, and OE-3) rice seedlings at three leaf stages under 10, 15, and 20 mM Na_2CO_3 and non-stress conditions (CK, pure nutrient solution) for 3, 5, and 7 d. Values are means ± SD, $n = 3$. The letters depicted on the column denote statistically significant differences among distinct rice lines subjected to identical treatment conditions based on Duncan's test ($p < 0.05$).

Alkaline stress also leads to a marked reduction in shoot dry weight and chlorophyll content in rice seedlings. OE-1, OE-2, and OE-3 maintained higher shoot dry weights and chlorophyll content in leaves than the WT under 15 mM and 20 mM Na_2CO_3 stress conditions for either 5 or 7 d ($p < 0.05$) (Figure 2B,C).

2.3. Overexpression of OsNCED3 Upregulated ABA Contents and the Expression of ABA Response-Related Genes under Na_2CO_3 Stress Conditions

Compared to the WT plants, overexpression of *OsNCED3* indicated a significant increase in ABA levels ($p < 0.05$) (Figure 3A). Under 10 mM Na_2CO_3 stress, the difference in ABA content between the transgenic lines and the WT remained relatively minimal. Nevertheless, when subjected to higher Na_2CO_3 stress concentrations of 15 and 20 mM, transgenic lines demonstrated strikingly elevated ABA content compared to the WT, indicating a significant accumulation effect. Among the transgenic lines, OE-2 exhibited the highest ABA content across different alkaline stress concentrations.

The transgenic lines exhibited significantly elevated expression levels of *OsNCED3* compared to the WT under alkaline stress concentrations ($p < 0.05$) (Figure 3B). The expression of *OsSalT* and *OsWsi18* was significantly upregulated in different rice lines under alkaline stress conditions, with higher upregulation observed in the transgenic lines than the WT plants ($p < 0.05$) (Figure 3C).

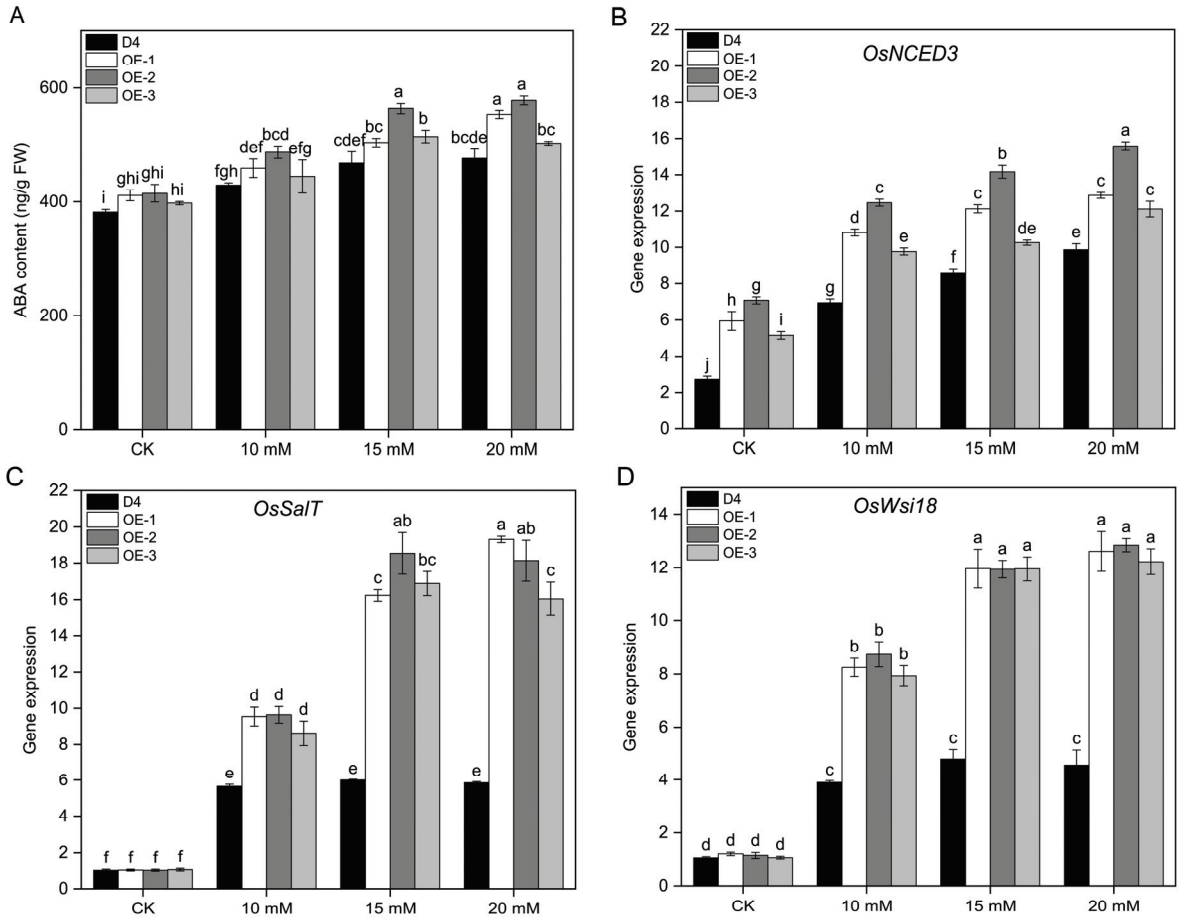


Figure 3. ABA contents and expression levels of *OsNCED3* and ABA-response genes of different rice seedling lines under alkaline conditions. The ABA contents (**A**) of D4 and transgenic line (OE-1, OE-2, and OE-3) rice seedlings at three leaf stages under 10, 15, and 20 mM Na_2CO_3 and non-stress conditions (CK, pure nutrient solution) for 3 d. The expression of *OsNCED3* (**B**), *OsSalT* (**C**), and *OsWsi18* (**D**) of D4 and transgenic line (OE-1, OE-2, and OE-3) rice seedlings at three leaf stages under 15 mM Na_2CO_3 and non-stress conditions (CK, pure nutrient solution) for 24 h. Values are means ± SD, $n = 3$. The letters depicted on the column denote statistically significant differences among distinct rice lines subjected to different treatment conditions based on Duncan's test ($p < 0.05$).

2.4. Overexpression of OsNCED3 Improved Contents of Osmotic Substances in Rice Seedlings under Na_2CO_3 Stress Conditions

Alkaline stress induces accumulation of proline, soluble sugars, and starch in rice seedlings. The transgenic lines OE-1, OE-2, and OE-3 exhibited significantly higher proline, soluble sugar, and starch contents in leaves than WT plants under different concentrations of Na_2CO_3 stress ($p < 0.05$) (Figure 4A–C). With an increase in Na_2CO_3 stress concentration and duration, differences in contents of proline and soluble sugars became more apparent. In addition, OE-1 and OE-2 accumulated higher contents of osmotic substances than OE-3.

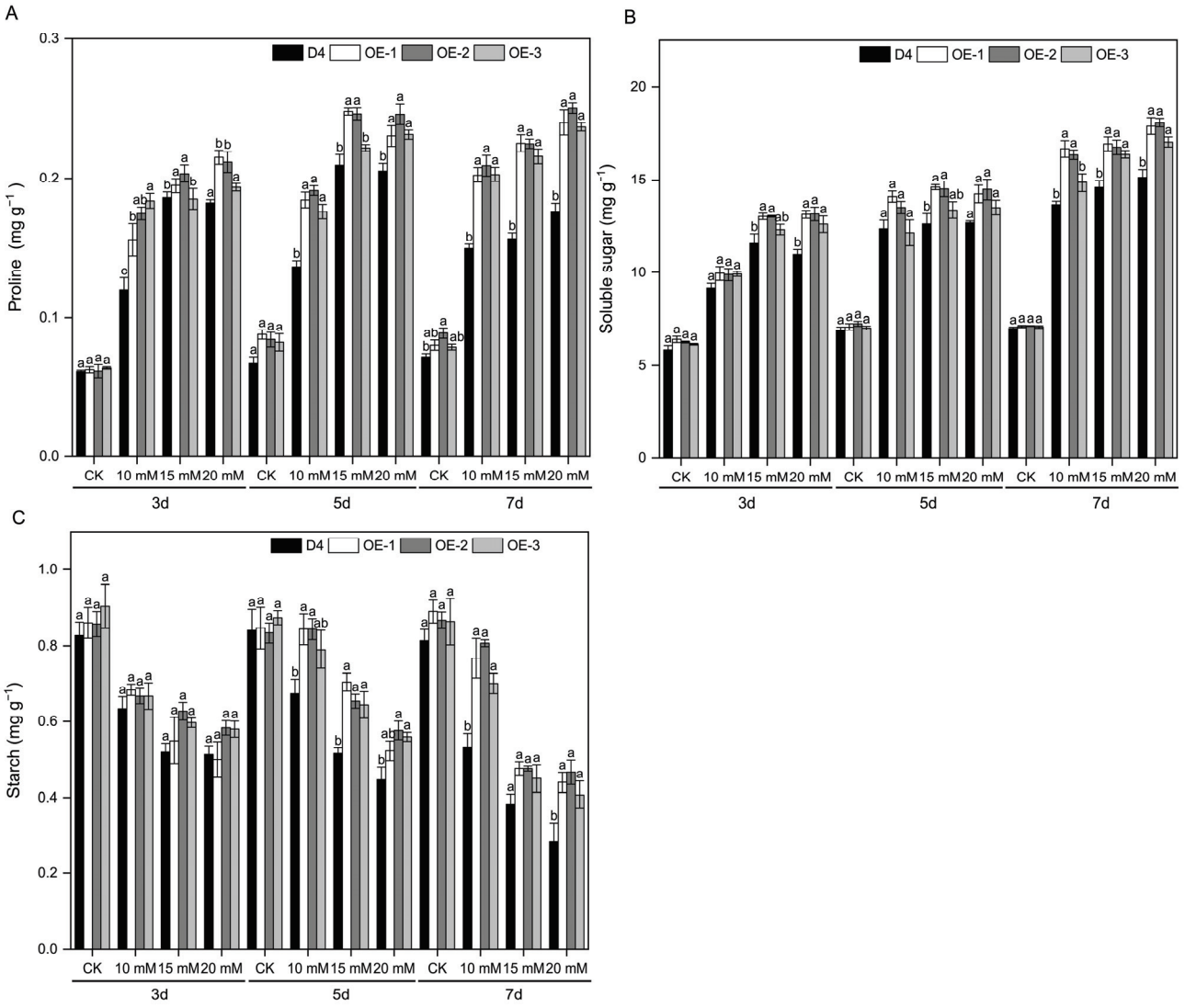


Figure 4. The contents of osmotic substances of different rice seedling lines under alkaline conditions. The contents of proline (**A**), soluble sugar (**B**), and starch (**C**) of D4 and transgenic line (OE-1, OE-2, and OE-3) rice seedlings at three leaf stages under 10, 15, and 20 mM Na_2CO_3 and non-stress conditions (CK, pure nutrient solution) for 3, 5, and 7 d. Values are means ± SD, $n = 3$. The letters depicted on the column denote statistically significant differences among distinct rice lines subjected to identical treatment conditions based on Duncan's test ($p < 0.05$).

2.5. Overexpression of OsNCED3 Regulated Ion Homeostasis of Rice Seedlings under Na_2CO_3 Stress Conditions

Alkaline stress resulted in an increased content of Na^+ of rice seedlings, accompanied by simultaneously decreased contents in both K^+ and Ca^{2+}. Overexpression of the *OsNCED3* gene demonstrated remarkable effectiveness in mitigating the accumulation of Na^+, enhancing the accumulation of K^+ and Ca^{2+}, elevating both Ca^{2+}/Na^+ and K^+/Na^+ ratios in rice leaves subjected to alkaline stress ($p < 0.05$). Specifically, OE-1 and OE-2 exhibited lower Na^+ content than OE-3 under varying concentrations of Na_2CO_3 stress conditions (Figure 5A–D). The Ca^{2+}/Na^+ ratio of OE-1, OE-2, and OE-3 increased by 62.96%, 58.89%, and 29.77%, respectively, compared to WT plants after 7 days of exposure to 20 mM Na_2CO_3 stress. Similarly, the K^+/Na^+ ratio increased by 1.7-, 2.2, and 1.0 times, respectively.

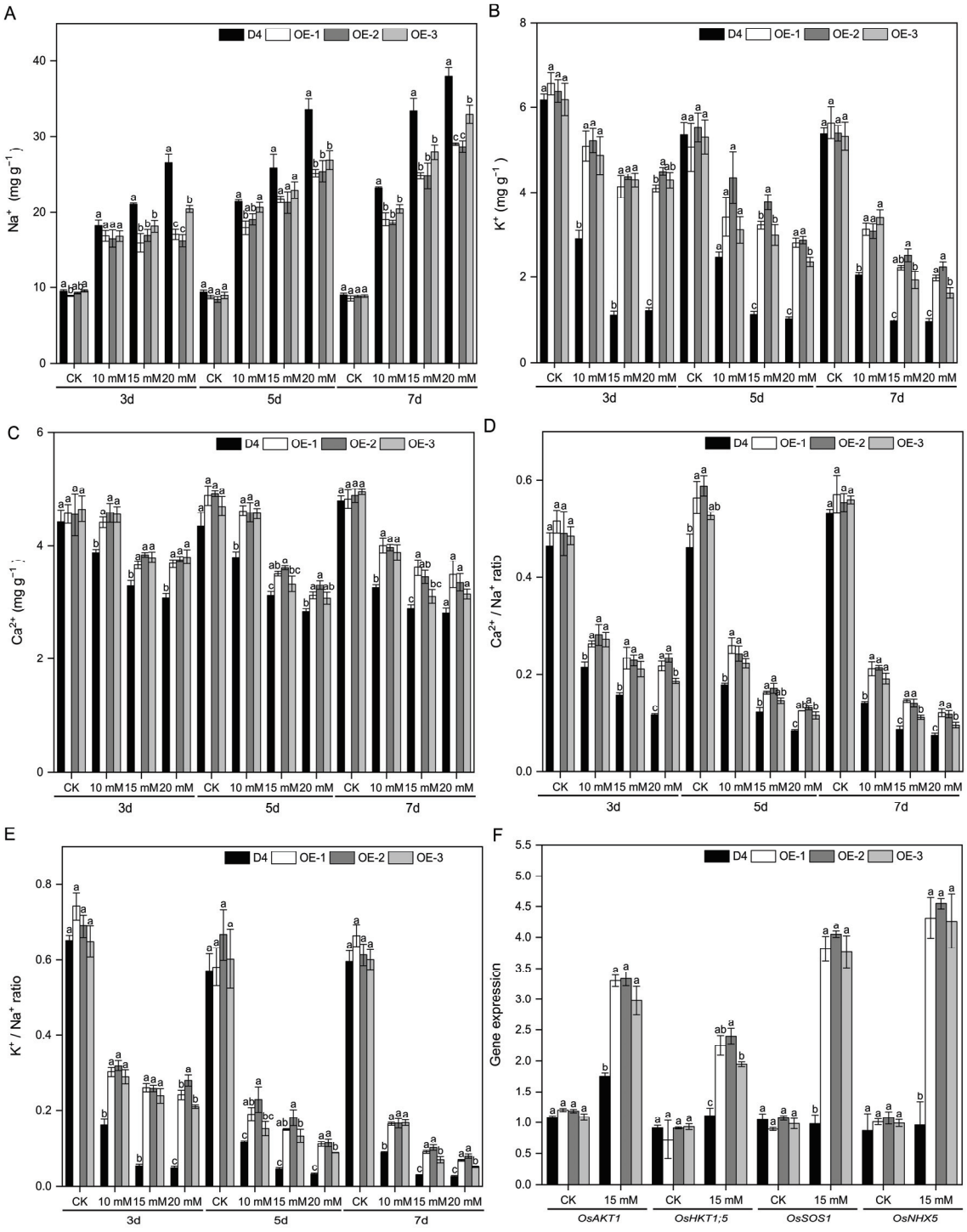


Figure 5. The ion contents and expression levels of ion homeostasis-relative genes of different rice lines under alkaline stress conditions. The contents of Na^+ (**A**), K^+ (**B**), Ca^{2+} (**C**), Ca^{2+}/Na^+ ratio (**D**), and K^+/Na^+ ratio (**E**) of D4 and transgenic line (OE-1, OE-2, and OE-3) rice seedlings at three leaf stages under 10, 15, and 20 mM Na_2CO_3 and non-stress conditions (CK, pure nutrient solution) for 3, 5, and 7 d. The expression of ion homeostasis-relative genes (**F**) of D4 and transgenic line (OE-1, OE-2, and OE-3) rice seedlings at three leaf stages under 15 mM Na_2CO_3 and non-stress conditions (CK, pure nutrient solution) for 24 h. Values are means ± SD, $n = 3$. The letters depicted on the column denote statistically significant differences among distinct rice lines subjected to identical treatment conditions based on Duncan's test ($p < 0.05$).

In comparison with the CK, alkaline stress significantly upregulated the expression of the ion homeostasis-related genes *OsAKT1*, *OsHKT1;5*, *OsSOS1*, and *OsNHX5* in the leaves of different lines ($p < 0.05$), and the expression levels of these genes were higher in the transgenic lines than in the WT plants (Figure 5E,F). Among the different transgenic lines, OE-2 exhibited the highest expression of ion homeostasis-related genes, and the expression levels of these genes were elevated in the transgenic lines compared to the WT plants.

2.6. Overexpression of OsNCED3 Reduced Plasma Membrane Damage and ROS Levels under Na_2CO_3 Stress Conditions

There was no substantial variation observed between the WT plants and transgenic lines in terms of plasma membrane injury (MI) or accumulation of reactive oxygen species (ROS) under non-stress conditions. Alkaline stress for 3 days led to increased plasma membrane injury in rice seedling leaves, elevated MDA content, and a sharp increase in the accumulation of $O_2 \cdot^-$ and H_2O_2. Overexpression of *OsNCED3* resulted in significantly reduced accumulation of $O_2 \cdot^-$ and H_2O_2, as well as lower MDA content and MI under alkaline stress conditions, among which OE-1 and OE-2 had lower plasma membrane injury and ROS accumulation than OE-3 ($p < 0.05$) (Figure 6A–D).

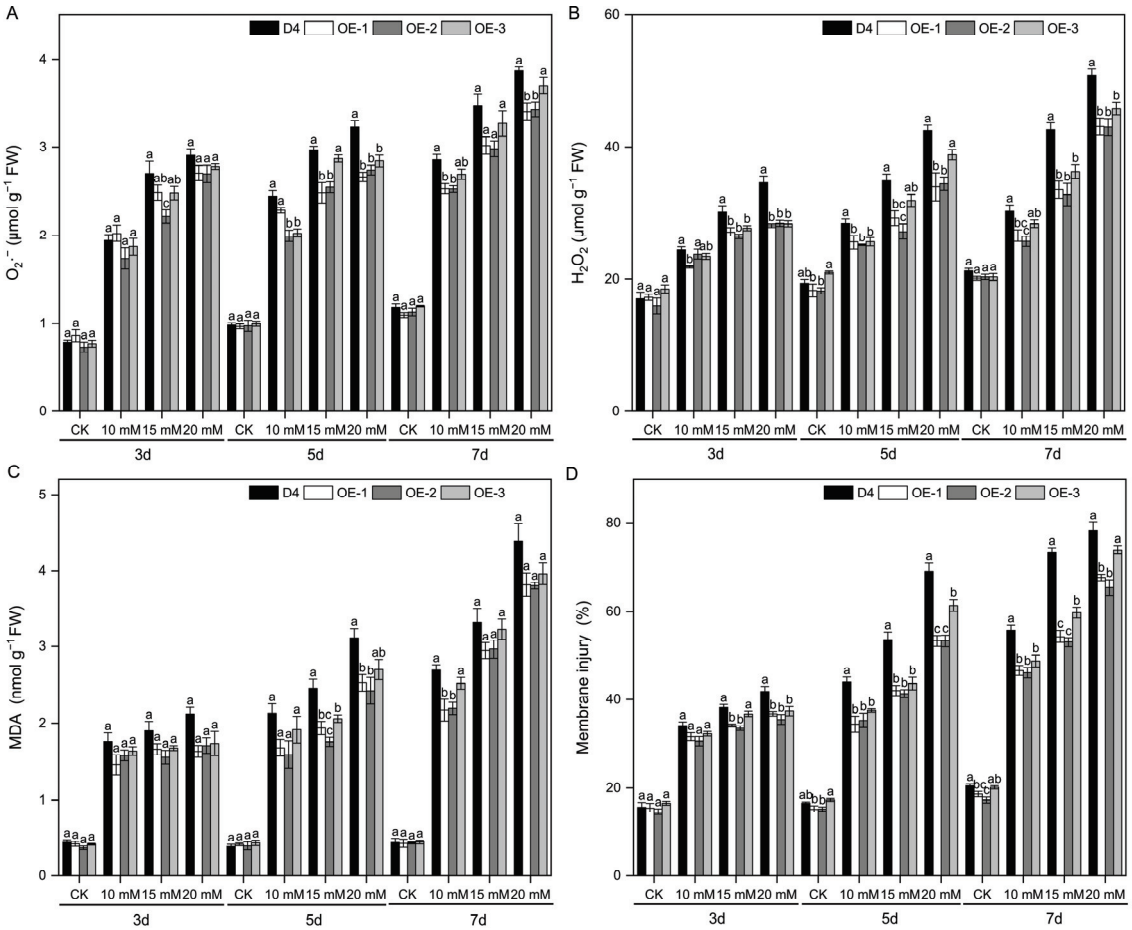


Figure 6. The ROS and MDA levels and membrane injury (MI) of different rice lines under alkaline stress conditions. The contents of $O_2 \cdot^-$ (**A**), H_2O_2 (**B**), MDA (**C**), and membrane injury (**D**) of D4 and transgenic line (OE-1, OE-2, and OE-3) rice seedlings at three leaf stages under 10, 15, and 20 mM Na_2CO_3 and non-stress conditions (CK, pure nutrient solution) for 3, 5, and 7 d. Values are means ± SD, $n = 3$. The letters depicted on the column denote statistically significant differences among distinct rice lines subjected to identical treatment conditions based on Duncan's test ($p < 0.05$).

2.7. Overexpression of OsNCED3 Enhanced Antioxidant Defense Capabilities under Na_2CO_3 Stress Conditions

There was no significant difference in the antioxidant enzyme activity of the leaves between the WT and transgenic lines under non-stress conditions. Alkaline stress for 3 d enhanced the antioxidant enzyme activities of SOD, POD, CAT, APX, GPX, and GR in rice seedling leaves. The antioxidant enzyme activities of the *OsNCED3* overexpression transgenic lines were significantly higher than those of the WT plants under alkaline stress ($p < 0.05$) (Figure 7A), with a more pronounced difference under 20 mM Na_2CO_3 stress.

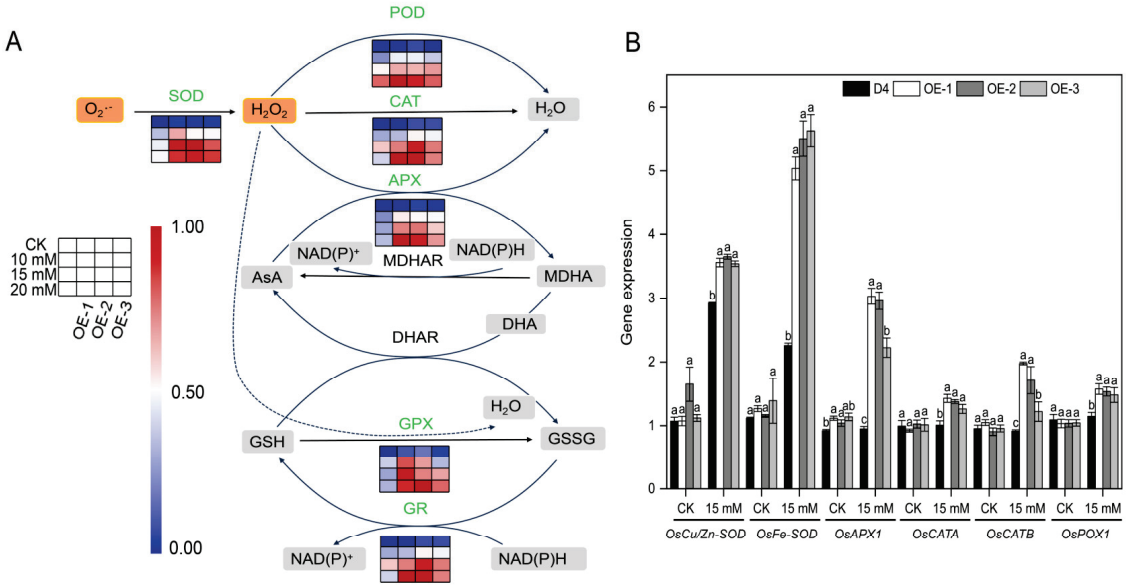


Figure 7. The ROS and MDA levels and membrane injury (MI) of different rice lines under alkaline stress conditions. Activities of antioxidant enzymes (**A**) of D4 and transgenic line (OE-1, OE-2, and OE-3) rice seedlings at three leaf stages under 10, 15, and 20 mM Na_2CO_3 and non-stress conditions (CK, pure nutrient solution) for 3 d. The expression of ion homeostasis-relative genes (**B**) of D4 and transgenic line (OE-1, OE-2, and OE-3) rice seedlings at three leaf stages under 15 mM Na_2CO_3 and non-stress conditions (CK, pure nutrient solution) for 24 h. Values are means ± SD, $n = 3$. The letters depicted on the column denote statistically significant differences among distinct rice lines subjected to identical treatment conditions based on Duncan's test ($p < 0.05$).

Furthermore, the expression of the ROS scavenging-related genes *OsCu/Zn-SOD*, *OsFe-SOD*, *OsPOX1*, *OsCATA*, *OsCATB*, and *OsAPX1* were significantly higher in the transgenic lines than in the WT plants ($p < 0.05$). Among the different genes, the upregulation of *OsCu/Zn-SOD*, *OsFe-SOD*, and *OsAPX1* was relatively high in the transgenic lines under alkaline stress (Figure 7B).

3. Discussion

Approximately 20% of cultivated land and 50% of irrigated land are affected by various degrees of soil salinization [42,43], posing a threat to global food security [44]. Saline–alkaline stress hinders the normal growth, development, and physiological functions of plants [45,46]. Many studies have shown that alkaline stress (dominated by $NaHCO_3$ and Na_2CO_3) has a much greater impact on plant growth and development than neutral salt stress (dominated by NaCl and Na_2SO_4) [3,47]. This is primarily due to the high pH caused by alkaline stress, in addition to osmotic stress and ionic toxicity [48,49].

ABA is a hormone that significantly affects plant growth and metabolism, and it is involved in physiological responses to environmental stresses [22,50,51]. The dynamic balance between endogenous ABA levels in plants is regulated by biosynthesis [52]. Modulating endogenous ABA levels in crops through genetic engineering techniques is one

approach to enhance their survival and stress resistance under saline–alkaline conditions. In most higher plants, ABA is synthesized from carotenoids through a C40 indirect pathway, which involves the catalysis of various crucial enzymes. Among these enzymes, 9-cis-epoxycarotenoid dioxygenase (NCED) is a crucial rate-limiting enzyme that plays a pivotal role in the biosynthesis pathway of ABA [53,54]. The rice *OsNCED* gene family comprises a series of genes ranging from *OsNCED1* to *OsNCED5*, all of which play a pivotal role in the modulation of plant resistance mechanisms. Therefore, a comprehensive exploration of the *OsNCED* gene family and its regulatory mechanisms is crucial for enhancing our understanding of alkaline tolerance mechanisms, thereby establishing a theoretical foundation for cultivating rice varieties that exhibit superior resistance. In the present study, we overexpressed the key ABA biosynthesis gene *OsNCED3* in the rice cultivar Dongdao 4 (D4) and obtained the three transgenic rice lines OE-1, OE-2, and OE-3. The results showed that under alkaline stress, transgenic rice seedlings exhibited superior growth trends compared to WT plants (D4), with less wilting and death. Among them, OE-2 exhibited the best phenotypic growth (Figure 1). The survival rates of the transgenic lines overexpressing *OsNCED3* were significantly higher than those of WT plants under alkaline stress ($p < 0.05$) (Figure 2A). Additionally, the overexpression of *OsNCED3* significantly increased the contents of dry weight and chlorophyll under alkaline stress (Figure 3A). Therefore, overexpression of the *OsNCED3* gene can significantly improve the growth of rice seedlings under alkaline stress, alleviate leaf wilting, and enhance seedling survival rates.

The ABA content and *OsNCED3* expression levels in the transgenic lines were significantly higher than those in the WT plants under alkaline stress, and the differences became more apparent with increasing concentrations and durations of alkaline stress ($p < 0.05$) (Figure 3A,B). The OE-2 line had the highest ABA content and *OsNCED3* gene expression levels compared to the other transgenic lines and WT plants under different alkaline stress concentrations. Furthermore, *OsSalT* and *OsWsi18* are key regulatory genes for plant tolerance to stress conditions, respond significantly to both salt stress and ABA treatment in rice, and are considered ABA-responsive genes [25,55]. In the present study, we found that the expression of the ABA-responsive genes *OsSalT* and *OsWsi18* was significantly upregulated in both the wild-type and transgenic lines. However, the transgenic lines exhibited a significantly higher amplitude of upregulation. This suggests that the transgenic lines had enhanced tolerance to alkaline stress, owing to an increase in endogenous ABA levels and activation of the ABA signaling pathway.

Under saline stress, osmolytes play a pivotal role in osmotic adjustment by decreasing the cellular osmotic potential and stabilizing proteins as well as cellular structures [56]. When rice is exposed to saline–alkaline stress, it accumulates osmolytes as osmoprotectants to enhance its resistance [57]. This study revealed that OE-1, OE-2, and OE-3 exhibited significantly higher levels of proline, soluble sugars, and starch in leaves under alkaline stress than the WT plants ($p < 0.05$) (Figure 4). The enhanced ABA biosynthesis in plants potentially modulates the osmotic adjustment mechanism in rice subjected to alkaline stress.

Excessive accumulation of Na^+ may lead to ion toxicity and damage to plants under saline and alkaline stress. The content of Na^+ and K^+ serve as important indicators for assessing plant resistance to saline–alkaline stress [58–60]. In the present study, we found that the overexpression of *OsNCED3* significantly reduced the accumulation of Na^+ in rice leaves under alkaline stress, increased the accumulation of K^+ and Ca^{2+}, and significantly improved the Ca^{2+}/Na^+ and K^+/Na^+ ratios ($p < 0.05$) (Figure 5A–E). Maintenance of ion homeostasis is closely related to the regulation of relevant genes. The cell membrane contains various ion channels and transporter proteins that regulate ion influx and efflux, thereby maintaining the ion concentration balance inside and outside the cell. Additionally, intracellular gene transcription regulatory systems are involved in regulating ion balance. For example, the high-affinity potassium (K^+) transporter 1;5 (*OsHKT1;5*) in rice functions as a Na^+-selective transporter that mediates Na^+ efflux through Na^+ removal from the xylem to maintain the Na^+/K^+ balance under salt stress [61]. Wang isolated a salt stress-

sensitive mutant, osbag4-1, which exhibited significantly reduced expression of *OsHKT1;5* and K^+ content, as well as increased Na^+ content in the shoots [62]. Salt overly sensitive protein 1 (SOS1) and the Na^+/H^+ exchanger (NHX) also played crucial roles in the Na^+ balance [63]. Exposure to high salinity stress triggers calcium signaling, which in turn activates the SOS pathway [64]. The expression of *SsSOS1* is significantly induced by NaCl [65].

The vacuolar Na^+/H^+ transporters *OsNHX1*, *OsNHX2*, *OsNHX3*, *OsNHX4*, and *OsNHX5* play an important role in the cytoplasmic accumulation of Na^+ and K^+, thereby determining salt tolerance in rice [66]. SOS1, the plasma membrane Na^+/H^+ exchanger, plays a key role in the salt tolerance response of rice by promoting Na^+ expulsion [67]. Members of the high-affinity K+ transporter (HKT) family in rice, including *OsHKT1;1*, *OsHKT1;4*, *OsHKT7*, *OsHKT8*, and *OsHKT1;5*, transport Na^+ or both Na^+ and K^+, assisting in maintaining the Na^+/K^+ balance in the cytoplasm and regulating the rice's response to saline and alkaline stresses [68,69]. In the present study, the overexpression of *OsNCED3* significantly upregulated the expression of the ion homeostasis-related genes *OsAKT1*, *OsHKT1;5*, *OsSOS1*, and *OsNHX5* in rice seedling leaves (Figure 5F). Moreover, exogenous ABA treatment can significantly reduce the Na^+ content and Na^+/K^+ ratios [70], which had similar regulatory effects with the overexpression of *OsNCED3* to change endogenous ABA level in this study on maintaining ion homeostasis in rice seedlings under alkaline stress.

NADPH oxidase (Rboh) is widely recognized as the primary source of H_2O_2. Studies have shown that when rice seedlings are subjected to NaCl stress, the *OsRbohA* gene is upregulated in both the shoot and root tissues. However, the tolerance of rice to saline stress is significantly reduced when the *OsRbohA* gene is knocked out [71]. Overexpression lines of *OsMn-SOD* and *OsCu/Zn-SOD* exhibit lower levels of H_2O_2 accumulation [72]. The upregulating expression of *OsAPX2*, *OsAPX7*, *OsAPX8*, *OsAPXa*, and *OsAPXb* enhance APX activity, reduce the levels of H_2O_2 and malondialdehyde (MDA), mitigate oxidative stress damage, and improve the salt tolerance of rice [73]. Additionally, *OsGR2*, *OsGR3*, and *OsGRX8* increase GSH content and enhance tolerance to various abiotic stresses [74]. In this study, the transgenic lines overexpressing *OsNCED3* exhibited significantly reduced accumulation of $O_2\cdot^-$, H_2O_2, and MDA, as well as lower plasma membrane injury in leaves under alkaline stress ($p < 0.05$) (Figure 6). To counter this damage, plants have gradually developed a complex antioxidant defense system during their long-term evolution that includes enzymatic and non-enzymatic ROS scavengers [75]. Enzymatic ROS scavengers include POD, CAT, SOD, APX, GPX, and GR [76]. This study also found that under alkaline stress, the transgenic lines had significantly higher antioxidant enzyme activities than the WT plants and higher expression levels of the ROS scavenging-related genes OsCu/Zn-SOD, *OsFe-SOD*, *OsPOX1*, *OsCATA*, *OsCATB*, and *OsAPX1* (Figure 7). Regulation of the antioxidant enzyme system by overexpressing *OsNCED3* plays a key role in maintaining ROS homeostasis within rice seedling cells, which helps rice adapt to alkaline stress environments. ABA could reduce the accumulation of $O_2\cdot^-$ and H_2O_2 in rice leaves under high pH conditions [74,77]. The tolerance of alfalfa to alkaline stress was enhanced by applying ABA to increase antioxidant enzyme activity [35], consistent with the findings of the present study. The overexpression of *OsNCED3* may significantly increase antioxidant enzyme activity and serve as an important defense mechanism against lipid peroxidation and membrane damage caused by alkaline stress.

4. Materials and Methods

4.1. Plant Material

In our experiment, a locally grown japonica rice cultivar named 'Dongdao 4' (D4) was utilized. The D4 was bred through the crossing of 'Akitakomachi' and 'Nongda-10' in Jilin, China.

4.2. DNA Construction and Plant Transformation

The genomic DNA in rice leaves was used as the template for PCR amplification. The full length of *OsNCED3* cDNA (Os03g0645900) sequence was cloned and constructed to the overexpression vector with 35S promoter. The rice cultivar D4 was transformed using the *Agrobacterium* strain EHA105 for rice transformation. For details on the technique used, refer to the protocol described by Toki [78]. Multiple primary transformants, which were designated as T0 plants, underwent self-fertilization to yield T1 generation seeds. T1 transgenic plants exhibiting resistance to hygromycin B were identified by subjecting them to conditions containing 30 μg mL^{-1} of hygromycin B in a medium containing 0.8% agar. These plants showed a segregation ratio of 3:1, favoring resistance to hygromycin B (Hyg-R vs. Hyg-S), which indicated the presence of a single transgene insertion. Subsequently, the selected plants were self-fertilized to produce T2 seeds that were homozygous for the transgene. From this process, three independent homozygous lines of T2 *OsNCED3*-OE were successfully isolated and designated OE-1, OE-2, and OE-3.

4.3. Plant Culture Conditions

The rice seeds were first disinfected for 10 min in a 0.1% (*w*/*v*) $HgCl_2$ solution, followed by thorough rinsing with distilled water. Then, the seeds were soaked in a beaker filled with distilled water and placed in a constant-temperature incubator at 30 °C for 48 h. After soaking, the seeds were spread at the bottom of a Petri dish and germinated in a constant-temperature incubator set at 28 °C for 24 h. Germinated rice seeds exhibiting uniform germination were planted in 96-well black culture plates and placed in a black plastic culture box 12 mm in length, 87 mm in width, and 114 mm in height. They were grown in distilled water for five days. Afterward, the seedlings were transferred to 1/2 Miyake B nutrient solution [79] and further cultivated in a growth chamber (HPG-400HX; Hadonglian Inc., Beijing, China) under conditions of 25 °C during the light period and 20 °C during the dark period, with a photoperiod of 12 h, until they reached the 3-leaf stage.

4.4. Stress Treatments

To simulate alkaline stress treatments with varying degrees, solutions of different concentrations of Na_2CO_3 were prepared using analytical grade reagents, specifically 10 mM (pH: 10.61 ± 0.024, EC: 2.33 ± 0.004 mS/cm), 15 mM (pH: 10.82 ± 0.032, EC: 2.80 ± 0.002 mS/cm), and 20 mM (pH: 11.14 ± 0.037, EC: 3.39 ± 0.002 mS/cm). The pH of the solutions was determined using a PHS-25 acidity meter, while the electrical conductivity (EC) was measured utilizing a DDS-12D conductivity meter. To assess the effects of alkaline stress, rice seedlings were treated with 10, 15, or 20 mM Na_2CO_3 solutions representing different stress gradients. The control group (CK) was cultivated in nutrient solution without stress. The growth indices and physiological characteristics of rice seedlings were measured on days 3, 5, and 7 under alkaline stress. Each treatment was replicated three times.

4.5. Measurement of Survival Rate and Seedling Growth

After six days of alkaline stress, the survival rate of each rice seedling was investigated. Seedlings were considered dead if their leaves were wilted and shriveled and the whole plant was curled up and wilted. Ten seedlings were randomly chosen and deactivated by exposing them to a temperature of 105 °C for an hour, subsequently maintaining them at 70 °C until they reached a constant mass to enable the measurement of their dry weight.

4.6. Measurement of Contents of Na^+, K^+, and Ca^{2+}

The rice samples underwent a drying process by being placed in an oven maintained at 80 °C. Subsequently, 0.1 g of the dried rice leaf samples were accurately measured and transferred into a flask. To facilitate digestion, 4 mL of HNO_3 and 2 mL of $HClO_4$ were added to the flask. Upon completion of the digestion process, the resulting solution was diluted to a total volume of 50 mL. The determination of Na^+, K^+, and Ca^{2+} contents in the

samples was achieved through use of inductively coupled plasma spectrometry (ICPS-7500, Shimadzu Corporation, Kyoto, Japan).

4.7. Measurement of Chlorophyll Content and Endogenous ABA Levels

Chlorophyll content was determined by extraction with a mixed solution of ethanol and acetone [80], with minor modifications. Rice seedling leaves (0.1 g fresh weight) from each treatment were weighed, shredded, and placed in a 15 mL centrifuge tube, and then 10 mL of ethanol–acetone mixed solution (volume ratio 1:1) was added to fully immerse the leaves. When the leaves were completely decolorized and turned white, the absorbance values of the extract at 645 and 663 nm were measured using a spectrophotometer and were denoted as A645 and A663, respectively. ABA content in rice seedlings was determined using an ELISA kit [81].

4.8. Measurement of Membrane Injury (MI), Malondialdehyde (MDA) Content, ROS Levels, and Antioxidant Enzyme Activities

The degree of membrane injury (MI) in seedlings was assessed by measuring their relative electrical conductivity, as described by Zhang [82]. The quantification of malondialdehyde (MDA) content was quantified using the thiobarbituric acid (TBA) reaction method [83]. The samples underwent pulverization twice, utilizing a high-throughput tissue crusher operating at 50 Hz for 30 s. Subsequently, 1 mL of a 50 mM phosphate buffer adjusted to a pH of 7.8 was introduced, and the mixture was vigorously vortexed. The homogenate was then centrifuged at 12,000 rpm for 15 min in a temperature-controlled environment of 4 °C. Following centrifugation, 400 µL of the supernatant was combined with 1 mL of 0.5% TBA. The mixture was incubated in a boiling water bath for 20 min, subsequently cooled rapidly, and centrifuged again. The optical density (OD) of the supernatant was assayed at 600 nm, 532 nm, and 450 nm to assess its spectrophotometric properties. The MDA content was calculated using the following formula: $6.45 \times (A532 - A600) - 0.56 \times A450$. Measurement of superoxide anion radical ($O_2 \cdot^-$) and hydrogen peroxide (H_2O_2) contents and the antioxidant enzyme activities were measured as described previously [16].

4.9. Measurement of Proline, Soluble Sugar, and Starch Contents

Dry leaf segments of rice seedlings were measured at 0.1 g, 80% ethanol was added, and the mixture was ground into a homogenous slurry. Afterwards, the slurry underwent a filtering process through filter paper in order to acquire sugar extracts. Subsequently, the content of soluble sugar (SS) was measure. This involved adding 0.2% anthrone to the extract, boiling it for 15 min in a water bath, allowing it to cool to room temperature, and measuring the absorbance value at 620 nm, as per the protocol described by Wei [84]. To determine proline, the ninhydrin colorimetric method was employed with modifications based on the approach outlined by Bates [85]. The starch content was determined by the protocol described by Wang [86].

4.10. qRT-PCR

The expression levels of genes related to the ABA response, ion homeostasis, and reactive oxygen species scavenging were detected in each leaf sample stressed for 24 h. The specific primer sequences for all genes are shown in Table S1. Total RNA was extracted (TRIzol reagent, TaKaRa Bio, Tokyo, Japan), followed by reverse transcription (M-MLV reverse transcriptase, Thermo Fisher Scientific, Carlsbad, CA, USA). The qRT-PCR procedure was performed following a previously reported method [16] with *β-actin* (GenBank ID: X15865.1) as an internal standard. The relative expression level was calculated using the $2^{-\triangle\triangle CT}$ method [87], with each treatment replicated in three biological replicates.

4.11. Statistical Analyses

We used IBM SPSS (version 21.0; IBM Corp., Armonk, NY, USA) to conduct comprehensive statistical analyses. Based on the outcomes of the one-way analysis of variance (ANOVA), Duncan's multiple range test (DMRT) was used to assess significant differences ($p < 0.05$). A graphical representation of the data was meticulously created using Origin 2021.

5. Conclusions

Alkaline stress significantly disrupts numerous biochemical and physiological processes, resulting in a reduced survival rate of rice seedlings. Abscisic acid (ABA) plays a positive role in regulating the tolerance of plants to alkaline stress. In summary, the overexpression of the rice ABA biosynthesis gene *OsNCED3* can increase endogenous ABA levels in rice, further activating the ABA signal transduction pathway to enhance osmotic adjustment, ion homeostasis, ROS scavenging, and antioxidant defense. It can also induce the expression of stress response genes, thereby reducing plasma membrane injury and ROS accumulation in seedling leaves, promoting osmotic accumulation, ion balance, and antioxidant defense. These findings provided a highly effective molecular approach to enhancing the alkaline tolerance of rice seedlings. By leveraging modern biotechnology and genetic breeding techniques, we can further explore and harness the potential of the *OsNCED* gene family, offering robust support to agricultural production on saline–alkaline soils. This molecular approach presents a sustainable means of enhancing crop tolerance, thereby revolutionizing agricultural production, even in challenging environments like saline–alkaline paddy fields. In this way, it is possible to help ensure food security and promote sustainable agriculture.

Supplementary Materials: The following supporting information can be downloaded at: https://www.mdpi.com/article/10.3390/plants13121713/s1. Table S1. List of primers used in quantitative real-time PCR analysis.

Author Contributions: W.L. and Z.L. designed and planned the research. Z.F. and Y.X. focused equally on writing and editing. Z.F., Y.X., Y.Y., G.L. and Y.J. performed experiments and analyzed the data. Z.X., M.W., M.L. and H.Y. helped with designing, executing, and interpreting experiments. Z.L. and W.L. edited the manuscript. W.L. and Z.L. agreed to serve as the authors responsible for contact and communication. All authors have read and agreed to the published version of the manuscript.

Funding: This work was funded by the Strategic Priority Research Program of the Chinese Academy of Sciences (Grant No. XDA28110100); the National Key Research and Development Program of China (Project No. 2022YFD1500500); the Science and Technology Project of the Education Department of Jilin Province (Project Number: JJKH20230019KJ); the Science and Technology Development Plan Project of Baicheng city (202206); the Key Scientific and Technological Project of Jilin Province (20240203002NC); the National Natural Science Foundation of China (42377040); and the Technology Cooperation High-Tech Industrialization Project of Jilin Province and the Chinese Academy of Sciences (2023SYHZ0045).

Data Availability Statement: Data are contained within the article and Supplementary Materials.

Acknowledgments: We express our sincere gratitude to Changjie Jiang and Xianzhi Xie from Shandong Academy of Agricultural Sciences (China) for their invaluable assistance in producing the transgenic rice lines.

Conflicts of Interest: The authors declare no conflicts of interest.

References

1. Food and Agriculture Organization. Management of Salt Affected Soils; Food and Agriculture Organization of the United Nations. 2016. Available online: http://www.fao.org/soils-portal/soil-management/management-of-some-problem-soils/salt-affected-soils/more-information-on-salt-affected-soils/en/ (accessed on 18 June 2024).
2. Pang, Q.; Zhang, A.; Zang, W.; Wei, L.; Yan, X. Integrated proteomics and metabolomics for dissecting the mechanism of global responses to salt and alkali stress in Suaeda corniculate. *Plant Soil* **2016**, *402*, 379–394. [CrossRef]

3. Lv, B.; Li, X.; Ma, H.; Sun, Y.; Wei, L.; Jiang, C.; Liang, Z. Differences in growth and physiology of rice in response to different saline-alkaline stress factors. *Agron. J.* **2013**, *105*, 1119–1128. [CrossRef]
4. Rao, Y.; Peng, T.; Xue, S. Mechanisms of plant saline-alkaline tolerance. *J. Plant Physiol.* **2023**, *281*, 153916. [CrossRef]
5. Wei, L.; Lv, B.; Wang, M.; Ma, H.; Yang, H.; Liu, X.; Jiang, C.; Liang, Z. Priming effect of abscisic acid on alkaline stress tolerance in rice (*Oryza sativa* L.) seedlings. *Plant Physiol. Biochem.* **2015**, *90*, 50–57. [CrossRef]
6. Liu, B.; Liu, Y.; Huang, G.; Jiang, X.; Liang, Y.; Yang, C.; Huang, L. Comparison of yield prediction models and estimation of the relative importance of main agronomic traits affecting rice yield formation in saline-sodic paddy fields. *Eur. J. Agron.* **2023**, *148*, 126870. [CrossRef]
7. Liu, M.; Liang, Z.; Yang, F.; Ma, H.; Huang, L.; Wang, M. Impacts of sand amendment on rice (*Oryza sativa* L.) growth and yield in saline-sodic soils of North-East China. *Food Agric. Environ.* **2010**, *8*, 412–418.
8. Munns, R.; Tester, M. Mechanisms of salinity tolerance. *Annu. Rev. Plant Biol.* **2008**, *59*, 651–681. [CrossRef]
9. Yu, J.; Zhu, C.; Xuan, W.; An, H.; Tian, Y.; Wang, B.; Chi, W.; Chen, G.; Ge, Y.; Li, J.; et al. Genome-wide association studies identify *OsWRKY53* as a key regulator of salt tolerance in rice. *Nat. Commun.* **2023**, *14*, 3550. [CrossRef]
10. Fang, S.; Hou, X.; Liang, X. Response mechanisms of plants under saline-alkali stress. *Front. Plant Sci.* **2021**, *12*, 667458. [CrossRef]
11. Summart, J.; Thanonkeo, P.; Panichajakul, S.; Prathepha, P.; McManus, M.T. Effect of salt stress on growth, inorganic ion and proline accumulation in Thai aromatic rice, Khao Dawk Mali 105, Callus Culture. *Afr. J. Biotechnol.* **2010**, *9*, 145–152.
12. James, R.; Munns, R.; von Caemmerer, S.; Trejo, C.; Miller, C.; Condon, T. Photosynthetic capacity is related to the cellular and subcellular partitioning of Na^+, K^+ and Cl^- in salt-affected barley and durum wheat. *Plant Cell Environ.* **2006**, *29*, 2185–2197. [CrossRef]
13. Wang, W.; Liu, Y.; Duan, H.; Yin, X.; Cui, Y.; Chai, W.; Song, X.; Flowers, T.J.; Wang, S. *SsHKT1;1* is coordinated with *SsSOS1* and *SsNHX1* to regulate Na^+ homeostasis in Suaeda salsa under saline conditions. *Plant Soil* **2020**, *449*, 117–131. [CrossRef]
14. Li, Q.; Yang, A.; Zhang, W. Comparative studies on tolerance of rice genotypes differing in their tolerance to moderate salt stress. *BMC Plant Biol.* **2017**, *17*, 141. [CrossRef]
15. Lu, X.; Min, W.; Shi, Y.; Tian, L.; Li, P.; Ma, T.; Zhang, Y.; Luo, C. Exogenous melatonin alleviates alkaline stress by removing reactive oxygen species and promoting antioxidant defence in rice seedlings. *Front. Plant Sci.* **2022**, *13*, 849553. [CrossRef]
16. Feng, N.; Yu, M.; Li, Y.; Jin, D.; Zheng, D. Prohexadione-calcium alleviates saline-alkali stress in soybean seedlings by improving the photosynthesis and up-regulating antioxidant defense. *Ecotoxicol. Environ. Saf.* **2021**, *220*, 112369. [CrossRef]
17. Li, H.; Shi, J.; Wang, Z.; Zhang, W.; Yang, H. H_2S pretreatment mitigates the alkaline salt stress on Malus hupehensis roots by regulating Na^+/K^+ homeostasis and oxidative stress. *Plant Physiol. Biochem.* **2020**, *156*, 233–241. [CrossRef]
18. Khan, M.; Abdullah, Z. Salinity–sodicity induced changes in reproductive physiology of rice (*Oryza sativa*) under dense soil conditions. *Environ. Exp. Bot.* **2003**, *49*, 145–157. [CrossRef]
19. Finkelstein, R. Abscisic acid synthesis and response. In *Arabidopsis Book*; American Society of Plant Biologists: Rockville, MD, USA, 2013; Volume 11, p. e0166.
20. Dar, N.; Amin, I.; Wani, W.; Wani, S.; Shikari, A.; Wani, S.; Masoodi, K. Abscisic acid: A key regulator of abiotic stress tolerance in plants. *Plant Gene* **2017**, *11*, 106–111. [CrossRef]
21. Singh, A.; Roychoudhury, A. Abscisic acid in plants under abiotic stress: Crosstalk with major phytohormones. *Plant Cell Rep.* **2023**, *42*, 961–974. [CrossRef]
22. Sybilska, E.; Daszkowska-Golec, A. Alternative splicing in ABA signaling during seed germination. *Front. Plant Sci.* **2023**, *14*, 1144990. [CrossRef]
23. Marusig, D.; Tombesi, S. Abscisic acid mediates drought and salt stress responses in Vitis vinifera—A review. *Int. J. Mol. Sci.* **2020**, *21*, 8648. [CrossRef] [PubMed]
24. Yang, J.; He, R.; Qu, Z.; Gu, J.; Jiang, L.; Zhan, X.; Gao, Y.; Adelson, D.; Li, S.; Wang, Z.; et al. Long noncoding RNA ARTA controls ABA response through MYB7 nuclear trafficking in *Arabidopsis*. *Dev. Cell.* **2023**, *58*, 1206–1217. [CrossRef]
25. Hartung, W.; Schraut, D.; Jiang, F. Physiology of abscisic acid (ABA) in roots under stress-a review of the relationship between root ABA and radial water and ABA flows. *Aust. J. Agr. Res.* **2005**, *56*, 1253–1259. [CrossRef]
26. Wahid, I.; Kumari, S.; Ahmad, R.; Hussain, S.; Alamri, S.; Khan, M. Silver nanoparticle regulates salt tolerance in wheat through changes in ABA concentration, ion homeostasis, and defense systems. *Biomolecules* **2020**, *10*, 1506. [CrossRef]
27. Gómez-Cadenas, A.; Arbona, V.; Jacas, J.; Primo-Millo, E.; Talon, M. Abscisic acid reduces leaf abscission and increases salt tolerance in citrus plants. *J. Plant Growth Regul.* **2002**, *21*, 234–240. [CrossRef]
28. Qin, X.; Zeevaart, J.A.D. The 9-*cis*-epoxycarotenoid cleavage reaction is the key regulatory step of abscisic acid biosynthesis in water-stressed bean. *Proc. Natl. Acad. Sci. USA* **1999**, *96*, 15354–15361. [CrossRef]
29. Vishwakarma, K.; Upadhyay, N.; Kumar, N.; Yadav, G.; Singh, J.; Mishra, R.K.; Kumar, V.; Verma, R.; Upadhyay, R.G.; Pandey, M.; et al. Abscisic acid signaling and abiotic stress tolerance in plants: A review on current knowledge and future prospects. *Front. Plant Sci.* **2017**, *8*, 161. [CrossRef] [PubMed]
30. Xu, Z.; Wang, J.; Zhen, W.; Sun, T.; Hu, X. Abscisic acid alleviates harmful effect of saline–alkaline stress on tomato seedlings. *Plant Physiol. Biochem.* **2022**, *175*, 58–67. [CrossRef] [PubMed]
31. Arango, J.; Wüst, F.; Beyer, P.; Welsch, R. Characterization of phytoene synthases from cassava and their involvement in abiotic stress-mediated responses. *Planta* **2010**, *232*, 1251–1262. [CrossRef]

32. Chen, Y.; Xiang, Z.; Liu, M.; Wang, S.; Zhang, L.; Cai, D.; Huang, Y.; Mao, D.; Fu, J.; Chen, L. ABA biosynthesis gene *OsNCED3* contributes to preharvest sprouting resistance and grain development in rice. *Plant Cell Environ.* **2023**, *46*, 1384–1401. [CrossRef]
33. Zhu, G.; Ye, N.; Zhang, J. Glucose-induced delay of seed germination in rice is mediated by the suppression of ABA catabolism rather than an enhancement of ABA biosynthesis. *Plant Cell Physiol.* **2009**, *50*, 644–651. [CrossRef] [PubMed]
34. Shi, L.; Guo, M.; Ye, N.; Liu, Y.; Liu, R.; Xia, Y.; Cui, S.; Zhang, J. Reduced ABA accumulation in the root system is caused by ABA exudation in upland rice (*Oryza sativa* L. var. Gaoshan1) and this enhanced drought adaptation. *Plant Cell Physiol.* **2015**, *56*, 951–964. [CrossRef] [PubMed]
35. Huang, Y.; Jiao, Y.; Xie, N.; Guo, Y.; Zhang, F.; Xiang, Z.; Wang, R.; Wang, F.; Gao, Q.; Tian, L.; et al. *OsNCED5*, a 9-*cis*-epoxycarotenoid dioxygenase gene, regulates salt and water stress tolerance and leaf senescence in rice. *Plant Sci.* **2019**, *287*, 110188. [CrossRef] [PubMed]
36. Bang, S.; Park, S.; Jeong, J.; Kim, Y.; Jung, H.; Ha, S.; Kim, J. Characterization of the stress-inducible *OsNCED3* promoter in different transgenic rice organs and over three homozygous generations. *Planta* **2013**, *237*, 211–224. [CrossRef] [PubMed]
37. Hwang, S.; Chen, H.; Huang, W.; Chu, Y.; Shii, C.; Cheng, W. Ectopic expression of rice *OsNCED3* in *Arabidopsis* increases ABA level and alters leaf morphology. *Plant Sci.* **2010**, *178*, 12–22. [CrossRef]
38. Hwang, S.; Lee, C.; Tseng, C. Heterologous expression of rice 9-*cis*-epoxycarotenoid dioxygenase 4 (*OsNCED4*) in *Arabidopsis* confers sugar oversensitivity and drought tolerance. *Bot. Stud.* **2018**, *59*, 2. [CrossRef] [PubMed]
39. Wei, L.; Lv, B.; Li, X.; Wang, M.; Ma, H.; Yang, H.; Yang, R.; Piao, Z.; Wang, Z.; Lou, J.; et al. Priming of rice (*Oryza sativa* L.) seedlings with abscisic acid enhances seedling survival, plant growth, and grain yield in saline-alkaline paddy fields. *Field Crops Res.* **2017**, *203*, 86–93. [CrossRef]
40. Feng, Z.; Lu, G.; Sun, M.; Jin, Y.; Xu, Y.; Liu, X.; Wang, M.; Liu, M.; Yang, H.; Guan, Y.; et al. Comparative study of the priming effect of abscisic acid on tolerance to saline and alkaline stresses in rice seedlings. *Agronomy* **2023**, *13*, 2698. [CrossRef]
41. Ji, X.; Dong, B.; Shiran, B.; Talbot, M.; Edlington, J.; Hughes, T.; White, R.; Gubler, F.; Dolferus, R. Control of abscisic acid catabolism and abscisic acid homeostasis is important for reproductive stage stress tolerance in cereals. *Plant Physiol.* **2011**, *156*, 647–662. [CrossRef]
42. Zhu, J. Plant salt tolerance. *Trends Plant Sci.* **2001**, *6*, 66–71. [CrossRef]
43. Bhatnagar-Mathur, P.; Vadez, V.; Sharma, K.K. Transgenic approaches for abiotic stress tolerance in plants: Retrospect and prospects. *Plant Cell Rep.* **2008**, *27*, 411–424. [CrossRef] [PubMed]
44. Peng, Y.; Gao, Z.; Gao, Y.; Liu, G.; Sheng, L.; Wang, D. Eco-physiological characteristics of alfalfa seedlings in response to various mixed salt-alkaline stresses. *J. Integr. Plant Biol.* **2008**, *50*, 29–39. [CrossRef] [PubMed]
45. Greenway, H.; Munns, R. Mechanisms of salt tolerance in nonhalophytes. *Annu. Rev. Plant Physiol.* **1980**, *31*, 149–190. [CrossRef]
46. Forni, C.; Duca, D.; Glick, B.R. Mechanisms of plant response to salt and drought stress and their alteration by rhizobacteria. *Plant Soil* **2017**, *410*, 335–356. [CrossRef]
47. Zhang, Z.; Zhang, L.; Gao, H.; Jia, Y.; Bu, J.; Meng, Q. Research of the photoinhibition of PS I and PS II in leaves of cucumber under chilling stress combined with different light intensities. *Sci. Agric. Sin.* **2009**, *42*, 4288–4293.
48. Guo, R.; Zhou, J.; Ren, G.X.; Hao, W. Physiological responses of linseed seedlings to iso osmotic polyethylene glycol, salt, and alkali stresses. *Agron. J.* **2013**, *105*, 764–772. [CrossRef]
49. Song, T.; Xu, H.; Sun, N.; Jiang, L.; Tian, P.; Yong, Y.; Yang, W.; Cai, H.; Cui, G. Metabolomic analysis of alfalfa (*Medicago sativa* L.) root-symbiotic rhizobia responses under alkali stress. *Front. Plant Sci.* **2017**, *8*, 1208. [CrossRef] [PubMed]
50. Lyu, J.; Li, B.; He, W.; Zhang, S.; Gou, Z.; Zhang, J.; Meng, L.; Li, X.; Tao, D.; Huang, W.; et al. A genomic perspective on the important genetic mechanisms of upland adaptation of rice. *BMC Plant Biol.* **2014**, *14*, 160. [CrossRef] [PubMed]
51. Hasan, M.; Liu, X.; Waseem, M.; Guang, Q.; Alabdallah, N.; Jahan, M.; Fang, X. ABA activated SnRK2 kinases: An emerging role in plant growth and physiology. *Plant Signal Behav.* **2022**, *17*, 2071024. [CrossRef]
52. Zeevaart, J.; Creelman, R. Metabolism and physiology of abscisic acid. *Annu. Rev. Plant Physiol. Plant Mol. Biol.* **1988**, *39*, 439–473. [CrossRef]
53. Nambara, E.; Marion-Poll, A. Abscisic acid biosynthesis and catabolism. *Annu. Rev. Plant Biol.* **2005**, *56*, 165–185. [CrossRef]
54. Pei, X.; Wang, X.; Fu, G.; Chen, B.; Nazir, M.F.; Pan, Z.; He, S.; Du, X. Identification and functional analysis of 9-cis-epoxy carotenoid dioxygenase (NCED) homologs in G. hirsutum. *Int. J. Biol. Macromol.* **2021**, *182*, 298–310. [CrossRef]
55. Jiang, C.; Liu, X.; Liu, X.; Zhang, H.; Yu, Y.; Liang, Z. Stunted growth caused by Blast Disease in rice seedlings is associated with changes in phytohormone signaling pathways. *Front. Plant Sci.* **2017**, *8*, 1558. [CrossRef] [PubMed]
56. Yang, Y.; Guo, Y. Elucidating the molecular mechanisms mediating plant salt-stress responses. *New Phytol.* **2018**, *217*, 523–539. [CrossRef]
57. Garg, A.; Kim, J.; Owens, T.; Ranwala, A.; Choi, Y.; Kochian, L.; Wu, R. Trehalose accumulation in rice plants confers high tolerance levels to different abiotic stresses. *Proc. Natl. Acad. Sci. USA* **2002**, *99*, 15898–15903. [CrossRef]
58. Serrano, R.; Rodriguez-Navarro, A. Ion homeostasis during salt stress in plants. *Curr. Opin. Cell Biol.* **2001**, *13*, 399–404. [CrossRef] [PubMed]
59. Zhang, J.; Flowers, T.; Wang, S. Mechanisms of sodium uptake by roots of higher plants. *Plant Soil* **2010**, *326*, 45–60. [CrossRef]
60. Ganapati, R.; Naveed, S.; Zafar, S.; Wang, W.; Xu, J. Saline-alkali tolerance in rice: Physiological response, molecular mechanism, and QTL identification and application to breeding. *Rice Sci.* **2022**, *29*, 412–434. [CrossRef]
61. Parida, A.; Das, A. Salt tolerance and salinity effects on plants: A review. *Ecotoxicol. Environ. Saf.* **2005**, *60*, 324–349. [CrossRef] [PubMed]

62. Wang, H.; Yang, S.; Lv, M.; Ding, S.; Li, J.; Xu, C.; Xie, H. RNA-Seq revealed that infection with white tip nematodes could downregulate rice photosynthetic genes. *Funct. Integr. Genomics* **2020**, *20*, 367–381. [CrossRef]
63. Ahmadi, F.; Samadi, A.; Sepehr, E.; Rahimi, A.; Rengel, Z.; Shabala, S. HKT1;5 transporter gene expression and NHX-type Na^+/H^+ exchanger activity regulate adaptation of Echinacea species to salt stress. *Environ. Exp. Bot.* **2023**, 105365. [CrossRef]
64. Brindha, C.; Vasantha, S.; Raja, A.K.; Tayade, A.S. Characterization of the salt overly sensitive pathway genes in sugarcane under salinity stress. *Physiol. Plant.* **2021**, *171*, 677–687. [CrossRef] [PubMed]
65. Diao, F.; Dang, Z.; Xu, J.; Ding, S.; Hao, B.; Zhang, Z.; Zhang, J.; Wang, L.; Guo, W. Effect of arbuscular mycorrhizal symbiosis on ion homeostasis and salt tolerance-related gene expression in halophyte *Suaeda salsa* under salt treatments. *Microbiol. Res.* **2021**, *245*, 126688. [CrossRef]
66. Farooq, M.; Park, J.; Jang, Y.; Kim, E.; Kim, K. Rice cultivars under salt stress Show differential expression of genes related to the regulation of Na^+/K^+ balance. *Front. Plant Sci.* **2021**, *12*, 680131. [CrossRef] [PubMed]
67. El Mahi, H.; Pérez-Hormaeche, J.; De Luca, A.; Villalta, I.; Espartero, J.; Gámez-Arjona, F.; Quintero, F. A critical role of sodium flux via the plasma membrane Na^+/H^+ exchanger SOS1 in the salt tolerance of rice. *Plant Physiol.* **2019**, *180*, 1046–1065. [CrossRef] [PubMed]
68. Suzuki, K.; Yamaji, N.; Costa, A.; Okuma, E.; Kobayashi, N.; Kashiwagi, T.; Katsuhara, M.; Wang, C.; Tanoi, K.; Murata, Y.; et al. *OsHKT1;4*-mediated Na^+ transport in stems contributes to Na^+ exclusion from leaf blades of rice at the reproductive growth stage upon salt stress. *BMC Plant Biol.* **2016**, *16*, 22. [CrossRef] [PubMed]
69. Zhao, C.; Zhang, H.; Song, C.; Zhu, J.; Shabala, S. Mechanisms of plant responses and adaptation to soil salinity. *Innovation* **2020**, *1*, 41. [CrossRef] [PubMed]
70. Liu, X.; Zhang, H.; Jin, Y.; Wang, M.; Yang, H.; Ma, H.; Jiang, C.; Liang, Z. Abscisic acid primes rice seedlings for enhanced tolerance to alkaline stress by upregulating antioxidant defense and stress tolerance-related genes. *Plant Soil.* **2019**, *438*, 39–55. [CrossRef]
71. Wang, Q.; Ni, L.; Cui, Z.; Jiang, J.; Chen, C.; Jiang, M. The NADPH oxidase *OsRbohA* increases salt tolerance by modulating K^+ homeostasis in rice. *Crop. J.* **2022**, *10*, 1611–1622. [CrossRef]
72. Li, C.; Liang, D.; Li, J.; Duan, Y.; Li, H.; Yang, Y.; Qin, R.; Li, L.; Wei, P.; Yang, J. Unravelling mitochondrial retrograde regulation in the abiotic stress induction of rice Alternative Oxidase 1 genes. *Plant Cell Environ.* **2013**, *36*, 775–788. [CrossRef]
73. Chou, T.; Chao, Y.; Kao, C. Involvement of hydrogen peroxide in heat shock-and cadmium-induced expression of ascorbate peroxidase and glutathione reductase in leaves of rice seedlings. *J. Plant Physiol.* **2012**, *165*, 478–486. [CrossRef] [PubMed]
74. Wu, T.; Lin, W.; Kao, C.; Hong, C. Gene knockout of glutathione reductase 3 results in increased sensitivity to salt stress in rice. *Plant Mol. Biol.* **2015**, *87*, 555–564. [CrossRef]
75. Bashri, G.; Prasad, S. Exogenous IAA differentially affects growth, oxidative stress and antioxidants system in Cd stressed *Trigonella foenum-Graecum* L. seedlings: Toxicity alleviation by up-regulation of ascorbate-glutathione cycle. *Ecotoxicol. Environ. Saf.* **2016**, *132*, 329–338. [CrossRef] [PubMed]
76. Postiglione, A.; Muday, G. The role of ROS homeostasis in ABA-induced guard cell signaling. *Front. Plant Sci.* **2020**, *11*, 968. [CrossRef]
77. Sah, S.; Reddy, K.; Li, J. Abscisic acid and abiotic stress tolerance in crop plants. *Front. Plant Sci.* **2016**, *7*, 571. [CrossRef]
78. Toki, S.; Hara, N.; Ono, K.; Onodera, H.; Tagiri, A.; Oka, S.; Tanaka, H. Early infection of scutellum tissue with Agrobacterium allows high-speed transformation of rice. *Plant J.* **2006**, *47*, 969–976. [CrossRef] [PubMed]
79. Miyake, Y.; Takahashi, E. Effect of silicon on the growth of solution-cultured cucumber plant. *Soil Sci. Plant Nutr.* **1983**, *29*, 71–83. [CrossRef]
80. Wellburn, A.; Lichtenthaler, H. Formulae and program to determine total carotenoids and chlorophylls A and B of leaf extracts in different solvents. In *Photosynthesis Research*; Springer: Dordrecht, The Netherlands, 1984; Volume 2, pp. 9–12.
81. Degenhardt, B.; Gimmler, H.; Hose, E.; Hartung, W. Effect of alkaline and saline substrates on ABA contents, distribution and transport in plant roots. *Plant Soil* **2000**, *225*, 83–94. [CrossRef]
82. Zhang, H.; Liu, X.; Zhang, R.; Yuan, H.; Wang, M.; Yang, H.; Ma, H.; Liu, D.; Jiang, C.; Liang, Z. Root damage under alkaline stress is associated with reactive oxygen species accumulation in rice (*Oryza sativa* L.). *Front. Plant Sci.* **2017**, *8*, 1580. [CrossRef]
83. Kumar, P.; Choudhary, M.; Halder, T.; Prakash, N.R.; Singh, V.; Vineeth, V.T.; Sheoran, S.; Longmei, N.; Rakshit, S.; Siddique, K.H. Salinity stress tolerance and omics approaches: Revisiting the progress and achievements in major cereal crops. *Heredity* **2022**, *128*, 497–518. [CrossRef]
84. Wei, T.; Li, G.; Wang, M.; Jin, Y.; Zhang, G.; Liu, M.; Yang, H.; Jiang, C.; Liang, Z. Physiological and transcriptomic analyses reveal novel insights into the cultivar-specific response to alkaline stress in alfalfa (*Medicago sativa* L.). *Ecotoxicol. Environ. Saf.* **2021**, *228*, 113017. [CrossRef] [PubMed]
85. Bates, L.; Waldren, R.; Teare, I. Rapid determination of free proline for water-stress studies. *Plant Soil* **1973**, *39*, 205–207. [CrossRef]
86. Wang, Y.; Hu, Y.; Chen, B.; Zhu, Y.; Dawuda, M.M.; Svetla, S. Physiological mechanisms of resistance to cold stress associated with 10 elite apple rootstocks. *J. Integr. Agric.* **2018**, *17*, 857–866. [CrossRef]
87. Livak, K.; Schmittgen, T. Analysis of relative gene expression data using real-time quantitative PCR and the $2^{-\Delta\Delta CT}$. *Methods* **2001**, *25*, 402–408. [CrossRef] [PubMed]

Disclaimer/Publisher's Note: The statements, opinions and data contained in all publications are solely those of the individual author(s) and contributor(s) and not of MDPI and/or the editor(s). MDPI and/or the editor(s) disclaim responsibility for any injury to people or property resulting from any ideas, methods, instructions or products referred to in the content.

plants

MDPI

Article

Overexpression of a '*Paulownia fortunei*' MYB Factor Gene, *PfMYB44*, Increases Salt and Drought Tolerance in *Arabidopsis thaliana*

Guijie Luo [1,†], Weijia Cai [1,†], Hao Wang [1], Wei Liu [1], Xu Liu [1], Shizheng Shi [2,*] and Lei Wang [2,*]

[1] Suqian Institute of Agricultural Sciences, Jiangsu Academy of Agricultural Sciences, Suqian 223800, China
[2] Jiangsu Academy of Forestry, Nanjing 211153, China
* Correspondence: shshzn@163.com (S.S.); wl_jaf1980@126.com (L.W.)
† These authors contributed equally to this work.

Abstract: *Paulownia fortunei (Seem.) Hemsl* is a *Paulownia* Sieb.et tree of the family Scrophulariaceae. It has become an important short-to-medium-term fast-growing multi-purpose tree species in China due to its rapid growth, strong adaptability, and excellent material properties. MYB transcription factors in plants have numerous and diverse functions, playing important roles in various aspects such as plant stress response. To investigate the function of MYB transcription factors in *Paulownia fortunei*, this study used PCR technology to clone the *PfMYB44* gene from *Paulownia fortunei*. The homology of PfMYB44 and SiMYB44 (*Sesamum indicum*) was the highest. Expression analysis results showed that *PfMYB44* was expressed in the root, stem, young leaf, and mature leaf of *Paulownia fortunei*, with the highest content in the root. Cold, drought, hot, salt, and ABA treatments could increase the expression level of *PfMYB44*. Overexpression-*PfMYB44* plants were constructed, and physiological and molecular analysis showed that *PfMYB44* could positively regulate salt and drought stresses. Under drought stress, the expression levels of *AtP5CS*, *AtCAT1*, *AtNCED3* and *AtSnRK2.4* in transgenic lines were significantly induced. Salt stress induced the expression of *AtNHX1*, *AtSOS1*, *AtSOS2* and *AtSOS3* genes, and the relative expression levels of these genes in transgenic *Arabidopsis* were higher. In conclusion, the functional study of *PfMYB44* laid a certain foundation for the study of *Paulownia* stress resistance, and was helpful to the study of its stress resistance mechanism and the cultivation of new stress resistance varieties.

Keywords: *Paulownia fortunei*; *PfMYB44*; salt stress; drought stress

1. Introduction

Drought, salinity, hot, and cold stresses can significantly alter the physiological and biochemical traits, gene expression patterns, and proteomic characteristics of plants, thereby having a significant impact on their growth, distribution, and yield formation. Drought seriously affects the growth and development of Paulownia, and can lead to various physiological and metabolic abnormalities of Paulownia plants, can even cause irreversible damage, eventually lead to the death of the whole plant, and seriously reduce the quality and yield of Paulownia. Under salt stress, paulownia is mainly affected by negative effects such as osmotic imbalance and ion toxicity [1,2]. Excessive Na^+ affects the absorption and transportation of water and nutrients by root cells, leading to a large accumulation of Na^+ in leaves and weakened photosynthesis, which in turn inhibits the growth and dry matter accumulation of paulownia [3]. Therefore, it is necessary to study the response mechanism of plants to abiotic stress in order to cultivate stress-resistant varieties.

Transcriptional regulation is one of the core links in plant resistance to adversity [4]. MYB transcription factors (TFs) are involved in plant growth and development, defense regulation, stress response, and play an active or negative regulatory role in these processes [5–8]. MYB TFs have a remarkable common feature: the N-terminal of its protein

structure contains the MYB domain [9]. The MYB domain generally contains 1–4 incomplete repeats of the sequence R, each consisting of 50–53 amino acid residues, which determine the binding of transcription factors to different acting elements [10]. There are three α helices; the second and third helices form HTH structures with hydrophobic fragments, which help transcription factors bind to specific target genes, while the third helix is responsible for directly binding to the DNA [11]. According to the number of R-structures in the N-terminal, it can be divided into R1/R2-MYB, R2R3-MYB, R1R2R3-MYB and 4R-MYB subclasses [12]. In addition, the C-terminal contains a transcriptional activation domain that ensures transcriptional activity and participates in interactions between other transcription factors or DNA, resulting in diverse of regulatory roles for the MYB gene family [6].

In 1987, Pazares identified the first gene encoding the MYB transcription factor in plants, COLORED1 (C1), which encodes the MYB domain protein required for anthocyanin synthesis in maize [13]. Afterwards, researchers isolated MYB TFs from various plants such as *Arabidopsis*, *Chrysanthemum morifolium*, *Gossypium hirsutum*, tomato and soybean, and studied their protein functions [14–18]. *AtMYB44* actively responds to drought stress by regulating ABA signaling, stomatal movement, and root growth [14]. Overexpression of the *AtMYB12* gene significantly increases the accumulation of flavonoids, which can enhance the survival ability of plants under drought and oxidative stresses [19]. The *TaMYBsdu1* gene regulates wheat tolerance to salt and drought stresses [20]. Overexpression of *XsMYB44* and *BcMYB44* can resist drought stress by enhancing plant osmotic regulation ability and ROS homeostasis [21,22]. In addition, MYB21, MYB24, and MYB57 affect anther development and anther cracking in *Arabidopsis* by regulating the biosynthesis of flavonols or jasmonic acid, and similar functions and regulatory mechanisms are present in *Capsicum annuum* and *Nicotiana tabacum* [23–27].

Paulownia fortunei is an important high-quality fast-growing timber tree species, naturally distributed in many provinces of China, commonly found in low-altitude hills and plains [28]. It has a cultivation history of over 2000 years in China. *Paulownia fortunei* is drought-resistant and salt-resistant, playing an important role in wind and sand fixation, landscaping, and improving the ecological environment. Its wood is a good material for furniture manufacturing and musical instrument production [29]. Therefore, *Paulownia fortunei* has important ecological and economic value. The phenomenon of cold and salt is widespread and increasingly severe, which seriously restricts the economic production and sustainable operation of *Paulownia fortunei*. With the further study of transcription factor MYB44, it has been found that it responds to both drought and salt stress. However, there is currently relatively little research on the stress resistance of *Paulownia fortune*; the mechanism of its response to cold and salt stresses is especially still unclear. The stress resistance gene *PfMYB44* was isolated from *Paulownia fortunei*, and its expression changes were determined after different stresses, which laid a certain foundation for the study of the stress resistance of *Paulownia fortunei*, and was helpful to the study of the stress resistance mechanism and the cultivation of new stress resistance varieties.

2. Results

2.1. Isolation and Bioinformatics Analysis of PfMYB44

The ORF (open reading frame) of the *PfMYB44* gene was obtained through PCR amplification, consisting of 1146 bp bases and encoding 381 aa (Figure S1). Domain analysis of *PfMYB44* revealed that it has two conserved SANT domains at the N-terminal, belonging to the R2R3 subfamily of MYB transcription factors. The first SANT domain contained 50 amino acid residues (positions 18–67), while the second SANT domain contained 49 amino acid residues (positions 70–118) (Figure S2B). The results of the secondary and tertiary structure of PfMYB44 predictions showed that the proportion of random coil was the highest at 63.25%, followed by the alpha helix (26.77%) (Figure S2A,C). In order to study the phylogenetic relationship between PfMYB44 and other species, Protein BLAST on the NCBI website was used to search for homologous genes of PfMYB44. A total of 11 homologous genes with higher alignment scores were selected for amino acid sequence alignment

with PfMYB44, and a phylogenetic tree was constructed (Figure 1). PfMYB44 showed high conservation with homologous proteins in different species, and the closest relative species to PfMYB44 was *Sesamum indicum* (Figure 1B). It is speculated that *PfMYB44* may have a similar function to other MYB44 transcription factors, responding to both drought and salt stresses.

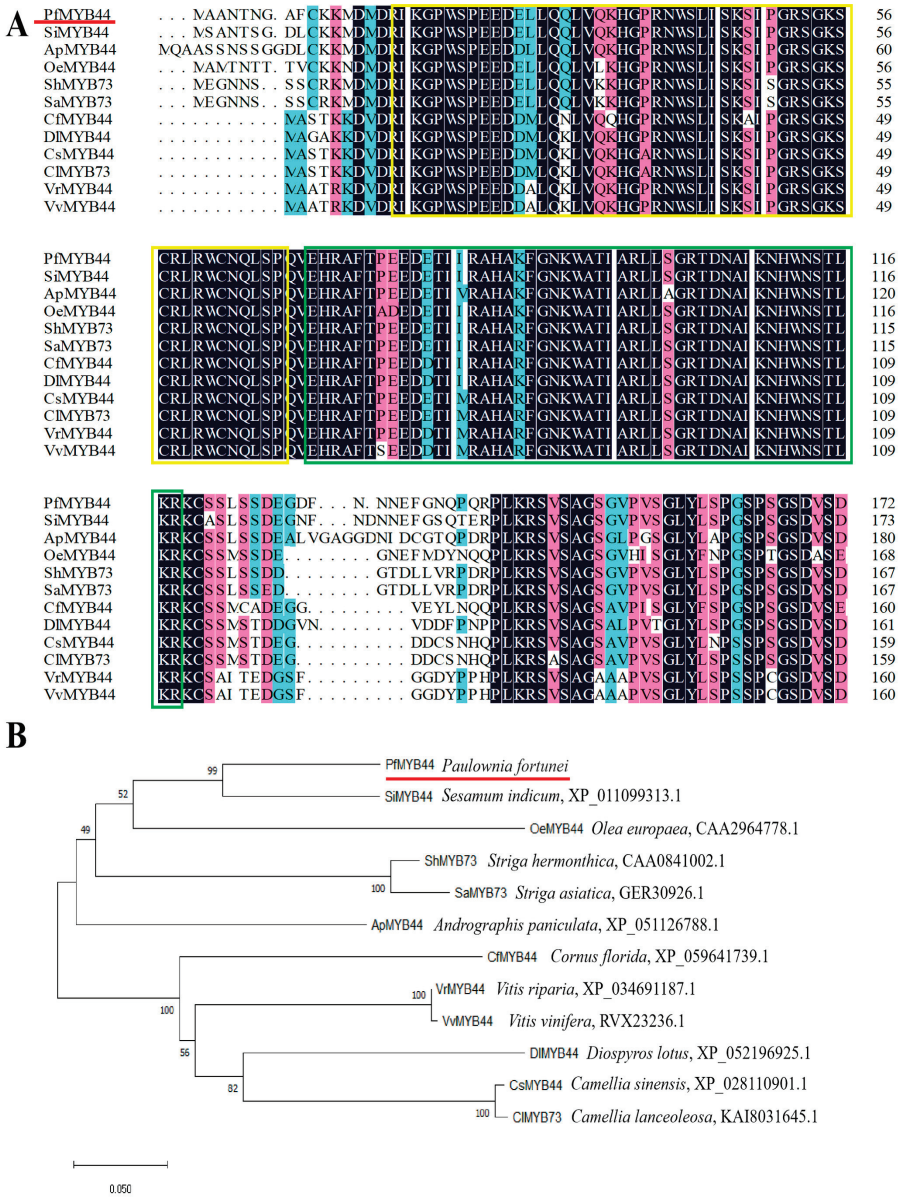


Figure 1. Homology analysis of PfMYB44. (**A**) Multiple-sequence alignment (**B**) and phylogenetic tree of PfMYB44 and other MYB protein species. The red line represents the target protein and the yellow and green boxes represent R-repeat structures.

2.2. Subcellular Localization of PfMYB44 Protein

Using the online software BUSCA, PfMYB44 was predicted to be located in the nucleus. In order to further validate the prediction results, this study constructed PfMYB44 into pCAMBIA1300-GFP vector and transformed it into Agrobacterium GV3101. The permeate was resuspended and injected into tobacco leaves, and the subcellular localization of PfMYB44 was observed in tobacco epidermal cells to see if it coincided with the fluorescence of mCherry (Figure 2). *PfMYB44*-GFP fluorescence was observed at the site of the nucleus, while control GFP fluorescence was distributed throughout the cell. The

subcellular localization results indicated that PfMYB44 was a protein that functions in the nucleus, consistent with the predicted results.

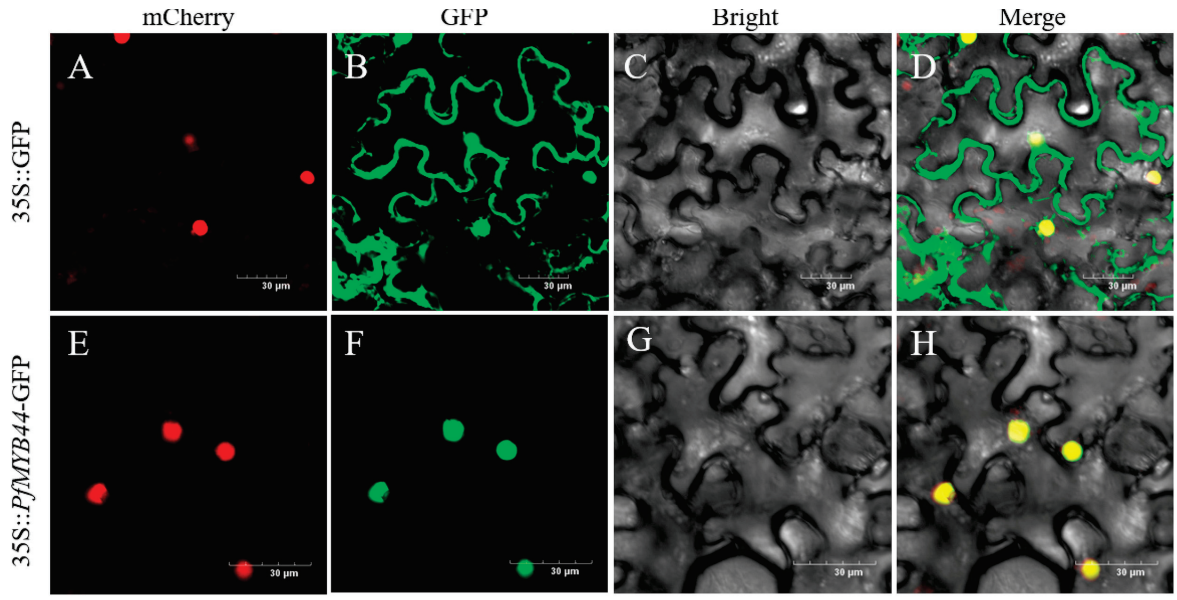


Figure 2. Subcellular localization of PfMYB44. (**A**,**E**) was mCherry, (**B**,**F**) was GFP, (**C**,**G**) was Bright, and (**D**,**H**) was Merge. Bar = 30 μm.

2.3. Expression of PfMYB44 in Paulownia fortunei

PfMYB44 gene was expressed in different tissues of *Paulownia fortunei*, but there were significant differences in expression patterns. Using the expression level of young leaf as a control, the *PfMYB44* gene had the highest expression level in root, approximately 6.0 times that of young leaf. Next were mature leaf and stem, which were 4.67 times and 2.0 times that of young leaf, respectively (Figure 3A).

Under salt, cold, drought, heat and ABA stresses, the expression of *PfMYB44* in mature leaf reached its peak at 5 h, 7 h, 7 h, 9 h and 7 h after treatment, and was 5.57, 5.07, 6.9, 4.9 and 3.07 times that of untreated leaf, respectively. In root, the expression of *PfMYB44* reached its peak value 3 h after drought treatment, while under salt, cold, hot and ABA treatments, the expression of *PfMYB44* reached its peak value at 7 h, which was 5.59, 6.16, 4.11, 3.43 and 3.07 times that of the control, respectively (Figure 3B,C).

2.4. Heterologous Expression of PfMYB44 in Arabidopsis-Improved Salinity Tolerance

Overexpression of *PfMYB44* in *Arabidopsis* was achieved through the flower soaking method. The homozygous screening and identification of *Arabidopsis* were carried out by kanamycin, and a total of six initially screened positive *Arabidopsis* lines were obtained. RNA was further extracted from these six *Arabidopsis* lines; RT-qPCR detection showed that *PfMYB44* transgenic was successful, and the expression levels of L2, L3 and L6 were higher (Figure 4A).

According to the difference in expression levels of *PfMYB44* in transgenic *Arabidopsis*, three homozygous lines L2, L3 and L6 with higher expression levels were selected in this study. As shown in Figure 4B, under normal culture conditions (Salt 0 d), transgenic *Arabidopsis*, wild-type (WT) and unloaded line (UL) *Arabidopsis* plants grew well and in the same growth state, without significant phenotypic differences. Compared to the control group, the experimental group (Salt 8 d) showed wilting and yellowing in *Arabidopsis*. However, compared to the WT and UL *Arabidopsis* with severe wilting and yellowing, transgenic *Arabidopsis* showed a healthier growth state and a significantly higher survival rate (Figure 4C).

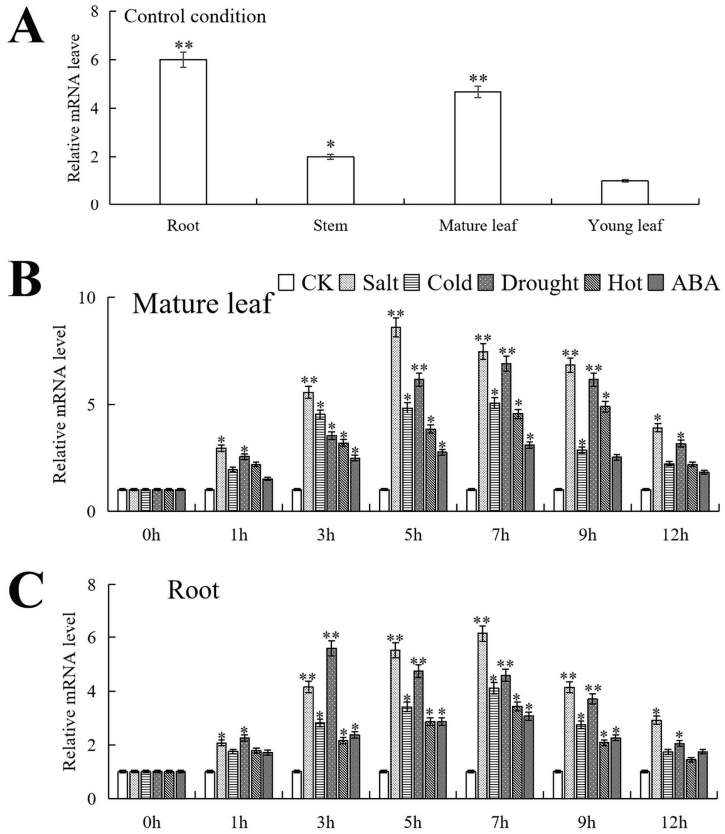


Figure 3. The expression of *PfMYB44* in *Paulownia fortunei*. (**A**) Expression levels of *PfMYB44* in different tissues of *Paulownia fortunei*. The expression level in young leaf was set to 1 for control. (**B**) Relative expression of *PfMYB44* under stresses in mature leaf and (**C**) root. The expression level of 0 h was set to 1 as the control. The SD represents error bar (n = 3). (*) $p \leq 0.05$; (**) $p \leq 0.01$.

Salt stress breaks down the chlorophyll of plants, which in turn causes them to fail to photosynthesize and die. However, the chlorophyll of overexpression-*PfMYB44 Arabidopsis* was less damaged (Figure 5D). Salt stress increased the content of MDA and proline, and the activity of antioxidant enzymes in the experimental group. The transgenic line had higher proline content (Figure 5C). The accumulation of ROS is one of the important indexes to evaluate the harm of salt to plants. Therefore, the content of MDA and the activities of antioxidant enzymes in different lines under salt stress were determined. There was no difference between the control groups. MDA content in WT and UL of the experimental group was higher, indicating that they suffered from more severe osmotic stress (Figure 5F). In addition, the activities of catalase (CAT), superoxide dismutase (SOD), and peroxidase (POD), which are related to antioxidant activity, were lower, indicating that they accumulated more reactive oxygen species in their bodies (Figure 5A,B,E). These results indicated that *PfMYBYB44* can indeed enhance plant survival under salt stress.

2.5. The Expression of Salt Tolerance-Related Genes

In order to investigate the molecular mechanism of *PfMYBYB44* to improve salt resistance in plants, the expression of genes related to ion transport in transgenic *Arabidopsis* was determined. The relative expression levels of *AtNHX1*, *AtSOS1*, *AtSOS2*, and *AtSOS3* were not significantly different in the control group. However, salt stress induced their expression, and the relative expression of these genes in transgenic *Arabidopsis* was higher in the experimental group (Figure 6). It is suggested that *PfMYBYB44* may enhance plant salt tolerance by upregulating the expression of these genes related to ion transport.

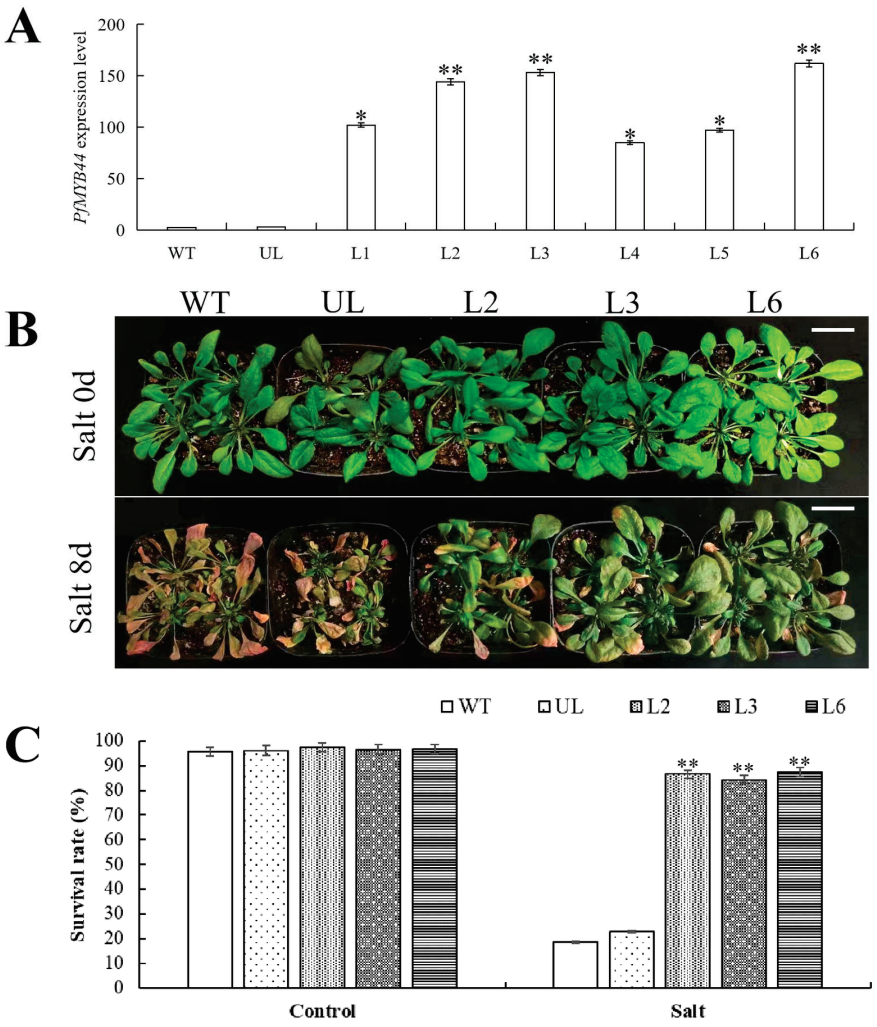


Figure 4. Overexpression-*PfMYB44* increased salt tolerance. (**A**) RNA level identification of transgenic plants. (**B**) Salt stress treatment for WT, UL and *PfMYB44* transgenic plants. Bar = 3 cm. (**C**) Survival rate statistical analysis of *Arabidopsis* under salt. The SD represents error bar (n = 3). (*) $p \leq 0.05$; (**) $p \leq 0.01$.

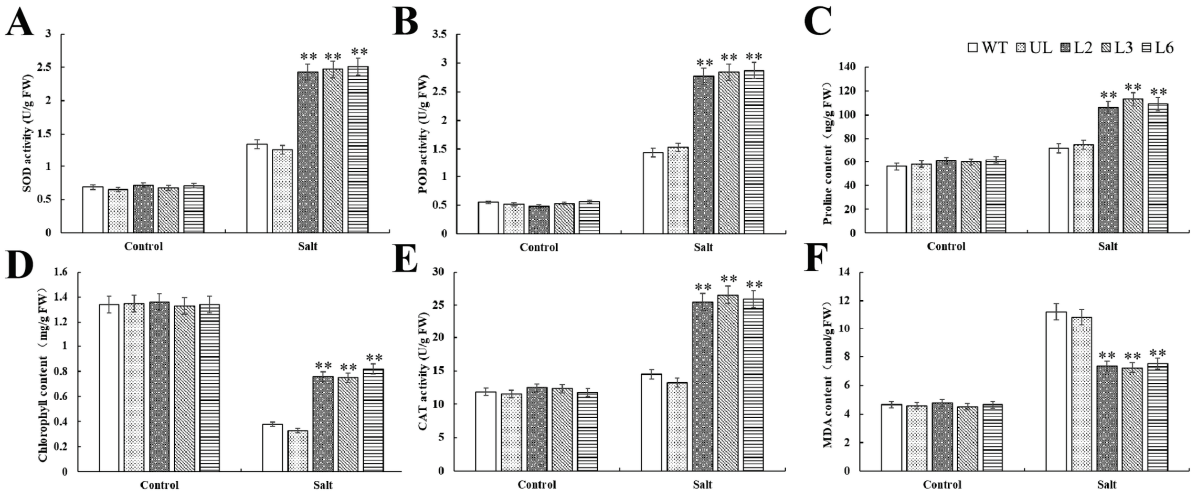


Figure 5. Statistical analysis of physiological indexes of plant stress resistance under salt stress. (**A**) SOD activity, (**B**) POD activity, (**C**) proline content, (**D**) chlorophyll content, (**E**) CAT activity, and (**F**) MDA content in *Arabidopsis* under salt stress. The SD represents error bar (n = 3). (**) $p \leq 0.01$.

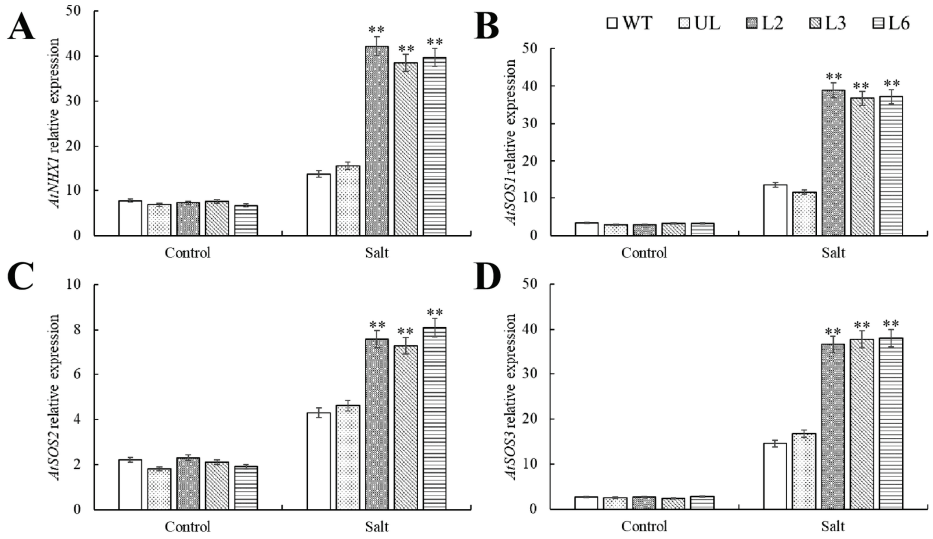


Figure 6. Expression of ion transport genes in WT, UL and transgenic plants under salt stress. The expression of (**A**) *AtNHX1*, (**B**) *AtSOS1*, (**C**) *AtSOS2*, and (**D**) *AtSOS3* under salt. The SD represents error bar (n = 3). (**) $p \leq 0.01$.

2.6. Heterologous Expression of PfMYBYB44 in Arabidopsis-Improved Drought Tolerance

As shown in Figure 7A, all *Arabidopsis* lines cultivated under normal conditions (Drought 0 d) had good growth status and consistent growth, with no obvious phenotypic differences. Compared with the Drought 0 d, the WT, UL and transgenic *Arabidopsis* in the experimental group (Drought 10 d) showed obvious poor growth, and WT and UL *Arabidopsis* leaves showed more severe wilting phenomenon than transgenic *Arabidopsis*. After 3 d of rewater treatment, compared with WT and UL, the leaf status of transgenic *Arabidopsis* was obviously restored, and showed a higher survival rate (Figure 7B).

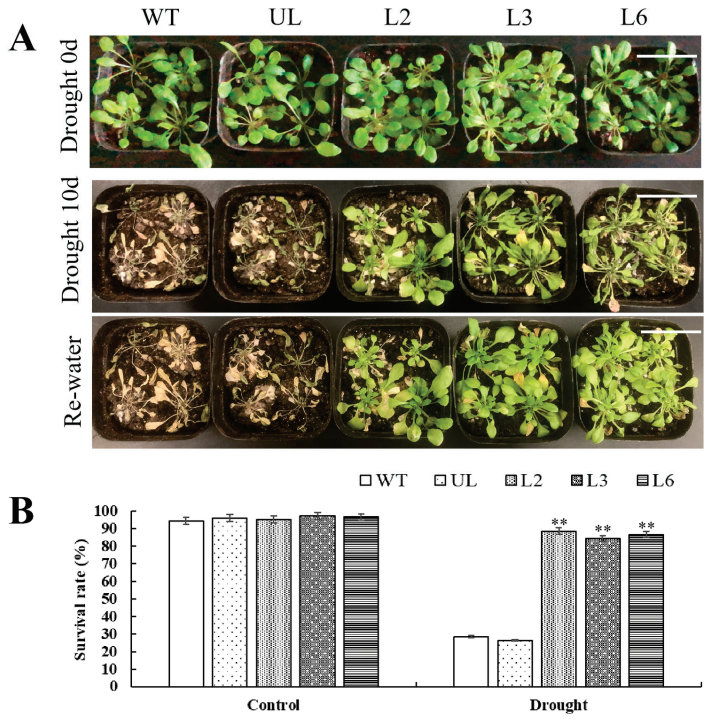


Figure 7. Overexpression-*PfMYB44* increased drought tolerance. (**A**) Drought stress treatment for WT, UL and *PfMYB44* transgenic plants. Bar = 3 cm. (**B**) Survival rate statistical analysis of *Arabidopsis* under drought. The SD represents error bar (n = 3). (**) $p \leq 0.01$.

There were no significant differences in chlorophyll, MDA and proline contents among all *Arabidopsis* lines. MDA content of transgenic *Arabidopsis* in the experimental group was significantly lower than that of WT and UL, while the contents of proline and chlorophyll were opposite (Figure 8C,D,F). Transgenic *Arabidopsis* showed a greater increase in SOD, POD, and CAT activities under drought stress. This indicates that the overexpression of the *PfMYBYB44* gene in *Arabidopsis* can significantly reduce the accumulation of harmful substances in plants after drought stress, and improve the content of osmotic regulatory substances and antioxidant enzyme activity in leaves of *Arabidopsis* (Figure 8A,B,E).

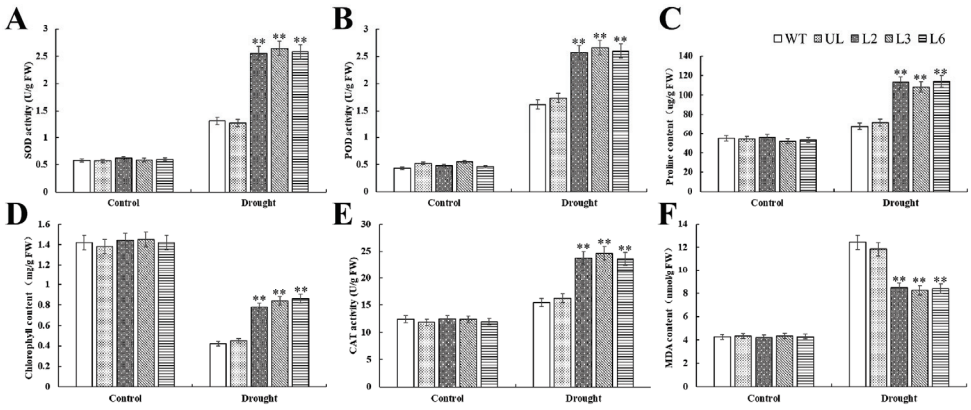


Figure 8. Statistical analysis of physiological indexes of plant stress resistance under drought stress. (**A**) SOD activity, (**B**) POD activity, (**C**) proline content, (**D**) chlorophyll content, (**E**) CAT activity, and (**F**) MDA content in *Arabidopsis* under drought stress. The SD represents error bar (n = 3). (**) $p \leq 0.01$.

2.7. The Expression of Drought Tolerance-Related Genes

In order to investigate the molecular mechanism of *PfMYBYB44* to improve drought resistance in plants, we detected the expression of stress-related genes such as *AtP5CS*, *AtCAT1*, *AtNCED3*, and *AtSnRK2.4* using RT-qPCR. The expression levels of the above genes under normal treatment were similar in all lines. On the contrary, the expression levels of these genes in transgenic lines were significantly induced in the experimental group. Under drought stress, *PfMYB44* may improve plant survival by regulating the expression of these stress-responsive genes (Figure 9).

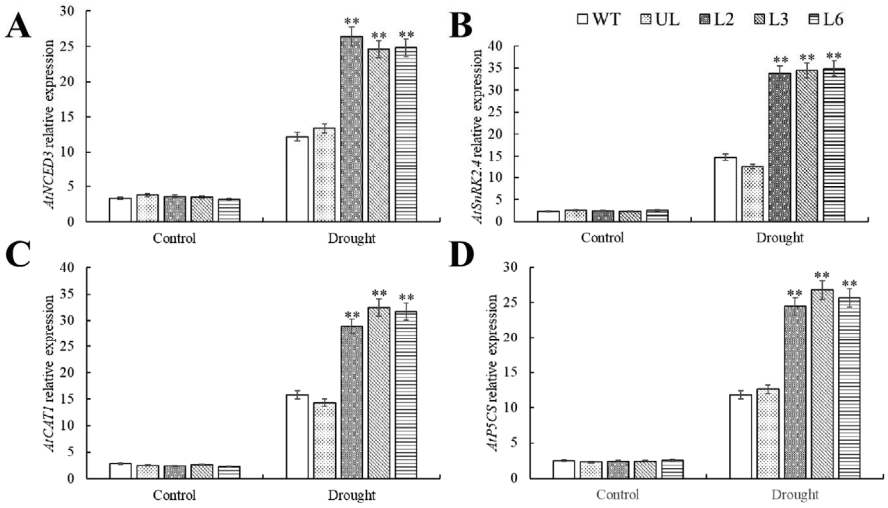


Figure 9. Expression of drought tolerance-related genes in WT, UL and transgenic plants under drought stress. Relative expression levels of (**A**) *AtNCED3*, (**B**) *AtSnRK2.4*, (**C**) *AtCAT1*, and (**D**) *AtP5CS* under drought stress. The SD represents error bar (n = 3). (**) $p \leq 0.01$.

3. Discussion

The role of WRKY, bHLH, MYB and other gene families in regulating plant growth and development and responding to stress has been confirmed [30]. MYB transcription factors have highly conserved MYB domains, each of which generally contains three regularly spaced tryptophan residues. This special domain can form an HTH configuration, which binds to DNA to participate in regulation [31]. This experiment cloned the full length of the *PfMYBYB44* gene from *Paulownia fortunei* and conducted bioinformatics analysis on it. The PfMYBYB44 had two SANT domains, indicating that the PfMYBYB44 belonged to the R2R3-MYB transcription factor (Figure 1). This study found for the first time that MYB44 may play a positive role in regulating the response of *Paulownia fortunei* stress resistance, which lays a good foundation for later analysis of the stress resistance pathway of *Paulownia fortunei*.

Previous studies have shown that most MYB proteins are located in the nucleus, such as the GbMYBFL protein identified in *Ginkgo biloba*, which is located in the nucleus [32]. The ApMYBs protein in *Agapanthus praecox*, which is partially involved in the flavonoid biosynthesis pathway, is localized in the nucleus [33]. The results of subcellular localization in this study showed that PfMYBYB44 was located in the nucleus, which is consistent with the predicted results and previous studies (Figure 2).

Overexpression of *TaMYB31* can promote wax synthesis and expression of drought resistance genes, thereby improving drought resistance in *Arabidopsis* [34]. *AtMYB96* can respond to ABA, drought and salt treatments, and overexpression of *AtMYB96* positively regulates plant tolerance to drought and cold stresses through the ABA signaling pathway [35]. Besides serving as a positive regulatory factor, *OsMYB30* negatively regulates the cold tolerance of rice by reducing the content of maltose [36]. In this paper, the relative expression of *PfMYB44* was analyzed under salt, drought, hot, cold stresses and external ABA treatment. The results showed that the expression of the *PfMYB44* gene showed a trend of first increasing and then decreasing under these treatments (Figure 3B,C). The PfMYBYB44 gene can be expressed in root, stem, young leaf, and mature leaf, but there were certain differences in expression levels. The *PfMYBYB44* gene had the highest expression level in root, and its homologous gene *VhMYB44* also had the highest expression level in root [37]. It is speculated that *PfMYBYB44* and *VhMYB44* genes have similar functions and play the greatest role in roots (Figure 3A). This may be related to the physiological regulation of plants in response to stress, such as adjusting their water-use efficiency, maintaining cell stability, and maintaining energy metabolism balance.

Plants that are exposed to adverse environments for a long time will lose balance in their ROS metabolism system, leading to a rapid increase in intracellular free-radical content and peroxidation of unsaturated fatty acids, resulting in the destruction of the cell membrane structure. In addition, it will also cause the dynamic balance of reactive oxygen species production and clearance system to be disrupted, accelerating the process of plant cell death. Proline has hydrophilicity and plays an important role in stabilizing metabolic processes within plant cells and tissues. Under adverse conditions, the content of MDA and proline in plants reflects their stress resistance to a certain extent. The MYB TF participates in plant response to drought stress through multiple pathways [38]. ABA is one of the main hormones regulating drought stress, which can reduce water transpiration, decrease the leaf water loss rate, and improve plant drought resistance by controlling the opening and closing of stomata [39]. It was found that the expression of *SiMYB56* was upregulated by drought induction in millet, and overexpression of *SiMYB56* in rice regulated lignin synthesis and the ABA signaling pathway to enhance the drought resistance of transgenic rice [40]. In this study, we found that overexpression of *PfMYBYB44* significantly enhanced salt and drought resistance in *Arabidopsis* compared to the WT (Figures 4 and 7). The determination of MDA content and free proline content showed that the degree of cell damage and plasma membrane peroxidation in transgenic lines was lower than that of the WT. This may be due to the stronger ability of transgenic *PfMYBYB44 Arabidopsis* to clear a large amount of harmful substances such as ROS produced by salt and drought

stresses, effectively increasing the content of protective substances such as polyamines and peroxidase, making the plant more resistant to salt and drought stresses. Overexpression of *PfMYBYB44* significantly increases the activities of POD, SOD, and CAT in *Arabidopsis*, quickly clearing the accumulation of hydrogen peroxide and superoxide ions caused by drought in the body, thus improving the salt- and drought-resistant ability of plants (Figures 5 and 8).

To cope with the disruption of ion dynamic balance caused by high salt environments, plants first choose to limit excessive Na^+ entry and absorb more K^+ to maintain intracellular homeostasis [41]. This process is usually handled by transport protein families such as SOS and HKT. SOS3 is usually located on the cell membrane and encodes Ca^{2+}-binding proteins, responsible for receiving Ca^{2+} signals induced by salt stress [42]. SOS2 is located in the cytoplasm and encodes a serine/threonine protein kinase, which usually receives the salt stress signal transmitted by SOS3 and can form a transcriptional complex with SOS3 to further phosphorylate the downstream Na^+/H^+ transporter SOS1, thereby accelerating intracellular Na^+ efflux and reducing the ion toxicity caused by salt stress [43]. NHX (Na^+/H^+ antiporter) is a cell membrane Na^+/H^+ antiporter protein that is located on the plasma membrane and vacuole membranes. It excretes Na^+ from the cytoplasm or isolates it into vacuoles through reverse concentration gradient transport, reducing the ion toxicity of salt stress to cells [44,45]. The expression of ion transport-related genes *AtSOS1*, *AtSOS2*, *AtSOS3* and *AtNHX1* in different transgenic lines was detected, and the results showed that under salt stress, the expression of these genes in overexpression-*PfMYBYB44* lines was significantly upregulated compared with that of WT (Figure 6). It was further suggested that *PfMYBYB44* enhanced plant salt tolerance, which may be related to the enhancement of plant ion transport capacity. It is speculated that *PfMYBYB44* not only transports excessive Na^+ to the extracellular space but also has a certain compartmentalization effect, causing plant vacuoles to receive certain salt ions to alleviate ion toxicity.

The expression pattern of NCED is closely related to the level of ABA in vivo. Rice *nced3* mutant is sensitive to salt and drought stresses, while overexpression of *OsNCED3* exhibits the opposite phenomenon [46]. *OsNCED4* and *OsNCED5* genes have also been confirmed to regulate the ABA level and stress resistance of rice under drought stress [47–49]. Catalase can directly act on H_2O_2, disproportionating it into H_2O and O_2, and protect cells from damage by ROS [50]. Proline is an amino acid synthesized in higher plants and plays a crucial role as a compatible osmotic substance under stress conditions. *P5CS*, as a key gene encoding proline synthesis, is significantly upregulated under osmotic stress induced by drought in species such as *Arabidopsis* and rice [51,52], and is highly responsive to osmotic stress. Protein kinase is an important core component of a plant stress defense mechanism, among which SnRK is a serine/threonine protein kinase, which plays an important role in plant stress response [53]. SnRK2 and SnRK3 are plant-specific protein kinases that actively participate in ABA signaling and various abiotic stresses in *Arabidopsis*, rice, wheat, and other plants [54,55]. In this study, *AtNCED3*, *AtP5CS*, *AtCAT1*, and *AtSnRK2.4*, four genes that have been shown to be mainly involved in drought stress, showed significantly higher expression levels in the overexpression of *Arabidopsis* after drought stress compared to WT (Figure 9). It can be inferred that under drought stress, *PfMYBYB44* is highly likely to affect the tolerance of *Paulownia fortunei* to drought stress by regulating the expression of key genes in these drought stress signaling pathways.

4. Materials and Methods

4.1. Sample Collection and Treatments

The *Paulownia fortunei* materials used in the experiment were cultured in the material culture room of the research group. The *Paulownia fortunei* seedlings (about 5–6 cm in height) with a good growth state and consistent growth were selected for stress treatment. Drought, salt, cold, hot and ABA treatment groups were set up, and the roots of the seedlings were immersed in Hoagland solution containing 15% PEG6000, 100 mM NaCl and 100 μM ABA for treatment, respectively. The seedlings cultured in Hoagland solutions

were placed under a constant temperature and in humidity incubators at 4 °C and 37 °C, respectively [56]. The seedlings under normal conditions without any treatment were used as the control group. After material treatment for 0 h, 1 h, 3 h, 5 h, 7 h, 9 h, and 12 h, samples were taken from the leaf and root of seedlings in each group. After being frozen in liquid nitrogen, they were stored in a −80 °C ultra-low temperature refrigerator for extracting leaf RNA and conducting gene expression analysis under stress. The root, stem, young leaf and mature leaf of *Paulownia fortunei* seedlings were collected and cryogenically frozen with liquid nitrogen for gene tissue expression analysis.

4.2. Cloning and Bioinformatic Analysis of PfMYB44

The RNA of the above samples was extracted using a column extraction kit and reverse-transcribed to synthesize cDNA. The reagent kit was purchased from Vazyme (Nanjing, China) with item numbers RC411-01 and r323, respectively. Specific primers for the PfMYB44 gene were designed based on the transcriptome data of *Paulownia fortunei*, pPfMYB44-F (5′-ATGGCAGCAAATACTAATGGTG-3′) and pPfMYB44-R (5′-TCAATCAA TCCTGCTGATTCC-3′). The complete *PfMYB44* gene fragment was obtained by PCR amplification using the cDNA. Purified PCR amplification products were transferred into T_5 vector and transformed into Escherichia coli DH5α receptor cells. After screening the monoclonal bacterial solution for PCR identification, positive clones were selected and sent to the company for sequencing verification.

The amino acid sequence of PfMYB44 was submitted to the NCBI database, and homologous sequences of other species with high similarity were screened by Blastp comparison, and the phylogenetic tree was constructed by the NJ (neighbor-joining) method of MEGA 11. Multiple sequences of PfMYB44 and its homologous proteins were compared by DNAMAN 5.2. ExPASy ProtParam was used to predict the physicochemical properties of protein. SOPMA was used to analyze the protein secondary structure, SWISS-MODEL was used to predict the protein tertiary structure, and BUSCA was used to predict the subcellular localization of PfMYB44.

4.3. Expression Analysis of PfMYB44

This study used the cDNA extracted from each sample group in Section 4.2 as a template and performed RT-qPCR using the fluorescent quantitative dye reagent ChamQ Universal SYBR qPCR Master Mix (Vazyme, Nanjing, China). The specific primers for RT-qPCR of the *PfMYB44* gene were pPfMYB44-qF: 5′-CCACAGCGACCTTTGAAGA-3′ and pPfMYB44-qR: 5′-GACATGCGAAGCC GACAC-3′. Using *PfActin* as the internal reference gene, the specific primer sequence was pPfActin-F: 5′-AATGGAATCTGCTGGAAT-3′ and pPfActin-R: 5′-ACTGAGGACAATGTTACC-3′ [57]. The PCR program was set up according to the instructions of the reagent kit. The relative gene expression was calculated using the $2^{-\Delta\Delta Ct}$ method.

4.4. Vector Construction and Subcellular Localization of PfMYB44

Primers pPfMYB44-OE-F (5′-GAGCTCGGTACCGGGGATCCATGGGGAGACAATAT ATAAT GGTG-3′) and pPfMYB44-OE-R (5′-GCCCTTGCTCACCATGTCGACATCATCCTG CTGATTCA AT-3′) were used to add homologous arms to both ends of the PfMYB44 sequence. The overexpression-*PfMYB44* vector was constructed with pCAMBIA1300-GFP plasmid as the skeleton by the homologous recombination method and named 35S:: PfMYB44-GFP. The plasmid vector, which was successfully sequenced and validated, was transformed into Agrobacterium and positive clones were selected. The bacterial liquid was identified by PCR.

Agrobacterium 35S::PfMYB44-GFP was injected into tobacco for nuclear localization and pCAMBIA1300-GFP Agrobacterium was used as blank control. The distribution and co-localization of GFP fluorescence and nuclear localization protein mCherry protein fluorescence in tobacco epidermal cells were observed by laser scanning confocal microscopy after 48 h of dark culture.

4.5. Generation of Transgenic Lines

The resuspension of Agrobacterium containing PfMYB44 was prepared and the dipping method was used to infect the flowering stage of *Arabidopsis* inflorescence. The seeds of T_1 generation were harvested, dried in a 37 °C oven for one week, and placed in a cold environment of 4 °C for vernalization. After, they were disinfected with 75% anhydrous ethanol for 30 s and washed with sterile water three times, and disinfected with 10% NaClO solution for 3 m, washed with sterile water three times, and then seeded on 1/2 MS solid medium containing kanamycin (50 mg L^{-1}). After 8–10 d, positive seedlings with robust roots and fresh green leaves were transplanted in the substrate (nutrient soil/vermiculite = 2:1). After 2 weeks of cultivation, T_1-generation transgenic *Arabidopsis* were obtained. Leaf samples were collected, their RNA was extracted, and cDNA was obtained by reverse transcription as a template for RT-qPCR expression detection. The specific sequence primers were pPfMYB44-qF: 5′-CCACAGCGACCTTTGAAGA-3′ and pPfMYB44-qR: 5′-GACATGCGAAGCCGACAC-3′. The internal reference primers were pAtActin-F: 5′-CCCGCTATGTATGTCGC-3′ and pAtActin-R: 5′-AAGGTCAAGA CGGAGGAT-3′. Individual transgenic positive plants with high expression and subculture were harvested to obtain T_3-generation homozygous plants for subsequent experiments.

4.6. Analysis of Related Physiological Indexes in Overexpression-PfMYB44 Arabidopsis

WT, UL and T_3 transgenic *Arabidopsis* (L2, L3 and L6) seedlings with similar root length and growth on 1/2 MS solid medium were selected and transplanted into soil. Control, salt treatment and drought treatment groups were set up, respectively. After 3 weeks of normal growth of *Arabidopsis* seedlings in the soil, the control group maintained normal watering treatment. After the salt treatment group was watered with 300 mmol L^{-1} NaCl for 8 d, the phenotype and survival rate were observed. After 10 d of natural drought and 3 d of rewater treatment, phenotype and survival rate were observed, respectively. After phenotypic observation, the contents of MDA, proline and chlorophyll were determined, and the activities of antioxidant enzymes SOD, POD and CAT were determined. The kit instructions were followed for specific steps. The specific kit numbers are as follows: chlorophyll (Solarbio, Beijing, China: mlsw-E0781), MDA (Solarbio: BC0020), proline (Solarbio: BC0295), SOD (Solarbio:HP-A101F), POD (Solarbio:ZY7POD-1-Y) and CAT (Solarbio:YBSH150).

4.7. Expression Analysis of Stress-Related Genes in Overexpression-PfMYB44 Arabidopsis

Samples were taken from the leaves of *Arabidopsis* (WT, UL, L2, L3 and L6) before and after stresses; the RNA was extracted and reverse-transcribed into cDNA for analyzing the expression changes in stress-related genes in *Arabidopsis*. The primer sequences used were as follows: pAtP5CS-F/R: GATACGGATATGGCAAAGCG/CCAAGTCCAAATCGGAAA CC; pAtCAT1-F/R: CGCCA TGCCGAAAAATACCC/CTTGCCTGTCTGAATCCCAGGAC; pAtNCED3-F/R: AGACAAATA CGCCGAAGA/CATACAGGACCCTATCACG; pAtSnRK 2.4-F/R: GAGGAAATGGGGATGCAG AT/TTCTCACTTCTCCACTTGCG; pAtSOS2-F/R: GCAAGGGAAGAAGAAGAAGT/TCTCCG CTACATAACTGCC; pAtSOS3-F/R: GAATC-CATCGCTCATCAA/CCATTTCTTCCTCTTCACA; pAtSOS1-F/R: TTCATCATCCTCA-CAATGGCTCTAA/CCCTCATCAAGCATCTCCCAGTA; pAtNHX1-F/R: AGCCTTCAGG GAACCACAAT/CTCCAAAGACGGGTCGCATG. The primers were from 5′ to 3′. Additionally, the *AtActin* was selected as the reference gene.

4.8. Statistical Analysis

All measurements were repeated three times. SPSS 26.0 software was used to conduct statistical scores of the data, and the ANOVA method was used to analyze the significant differences (* $p \leq 0.05$, ** $p \leq 0.01$).

5. Conclusions

This study preliminarily analyzed the bioinformatics characteristics and expression patterns of the *PfMYB44* gene in response to abiotic stress and ABA. It was found that *PfMYB44* belongs to R2R3-MYB and positively responds to drought, cold, hot, salt, and ABA stresses. Overexpression in *Arabidopsis* further confirms that *PfMYB44* is a positive regulatory factor for drought and salt stresses. Under salt stress, *PfMYBYB44* enhanced the ability of plants to transport Na^+ and improve salt tolerance by upregulating the expression of ion transport-related genes *AtSOS1*, *AtSOS2*, *AtSOS3*, and *AtNHX1*. Under drought stress, *PfMYBYB44* was highly likely to affect paulownia's tolerance to drought stress through the ABA pathway by regulating the expression of key genes in drought stress signaling pathways such as *AtNCED3*, *AtP5CS*, *AtCAT1*, and *AtSnRK2.4*. This provides an important reference for future exploration and exploration of such transcription factors, and further in-depth research is needed on their biological functions and molecular mechanisms in *Paulownia fortunei*.

Supplementary Materials: The following supporting information can be downloaded at https://www.mdpi.com/article/10.3390/plants13162264/s1, Figure S1: Nucleotide and amino acid sequence of *PfMYB44*. The red underlined part was the R-repeated conserved domain; Figure S2: Structure analysis of PfMYB44 protein. (A) The secondary structure; (B) functional domain; and (C) tertiary structure of PfMYB44.

Author Contributions: Conceptualization, G.L. and W.C.; formal analysis, H.W. and W.L.; funding acquisition, S.S. and L.W.; methodology, H.W., W.L. and X.L.; methodology, W.L. and X.L.; supervision, L.W.; investigation, G.L., W.C. and L.W.; writing—original draft preparation, G.L. and W.C.; writing—review and editing, G.L. All authors have read and agreed to the published version of the manuscript.

Funding: This work was supported by the independent research project of Jiangsu Academy of Forestry Sciences "Selection of High Quality Wood and Landscape Greening Varieties of *Paulownia* and *Taxodium mucronatum* Ten" (ZZKY202102), and Jiangsu Forestry Science and Technology Innovation and Promotion Project "Jiangsu Paulownia cultivation technology long-term scientific research base" (LYKJ [2020]23).

Informed Consent Statement: Not applicable.

Data Availability Statement: The original data for this present study are available from the corresponding authors.

Conflicts of Interest: The authors declare no conflicts of interest.

References

1. Jiang, H.; Okoye, C.O.; Chen, X.; Zhang, F.; Jiang, J. High-throughput 16S rRNA gene-based amplicon sequencing reveals the functional divergence of halophilic bacterial communities in the Suaeda salsa root compartments on the eastern coast of China. *Sci. Total Environ.* **2024**, *942*, 173775. [CrossRef] [PubMed]
2. Zhang, X.; Zhai, X.; Deng, M.; Dong, Y.; Zhao, Z.; Fan, G. Comparative studies on physiological responses of diploid paulowniaand its tetraploid to drought stress. *J. Henan Agric. Sci.* **2013**, *42*, 118–123.
3. Wang, Y.; Cao, L.; Deng, M.; Ma, Y.; Zhao, Z.; Niu, S.; Wang, X.; Fan, G. Analysis of salt stress-responsive microRNAs in *Paulownia fortunei* by high-throughput sequencing. *J. Henan Agric. Univ.* **2015**, *49*, 461–467.
4. Ng, D.W.K.; Abeysinghe, J.K.; Kamali, M. Regulating the regulators: The control of transcription factors in plant defense signaling. *Int. J. Mol. Sci.* **2018**, *19*, 3737. [CrossRef]
5. Dubos, C.; Stracke, R.; Grotewold, E.; Weisshaar, B.; Martin, C.; Lepiniec, L. MYB transcription factors in *Arabidopsis*. *Trends Plant Sci.* **2010**, *15*, 573–581. [CrossRef] [PubMed]
6. Feller, A.; Machemer, K.; Braun, E.L.; Grotewold, E. Evolutionary and comparative analysis of MYB and bHLH plant transcription factors. *Plant J.* **2011**, *66*, 94–116. [CrossRef]
7. Li, Y.; Leng, N.; Mu, Z.; Wang, H.; Chao, Y. Cloning and expression analysis of transcription factor *MtMYB* and transformation of *Arabidopsis thaliana*. *Mol. Plant Breed.* **2020**, *18*, 2769–2775.
8. Wang, J.; Liu, Y.; Tang, B.; Dai, X.; Xie, L.; Liu, F.; Zou, X. Genome-wide identification and capsaicinoid biosynthesis-related expression analysis of the R2R3 MYB gene family in *Capsicum annuum*. *Front. Genet.* **2020**, *11*, 598183. [CrossRef] [PubMed]

9. Grotewold, E.; Sainz, M.B.; Tagliani, L.; Hernandez, J.M.; Bowen, B.; Chandler, V. Identification of the residues in the Myb domain of maize C1 that specify the interaction with the bHLH cofactor R. *Proc. Natl. Acad. Sci. USA* **2000**, *97*, 13579–13584. [CrossRef]
10. Liu, L.; Du, H.; Tang, X.F.; Wu, Y.M.; Huang, Y.B.; Tang, Y.X. The roles of MYB transcription factors on plant defense responses and its molecular mechanism. *Hereditas* **2008**, *30*, 1265–1271. [CrossRef]
11. Ogata, K.; Kanei-Ishii, C.; Sasaki, M.; Hatanaka, H.; Nagadoi, A.; Enari, M.; Nakamura, H.; Nishimura, Y.; Ishii, S.; Sarai, A. The cavity in the hydrophobic core of Myb DNA-binding domain is reserved for DNA recognition and transactivation. *Nat. Struct. Biol.* **1996**, *3*, 178–187. [CrossRef]
12. Stracke, R.; Werber, M.; Weisshaar, B. The R2R3-MYB gene family in *Arabidopsis thaliana*. *Curr. Opin. Plant Biol.* **2001**, *4*, 447–456. [CrossRef]
13. Pazares, J.; Ghosal, D.; Wienand, U.; Peterson, P.A.; Saedler, H. The regulatory C1 locus of *Zea mays* encodes a protein with homology to MYB proto-oncogene products and with structural simiarities to transcriptional activators. *EMBO J.* **1987**, *6*, 3553–3558. [CrossRef] [PubMed]
14. Seo, J.; Sohn, H.B.; Noh, K.; Jung, C.; An, J.H.; Donovan, C.M.; Somers, D.A.; Kim, D.I.; Jeong, S.C.; Kim, C.g.; et al. Expression of the *Arabidopsis AtMYB44* gene confers drought/salt-stress tolerance in transgenic soybean. *Mol. Breed.* **2012**, *29*, 601–608. [CrossRef]
15. An, C.; Sheng, L.; Du, X.; Wang, Y.; Zhang, Y.; Song, A.; Jiang, J.; Guan, Z.; Fang, W.; Chen, F.; et al. Overexpression of *CmMYB15* provides chrysanthemum resistance to aphids by regulating the biosynthesis of lignin. *Hortic. Res.* **2019**, *6*, 84. [CrossRef]
16. Yuan, Y.; Xu, X.; Luo, Y.; Gong, Z.; Hu, X.; Wu, M.; Liu, Y.; Yan, F.; Zhang, X.; Zhang, W.; et al. R2R3 MYB-dependent auxin signalling regulates trichome formation, and increased trichome density confers spider mite tolerance on tomato. *Plant Biotechnol. J.* **2021**, *19*, 138–152. [CrossRef]
17. Hu, Z.; Zhong, X.; Zhang, H.; Luo, X.; Wang, Y.; Wang, Y.; Liu, T.; Zhang, Y.; Wang, X.; An, H.; et al. *GhMYB18* confers aphis gossypii glover resistance through regulating the synthesis of salicylic acid and flavonoids in cotton plants. *Plant Cell Rep.* **2023**, *42*, 355–369. [CrossRef]
18. Gao, R.F.; Han, T.T.; Xun, H.W.; Zeng, X.S.; Li, P.H.; Li, Y.Q.; Wang, Y.N.; Shao, Y.; Cheng, X.; Feng, X.Z.; et al. MYB transcription factors *GmMYBA2* and *GmMYBR* function in a feedback loop to control pigmentation of seed coat in soybean. *J. Exp. Bot.* **2021**, *72*, 4401–4418. [CrossRef]
19. Wang, F.; Kong, W.; Wong, G.; Fu, L.; Peng, R.; Li, Z.; Yao, Q. *AtMYB12* regulates flavonoids accumulation and abiotic stress tolerance in transgenic *Arabidopsis thaliana*. *Mol. Genet. Genom.* **2016**, *291*, 1545–1559. [CrossRef] [PubMed]
20. Rahaie, M.; Xue, G.P.; Naghavi, M.R.; Alizadeh, H.; Schenk, P.M. A MYB gene from wheat (*Triticum aestivum* L.) is up-regulated during salt and drought stresses and differentially regulated between salt-tolerant and sensitive genotypes. *Plant Cell Rep.* **2010**, *29*, 835–844. [CrossRef] [PubMed]
21. Li, J.; Zhao, S.; Yu, X.; Du, W.; Li, H.; Sun, Y.; Sun, H.; Ruan, C. Role of *Xanthoceras sorbifolium* MYB44 in tolerance to combined drought and heat stress via modulation of stomatal closure and ROS homeostasis. *Plant Physiol. Biochem.* **2021**, *162*, 410–420. [CrossRef] [PubMed]
22. Hao, Y.; Wang, J.; Hu, C.; Zhou, Q.; Mubeen, H.; Hou, X. Regulation of *BcMYB44* on anthocyanin synthesis and drought tolerance in non-heading Chinese cabbage (*Brassica campestris ssp.* chinensis Makino). *Horticulturae* **2022**, *8*, 351. [CrossRef]
23. Qi, T.C.; Huang, H.; Song, S.S.; Xie, D.X. Regulation of jasmonate-mediated stamen development and seed production by a bHLH-MYB complex in *Arabidopsis*. *Plant Cell* **2015**, *27*, 1620–1633. [CrossRef]
24. Rahim, M.A.; Resentini, F.; Dalla, V.F.; Trainotti, L. Effects on plant growth and reproduction of a peach R2R3-MYB transcription factor overexpressed in tobacco. *Front. Plant Sci.* **2019**, *10*, 1143. [CrossRef]
25. Song, S.S.; Qi, T.C.; Huang, H.; Ren, Q.C.; Wu, D.W.; Chang, C.Q.; Peng, W.; Liu, Y.L.; Peng, J.R.; Xie, D.X. The jasmonate-zim domain proteins interact with the R2R3-MYB transcription factors MYB21 and MYB24 to affect jasmonate-regulated stamen development in *Arabidopsis*. *Plant Cell* **2011**, *23*, 1000–1013. [CrossRef]
26. Sun, B.M.; Zhu, Z.S.; Chen, C.J.; Chen, G.J.; Cao, B.H.; Chen, C.M.; Lei, J.J. Jasmonate-inducible R2R3-MYB transcription factor regulates capsaicinoid biosynthesis and stamen development in *Capsicum*. *J. Agric. Food Chem.* **2019**, *67*, 10891–10903. [CrossRef]
27. Zhang, X.Y.; He, Y.Q.; Li, L.Y.; Liu, H.R.; Hong, G.J. Involvement of the R2R3-MYB transcription factor MYB21 and its homologs in regulating flavonol accumulation in *Arabidopsis* stamen. y. *Exp. Bot.* **2021**, *72*, 4319–4332. [CrossRef] [PubMed]
28. Zhao, Z.L.; Zhai, X.Q. The agroforestry compound management model of *Paulownia* and it's benefit evaluation. *J. Henan For. Sci. Technol.* **2020**, *40*, 6–7.
29. Rodríguez-Seoane, P.; Díaz-Reinoso, B.; Moure, A.; Domínguez, H. Potential of *Paulownia* sp. for biorefinery. *Ind. Crop. Prod.* **2020**, *155*, 112739. [CrossRef]
30. Li, W.; Zhong, J.; Zhang, L.; Wang, Y.; Song, P.; Liu, W.; Li, X.; Han, D. Overexpression of a *Fragaria vesca* MYB transcription factor gene (*FvMYB82*) increases salt and cold tolerance in *Arabidopsis thaliana*. *Int. J. Mol. Sci.* **2022**, *23*, 10538. [CrossRef] [PubMed]
31. Yang, X.; Luo, J.; Wang, Y.Q. MYB transcription factors involved in regulation of flavonoid biosynthesis of medicinal plants. *J. Gansu Univ. Chin. Med.* **2018**, *35*, 77–81.
32. Zhang, W.; Xu, F.; Cheng, S.; Liao, Y. Characterization and functional analysis of a *MYB* gene (*GbMYBFL*) related to flavonoid accumulation in *Ginkgo biloba*. *Genes Genom.* **2018**, *40*, 49–61. [CrossRef] [PubMed]
33. He, W.; Lei, W.; Guo, X.; Li, R.; Chen, G. Identification of the MYB gene family and functional analysis of key genes related to blue flower coloration in *Agapanthus praecox*. *Acta Hortic. Sin.* **2023**, *50*, 1255–1268.

34. Zhao, Y.; Cheng, X.; Liu, X.; Wu, H.; Bi, H.; Xu, H. The wheat MYB transcription factor *TaMYB31* is involved in drought stress responses in *Arabidopsis*. *Front. Plant Sci.* **2018**, *9*, 1426. [CrossRef]
35. Lee, H.G.; Seo, P.J. The MYB96-HHP module integrates cold and abscisic acid signaling to activate the CBF-COR pathway in *Arabidopsis*. *Plant J.* **2015**, *82*, 962–977. [CrossRef]
36. Lv, Y.; Yang, M.; Hu, D.; Yang, Z.; Ma, S.; Li, X.; Xiong, L. The *OsMYB30* transcription factor suppresses cold tolerance by interacting with a JAZ protein and suppressing beta-amylase expression. *Plant Physiol.* **2017**, *173*, 1475–1491. [CrossRef]
37. Zhang, H.; Hu, Y.; Gu, B.; Cui, X.; Zhang, J. *VaMYB44* transcription factor from Chinese wild *Vitis amurensis* negatively regulates cold tolerance in transgenic *Arabidopsis thaliana* and *V. vinifera*. *Plant Cell Rep.* **2022**, *41*, 1673–1691. [CrossRef]
38. Wang, X.P.; Niu, Y.L.; Zheng, Y. Multiple functions of MYB transcription factors in abiotic stress responses. *Int. J. Mol. Sci.* **2021**, *22*, 6125. [CrossRef] [PubMed]
39. Chen, K.; Li, G.J.; A Bressan, R.; Song, C.P.; Zhu, J.K. Abscisic acid dynamics, signaling, and functions in plants. *J. Integr. Plant Biol.* **2020**, *62*, 27–56. [CrossRef]
40. Xu, W.; Tang, W.; Wang, C.; Ge, L.; Sun, J.; Qi, X.; He, Z.; Zhou, Y.; Chen, J.; Xu, Z.; et al. *SiMYB56* confers drought stress tolerance in transgenic rice by regulating lignin biosynthesis and ABA signaling pathway. *Front. Plant Sci.* **2020**, *11*, 785. [CrossRef]
41. Xiong, L.; Schumaker, K.S.; Zhu, J.K. Cell signaling during cold, drought, and salt stress. *Plant Cell* **2002**, *14*, S165–S183. [CrossRef] [PubMed]
42. Ma, L.; Ye, J.; Yang, Y.; Lin, H.; Yue, L.; Luo, J.; Long, Y.; Fu, H.H.; Liu, X.G.; Zhang, Y.L.; et al. The *SOS2-SCaBP8* complex generates and fine-tunes an *AtANN4*-dependent calcium signature under salt stress. *Dev. Cell* **2019**, *48*, 697–709. [CrossRef]
43. Quan, R.; Lin, H. *SCABP8/CBL10*, aputative calcium sensor, interacts with the protein kinase *AtSOS2* to protect *Arabidopsis* shoots from salt stress. *Plant Cell* **2007**, *19*, 1415–1431. [CrossRef]
44. Munns, R.; Tester, M. Mechanisms of salinity tolerance. *Annu. Rev. Plant Biol.* **2008**, *59*, 651–681. [CrossRef]
45. Krishna, R.; Karkute, S.G.; Ansari, W.A.; Jaiswal, D.K.; Verma, J.P.; Singh, M. Transgenic tomatoes for abiotic stress tolerance: Status and way ahead. *3 Biotech* **2019**, *9*, 143. [CrossRef]
46. Huang, Y.; Guo, Y.M.; Liu, Y.T.; Zhang, F.; Wang, Z.K.; Wang, H.Y.; Wang, F.; Li, D.P.; Mao, D.D.; Luan, S.; et al. 9-*cis*-epoxycarotenoid dioxygenase 3 regulates plant growth and enhances multi-abiotic stress tolerance in rice. *Front. Plant Sci.* **2018**, *9*, 162. [CrossRef]
47. Hwang, S.G.; Lee, C.Y.; Tseng, C.S. Heterologous expression of rice 9-*cis*-epoxycarotenoid dioxygenase 4 (*OsNCED4*) in *Arabidopsis* confers sugar oversensitivity and drought tolerance. *Bot. Stud.* **2018**, *59*, 2. [CrossRef] [PubMed]
48. Huang, Y.; Jiao, Y.; Xie, N.; Guo, Y.; Zhang, F.; Xiang, Z.; Wang, R.; Wang, F.; Gao, Q.; Tian, L.; et al. *OsNCED5*, a 9-*cis*-epoxycarotenoid dioxygenase gene, regulates salt and water stress tolerance and leaf senescence in rice. *Plant Sci.* **2019**, *287*, 110188. [CrossRef] [PubMed]
49. Zong, W.; Tang, N.; Yang, J.; Peng, L.; Ma, S.Q.; Xu, Y.; Li, G.L.; Xiong, L.Z. Feedback regulation of ABA signaling and biosynthesis by a bZIP transcription factor targets drought-resistance-related genes. *Plant Physiol.* **2016**, *171*, 2810–2825. [CrossRef] [PubMed]
50. Scandalios, J.G. Oxidative stress molecular perception and transduction of signal triggering antioxidant gene defenses. *Braz. J. Med. Biol. Res.* **2005**, *38*, 995–1001. [CrossRef]
51. Verslues, P.E.; Sharma, S. Proline metabolism and its implications for plant-environment interaction. *Arab. Book* **2010**, *8*, e140. [CrossRef] [PubMed]
52. Hur, J.; Jung, K.H.; Lee, C.H.; An, G.H. Stress-inducible *OsP5CS2* gene is essential for salt and cold tolerance in rice. *Plant Sci.* **2004**, *167*, 417–426. [CrossRef]
53. Coello, P.; Hey, S.J.; Halford, N.G. The sucrose non-fermenting-1-related (SnRK) family of protein kinases: Potential for manipulation to improve stress tolerance and increase yield. *J. Exp. Bot.* **2011**, *62*, 883–893. [CrossRef] [PubMed]
54. Lu, K.; Zhang, Y.D.; Zhao, C.F.; Zhou, L.H.; Zhao, Q.Y.; Chen, T.; Wang, C.L. The *Arabidopsis* kinase-associated protein phosphatase KAPP, interacting with protein kinases SnRK2.2/2.3/2.6, negatively regulates abscisic acid signaling. *Plant Mol. Biol.* **2020**, *102*, 199–212. [CrossRef] [PubMed]
55. Ma, X.; Li, Q.H.; Yu, Y.N.; Qiao, Y.M.; Haq, S.U.; Gong, Z.H. The CBL CIPK pathway in plant response to stress signals. *Int. J. Mol. Sci.* **2020**, *21*, 5668. [CrossRef] [PubMed]
56. Duan, Y.; Han, J.; Guo, B.; Zhao, W.; Zhou, S.; Zhou, C.; Zhang, L.; Li, X.; Han, D. *MbICE1* confers drought and cold tolerance through up–regulating antioxidant capacity and stress–resistant genes in *Arabidopsis thaliana*. *Int. J. Mol. Sci.* **2022**, *23*, 16072. [CrossRef]
57. Zhao, X.; Li, B.; Zhai, X.; Liu, H.; Deng, M.; Fan, G. Genome-Wide analysis of specific *PfR2R3-MYB* genes related to *Paulownia* witches' broom. *Genes* **2023**, *14*, 7. [CrossRef]

Disclaimer/Publisher's Note: The statements, opinions and data contained in all publications are solely those of the individual author(s) and contributor(s) and not of MDPI and/or the editor(s). MDPI and/or the editor(s) disclaim responsibility for any injury to people or property resulting from any ideas, methods, instructions or products referred to in the content.

plants

MDPI

Article

Genome-Wide Identification and Analysis of Maize *DnaJ* Family Genes in Response to Salt, Heat, and Cold at the Seedling Stage

Gang Li †, Ziqiang Chen †, Xinrui Guo, Dagang Tian, Chenchen Li, Min Lin, Changquan Hu * and Jingwan Yan *

Biotechnology Research Institute, Fujian Academy of Agricultural Sciences, Fuzhou 350003, China; ligang4439@163.com (G.L.); czq@fjage.org (Z.C.); guoxinrui1@163.com (X.G.); tdg@fjage.org (D.T.); lcc823j@163.com (C.L.); linmin_0916@163.com (M.L.)

* Correspondence: hcq@fjage.org (C.H.); yjw@fjage.org (J.Y.)

† These authors contributed equally to this work.

Abstract: DnaJ proteins, also known as HSP40s, play a key role in plant growth and development, and response to environmental stress. However, little comprehensive research has been conducted on the *DnaJ* gene family in maize. Here, we identify 91 *ZmDnaJ* genes from maize, which are likely distributed in the chloroplast, nucleus, and cytoplasm. Our analysis revealed that *ZmDnaJs* were classified into three types, with conserved protein motifs and gene structures within the same type, particularly among members of the same subfamily. Gene duplication events have likely contributed to the expansion of the *ZmDnaJ* family in maize. Analysis of cis-regulatory elements in *ZmDnaJ* promoters suggested involvement in stress responses, growth and development, and phytohormone sensitivity in maize. Specifically, four cis-acting regulatory elements associated with stress responses and phytohormone regulation indicated a role in adaptation. RNA-seq analysis showed constitutive expression of most *ZmDnaJ* genes, some specifically in pollen and endosperm. More importantly, certain genes also responded to salt, heat, and cold stresses, indicating potential interaction between stress regulatory networks. Furthermore, early responses to heat stress varied among five inbred lines, with upregulation of almost tested *ZmDnaJ* genes in B73 and B104 after 6 h, and fewer genes upregulated in QB1314, MD108, and Zheng58. After 72 h, most *ZmDnaJ* genes in the heat-sensitive inbred lines (B73 and B104) returned to normal levels, while many genes, including ZmDnaJ55, 79, 88, 90, and 91, remained upregulated in the heat-tolerant inbred lines (QB1314, MD108, and Zheng58) suggesting a synergistic function for prolonged protection against heat stress. In conclusion, our study provides a comprehensive analysis of the *ZmDnaJ* family in maize and demonstrates a correlation between heat stress tolerance and the regulation of gene expression within this family. These offer a theoretical basis for future functional validation of these genes.

Keywords: *DnaJ* gene family; abiotic stress; maize; gene expression

1. Introduction

Plants are subjected to a range of stresses, including drought, heat, salinity, cold, and pathogens, all of which have the potential to impede their growth and reduce yield [1]. A 1 °C increase in temperature is reported to potentially reduce the production of maize (*Zea mays* L.), wheat (*Triticum aestivum* L.), rice (*Oryza sativa* L.), and soybean (*Glycine max* (L.) *Merr.*) by 7.4%, 6%, 3.2%, and 3.1%, respectively [2]. In response to such stresses, plants produce heat shock proteins (Hsps), which are essential for cell survival during periods of stress [3,4]. Previous studies have shown that Hsps, classified as Hsp100, Hsp90, Hsp70, Hsp60, Hsp40, and Hsp20, based on molecular weight, function in a variety of cellular processes, such as maintaining protein folding, facilitating membrane transport, and disaggregating protein complexes [5,6]. Among these, Hsp40 proteins are the most prevalent in eukaryotic organisms. For example, yeast is reported to have 22 Hsp40 members [7], while *Arabidopsis thaliana* and rice contain 109 and 104 Hsp40 members, respectively [8,9].

Hsp40s, also known as DnaJ proteins (DnaJs), are characterized by a conserved J-domain featuring a histidine/proline/aspartic (HPD) signature motif. This motif is crucial for interacting with Hsp70, which regulates its ATPase activity and facilitates the refolding of stress-damaged proteins [10,11]. Except for the common J-domain, DnaJ proteins exhibit extensive structural diversity. Based on their domains, DnaJ proteins can generally be divided into three types: type I, type II, and type III. Type I DnaJ proteins include three typical domains, namely the J-domain, G/F domain, and C-terminal domain. Type II DnaJ proteins are similar to type I but lack the G/F domain. Type III DnaJ proteins, the most diverse group, present only the J-domain or are accompanied by other diverse domains like the TPR domain, Fe-S cluster, or AT-hook domain, which may lead to more specialized functions [8,9,11]. The different types of DnaJ proteins reflect their functional diversity.

Studies showed that plant DnaJ proteins are widely involved in various biological processes, including chloroplast function and plant stress responses. For example, DJA6 and DJA5 proteins in *Arabidopsis* facilitate chloroplast iron-sulfur cluster biogenesis [12,13]. DnaJ proteins, such as AtJ8, AtJ11, and AtJ20, are essential for optimizing photosynthesis and chloroplast efficiency [14]. In stress responses, the AtJ3 protein in *Arabidopsis* regulates pH homeostasis and influences stress sensitivity, particularly under alkaline conditions and high salt [15]. The tomato SlDnaJ20 protein enhances thermo-tolerance and reduces photosystem II photoinhibition under heat stress [16]. LeCDJ1, a tomato chloroplast-targeted DnaJ protein, could improve tolerance to heat, chilling, and drought stress, as well as resistance to *Pseudomonas solanacearum* [17–19]. In addition, two ER-localized DnaJ proteins, ERdj3B and TMS1, are crucial for the development of anthers and pollen tubes under high-temperature stress [20–22]. These findings indicate the significance of DnaJ proteins in stress responses.

Currently, identification efforts for the *DnaJ* gene family have primarily focused on *Arabidopsis*, rice, cucumber, and pepper [8,9,23,24]. However, there were no reports on maize, a globally significant crop that frequently faces biotic and abiotic stress. In the present work, we systematically identify and characterize *ZmDnaJs* in the maize genome, including the gene structure, conserved motif, cis-element in the promoter, and phylogenetic relationship. We also analyze the expression patterns of *ZmDnaJs* in various tissues and under abiotic stresses, especially for expression levels under high temperatures. This work provides a thorough examination of the *ZmDnaJ* family in maize and lays the foundation for further investigations to determine whether the *ZmDnaJ* gene family members are involved in the response to environmental stress.

2. Results

2.1. ZmDnaJ Gene Family in the Maize Genome and Their Physiochemical Properties

In this study, 91 *ZmDnaJ* genes were identified in the maize genome using the hidden Markov model (HMM) of the DnaJ structural domain (PF00226). Based on the Pfam and NCBI CDD databases, we confirmed that these proteins contained the full DnaJ domain. These genes were renamed *ZmDnaJ1~ZmDnaJ91* according to their locations on the chromosome (Table S1).

The physicochemical properties of these genes and their corresponding proteins were further analyzed, including gene ID, location, protein length (aa), molecular weight (MW), theoretical isoelectric point (pI), instability index, grand average of hydropathicity, and subcellular location. The number of amino acids ranged greatly from 121aa (ZmDnaJ43) to 2574aa (ZmDnaJ6). The molecular weights ranged from 13,812.54 Da (ZmDnaJ38) to 281,715.97 Da (ZmDnaJ6), pI from 4.41 (ZmDnaJ18) to 10.8 (ZmDnaJ32), and the instability index from 24.94 (ZmDnaJ43) to 97.37 (ZmDnaJ65). The grand average of hydropathicity was <0, indicating that all members of the ZmDnaJ family were hydrophilic proteins. Subcellular localization prediction showed that the majority of ZmDnaJ members were located in the cytoplasm, chloroplast, or nucleus, with few members in the mitochondrion or endoplasmic reticulum or vacuole, indicating their various functions (Table S1).

2.2. Phylogenetic and Conserved Domain Analysis of the ZmDnaJ Gene Family

To understand the phylogenetic relationships of the *ZmDnaJ* gene family, a phylogenetic tree was constructed based on the 91 ZmDnaJ and 101 *Arabidopsis* DnaJ protein sequences using MEGA-X with the maximum likelihood (ML) method. The phylogenetic tree of *DnaJ* gene members from *Arabidopsis* and maize showed different clades, based on their conserved protein sequences. According to the classification of the *AtDnaJ* members, the maize *ZmDnaJ* members were divided into three types (type I, type II, and type III) with the related *Arabidopsis* homeobox genes. Type I contains nine *AtDnaJs* from *Arabidopsis* and eight *ZmDnaJs* from maize. Type II presents 11 *AtDnaJs* and 12 *ZmDnaJs*. These two types have a close evolutionary relationship, indicating that they are relatively conserved in their evolution and functions. The remaining *DnaJ* genes from *Arabidopsis* and maize were clustered into type III, constituting the largest group. It is worth noting that type III could be further divided into several subgroups, which may exhibit the most diverse functions (Figure 1).

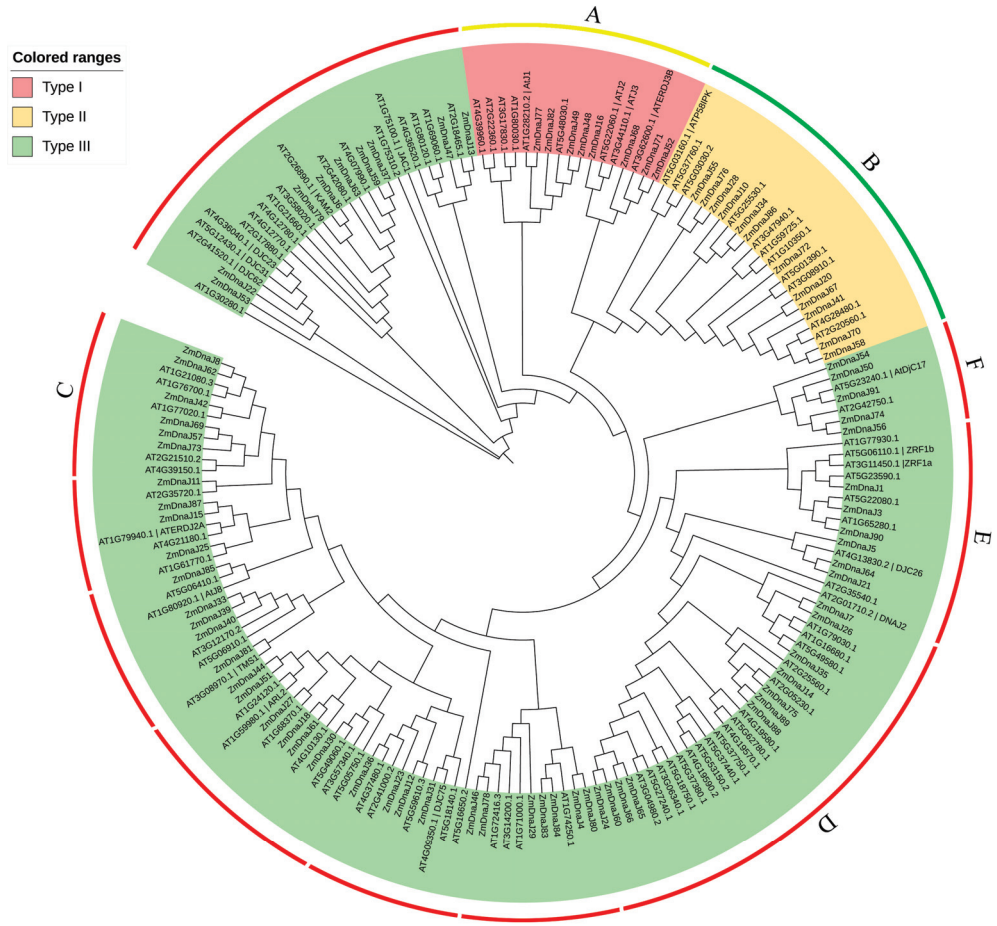


Figure 1. Phylogenetic tree of ZmDnaJ and AtDnaJ proteins. The phylogenetic tree was constructed using MEGA X with 1000 bootstrap replications and an optimal Jones–Taylor–Thornton (JTT) model, incorporating the DnaJ proteins from maize and *Arabidopsis*. The new names for maize proteins are listed in Table S1, and the accession numbers for *Arabidopsis* proteins are based on Rajan et al. [8]. Different background colors represent the three types. A and B represent the DnaJ_C subfamily; C represents the DnaJ-X subfamily; D represents the DUF3444 subfamily; E represents the Jiv90 subfamily; F represents the Fer4_8 subfamily.

To understand the relationship between evolution and conserved domains among ZmDnaJ proteins, we further analyzed their conserved domains using the NCBI-CDD website. The evolutionary tree of ZmDnaJ proteins was conducted by MEGA-X to distinguish different clades. As shown in Figure S1, we found that ZmDnaJ pro-

teins belonging to types I and II (Figure 1) generally consist of a J-domain followed by a C-terminal domain (DnaJ_C), apart from ZmDnaJ20. In addition to the signature J-domain, type III J-proteins contain diverse domains such as DnaJ-X, DUF3444, TPR domain, Fer4_8 cluster, or Jiv90, which confer additional specificity. These results indicate that the conserved domains of ZmDnaJ proteins within the same group exhibit similar compositions.

2.3. Conserved Motif and Gene Structure Analysis of the ZmDnaJ Gene Family

We further analyzed the conserved motifs of ZmDnaJ proteins to evaluate their functional regions. Using the MEME website, 10 conserved motifs were identified, and their distribution in ZmDnaJ proteins, along with a phylogenetic tree is shown in Figure 2. We found that 32 ZmDnaJ proteins contain a complete J domain, including motifs 1, 2, 3, and 8. Among these, motif 1, with a stable HPD structure (the core of the J domain), is present in all proteins. Motifs 2 and 8, which form an α-helical structure, are located within the C-terminal region of the J-domain (Figures 2 and S2). The remaining proteins only possess the HPD structure and an incomplete α-helical structure. In addition, some motifs are specific to particular groups, which might be related to distinct biological functions. For example, motifs 4, 5, and 6 are present in type I and type II, motif 7 is specific to the DnaJ-X subgroup, and motifs 9 and 10 are unique to the DUF3444 subgroup (Figures 2 and S1). The above results would facilitate the prediction of *ZmDnaJ* gene functions.

Furthermore, the gene structure of the ZmDnaJ family was analyzed to better understand its characterization. The results showed significant variation in the number of exons (ranging from 1 to 22) and introns (ranging from 0 to 21) in individual *ZmDnaJ* genes (Figure 2). Most *ZmDnaJ* genes within the same group have similar exon numbers and structures. However, there are significant differences in intron lengths, as seen in *ZmDnaJ86* and *ZmDnaJ34* in type I; *ZmDnaJ24* and *ZmDnaJ60* in the DUF3444 subgroup, and *ZmDnaJ24* and *ZmDnaJ60* in another subgroup.

2.4. Gene Duplication Analysis of the ZmDnaJ Gene Family

To illustrate the replication patterns of *ZmDnaJ* gene family, we analyzed duplication events using MCScanX. We detected 18 pairs of duplication events involving 29 *ZmDnaJs* (Figure 3), indicating that these gene duplications contributed to the expansion of *the ZmDnaJ* gene family in maize. Further, we calculated nonsynonymous (Ka), synonymous substitutions (Ks), as well as the Ka/Ks ratios for these gene pairs to assess the evolutionary selection in the *ZmDnaJ* gene family. The results show that, except for three gene pairs (*ZmDnaJ14* and *ZmDnaJ75*; *ZmDnaJ14* and *ZmDnaJ88*; *ZmDnaJ48* and *ZmDnaJ77*), for which Ka/Ks values were not obtained, the Ka/Ks values of the remaining *ZmDnaJ* gene pairs are all less than 1, ranging from 0.091 to 0.615 (Table S2). This suggests that these genes have undergone purifying selection during evolution.

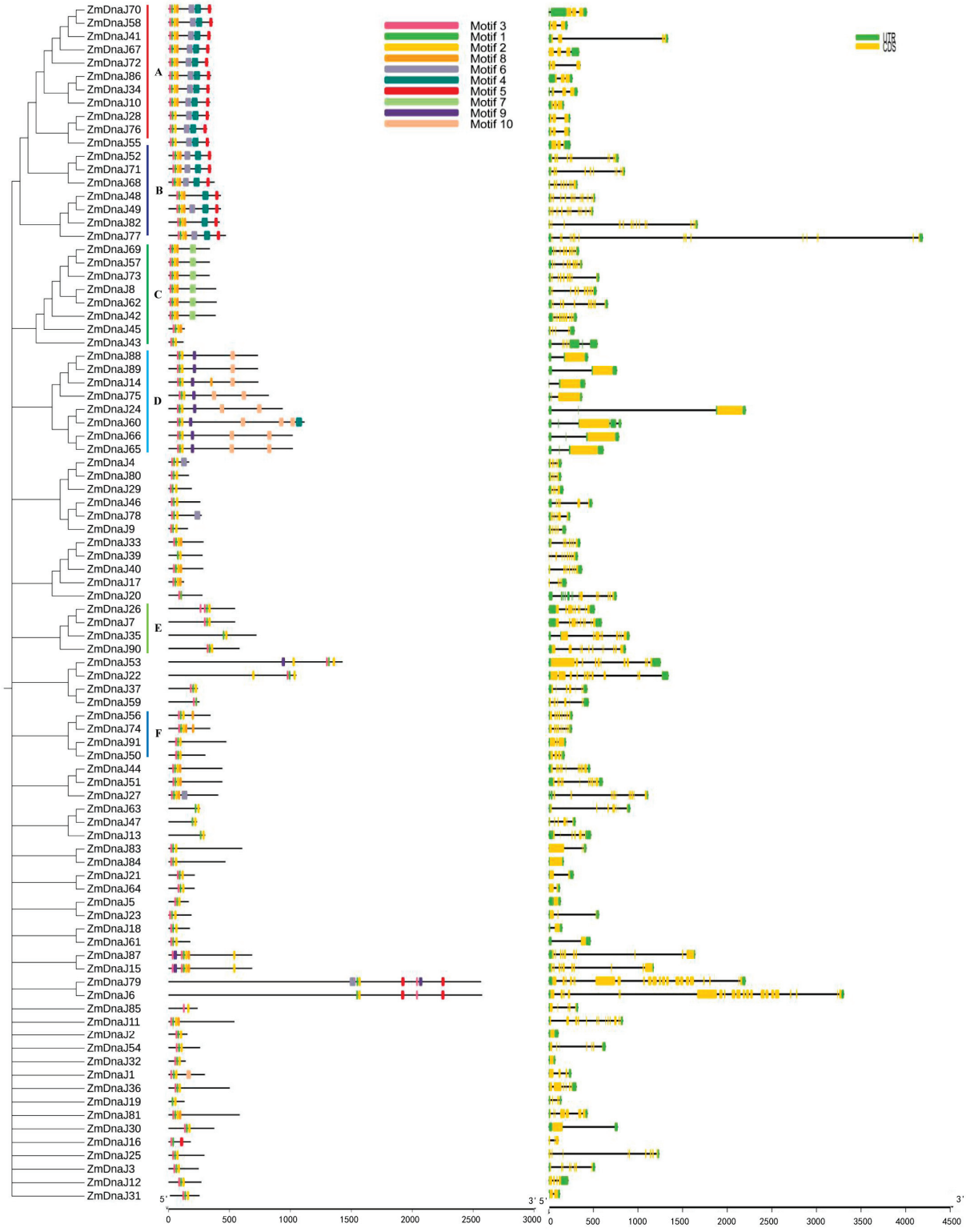


Figure 2. Phylogenetic relationship, conserved motif, and gene structure of *ZmDnaJ* members. Different colored boxes represent various motifs or exons, while black lines indicate non-conserved sequences and introns. A and B represent the DnaJ_C subfamily; C represents the DnaJ-X subfamily; D represents the DUF3444 subfamily; E represents the Jiv90 subfamily; F represents the Fer4_8 subfamily.

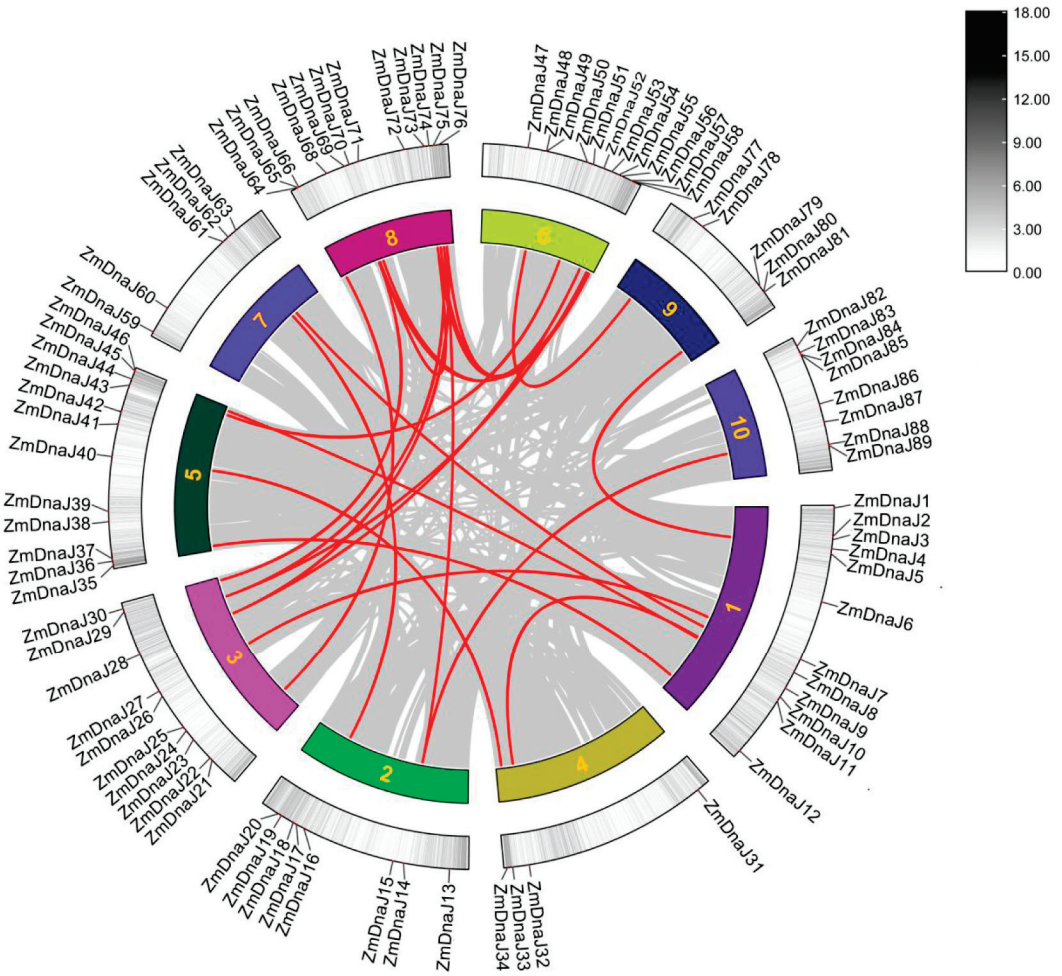


Figure 3. Gene duplication of *ZmDnaJ* genes on the 10 chromosomes of the maize genome. Red lines connect the duplicated gene pairs, while gray lines represent all synteny blocks within the maize genome. Detailed relationships of the duplicated genes are provided in Table S2.

2.5. Cis-Regulating Elements in Maize ZmDnaJ Promoters

The cis-regulatory elements of the proximal promoter play key roles in the initiation of gene expression. Therefore, we identified the conserved cis-elements present in the promoter of *ZmDnaJs* using PlantCARE [25]. A total of 66 conserved cis-elements were generated, as shown in Figure 4. These cis-elements could be classified into three categories: abiotic and biotic stress, plant growth and development, and phytohormone responsiveness. In the abiotic and biotic stress category, most elements are related to three general stress-responsive motifs: the stress-responsive element (STRE), MYB (CCAAT box), and MYC (CACATG box) binding sites, which account for 11%, 9.4% and 10% of the total identified cis-elements, respectively (Table S3). Other stress-responsive elements observed include the anaerobic-responsive element (ARE) motif, low-temperature-responsive (LTR) motifs, MYB binding site (MBS), TC-rich repeat, WRKY-box (W-box), dehydration-responsive element (DRE)-core, and the wound-responsive motif (WUN-motif). In the phytohormone-responsive category, 10 related cis-elements were identified, with the G-box occupying the highest percentage at 8.5%. In the phytohormone-responsive category, the ABRE element (~9.7%), involved in ABA responsiveness, was the most prominent, followed by two MeJA-responsiveness elements (the CGTCA motif (5.5%) and TGACG motif (5.5%)), as well as the as-1 motif involved in SA response (Figure 4, Table S3). These elements may play important roles in regulating the differential expression of *ZmDnaJs* during plant growth and development, especially under various biotic and abiotic stresses.

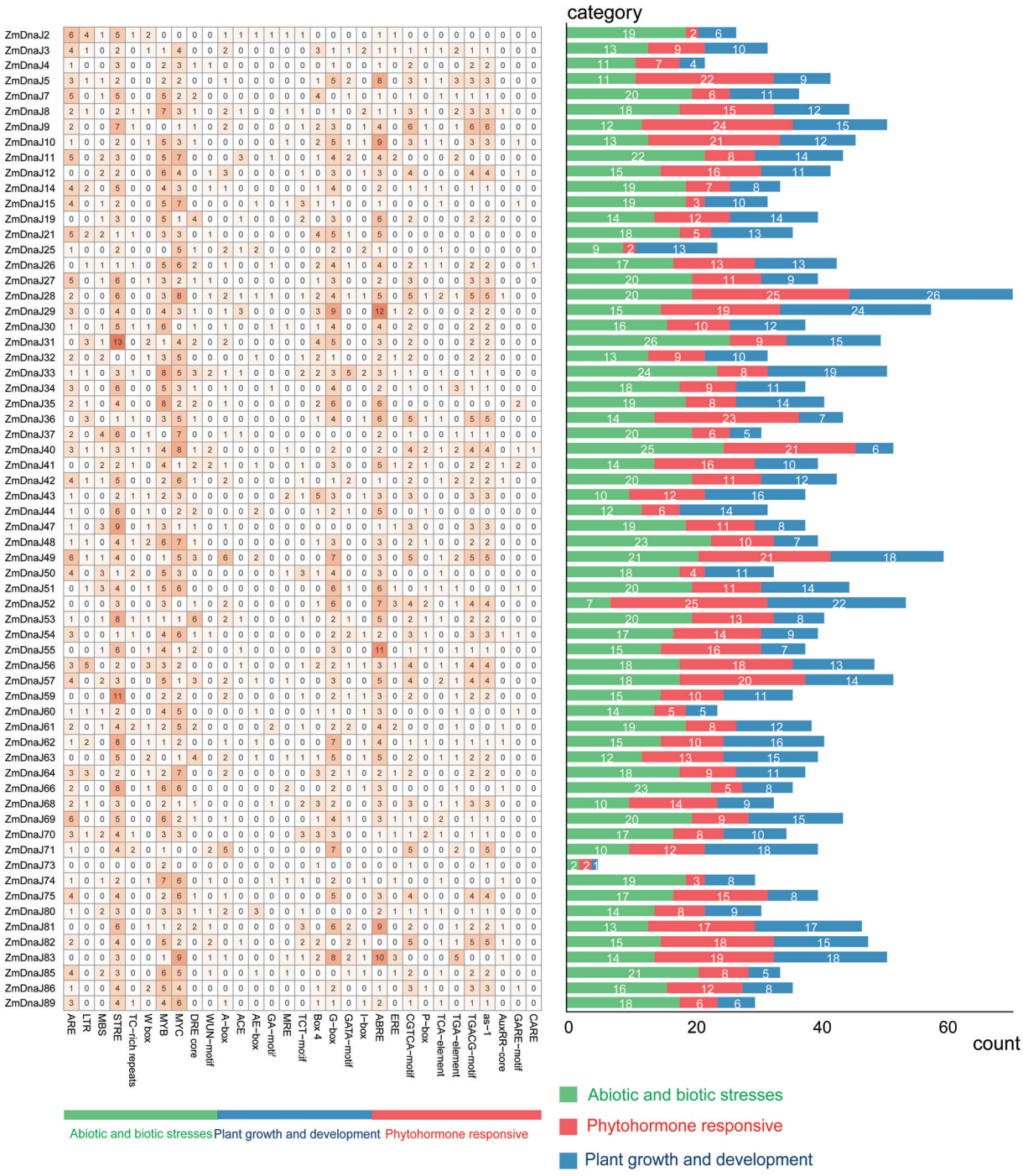


Figure 4. Cis-element number analysis in the *ZmDnaJ* gene family. The grid's varying color intensities and numbers represent the number of different promoter elements within the *ZmDnaJ* genes. The histogram, with its different colors, shows the total number of cis-acting elements for each category.

2.6. Expression Patterns of ZmDnaJ Gene Family Members in Different Tissues

To assess the temporal expression patterns of *ZmDnaJs*, we investigated the transcriptome data of *ZmDnaJs* from various maize tissues and development stages, as reported by Walley et al. [26]. The expression level of each gene was normalized using the RPKM method. As shown in Figure 5, 39 *ZmDnaJs* were expressed across all tested tissues, including the root, internode, leaf, mature pollen, silk, embryos, and endosperm. Among these, 26 genes, such as *ZmDnaJ79*, *20*, *37*, *8*, *47*, *3*, and *63*, showed relatively high expression levels. Some *ZmDnaJs*, including *ZmDnaJ38*, *51*, *90*, *81*, *40*, *56*, *11*, and *14*, were not detected

in mature pollen. The expression levels of *ZmDnaJ39*, *33*, *68*, *41*, *62*, *26*, *9*, *84*, and *88* were higher in the mature leaf than in the leaf zone (symmetrical), leaf zone 2 (stomatal), and leaf zone 2 (growth), indicating their involvement in leaf growth and development. In addition, pollen-specific expression was observed in *ZmDnaJ10*, while *ZmDnaJ32* and *ZmDnaJ78* were specifically expressed in the endosperms. *ZmDnaJ15* and *ZmDnaJ49* were barely detected in all tested tissues. The results indicated functional diversity among *ZmDnaJ* family members during maize growth and development.

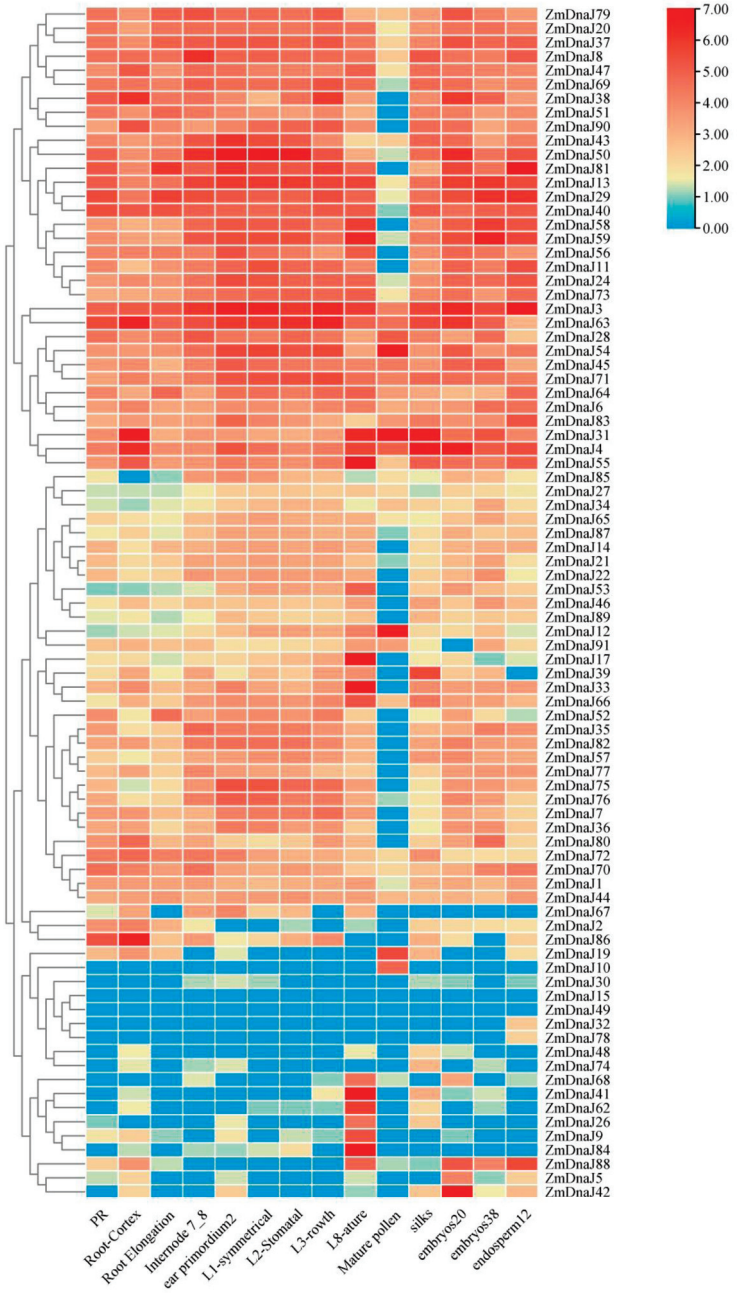


Figure 5. Expression pattern analysis of *ZmDnaJ* family genes in different tissues and developmental stages based on transcript data. The expression patterns of 91 genes were examined across 13 different tissues and developmental stages using public transcriptome data. The FPKM values (fragments per kilobase of transcript per million fragments) of all genes were transformed to the log2 scale. Red and blue colors indicate higher and lower relative transcript enrichment, respectively.

2.7. Expression Patterns of ZmDnaJ Gene Family Members under Abiotic Stress

To analyze the expression patterns of *ZmDnaJs* in response to abiotic stress, we investigated the gene expression by using TBtools, based on transcriptome data reported by Makarevitch et al. [27]. Relative expression values were calculated by comparing treated samples to control samples. The results showed that, compared with the control group, 12 genes (*ZmDnaJ39*, *62*, *4*, *90*, *56*, *91*, *88*, *5*, *70*, *80*, *58*, and *59*) were upregulated, while 15 genes (*30*, *67*, *52*, *43*, *86*, *50*, *63*, *48*, *38*, *42*, *19*, *9* and *74*) were downregulated under heat and salt stresses. The parallel expression profiles of *ZmDnaJs* under these conditions suggested an extensive overlap between heat and salt stress response pathways. In response to cold stress, eight genes, (*ZmDnaJ19*, *9*, *74*, *26*, *62*, *39*, *4*, and *90*) showed more than a two-fold upregulation, while five genes, (*ZmDnaJ88*, *5*, *2*, *33*, and *68*) exhibited more than a two-fold downregulation. Notably, *ZmDnaJ39* was upregulated in response to salt, heat, and cold stresses (Figure 6). These findings indicate that *ZmDnaJ* genes play complex and significant regulatory roles in response to various abiotic stresses in maize, with extensive overlap between the pathways responding to heat and salt stresses.

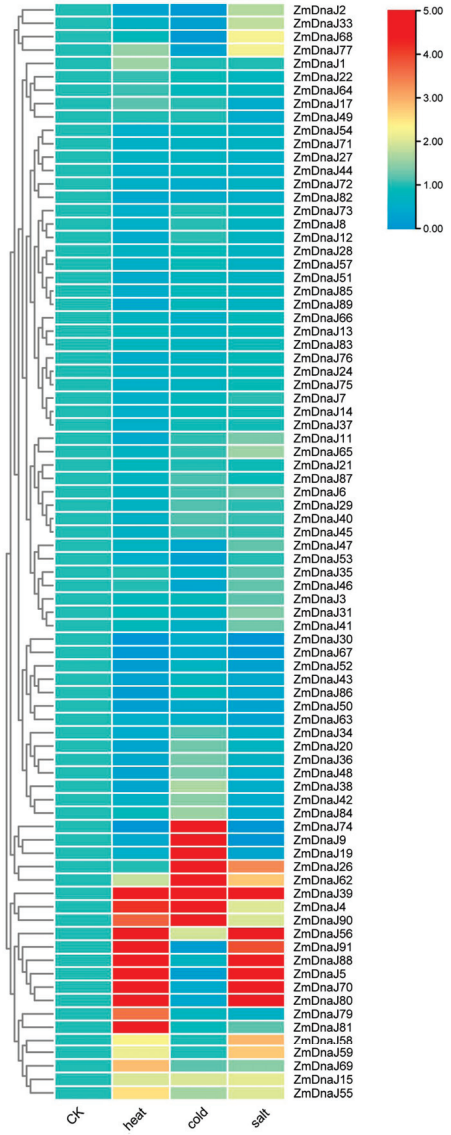


Figure 6. Gene expression profiles of *ZmDnaJ* genes in response to salt, heat, and cold stress treatments based on transcript data. The changes in expression of *ZmDnaJ* genes under salt, heat, and cold stress compared to normal conditions were calculated. Blue and red scales indicate low and high expression levels, respectively.

2.8. Expression Patterns of 17 ZmDnaJs of Five Inbred Maize Lines under Heat Stress

To further explore the potential roles of the 16 upregulated *ZmDnaJs* (*39*, *4*, *90*, *56*, *91*, *88*, *5*, *70*, *80*, *79*, *81*, *58*, *59*, *69*, *15*, and *55*) in heat stress tolerance in maize, we conducted qRT-PCR to assess their expressions before and after heat treatment at the seedling stage across five inbred lines. RNA quality (Figure S3, Table S4) and melting curves (Figure S4) ensured the reliability of the qRT-PCR results. The results showed that, compared to normal conditions, nearly all *ZmDnaJs* showed significantly increased expressions in B73 and B104 at 6 h after heat treatment, which was consistent with the transcriptome data. In the other inbred lines, only a few *ZmDnaJs* were upregulated at this time point. For example, *ZmDnaJ88*, *81*, and *90* were upregulated in Z58, *ZmDnaJ55*, *88*, *81*, and *90* in QB1314, and *ZmDnaJ58*, *79*, *88*, and *81* in MD108, with two- to five-fold increases (Figure 7A). Additionally, *ZmDnaJ70*, and *15* did not show detectable expression.

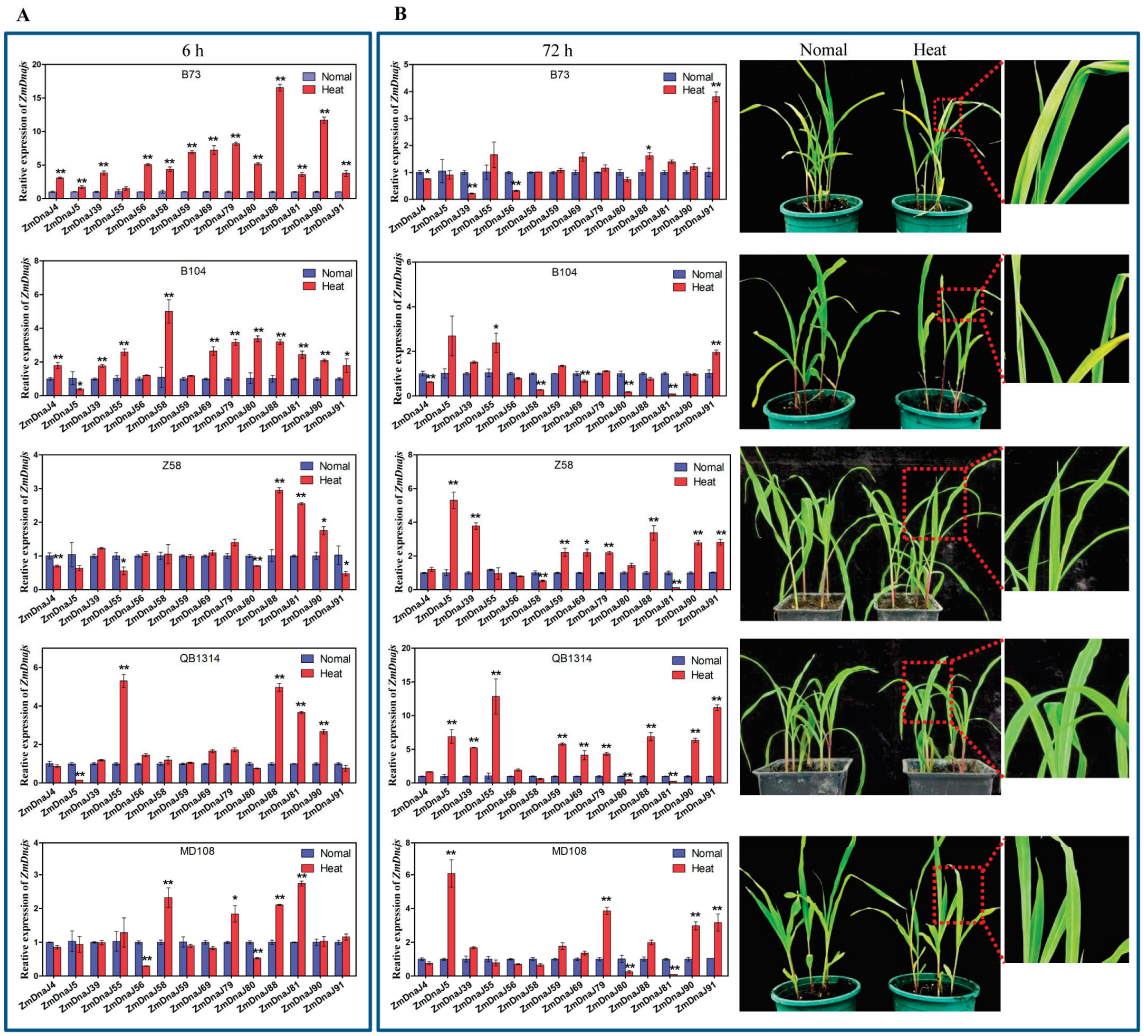


Figure 7. Relative expression levels of 14 selected *ZmDnaJ* genes and the phenotypes of five inbred maize lines under heat treatment. (**A**) The relative expression levels of 14 *ZmDnaJ* genes in the seedling leaves of five inbred lines were measured using qRT-PCR, with ZmUbi as the reference gene. Results are shown as mean ± standard deviation, with significance indicated by * $p < 0.05$ and ** $p < 0.01$ (Student's *t*-test). Leaf samples were collected 6 h after heat treatment. (**B**) Left panel: Relative expression levels of the 14 *ZmDnaJ* genes in seedling leaves at 72 h after heat treatment. Right panel: Phenotypes of the five inbred lines (B73, B104, Zheng 58, QB1314, and MD108) at 72 h after heat treatment.

After 72 h of continuous heat stress, the leaves of B73 and B104 were severely curled or wilted, whereas Z58, QB1314, and MD108 still grew normally (Figure 7B). Notably, qRT-PCR results showed that, except for *ZmDnaJ91*, the expression levels of most *ZmDnaJs* in B73 and B104 returned to normal levels after 72 h of heat treatment, with some even lower than untreated levels. However, in Z58, QB1314, and MD108, many *ZmDnaJs*, including *ZmDnaJ55*, *79*, *88*, *90*, and *91*, were upregulated after 72 h of heat treatment, with expression levels increasing by 2- to 12-fold compared to normal conditions (Figure 7B, Table 1), indicating these *ZmDnaJs* function against prolonged heat stress. The above results suggest that multiple *ZmDnaJ* genes may enhance maize heat tolerance through synergistic interactions.

Table 1. The expression profiles of 14 selected *ZmDnaJ* genes of five maize inbred lines under heat treatment.

Heat Stress Gene	Heat-Sensitive Inbred Lines				Heat-Tolerant Inbred Lines					
	B73		B104		Z58		QB1314		MD108	
	6 h	72 h	6 h	72 h	6 h	72 h	6 h	72 h	6 h	72 h
ZmDnaJ4	up	-	up	down	down	-	-	-	-	-
ZmDnaJ5	up	-	down	-	-	up	down	up	-	down
ZmDnaJ39	up	down	up	-	-	up	-	up	-	-
ZmDnaJ55	up	-	up	up	down		up	up	-	-
ZmDnaJ56	up	down	-	-	-	-	-		down	-
ZmDnaJ58	up	-	up	down	-	down	-		up	-
ZmDnaJ59	up	-	-	-	-	up	-	up	-	up
ZmDnaJ69	up	-	up	-	-	up	-	up	-	-
ZmDnaJ79	up	-	up	-	-	up	-	up	up	up
ZmDnaJ80	up	-	up	down	down	-	-	-	down	-
ZmDnaJ81	up	-	up	down	up	down	up	down	up	-
ZmDnaJ88	up	up	up	-	up	up	up	up	up	up
ZmDnaJ90	up	-	up	-	up	up	up	up	-	up
ZmDnaJ91	up	up	up	up	down	up	-	up	-	up

Note: red box represents up-regulated, green box represents down-regulated, - indicates no difference.

3. Discussion

DnaJ proteins, as types of heat shock proteins, are widely present in plant tissues and cells as stress response factors. They play important roles in plant responses to both biotic and abiotic stresses. For instance, the overexpression of a tobacco J-domain protein was shown to enhance drought tolerance in transgenic *Arabidopsis* [28]. The tomato chloroplast-targeted DnaJ protein was found to protect Rubisco activity under heat stress [29]. The identification and characterization of the *DnaJ* gene family have been reported in many plant species, such as *Arabidopsis*, rice, cucumber, pepper, *sorghum bicolor*, and *Catalpa bungei* [8,9,23,24,30,31]. In this study, we identified 91 *ZmDnaJ* genes in maize using bioinformatics methods and conducted a comprehensive analysis of their phylogeny, sequence structure, conserved domain, collinearity, and expression patterns during different tissues and under abiotic stresses. This research provides a theoretical foundation and valuable data for further functional studies.

Previous studies have indicated that ZmDnaJ proteins facilitate the refolding of proteins damaged by stress and regulate the activity of many regulatory proteins in various cellular compartments, including the mitochondrial matrix, the lumen of the endoplasmic reticulum, the cytosol, and the nucleus [8,9]. For example, it is reported that chloroplast-localized DnaJ proteins are well-characterized as key mediators in plant stress responses [23,24,32]. Bekh-Ochir et al. reported that the mitochondrial DnaJ/Hsp40 family protein BIL2 promotes plant growth and resistance against environmental stress

in brassinosteroid signaling [33]. Our subcellular localization predictions for ZmDnaJ proteins (Table S1) similarly indicated their probable role in maize's response to environmental stress.

The phylogenetic relationship of gene family members helps elucidate their evolutionary history, classification, functional prediction, and the adaptation and speciation processes in both organisms and genes. J-proteins have traditionally been classified into three types (type I, type II, and type III) based on the bacterial DnaJ classification [34]. The signature of all DnaJs is the J-domain, characterized by a highly conserved and functionally essential HPD motif. Type I and Type II proteins also contain a conserved C-terminal region, with Type I additionally characterized by zinc finger domains. Type III proteins can be further classified based on secondary structural elements, such as tetratricopeptide repeats and Fe-S clusters [8,9]. Further studies have identified "J-like proteins" that have significant sequence and structural similarities to the J-domain but lack the HPD motif [6]. In our study, all 91 identified ZmDnaJ proteins contained the HPD motif, with no J-like proteins detected (Figure 2 and Figure S2), likely due to the exclusion of sequences that did not have a fully conserved domain. We classified the 91 *ZmDnaJs* into three types: eight in Type I, twelve in Type II, and the remaining in Type III, consistent with the clustering observed in *Arabidopsis* and other plants [9,13]. Gene duplication is recognized as a major evolutionary force in the development of genetic systems and genomes [35]. In evolutionary biology, the ratio of Ka/Ks in a gene can provide insights into the type of selection acting on that gene. A Ka/Ks ratio of more than one indicates positive selection, a ratio of one implies neutral evolution, and a ratio of less than one suggests purifying selection [36]. Our results showed that 18 pairs of *ZmDnaJ* genes, located on different chromosomes, have undergone successive duplication events (Figure 3), indicating gene expansion during evolution. The Ka/Ks ratio for all duplicated genes was less than one (Figure 3), suggesting that these gene pairs may have undergone purifying selection, resulting in limited functional divergence following duplication.

The cis-elements within promoters play a crucial role in initiating gene expression. Our analysis of the cis-acting elements within promoters of *ZmDnaJ* genes revealed a diverse array of regulatory elements involved in plant growth, stress responses, and phytohormone signaling (Figure 4). Elements such as STRE, MYB, MYC, and ABRE in the promoters of *ZmDnaJ* genes have been shown to be involved in complex regulatory networks that govern stress tolerance [37–39]. Additionally, RNA-seq data [26,27] analysis revealed distinct expression patterns of *ZmDnaJ* genes across different tissues, developmental stages, and in response to three stresses (Figures 5 and 6). This is consistent with the established roles of cis-elements in modulating gene expression in response to various internal and external cues. The distinct tissue-specific and stress-responsive expression patterns observed in RNA-seq data suggest that *ZmDnaJ* genes are finely regulated to respond to different physiological conditions, indicating their functional diversification and critical roles in maize adaptability.

High temperature has emerged as one of the most critical abiotic stresses impacting crop plants. Heat shock proteins (Hsps), including Hsp100, Hsp90, Hsp70, Hsp60, Hsp40, and Hsp20, are key components of the heat shock regulatory network that help plants cope with this stress [40]. Our study revealed the differences in expression patterns of *ZmDnaJ* genes and their response to heat stress among five inbred lines. The heat-tolerant inbred lines (QB1314, MD108, and Zheng58) show a greater number of upregulated *ZmDnaJ* genes and higher expression levels compared to the heat-sensitive lines (B73 and B104) after 72 h of heat stress (Figure 7, Table 1). These indicated that they may function synergistically to provide sustained protection against prolonged heat stress. Apart from heat stress, *Hsp* expression was strongly induced by cold, salt, and drought stress [41]. Moreover, many *Hsps* had highly similar or overlapped response and regulation patterns under different stresses [41–43]. Here, we found that many *ZmDnaJs* exhibited high similarities in expression patterns in response to heat and salt stresses (Figure 6). These suggested considerable cross-talk among the regulatory networks of various stresses.

In conclusion, the differential expression of *ZmDnaJ* genes and their responses to various stresses indicate their critical roles in maize adaptation. The above analysis offers a theoretical basis for future functional validation of these genes.

4. Materials and Methods

4.1. Genome-Wide Identification of ZmDnaJ Gene Family in Maize

The genome sequences of maize were downloaded from the MaizeGDB database (https://www.maizegdb.org/ (accessed on 23 October 2023)). Subsequently, the hidden Markov model (HMM) profile of the J-domain (PF00226) was downloaded from the Pfam database (http://pfam.xfam.org/ (accessed on 23 October 2023)) to search the putative protein sequence containing DnaJ domain in maize (e-value < 10^{-10}). To validate the accuracy of these DnaJ proteins, the redundant protein sequences were removed manually, and then the remaining protein sequences were confirmed as the final ZmDnaJ protein sequences based on the Conserved Domain Database (CDD) of NCBI (https://www.ncbi.nlm.nih.gov/cdd/ (accessed on 23 October 2023)). Molecular weight, theoretical isoelectric point (pI), Instability Index, and Grand Average of Hydropathicity of the *ZmDnaJ* gene family members were analyzed with EXPASY PROTOPARAM (https://web.expasy.org/protparam/ (accessed on 2 November 2023)). The WoLF PSORT (https://wolfpsort.hgc.jp/ (accessed on 8 November 2023)) was used to predict protein subcellular localization.

4.2. Phylogenetic Tree and Conserved Domain Analysis of ZmDnaJ Gene Family

To explore the evolutionary relationship of the *ZmDnaJ* gene family between maize and *Arabidopsis*, the DnaJ protein sequences from *Arabidopsis* and 89 *ZmDnaJs* were used for the phylogenetic tree construction with MEGA-X (v1.2.6) software [44]. The phylogenetic tree was constructed using the neighbor-joining phylogenetic tree (NJ) and the Jones–Taylor–Thorton (JTT) model with 1000 bootstraps. The phylogenetic tree was modified using the online software iTOL (https://itol.embl.de/ (accessed on 8 November 2023)) [45]. To understand the relationship between evolution and conserved domains among ZmDnaJ proteins, the conserved domains of ZmDnaJ proteins were obtained using the NCBI-CDD website. The above files were optimized using TBtools (v2.096) [46].

4.3. Analysis of Protein Motif, Gene Structure, and Gene Duplication of the ZmDnaJ Gene Family

The gff3 file (Zea mays. Zm-B73-REFERENCE-NAM-5.0.51.gff3), downloaded from NCBI, was used to analyze the gene structure of *ZmDnaJ* genes. The motifs of ZmDnaJ proteins were analyzed via the online MEME tool (http://meme-suite.org/tools/meme (accessed on 15 November 2023)) based on their protein sequences (the number of different motifs, 10; minimum width of motifs, 6; maximum width of motifs, 50). To identify the gene duplication pattern, ZmDnaJ genes in maize were analyzed using the one-step MCScanX tool from TBtools with default parameters, including an E-value cut-off < 1×10^{-10} and the number of BLAST hits at 5.

4.4. Cis-Acting Element Analysis of ZmDnaJ Genes

The upstream regulatory regions (~2000 bp) of *ZmDnaJ* gene sequences were retrieved from the MaizeGDB database and subsequently used to search for cis-regulating elements in the PlantCARE website https://bioinformatics.psb.ugent.be/webtools/plantcare/html/ (accessed on 3 December 2023) [25].

4.5. Expression of ZmDnaJ Genes Based on RNA-Seq in Maize cv. B73

In this paper, RNA-seq data reported by Walley et al. [26] were used to investigate the expression patterns of putative *ZmDnaJ* genes in maize. Different tissues were selected: primary root 5 days, root cortex 5 days, root elongation zone 5 days, 7–8 internode, ear primordium 2–4 mm, leaf zone 1 (symmetrical), leaf zone 2 (Stomatal), leaf zone 3 (growth), mature leaf 8, mature pollen, silk, embryo 20 days after pollination (DAP), embryo 38 DAP, endosperm crown 12 DAP. RPKM values (reads per kilo bases per million mapped reads)

of *ZmDnaJ* genes were log2-transformed. Additionally, we also analyzed the change of expression of *ZmDnaJ* genes under salt, heat, and cold stress based on RNA-seq data reported by Makarevitch et al. [27]. Heat maps of *ZmDnaJ* genes in different tissues or under abiotic stresses were performed using the software TBtools (v2.096) [46].

4.6. Plant Material and Stress Treatment

The maize inbred lines, including B73, B104, QB1314 (obtained from Guizhou Academy of Agricultural Sciences, Guiyang, China), MD108, and Zheng58, were grown in a chamber (JIUPO, Fuzhou, China; Catalog: BPC500H) under normal conditions (32 °C/22 °C, day/night) with a photoperiod of 14 h light and 10 h dark. The light intensities were ramped up to 300 μmol/m^2/s. Half of the plants at the two-leaf stage (V2, 10 days after seed germination) were cultivated under consistent conditions to ensure their growth and development, while others were moved to a higher temperature circumstance (42 °C/32 °C, day/night) for the heat stress treatment. The photoperiod and light intensities under the higher temperature conditions were set as the control conditions. In order to avoid drought stress, the trays were adequately watered during the treatment. Samples were collected from the plants under the two conditions after 6 or 72 h of treatment for the mRNA-seq. Leaves under each condition were collected and stored at −80 °C after the evaporation of liquid nitrogen.

4.7. RNA Extraction, and Quantitative Real-Time PCR Analysis (qRT-PCR)

Total RNA was extracted using RNA-easy Isolation Reagent (Vazyme, Nanjing, China) and reverse-transcribed using HiScript III RT SuperMix kit qPCR (+gDNA wiper) (Vazyme, Nanjing, China), the operational procedure followed the manufacturer's procedure. qRT-PCR was performed on ABI Prism 7500 Sequence Detection System (Applied Biosystems) using 2× Taq Master Mix (Vazyme, Nanjing, China) in 10 μL qRT-PCR reactions. The UBI gene was used as an internal control [47]. The relative expression values of genes were calculated using the $2^{-\Delta\Delta Ct}$ method [48]. Three biological repeats were performed for each sample. The primers for qRT-PCR are listed in Table S5.

5. Conclusions

This study identified 91 *ZmDnaJ* genes in the maize genome and analyzed their physicochemical properties, phylogenetic relationships, conserved motifs, gene structures, and expression patterns. The *ZmDnaJ* genes showed significant diversity in their expression across different tissues, developmental stages, and in response to various abiotic stresses, including heat, salt, and cold. Our findings highlight the potential role of *ZmDnaJ* genes in enhancing stress tolerance, with certain genes, such as *ZmDnaJ39*, consistently upregulated under multiple stresses. Additionally, heat-tolerant maize inbred lines exhibited higher expression levels of multiple *ZmDnaJ* genes compared to heat-sensitive lines, suggesting a synergistic function in stress response. These insights provide a valuable foundation for further exploration of *ZmDnaJ* genes in improving maize resilience to environmental stresses.

Supplementary Materials: The following supporting information can be downloaded at https://www.mdpi.com/article/10.3390/plants13172488/s1, Figure S1 Phylogenetic relationship and conserved domain of ZmDnaJ members. Different colored boxes represent different subfamilies, while black lines indicate non-conserved sequences. Figure S2 Sequence logos of J-domains of ZmDnaJ proteins. The J-domains include motifs 1, 2, 3, and 8. Asterisks indicate the conserved histidine/proline/aspartic (HPD) residues in the J-domains among ZmDnaJ proteins. Figure S3 The electropherograms of RNA bands in agarose gels from the maize inbred lines. Figure S4 Melting curves of transcripts targeted for qRT-PCR. Table S1. The list of *ZmDnaJ* members identified in maize. Table S2. Inference of duplication time in paralogous pairs. Table S3. Statistics of the Proportions of four cis-Elements distributed in the promoters of ZmDnaJ genes. Table S4. The information regarding quality of total RNA samples. Table S5. Primers used in this study.

Author Contributions: G.L. and Z.C. contributed the plant materials, conducted the experiments, analyzed the data, and wrote the manuscript; X.G., D.T. and M.L. contributed the analysis tools and analyzed the data; C.L. performed the experiments; C.H. and J.Y. designed the experiments and wrote the manuscript. All authors have read and agreed to the published version of the manuscript.

Funding: This research was funded by Fujian Province Public Welfare Scientific Research Program (2023R1025001, 2021R1027001, and 2022R1027002).

Data Availability Statement: Data are contained within the article and Supplementary Materials.

Conflicts of Interest: The authors declare no conflict of interest.

References

1. Godara, H.; Ramakrishna, W. Endophytes as nature's gift to plants to combat abiotic stresses. *Lett. Appl. Microbiol.* **2023**, *76*, ovac067. [CrossRef] [PubMed]
2. Zhao, C.; Liu, B.; Piao, S.L.; Wang, X.H.; Lobell, D.B.; Huang, Y.; Huang, M.T.; Yao, Y.T.; Bassu, S.; Ciais, P.; et al. Temperature increase reduces global yields of major crops in four independent estimates. *Proc. Natl. Acad. Sci. USA* **2017**, *114*, 9326–9331. [CrossRef] [PubMed]
3. Haq, S.U.; Khan, A.; Ali, M.; Khattak, A.M.; Gai, W.-X.; Zhang, H.-X.; Wei, A.-M.; Gong, Z.-H. Heat shock proteins: Dynamic biomolecules to counter plant biotic and abiotic stresses. *Int. J. Mol. Sci.* **2019**, *20*, 5321. [CrossRef]
4. Jin, J.; Zhao, M.T.; Wang, Y.; Zhou, Z.S.; Wan, F.H.; Guo, J.Y. Induced thermotolerance and expression of three key *Hsp* genes (*Hsp70*, *Hsp21*, and *sHsp21*) and their roles in the high temperature tolerance of *Agasicles hygrophila*. *Front. Physiol.* **2020**, *10*, 1593. [CrossRef] [PubMed]
5. Jacob, P.; Hirt, H.; Bendahmane, A. The heat-shock protein/chaperone network and multiple stress resistance. *Plant Biotechnol. J.* **2017**, *15*, 405–414. [CrossRef]
6. Feder, M.E.; Hofmann, G.E. Heat-shock proteins, molecular chaperones, and the stress response: Evolutionary and ecological physiology. *Annu. Rev. Physiol.* **1999**, *61*, 243–282. [CrossRef]
7. Walsh, P.; Bursac, D.; Law, Y.C.; Cyr, D.; Lithgow, T. The J-protein family: Modulating protein assembly, disassembly and translocation. *EMBO Rep.* **2004**, *5*, 567–571. [CrossRef]
8. Rajan, V.B.; D'Silva, P. *Arabidopsis thaliana* J-class heat shock proteins: Cellular stress sensors. *Funct. Integr. Genom.* **2009**, *9*, 433–446. [CrossRef]
9. Sarkar, N.K.; Thapar, U.; Kundnani, P.; Panwar, P.; Grover, A. Functional relevance of J-protein family of rice (*Oryza sativa*). *Cell Stress Chaperones* **2013**, *18*, 321–331. [CrossRef]
10. Craig, E.A.; Huang, P.; Aron, R.; Andrew, A. The diverse roles of J-proteins, the obligate Hsp70 co-chaperone. *Rev. Physiol. Biochem. Pharmacol.* **2006**, *156*, 1–21.
11. Verma, A.K.; Diwan, D.; Raut, S.; Dobriyal, N.; Brown, R.E.; Gowda, V.; Hines, J.K.; Sahi, C. Evolutionary conservation and emerging functional diversity of the cytosolic Hsp70:J protein chaperone network of *Arabidopsis thaliana*. *G3* **2017**, *7*, 1941–1954. [CrossRef]
12. Zhang, J.; Bai, Z.C.; Ouyang, M.; Xu, X.M.; Xiong, H.B.; Wang, Q.; Grimm, B.; Rochaix, J.D.; Zhang, L.X. The DnaJ proteins DJA6 and DJA5 are essential for chloroplast iron-sulfur cluster biogenesis. *EMBO J.* **2021**, *40*, e106742. [CrossRef] [PubMed]
13. Zhao, L.; Jia, T.; Jiao, Q.S.; Hu, X.Y. Research Progress in J-Proteins in the Chloroplast. *Genes* **2022**, *13*, 1469. [CrossRef] [PubMed]
14. Chen, K.M.; Holmström, M.; Raksajit, W.; Suorsa, M.; Piippo, M.; Aro, E.M. Small chloroplast-targeted DnaJ proteins are involved in optimization of photosynthetic reactions in *Arabidopsis thaliana*. *BMC Plant Biol.* **2010**, *10*, 43. [CrossRef] [PubMed]
15. Yang, Y.Q.; Qin, Y.X.; Xie, C.G.; Zhao, F.Y.; Zhao, J.F.; Liu, D.F.; Chen, S.Y.; Fuglsang, A.T.; Palmgren, M.G.; Schumaker, K.S.; et al. The *Arabidopsis* chaperone J3 regulates the plasma membrane H^+-ATPase through interaction with the PKS5 kinase. *Plant Cell* **2010**, *22*, 1313–1332. [CrossRef]
16. Wang, G.D.; Cai, G.H.; Xu, N.; Zhang, L.T.; Sun, X.L.; Guan, J.; Meng, Q.W. Novel DnaJ protein facilitates thermotolerance of transgenic tomatoes. *Int. J. Mol. Sci.* **2019**, *20*, 367. [CrossRef]
17. Kong, F.Y.; Deng, Y.S.; Wang, G.D.; Wang, J.R.; Liang, X.Q.; Meng, Q.W. LeCDJ1, a chloroplast DnaJ protein, facilitates heat tolerance in transgenic tomatoes. *J. Integr. Plant Biol.* **2014**, *56*, 63–74. [CrossRef]
18. Kong, F.Y.; Deng, Y.S.; Zhou, B.; Wang, G.D.; Wang, Y.; Meng, Q.W. A chloroplast-targeted DnaJ protein contributes to maintenance of photosystem II under chilling stress. *J. Exp. Bot.* **2014**, *65*, 143–158. [CrossRef]
19. Wang, G.D.; Cai, G.H.; Kong, F.Y.; Deng, Y.S.; Ma, N.N.; Meng, Q.W. Overexpression of tomato chloroplast-targeted DnaJ protein enhances tolerance to drought stress and resistance to *Pseudomonas solanacearum* in transgenic tobacco. *Plant Physiol. Biochem.* **2014**, *82*, 95–104. [CrossRef]
20. Yamamoto, M.; Uji, S.; Sugiyama, T.; Sakamoto, T.; Kimura, S.; Endo, T.; Nishikawa, S.I. ERdj3B-Mediated Quality Control Maintains Anther Development at High Temperatures. *Plant Physiol.* **2020**, *182*, 1979–1990. [CrossRef]
21. Leng, Y.J.; Yao, Y.S.; Yang, K.Z.; Wu, P.X.; Xia, Y.X.; Zuo, C.R.; Luo, J.H.; Wang, P.; Liu, Y.Y.; Zhang, X.Q.; et al. *Arabidopsis* ERdj3B coordinates with ERECTA-family receptor kinases to regulate ovule development and the heat stress response. *Plant Cell* **2022**, *34*, 3665–3684. [CrossRef] [PubMed]

22. Yang, K.Z.; Xia, C.; Liu, X.L.; Dou, X.Y.; Wang, W.; Chen, L.Q.; Zhang, X.Q.; Xie, L.F.; He, L.; Ma, X.; et al. A mutation in Thermosensitive Male Sterile 1, encoding a heat shock protein with DnaJ and PDI domains, leads to thermosensitive gametophytic male sterility in *Arabidopsis*. *Plant J.* **2009**, *57*, 870–882. [CrossRef]
23. Fan, F.F.; Yang, X.; Cheng, Y.; Kang, Y.Y.; Chai, X.R. The *DnaJ* Gene Family in Pepper (*Capsicum annuum* L.): Comprehensive Identification, Characterization and Expression Profiles. *Front. Plant Sci.* **2017**, *8*, 689. [CrossRef]
24. Song, M.F.; Wang, X.; Zhang, K.J.; Chen, F.J.; Lou, Q.F. Identification of DnaJ gene family in cucumber and its expression response to high-temperature stress. *J. Nanjing Agric. Univ.* **2021**, *44*, 267–277.
25. Lescot, M.; Déhais, P.; Thijs, G.; Marchal, K.; Moreau, Y.; Van de Peer, Y.; Rouzé, P.; Rombauts, S. PlantCARE, a database of plant cis-acting regulatory elements and a portal to tools for in silico analysis of promoter sequences. *Nucleic Acids Res.* **2002**, *30*, 325–327. [CrossRef]
26. Walley, J.W.; Sartor, R.C.; Shen, Z.; Schmitz, R.J.; Wu, K.J.; Urich, M.A.; Nery, J.R.; Smith, L.G.; Schnable, J.C.; Ecker, J.R.; et al. Integration of omic networks in a developmental atlas of maize. *Science* **2016**, *353*, 814–818. [CrossRef] [PubMed]
27. Makarevitch, I.; Waters, A.J.; West, P.T.; Stitzer, M.; Hirsch, C.N.; Ross-Ibarra, J.; Springer, N.M. Transposable elements contribute to activation of maize genes in response to abiotic stress. *PLoS Genet.* **2015**, *11*, e1004915.
28. Xia, Z.L.; Zhang, X.Q.; Li, J.Q.; Su, X.H.; Liu, J.J. Overexpression of a tobacco J-domain protein enhances drought tolerance in transgenic *Arabidopsis*. *Plant Physiol. Biochem.* **2014**, *83*, 100–106. [CrossRef]
29. Wang, G.D.; Kong, F.Y.; Zhang, S.; Meng, X.; Wang, Y.; Meng, Q.W. A tomato chloroplast-targeted DnaJ protein protects Rubisco activity under heat stress. *J. Exp. Bot.* **2015**, *66*, 3027–3040. [CrossRef]
30. Yang, Y.Y.; Zhao, L.J.; Wang, J.H.; Lu, N.; Ma, W.J.; Ma, J.; Zhang, Y.; Fu, P.Y.; Yao, C.C.; Hu, J.W.; et al. Genome-wide identification of *DnaJ* gene family in *Catalpa bungei* and functional analysis of *CbuDnaJ49* in leaf color formation. *Front. Plant Sci.* **2023**, *14*, 1116063.
31. Nagaraju, M.; Kumar, A.; Rajasheker, G.; ManoharRao, D.; KaviKishor, P.B. DnaJs, the critical drivers of Hsp70s: Genome-wide screening, characterization and expression of *DnaJ* family genes in *Sorghum bicolor*. *Mol. Biol. Rep.* **2020**, *47*, 7379–7390. [CrossRef] [PubMed]
32. Cai, G.H.; Xu, Y.J.; Zhang, S.X.; Chen, T.T.; Liu, G.; Li, Z.Y.; Zhu, Y.S.; Wang, G.D. A tomato chloroplast-targeted DnaJ protein, SlDnaJ20 maintains the stability of photosystem I/II under chilling stress. *Plant Signal. Behav.* **2022**, *17*, 2139116. [CrossRef] [PubMed]
33. Bekh-Ochir, D.; Shimada, S.; Yamagami, A.; Kanda, S.; Ogawa, K.; Nakazawa, M.; Matsui, M.; Sakuta, M.; Osada, H.; Asami, T.; et al. A novel mitochondrial DnaJ/Hsp40 family protein BIL2 promotes plant growth and resistance against environmental stress in brassinosteroid signaling. *Planta* **2013**, *237*, 1509–1525. [CrossRef]
34. Cheetham, M.E.; Caplan, A.J. Structure, function and evolution of DnaJ: Conservation and adaptation of chaperone function. *Cell Stress Chaperones* **1998**, *3*, 28–36. [CrossRef] [PubMed]
35. Magadum, S.; Banerjee, U.; Murugan, P.; Gangapur, D.; Ravikesavan, R. Gene duplication as a major force in evolution. *J. Genet.* **2013**, *92*, 155–161. [CrossRef]
36. Navarro, A.; Barton, N.H. Chromosomal speciation and molecular divergence-accelerated evolution in rearranged chromosomes. *Science* **2003**, *300*, 321–324. [CrossRef]
37. Varela, J.C.; Praekelt, U.M.; Meacock, P.A.; Planta, R.J.; Mager, W.H. The *Saccharomyces cerevisiae HSP12* gene is activated by the high-osmolarity glycerol pathway and negatively regulated by protein kinase A. *Mol. Cell. Biol.* **1995**, *15*, 6232–6245. [CrossRef]
38. Narusaka, Y.; Nakashima, K.; Shinwari, Z.K.; Sakuma, Y.; Furihata, T.; Abe, H.; Narusaka, M.; Shinozaki, K.; Yamaguchi-Shinozaki, K. Interaction between two cis-acting elements, ABRE and DRE, in ABA-dependent expression of *Arabidopsis rd29A* gene in response to dehydration and high-salinity stresses. *Plant J.* **2003**, *34*, 137–148. [CrossRef]
39. Zhang, L.; Song, Z.Q.; Li, F.F.; Li, X.X.; Ji, H.K.; Yang, S.S. The specific MYB binding sites bound by TaMYB in the GAPCp2/3 promoters are involved in the drought stress response in wheat. *BMC Plant Biol.* **2019**, *19*, 366. [CrossRef]
40. Huang, B.R.; Xu, C.P. Identification and characterization of proteins associated with plant tolerance to heat stress. *J. Integr. Plant Biol.* **2008**, *50*, 1230–1237. [CrossRef]
41. Hu, W.H.; Hu, G.C.; Han, B. Genome-wide survey and expression profiling of heat shock proteins and heat shock factors revealed overlapped and stress specific response under abiotic stresses in rice. *Plant Sci.* **2009**, *176*, 583–590. [CrossRef]
42. Fragkostefanakis, S.; Röth, S.; Schleiff, E.; Scharf, K.D. Prospects of engineering thermotolerance in crops through modulation of heat stress transcription factor and heat shock protein networks. *Plant Cell Environ.* **2015**, *38*, 1881–1895. [CrossRef] [PubMed]
43. Swindell, W.R.; Huebner, M.; Weber, A.P. Transcriptional profiling of *Arabidopsis* heat shock proteins and transcription factors reveals extensive overlap between heat and non-heat stress response pathways. *BMC Genom.* **2007**, *8*, 125. [CrossRef] [PubMed]
44. Kumar, S.; Stecher, G.; Li, M.; Knyaz, C.; Tamura, K. MEGA X: Molecular evolutionary genetics analysis across computing platforms. *Mol. Biol. Evol.* **2018**, *35*, 1547–1549. [CrossRef] [PubMed]
45. Letunic, I.; Bork, P. Interactive Tree Of Life (ITOL) v5: An online tool for phylogenetic tree display and annotation. *Nucleic Acids Res.* **2021**, *49*, W293–W296. [CrossRef]
46. Chen, C.J.; Chen, H.; Zhang, Y.; Thomas, H.R.; Frank, M.H.; He, Y.H.; Rui, X. TBtools: An integrative toolkit developed for interactive analyses of big biological data. *Mol. Plant* **2020**, *13*, 1194–1202. [CrossRef]

47. Zeng, R.; Li, Z.Y.; Shi, Y.T.; Fu, D.Y.; Yin, P.; Cheng, J.K.; Jiang, C.F.; Yang, S.H. Natural variation in a type—A response regulator confers maize chilling tolerance. *Nat Commun.* **2021**, *12*, 4713. [CrossRef]
48. Livak, K.J.; Schmittgen, T.D. Analysis of relative gene expression data using real-time quantitative PCR and the 2(-Delta DeltaC(T)) method. *Methods* **2001**, *25*, 402–408. [CrossRef]

Disclaimer/Publisher's Note: The statements, opinions and data contained in all publications are solely those of the individual author(s) and contributor(s) and not of MDPI and/or the editor(s). MDPI and/or the editor(s) disclaim responsibility for any injury to people or property resulting from any ideas, methods, instructions or products referred to in the content.

plants

MDPI

Article

Comparative Analysis of Water Stress Regimes in Avocado Plants during the Early Development Stage

Tatiana Rondon [1,*], Manuel Guzmán-Hernández [1], Maria C. Torres-Madronero [2,3], Maria Casamitjana [1,4], Lucas Cano [1], July Galeano [5] and Manuel Goez [2]

[1] Corporación Colombiana de Investigación Agropecuaria (AGROSAVIA), Centro de Investigación La Selva, Rionegro 054040, Colombia; maguzman@agrosavia.co (M.G.-H.); casmi242@hotmail.com (M.C.); lcanog@agrosavia.co (L.C.)
[2] MRP Laboratory, Research Group on Smart Machine and Pattem Recognition, Department of Electronic and Telecommunications Engineering, Instituto Tecnológico Metropolitano (ITM), Medellín 050034, Colombia; mctorresm@unal.edu.co (M.C.T.-M.); manuelgoez@itm.edu.co (M.G.)
[3] Department of Computer and Decision Sciences, Faculty of Mines, Universidad Nacional de Colombia, Medellín 050034, Colombia
[4] Laboratori d'Anàlisi i Gestió del Paisatge, Universitat de Girona, 17071 Girona, Spain
[5] Research Group Materiales Avanzados y Energía MatyEr, Instituto Tecnológico Metropolitano (ITM), Medellín 050013, Colombia; julygaleano@itm.edu.co
* Correspondence: trondon@agrosavia.co

Abstract: The avocado cv. Hass requires a suitable rootstock for optimal development under water stress. This study evaluated the performance of two avocado rootstocks (ANRR88 and ANGI52) grafted onto cv. Hass under four water stress conditions, 50% and 25% deficit, and 50% and 25% excess during the nursery stage. Plant height, leaf area (LA), dry matter (DM), and Carbon (OC) content in the roots, stems, and leaves were measured. Root traits were evaluated using digital imaging, and three vegetation indices (NDVI, CI_{RE}, and MTCI) were used to quantify stress. The results showed that genotype significantly influenced the response to water stress. ANRR88 exhibited adaptation to moderate to high water deficits. ANGI52 adapted better to both water deficit and excess, and showed greater root exploration. LA and DM reductions of up to 60% were observed in ANRR88, suggesting a higher sensitivity to extreme changes in water availability. More than 90% of the total OC accumulation was observed in the stem and roots. The NDVI and the MTCI quantified the presence and levels of stress applied, and the 720 nm band provided high precision and speed for detecting stress. These insights are crucial for selecting rootstocks that ensure optimal performance under varying water availability, enhancing productivity and sustainability.

Keywords: avocado seedling; phenotyping; spectral images; vegetation index; water stress

1. Introduction

Over the last 20 years, the international avocado (*Persea americana* Mill.) trade has grown from USD 331 million to USD 7.59 billion, and the United States and some European countries, such as the Netherlands, Spain, and France, lead the importation markets [1]. Avocados have a huge market demand due to their highly nutrition-dense compounds and benefits to human health [2–4]. The avocado cv. Hass is the most popular variety of avocado worldwide, and its consumption has tripled since the early 2000s [3,5]. In the United States, per capita consumption has increased more than 300% since 2000, from 1.02 to 4.01 kg person^{-1} yr^{-1} [6,7].

Colombia is included in the top five avocado cv. Hass producers and exporters worldwide, with a high expansion rate of fresh fruit suppliers to Europe and the United States. In Colombia, the Hass variety represents 26% of the planted area, equivalent to 20.000 ha, approx. [8]. Moreover, it is cultivated in different ecosystems and at different

technological levels [9]; mainly in the Andean's mid-altitude ranges from 1100 to 2250 m above sea level. Therefore, it is essential to study the behavior of this plant species under different stress conditions.

Climate variables are shifting as a result of global warming, making Colombia particularly vulnerable to its effects. A variable precipitation pattern, temperature, and carbon dioxide (CO_2) concentration increases, and air humidity variation constantly change and affect plant water use [10]. In addition, population growth, land use change, and increasing demand in non-agricultural sectors impact the availability and quality of water [11,12].

Freshwater resources are increasingly over-exploited in many parts of the world [13]. In regions of the world where avocados are cultivated, such as the Mediterranean region and southeast California, drier conditions and water stress are on the increase due to climate change, and fluctuations in these factors directly affect crop development [14,15]. Meanwhile, Colombia has significantly increased its agricultural water consumption over the past two decades, rising from 4.92 to 25.04 km^3 $year^{-1}$ [16,17], mainly due to the use of empirical irrigation practices by farmers and the lack of water requirement information.

Avocado plants are susceptible to events associated with water stress [18,19], which can significantly impact fruit production. Both water deficits and excesses can induce alterations in the plant and its physiological processes, primarily due to its sensitive shallow root system, affecting shoot and root growth, flowering time, and biomass production [20–22]. The duration and severity of water stress are other relevant factors when stress responses are analyzed, and several studies have explained the mechanisms plants use to cope with water stress [14,15,23]. Complex physiological and biochemical adaptations are developed by the avocado plants in response to the stress level applied, which results in fruit drop during formation and decreases in fruit weight and quality [24–26].

Avocado productivity and fruit quality decrease when the plants are grown in soils with high water retention [27], as this promotes root damage by anoxia [28]. Understanding the effect of abiotic stress on the roots of a permanent crop, such as avocado, is essential to guarantee the sustainability of the productive system, since it allows us to know the "tolerance capacity" of plant materials to stress conditions directly and indirectly, which allows for the selection of rootstocks suitable to specific production areas. Anchoring and support in the soil, water, nutrient assimilation, and a beneficial relationship with the soil microbiota are some of the main functions of the roots, which are in direct contact with soil and can quickly detect changes or alterations caused by abiotic stresses, such as drought, waterlogging, and salinity, among other factors [29,30].

Plant phenotyping is a powerful tool for studying the water stress that significantly impacts avocado productivity. In this regard, several studies in morphological [31,32], physiological [26,33,34], biochemical [35,36], and molecular [37–39] traits were reported to assess the responses of avocado plants under water stress.

Recently, advanced imaging technologies, such as thermal, multispectral, and hyperspectral cameras, have enabled the precise measurement of traits [40–42]. These non-invasive and non-destructive measurements help to identify early stress responses and to quantify traits more efficiently.

Commercial avocado orchards use asexual propagation via grafting. This method is the most recommended, and is used by farmers and academics. It involves a commercial cultivar as a scion and usually a local landrace as a rootstock. The use of grafted rootstocks is ideal for mitigating root pathogen effects [43–45] or abiotic stresses [46,47]. In this study, we used two experimental avocado rootstocks that show potential for use under water stress.

Previous studies have provided evidence of the avocado rootstock effect on the performance of cv. Hass. However, a more in-depth evaluation and quantification of the biometrical, physiological, and spectral responses of both rootstock and scion during the initial growth stages are required to guarantee optimal plant development. The aim of this study was to assess the performance of two creole avocado rootstocks grafted onto cv. Hass under different water stress conditions during the early growth stage. This

evaluation was important to identify rootstocks suitable for specific water regimes, and contributes to research focused on physiological and omics approaches, as well as water management practices.

2. Results

2.1. Root Analyses

An analysis of variance was performed for root traits (Table 1). Statistical differences ($p \leq 0.05$) were observed between rootstock effects for the size of the entire root system (AREA), total root length (TRL), right root angle (RRA), and root angle opening (RAO). Among the different water regimes evaluated, statistical differences ($p \leq 0.05$) were observed in the following traits: depth with a maximum proportion of roots (DPR), AREA, TRL, left root angle (LRA), and RRA. For the effects of rootstock–water regime interactions, TRL, LRA, RRA, and RAO were statistically different at the 0.05 level.

Table 1. Mean squares for root traits of avocado plants evaluated under five water regimes.

Source of Variation	DPR (cm)	AREA (cm^2) ($\times$1000)	TRL (mm) ($\times$1000)	LRA (°)	RRA (°)	RAO (°)
Repetition (Rep)	18.41	0.9	246.1	179.2	80.7	157.40
Rootstock (RS)	20.81 ^{ns}	37.3 *	4772.6 ***	139.8 ^{ns}	1040.7 **	508.77 **
Error A (Rep × RS)	0.34	2.0	74.4	85.72	95.1	415.81
Water regime (WR)	65.58 *	9.9 *	6920.6 ***	300.7 *	5101.0 ***	139.36 ^{ns}
RS × WR	65.47 ^{ns}	3.3 ^{ns}	1411.0 ***	1266.9 ***	2491.0 ***	619.92 *
Error B (Rep × RS × WR)	21.43	3.3	259.2	114.14	84.8	126.37
CV, % A	21.4	15.2	13.2	14.2	15.1	22.4
CV% B	28.1	19.0	24.6	16.4	14.3	31.3

DPR: depth with a maximum proportion of roots, AREA: the size of the entire root system, TRL: total root length, LRA: left root angle, RRA: right root angle, RAO: root angle opening. *, **, and *** are significant at the 0.05, 0.01, and 0.001 probability levels, respectively. ns, non-significant at the 0.05 probability level according to the Tukey test.

DPR ranged from 15.24 to 31.77 cm (Table 2). The lower value of DPR for genotype ANRR88 was observed in T4 (50% of water excess) with 15.24 cm, while for ANGI52, it was 22.94 cm in T3 (25% of water excess). Overall, a higher root exploration was observed in ANGI52 across all the treatments, with a mean value of 25.58 cm. AREA represents the size of the entire root system, expressed in cm^2. Between genotypes, AREA was higher for ANGI52 than ANRR88, with mean values of 264.3 cm^2 and 339.6 cm^2, respectively. The minimum root exploration in the soil was observed for ANRR88 under treatment T4 (50% of water excess) at 190.09 cm^2. However, the maximum AREA was observed in ANGI52 under treatment T3 (25% of water stress), with a value of 397.23 cm^2.

For both genotypes, the treatment values of TRL were lower than those observed for the control treatment (T5). For ANRR88, a reduction of 18% on average was observed for TRL compared with T5, making it the treatment with the smallest reduction in root length. A higher decrease in TRL values was observed for ANGI52, particularly for treatments T1 (50% of water restriction) and T2 (25% of water restriction), with values of 1680.4 and 1560.5 mm, respectively.

LRA and RRA indicate the outermost angle to the horizontal along an arc of 10 cm. Root angle opening (RAO) is the opening of the angle between LRA and RRA. In both genotypes, T5 showed the maximum values of LRA and RRA among the treatments evaluated. For the genotype ANRR88, mean opening angles of 65.1° and 64.7° were observed for LRA and RRA, respectively. The lowest value of LRA was observed in T1 (49.0°), while the lowest value of RRA was observed in T3 (32.8°). Similar values were observed for ANGI52, with mean values of 64.5° and 66.4° for LRA and RRA, respectively.

Maximum values of RAO were observed for water restriction treatments in T1 (61.5°) for ANRR88, and in T3 (63.3°) for ANGI52.

Table 2. Mean values for root traits of avocado plants under different water regimes.

Genotype	Treatments	DPR (cm)	AREA (cm^2)	TRL (mm)	LRA (°)	RRA (°)	RAO (°)
ANRR88	T1	26.45 ^{ab}	295.38 ^{bc}	2353.9 ^{abc}	49.03 ^{c}	69.41 ^{abc}	61.56 ^{ab}
	T2	23.03 ^{bc}	253.22 ^{c}	2240.6 ^{bc}	68.04 ^{a}	77.60 ^{a}	34.38 ^{c}
	T3	31.77 ^{a}	281.08 ^{c}	2317.6 ^{bc}	70.37 ^{a}	32.83 ^{d}	32.83 ^{c}
	T4	15.24 ^{c}	190.09 ^{d}	1805.5 ^{cd}	67.77 ^{a}	66.05 ^{bc}	46.17 ^{bc}
	T5 (Control)	23.54 ^{ab}	301.95 ^{bc}	2644.9 ^{ab}	70.56 ^{a}	77.98 ^{a}	31.48 ^{c}
ANGI52	T1	28.77 ^{ab}	290.69 ^{c}	1680.4 ^{d}	70.23 ^{a}	72.34 ^{ab}	38.43 ^{c}
	T2	23.27 ^{bc}	354.82 ^{ab}	1560.5 ^{d}	63.96 ^{ab}	69.53 ^{ab}	46.51 ^{bc}
	T3	22.94 ^{bc}	397.23 ^{a}	1848.9 ^{cd}	56.51 ^{bc}	60.21 ^{c}	63.30 ^{a}
	T4	24.29 ^{b}	298.46 ^{bc}	1779.9 ^{cd}	63.92 ^{ab}	63.58 ^{bc}	52.53 ^{ab}
	T5 (Control)	28.63 ^{ab}	357.26 ^{ab}	2904.0 ^{a}	68.09 ^{a}	66.36 ^{bc}	45.57 ^{bc}
	Mean	24.95	303.14	2071.78	65.29	64.60	45.11

T1: water restriction of 50%, T2: water restriction of 25%, T3: water excess of 25%, T4: water excess of 50%, and T5: control. DPR: depth with a maximum proportion of roots, AREA: the size of the entire root system, TRL: total root length, LRA: left root angle, RRA: right root angle, and RAO: root angle opening. Different letters indicate statistical differences at a significance of $p \leq 0.05$ according to the Tukey test.

The results shown below in Section 2.2 validate the selection of genotypes ANRR88 and ANGI52 based on the results of the root phenotyping. The information provided by the variables plant height, leaf area, dry matter, and organic Carbon per organ (root, stem, and leaf) allowed us to know the effect of water stress on the entire avocado plant, from the roots, represented by ANRR88 and ANGI52, to the aerial part, represented by the cv. Hass.

2.2. Plant Height, Leaf Area, Dry Matter Accumulation, and Organic Carbon Content

Averaged data across plots were used to conduct an analysis of variance for plant height (PH), leaf area (LA), dry matter accumulation, and organic Carbon (OC) content for leaves, stems, and roots (Table 3). No significant differences were observed between rootstocks (RS) for these traits. However, water stress regimes (WR) had a significant effect on all traits. The interaction RS × WR effect was significant only for stem dry matter at a significance level of 0.05.

Table 3. Mean squares for plant height (PH), leaf area (LA), dry matter partition, and Organic Carbon (OC) of avocado plants under different water stress regimes.

Source of Variation	PH	LA (×1000)	Dry Matter (×1000)				Organic Carbon		
			Leaves	Stems	Roots	Total	Leaves	Stems	Roots
Repetition (Rep)	35.9	66.4	7.0	8.0	27.6	198.6	0.06	1.53	0.37
Rootstock (RS)	2.1 ^{ns}	1679 ^{ns}	10.6 ^{ns}	5.3 ^{ns}	332 ^{ns}	602.8 ^{ns}	0.10 *	615.3 ***	5.33 *
Error A (Rep × RS)	14.5	206.2	8.8	20.9	40.4	202.8	0.01	4.92	0.46
Water regime (WR)	107.9 *	2952 ***	280.8 ***	116.1 ***	202.6 *	1705.1 ***	0.50 ***	58.08 ***	3.09 ***
RS × WR	26.9 ^{ns}	521.8 ^{ns}	31.2 ^{ns}	47.3 *	10.4 ^{ns}	111.9 ^{ns}	0.07 ^{ns}	18.07 ***	1.15 ^{ns}
Error B (Rep × RS × WR)	32.0	290.6	26.0	10.7	59.2	166.5	0.05	1.55	0.43
Mean	61.3	1.563	19.14	19.59	23.46	61.34	0.46	5.48	1.75
CV, % A	6.22	29.05	15.53	23.35	27.10	23.22	23.93	40.5	38.79
CV% B	9.22	34.48	26.68	16.74	32.81	21.04	51.67	22.78	37.69

*, and *** are significant at the 0.05, and 0.001 probability levels, respectively. ns, non-significant at the 0.05 probability level.

Plant height (PH) showed statistically significant differences ($p \leq 0.05$) among the treatments, but not between the genotypes evaluated. Genotype ANRR88 showed more height at 61.68 cm (±1.32), while ANGI52 reached 60.24 cm (±1.37). For both genotypes, the treatment with the highest PH was T5 with an average of 69.24 cm (±2.48), while the lowest PH was observed in T1, with 55.40 cm (±2.21) (Figure 1). The PH variable decreased because of the treatments. In cases of severe stress due to water deficit or excess, the lowest values were recorded, 55.40 cm (±2.21) and 56.67 (±2.02) cm, respectively.

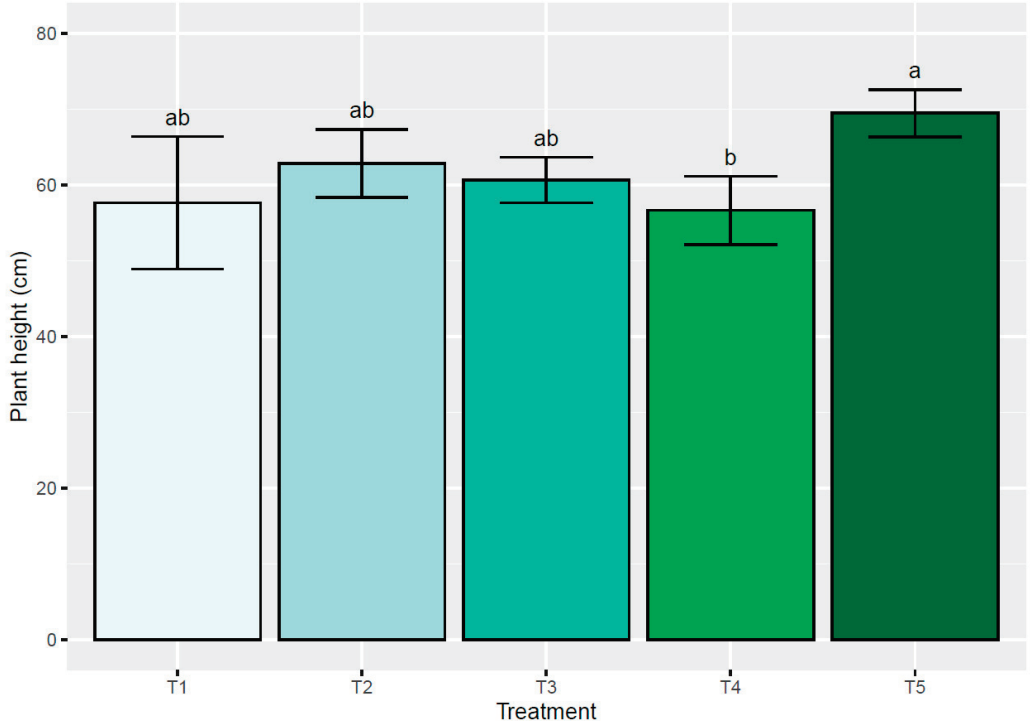


Figure 1. Average plant height (cm) for the different treatments evaluated: water restriction of (T1) 50% and (T2) 25%, water excess of (T3) 25% and (T4) 50%, and (T5) control. Values represent the mean of the two rootstocks evaluated. Both rootstocks were combined with a common cv. Hass scion. Different letters indicate statistical differences at a significance of $p \leq 0.05$ according to the Tukey test.

Highly significant differences were found for leaf area (LA) under the water stress treatments evaluated for the genotypes. ANGI52 presented the lowest values for this variable, with 650 cm^2. For leaf area (LA), statistically significant differences ($p \leq 0.05$) were observed among genotypes and treatment effects (Figure 2). The control (T5) showed a mean value for rootstock of 3053.2 cm^2, superior to all the treatments evaluated. A higher reduction in LA was observed for ANRR88 compared with ANGI52, ranging from 12.2% (T1) to 65.7% (T2). A higher LA reduction was observed for ANRR88 in T4 when compared to the other treatments, with a value of 711.1 cm^2. The highest value of LA was observed in ANGI52 for T2, 2204.5 cm^2.

The dry matter accumulation was quantified to leaves, stems, and roots (Figure 3). In both rootstocks, the control treatment (T5) showed higher values of dry matter accumulation, ranging from 1396.89 (ANGI52) to 1443.79 g m^{-2} (ANRR88). A higher variation in dry matter accumulation among treatments and organs was observed in ANRR88, where T4 (50% of water excess) showed a maximum reduction of 57.3% in dry matter accumulation compared with the control treatment (T5). However, when the same treatment (T4) was applied to the rootstock ANGI52, a smaller reduction in dry matter accumulation was observed, with a decrease of 38% compared with T5 (Figure 3).

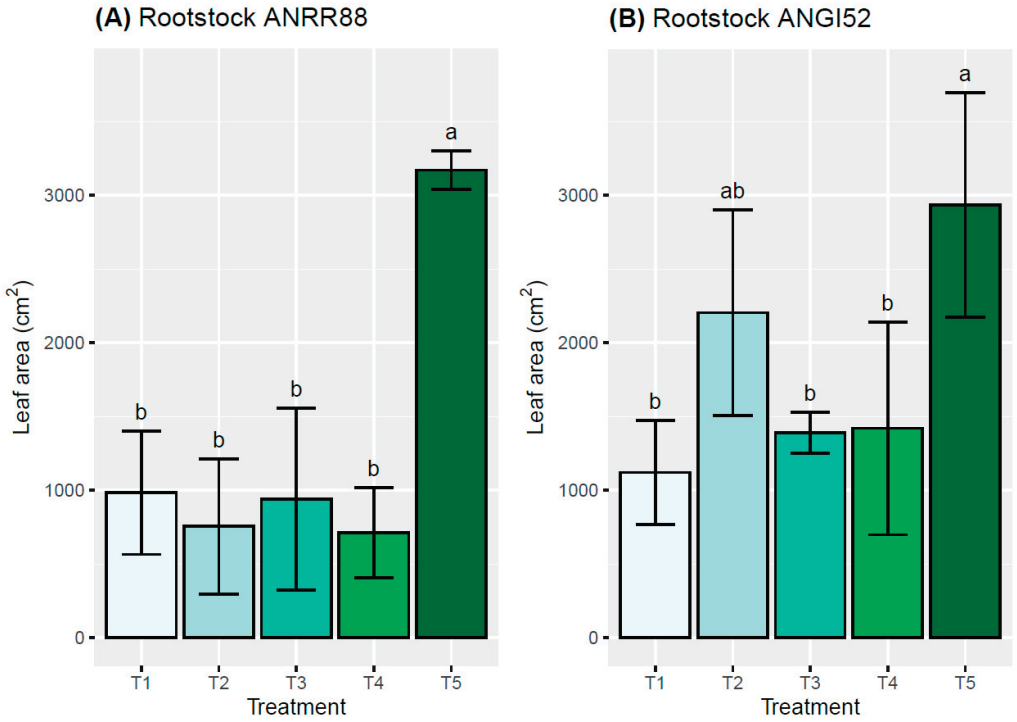


Figure 2. Leaf area (cm^2) of the avocado plants using rootstock (**A**) ANRR88 and (**B**) ANGI52 for the different treatments evaluated: water restriction of (T1) 50% and (T2) 25%, water excess of (T3) 25% and (T4) 50%, and (T5) control. Both rootstocks were combined with a common cv. Hass scion. Different letters indicate statistical differences at a significance of $p \leq 0.05$ according to the Tukey test.

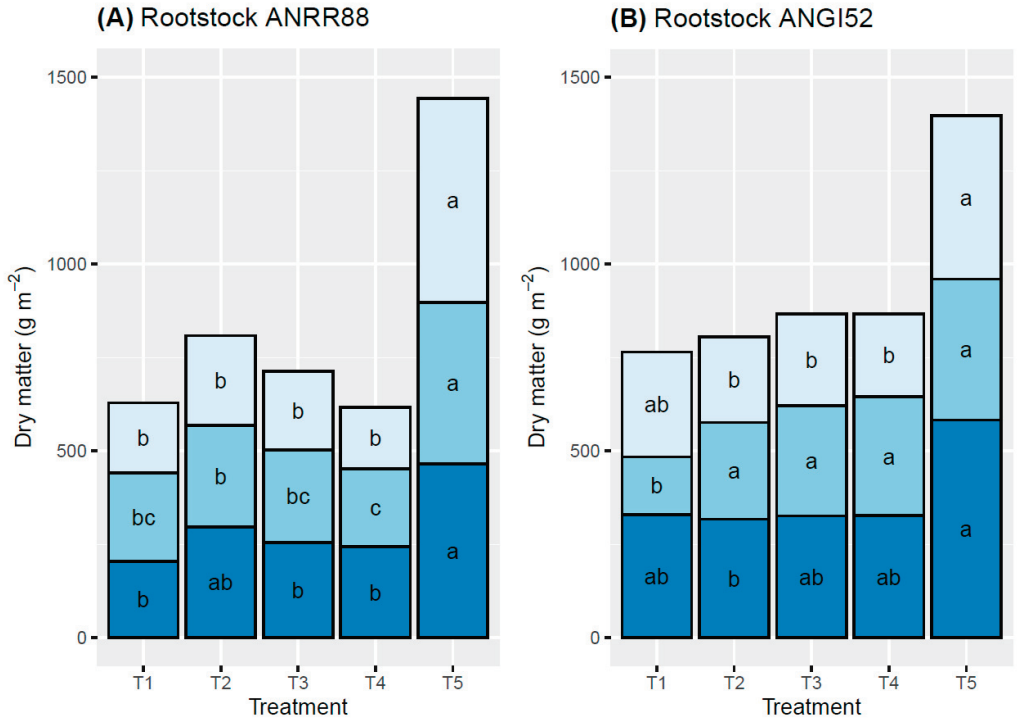


Figure 3. Dry matter (g m^{-2}) partitioning per plant organ: leaves (light blue), stem (medium blue), and roots (dark blue) for ANRR88 (**A**) and ANGI52 (**B**). Treatments: water restriction of (T1) 50% and (T2) 25%, water excess of (T3) 25% and (T4) 50%, and (T5) control. Both rootstocks were combined with a common cv. Hass scion. Different letters indicate statistical differences at a significance of $p \leq 0.05$ according to the Tukey test.

The leaves were the plant organ with the highest decrease in dry matter, ranging from 44.1% (ANGI52) to 63.3% (ANRR88). A maximum reduction in stem and root dry matter was observed for ANRR88, 44.1 and 46.3%, respectively.

The organic Carbon (OC) content was determined for both rootstocks and in each plant organ (Figure 4). ANRR88 accumulated a higher Carbon content amount than ANGI52 in all plant organs, with average values of 10.94 and 4.66 mg OC g^{-1} of DT, respectively. At the plant organ dissertation level, high Carbon accumulation was observed in the stem and roots, where both organs accumulated more than 90% of the total Carbon determined. However, a higher Carbon accumulation proportion in the stem was observed for ANRR88, ranging from 68.1 to 88.4%, for all the treatments.

T3 caused a lower accumulation of OC in roots for ANRR88; even so, all the treatments, due to a deficit or excess of water, strongly affected the accumulation of OC in the roots, while ANGI52 was affected by T1 (Figure 4). In both genotypes, the highest concentration of OC in the stem was in T5. ANRR88 and ANGI52 had the lowest values of OC in the stem under T1 with 3.10 and 0.27 mg of OC g^{-1} DT, respectively. The OC content in leaves was higher in T4 for both genotypes.

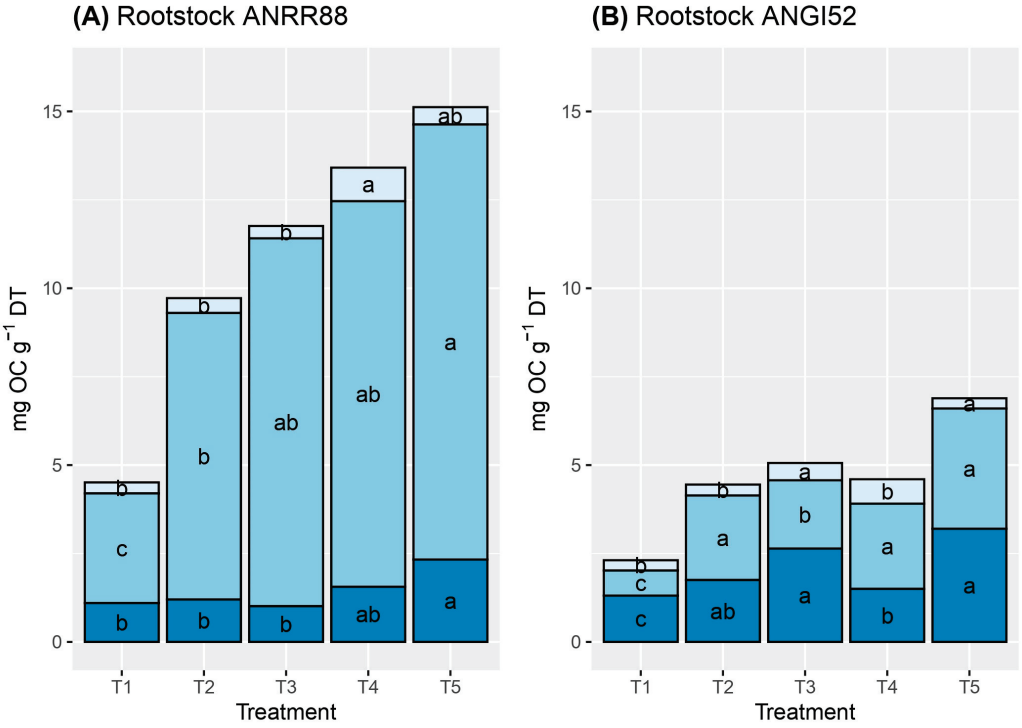


Figure 4. Organic Carbon (mg OC g^{-1} DT) partitioning per plant organ: leaves (light blue), stem (medium blue), and roots (dark blue) for ANRR88 (**A**) and ANGI52 (**B**). Treatments: water restriction of (T1) 50% and (T2) 25%, water excess of (T3) 25% and (T4) 50%, and (T5) control. Both rootstocks were combined with a common cv. Hass scion. Different letters indicate statistical differences at a significance at the $p \leq 0.05$ according to the Tukey test.

2.3. Analysis of Vegetation Indices

The vegetation indices were evaluated as the mean values across both rootstocks, and the results are presented per treatment (Table 4). Statistical differences ($p > 0.05$) were observed among the treatments for the three vegetation indices evaluated. The coefficient of variation ranged between 1.09% and 16.72% for the normalized difference vegetation index (NDVI) and the MERIS Terrestrial chlorophyll index (MTCI), respectively.

Table 4. Summary of ANOVA for three vegetation indices applied to avocado plants under different water stress regimes.

Vegetation Index	Sum Square	Mean Square	F	Prob > F	CV%
NDVI	0.02297	0.00574	19.59	5.13×10^{-16} ***	1.09
MTCI	186.69	46.6718	23.76	1.71×10^{-19} ***	10.52
CI_{RE}	1639.1	409.769	5.87	0.0001 **	16.72

NDVI: Normalized difference vegetation index, CI_{RE}: Chlorophyll estimation red edge, and MTCI: MERIS Terrestrial chlorophyll index. **, and *** are significant at the 0.01, and 0.001 probability levels, respectively.

Figure 5 summarizes the mean and standard deviation for the NDVI, the CI_{RE} index, and the MTCI. For the NDVI, differences were observed among treatments, with T5 (control) showing a higher value (0.9318) compared to the other treatments. T2 was the treatment that most significantly affected the rootstocks according to the NDVI values. With the data obtained in our experiments, T1, T3, and T4 could not be statistically differentiated from each other. The MTCI found a significant difference between T3 and the rest of the treatments. T1, T2, and T4 were not statistically different ($p \leq 0.05$). T2 was the treatment with higher MTCI values of 5.8324. Finally, the CI_{RE} index indicated that T3 significantly differed from the other treatments evaluated.

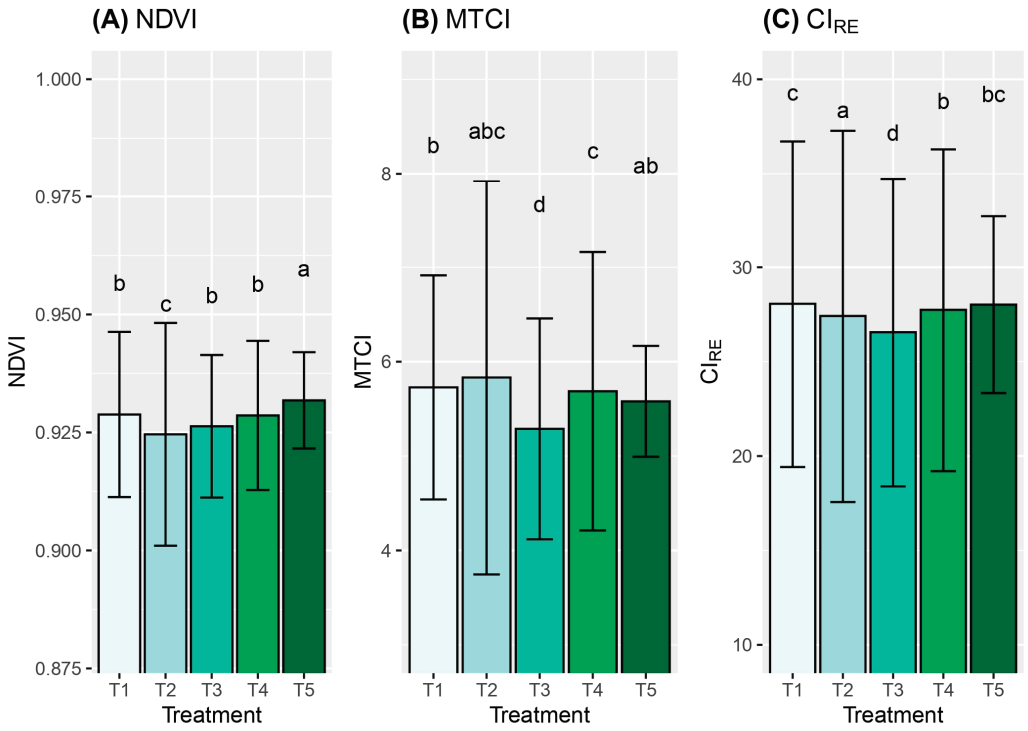


Figure 5. Mean values per treatment for (**A**) NDVI, (**B**) MTCI, and (**C**) CI_{RE}. Treatments: water restriction of (T1) 50% and (T2) 25%, water excess of (T3) 25% and (T4) 50%, and (T5) control. Both rootstocks were combined with a common cv. Hass scion. Different letters indicate statistical differences at a significance of 0.05 level, according to the Tukey test.

The NDVI and the MTCI were more effective than the CI_{RE} index at quantifying stress, distinguishing not only between water excess and deficit stress, but also between different levels of these stresses. Stress detection was achieved using all vegetative indices including the NDVI, the CI_{RE} index, and the MTCI.

3. Discussion

This study evaluated the responses of two avocado rootstocks, ANRR88 and ANGI52, under different water regimes, analyzing both root and plant phenotypic traits and vegetation indices. The results provide valuable insight into how each rootstock responds

to conditions of water deficit or excess, which is crucial for the identification and selection of rootstocks, improving crop management practices under variable nursery and field conditions.

Several techniques and software were used for crop root phenotyping, increasing the accuracy and timing of the data acquisition [48–50]. Digital imaging utilization for avocado root phenotyping allows for the quantification of root traits like architecture, root growth dynamics, and root interaction with the soil. However, there are no published studies on avocado root phenotyping; it is costly in terms of resources and time, limiting factors in the research programs. The REST v1.0.1 software was used in this study to facilitate the acquisition and data processing of several root traits. The accuracy of this software was previously validated by [50–52], which found a high correlation between manually measured traits and image-derived traits.

The statistical differences observed in root traits (DPR, AREA, TRL, LRA, RRA, and RAO) among the different water regimes evaluated, using the REST software, suggest a significant phenotypic plasticity in response to soil condition. For each treatment applied, ANGI52 showed greater root exploration and root size systems (AREA) compared to ANRR88 (Table 2), indicating better anchoring, and water and nutrient uptake capacity under water excess conditions (T3). For the RAO, root behavior varied depending on the stress applied. Severe water stress to avocado plants changes root architecture, resulting in both a larger root angle opening and a higher proportion of shallow roots.

The difference in plant height (PH) and leaf area (LA) between rootstocks and treatments indicates that water deficit and excess differently affect the vegetative growth of the avocado plant. Water stress inhibits cell division and growth, as well as some developmental processes of the plants [53]. The reduction in LA was more significant in ANRR88 than in ANGI52, suggesting ANRR88 has a higher sensitivity to extreme changes in water availability.

Dry matter partitioning was affected when the water regime was modified, particularly in the roots and stem. The dry matter accumulation in ANGI52 was similar among treatments for each plant organ evaluated. However, a significant reduction was observed in T1, with a decrease of 43% compared to the control treatment. Several authors have explained that the variation in dry matter partitioning and accumulation is caused both by a competitive growth under limitations of assimilates and by hormone regulation [54–56]. PH, LA, and dry matter accumulation are closely correlated with crop productivity [57]. These results suggest the need for complete differential soil management according to the genotype used as rootstock, and special attention to the substrate composition such as soil texture, in the case of field conditions and nursery, respectively.

Variations in organic Carbon accumulation among plant organs and genotypes were observed. ANRR88 was highly affected in terms of OC content by treatments associated with water restriction, T1 and T2, compared with the water excess treatments. Meanwhile, ANGI52 showed low OC accumulation but similar content per organ among the treatments. In plants subjected to abiotic stress, photosynthetic Carbon uptake is limited [58], growth decreases or stops, and non-structural carbohydrates (e.g., glucose, fructose, sucrose, and starch) are accumulated [59,60]. When Carbon is stored instead of being used to increase dry matter, there is a notable reduction in light capture and photosynthetic capacity. In our study, more than 90% of Carbon accumulation was observed in both stem and roots. Root architecture, whether deep or shallow, affects Carbon stocks, resulting in a higher adaptation capability to environmental changes [61,62]. Plant storage accumulation starts as soon as abiotic stress is detected, leading to the accumulation of photoassimilates in lower organs, such as the stem and roots, while the leaves reduce their photosynthetic area to avoid excess evapotranspiration. In this study, this indirect relationship was observed to be overlapping in Figures 3 and 5.

Water restriction has a progressive effect on plants, causing a distinct response that eventually results in reduced leaf expansion and increased root growth. Other effects of

water stress are the alterations in gene expression, particularly in relation to the synthesis of enzymes [63].

Rocha-Arroyo et al. [64] indicate that root development occurs in phases opposite to vegetative shoots development. Both processes can be affected in the presence of water stress, as evidenced by the results showing reduced leaf development under stress conditions.

Water is not the only stress that affects the normal physiological behavior of plants. Variations in temperature, light, and atmospheric CO_2 concentration impact the distribution of photoassimilates and the generation of biomass [28,65].

In orange trees, another grafted fruit tree, Garzón et al. [66] showed that water deficit stress can impact fruit setting in citrus cv. Valencia. However, when the stress is removed after the first flowering, the plant can increase its fruit set efficiency compared with plants that continue to experience water deficit stress after flowering. Since the greatest proportion of vegetative development occurs when there is an adequate water supply and stops when there is not, once produced, the vegetative structures compete with the fruits for OC.

The leaf is the organ of the plant that exhibits the greatest negative water potential when excessive transpiration occurs, and the plant vigor can primarily be impacted in the leaves during water deficiency stress [67]. The spectral response of the leaves can also change in response to the type of stress and its intensity, as evidenced by comparing different vegetation indices (NDVI, MCTI, and CI_{RE}). The obtention of precise wavelength ranges by type of stress, as identified in this study, allows for early intervention in several aspects: (i) remediating stress, (ii) early selection of plant materials with tolerance to specific stresses, (iii) selecting efficient predictive variables, and (iv) designing stress prediction models, among others.

The spectral response to mild level and short-term stresses may not be as expected. Plants have different mechanisms to cope with stress, such as decreasing the water potential of the tissues, such as osmotic adjustment, which maintains turgor in the cell wall, and is reflected as "vigor" [68]. Additionally, mechanisms such as gene expression can cause some genes to be turned off in the presence of excess stress and others to be activated by deficit stress [63]. This could alter both the spectral response and the accumulation of biomass and organic Carbon.

The metric that best quantified stress among treatments in this investigation was the CI_{RE} index, which is based on the amount of chlorophyll between the NIR bands and the red edge, specifically between 700 nm and 1000 nm in wavelength. We suggest that simultaneous spectral alterations occur in multiple electromagnetic regions, with the most remarkable changes occurring in the infrared region. The reflectance in this region is attributed to cell structure and water content due to the intricate interaction between the reflectance of the cavities between the leaf and the internal reflection of infrared radiation from these cavities [69].

Currently, our research program involves the constant monitoring of the rootstocks under both controlled and field conditions. Data from physiological traits, genetic characterization, and spectral (multi and hyperspectral) imaging are being processed for an integration analysis in the next phase. Different artificial intelligence (AI)-based methods such as machine learning (ML) and deep learning techniques (e.g., convolutional neural networks—CNNs) have been used preliminarily for the efficient processing of large and complex datasets. These approaches will be applied to model the rootstocks and scion responses to varying water availability by identifying key stress markers. The use of ML and CNN techniques in the identification, classification, and prediction of water stress in crops is rapidly increasing, making their application both feasible and highly promising.

4. Materials and Methods

4.1. Genetic Material and Experimental Conditions

This study used two experimental avocado rootstocks, ANRR88 (Genotype 1) and ANGI52 (Genotype 2). Both rootstocks were selected previously by AGROSAVIA from

local landraces of Antioquia, a northwest department of Colombia. These landraces were collected and evaluated for their agronomic performance and genetic structure in previous studies [70–72]. Seeds from selected avocado trees were germinated in a nursery, and after three months, those with uniform sizes were grafted with cv. Hass scions. Grafted plants were grown in a greenhouse (19 ± 3 °C, 72 ± 4% RH) for five months. They were transplanted to buckets of 20 L capacity filled with a commercial substrate. Chemical and physical analyses of the substrate (Table S1) were carried out before the installation of the experiment to determine the initial properties of the substrate and adjust the fertilization doses administered for plant nutrition. The substrate used in this study shares soil properties similar to those in the region. Ten months after grafting, healthy and vigorous plants were selected for the experiment. Seedlings and grafted plants were irrigated twice weekly to ensure the correct development of the plants.

The experiment was performed in 2021, in a greenhouse of AGROSAVIA, located at La Selva Research Center, Colombia (6°7′46.5″ N, 75°24′55.6″ W, 2110 m.a.s.l). Based on the average of 40 years of meteorological data, the climate in the area featured an average annual temperature of 17.8 °C, precipitation of 1917 mm, relative humidity of 78%, daylight duration of 1726 h yr^{-1}, and evapotranspiration of 1202 mm.

4.2. Treatments and Experimental Design

Grafted plants were exposed to five water levels: a control treatment (T5) with non-stressing water conditions, which consisted of a constant water application of 222 mL day^{-1} $plant^{-1}$ according to Dorado-Guerra et al. [73] for the volume of soil used; a water restriction treatment of 50% (T1) and 25% (T2) less water than the control amount, with a twice a week watering regime; and a water excess treatment with 25% (T3) and 50% (T4) more water than the control amount, with a daily irrigation regime.

All treatments were laid out in a split-plot arrangement under a randomized complete block design with nine replications, where the whole plot and sub-plots were rootstocks and water regimes, respectively, resulting in a total of 90 plots, where each plant represented each experimental unit.

4.3. Trial Management

Prior to the experiment, the substrate was saturated with water and drained for 24 h. Tensiometers were placed in each bucket to monitor daily soil moisture and water content at 10 cm depth during the trial. Soil water drainage was ensured through holes at the bottom of the buckets. Treatments were maintained for 180 days until non-destructive and destructive sampling.

The plants received the recommended fertilization rates of 87.7 g $plant^{-1}$ of nitrogen (N), 64.4 g $plant^{-1}$ of phosphate (P_2O_5), and 84.7 g $plant^{-1}$ of potassium (K_2O) per bucket. The fertilization was divided and applied as follows: 50% one week before the experiment started, 25% 30 days after experiment started, and the remaining 25% 90 days after the experiment started.

4.4. Data Collection

Soil moisture per bucket was monitored at 10-day intervals (n = 3 per plot) using a FieldScout® TDR 300 (Spectrum® Technologies Inc., Aurora, IL, USA) and expressed as a percentage (%). At 180 days, plants were sampled for both non-destructive and destructive assessments in each plot. Plant height (PH, cm) was measured on the main stem from the ground level to the canopy terminal. Entire plants were harvested and divided into leaves, stems, and roots. Leaf area (cm^2) was measured for all the leaves harvested from each plot and scanned in triplicate using a LI-3000C (LI-COR® Bioscience, Lincoln, NE, USA) portable leaf area meter.

Roots were extracted one at a time to avoid moisture loss and changes in the architecture of the roots before imaging. The roots were carefully shaken briefly and washed with regular water to remove the remaining soil. Following the method described by Colombi

et al. [52], the roots were photographed in a custom-made imaging tent with modifications. Plastic tubes for the structure and a combination of cold and warm white regular LED panel lights were used in place of aluminum bars and flashlights, respectively. A 24.2 megapixel Nikon D5500 digital camera (Nikon®, Tokyo, Japan) with a 35 mm fixed focal objective was used to photograph the root architecture. The camera was mounted on a tripod and placed in the center of the tent, 70 cm above the ground, and at a fixed distance of 100 cm from the roots. Uniform distance from the camera to roots, exposure time, and illumination settings were fixed to normalize and optimize image quality. A minimum of 25 photographs were taken per root sample. Images were recorded, stored in JPEG format, and immediately renamed with an ID code. The details of the root capture, image acquisition, and analysis of avocado roots subjected to water stress are shown in Figure 6.

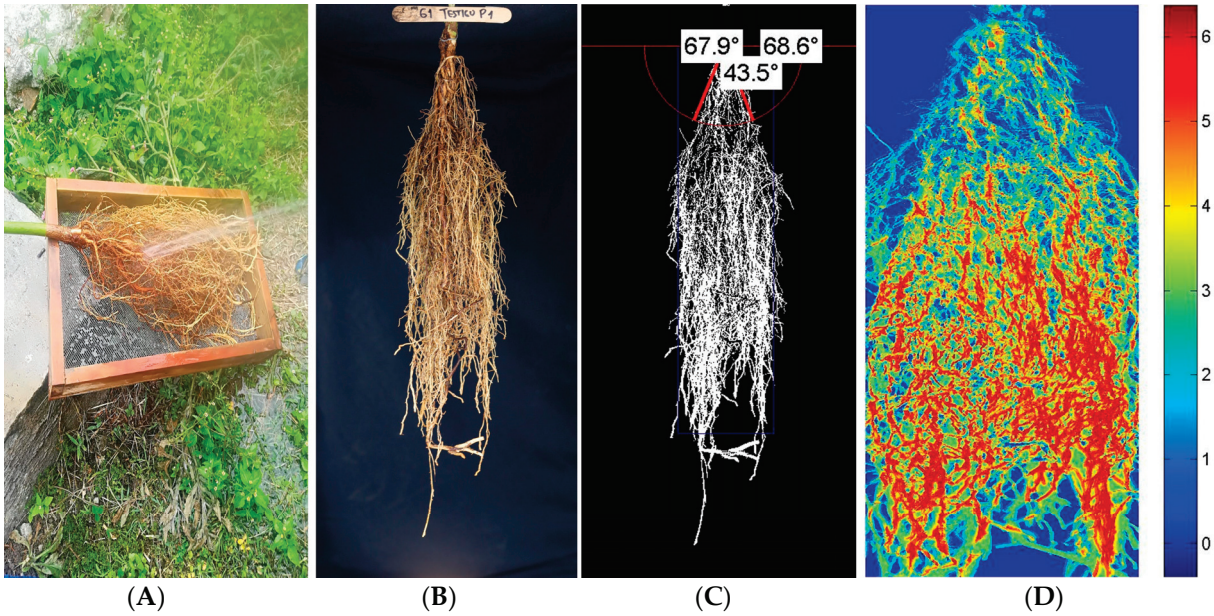


Figure 6. Process of avocado root conditioning for imaging: (**A**) washing, (**B**) sample before imaging, (**C**) angle opening data calculated by the software, and (**D**) density area occupied estimated by the software.

The quantitative traits of the root system architecture were obtained from the images. Depth with a maximum proportion of roots (DPR, cm) was estimated. The size of the entire root system (AREA, cm^2) was calculated as the sum of all pixels within the convex hull. Total root length (TRL, mm) was the total projected structure length within the convex hull. The left (LRA, °) and right root angle (RRA, °) were determined as the outermost angle to the horizontal along an arc of 10 cm. The root angle opening (RAO, °) was determined as the opening angle between LRA and RRA.

Plant organs (roots, stems, and leaves) were assessed for estimated dry matter production and organic Carbon (OC). Samples were air-dried for 120 h and further dried using an electric stove at 45 °C until constant weight for dry matter was attained. OC was estimated for each organ, using wet digestion with the dichromate method [74] in triplicate.

4.5. Hyperspectral Image Acquisition and Vegetation Index

A hyperspectral image was captured on 18 November 2021 using a Dual HySpex Mjolnir VS-620 (HySpex®, Oslo, Norway) system. At the time of imaging, the plants had been under stress for 155 days. The system included a V-1240 (HySpex®, Oslo, Norway) sensor with a spectral range between 400 and 1000 nm and comprising 200 spectral bands with a bandwidth of 3.0 nm. The image was captured by a drone at an altitude of 2140 m.a.s.l, approximately 40 m from the surface. The images were orthorectified and atmospherically corrected. Manual labeling was performed to match each section of pixels corresponding

to each avocado rootstock and treatment. From these spectral signatures, three vegetation indices were calculated and subjected to statistical analysis: normalized difference vegetation index (NDVI), Chlorophyll estimation red edge (CI_{RE}), and the MERIS Terrestrial chlorophyll index (MTCI). These indices were selected for their sensitivity to chlorophyll and irrigation levels [75]:

$$NDVI = \frac{R_{NIR} - R_R}{R_{NIR} + R_R} \quad (1)$$

$$MTCI = \frac{R_{NIR} - R_{RE}}{R_{RE} - R_R} \quad (2)$$

$$CI_{RE} = \frac{R_{NIR}}{R_R} - 1 \quad (3)$$

where R_{NIR}, R_{RE}, and R_R correspond to the reflectance in the near-infrared (780 to 900 nm), red edge (690 to 710 nm), and red (650 to 680 nm), respectively.

4.6. Data Analysis and Statistics

For root image analyses, the Root Estimator for Shovelomics Traits (REST, v1.0.1 Institute of Agricultural Science, ETH, Zurich, Switzerland) software was utilized in MatLab 7.12 (The MathWorks, Inc., Natick, MA, USA). The image pre-processing process was realized as described by [76].

A two-way ANOVA was performed for each dependent variable, with rootstocks and water regimes treated as fixed effects in the model. Where significant effects were observed, paired comparisons were conducted using the Tukey test at a significance level of $p \leq 0.05$. The normality assumption was confirmed based on the Shapiro–Wilk test. All data, including those from the REST software, were analyzed in R v4.1.1 (R Core Team 2021).

5. Conclusions

This study allowed us to characterize the behavior of two avocado rootstocks during the nursery phase under abiotic stress, such as water stress. The response to water stress was conditioned by the genotype. ANRR88 presents a greater ability to adapt to stress conditions due to moderate to high water deficit for medium-term periods, while ANGI52, shows better adaptation to both deficit and excess stress conditions, with a larger root system and greater root length. Both genotypes showed significant reductions in plant height and leaf area under severe water stress. The leaves experienced the highest decrease in dry matter accumulation under water stress. More than 90% of the total Carbon was stored in the stem and roots, with ANRR88 showing a higher proportion of Carbon accumulation in the stem across all treatments.

Water stress affected the spectral responses of avocado plants. The spectral bands near the red edge, around 720 nm, were shown to be more efficient in quantifying this stress. These spectral tools support faster measurements with high precision and in a shorter time than conventional techniques require. All vegetation indices used in this study detected stress, but their effectiveness varied in distinguishing among different levels of stress. The MTCI and the NDVI were more effective for detecting and quantifying stress under varying water conditions.

These findings enhance our understanding of how avocado plants respond to water stress, using simple and accessible tools that are highly precise and effective in detecting and quantifying stress. This knowledge will allow for improvements in future water management practices by aligning them with the plant's natural stress regulation strategies.

Further investigations, including additional physiological variables and AI-based approaches, are necessary to elucidate the mechanism by which water deficit or excess influences the behavior and response of the rootstock–scion interaction.

Supplementary Materials: The following supporting information can be downloaded at https://www.mdpi.com/article/10.3390/plants13182660/s1: Table S1. Chemical and physical characteristics of soil substrate used in avocado nursery.

Author Contributions: Conceptualization, T.R., M.G.-H., M.C.T.-M. and M.C.; data curation, T.R., M.G.-H., M.C.T.-M., L.C., J.G. and M.G.; formal analysis, T.R., M.G.-H., M.C.T.-M. and M.G.; investigation, T.R., M.G.-H., M.C.T.-M., M.C., L.C., J.G. and M.G.; resources, T.R. and M.C.T.-M.; methodology, T.R., M.G.-H., M.C.T.-M., M.C., J.G. and M.G.; project administration, T.R.; supervision, T.R. and M.C.T.-M.; writing—original draft preparation, T.R. and M.G.-H.; writing—review and editing, T.R., M.G.-H., M.C.T.-M., M.C., L.C., J.G. and M.G.; visualization, M.G.-H.; project administration, M.C.T.-M. All authors have read and agreed to the published version of the manuscript.

Funding: This research and APC were funded by the Ministerio de Ciencia, Tecnología e Innovación Minciencias, Colombia (grant number RC 80740-475-2020).

Data Availability Statement: The datasets generated and/or analyzed during the current study are available from the corresponding author on reasonable request.

Acknowledgments: The authors thank María Vargas, Albeiro Macias, Carolina Zuluaga, and Alba Sanchez for their support in managing and monitoring the experiments. Their assistance was essential for the successful completion of this study.

Conflicts of Interest: The authors declare no conflicts of interest. The funders had no role in the design of this study; in the collection, analyses, or interpretation of data; in the writing of the manuscript; or in the decision to publish the results.

References

1. FAOSTAT. Avocado Trade–Crops and Livestock Products. 2023. Available online: https://www.fao.org/faostat/en/#data/TCL/visualize (accessed on 11 April 2024).
2. USDA; Nutrient Data Laboratory. Avocado, Almond, Pistachio and Walnut Composition. In *USDA National Nutrient Database for Standard Reference, Release 24*; U.S. Department of Agriculture: Washington, DC, USA, 2011.
3. Dreher, M.L.; Davenport, A.J. Hass avocado composition and potential health effects. *Crit. Rev. Food Sci. Nutr.* **2013**, *53*, 738–750. [CrossRef]
4. Ford, N.A.; Liu, A.G. The forgotten fruit: A case for consuming avocado within the traditional Mediterranean diet. *Front. Nutr.* **2020**, *7*, 78. [CrossRef]
5. CBI. The European Market Potential for Avocados. *Centre for the Promotion of Imports from Developing Countries. The Netherlands Ministry of Foreign Affairs.* Available online: https://www.cbi.eu/market-information/fresh-fruit-vegetables/avocados/market-potential (accessed on 9 March 2024).
6. Ferreira, G.; Perez, A. *Fruit and Tree Nuts Outlook*; Economic Research Service U.S. Department of Agriculture: Washington, DC, USA, 2017; 28p. Available online: https://www.ers.usda.gov/webdocs/outlooks/83036/fts-364.pdf?v=631.3 (accessed on 16 April 2024).
7. USDA. Imports Play Dominant Role as U.S. Demand for Avocados Climbs. Economic Research Service U.S. Department of Agriculture. Available online: https://www.ers.usda.gov/data-products/chart-gallery/gallery/chart-detail/?chartId=103810 (accessed on 14 May 2024).
8. MADR. Evaluaciones Agropecuarias Municipales—EVA. Ministerio de Agricultura y Desarrollo Rural. Available online: https://www.datos.gov.co/Agricultura-y-Desarrollo-Rural/Evaluaciones-Agropecuarias-Municipales-EVA/2pnw-mmge (accessed on 10 July 2024).
9. Rondón, T.; Builes, S.; Casamitjana, M.; Duque, M.; Rodríguez-León, A.K.; Vega, C.; Ruiz, D.; Rodríguez, G.A. Perspectiva del ordenamiento productivo del aguacate cv. Hass en Antioquia. In *Actualización Tecnológica y Buenas Prácticas Agrícolas (BPA) en el Cultivo de Aguacate*; Bernal, J., Diaz, C., Eds.; Editorial AGROSAVIA: Bogotá, Colombia, 2020; pp. 715–758. [CrossRef]
10. Hatfield, J.L.; Dold, C. Water-Use Efficiency: Advances and challenges in a changing climate. *Front. Plant Sci.* **2019**, *10*, 103. [CrossRef]
11. Soothar, R.K.; Singha, A.; Soomro, S.A.; Chachar, A.; Kalhoro, F.; Rahaman, M.A. Effect of different soil moisture regimes on plant growth and water use efficiency of Sunflower: Experimental study and modeling. *Natl. Bull. Res. Cent.* **2021**, *45*, 121. [CrossRef]
12. Zhao, M.; Boll, J. Adaptation of water resources management under climate change. *Front. Water* **2022**, *4*, 983228. [CrossRef]
13. Marquez, A. Sobreexplotación del Agua: Causas, Consecuencias y Soluciones. Available online: https://www.ecologiaverde.com/sobreexplotacion-del-agua-causas-consecuencias-y-soluciones-3158.html (accessed on 15 July 2024).
14. Iglesias, A.; Garrote, L. Adaptation strategies for agricultural water management under climate change in Europe. *Agric. Water Manag.* **2015**, *155*, 113–124. [CrossRef]
15. Prein, A.F.; Holland, G.J.; Rasmussen, R.M.; Clark, M.P.; Tye, M.R. Running dry: The U.S. Southwest's drift into a drier climate state. *Geophys. Res. Lett.* **2016**, *43*, 1272–1279. [CrossRef]

16. ICF. Interactive Country Fiches. Available online: https://dicf.unepgrid.ch/colombia/water#section-pressures (accessed on 5 August 2024).
17. AQUASTAT. AQUASTAT Database. AQUASTAT Dissemination System. Available online: https://data.apps.fao.org/aquastat/?lang=en (accessed on 18 August 2024).
18. Erazo-Mesa, E.; Ramírez-Gil, J.G.; Sánchez, A.E. Avocado cv. Hass needs water irrigation in tropical precipitation regime: Evidence from Colombia. *Water* **2021**, *12*, 1942. [CrossRef]
19. Zuazo, V.H.D.; Lipan, L.; Rodríguez, B.C.; Sendra, E.; Franco Tarifa, D.; Nemś, A.; Gálvez Ruiz, B.; Carbonell–Barrachina, A.A.; García–Tejero, I.F. Impact of deficit irrigation on fruit yield and lipid profile of terraced avocado orchards. *Agron. Sustain. Dev.* **2021**, *41*, 69. [CrossRef]
20. Li, T.; Hasegawa, T.; Yin, X.; Zhu, Y.; Boote, K.; Adam, M. Uncertainties in predicting rice yield by current crop models under a wide range of climatic conditions. *Glob. Chang. Biol.* **2015**, *21*, 1328–1341. [CrossRef]
21. Schaffer, B.; Gil, P.; Micklbart, M.V.; Whiley, A.W. Ecophysiology. In *Avocado: Botany, Production and Uses*; Schaffer, B., Wolstenholme, B.N., Whiley, A.W., Eds.; CABI: Croydon, UK, 2013; pp. 168–199. [CrossRef]
22. Ramírez-Gil, J.G.; Cobos, M.E.; Jiménez-García, D.; Morales-Osorio, J.G.; Peterson, A.T. Current and potential future distributions of Hass avocados in the face of climate change across the Americas. *Crop Pasture Sci.* **2019**, *70*, 694. [CrossRef]
23. da Silva, S.R.; Cantuarias-Avilés, T.E.; Chiavelli, B.; Martins, M.A.; Oliveira, M.S. Phenological models for implementing management practices in rain-fed avocado orchards. *Pesq. Agropec. Trop.* **2017**, *47*, 321–327. [CrossRef]
24. Ferreyra, R.; Selles, G. Avocado. In *Crop Yield Response to Water. FAO Irrigation and Drainage Paper 66*; Steduto, P., Hsiao, T.C., Fereres, E., Raes, D., Eds.; FAO: Rome, Italy, 2012; pp. 442–447.
25. Carr, M.K.V. The water relations and irrigation requirements of avocado (*Persea americana* Mill.): A review. *Exp. Agric.* **2013**, *49*, 256–278. [CrossRef]
26. Holzapfel, E.; de Souza, J.A.; Jara, J.; Guerra, H.C. Responses of avocado production to variation in irrigation levels. *Irrig. Sci.* **2017**, *35*, 205–215. [CrossRef]
27. Escobar, V.; Cortes, M.; Correa, A.; Rondon, T.; Rodríguez, P. Hass avocado internal disorders under simulated export conditions and its relationship with flesh mineral content and preharvest variables. *Horticulturae* **2021**, *7*, 77. [CrossRef]
28. Schaffer, B. Effects of soil oxygen deficiency on avocado (*Persea americana* Mill.) trees. In Proceedings of the International Seminar: Irrigation and Soil Management in Avocado Cultivation, La Cruz, Chile, 27–28 September 2006.
29. Davies, W.J.; Bacon, M.A. Adaptation of roots to drought. In *Root Ecology. Ecological Studies*; de Kroon, H., Visser, E.J.W., Eds.; Springer: Berlin/Heidelberg, Germany, 2003; pp. 173–192. [CrossRef]
30. Shekhar, V.; Stöckle, D.; Thellmann, M.; Vermeer, J.E.M. The role of plant root systems in evolutionary adaptation. *Curr. Top. Dev. Biol.* **2019**, *131*, 55–80. [CrossRef]
31. Kofidis, G.; Bosabalidis, A.M.; Chartzoulakis, K. Leaf anatomical alterations induced by drought stress in two avocado cultivars. *J. Biol. Res.* **2004**, *1*, 115–120.
32. Kaneko, T.; Gould, N.; Campbell, D.; Clearwater, M.J. Isohydric stomatal behaviour alters fruit vascular flows and minimizes fruit size reductions in drought-stressed 'Hass' avocado (*Persea americana* Mill.). *Ann. Bot.* **2024**, *133*, 969–982. [CrossRef]
33. Chartzoulakis, K.; Patakas, A.; Kofidis, G.; Bosabalidis, A.; Nastou, A. Water stress affects leaf anatomy, gas exchange, water relations and growth of two avocado cultivars. *Sci. Hortic.* **2002**, *95*, 39–50. [CrossRef]
34. Reeksting, B.J.; Taylor, N.J.; van den Berg, N. Flooding and *Phytophthora cinnamomi*: Effects on photosynthesis and chlorophyll fluorescence in shoots of non-grafted *Persea americana* (mill.) rootstocks differing in tolerance to Phytophthora root rot. *S. Afr. J. Bot.* **2014**, *95*, 40–53. [CrossRef]
35. Sanclemente, M.A.; Schaffer, B.; Gil, P.M.; Vargas, A.I.; Davies, F.S. Pruning after flooding hastens recovery of flood-stressed avocado (*Persea americana* Mill.) trees. *Sci. Hortic.* **2014**, *169*, 27–35. [CrossRef]
36. Chung, S.W.; Rho, H.; Lim, C.K.; Jeon, M.K.; Kim, S.; Jang, Y.J.; An, J.H. Photosynthetic response and antioxidative activity of 'Hass' avocado cultivar treated with short-term low temperature. *Sci. Rep.* **2022**, *12*, 11593. [CrossRef] [PubMed]
37. Wang, H.; Wang, H.; Shao, H.; Tang, X. Recent advances in utilizing transcription factors to improve plant abiotic stress tolerance by transgenic technology. *Front. Plant Sci.* **2016**, *7*, 67. [CrossRef]
38. van den Berg, N.; Mahomed, W.; Olivier, N.A.; Swart, V.; Crampton, B.G. Transcriptome analysis of an incompatible *Persea americana-Phytophthora cinnamomi* interaction reveals the involvement of SA- and JA-pathways in a successful defense response. *PLoS ONE* **2018**, *13*, e0205705. [CrossRef]
39. Moreno-Ortega, G.; Zumaquero, A.; Matas, A.; Nicholas, O.A.; van den Berg, N.; Palomo-Ríos, E.; Martínez-Ferri, E.; Pliego, C. Physiological and Molecular Responses of 'Dusa' Avocado Rootstock to Water Stress: Insights for Drought Adaptation. *Plants* **2021**, *10*, 2077. [CrossRef]
40. Granum, E.; Pérez-Bueno, M.L.; Calderón, C.E.; Ramos, C.; de Vicente, A.; Cazorla, F.M.; Barón, M. Metabolic responses of avocado plants to stress induced by *Rosellinia necatrix* analysed by fluorescence and thermal imaging. *Eur. J. Plant Pathol.* **2015**, *142*, 625–632. [CrossRef]
41. Guo, X.; Tseung, C.; Zare, A.; Liu, T. Hyperspectral image analysis for the evaluation of chilling injury in avocado fruit during cold storage. *Postharvest Biol. Technol.* **2023**, *206*, 112548. [CrossRef]

42. Torres-Madronero, M.C.; Rondón, T.; Franco, R.; Casamitjana, M.; González, J.T. Spectral characterization of avocado *Persea americana* Mill. cv. Hass using spectrometry and imagery from the visible to near-infrared range. *TecnoLógicas* **2023**, *26*, e208. [CrossRef]
43. Andrade-Hoyos, P. Selection of Avocado Rootstocks for Tolerance-Resistance to *Phytophthora cinnamomi* (Rands). Ph.D. Thesis, Colegio de Postgraduados, Montecillo, Mexico, 2012. Available online: http://colposdigital.colpos.mx:8080/xmlui/bitstream/handle/10521/1769/Andrade_Hoyos_P_DC_Fitopatolog%C3%ADa_2012.pdf?sequence=1&isAllowed=y (accessed on 1 August 2023).
44. Engelbrecht, J.; van den Berg, N. Expression of defense-related genes against *Phytophthora cinnamomi* in five avocado rootstocks. *S. Afr. J. Sci.* **2013**, *109*, 8. [CrossRef]
45. Sánchez-González, E.I.; Gutiérrez-Soto, J.G.; Olivares-Sáenz, E.; Gutiérrez-Díez, A.; Barrientos-Priego, A.F.; Ochoa-Ascencio, S. Screening progenies of Mexican race avocado genotypes for resistance to *Phytophthora cinnamomi* Rands. *HortScience* **2019**, *54*, 809–813. [CrossRef]
46. Mickelbart, M.V.; Arpaia, M.L. Rootstock influences changes in ion concentrations, growth, and photosynthesis of 'Hass' avocado trees in response to salinity. *J. Am. Soc. Hortic. Sci.* **2002**, *127*, 649–655. [CrossRef]
47. Calderón-Vázquez, C.; Durbin, M.L.; Ashworth, V.E.T.M.; Tommasini, L.; Meyer, K.K.T.; Clegg, M.T. Quantitative genetic analysis of three important nutritive traits in the fruit of Avocado. *J. Am. Soc. Hortic. Sci.* **2013**, *138*, 283–289. [CrossRef]
48. Jeudy, C.; Adrian, M.; Baussard, C.; Bernard, C.; Bernaud, E.; Bourion, V.; Busset, H.; Cabrera-Bosquet, L.; Cointault, F.; Han, S.; et al. RhizoTubes as a new tool for high throughput imaging of plant root development and architecture: Test, comparison with pot grown plants and validation. *Plant Methods* **2016**, *12*, 31. [CrossRef] [PubMed]
49. Martins, S.M.; de Brito, G.G.; Gonçalves, W.C.; Tripode, B.M.D.; Lartaud, M.; Duarte, J.B.; Morello, C.L.; Giband, M. PhenoRoots: An inexpensive non-invasive phenotyping system to assess the variability of the root system architecture. *Sci. Agric.* **2020**, *77*, e20180420. [CrossRef]
50. Coronado, V.; Barrera-Sánchez, C.F.; Guzmán, M. High-throughput phenotyping of maize roots using digital image analysis. *Cienc. Tecnol. Agropecu.* **2024**, *25*, e3312. [CrossRef]
51. Trachsel, S.; Kaeppler, S.M.; Brown, K.M.; Lynch, J.P. Shovelomics: High throughput phenotyping of maize (*Zea mays* L.) root architecture in the field. *Plant Soil* **2011**, *341*, 75–87. [CrossRef]
52. Colombi, T.; Kirchgessner, N.; Le Marié, C.A.; York, L.M.; Lynch, J.P.; Hund, A. Next generation shovelomics: Set up a tent and REST. *Plant Soil* **2015**, *388*, 1–20. [CrossRef]
53. Derebe, A.D.; Dema, M.W.; Roro, A.G. Impact of waterlogging stress on grafted avocado (*Persea americana*) seedlings growth and physiological performance. *Cogent Food Agric.* **2023**, *9*, 2261837. [CrossRef]
54. Marcelis, L.F.M.; Heuvelink, E.; Goudriaan, J. Modelling biomass production and yield of horticultural crops: A review. *Sci. Hortic.* **1998**, *74*, 83–111. [CrossRef]
55. Higashide, T.; Heuvelink, E. Physiological and morphological changes over the past 50 years in yield components in tomato. *J. Am. Soc. Hortic. Sci.* **2009**, *134*, 460–465. [CrossRef]
56. Homma, M.; Higashide, T.; Dong-Hyuk, A. Modeling short-term yield changes in sweet pepper based on dry matter production and fruit growth. *J. Am. Soc. Hortic. Sci.* **2023**, *148*, 292–303. [CrossRef]
57. Liu, Y.; Su, L.; Quanjiu, W.; Zhang, J.; Shan, Y.; Deng, M. Comprehensive and quantitative analysis of growth characteristics of winter wheat in China based on growing degree days. In *Advances in Agronomy*; Sparks, D.L., Ed.; Academic Press: Cambridge, MA, USA, 2020; Volume 59, pp. 237–273. [CrossRef]
58. Ferner, E.; Rennenberg, H.; Kreuzwieser, J. Effect of flooding on C metabolism of flood-tolerant (*Quercus robur*) and non-tolerant (*Fagus sylvatica*) tree species. *Tree Physiol.* **2012**, *32*, 135–145. [CrossRef]
59. Tardieu, F.; Granier, C.; Muller, B. Water deficit and growth. Coordinating processes without an orchestrator? *Curr. Opin. Plant Biol.* **2011**, *14*, 283–289. [CrossRef]
60. Stefaniak, E.; Tissue, D.T.; Dewar, R.C.; Medlyn, B.E. Optimal carbon storage during drought. *Tree Physiol.* **2024**, tpae032. [CrossRef] [PubMed]
61. Paula, S.; Pausas, J.G. Root traits explain different foraging strategies between resprouting life strategies. *Oecologia* **2011**, *165*, 321–331. [CrossRef] [PubMed]
62. Tariq, A.; Graciano, C.; Sardans, J.; Zeng, F.; Hughes, A.C.; Ahmed, Z.; Ullah, A.; Ali, S.; Gao, Y.; Peñuelas, J. Plant root mechanisms and their effects on carbon and nutrient accumulation in desert ecosystems under changes in land use and climate. *New Phytol.* **2024**, *242*, 916–934. [CrossRef]
63. Moreno, L. Respuestas de las plantas al estrés por déficit hídrico. Una revisión. *Agron. Colomb.* **2009**, *27*, 179–191.
64. Rocha-Arroyo, J.L.; Salazar-García, S.; Bárcenas-Ortega, A.E.; González-Durán, I.J.; Cossio-Vargas, L.E. Fenología del aguacate 'Hass' en Michoacán. *Rev. Mex. Cienc. Agrícolas* **2011**, *2*, 303–316.
65. Schaffer, B.; Whiley, A. Environmental physiology. In *The Avocado, Botany, Production and Uses*; Whiley, A., Schaffer, B., Wolstenholme, B., Eds.; CABI Publishing: London, UK, 2002; pp. 133–154.
66. Garzón, D.; Vélez-Sanchez, J.; Orduz, J. Efecto del déficit hídrico en el crecimiento y desarrollo de los frutos de naranja Valencia (*Citrus sinensis* Osbeck) en el piedemonte del Meta, Colombia. *Acta Agronómica* **2013**, *62*, 136–147.
67. Zyalalov, A.A. Water flows in higher plants: Physiology, evolution, and system analysis. *Russ. J. Plant Physiol.* **2004**, *51*, 547–555. [CrossRef]

68. Cushman, J.C. Osmoregulation in plants: Implications for agriculture. *Amer. Zool.* **2001**, *41*, 758–769. [CrossRef]
69. Campbell, J.B.; Wynne, R.H. *Introduction to Remote Sensing*, 5th ed.; The Guilford Press: New York, NY, USA, 2013; 717p.
70. Cañas-Gutiérrez, G.P.; Arango-Isaza, R.E.; Saldamanto-Benjumea, C.I. Microsatellites revealed genetic diversity and population structure in Colombian avocado (*Persea americana* Mill.) germplasm collection and its natural populations. *J. Plant Breed. Crop Sci.* **2019**, *11*, 106–119. [CrossRef]
71. Reyes-Herrera, P.H.; Muñoz-Baena, L.; Velásquez-Zapata, V.; Patiño, L.; Delgado-Paz, O.A.; Diaz-Diez, C.A.; Navas-Arboleda, A.A.; Cortés, A.J. Inheritance of Rootstock Effects in Avocado (*Persea americana* Mill.) cv. Hass. *Front. Plants Sci.* **2020**, *11*, 555071. [CrossRef] [PubMed]
72. Cañas-Gutiérrez, G.P.; Sepulveda-Ortega, S.; López-Hernández, F.; Navas-Arboleda, A.A.; Cortés, A.J. Inheritance of yield components and morphological traits in avocado cv. Hass from "Criollo" "Elite trees" via half-sib seedling rootstocks. *Front. Plants Sci.* **2022**, *13*, 43099. [CrossRef] [PubMed]
73. Dorado-Guerra, D.; Grajales-Guzmán, L.C.; Rebolledo-Roa, A. *Requerimientos Hídricos del Cultivo de Aguacate (Persea americana) Variedad Hass en Zonas Productoras de Colombia*; Corporación Colombiana de Investigación Agropecuaria: Mosquera, Colombia, 2016; 92p. Available online: https://editorial.agrosavia.co/index.php/publicaciones/catalog/download/14/12/115-1?inline=1?inline=1 (accessed on 16 November 2023).
74. UCV. *Métodos de Análisis de Suelos y Plantas Utilizados en el Laboratorio General de Suelos del Instituto de Edafología*; Cuadernos de Agronomía, Facultad de Agronomía, UCV: Maracay, Venezuela, 1993; Year 1, Number 6; 89p.
75. López-Calderón, M.J.; Estrada-Ávalos, J.; Rodríguez-Moreno, V.M.; Mauricio-Ruvalcaba, J.E.; Martínez-Sifuentes, A.R.; Delgado-Ramírez, G.; Miguel-Valle, E. Estimation of total nitrogen content in forage maize (*Zea mays* L.) using spectral indices: Analysis by random forest. *Agriculture* **2020**, *10*, 451. [CrossRef]
76. Shao, H.; Shi, D.; Shi, W.; Ban, X.; Chen, Y.; Ren, W.; Chen, F.; Mi, G. Genotypic difference in the plasticity of root system architecture of field-grown maize in response to plant density. *Plant Soil* **2019**, *439*, 201–217. [CrossRef]

Disclaimer/Publisher's Note: The statements, opinions and data contained in all publications are solely those of the individual author(s) and contributor(s) and not of MDPI and/or the editor(s). MDPI and/or the editor(s) disclaim responsibility for any injury to people or property resulting from any ideas, methods, instructions or products referred to in the content.

plants

MDPI

Article

Genome-Wide Identification and Expression Analysis of the Melon Aldehyde Dehydrogenase (ALDH) Gene Family in Response to Abiotic and Biotic Stresses

Dekun Yang [1,2,4,†], Hongli Chen [1,2,4,†], Yu Zhang [1,2,3], Yan Wang [1,2], Yongqi Zhai [1,2], Gang Xu [1,2], Qiangqiang Ding [1,2], Mingxia Wang [1,2], Qi-an Zhang [1,2], Xiaomin Lu [3,*] and Congsheng Yan [1,2,*]

[1] Institute of Vegetables, Anhui Academy of Agricultural Sciences, Hefei 230001, China
[2] Key Laboratory of Genetic Improvement and Ecophysiology of Horticultural Crop, Hefei 230001, China
[3] College of Agriculture, Anhui Science and Technology University, Fengyang 233100, China
[4] Anhui Society for Horticultural Science, Hefei 230001, China
* Correspondence: luxm@ahstu.edu.cn (X.L.); congshengyan@126.com (C.Y.)
† These authors contributed equally to this work.

Abstract: Through the integration of genomic information, transcriptome sequencing data, and bioinformatics methods, we conducted a comprehensive identification of the ALDH gene family in melon. We explored the impact of this gene family on melon growth, development, and their expression patterns in various tissues and under different stress conditions. Our study discovered a total of 17 ALDH genes spread across chromosomes 1, 2, 3, 4, 5, 7, 8, 11, and 12 in the melon genome. Through a phylogenetic analysis, these genes were classified into 10 distinct subfamilies. Notably, genes within the same subfamily exhibited consistent gene structures and conserved motifs. Our study discovered a pair of fragmental duplications within the melon ALDH gene. Furthermore, there was a noticeable collinearity relationship between the melon's ALDH gene and that of *Arabidopsis* (12 times), and rice (3 times). Transcriptome data reanalysis revealed that some ALDH genes consistently expressed highly across all tissues and developmental stages, while others were tissue- or stage-specific. We analyzed the ALDH gene's expression patterns under six stress types, namely salt, cold, waterlogged, powdery mildew, *Fusarium* wilt, and gummy stem blight. The results showed differential expression of *CmALDH2C4* and *CmALDH11A3* under all stress conditions, signifying their crucial roles in melon growth and stress response. RT-qPCR (quantitative reverse transcription PCR) analysis further corroborated these findings. This study paves the way for future genetic improvements in melon molecular breeding.

Keywords: ALDH gene family; melon; abiotic and biotic stress; RNA-seq

1. Introduction

Throughout their lifecycle, plants are subjected to various forms of abiotic and biological stresses. These stresses promptly induce the synthesis of reactive oxygen species (ROS) within the plants, subsequently leading to an accumulation of aldehydes [1]. Aldehydes, which are metabolic byproducts of carbohydrates, lipids, and amino acids, can, in appropriate quantities, positively influence the physiological metabolism of plants. However, excessive concentrations of aldehydes can cause cellular damage, disrupt metabolic processes, and lead to the formation of toxic substances detrimental to plant health, compromising their normal growth [2]. Hence, the selective removal and regulation of aldehyde concentrations within plants hold significant implications for their growth and development, mandating strict regulation [3].

Aldehyde dehydrogenase (ALDH), often referred to as the "aldehyde scavenger", is effective in eliminating active aldehyde molecules in plants [4]. ALDH is a category of enzymes that encode NAD(P)+-dependent reactions, showcasing a diversity of amino acid

sequences and incorporating different motifs such as the cysteine active site (PS00070), glutamic acid active site (PS00687), and the Rossmann fold [5]. To mitigate the damage inflicted by excessive aldehyde accumulation during plant growth, the ALDH gene is induced to express differently under stress, subsequently leading to a substantial increase in aldehyde dehydrogenase proteins [6]. Consequently, the toxic aldehydes generated due to stress are irreversibly oxidized into their non-toxic carboxylic acid counterparts, thus enhancing the plant's stress tolerance and reducing stress-induced damage. This indicates a critical detoxification mechanism in plants [7]. Additionally, ALDH is crucial for various metabolic processes in plants, including glycolysis, amino acid synthesis, and the production of carnitine [8]. Under osmotic stress, ALDH helps maintain cellular osmotic equilibrium in plants through the synthesis of osmoregulators [9].

Aldehyde dehydrogenase (ALDH) is predominantly found in both eukaryotes and prokaryotes. As the genome sequencing information for an ever-increasing number of species becomes available, the presence of ALDH genes in more species is being discovered. The ALDH Gene Naming Committee (ANGC) defines a classification system based on protein sequence similarity between a new gene and an identified gene. If this similarity is less than 40%, the gene is considered as part of a new family; if the similarity ranges between 40% and 60%, it is classified within a family; if the similarity exceeds 60%, it is allocated to a subfamily [10]. Currently, the identified ALDH genes are categorized into 24 families, namely ALDH1-ALDH24, with 14 families found in plants. These 14 include ALDH2, ALDH3, ALDH5, ALDH6, ALDH7, ALDH10, ALDH11, ALDH12, ALDH18, ALDH19, ALDH21, ALDH22, ALDH23, and ALDH24, with the last seven exclusive to plants [11,12]. Over recent years, we have seen an increasing number of ALDH genes being identified in various plants, each with varying quantities, such as 14, 20, 28, 29, 53, 19, 27, 23, 22, and 39 in *Arabidopsis* [5], rice [13], maize [14], tomato [15], soybean [16], sorghum [17], Chinese cabbage [18], grape [19], potato [20], and apple [21], respectively. These genes play a significant role in the regulation of stress response, growth, and development in plants, hence are critical for normal plant growth [22,23]. For instance, *AtALDH3I1* and *AtALDH7B4* in *Arabidopsis* are seen to reduce MDA (malondialdehyde) and lipid peroxidation when their expression is upregulated, improving the plant's tolerance to drought and salt stress [24]. Overexpression of *BrALDH7B2* in tobacco can enhance photosynthesis and reduce ROS production, thereby improving salt tolerance [25]. When wheat is subjected to drought and salt stress, *TraeALDH7B1-5A* is highly expressed in various parts of the plant, and overexpression of this gene in transgenic *Arabidopsis* significantly improves plant tolerance to drought stress [26]. Similarly, rice exhibited elevated expression levels of *OsALDH2*-4, *OsALDH3*-4, *OsALDH7*, *OsALDH18*-2, and *OsALDH12* when subjected to drought stress, surpassing control levels by twofold [13]. A Virus-Induced Gene Silencing (VIGS) experiment performed on the cotton genes *Gohir.A11G040800* and *Gohir.D06G046200* demonstrated increased sensitivity of the silenced plants to salt stress as compared to the control, indicating the potential involvement of these genes in cotton's salt stress response [27]. In soybeans, acetaldehyde dehydrogenase can reduce the content of toxic MDA (malondialdehyde), and overexpression of *ALDH3H1* increases soybean resistance to salt stress [28]. *ZmALDH9*, *ZmALDH13*, and *ZmALDH17* have been reported to participate in the maize response to drought stress and are involved in plant acid tolerance and pathogen infection response [14].

Cucumis melo L., a member of the genus Cucumis in the Cucurbitaceae family, is an annual horticultural crop of high economic worth, primarily due to its flavorful fruits and substantial nutritional value [29–31]. In 2012, the genome of Muskmelon DHL92 was sequenced by the Spanish Agricultural Genomics Research Center, paving the way for bioinformatics research related to melon [32]. As bioinformatics technology continued to advance, Ruggieri carried out an upgrade of the DHL92 genome to version V3.6.1 in 2018, resulting in an enhanced sequence and annotation information [33]. Later in 2019, Castanera further improved the V3.6.1 version of DHL92 to version V4.0 [34]. Exploiting the melon genome data, a substantial volume of transcriptome sequencing and

analysis has been executed by scholars [35]. This approach in transcriptomics research empowers the scientific community with a comprehensive understanding of relevant gene expression, allowing us to delve into the related metabolic networks and regulatory mechanisms at the transcription level [36]. The Cucurbitaceae genome database (CuGenDBv2, http://cucurbitgenomics.org/v2/, accessed 1 May 2024) has already made available a total of 41 published transcriptome data points related to melons. This wealth of data not only evidences the rapid progression in melon research but also facilitates the work of an increasingly large number of researchers. Through deep mining of the available transcriptome data, we can identify beneficial genes. In recent years, researchers worldwide have conducted numerous gene family studies, focusing on gene families such as LBD [37], SUN [38], and JMJ-C [39]. However, no research has yet been reported on the ALDH gene family in melon. In this bioinformatic analysis, we identified 17 ALDH genes in the melon genome using the available genomic data and conducted a thorough biogenic analysis, examining aspects such as chromosome localization, phylogeny, gene structure, and collinearity. To explore the expression patterns of the ALDH gene in different melon tissues under various stresses, we utilized published transcriptome data to analyze ALDH gene expression levels. The findings of this study establish a basis for future research on the ALDH gene family in melon and provide potential target candidate genes for resistance breeding in melon.

2. Results

2.1. Identification and Physicochemical Characteristics of the ALDH Family Members in Melon

This research identified 17 ALDH genes in the melon genome (DHL92V4) through the use of the hidden Markov model PF00171, and discovered conserved ALDH domains in Pfam, SMART, and NCBI conserved domain databases. An analysis of the physical and chemical properties of the ALDH family members in melon revealed that the smallest CDS gene was *CmALDH2B1* (1149 bp), while the largest was *CmALDH6B1* (3132 bp). The encoded amino acid length ranged from 382 (*CmALDH2B1*) to 1043 (*CmALDH6B1*); molecular weights fell between 41.81 kD (*CmALDH2B1*) and 114.38 kD (*CmALDH6B1*); and theoretical isoelectric point values varied from 5.32 (*CmALDH10A8*) to 8.89 (*CmALDH3H2*). Our instability index analysis indicated that only one ALDH gene in melon, *CmALDH6B1*, yielded a stable protein (instability coefficient > 40), while the rest were classified as unstable proteins (instability coefficient < 40). The aliphatic index (abundance and relative content of nonpolar amino acids in proteins) for the 17 ALDH genes spanned a range from 77.52 (*CmALDH6B1*) to 105.54 (*CmALDH18B2*). An evaluation of their average hydrophilic values revealed that 12 ALDH genes had discernible hydrophilic values (mean hydrophilic value < 0), with the remaining five classified as hydrophobic proteins. The mitochondria housed the most ALDH genes, with a total of six. This was followed by the chloroplast with five genes, the cytoplasm with four, and the nuclear and plasma membrane regions each containing one (Table 1).

Table 1. Information and physicochemical properties of 17 *CmALDH* members.

Gene Name	Locus Name	CDS Size (bp)	Number of Amino Acids (aa)	Molecular Weight (kDa)	TheoreticalpI	Instability Index	Aliphatic Index	Grand Average of Hydropathicity	Prediction of Subcellular Location
CmALDH2B1	*MELO3C004383*	1149	382	41.81	8.30	26.07	93.19	−0.022	Chloroplast
CmALDH2B2	*MELO3C017100*	1665	554	60.07	7.23	33.22	89.10	−0.084	Chloroplast
CmALDH2C4	*MELO3C025328*	1701	566	61.73	8.81	31.75	87.05	−0.069	Mitochondrial
CmALDH3F1	*MELO3C017542*	1395	464	51.87	8.76	37.35	97.93	−0.06	Cytoplasmic
CmALDH3F2	*MELO3C014601*	1446	481	54.04	8.55	39.02	95.90	−0.043	Plasma Membrane
CmALDH3H1	*MELO3C010494*	1296	431	47.24	8.11	34.49	104.29	0.046	Cytoplasmic
CmALDH3H2	*MELO3C010493*	1560	519	57.19	8.89	35.71	99.79	0.02	Mitochondrial
CmALDH5F1	*MELO3C019622*	1626	541	57.94	6.98	38.09	95.21	0.039	Chloroplast
CmALDH6B1	*MELO3C007705*	3132	1043	114.38	8.10	48.04	77.52	−0.38	Nuclear

Table 1. *Cont.*

Gene Name	Locus Name	CDS Size (bp)	Number of Amino Acids (aa)	Molecular Weight (kDa)	TheoreticalpI	Instability Index	Aliphatic Index	Grand Average of Hydro-pathicity	Prediction of Subcellular Location
CmALDH6B2	*MELO3C018583*	1614	537	57.55	6.47	34.29	90.63	0.041	Mitochondrial
CmALDH7B1	*MELO3C024345*	1365	454	48.7	6.19	37.34	96.17	0.085	Chloroplast
CmALDH10A8	*MELO3C017125*	1512	503	54.56	5.32	25.17	92.94	−0.001	Cytoplasmic
CmALDH11A3	*MELO3C004430*	1620	539	58.48	7.60	37.92	91.37	−0.002	Chloroplast
CmALDH12A1	*MELO3C002203*	1620	539	60.37	6.33	39.65	95.45	−0.09	Mitochondrial
CmALDH18B1	*MELO3C009229*	1941	646	69.86	5.45	34.89	104.78	−0.032	Cytoplasmic
CmALDH18B2	*MELO3C008245*	2154	717	77.67	6.20	32.92	105.54	−0.096	Mitochondrial
CmALDH22A1	*MELO3C021272*	1815	604	66.88	7.20	36.64	92.33	−0.032	Mitochondrial

2.2. Chromosome Distribution of Melon ALDH Genes

Utilizing the location information of ALDH gene family members on melon chromosomes, a distribution map of the ALDH gene in melon was constructed using TBtools software 2.136 (Figure 1). The findings revealed that ALDH genes were present on all chromosomes except for 6, 9, and 10, which lacked these genes, and a certain degree of variation in distribution quantity. For instance, the highest number of distributed genes was found on chromosomes 2 and 7, with three on each. Conversely, chromosomes 3, 4, 8, and 12 harbored the fewest genes, each with only one. This suggests that chromosomes 2 and 7 may play a significant role in the evolution of ALDH in melon. By observing gene positioning on the chromosomes, it was observed that ALDH genes in melon predominantly resided on the termini of chromosomes, with some located centrally. Furthermore, one pair of tandem repeat genes and fragment repeat genes, namely *CmALDH3H1/CmALDH3H2* and *CmALDH18B2/CmALDH18B1*, respectively, were identified within the 17 ALDH genes of melon.

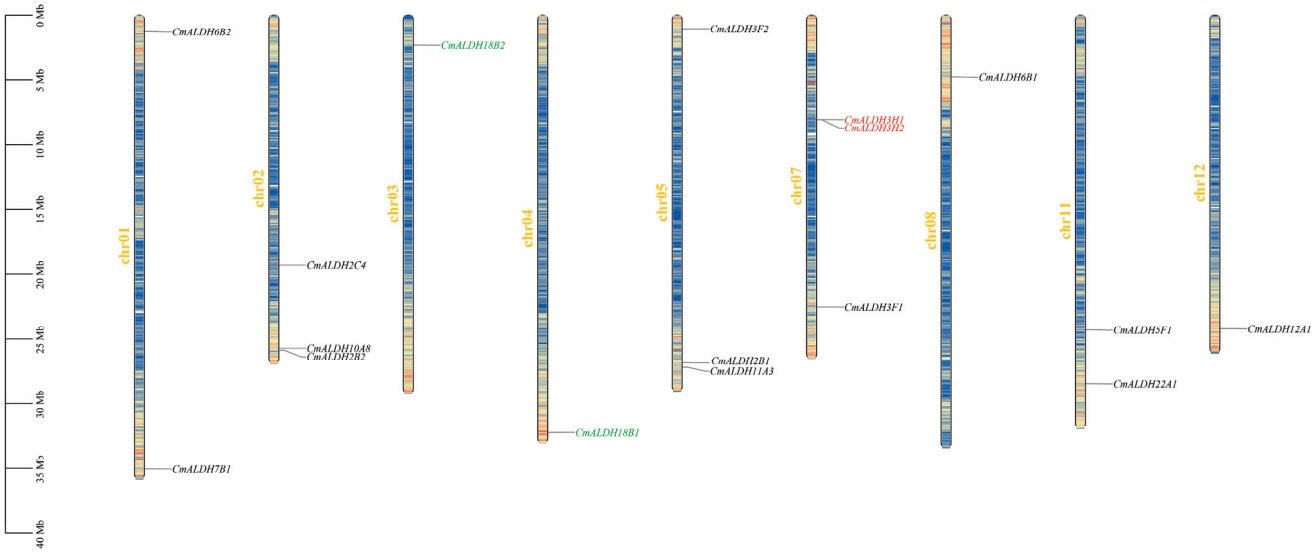


Figure 1. Distribution of the melon ALDH family genes on the chromosomes. The genes marked in red color were tandem duplication gene pairs, and the genes marked in green color were segmental duplication genes. The blue part on the chromosome indicates a small number of distributed genes, the yellow part indicates a moderate number of distributed genes, while the red part indicates a large number of distributed genes.

2.3. Phylogenetic Tree Analysis of ALDH Family Genes

To elucidate the phylogenetic relationship of ALDH genes in melon, we procured the protein sequences of acknowledged ALDH genes from *Arabidopsis* and rice genome databases. These sequences were aligned with the 17 ALDH protein sequences in melon to

facilitate phylogenetic analysis and construct a phylogenetic tree (Figure 2). Subsequently, melon's ALDH genes were partitioned into 10 subfamilies based on *Arabidopsis* and rice groupings. Family 3 was identified as the most abundant, containing four melon ALDH genes, followed by Family 2 with three. Aside from Family 6 and 18, which each comprised two melon ALDH genes, the remaining six subfamilies each held a single ALDH gene.

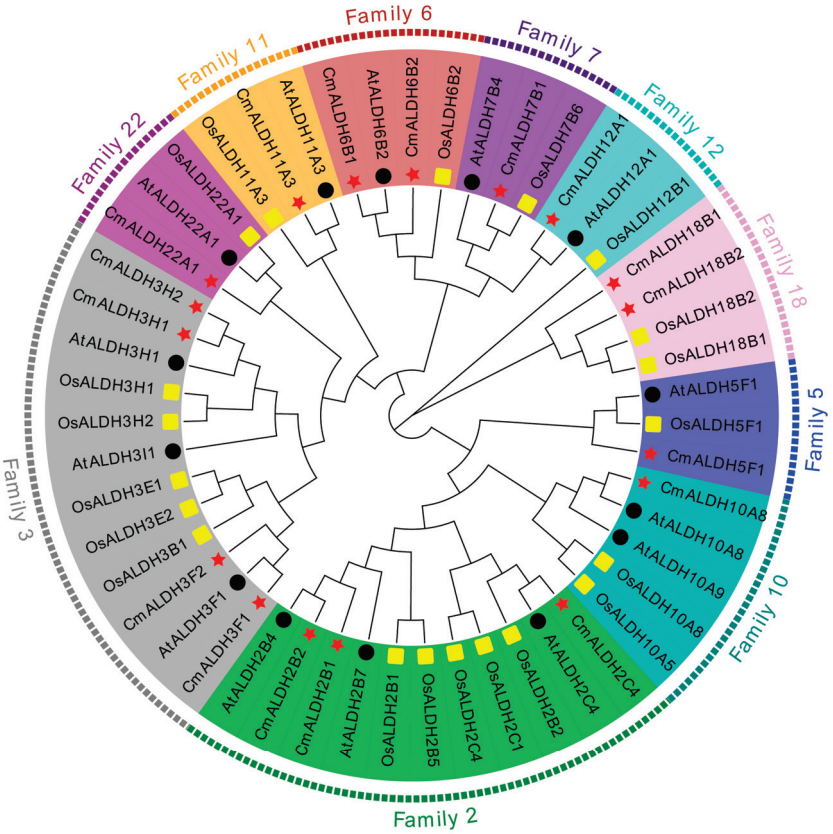


Figure 2. Phylogenetic relationships of melon, rice, and *Arabidopsis* ALDH proteins. The red star represents the protein in melon. The black circle represents the protein in *Arabidopsis*. The yellow rectangle represents the protein in rice.

We discovered seven pairs of direct homologous genes between the ALDH family of melon and *Arabidopsis*, namely *CmALDH11A3*/*AtALDH11A3*, *CmALDH10A8*/*AtALDH10A8*, *CmALDH2C4*/*AtALDH2C4*, *CmALDH2B2*/*AtALDH2B4*, *CmALDH12A1*/*AtALDH12A1*, *CmALDH6B1*/*AtALDH6B2*, and *CmALDH3F1*/*AtALDH3F1*. Additionally, we found one family of orthologous genes between melon and rice ALDH, specifically *CmALDH7B1*/*OsALDH7B6*. In the melon ALDH gene family, only one pair of paralog genes, *CmALDH3H2*/*CmALDH3H1*, was identified. Evolutionarily related ALDH genes, which exhibit similar biological functions and gene structures, were noted. Future studies can predict the biological function of the melon ALDH gene based on previously reported ALDH genes in *Arabidopsis* and rice.

2.4. Gene Structure and Conserved Motif Analysis of Melon ALDH Genes

We conducted a phylogenetic tree construction using the protein sequences from 17 melon ALDH genes, underpinned by gene structure and conserved motif analysis in correlation with melon genome files (Figure 3). The findings demonstrated that melon's ALDH gene family could be segregated into 10 distinct subfamilies. ALDH genes originating from the same subfamily exhibited a tendency to cluster, which essentially aligns with the ALDH gene clustering outcomes from melon, *Arabidopsis*, and rice (Figure 2).

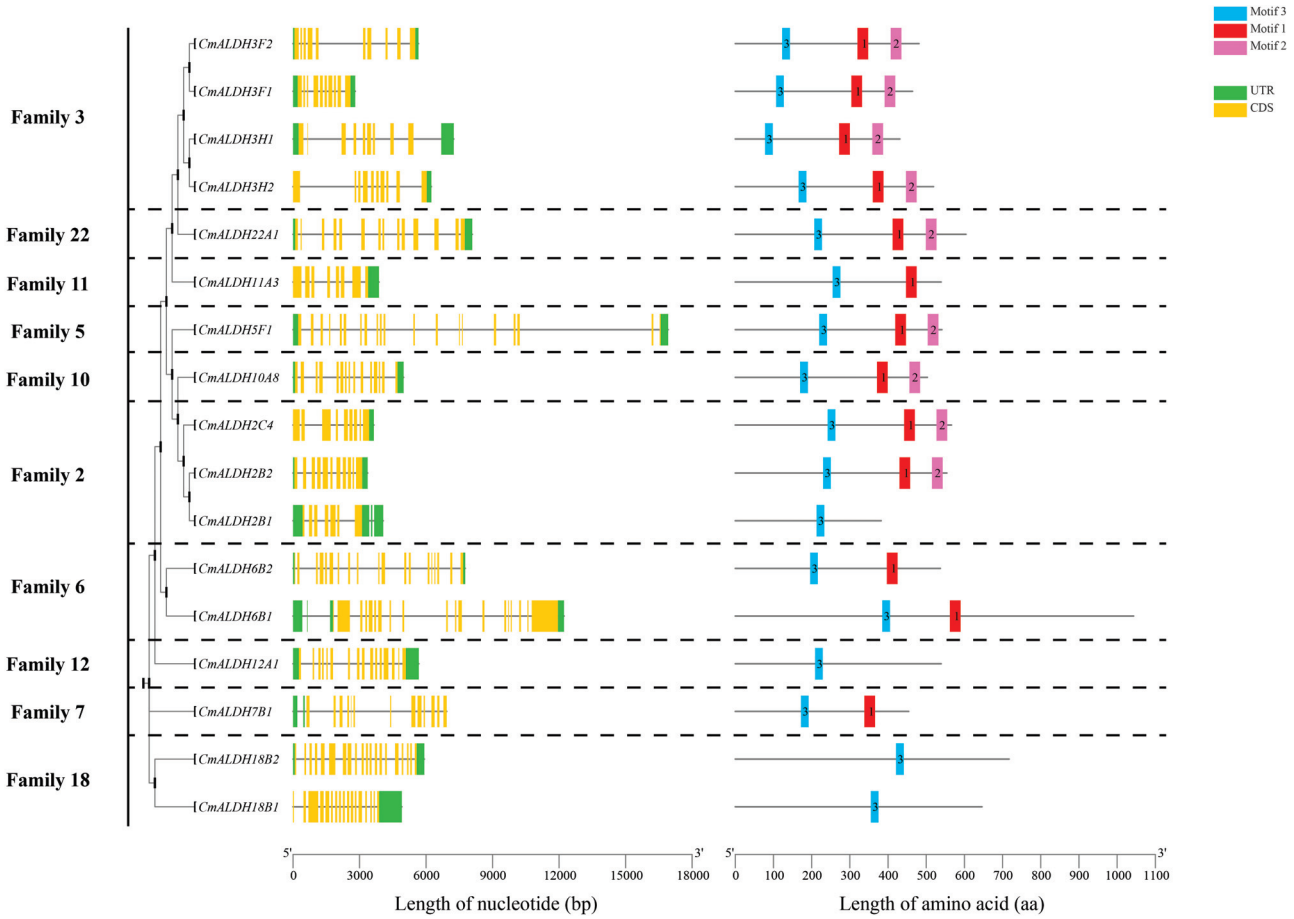


Figure 3. Gene structures and protein motifs of the melon ALDH gene family.

In the context of multi-gene families, the structural disparities in exon-introns within the same family serve as pivotal factors in the evolutionary process. As per the gene structure of ALDH genes in the melon family, the exon count fluctuates between 7 and 20. The genes *CmALDH5F1* and *CmALDH18B2* are characterized by the highest number of exons, tallying at 20, succeeded by *CmALDH6B2* and *CmALDH6B1* from the same subfamily, each having 19 exons. The lowest count is attributed to *CmALDH2B1*, with a mere 7 exons. Genes within the same subfamily generally exhibit similarities in their exon-intron structure. The resemblance in these gene structures, coupled with high sequence homology, suggests that gene duplication events transpired in the evolution of the melon's ALDH gene family.

Conserved motif analysis revealed that the motif sequences of Families 3, 22, 11, 5, 10, and 2 were nearly identical, in the sequence of 3, 1, and 2. The motifs in Family 6 and Family 7 displayed the same sequence, 3, 1. Similarly, the motifs in Family 12 and Family 18 followed the same sequence, incorporating only motif 3. This suggests that ALDH genes within these similar subfamilies could potentially share similar biological functions.

2.5. Synteny Analysis of ALDH Genes Among Melon, Arabidopsis, and Rice

To deepen our understanding of the evolutionary details of ALDH genes in melon, we conducted a synteny analysis of these genes (Figure 4). Our findings revealed that, out of the 17 ALDH genes in melon, there was only one pair of repeated gene fragments, specifically *CmALDH18B2/CmALDH18B1*. Nine melon ALDH genes (*CmALDH6B2*, *CmALDH7B1*, *CmALDH2C4*, *CmALDH2B2*, *CmALDH18B2*, *CmALDH3H1*, *CmALDH3F1*, *CmALDH5F1*, *CmALDH22A1*) displayed twelve types of collinearity relationships with the twelve genes in *Arabidopsis* (*AtALDH2B7*, *AtALDH3H1*, *AtALDH7B4*, *AtALDH10A8*, *AtALDH5F1*, *AtALDH6B2*, *P5CS1*, *AtALDH22A1*, *AtALDH2C4*, *AtALDH10A9*, *P5CS2*,

AtALDH3F1). We also discovered three collinearity relationships between three melon ALDH genes (*CmALDH7B1*, *CmALDH10A8*, *CmALDH18B2*) and three rice ALDH genes (*OsALDH18B2*, *OsALDH10A5*, *OsALDH7B6*). However, the remaining six ALDH genes in melon (*CmALDH3F2*, *CmALDH2B1*, *CmALDH11A3*, *CmALDH3H2*, *CmALDH6B1*, *CmALDH12A1*) exhibited no collinearity with those in Arabidopsis and rice. This indicates that these genes demonstrate a certain degree of conservation within the ALDH family.

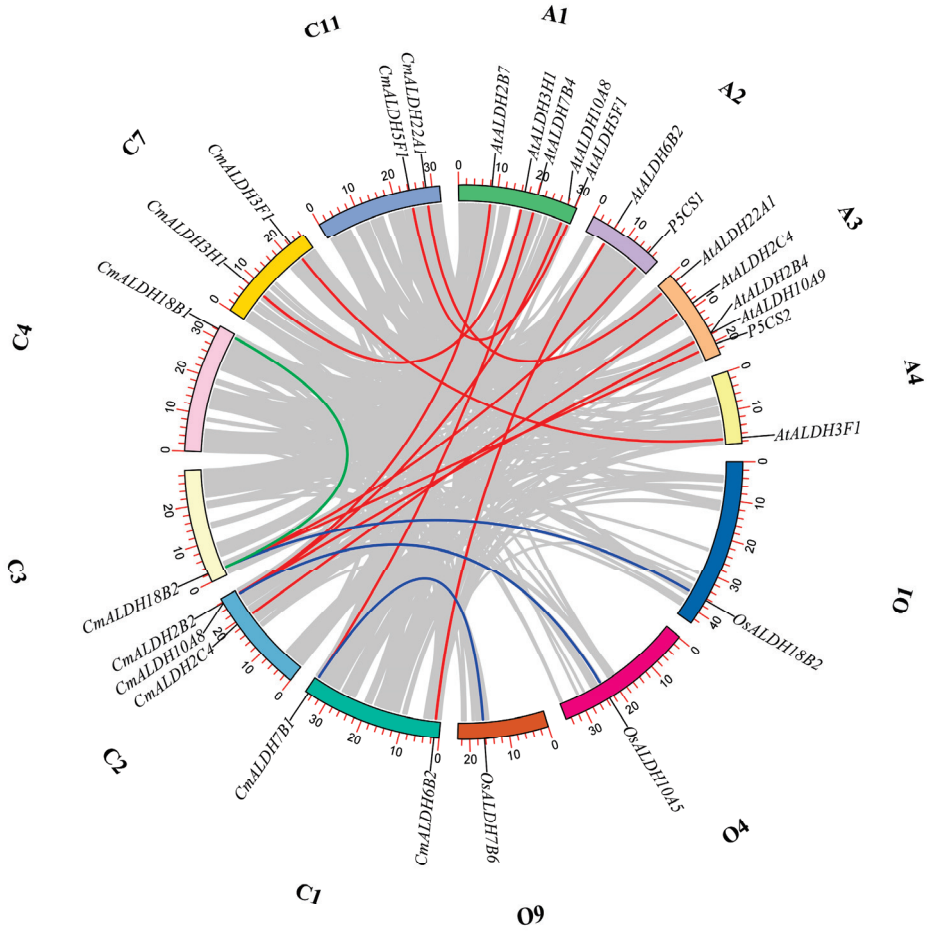


Figure 4. Assessment of the ALDH gene duplication between melon, *Arabidopsis*, and rice. The green lines represent the segmentally duplicated ALDH genes in melon. The red lines represent the orthologous relationships of the ALDH genes between melon and *Arabidopsis*. The blue lines represent the orthologous relationships of the ALDH genes between melon and rice. The gray lines represent the orthologous relationships of the genes between melon, *Arabidopsis*, and rice. The scale on the chromosome represents the physical location.

2.6. Analysis of the Cis-Acting Elements in Melon ALDH Genes

Based on the cis-acting element analysis, we identified 12 distinct cis-acting elements in the promoter sequences of the melon ALDH genes (Figure 5A). Light-responsiveness elements constituted the majority, accounting for 45.6% of the total, and were uniformly distributed among all 17 ALDH genes in melon. The second most prevalent were the hormone-related cis-acting elements (abscisic acid responsiveness, MeJA-responsiveness, and salicylic acid responsiveness), contributing to 28.6% of the total, following photoresponsive elements (Figure 5B). Additionally, we examined elements related to stress response and endosperm expression. Our findings suggest that the ALDH gene could respond to a range of hormones and stress conditions. Thus, the identified response elements could significantly impact the stress response capability of the ALDH gene under stress conditions.

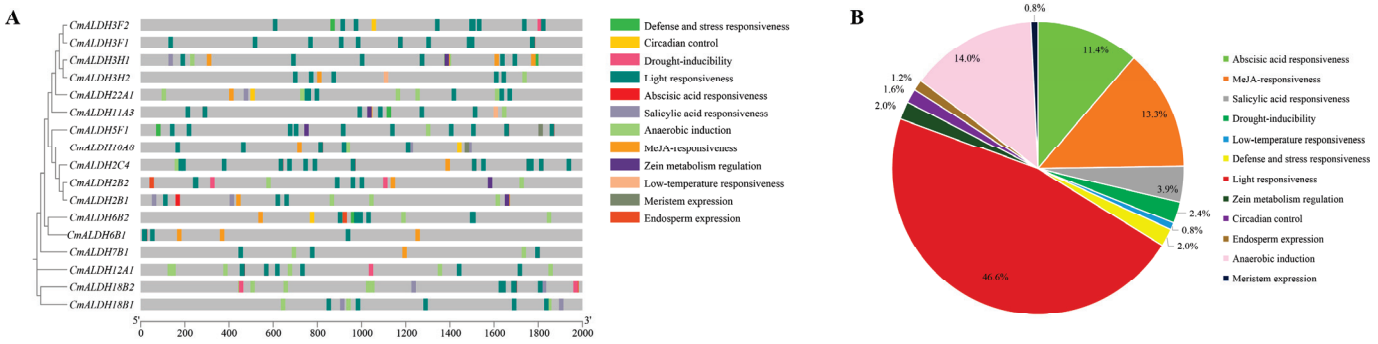


Figure 5. *Cis*-regulatory elements in promoter region of melon ALDH genes (**A**) and their proportions (**B**).

2.7. Tissue-Specific Expression Analysis of Melon ALDH Genes

Utilizing previously published transcriptome data from an array of melon tissues and fruit at different developmental stages, we were able to analyze the tissue-specific expression profiles of the melon's ALDH gene family members during various stages of development (Figure 6). The histospecificity analysis of the ALDH gene family revealed high expression levels of *CmALDH6B2* and *CmALDH10A8* across all organs. Notably, *CmALDH3H2* is expressed specifically in male flowers and showed nearly an 8-fold greater expression level compared to other organs. This is similar to *CmALDH2C4* and *CmALDH18B1*, which presented specific expression only in the roots and male flowers. Conversely, *CmALDH18B2* and *CmALDH22A1* exhibited low expression in male flowers, but high expression in other organs. *CmALDH7B1* and *CmALDH2B1* were highly expressed in all organs except the ovary, where expression levels were significantly lower. The expression of *CmALDH5F1* and *CmALDH12A1* were more evenly distributed across all organs. Interestingly, *CmALDH11A3* displayed significantly higher expression levels in both male and female flowers than other organs, which suggests it may play a role in the formation of melon flower organs and fruits. Among the 17 ALDH genes, only *CmALDH6B1* showed no specific organ expression and maintained low expression levels, suggesting this gene is not involved in the growth and development of melon organs.

The expression profiles of ALDH family genes during different stages of fruit development showed that *CmALDH6B2* and *CmALDH10A8* were highly expressed at all four stages (growing, ripening, climacteric, and post-climacteric). This pattern, combined with their organ-specific expression, suggests these genes participate in melon organ development and have a role in fruit ripening and development. *CmALDH7B1*, *CmALDH3H1*, *CmALDH5F1*, and *CmALDH12A1* also displayed high expression levels in all four stages, second only to *CmALDH6B2* and *CmALDH10A8*. However, *CmALDH2C4*, *CmALDH18B1*, *CmALDH3F2*, and *CmALDH3F1* exhibited very low or no expression throughout the entire fruit development stage. *CmALDH3H2* and *CmALDH2B1* showed stage-specific expression during the ripening and growing stages, respectively, while *CmALDH2B2* was significantly more expressed during the growing stage than at other stages. No expression was observed during the climacteric and post-climacteric stages, suggesting this gene may be involved only in the growth and ripening of melon fruits.

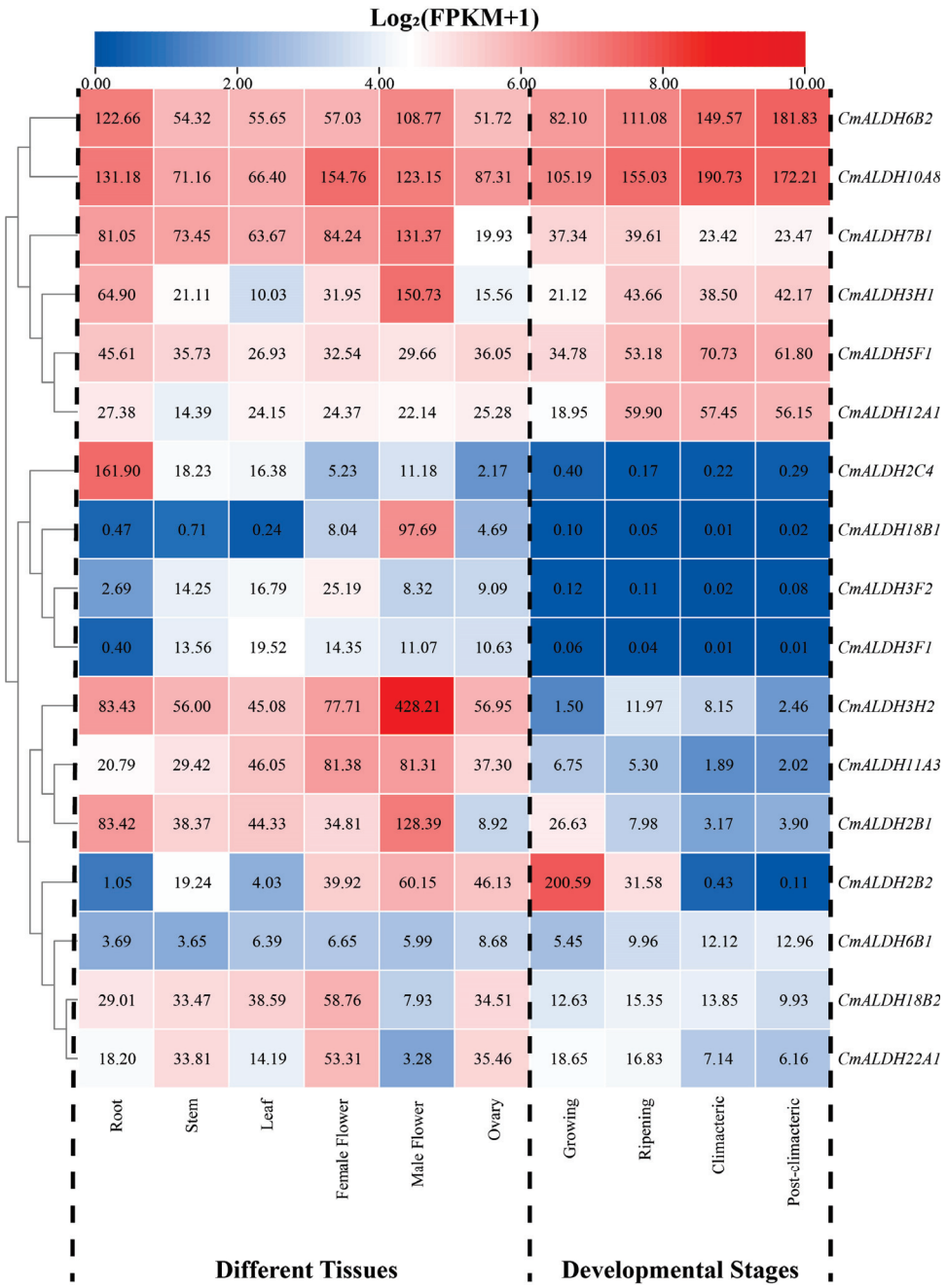


Figure 6. Expression analysis of melon ALDH genes in different tissues and developmental stages.

2.8. Expression Patterns Analysis of Melon ALDH Genes Under Abiotic Stresses

To investigate the expression patterns of the ALDH gene in melon under varying abiotic stress conditions, we used published transcriptome sequencing data from melon studies conducted under salt, cold, and waterlogged stress. This allowed us to analyze ALDH gene expression levels under these stresses (Figure 7).

Under salt stress (Figure 7A), only five ALDH genes—*CmALDH22A1*, *CmALDH6B1*, *CmALDH3F2*, *CmALDH3F1*, and *CmALDH3H2*—were not differentially expressed compared to the control. Conversely, *CmALDH2B2*, *CmALDH2C4*, and *CmALDH11A3* showed significant downregulation in both salt-sensitive and salt-resistant materials. Other genes, particularly *CmALDH2B1* and *CmALDH7B1*, were significantly upregulated in these same materials.

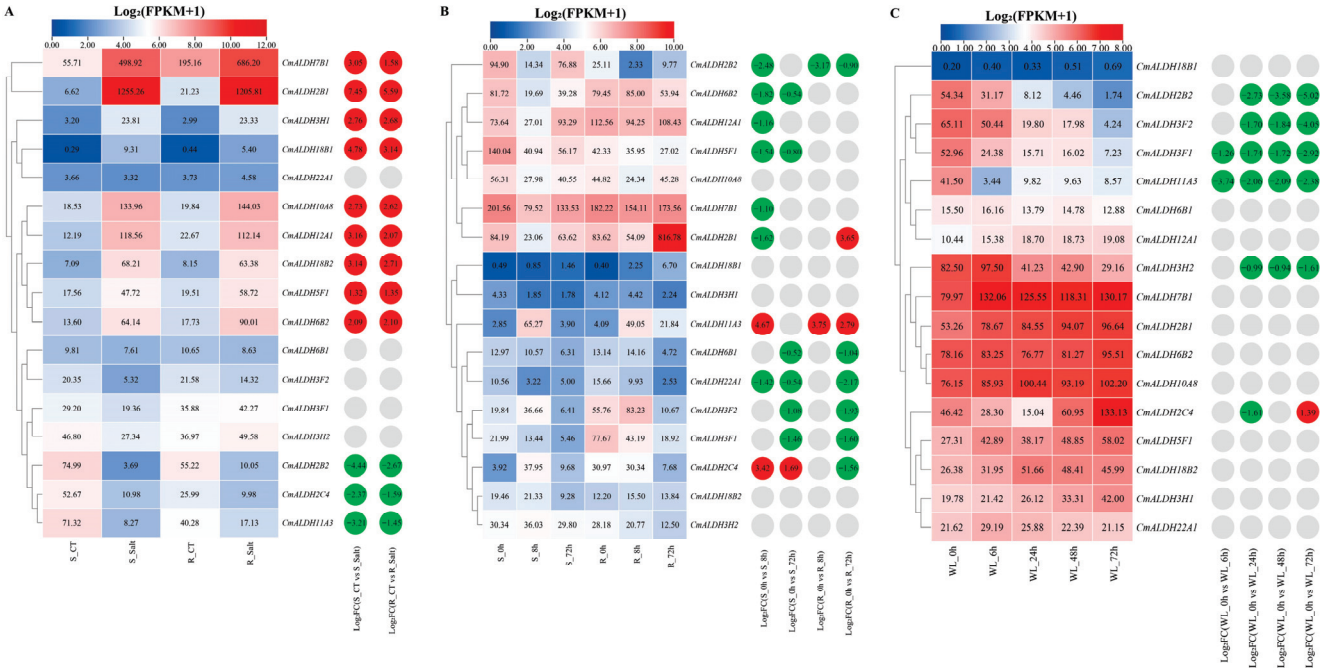


Figure 7. The expression patterns of melon ALDH genes in response to abiotic stresses. (**A**) The expression heatmap of melon ALDH genes in response to salt stress. S: susceptible plant; R: resistant plant; CT: control treatment; Salt: salt treatment. (**B**) The expression heatmap of melon ALDH genes in response to cold stress. S: susceptible plant; R: resistant plant; 0 h, 8 h and 72 h were treatment for 0 h, 8 h and 72 h. (**C**) The expression heatmap of melon ALDH genes in response to waterlogging stress. 0 h, 6 h, 24 h, 48 h and 72 h were treatment for 0 h, 6 h, 24 h, 48 h and 72 h hours. The data in the left expression heatmaps are the original FPKM values; the data in the right boxes are log2 (fold change) values highlighted by red (upregulation) and green (downregulation) colors.

In response to cold stress (Figure 7B), only *CmALDH11A3* was significantly upregulated in both cold-sensitive and resistant materials when compared with the control. *CmALDH2B1* showed a downregulation in sensitive materials and an upregulation in resistant materials, whereas *CmALDH2C4* exhibited an opposed pattern of upregulation in sensitive and downregulation in resistant materials. Other genes—*CmALDH2B2*, *CmALDH6B1*, *CmALDH22A1*, *CmALDH3F2*, and *CmALDH3F1*—were significantly downregulated in both types of materials. However, downregulated expressions of *CmALDH6B2*, *CmALDH12A1*, *CmALDH5F1*, and *CmALDH7B1* were only observed in sensitive materials.

When under waterlogging stress (Figure 7C), *CmALDH2C4* was significantly downregulated after 24 h of treatment, but showed a significant upregulation after 72 h. Both *CmALDH3F1* and *CmALDH11A3* showed significant downregulation in all four treatments. *CmALDH2B2*, *CmALDH3F2*, and *CmALDH3H2* did not present differential expression at the 6 h mark but demonstrated downregulation at 24, 48, and 72 h.

2.9. Expression Patterns Analysis of Melon ALDH Genes Under Biotic Stresses

To comprehend the expression patterns of melon under various biological stresses, we reanalyzed the published transcriptomic data of melon under powdery mildew, *Fusarium* wilt, and gummy stem blight stress. This reanalysis was performed in conjunction with the melon genome data (DHL92 V4) using TBtools software to generate expression heat maps (Figure 8).

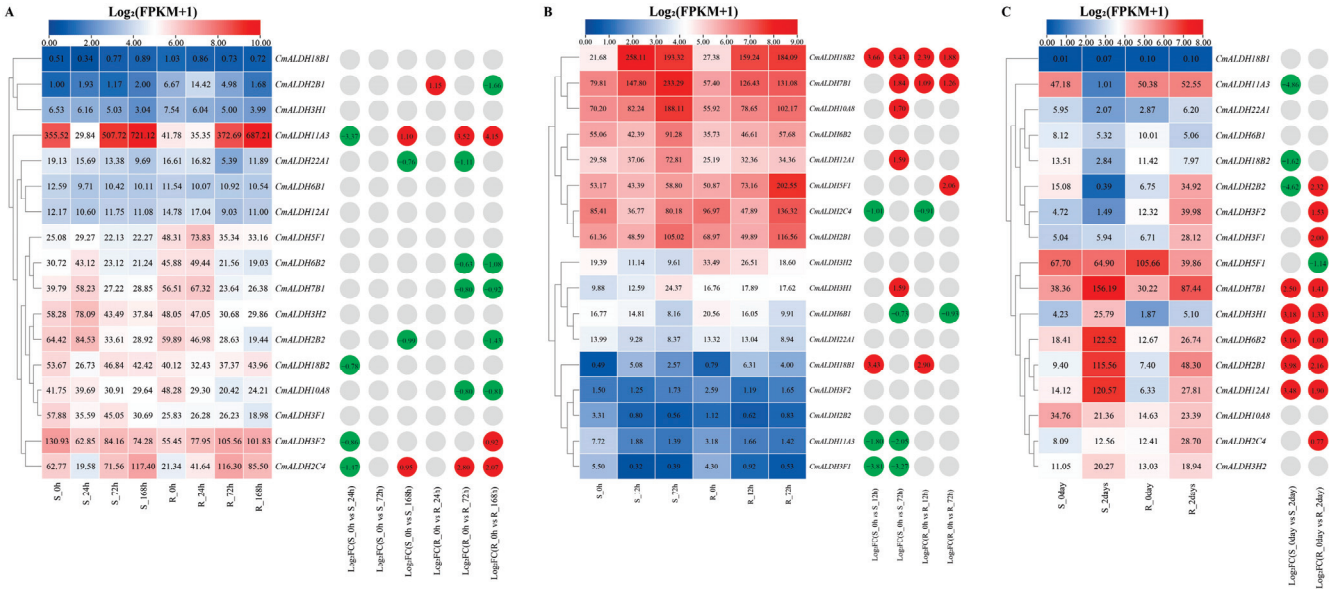


Figure 8. The expression patterns of melon ALDH genes in response to biotic stresses. (**A**) The expression heatmap of melon ALDH genes in response to downy mildew stress. S: susceptible plant; R: resistant plant; 0 h, 24 h, 72 h and 168 h were 0, 24, 72, and 168 h post-inoculation, respectively. (**B**) The expression heatmap of melon ALDH genes in response to *Fusarium* wilt stress. S: susceptible plant; R: resistant plant; 0 h, 12 h, and 72 h were 0, 12, and 72 h post-inoculation, respectively. (**C**) The expression heatmap of melon ALDH genes in response to gummy stem blight stress. S: susceptible plant; R: resistant plant; 0 day and 2 days were 0 and 2 days post-inoculation, respectively. The data in the left expression heatmaps are the original FPKM values; the data in the right boxes are log2 (fold change) values highlighted by red (upregulation) and green (downregulation) colors.

During powdery mildew stress (Figure 8A), *CmALDH11A3* and *CmALDH2C4* exhibited identical differential expression patterns. Their expression levels significantly decreased and were downregulated after 24 h of treatment in the sensitive material, then increased significantly and were upregulated following 168 h of treatment. *CmALDH3F2* showed downregulation in sensitive materials but upregulation in resistant materials. *CmALDH2B1* demonstrated a conflux of both upregulated and downregulated expressions in resistant materials. Both *CmALDH22A1* and *CmALDH2B2* were significantly downregulated in both sensitive and resistant materials, while *CmALDH18B2* showed significant downregulation only in sensitive materials. Conversely, *CmALDH6B2*, *CmALDH7B1*, and *CmALDH10A8* were significantly downregulated in resistant materials.

Under *Fusarium* wilt stress (Figure 8B), compared with the control materials, *CmALDH18B2*, *CmALDH7B1*, and *CmALDH10A8* showed the highest expression and significantly upregulated in both sensitive and resistant materials. Similarly, *CmALDH18B1* was significantly upregulated in both sensitive and resistant materials. In contrast, *CmALDH2C4* and *CmALDH6B1* demonstrated significant downregulation in both types of materials. *CmALDH10A8*, *CmALDH12A1*, and *CmALDH3H1* were significantly upregulated in sensitive materials, while *CmALDH11A3* and *CmALDH3F1* were significantly downregulated. Notably, *CmALDH5F1* was only significantly upregulated in resistant materials.

Under gummy stem blight stress (Figure 8C), five ALDH genes—*CmALDH7B1*, *CmALDH3H1*, *CmALDH6B2*, *CmALDH2B1*, and *CmALDH12A1*—were significantly upregulated in both sensitive and resistant materials compared with control materials. Excluding *CmALDH3H1*, the expression levels of the other four ALDH genes showed significant changes in sensitive materials. *CmALDH2B2* was downregulated in sensitive materials yet significantly upregulated in resistant ones. Conversely, *CmALDH11A3* and *CmALDH18B2* were significantly downregulated in sensitive materials. *CmALDH3F2*, *CmALDH3F1*, and

CmALDH2C4 were significantly upregulated in resistant materials. Lastly, *CmALDH5F1* demonstrated a significant downregulation in resistant materials.

2.10. Regulation Patterns of Melon ALDH Genes Under Stresses

The expression profiles of the melon ALDH gene family under various stresses were utilized to summarize and label the stress response of the ALDH gene family, and a heat map of ALDH genes under differing stresses was created using TBtools software (Figure 9). As indicated in the figure, 17 ALDH genes in melon participate in the plant's stress response to varying extents. Notably, the ALDH genes *CmALDH2C4* and *CmALDH11A3* exhibited significant differential expression in both abiotic and biotic stress scenarios. This indicates that these two genes are capable of initiating a positive response under stress conditions. Hence, they may serve as key candidate genes for future studies examining melon's stress responses. Interestingly, while *CmALDH2B2* did not exhibit different expression under *Fusarium* wilt stress, it was significantly downregulated under all other five forms of stress. Some ALDH genes in melon, such as *CmALDH3H2*, only showed downregulation under waterlogging stress conditions. In the context of abiotic stress, most of the 17 ALDH genes were upregulated under salt stress, but downregulated under cold and waterlogging stress. Under biological stress, the majority of these ALDH genes were downregulated in response to powdery mildew stress but upregulated in response to *Fusarium* wilt and gummy stem blight stress. These findings highlight the differential expression of melon's ALDH gene family under abiotic and biological stresses, providing a favorable starting point for further research into the molecular biological functions of the ALDH gene family in melons.

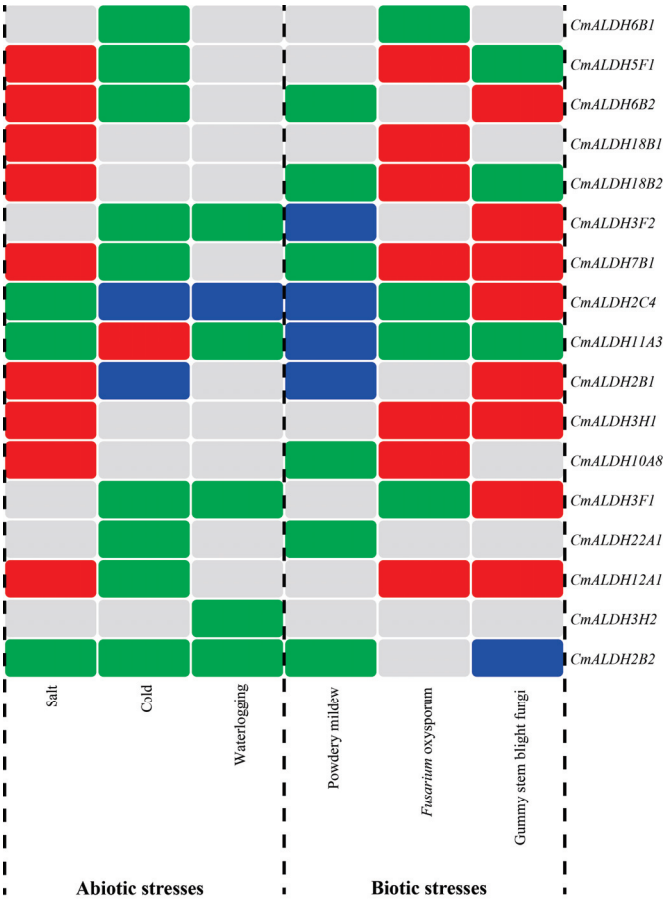


Figure 9. An expression pattern heatmap of the melon ALDH genes under abiotic and biotic stresses. The gray color represents unchanged expression, red represents upregulated expression, green represents downregulated expression, and blue represents both upregulated and downregulated expression.

2.11. RT-qPCR Analysis of the Melon ALDH Gene Family

To evaluate the precision of our transcriptomic data analysis, we selected all genes from the *CmALDH* gene family. We assessed the impact of salt stress treatment (300 mM) at varying time intervals (0 h, 3 h, 6 h, 12 h, and 24 h) on their expression levels using the RT-qPCR method (Figure 10). In this investigation, the transcriptomic data was salt stress treatment after 24 h. According to our RT-qPCR test results, the expression patterns were generally consistent for the two sets of data we focused on. Genes such as *CmALDH3F1*, *CmALDH6B1*, *CmALDH6B2*, *CmALDH7B1*, *CmALDH12A1* and *CmALDH18B1*, peaked in expression after 6 h of NaCl treatment (with CK serving as the control), showing significant differences in comparison to the control. Conversely, other genes, including *CmALDH2B1*, *CmALDH2C4*, *CmALDH3F2*, *CmALDH3H1*, *CmALDH3H2*, *CmALDH10A8*, and *CmALDH18B2* exhibited their highest expression levels and significant differences at the 12 h mark. Of these, the gene *CmALDH2B2* displayed a substantial decrease in expression following stress treatment, reaching its lowest point after 9 h, before demonstrating an increasing trend. The expression level of *CmALDH2B1* showed a rising pattern post-stress, exhibiting significant differences compared to the control. This increase was particularly notable at the 12 h point, after which it started to decrease.

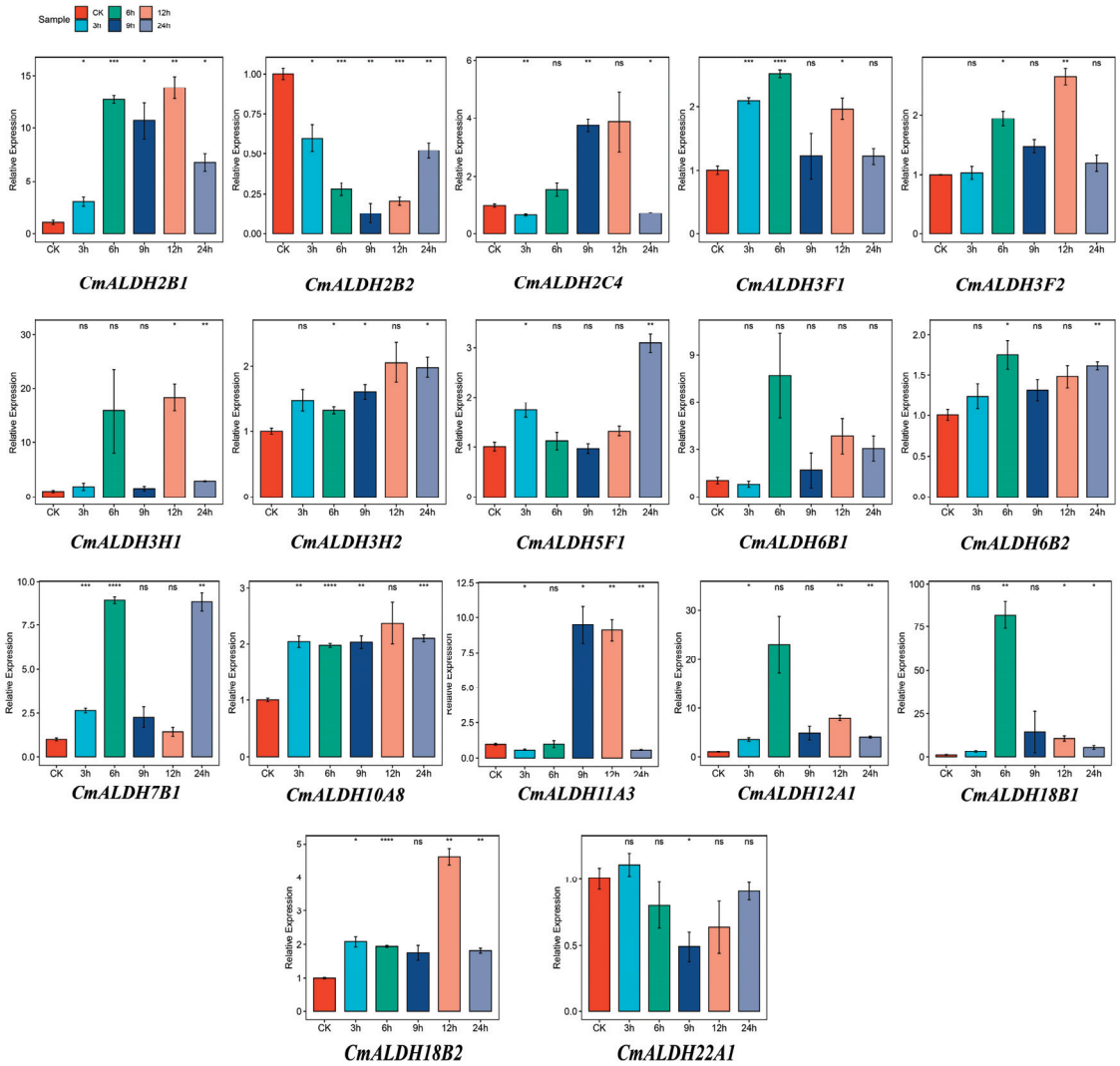


Figure 10. Relative expression level of 17 *CmALDH* genes in response to salt treatments. Error bars are the average error of three biological replicates. Asterisks are used to indicate the significant degree of the expression level compared to the value of the control (* $p < 0.05$, ** $p < 0.01$, *** $p < 0.001$, **** $p < 0.0001$).

3. Discussion

Research into plant responses to both abiotic and biotic stresses has consistently attracted the attention of scientists. Stress has the potential to not only diminish the yield and quality of food crops [40] but also, in severe instances, result in plant death, thereby incurring substantial losses in agricultural production [41]. The ALDH enzyme, aside from its protective and detoxifying influence, also plays a crucial role in plant stress response [42]. The most prominently studied gene within the ALDH gene family is the betaine aldehyde dehydrogenase gene. This gene, belonging to the ALDH10 family, is a well-established osmoregulator and has demonstrated an effective response to adversity. It becomes upregulated in response to both drought and salt stress, enhancing plant resilience to these stresses [43]. As scientific and technological progress has allowed for the publication of an increasing amount of genome and transcriptome sequencing information, it has become particularly valuable to utilize this data to identify stress-related genes. This approach not only increases the usefulness of the existing data but also holds significant implications for related research [44]. Melon, the second cucurbit crop to have its whole genome sequenced (as early as 2012) [32], has yet to have any studies published on its ALDH gene family. This lack of information significantly hinders research into melon's biological functions linked to ALDH genes. Therefore, this study aims to fill this gap by conducting a whole genome identification and expression pattern analysis of the ALDH gene family in melons. The results will provide a theoretical framework for future ALDH gene family studies in melons and contribute to the identification of advantageous genes for resistance breeding in melons.

In this study, we identified 17 ALDH genes in the melon genome using the latest genomic information and advanced bioinformatics analysis methods. These findings differ from the number of ALDH genes identified in other species, which may be due to variations in the number of ALDH gene family members across different species and distinct stages of evolution [45]. It could also be linked to the specific characteristics of the melon's chromosomes and genome [46]. In our phylogenetic analysis, these 17 melon ALDH genes were classified into 10 subfamilies, each with a largely consistent gene structure and motif arrangement. Comparative analysis with the model plants *Arabidopsis* and rice revealed that there are seven pairs of directly homologous genes with *Arabidopsis*, and only one pair with rice's ALDH gene family. This suggests potential similarities in biological functions, allowing for future melon studies to refer to the homologous genes in *Arabidopsis* and rice. Our gene duplication analysis within the melon's ALDH gene family revealed a pair of tandem and fragment repeats, suggesting that the amplification of the melon's ALDH gene was solely due to these repeats, a finding that aligns with reports on gene families in other plants [47].

Transcriptomics forms a critical component of genomics research. Bolstered by the ongoing advancements in high-throughput sequencing technology, transcriptome sequencing is becoming increasingly prevalent in plant-related studies. This has led to deepened insights into gene expression regulatory mechanisms and cellular functional diversity in plants [48,49]. Numerous transcriptome sequencing projects have used melons as their subject, with the resulting data undergoing validation via RT-qPCR and rigorous peer review before publication [50,51]. This process has led to an extensive database of melon transcriptomes. This study leverages this wealth of published transcriptome sequencing data to analyze the expression patterns of 17 ALDH genes in melons across different tissues, developmental stages, and stress conditions.

ALDH's role in plant organ development has been widely reported. For instance, the *ALDH2B2* (*Rf2a*) gene is linked to cytoplasmic male sterility in maize and plays a key role in another development [52]. ALDH is also highly expressed in rice anthers during early meiosis to microspore [53]. The *ALDH3F1* mutant triggers early flowering in plants, while its overexpression causes delayed flowering [54]. In grapes, the expression levels of three genes (*ALDH2B8*, *ALDH3H5*, and *ALDH18B1*) noticeably increase during fruit development and maturation, while the levels of *ALDH2B4* and *ALDH5F1* significantly

decrease [11]. In this study, we found that all 17 ALDH genes in melon were expressed to varying degrees in different melon tissues, with some genes exhibiting tissue-specific expression. This specific expression pattern across various melon tissues contributes to the synergistic regulation of melon growth and development. Only four ALDH genes were not expressed at different developmental stages of melon fruit. Notably, the *CmALDH2B2* gene exhibited the highest expression level during the fruit growth stage and in male and female flowers and the ovary. However, its expression level dropped dramatically as the fruit matured, indicating that this gene primarily contributes to melon fruit growth.

The ALDH gene family's response to stress in plants has become a key focus of recent studies, suggesting that this gene family is crucial for plant stress resistance. In European sweet cherry, fluorescence quantitative experiments confirmed that *PaALDH17*'s expression under salt stress was significantly higher than that of other genes. *PaALDH17* was subsequently cloned and transferred to *Arabidopsis*, where transgenic *PaALDH17* plants exhibited stronger stress resistance and fewer changes in various physiological indices under salt stress, compared to wild-type plants [55]. In grapes, *VvALDH2B4* and *VvALDH2B8* expression levels significantly increased under drought and salt stress [11]. Moreover, overexpressing *VvALDH2B4* in wild Chinese grapes led to a decrease in MDA levels, significantly improving resistance to pathogenic bacteria [56]. In bamboo, ALDH gene expression significantly increased under drought stress compared to the control, with *PeALDH2B2* responding to drought stress by interacting with *PeGPB1* [57]. Wang et al. [16] discovered that the wheat ALDH gene *TraeALDH7B1-5A* exhibited significant differences under both drought and salt stress. Its soybean homologous gene, *GmALDH7B1*, was significantly upregulated in both roots and leaves under 20% PEG treatment. To understand the melon ALDH gene family's role in abiotic stress, this study analyzed the ALDH family genes' expression patterns under salt, cold, and waterlogging stress using published melon transcriptome sequencing data. It was revealed that over half of the melon ALDH genes displayed significantly upregulated expression under salt stress, in line with previous reports on plant ALDH genes' upregulated expression under salt and drought stress [20]. In contrast, most melon ALDH genes' expression was significantly downregulated under cold and waterlogging stress. This suggests that these ALDH genes are negatively regulated when transcribed into mRNA under stress, leading to reduced expression [58]. Interestingly, some melon ALDH genes were differentially expressed under all three abiotic stresses, while others were only differentially expressed under one stress. For instance, *CmALDH10A8*, *CmALDH18B1*, *CmALDH3H1*, and *CmALDH18B2* were differentially expressed solely under salt stress, while their expression levels remained unchanged under cold and waterlogged stress. *CmALDH22A1* and *CmALDH6B1* were differentially expressed only under cold stress, and *CmALDH3H2* was differentially expressed only under waterlogging stress. These results suggest that while some ALDH genes can be induced under various abiotic stresses, others are only induced by a specific abiotic stress. In addition to abiotic stress analysis, this study also examined the ALDH gene family's expression patterns in melons under biological stress. It was observed that the 17 melon ALDH genes were primarily downregulated under powdery mildew stress and primarily upregulated under *Fusarium* wilt stress, with a higher number of differentially expressed genes than under powdery mildew stress. These ALDH genes were positively responsive to these stresses and played a role in plant disease resistance [59]. Among these, *CmALDH22A1* was significantly downregulated under powdery mildew stress but not expressed under *Fusarium* wilt stress. Similarly, *CmALDH6B1* and *CmALDH18B1* were differentially expressed under *Fusarium* wilt stress. However, *CmALDH3H2* was not differentially expressed under any of these three biological stresses, suggesting that this gene did not contribute to melon's response to these biological stresses. The functional characteristics of melon ALDH genes showed that 17 ALDH genes were differentially expressed under both abiotic and biological stresses, with *CmALDH2C4* and *CmALDH11A3* being differentially expressed under all stresses (salt, cold, waterlogging, powdery mildew, *Fusarium* wilt, and gummy stem blight). Interestingly, *CmALDH2C4* was upregulated and

downregulated in cold, waterlogged, and powdery mildew stress, suggesting that these two melon ALDH genes play a role in plants facing these stresses.

4. Materials and Methods

4.1. Identification and Chromosomal Distribution of Melon ALDH Gene Family Members

We retrieved the melon DHL92 protein group sequence file from the Cucurbitaceae genome database (http://cucurbitgenomics.org/v2/, accessed 5 May 2024), and constructed a local database [60]. Subsequently, the HMM model file for the ALDH gene family (PF00171) was downloaded from the InterPro database (https://www.ebi.ac.uk/interpro/, accessed 5 May 2024) [61]. We utilized the hmmsearch program [62] to screen the ALDH gene ID ($E < 1 \times 10^5$) in the melon protein database, and a Perl script was employed to extract the protein sequence data of the candidate genes. These sequences were then uploaded to the online platforms Pfan [63], SMART [64], and NCBI [65] for domain verification of identified ALDH gene candidates in melon. Sequences that did not contain the ALDH domain were eliminated, aiding in the identification of ALDH gene family members in melon. The ExPASy online tool [66] (https://web.expasy.org/protparam/, accessed 5 May 2024) was used to analyze the physical and chemical properties of the melon ALDH family genetic information. Lastly, the chromosome distribution map of the ALDH family genes in melon was constructed using the TBtools software [67].

4.2. Phylogenetic Analysis of ALDH Family Genes from Melon, Arabidopsis, and Rice

The sequence data for the ALDH gene family members in melon were uploaded to the online platform, GSDS (http://gsds.cbi.pku.edu.cn/, accessed 8 May 2024) [68], to execute a gene structure analysis. For the examination of conserved motifs within the ALDH gene family, the same sequence information was submitted to the online resource, MEME (http://meme-suite.org/tools/meme, accessed 8 May 2024) [69], with all parameters set to their default values. In order to construct a phylogenetic tree, we combined ALDH protein sequences of *Arabidopsis* and rice with those of melon. This collective dataset was then imported into the MEGA11 software (version 11.0.13) [70]. The construction process employed the maximum likelihood method, with all parameters set to their default values.

4.3. Genetic Characterization and Phylogenetic Analysis of ALDH Family in Melon

The MCScanX software (using built-in parameters) [71] was employed to examine tandem and fragment duplications within the ALDH gene family in melon. Furthermore, it was used to investigate the collinearity relationship among the ALDH gene families in *Arabidopsis*, rice, and melon. The findings were then visualized using the TBtools software. The cis-acting elements of the promoters of the melon ALDH family genes were analyzed within the 2.0 kb upstream sequences from the transcription start sites of the melon ALDH family genes using the online website PlantCare (https://bioinformatics.psb.ugent.be/webtools/plantcare/html/, accessed 8 May 2024).

4.4. Tissue-Specific Expression of Melon ALDH Family Genes

We reanalyzed publicly available melon transcriptome data from different tissues (PRJNA803327) [30] and developmental stages (PRJNA543288) [72] in conjunction with melon genome information. Subsequently, TBtools was utilized to generate a heatmap representation of ALDH gene family expression in various melon tissues and at different stages.

4.5. Analysis of Expression Patterns of Melon ALDH Gene Family Under Various Stresses

In order to investigate the effect of different stresses, we evaluated published melon transcriptome data under conditions including salt stress (PRJNA296827) [73], cold stress (PRJNA553119) [74], waterlogging stress (PRJNA726294) [75], powdery mildew (PRJNA358655) [76], *Fusarium* wilt (PRJNA842515) [77], and gummy stem blight (PRJNA681992) [78]. This data was reanalyzed in combination with melon genomic data, enabling us to identify differen-

tially expressed genes. A heatmap of their expression under different stress conditions in melon was again visualized using TBtools.

4.6. RT-qPCR Analysis of Melon Under Salt Stress

We used "TQ1", a highly inbred melon strain, provided by the Institute of Vegetables, Anhui Academy of Agricultural Sciences, as the experimental subject. Melon seedlings, possessing uniform growth potential and exhibiting five cotyledon leaves and one true leaf, were exposed to a 300 mM NaCl stress for periods of 0, 3, 6, 9, 12, and 24 h. Subsequently, the young leaves were harvested for further analysis. The leaves were then flash-frozen in liquid nitrogen for RNA extraction and reverse transcription. Total RNA extraction was performed utilizing the HiPure Plant RNA Mini Kit (Magen Biotech, Shanghai, China), followed by cDNA synthesis via the SMART kit (Takara Bio, Shiga, Japan), all in strict adherence to the manufacturer's guidelines. The real-time quantitative RT-PCR (RT-qPCR) was conducted employing SYBR Green qPCR Premix (Low ROX) on an IQ5 real-time PCR detection system (Bio-Rad, Hercules, CA, USA). *Actin3* (GenBank accession number XM_008449644.2) was utilized as the reference gene (Table S1). The reaction system consisted of the following: ddH2O (7 μL), 2 × Mix (10 μL), cDNA (1 μL), and both positive and negative primers (1 μL each), the reaction system was 20 μL and the reaction procedure was 95 °C for 30 s, 95 °C for 5 s, 60 °C for 34 s, 40 cycles; 72 °C for 10 s. The results from three biological replicates were analyzed using the $2^{-\Delta\Delta Ct}$ method and processed with Excel 2021. A *t*-test in SPSS 19.0 was employed to assess the significance of differences in the data, and GraphPad 9.0 Prism was utilized for plotting.

5. Conclusions

In this research, we undertook the first-ever identification of the ALDH gene family within the melon genome. We identified a total of 17 ALDH gene members, which were scattered across chromosomes 1, 2, 3, 4, 5, 7, 8, 11, and 12. Phylogenetic analysis grouped these genes into 10 distinct subfamilies, each exhibiting a largely similar gene structure. Collinearity analysis revealed a pair of fragment repeats among the 17 melon ALDH genes. Additionally, there were 12 collinear relationships between melon and *Arabidopsis* and three collinear relationships between melon and rice. Analysis of ALDH gene expression patterns during different developmental stages and in various melon tissues suggested that these genes contribute to melon growth, development, and fruit ripening. The examination of ALDH gene expression patterns under diverse stress conditions showed that these genes were differentially expressed at varying degrees in response to different stresses in melons. Particularly, the distinct expressions of *CmALDH2C4* and *CmALDH11A3* signpost these genes' crucial role in melon growth and development. RT-qPCR analysis results showed that most genes were highly expressed, signifying their participation in salt stress responses. Together, these findings pave the way for further exploration of the ALDH gene family in melons and offer promising genes for enhancing melon resistance breeding.

Supplementary Materials: The following supporting information can be downloaded at: https://www.mdpi.com/article/10.3390/plants13202939/s1, Table S1: Primers used for RT-qPCR.

Author Contributions: C.Y. and X.L. conceived the research and designed the experiments. D.Y. performed the research, analyzed the data, and wrote the manuscript. H.C., Y.Z. (Yu Zhang) and Q.D. participated in downloading the transcriptome sequencing data and helped with the bioinformatics analysis. Y.W., M.W. and Y.Z. (Yongqi Zhai) reviewed and edited the manuscript. Q.-a.Z. and G.X. provided constructive suggestions. All authors have read and agreed to the published version of the manuscript.

Funding: This research was funded by Anhui Province Key Research and Development Plan Basic Field Project (2023z04020019); the Youth Development Fund from Anhui Academy of Agricultural Sciences (QNYC-202110); the National Modern Agricultural Industrial Technology System Project (CARS-25); and the Anhui Province Vegetable Industry Technology System.

Data Availability Statement: The data presented in this study are available on request from the corresponding author. Congsheng Yan (congshengyan@126.com).

Conflicts of Interest: The authors declare no conflicts of interest.

References

1. Bartels, D. Targeting detoxification pathways: An efficient approach to obtain plants with multiple stress tolerance? *Trends Plant Sci.* **2001**, *6*, 284–286. [CrossRef] [PubMed]
2. Lindahl, R. Aldehyde dehydrogenases and their role in carcinogenesis. *Crit. Rev. Biochem. Mol.* **1992**, *27*, 283–335. [CrossRef] [PubMed]
3. Singh, S.; Brocker, C.; Koppaka, V.; Chen, Y.; Jackson, B.; Matsumoto, A.; Thompson, D.; Vasiliou, V. Aldehyde dehydrogenases in cellular responses to oxidative/electrophilic stress. *Free. Radic. Biol. Med.* **2013**, *56*, 89–101. [CrossRef] [PubMed]
4. Yoshida, A.; Rzhetsky, A.; Hsu, L.C.; Chang, C. Human aldehyde dehydrogenase gene family. *Eur. J. Biochem.* **1998**, *251*, 549–557. [CrossRef]
5. Kirch, H.H.; Bartels, D.; Wei, Y.; Schnable, P.; Wood, A. The ALDH gene superfamily of *Arabidopsis*. *Trends Plant Sci.* **2004**, *9*, 371–377. [CrossRef]
6. Perozich, J.; Nicholas, H.; Wang, B.C.; Lindahl, R.; Hempel, J. Relationships within the aldehyde dehydrogenase extended family. *Protein Sci.* **1999**, *8*, 137–146. [CrossRef]
7. Kopečný, D.; Končitíková, R.; Tylichová, M.; Vigouroux, A.; Moskalíková, H.; Soural, M.; Šebela, M.; Moréra, S. Plant ALDH10 family. *J. Biol. Chem.* **2013**, *288*, 9491–9507. [CrossRef]
8. Islam, M.S.; Ghosh, A. Evolution, family expansion, and functional diversification of plant aldehyde dehydrogenases. *Gene* **2022**, *829*, 146522. [CrossRef]
9. Brocker, C.; Lassen, N.; Estey, T.; Pappa, A.; Cantore, M.; Orlova, V.; Chavakis, T.; Kavanagh, K.; Oppermann, U.; Vasiliou, V. Aldehyde dehydrogenase 7A1 (ALDH7A1) is a novel enzyme involved in cellular defense against hyperosmotic stress. *J. Biol. Chem.* **2010**, *285*, 18452–18463. [CrossRef]
10. Vasiliou, V.; Bairoch, A.; Tipton, K.F.; Nebert, D.W. Eukaryotic aldehyde dehydrogenase (ALDH) genes: Human polymorphisms, and recommended nomenclature based on divergent evolution and chromosomal mapping. *Pharmacogenetics* **1999**, *9*, 421–434.
11. Kopečná, M.; Vigouroux, A.; Vilím, J.; Končitíková, R.; Briozzo, P.; Hájková, E.; Jašková, L.; Schwartzenberg, K.; Šebela, M.; Moréraet, S.; et al. The *ALDH21* gene found in lower plants and some vascular plants codes for a $NADP^+$—Dependent succinic semialdehyde dehydrogenase. *Plant J.* **2017**, *92*, 229–243. [CrossRef] [PubMed]
12. Hou, Q.; Bartels, D. Comparative study of the aldehyde dehydrogenase (ALDH) gene superfamily in the glycophyte *Arabidopsis thaliana* and *Eutrema* halophytes. *Ann. Bot.* **2015**, *115*, 465–479. [CrossRef] [PubMed]
13. Gao, C.; Han, B. Evolutionary and expression study of the aldehyde dehydrogenase (ALDH) gene superfamily in rice (*Oryza sativa*). *Gene* **2009**, *431*, 86–94. [CrossRef] [PubMed]
14. Zhou, M.L.; Zhang, Q.; Zhou, M.; Qi, L.P.; Yang, X.B.; Zhang, K.X.; Pang, J.F.; Zhu, X.M.; Shao, J.R.; Tang, Y.X.; et al. Aldehyde dehydrogenase protein superfamily in maize. *Funct. Integr. Genom.* **2012**, *12*, 683–691. [CrossRef] [PubMed]
15. Jimenez-Lopez, J.C.; Lopez-Valverde, F.J.; Robles-Bolivar, P.; Lima-Cabello, E.W.; Gachomo, E.O.; Kotchoni, S. Genome-Wide Identification and Functional Classification of Tomato (*Solanum lycopersicum*) Aldehyde Dehydrogenase (ALDH) Gene Superfamily. *PLoS ONE* **2016**, *11*, e0164798. [CrossRef]
16. Wang, W.; Jiang, W.; Liu, J.; Li, Y.; Gai, J.; Li, Y. Genome-wide characterization of the aldehyde dehydrogenase gene superfamily in soybean and its potential role in drought stress response. *BMC Genom.* **2017**, *18*, 518. [CrossRef]
17. Islam, M.S.; Mohtasim, M.; Islam, T.; Ghosh, A. Aldehyde dehydrogenase superfamily in sorghum: Genome-wide identification, evolution, and transcript profiling during development stages and stress conditions. *BMC Plant Biol.* **2022**, *22*, 316. [CrossRef]
18. Jiang, X.; Ren, J.; Ye, X.; Liu, M.; Li, Q.; Wang, L.; Liu, Z. Genome-wide identification and analysis of the aldehyde dehydrogenase gene superfamily in Chinese cabbage (*Brassica rapa* subsp. *pekinensis*). *Can. J. Plant Sci.* **2019**, *99*, 420–436. [CrossRef]
19. Zhang, Y.; Mao, L.; Wang, H.; Brocker, C.; Yin, X.; Vasiliou, V.; Fei, Z.; Wang, X. Genome-wide identification and analysis of grape aldehyde dehydrogenase (ALDH) gene superfamily. *PLoS ONE* **2012**, *7*, e32153. [CrossRef]
20. Islam, M.S.; Hasan, M.S.; Hasan, M.N.H.; Prodhan, S.; Islam, T.; Ghosh, A. Genome-wide identification, evolution, and transcript profiling of Aldehyde dehydrogenase superfamily in potato during development stages and stress conditions. *Sci. Rep.* **2021**, *11*, 18217–18284. [CrossRef]
21. Li, X.; Guo, R.; Li, J.; Singer Stacy, D.; Zhang, Y.; Yin, X.; Zheng, Y.; Fan, C.; Wang, X. Genome-wide identification and analysis of the aldehyde dehydrogenase (*ALDH*) gene superfamily in apple (*Malus* × *domestica* Borkh.). *Plant Physiol. Biochem.* **2013**, *71*, 268–282. [CrossRef] [PubMed]
22. Tola, A.J.; Jaballi, A.; Germain, H.D.; Missihoun, T. Recent Development on Plant Aldehyde Dehydrogenase Enzymes and Their Functions in Plant Development and Stress Signaling. *Genes* **2020**, *12*, 51. [CrossRef]
23. Brocker, C.; Vasiliou, M.; Carpenter, S.; Carpenter, C.; Zhang, Y.; Wang, X.O.; Kotchoni, S.J.; Wood, A.; Kirch, H.; Kopečný, D.; et al. Aldehyde dehydrogenase (ALDH) superfamily in plants: Gene nomenclature and comparative genomics. *Planta* **2013**, *237*, 189–210. [CrossRef] [PubMed]

24. Kotchoni, S.O.; Kuhns, C.; Ditzer, A.; KIRCH, H.; BARTELS, D. Over-expression of different aldehyde dehydrogenase genes in *Arabidopsis thaliana* confers tolerance to abiotic stress and protects plants against lipid peroxidation and oxidative stress. *Plant Cell Environ.* **2006**, *29*, 1033–1048. [CrossRef] [PubMed]
25. Gautam, R.; Meena, R.K.; Woch, N.; Kirti, P. Ectopic expression of BrALDH7B2 gene encoding an antiquitin from *Brassica rapa* confers tolerance to abiotic stresses and improves photosynthetic performance under salt stress in tobacco. *Environ. Exp. Bot.* **2020**, *180*, 104223. [CrossRef]
26. Chen, J.; Wei, B.; Li, G.; Fan, R.; Zhong, Y.; Wang, X.; Zhang, X. TraeALDH7B1-5A, encoding aldehyde dehydrogenase 7 in wheat, confers improved drought tolerance in *Arabidopsis*. *Planta* **2015**, *242*, 137–151. [CrossRef] [PubMed]
27. Gu, H.; Pan, Z.; Jia, M.; Fang, H.; Li, J.; Qi, Y.; Yang, Y.; Feng, W.; Gao, X.; Ditta, A.; et al. Genome-wide identification and analysis of the cotton ALDH gene family. *BMC Genom.* **2024**, *25*, 513. [CrossRef]
28. Cao, Y.; Wang, J.; Zhao, S.; Fang, Q.; Ruan, J.; Li, S.; Liu, T.; Qi, Y.; Zhang, L.; Zhang, X.; et al. Overexpression of the aldehyde dehydrogenase *AhALDH3H1* from *Arachis hypogaea* in soybean increases saline-alkali stress tolerance. *Front. Plant Sci.* **2023**, *14*, 1165384. [CrossRef]
29. Rolim, P.M.; Fidelis, G.P.; Padilha, C.; Santos, E.S.; Rocha, H.; Macedo, G.R. Phenolic profile and antioxidant activity from peels and seeds of melon (*Cucumis melo* L. var. *reticulatus*) and their antiproliferative effect in cancer cells. *Braz. J. Med. Biol. Res.* **2018**, *51*, e6069. [CrossRef]
30. Lija, M.; Beevy, S.S. A Review on the diversity of Melon. *Plant Sci. Today* **2021**, *8*, 995–1003. [CrossRef]
31. Pujol, M.; Garcia-Mas, J. Regulation of climacteric fruit ripening in melon: Recent advances and future challenges. *J. Exp. Bot.* **2023**, *74*, 6224–6236. [CrossRef] [PubMed]
32. Garcia-Mas, J.; Benjak, A.; Sanseverino, W.; Puigdomènech, P. The genome of melon (*Cucumis melo* L.). *Proc. Natl. Acad. Sci. USA* **2012**, *109*, 11872–11877. [CrossRef] [PubMed]
33. Ruggieri, V.; Alexiou, K.G.; Morata, J.; Argyris, J.; Pujol, M.; Yano, R.; Nonaka, S.; Ezura, H.; Latrasse, D.; Boualem, A.; et al. An improved assembly and annotation of the melon (*Cucumis melo* L.) reference genome. *Sci. Rep.* **2018**, *8*, 8088. [CrossRef] [PubMed]
34. Castanera, R.; Ruggieri, V.; Pujol, M.; Garcia-Mas, J.M.; Casacuberta, J. An Improved Melon Reference Genome with Single-Molecule Sequencing Uncovers a Recent Burst of Transposable Elements with Potential Impact on Genes. *Front. Plant Sci.* **2019**, *10*, 1815. [CrossRef]
35. Ge, C.; Zhao, W.; Nie, L.; Niu, S.; Fang, S.; Duan, Y.; Zhao, J.; Guo, K.; Zhang, Q. Transcriptome profiling reveals the occurrence mechanism of bisexual flowers in melon (*Cucumis melo* L.). *Plant Sci.* **2020**, *301*, 110694. [CrossRef]
36. Lv, Y.; Amanullah, S.; Liu, S.; Zhang, C.; Liu, H.; Zhu, Z.; Zhang, X.; Gao, P.; Luan, F. Comparative Transcriptome Analysis Identified Key Pathways and Genes Regulating Differentiated Stigma Color in Melon (*Cucumis melo* L.). *Int. J. Mol. Sci.* **2022**, *23*, 6721. [CrossRef]
37. Zheng, L.; Chao, Y.; Wang, Y.; Xu, Y.; Li, S. Genome-Wide Analysis of the LBD Gene Family in Melon and Expression Analysis in Response to Wilt Disease Infection. *Genes* **2024**, *15*, 442. [CrossRef]
38. Ma, M.; Liu, S.; Wang, Z.; Shao, R.; Ye, J.; Yan, W.; Lv, H.; Hasi, A.; Che, G. Genome-Wide Identification of the SUN Gene Family in Melon (*Cucumis melo*) and Functional Characterization of Two CmSUN Genes in Regulating Fruit Shape Variation. *Int. J. Mol. Sci.* **2022**, *23*, 16047. [CrossRef]
39. Jin, W.; Yan, W.; Ma, M.; Agula, H.; Che, G. Genome-wide identification and expression analysis of the JMJ-C gene family in melon (*Cucumis melo* L.) reveals their potential role in fruit development. *BMC Genom.* **2023**, *24*, 771. [CrossRef]
40. Strzemski, M.; Dresler, S. Impact of Biotic/Abiotic Stress Factors on Plant Specialized Metabolites. *Int. J. Mol. Sci.* **2024**, *25*, 5742. [CrossRef]
41. Fang, Y.; Jiang, J.; Ding, H.; Li, X.; Xie, X. Phospholipase C: Diverse functions in plant biotic stress resistance and fungal pathogenicity. *Mol. Plant Pathol.* **2023**, *24*, 1192–1202. [CrossRef] [PubMed]
42. Jacques, F.; Zhao, Y.; Kopecna, M.; Končitíková, R.; Kopečný, D.; Rippa, S.; Perrin, Y. Roles for ALDH10 enzymes in gamma-butyrobetaine synthesis, seed development, germination, and salt tolerance in *Arabidopsis*. *J. Exp. Bot.* **2020**, *71*, 7088–7102. [CrossRef] [PubMed]
43. Diaz-Sanchez, A.G.; Gonzalez-Segura, L.; Mujica-Jimenez, C.; Rudiño-Piñera, E.; Montiel, C.P.; Martínez-Castilla, L.; Muñoz-Clares, R.A. Amino acid residues critical for the specificity for betaine aldehyde of the plant ALDH10 isoenzyme involved in the synthesis of glycine betaine. *Plant Physiol.* **2012**, *158*, 1570–1582. [CrossRef] [PubMed]
44. Dmitriev, A.A.; Pushkova, E.N.; Melnikova, N.V. Plant Genome Sequencing: Modern Technologies and Novel Opportunities for Breeding. *Mol. Biol.* **2022**, *56*, 531–545. [CrossRef]
45. Jain, M.; Tyagi, A.K.; Khurana, J.P. Genome-wide analysis, evolutionary expansion, and expression of early auxin-responsive SAUR gene family in rice (*Oryza sativa*). *Genomics* **2006**, *88*, 360–371. [CrossRef]
46. Yang, L.; Koo, D.H.; Li, Y.; Zhang, X.; Luan, F.; Havey, M.J.; Jiang, J.; Weng, Y. Chromosome rearrangements during domestication of cucumber as revealed by high-density genetic mapping and draft genome assembly. *Plant J.* **2012**, *71*, 895–906. [CrossRef]
47. Zhang, S.; Chen, C.; Li, L.; Meng, L.; Singh, J.; Jiang, N.; Deng, X.; He, Z.; Lemaux, P.G. Evolutionary expansion, gene structure, and expression of the rice wall-associated kinase gene family. *Plant Physiol.* **2005**, *139*, 1107–1124. [CrossRef]

48. Wang, L.; Li, P.; Brutnell, T.P. Exploring plant transcriptomes using ultra high-throughput sequencing. *Brief Funct. Genom.* **2010**, *9*, 118–128. [CrossRef]
49. Shulse, C.N.; Cole, B.J.; Ciobanu, D.; Lin, J.; Yoshinaga, Y.; Gouran, M.; Turco, G.; Zhu, Y.; O'Malley, R.; Brady, S.; et al. High-Throughput Single-Cell Transcriptome Profiling of Plant Cell Types. *Cell Rep.* **2019**, *27*, 2241–2247. [CrossRef]
50. Yang, D.; Li, Y.; Zhu, M.; Cui, R.; Gao, J.; Shu, Y.; Lu, X.; Zhang, H.; Zhang, K. Genome-Wide Identification and Expression Analysis of the Cucumber FKBP Gene Family in Response to Abiotic and Biotic Stresses. *Genes* **2023**, *14*, 2006. [CrossRef]
51. Zhang, K.; He, S.; Sui, Y.; Gao, Q.; Jia, S.; Lu, X.; Jia, L. Genome-Wide Characterization of HSP90 Gene Family in Cucumber and Their Potential Roles in Response to Abiotic and Biotic Stresses. *Front. Genet.* **2021**, *12*, 584886. [CrossRef] [PubMed]
52. Liu, F.; Cui, X.; Horner, H.T.; Weiner, H.; Schnable, P.S. Mitochondrial aldehyde dehydrogenase activity is required for male fertility in maize. *Plant Cell* **2001**, *13*, 1063–1078. [CrossRef] [PubMed]
53. Xie, X.; Zhang, Z.; Zhao, Z.; Xie, Y.; Li, H.; Ma, X.; Liu, Y.G.; Chen, L. The mitochondrial aldehyde dehydrogenase OsALDH2b negatively regulates tapetum degeneration in rice. *J. Exp. Bot.* **2020**, *71*, 2551–2560. [CrossRef] [PubMed]
54. Gan, Q.; Luan, M.; Hu, M.; Liu, Z.; Zhang, Z. Functional study of CYP90A1 and ALDH3F1 gene obtained by transcriptome sequencing analysis of Brassica napus seedlings treated with brassinolide. *Front. Plant Sci.* **2022**, *13*, 1040511. [CrossRef]
55. Li, S.; Wang, X.; Wang, W.; Zhang, Z.; Wang, X.; Zhang, Q.; Wang, Y. Genome-wide identification and expression analysis of the ALDH gene family and functional analysis of PaALDH17 in Prunus avium. *Physiol. Mol. Biol. Plants* **2024**, *30*, 633–645. [CrossRef]
56. Wen, Y.; Wang, X.; Xiao, S.; Wang, Y. Ectopic expression of VpALDH2B4, a novel aldehyde dehydrogenase gene from Chinese wild grapevine (*Vitis pseudoreticulata*), enhances resistance to mildew pathogens and salt stress in *Arabidopsis*. *Planta* **2012**, *236*, 525–539. [CrossRef]
57. Xu, J.; Liu, L.; Huang, H.; Shang, C.; Pan, H.; Fan, H.; Han, X.; Qiu, W.; Lu, Z.; Qiao, G.; et al. Genome-wide characterization and gene expression analyses of ALDH gene family in response to drought stress in moso bamboo (*Phyllostachys edulis*). *Plant Physiol. Biochem.* **2023**, *202*, 107954. [CrossRef]
58. Wang, L.; Dai, W.; Shi, Y.; Wang, Y.; Zhang, C. Cloning and activity analysis of the highly expressed gene VviABCG20 promoter in seed and its activity is negatively regulated by the transcription factor VviDof14. *Plant Sci.* **2022**, *315*, 111152. [CrossRef]
59. Arick, M.N.; Hsu, C.Y. Differential Gene Expression Analysis of Plants. *Methods Mol. Biol.* **2018**, *1783*, 279–298. [CrossRef]
60. Yu, J.; Wu, S.; Sun, H.; Wang, X.; Tang, X.; Guo, S.; Zhang, Z.; Huang, S.; Xu, Y.; Weng, Y.; et al. CuGenDBv2: An updated database for cucurbit genomics. *Nucleic Acids Res.* **2023**, *51*, D1457–D1464. [CrossRef]
61. Paysan-Lafosse, T.; Blum, M.; Chuguransky, S.; Grego, T.; Pinto, B.L.; Salazar, G.A.; Bileschi, M.L.; Bork, P.; Bridge, A.; Colwell, L.; et al. InterPro in 2022. *Nucleic Acids Res.* **2023**, *51*, D418–D427. [CrossRef] [PubMed]
62. Finn, R.D.; Clements, J.; Eddy, S.R. HMMER web server: Interactive sequence similarity searching. *Nucleic Acids Res.* **2011**, *39*, W29–W37. [CrossRef] [PubMed]
63. Mistry, J.; Chuguransky, S.; Williams, L.; Qureshi, M.; Salazar, G.A.; Sonnhammer, E.L.L.; Tosatto, S.C.E.; Paladin, L.; Raj, S.; Richardson, L.J.; et al. Pfam: The protein families database in 2021. *Nucleic Acids Res.* **2021**, *49*, D412–D419. [CrossRef] [PubMed]
64. Letunic, I.; Khedkar, S.; Bork, P. SMART: Recent updates, new developments and status in 2020. *Nucleic Acids Res.* **2021**, *49*, D458–D460. [CrossRef]
65. Marchler-Bauer, A.; Bryant, S.H. CD-Search: Protein domain annotations on the fly. *Nucleic Acids Res.* **2004**, *32*, W327–W331. [CrossRef] [PubMed]
66. Duvaud, S.; Gabella, C.; Lisacek, F.; Stockinger, H.; Ioannidis, V.; Durinx, C. Expasy, the Swiss Bioinformatics Resource Portal, as designed by its users. *Nucleic Acids Res.* **2021**, *49*, W216–W227. [CrossRef] [PubMed]
67. Chen, C.; Wu, Y.; Li, J.; Wang, X.; Zeng, Z.; Xu, J.; Liu, Y.; Feng, J.; Chen, H.; He, Y.; et al. TBtools-II: A "one for all, all for one" bioinformatics platform for biological big-data mining. *Mol. Plant* **2023**, *16*, 1733–1742. [CrossRef]
68. Hu, B.; Jin, J.; Guo, A.Y.; Zhang, H.; Luo, J.; Gao, G. GSDS 2.0: An upgraded gene feature visualization server. *Bioinformatics* **2015**, *31*, 1296–1297. [CrossRef]
69. Bailey, T.L.; Johnson, J.; Grant, C.E.; Noble, W. The MEME Suite. *Nucleic Acids Res.* **2015**, *43*, W39–W49. [CrossRef]
70. Tamura, K.; Stecher, G.; Kumar, S. MEGA11: Molecular Evolutionary Genetics Analysis Version 11. *Mol. Biol. Evol.* **2021**, *38*, 3022–3027. [CrossRef]
71. Wang, Y.; Tang, H.; Wang, X.; Sun, Y.; Joseph, P.V.; Paterson, A.H. Detection of colinear blocks and synteny and evolutionary analyses based on utilization of MCScanX. *Nat. Protoc.* **2024**, *19*, 2206–2229. [CrossRef] [PubMed]
72. Tian, Y.; Bai, S.; Dang, Z.; Hao, J.; Zhang, J.; Hasi, A. Genome-wide identification and characterization of long non-coding RNAs involved in fruit ripening and the climacteric in *Cucumis melo*. *BMC Plant Biol.* **2019**, *19*, 369. [CrossRef] [PubMed]
73. Tian, Z.; Han, J.; Che, G.; Hasi, A. Genome-wide characterization and expression analysis of SAUR gene family in Melon (*Cucumis melo* L.). *Planta* **2022**, *255*, 123. [CrossRef] [PubMed]
74. Diao, Q.; Cao, Y.; Fan, H.; Zhang, Y. Transcriptome analysis deciphers the mechanisms of exogenous nitric oxide action on the response of melon leaves to chilling stress. *Biol. Plant.* **2020**, *64*, 465–472. [CrossRef]
75. Zhang, H.; Li, G.; Yan, C.; Cao, N.; Yang, H.; Le, M.; Zhu, F. Depicting the molecular responses of adventitious rooting to waterlogging in melon hypocotyls by transcriptome profiling. *3 Biotech* **2021**, *11*, 351. [CrossRef]
76. Zhu, Q.; Gao, P.; Wan, Y.; Cui, H.; Fan, C.; Liu, S.; Luan, F. Comparative transcriptome profiling of genes and pathways related to resistance against powdery mildew in two contrasting melon genotypes. *Sci. Hortic.* **2018**, *227*, 169–180. [CrossRef]

77. Yang, T.; Liu, J.; Li, X.; Amanullah, S.; Lu, X.; Zhang, M.; Zhang, Y.; Luan, F.; Liu, H.; Wang, X. Transcriptomic Analysis of *Fusarium* oxysporum Stress-Induced Pathosystem and Screening of Fom-2 Interaction Factors in Contrasted Melon Plants. *Front. Plant Sci.* **2022**, *13*, 961586. [CrossRef]
78. Intana, W.; Wonglom, P.; Suwannarach, N.; Sunpapao, A. Trichoderma asperelloides PSU-P1 Induced Expression of Pathogenesis-Related Protein Genes against Gummy Stem Blight of Muskmelon (*Cucumis melo*) in Field Evaluation. *J. Fungi* **2022**, *8*, 156. [CrossRef]

Disclaimer/Publisher's Note: The statements, opinions and data contained in all publications are solely those of the individual author(s) and contributor(s) and not of MDPI and/or the editor(s). MDPI and/or the editor(s) disclaim responsibility for any injury to people or property resulting from any ideas, methods, instructions or products referred to in the content.

plants

MDPI

Article

Multi-Omics Research Reveals the Effects of the ABA-Regulated Phenylpropanoid Biosynthesis Pathway on the UV-B Response in *Rhododendron chrysanthum* Pall.

Wang Yu, Xiangru Zhou, Jinhao Meng, Xiaofu Zhou * and Hongwei Xu *

Jilin Provincial Key Laboratory of Plant Resource Science and Green Production, Jilin Normal University, Siping 136000, China; 15043512434@163.com (W.Y.); 17604342645@163.com (X.Z.)
* Correspondence: zhouxiaofu@jlnu.edu.cn (X.Z.); xuhongwei@jlnu.edu.cn (H.X.)

Abstract: The growing depletion of the ozone layer has led to increased ultraviolet B (UV-B) radiation, prompting plants like the alpine *Rhododendron chrysanthum* Pall. (*R. chrysanthum*) to adapt to these harsh conditions. This study explored how abscisic acid (ABA) signaling influences *R. chrysanthum*'s metabolic responses under UV-B stress. *R. chrysanthum* was treated with UV-B radiation and exogenous ABA for widely targeted metabolomics, transcriptomics, and proteomics assays, and relevant chlorophyll fluorescence parameters were also determined. It was observed that UV-B stress negatively impacts the plant's photosynthetic machinery, disrupting multiple metabolic processes. Multi-omics analysis revealed that ABA application mitigates the detrimental effects of UV-B on photosynthesis and bolsters the plant's antioxidant defenses. Additionally, both UV-B exposure and ABA treatment significantly influenced the phenylpropanoid biosynthesis pathway, activating key enzyme genes, such as 4CL, CCR, and HCT. The study also highlighted the MYB–bHLH–WD40 (MBW) complex's role in regulating this pathway and its interaction with ABA signaling components. These findings underscore ABA's crucial function in improving plant resistance to UV-B stress and offer novel insights into plant stress biology.

Keywords: UV-B; *R. chrysanthum*; phenylpropanoid biosynthesis pathway

1. Introduction

In recent years, substantial degradation of the ozone layer due to increasing environmental pollution has led to excessive ultraviolet B (UV-B) radiation (280 to 315 nm) exposure on the earth's surface [1]. Excess UV-B radiation has substantial adverse effects on plants [2]. UV-B stress is currently demonstrated to produce reduced leaf area and even defoliation in plants [3]. UV-B stress can also disrupt photosynthesis in plants by degrading plant Photosystem II (PSII) proteins, impairing PS electron donors, and even interfering with stomatal function, resulting in a decrease in photosynthesis rates [4–6]. UV-B stress causes the production of reactive oxygen species (ROS) in plants, and excessive accumulation of these substances disrupts various metabolic processes in plant cells [7,8]. UV-B stress also alters plant metabolite content, causing significant changes in the total sugar and starch content, as well as a significant increase in carotenoid and phenolic levels [9–11]. As a result, in response to the environmental changes caused by the ever-increasing UV-B radiation, various plants have gradually developed their own distinct adaptive mechanisms to cope with UV-B stress.

Rhododendron chrysanthum Pall. (*R. chrysanthum*), a perennial evergreen dwarf shrub, mainly grows in the high altitudes of Changbai Mountains [12]. Because of the harsh envi-

ronmental conditions in the Changbai Mountains, *R. chrysanthum* has evolved resistance to strong UV radiation, low temperatures, and other abiotic stresses. Previous research on *R. chrysanthum* revealed that UV-B stress causes reprogramming of its major primary metabolism pathways [13]. *R. chrysanthum*'s PSII proteins undergo acetylation alteration in response to UV-B stress, and this modification partially offsets the plant's UV-B damage [14]. However, few studies have been conducted on the phenylpropanoid biosynthesis pathway in the reaction to UV-B stress in *R. chrysanthum*, which is ubiquitous and plays a vital function in plants and hence warrants more investigation.

The phenylpropanoid biosynthesis pathway acts as a crucial part in plant metabolism. This pathway is capable of efficiently producing a diverse range of important secondary metabolites that play critical roles in plant reactions to varied environmental stressors [15,16]. The phenylpropanoid biosynthesis pathway is a major source of most defensive secondary metabolites (flavonoids, lignans, salicylic acid, etc.) and is capable of efficiently scavenging reactive oxygen species accumulated as a result of various stresses, as well as playing an important regulatory role in the reorientation of metabolic streams in different pathways [17]. Among these metabolites, flavonoids, as an important class of derivatives in the phenylpropanoid biosynthesis pathway, are able to absorb UV-B rays at 280–315 nm so that plant organs and tissues, especially photosynthetic tissues, can be protected from UV-B damage, and are important protective barriers against the absorption of ultraviolet radiation in plants [18]. Furthermore, flavonoids have strong antioxidant activity, which can scavenge reactive oxygen species produced during stress and increase plant survival [19]. Therefore, the study of the dynamics of the phenylpropanoid biosynthesis pathway under abiotic stress in *R. chrysanthum* is of great importance.

Abscisic acid (ABA), an abiotic stress hormone that increases plant resistance, serves as both a signal for the plant response to abiotic stress and an important factor in eliciting adaptive regulatory responses and gene expression in plants [20]. Plants are able to regulate the degree of stomatal opening and closing through ABA to reduce the plant transpiration rate in order to counteract the damage caused by abiotic stresses on plants [21]. ABA can also activate the antioxidant defense system, which scavenges reactive oxygen species produced by environmental stress [22]. Numerous experiments on exogenous ABA have shown that exogenous ABA can significantly enhance the stress tolerance performance of plants [23–25]. Few studies have been carried out on the synergistic responses of the phenylpropanoid biosynthesis pathway in plants to UV-B stress that are regulated by ABA, despite the fact that the function of this pathway in plants cannot be overlooked and that ABA is crucial for improving plant stress tolerance.

The benefits of both targeted and untargeted metabolomics are combined in widely targeted metabolomics analysis, which has the ability to accurately respond to the dynamic changes in plant metabolites. Its features include high throughput, ultra-sensitivity, wide coverage, and accurate qualitative and quantitative analysis [26,27]. The transcriptome can accurately reflect changes in the expression of various genes in plants as a result of environmental changes, aiding in the discovery of regulatory relationships between genes and networks [28]. Protein acetylation, a widespread post-translational modification on lysine, tweaks protein properties, influencing activity and cell signaling [29,30]. Protein acetylation modificationomics is precisely the most important research tool to reveal protein acetylation, providing new perspectives for understanding life processes [31].

Given the crucial role of the abscisic acid and phenylpropanoid biosynthesis pathways in plant reactions to adversity stress, this study investigated the molecular mechanisms governing how ABA regulates the phenylpropanoid biosynthesis route in *R. chrysanthum* in response to UV-B radiation. The dynamic alterations in *R. chrysanthum* ABA biosynthesis and signaling under UV-B stress were investigated further via a joint multi-strategyomics analysis.

2. Results

2.1. R. chrysanthum's Photosynthetic System Is Injured by UV-B Exposure

In order to demonstrate the detrimental impact of UV-B stress on *R. chrysanthum*'s photosynthetic system, radargrams illustrating the pertinent OJIP (fast chlorophyll a fluorescence induction curve) test parameters were created (Supplementary Figure S1A). The findings indicated that following exposure to UV-B radiation, the levels of φD_o (quantum yield at t = Fo for energy dissipation), Fo (minimal fluorescence), and S_m (normalised total complementary area) rise, whereas Ψ_o (probability that a trapped exciton moves an electron into the electron), φE_o (quantum yield at t = Fo for electron transport), and Fm (fluorescence maximum) all fall. UV-B radiation also resulted in a significant decrease in PI_{ABS} (performance index on absorption basis) and Fv/Fm (maximal photochemical efficiency of PSII) and a significant increase in DIo/RC (dissipated energy flux per RC at t = Fo) in *R. chrysanthum* (Supplementary Figure S1B–D).

2.2. Response of Key Metabolites in R. chrysanthum to UV-B Radiation

UV-B radiation resulted in an increase in L-tryptophan content and a decrease in ABA content in *R. chrysanthum*, and the differences in these changes were not significant (Figure 1A,B). L-tryptophan is able to participate in the signaling process of plants in response to UV-B stress, and the increase in its content due to UV-B radiation indicates that *R. chrysanthum* switched on a response mechanism upon exposure to UV-B radiation. L-glutamine is associated with photosynthetic pigments, and UV-B caused a decrease in its content, suggesting that UV-B can have some effect on the photosynthetic system of *R. chrysanthum*, which is consistent with the aforementioned results, indicating that UV-B can disrupt the photosynthetic system of *R. chrysanthum* (Figure 1C).

The biosynthetic process of phenylpropanoid involves critical roles of L-phenylalanine and 3-hydroxycinnamic acid. The results of the study showed a significant increase in L-phenylalanine content due to UV-B radiation, and 3-hydroxycinnamic acid also increased but not significantly (Figure 1D,E). This occurrence reveals that the phenylpropanoid biosynthesis pathway may be activated in *R. chrysanthum* in its reaction to UV-B exposure.

Correlation analyses showed that the aforementioned key metabolites in *R. chrysanthum* were closely linked to each other under UV-B radiation, among which L-phenylalanine was more strongly correlated with L-tryptophan and ABA (Figure 1F). Consequently, through dynamic alterations in ABA and phenylalanine biosynthesis, *R. chrysanthum* may react favorably to UV-B stress (Figure 1G).

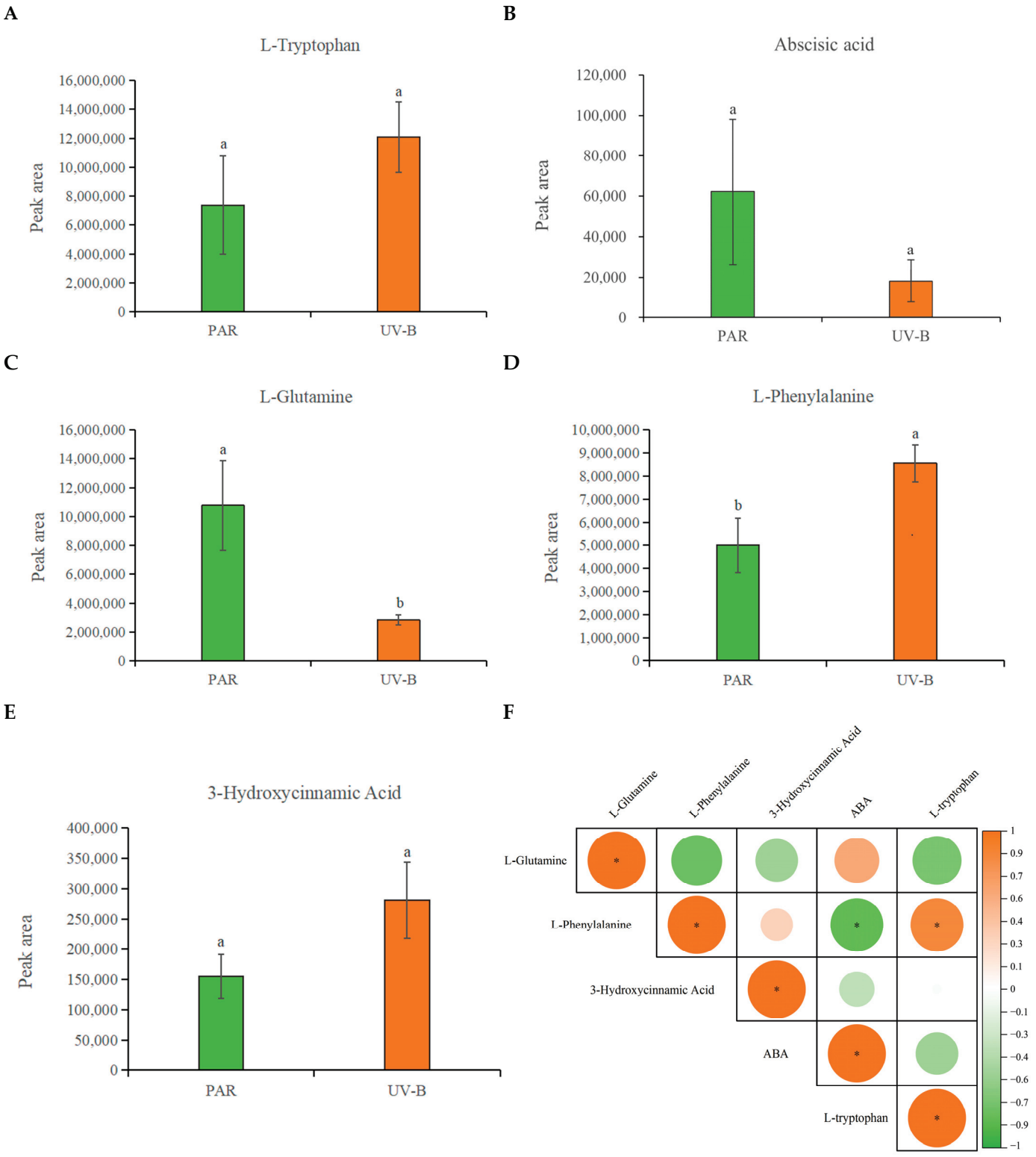


Figure 1. *Cont.*

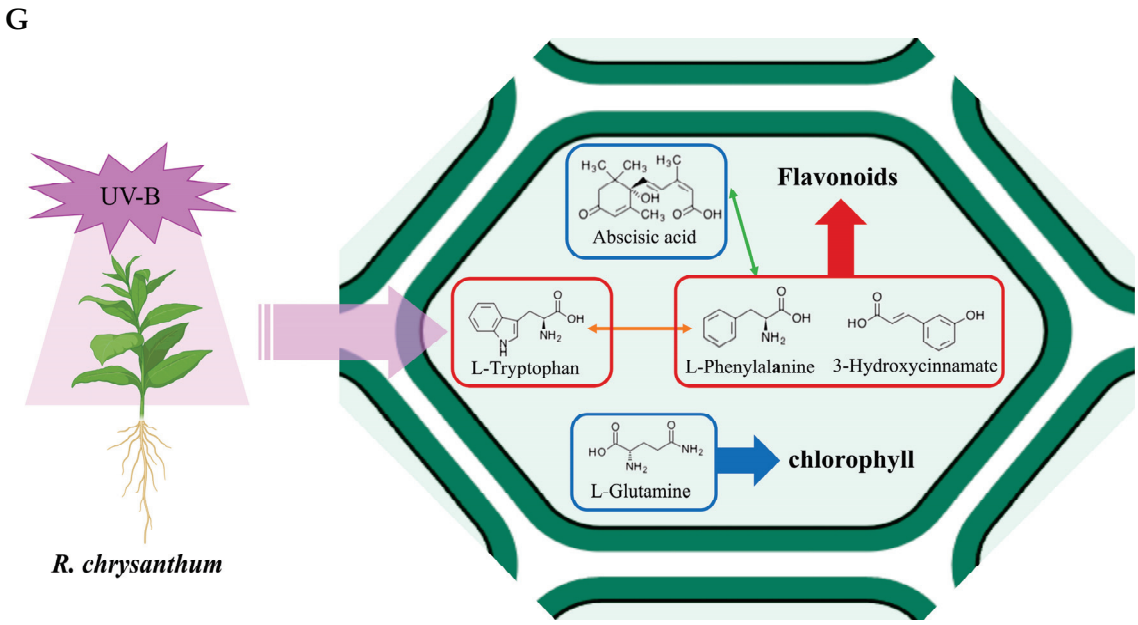


Figure 1. After UV-B radiation exposure, *R. chrysanthum*'s ABA and key metabolites act together. (**A**–**E**) Bar graphs representing the changes in L-tryptophan, ABA, L-glutamine, L-phenylalanine, and 3-hydroxycinnamic acid after UV-B radiation exposure, respectively. The peak area is used to estimate the relative amount of a specific metabolite in a sample. The larger the peak area, the higher the amount of that metabolite in the sample. The three biological duplicate experiments' means are shown by the heights of the bar graphs (n = 3), and the SDs of the three samples are shown by the error bars. Significant changes across data groups are indicated by different letter markers ($p < 0.05$). (**F**) Correlation analysis between key substances in *R. chrysanthum* under UV-B radiation. Correlation analyses were performed on the data involved for each metabolite in (**A**–**E**). Orange and green circles represent positive and negative correlations, respectively, and the sizes and color shades of the circles indicate the strength of the correlation, with "*" representing $r^2 \geq 0.8$ and $p < 0.05$. (**G**) Mechanogram of changes in ABA and key metabolites in *R. chrysanthum* after UV-B radiation exposure. Orange bi-directional arrows represent positive correlations, and green bi-directional arrows represent negative correlations.

2.3. Treatment with Exogenous ABA Protects R. chrysanthum's Photosynthetic System

This study revealed that while UV-B exposure decreased *R. chrysanthum*'s actual electron transport rate (ETR), exogenous ABA prevented this downward trend, hence minimizing the effect (Figure 2A). Non-photochemical quenching (NPQ) is a protective mechanism for plants to avoid damage to the photosynthetic apparatus caused by excess excitation energy produced during photosynthesis. The rise in NPQ after UV-B radiation exposure suggests that *R. chrysanthum* protects the photosynthetic apparatus from damage by UV-B radiation by enhancing energy dissipation. In contrast, the decrease in NPQ after exogenous ABA treatment suggests that ABA may disperse too much excess excitation energy by regulating the phenylpropanoid biosynthesis pathway, thus helping *R. chrysanthum* to respond positively to UV-B radiation (Figure 2B).

All of the assessed chlorophyll fluorescence parameters dramatically decreased, having been exposed to UV-B radiation; nonetheless, exogenous ABA significantly reversed this trend and increased *R. chrysanthum*'s potential to withstand stress (Figure 2C,D). All things considered, the findings demonstrate that *R. chrysanthum*'s photosynthetic system is negatively impacted by UV-B radiation and that exogenous ABA could improve *R. chrysanthum*'s resistance to stress.

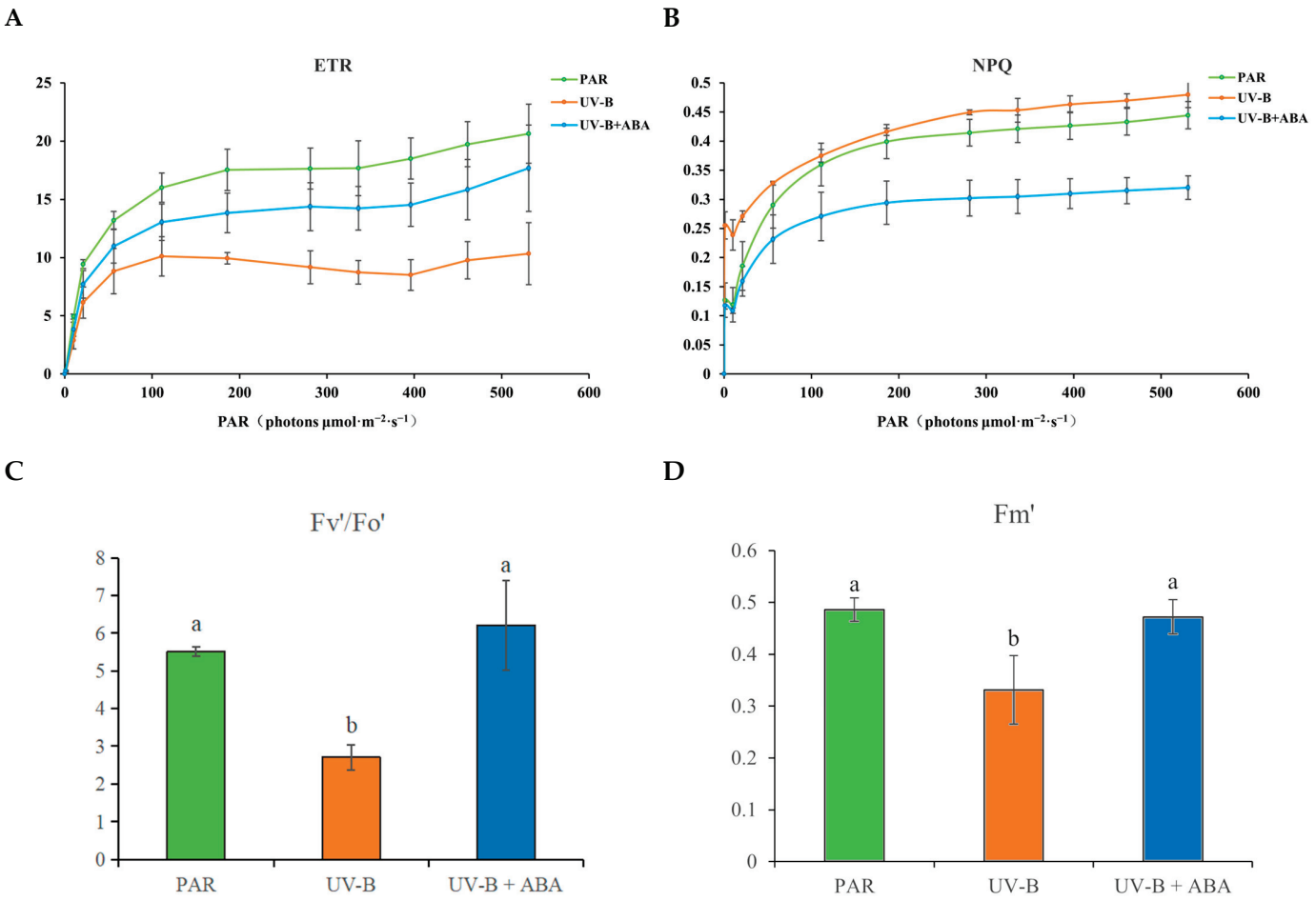


Figure 2. Dynamics of *R. chrysanthum*'s chlorophyll fluorescence characteristics. (**A**,**B**) Line plots of NPQ and ETR in *R. chrysanthum* after exogenous ABA and UV-B radiation treatments. (**C**,**D**) Histograms of Fv′/Fo′ (variable fluorescence ratio in the light) and Fm′ (maximum fluorescence in the light) of PSII of *R. chrysanthum* after treatment with exogenous ABA and UV-B radiation. The three biological duplicate experiments' means are shown by the heights of the bar graphs (n = 3), and the SDs of the three samples are shown by the error bars. Significant changes across data groups are indicated by different letter markers ($p < 0.05$).

2.4. Alteration of the Phenylpropanoid Biosynthesis Pathway and the Derivative Flavonoids of This Pathway in R. chrysanthum

The findings from widely targeted metabolomics revealed 2148 *R. chrysanthum* metabolites in total. With 487 species, the majority of them were flavonoids and could be divided into nine main families (Figure 3A). Different metabolites (DMs) and different flavonoids (DFs) were screened according to variable importance in the projection (VIP) and fold change (FC) values. UV-B radiation (MvsN) resulted in 522 DMs (355 raised and 167 reduced) in *R. chrysanthum*, while exogenous ABA treatment (NvsQ) resulted in 289 DMs (183 raised and 106 reduced) (Figure 3B,C). KEGG enrichment analyses showed that post-UV-B, the DMs of *R. chrysanthum* were mainly enriched in phenylpropanoid biosynthesis, flavonoid biosynthesis, and flavone and flavonol biosynthesis, and the DMs after exogenous ABA treatment were similarly mainly concentrated in the phenylpropanoid biosynthesis and flavonoid biosynthesis (Figure 3D,E). This suggests that UV-B radiation activates phenylpropanoid biosynthesis in *R. chrysanthum*, while exogenous ABA modulates the phenylpropanoid biosynthesis pathway, thereby inducing a positive response to UV-B in *R. chrysanthum*.

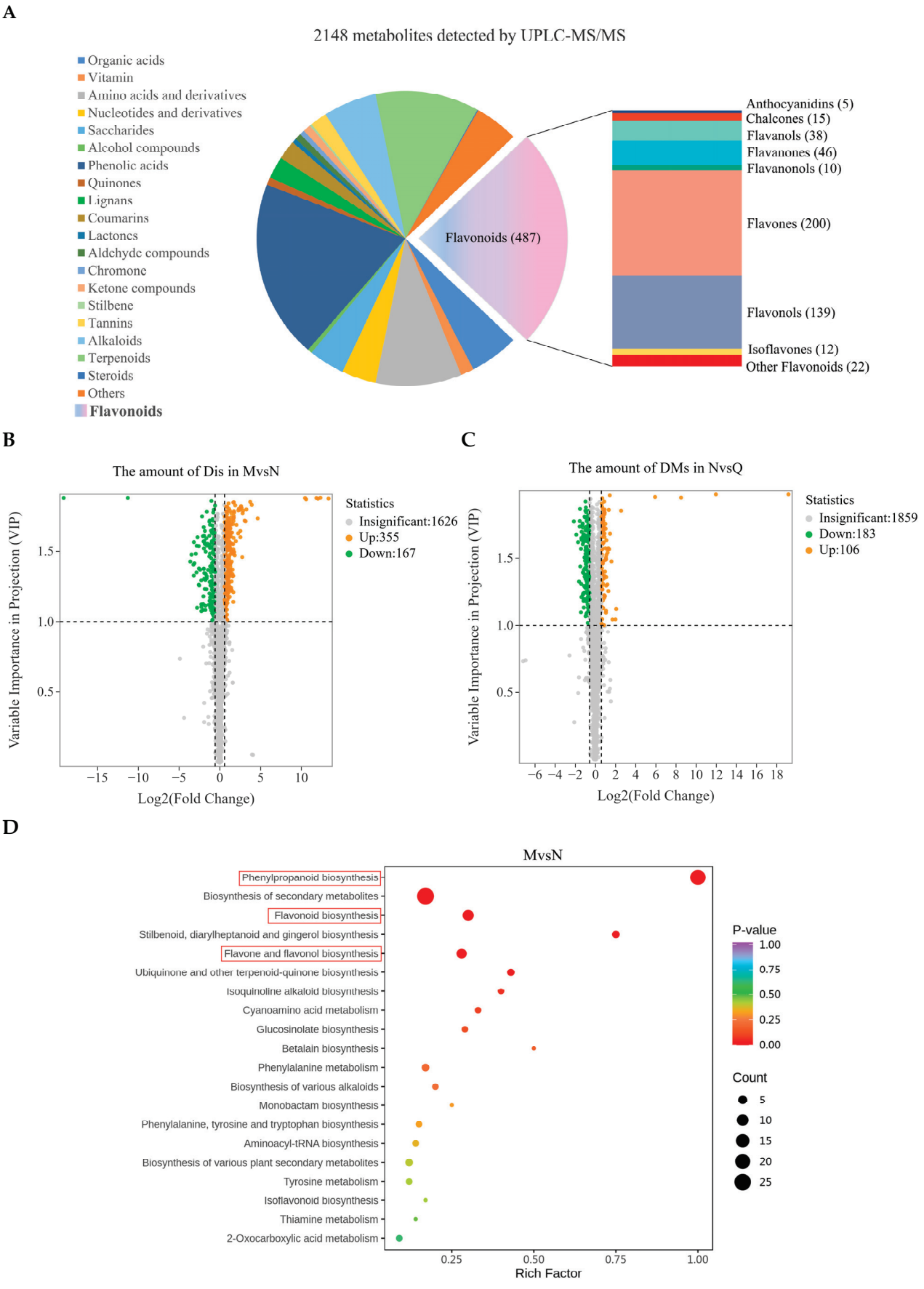


Figure 3. *Cont.*

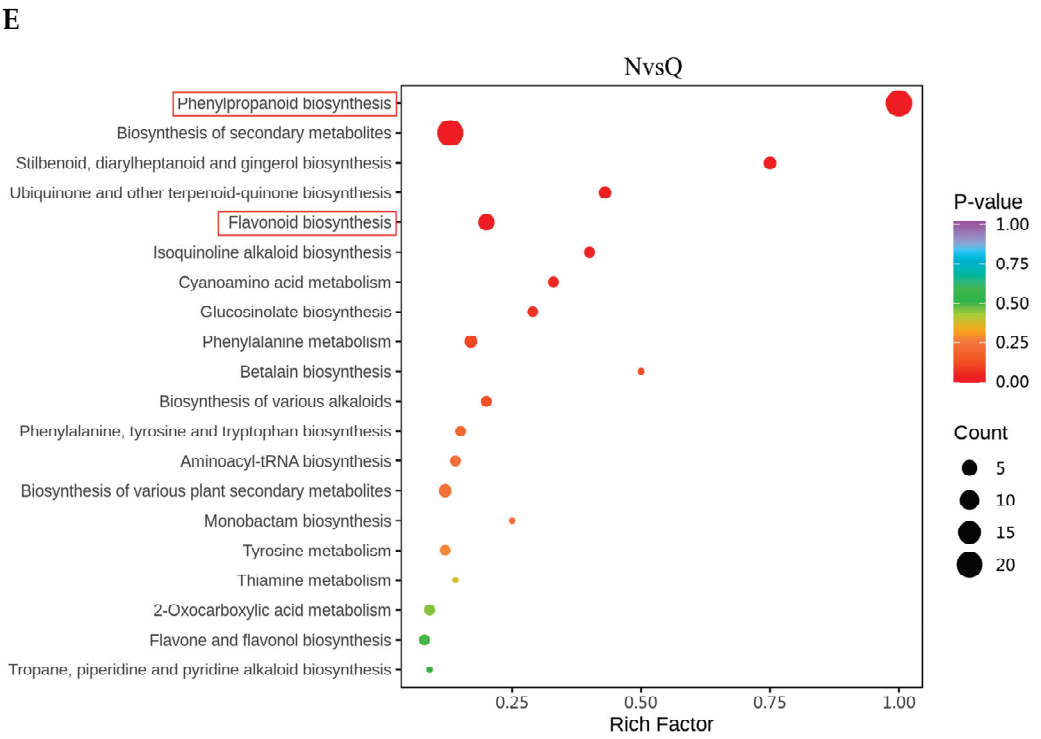


Figure 3. Information related to metabolites in *R. chrysanthum* detected by widely targeted metabolomics. Group M (PAR treated), group N (UV-B radiation treated), and group Q (exogenous ABA and UV-B treated) were the three groups being studied. (**A**) Classification statistics of detected flavonoids and their percentage in total metabolites. (**B**) Volcano plots of DM counts in *R. chrysanthum* under UV-B radiation. (**C**) Volcano plots of DM counts in *R. chrysanthum* after exogenous ABA treatment. (**D**) Bubble plots of KEGG enrichment analysis of DMs in *R. chrysanthum* under UV-B radiation. (**E**) Bubble plots of KEGG enrichment analysis of DMs in *R. chrysanthum* after exogenous ABA treatment.

2.5. Two Experimental Treatments Cause Reprogramming of the Phenylpropanoid Biosynthesis Pathway (ko00940) in R. chrysanthum

This experiment was conducted on *R. chrysanthum* leaf samples for transcriptomics to investigate the dynamics of genes involved in the phenylpropanoid biosynthesis pathway and its internal ABA biosynthesis, as well as the response of genes related to the signaling pathway to UV-B. KEGG enrichment analyses of DEGs produced by the two treatments showed that UV-B radiation mainly led to the production of 35 differentially expressed genes (DEGs) in the phenylpropanoid biosynthesis of *R. chrysanthum*, and exogenous ABA treatment resulted in the production of 3 DEGs (Supplementary Figure S2).

The simplified model of the phenylpropanoid biosynthesis pathway illustrated alterations in DMs and DEGs in phenylpropanoid biosynthesis in *R. chrysanthum* following the two experimental treatments, as well as the regulatory link between them (Figure 4A). ABA and UV-B led to the differential expression of a large number of metabolites in the phenylpropanoid biosynthesis pathway. Among them, the expression of most DMs increased under the influence of UV-B and further increased after ABA treatment, such as the initiating metabolites L-phenylalanine and L-tyrosine (Figure 4B). Following the two experimental treatments, DEGs encoding three enzymes involved in the pathway of phenylpropanoid biosynthesis were generated. There were four DEGs involved in encoding 4-coumarate-CoA ligase (4CL, [EC:6.2.1.12]), and two DEGs were up-regulated in MvsN and consistently up-regulated in NvsQ. There were seven DEGs involved in encoding cinnamoyl-CoA reductase (CCR, [EC:1.2.1.44]), five DEGs were up-regulated in MvsN and consistently up-regulated in NvsQ, and two DEGs were down-regulated in MvsN and con-

sistently down-regulated in NvsQ. There were six DEGs involved in encoding shikimate. There were six DEGs involved in encoding shikimate O-hydroxycinnamoyltransferase (HCT, [EC:2.3.1.133]), of which one DEG was up-regulated in MvsN and consistently up-regulated in NvsQ, and four DEGs were down-regulated in MvsN and consistently down-regulated in NvsQ (Figure 4C).

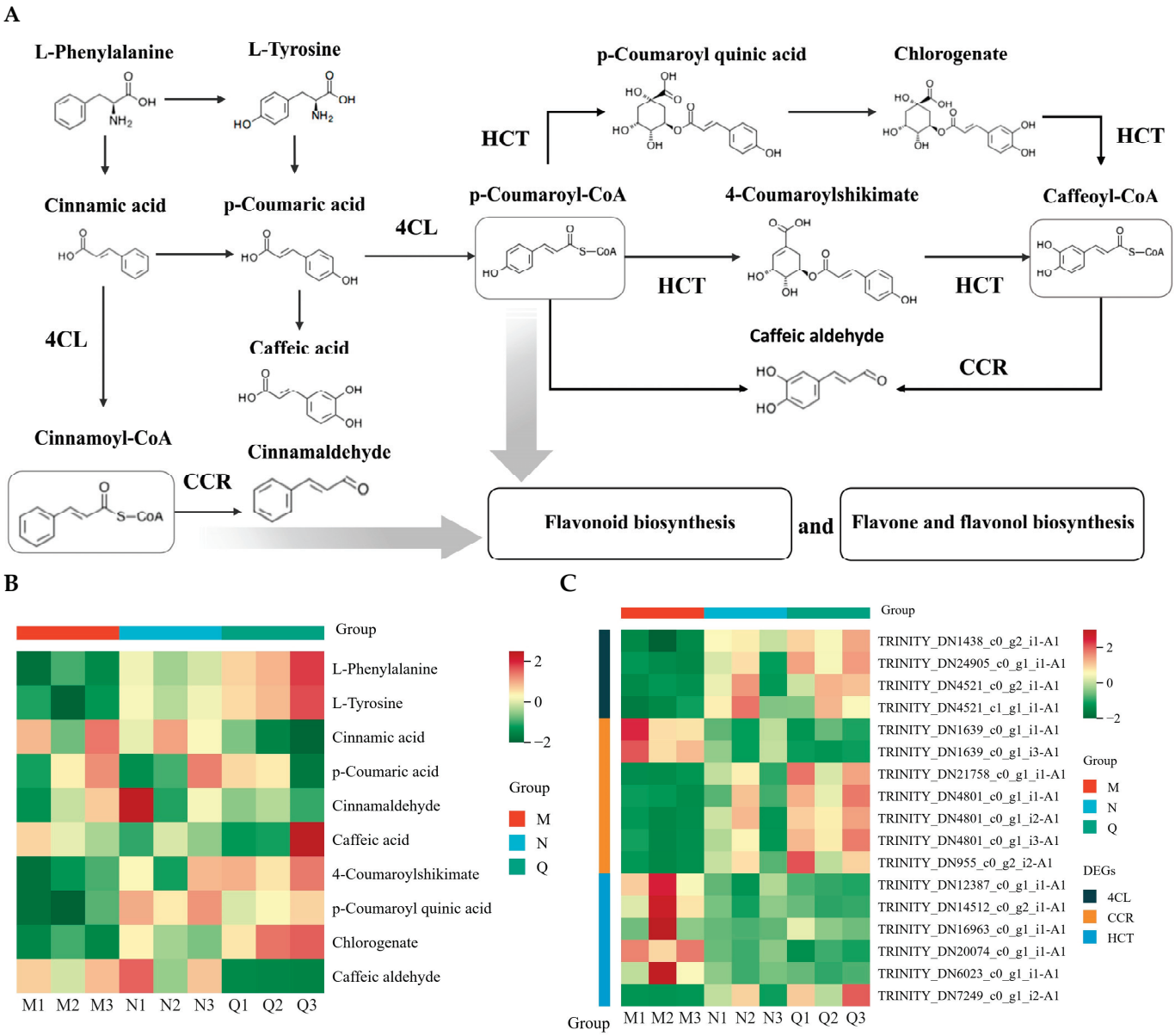


Figure 4. Two experimental treatments prompted reprogramming of the phenylpropanoid biosynthesis pathway in *R. chrysanthum*. Group M (PAR treated), group N (UV-B radiation treated), and group Q (exogenous ABA and UV-B treated) were the three groups being studied. (**A**) Simplified modeling of the phenylpropanoid biosynthesis pathway in *R. chrysanthum*. (**B**,**C**) Clustering heatmap of DMs and DEGs. The expression of DMs and DEGs involved in enzymes in the pathway is presented as a clustered heatmap; the higher the expression, the more reddish the color, and the lower the expression, the more greenish the color. From left to right, each of the adjacent three squares represents three biological replicates of each of the three comparison groups (M, N, and Q).

The findings reveal that the phenylpropanoid biosynthesis pathway is activated in the presence of UV-B exposure in *R. chrysanthum* and exogenous ABA plays an important role in the regulation of enzymes and metabolites related to the phenylpropanoid biosynthesis

pathway. This phenomenon is also consistent with the results of metabolomics KEGG analyses, suggesting that UV-B radiation and exogenous ABA mainly affect the phenylpropanoid biosynthesis pathway in *R. chrysanthum*. This phenomenon is also consistent with the results of metabolomics KEGG analysis, suggesting that the two experimental treatments mainly affected the phenylpropanoid biosynthesis pathway in *R. chrysanthum*.

2.6. MBW Complex Is Involved in the Transcriptional Regulation of the Phenylpropanoid Biosynthesis Pathway in R. chrysanthum

The phenylpropanoid biosynthesis pathway is regulated by a variety of signaling pathways and multiple regulatory mechanisms, among which the MBW complex, consisting of transcription factors and regulatory proteins (R2R3-MYB, bHLH, and WD40), plays an important role in regulating the phenylpropanoid biosynthesis pathway. In this study, we found that a total of 5 R2R3-MYB, 10 bHLH, and 4 WD40-related genes were differentially accumulated in *R. chrysanthum* after two experimental treatments (UV-B and exogenous ABA treatments) (Figure 5A). Most bHLH-related genes were down-regulated after UV-B radiation exposure and consistently down-regulated after exogenous ABA treatment, and only one related gene was consistently elevated after both treatments. In contrast, most WD40-related genes were up-regulated after UV-B radiation exposure and persistently up-regulated after exogenous ABA treatment. Two of the MYB-related genes were consistently up-regulated and one consistently down-regulated after both treatments (Figure 5B–D) (Table 1).

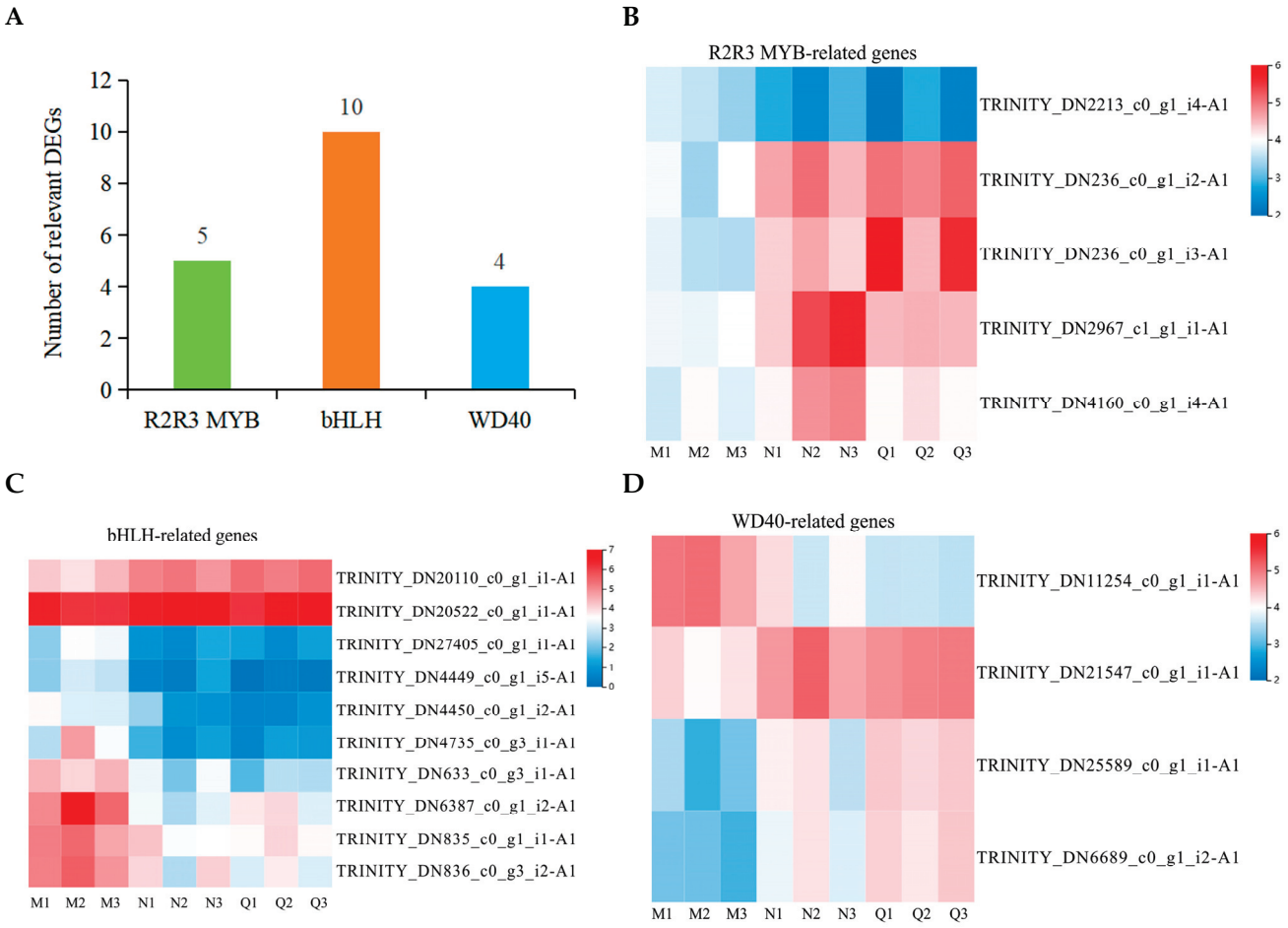


Figure 5. Dynamics of the MBW complex after two experimental treatments. (**A**) Quantitative statistics of MYB, bHLH, and WD40-associated DEGs in *R. chrysanthum* after two experimental treatments. (**B**–**D**) The heatmap of clustering of the expression of MYB, bHLH, and WD40-related DEGs.

Table 1. Information about MBW-related DEGs.

Gene Annotation	Gene ID	M (FPKM)	N (FPKM)	Q (FPKM)	Type (MvsN)	Type (NvsQ)
MYB	TRINITY_DN2213_c0_g1_i4-A1	10.88	5.71	4.57	DOWN	DOWN
	TRINITY_DN236_c0_g1_i2-A1	13.27	23.93	16.35	UP	DOWN
	TRINITY_DN236_c0_g1_i3-A1	14.03	36.31	21.96	UP	DOWN
	TRINITY_DN2967_c1_g1_i1-A1	11.42	20.69	40.91	UP	UP
	TRINITY_DN4160_c0_g1_i4-A1	12.90	26.01	31.85	UP	UP
bHLH	TRINITY_DN20110_c0_g1_i1-A1	76.00	112.60	87.31	UP	DOWN
	TRINITY_DN20522_c0_g1_i1-A1	13.75	1.39	1.01	DOWN	DOWN
	TRINITY_DN27405_c0_g1_i1-A1	62.73	7.33	11.73	DOWN	UP
	TRINITY_DN4449_c0_g1_i5-A1	17.04	32.66	39.16	UP	UP
	TRINITY_DN4450_c0_g1_i2-A1	19.06	7.08	4.35	DOWN	DOWN
	TRINITY_DN4735_c0_g3_i1-A1	33.49	12.73	12.31	DOWN	DOWN
	TRINITY_DN633_c0_g3_i1-A1	36.53	12.17	9.00	DOWN	DOWN
	TRINITY_DN6387_c0_g1_i2-A1	16.49	7.62	6.37	DOWN	DOWN
	TRINITY_DN835_c0_g1_i1-A1	43.89	15.00	11.09	DOWN	DOWN
	TRINITY_DN836_c0_g3_i2-A1	23.60	15.07	13.38	DOWN	DOWN
WD40	TRINITY_DN11254_c0_g1_i1-A1	17.24	28.36	29.08	UP	UP
	TRINITY_DN21547_c0_g1_i1-A1	29.21	15.10	11.10	DOWN	DOWN
	TRINITY_DN25589_c0_g1_i1-A1	7.41	14.59	18.75	UP	UP
	TRINITY_DN6689_c0_g1_i2-A1	8.09	14.91	19.52	UP	UP

Correlation analyses of DMs and DEGs in the phenylpropanoid biosynthesis pathway in *R. chrysanthum* were performed to explore the link between the MBW complex and phenylpropanoid biosynthesis (Supplementary Figure S3). The results showed that the MBW complex was significantly associated with genes related to 4CL, CCR, and HCT. In addition, the MBW complex was significantly correlated with L-phenylalanine and L-tyrosine, the initiating metabolites of the phenylpropanoid biosynthesis pathway, suggesting that there is a close association between the MBW complex of *R. chrysanthum* and the phenylpropanoid biosynthesis pathway under both experimental treatments.

2.7. ABA Production and Signaling in R. chrysanthum Regulate the Phenylpropanoid Biosynthesis Pathway in the Aftermath of UV-B Stress

In addition to the phenylpropanoid biosynthesis pathway being regulated by transcription factors, phytohormone-signaling-related pathways play an important role. The phenylpropanoid biosynthesis pathway in *R. chrysanthum* is, indeed, regulated by ABA, as demonstrated by the preceding exogenous ABA-related data. In this experiment, we further investigated the biosynthesis process of ABA in *R. chrysanthum* under UV-B radiation and its alterations in key genes associated with it as a signal during signal transduction in order to present a complete picture of the dynamics of ABA in regulating the phenylpropanoid biosynthesis pathway in response to UV-B stress.

The findings demonstrated that during *R. chrysanthum*'s ABA biosynthesis, UV-B raised the majority of the important enzymes (CYP97A3, ZEP, and ABA2). UV-B radiation caused differential accumulation of two PYL-related genes (one up-regulated and one down-regulated) and one PP2C-related gene during ABA signaling in *R. chrysanthum* (Figure 6, Table 2). It is thus evident that changes in these key ABA-related genes in *R. chrysanthum* turn on their own ABA signaling pathways to respond positively to UV-B stress.

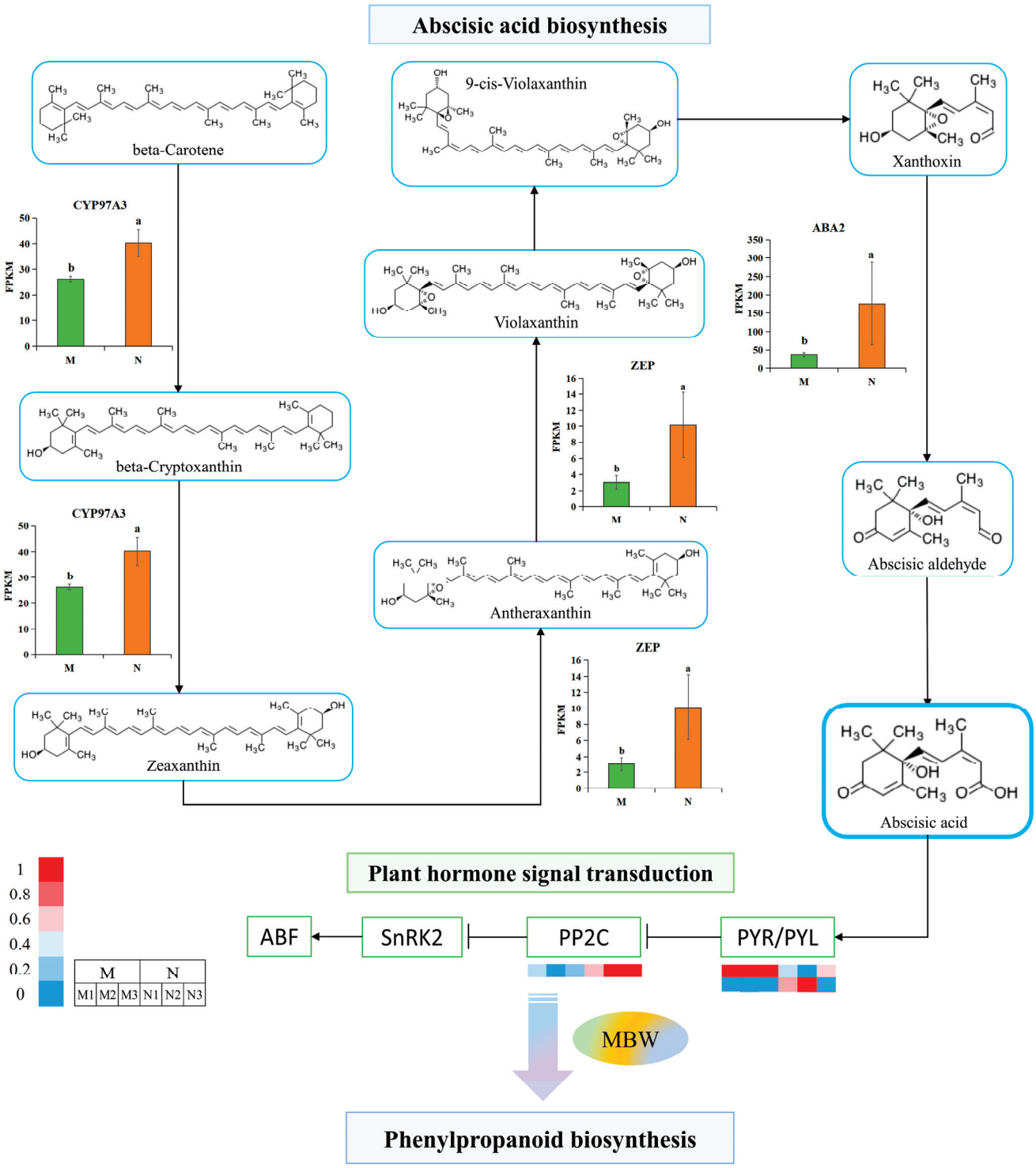


Figure 6. A simplified model of ABA biosynthesis and signal transduction in *R. chrysanthum*. The three biological duplicate experiments' means are shown by the heights of the bar graphs (n = 3), and SDs of the three samples are shown by the error bars. Significant changes across data groups are indicated by different letter markers ($p < 0.05$). The expression of DEGs in the ABA signal transduction pathway is presented as a clustered heatmap; the higher the expression, the more reddish the color, and the lower the expression, the more bluish the color. From left to right, each of the adjacent three squares represents the respective three biological replicates of the two comparison groups, M and N, respectively.

Table 2. Information about DEGs related to the ABA biosynthesis and signal transduction pathway.

Abbreviations for Enzymes	Gene ID	M (FPKM)	N (FPKM)	Type
CYP97A3	TRINITY_DN283_c2_g1_i6-A1	26.24	40.18	UP
ZEP	TRINITY_DN23876_c0_g1_i1-A1	3.04	10.17	UP
ABA2	TRINITY_DN4090_c0_g1_i1-A1	37.36	176.22	UP
PYL	TRINITY_DN3386_c0_g3_i3-A1	15.57	9.31	DOWN
	TRINITY_DN6964_c0_g1_i1-A1	5.73	517.12	UP
PP2C	TRINITY_DN26715_c0_g1_i1-A1	11.47	23.36	UP

2.8. Acetylation Modification of SnRK2, a Key Enzyme in the ABA Signal Transduction Pathway in R. chrysanthum, Under UV-B Stress

Protein acetylation modifications exert a significant impact on the activation of the signal transduction pathway, as well as the activity of signaling molecules. In this study, we performed acetylation proteomics of proteins related to the ABA signal transduction process in *R. chrysanthum* under UV-B radiation in order to reveal the effect of UV-B radiation on the related proteins in ABA signal transduction at the level of acetylation modification.

The results showed that lysine residue 140 of the SnRK2 protein in the ABA signal transduction pathway in *R. chrysanthum* underwent significant acetylation modification, and its expression was significantly increased after UV-B radiation treatment (Figure 7A). Based on this, a three-dimensional structure of SnRK2 was constructed in this experiment, and the acetylation site was labeled (Figure 7B).

Serine/threonine-protein kinase SRK2 (SnRK2) is able to perform its corresponding biological functions, thanks to its natural structure, and the driving of various non-covalent interactions is crucial for the stabilization of its natural structure. Therefore, this experiment used ProteinTools to visualize and analyze these structures (Figure 7C,D). The results showed that SnRK2 contained 38 hydrophobic clusters, of which the largest hydrophobic cluster area was 4014.6^2 (cluster 3), and the smallest hydrophobic cluster area was 38.12^2 (cluster 14). Cluster 3 contained 28 residues, with an area of 39.75^2 per residue and 101 interactions between residues, and cluster 14 contained 2 residues, with an area of 38.12^2 per residue and 2 interactions between residues (Supplementary Table S1). In addition, 70 salt bridge networks were found to exist in the protein, and charge separation parameters were calculated. The findings revealed that the kappa value was 0.13 and the FCR was 0.26.

Accordingly, *R. chrysanthum* is likely to activate the downstream phenylpropanoid biosynthesis pathway under UV-B stress conditions, probably by regulating ABA biosynthesis and interacting with the ABA signaling pathway and ultimately activating the downstream phenylpropanoid biosynthesis pathway through the modification of the acetylation of SnRK2 proteins, which in turn triggers a series of positive responses.

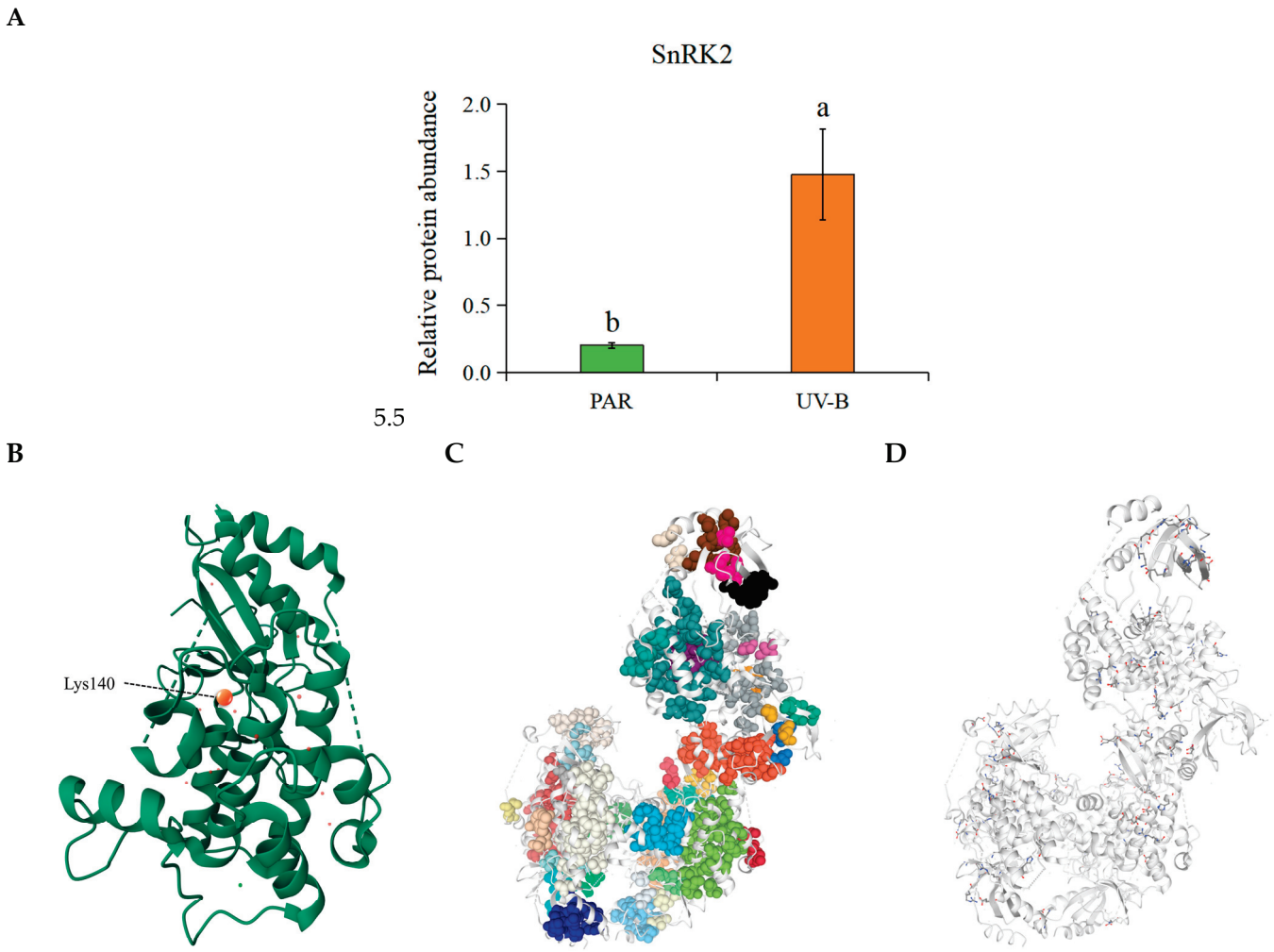


Figure 7. Information about SnRK2 in *R. chrysanthum* under UV-B stress. (**A**) Bar chart of SnRK2 expression under UV-B stress. The three biological duplicate experiments' means are shown by the heights of the bar graphs (n = 3), and the SDs of the three samples are shown by the error bars. Significant changes across data groups are indicated by different letter markers ($p < 0.05$). (**B**) Visualization of the three-dimensional structure of SnRK2 and labeling of its acetylation sites. (**C**) Visualization of SnRK2 hydrophobic clusters. (**D**) Visualization of SnRK2 salt bridges.

3. Discussion

The ozone layer absorbs the majority of UV-B rays in solar radiation and serves as the earth's primary barrier to UV radiation; hence, its loss has resulted in severe UV-B stress for all life on earth [32]. Plants cannot actively avoid hazards but can only face the environmental stresses they face through different specialized adaptive mechanisms [33]. Therefore, in the face of environmental stresses, plants regulate their key metabolic pathways to synthesize important secondary metabolites to ensure that they can survive [34,35].

Photosynthesis in plants converts solar energy into chemical energy and is a direct source of the materials and energy needed for growth and development [36]. Fo is the fluorescence intensity of the chlorophyll molecule in its most basal state, which rises when the plant is subjected to environmental stresses; Ψ_o represents the plant's use of light energy and the efficiency of energy conversion during photosynthesis [37]. φD_o can show the quantum ratio used for heat dissipation, S_m responds to the capacity of the electron acceptor reservoir on the acceptor side, and φEo indicates the quantum yield used for electron transfer [38]. This demonstrates that UV-B radiation degrades *R. chrysanthum*'s antenna pigments, and excess light energy is lost as heat, disrupting the normal operation of

the photosynthetic electron transport chain and impeding photosynthesis (Supplementary Figure S1A). PI_{ABS} is an index of PSII performance based on absorbed light energy that provides an integrated response to the state of the photosynthetic apparatus, Fv/Fm is the maximum photochemical efficiency, and DIo/RC represents the degree of heat dissipation per reaction center [39,40]. The results of this study illustrate that UV-B radiation caused some damage to electron transfer in the PSII of *R. chrysanthum*, and the increase in the burden on the active reaction center forced an increase in the energy dissipation efficiency and heat dissipation (Supplementary Figure S1B–D).

The maximum absorption peak of L-tryptophan in solution is near 280 nm, so it is considered as one of the candidates for sensing UV-B chromophores [41]. L-glutamine is involved in the conversion process from amino acids to chlorophyll precursors and is one of the key nitrogen sources for chlorophyll biosynthesis [42,43]. L-phenylalanine is the initiating metabolite of the phenylpropanoid biosynthesis pathway, and the key precursor for flavonol synthesis is 3-hydroxyphenylpropionic acid, which consists of 3-hydroxycinnamic acid, able to pass through shikimate O-hydroxycinnamoyl transferase (HCT)-catalyzed synthesis [44,45]. The results of this study showed that these key metabolites were altered to different extents after UV-B radiation exposure, while correlation analyses indicated that ABA was likely involved in regulating the phenylpropanoid biosynthesis pathway in *R. chrysanthum* under UV-B stress (Figure 1).

It has been shown that oilseed rape is able to activate its own phenylpropanoid biosynthesis pathway and thus regulate the phenolic acid biosynthesis pathway in order to respond positively to drought stress [46]. Under salt stress, the soybean's phenylpropanoid biosynthesis pathway is activated, which helps control flavonoid synthesis and prevent the formation of reactive oxygen species in the body [47]. The results of this study showed that UV-B radiation and exogenous ABA treatment mainly altered the phenylpropanoid biosynthesis pathway in *R. chrysanthum* (Figure 3B,C). Combined with the results of chlorophyll fluorescence parameters, it is likely that exogenous ABA affects flavonoid biosynthesis by regulating the phenylpropanoid biosynthesis pathway, thereby protecting the photosynthetic system of *R. chrysanthum* (Figure 2). In addition, metabolomics analyses showed that flavonoids accounted for the largest proportion of all metabolites detected in *R. chrysanthum*, which also coincided with a significant increase in 3-hydroxycinnamic acid after UV-B radiation exposure (Figures 1E and 3A). The phenylpropane biosynthesis pathway relies on the regulation of a series of enzymes to ensure that the pathway proceeds properly [48]. It has been shown that the activation of the 4CL gene is closely related to plant defense mechanisms [49]. The results of this study are consistent with previous findings that UV-B radiation and exogenous ABA are able to differentially express 4CL-related genes in *R. chrysanthum* (Figure 4C). This is further evidence from a transcriptomic perspective that the phenylpropanoid biosynthesis pathway in *R. chrysanthum* responds to UV-B stress and that ABA plays an important role in regulating the phenylpropanoid biosynthesis pathway.

It has been shown that the MBW complex, composed of three regulatory proteins (MYB, bHLH, and WD40), is able to regulate the entire phenylpropane metabolic pathway in Arabidopsis [50]. Not only that, one of the R2R3-MYB transcription factors is also closely related to flavonoid regulation [51]. While the bHLH transcription factor does not actually alter flavonoid production pathways, it can dramatically regulate these pathways when combined with the MYB transcription factor [52]. WD40 transcription factors, also known as WDR proteins, play an important role in the regulation of flavonoid metabolism and are also able to assist plants in responding positively to the various stresses they face [53]. In this study, we found that exogenous ABA was able to further alter most of the relevant DEGs of the MBW complex in *R. chrysanthum* after UV-B radiation exposure in the same trend (Table 1). Correlation analyses showed that the MBW complex was

strongly associated with key enzymes in the phenylpropanoid biosynthesis pathway (4CL, CCR, and HCT), as well as with key metabolites, such as L-phenylalanine (Supplementary Figure S3). These results suggest that the MBW complex, indeed, has an important effect on the phenylpropanoid biosynthesis pathway in *R. chrysanthum*.

It has been shown that the expression of genes, such as C4H, DFR, and LDOC, in Arabidopsis seedlings after treatment with exogenous ABA elevated the content of anthocyanins in *Arabidopsis thaliana* [54]. Plant ABA signaling can regulate ionic and osmotic homeostatic signaling-related pathways to maintain its own cellular homeostasis under salt stress [55]. In this study, we found that five key enzymes in ABA biosynthesis were differentially expressed after UV-B radiation exposure (CYP97A3, ZEP, and ABA2, as well as PYL and PP2C) in the ABA signaling pathway (Figure 6). This suggests that UV-B radiation induces changes in ABA biosynthesis and signal transduction in *R. chrysanthum* and thus regulates the downstream phenylpropanoid biosynthesis pathway.

Serine/threonine-protein kinase SRK2 (SnRK2) and PP2C are able to interact with each other, and in general, PP2C inhibits SnRK2 activity, which in turn silences ABA signaling [56]. In contrast, environmental stress can stimulate PYR/PYL to interact with and inhibit the activity of PP2C, leading to the release of SnRK2 from the negative regulatory system by PP2C and the conversion of signaling molecules by the phosphorylation of the downstream factors of SnRK2 and PP2C, which in turn has an impact on subsequent metabolic pathways [57]. This investigation found that PP2C-associated DEGs increased with UV-B, while SnRK2 itself underwent acetylation (Figures 6 and 7). Although UV-B increased the expression of PP2C-related genes capable of inhibiting the activity of SnRK2, it also caused the acetylation of SnRK2. This twofold effect on SnRK2 mediated by UV-B radiation is most likely a unique response style of *R. chrysanthum* to UV-B, and the way it works warrants further exploration.

The results of this study are of great significance for the conservation of *R. chrysanthum* germplasm resources and obtaining new perspectives for understanding the changing patterns of metabolites and their regulatory mechanisms in plants under adverse conditions. The results highlight the key role of ABA in regulating the phenylpropanoid biosynthesis pathway in plants in response to UV-B stress, which broadens research in the field of plant adversity biology. In addition, a deeper understanding of the mechanisms of plant adaptation to UV-B radiation is crucial for the maintenance of biodiversity, especially in ecosystems that are extremely sensitive to changes in UV-B radiation. As global climate change continues, these findings have long-term implications for enhancing agricultural productivity.

4. Materials and Methods

4.1. The Cultivation and Radiation Treatment of Experimental Material

The experimental material in this study was *R. chrysanthum*. To ensure optimal growth of experimental materials, they were kept in an intelligent artificial climate room that simulated an alpine environment. Samples were cultured in 1/4 MS medium. The smart artificial climate chamber simulated the natural light–dark cycle (14 h light/10 h dark) and maintained appropriate temperature conditions (18 °C daytime/16 °C nighttime) and a photon flux density of 50 μmol (photon) m^{-2} s^{-1}. The experiment was conducted on 8-month-old and similarly growing cultured seedlings of *R. chrysanthum*.

The UV-B radiation and exogenous ABA method was grounded in earlier research with appropriate adjustments [58,59]. The experiment was divided into three groups, each of which was subjected to three biological replications (n = 3). *R. chrysanthum* samples from M and N groups were grown in 1/4 MS medium. The culture of *R. chrysanthum* in 1/4 MS medium supplemented with ABA (at a concentration of 100 μmol/L) was group Q.

After transplantation, all samples were incubated in a smart artificial climate chamber for one week before subsequent radiation treatments: group M (PAR treatment only), group N (UV-B radiation treatment), and group Q (UV-B radiation with exogenous ABA treatment).

Using a light meter (Tes-1339 Light Meter Pro.; TES Electrical Electronic Corp., Taipei, China) and a UV intensity meter (ST-513, SHH; Sentry Optron-ICS Corp., New Taipei City, China), the irradiance of the samples treated with UV-B was measured in accordance with the transmission function of the long-pass filter. Group M received only PAR treatment (50 μmol (photon) m^{-2} s^{-1}) for 8 h per day for two days. For two days, groups N and Q were exposed to UV-B radiation for 8 h each day. UV-B radiation was provided by synthetic UV-B lamps in the wavelength range of 280–320 nm. To ensure effective UV-B radiation while excluding other light interferences, the 295 nm filter was mounted above groups N and Q. The 400 nm filter was installed in group M to remove undesired radiation. At the end of the experiment, the sample leaves were frozen in liquid nitrogen for subsequent multi-omics testing (Supplementary Figure S4).

4.2. Widely Targeted Metabolomics

Widely targeted metabolomics analysis of this experiment was performed by Metware Biotech Inc. (Wuhan, China). Experimental procedures and conditions closely followed the descriptions of previous studies [60]. Briefly, Analyst 1.6.3 software and Multial Quant 3.0.2 software were used to qualify and quantify the mass spectrometry data and to perform chromatographic peak integrals. Based on the Metware database (MWDB), the characterization of substances was performed based on the primary and secondary spectral data detected by mass spectrometry. Metabolite quantification was accomplished by MRM analysis using triple quadrupole mass spectrometry, during which the mass spectra of the same metabolite in different samples were integrally corrected for outgoing peaks to obtain metabolite-related data metrics.

Differential metabolites (DMs) were screened based on VIP > 1 and FC $\geq$ 1.5/FC $\leq$ 0.67. These DMs were then tagged in the KEGG database for researching the phenylpropanoid biosynthesis pathway.

4.3. Transcriptomics Testing

The transcriptomics assays in this work were performed by BGI Genomics Co., Ltd., Shenzhen, China. The analytical approaches and settings of the experiments strictly followed the detailed descriptions of previous studies [61].

The total RNA extraction of the samples was carried out by the CTAB method. Single-stranded circular DNA libraries were subsequently constructed and analyzed by RNA-seq.

The MGISEQ-2000 platform was used to perform RNA-seq experiments. Raw sequencing data were initially counted and filtered by SOAPnuke software (v1.4.0) to remove low-quality sequences. Subsequently, further sequence trimming was performed using trimmomatic to ensure the purity of the data. Clean reads were aligned to reference gene sequences by Bowtie2 software (v2.2.5), and the expression levels of genes and transcripts were estimated using RSEM (v1.2.8). To determine the differences in gene expression after the experimental treatments, the FPKM method was used to determine the gene expression of each transcript. The Deseq2 method based on the negative binomial distribution principle was used to explore the differential genes of *R. chrysanthum* after the corresponding experimental treatments. Differentially expressed genes were screened using FC > 1 and q-value (adjusted *p*-value) < 0.05 as standard screening criteria.

Functional annotation and classification of Unigenes used public database resources, such as KEGG, Pfam, and Swissprot. Annotation and classification of information was

achieved by comparing Unigene sequences with sequences in these databases through BLAST comparison.

In this experiment, a total of nine cDNA libraries of *R. chrysanthum* samples were created, and 76.65 GB of data were acquired, with 47,598 Unigenes obtained after assembly and de-redundancy. The size of raw reads obtained was 43.69–45.44 million. After data cleaning and quality checking, the size of clean reads was 42.34–43.46 million. Q20 was more than or equal to 97.83%, whereas Q30 was greater than or equal to 92.4% (Supplementary Table S2). Unigenes had N50, N70, and N90 of not less than 1675, 1106, and 431, respectively, and a GC content of not less than 43.63% (Supplementary Table S3).

4.4. Quantitative Proteomic Detection of Acetylation Modifications

The quantitative proteomics assay for acetylation modifications in this study was carried out by Jingjie PTM BioLab Co. (Hangzhou, China). The assay procedure and experimental conditions were carried out in accordance with the previous experimental description [14]. A brief description is given next.

R. chrysanthum leaves that had been exposed to the relevant experimental treatments were subjected to protein extraction, and the levels of protein were calculated using the two-dimensional quantitative analytical kit. This was followed by trypsinization, a process that desalted the peptides using a Strata X SPE column. The treated peptides were then affinity-enriched, and the resulting peptides were desalted for LCMS/MS analysis using C18 ZipTips according to the manufacturer's instructions. During LCMS/MS analysis, peptides were processed through a capillary source and analyzed by mass spectrometry using timsTOF Pro. The obtained mass spectrometry data were then further analyzed and annotated in the Kyoto Encyclopedia of Genes and Genomes (KEGG) database using the MaxQuant search engine (v.1.6.6.0). The FDR adjustment was set to <1%, and the differential protein screening criteria were set to $p < 0.05$; fold change (FC) ≥ 1.5.

A total of 807 differentially expressed proteins (450 with increased abundance and 357 with decreased abundance) were obtained after UV-B radiation exposure according to the differential protein screening criteria (Supplementary Figure S5A). Of the 685 acetylated differentially expressed proteins after UV-B radiation exposure, 95 increased in abundance and 590 decreased in abundance and of the 945 acetylation sites, 104 were up-regulated and 841 were down-regulated) (Supplementary Figure S5B,C).

Homology modeling of acetylated proteins followed the previous method, using NCBI BLAST to search for homologous sequences [14]. The 3D structural model of the acetylated protein was then created using the comparative protein modeling server SWISS-MODEL.

4.5. Determination of the OJIP Curve

With reference to the previous method [62], the dark adaption period lasted 30 min, and the fast chlorophyll fluorescence induction kinetic curve (O-J-I-P fluorescence induction curve) was measured by a Handy-PEA continuous excitation fluorometer (Hansatech, UK), with a saturated pulsed light intensity of 3000 μmol·m^{-2} s^{-1} and a measurement time of 1 s. The relevant parameters listed later were determined using JIP-test analysis, as described previously [63].

$$\Psi_o \text{ (probability that a trapped exciton moves an electron into the electron)} = 1 - V_j$$
$$(V_j \text{ (relative variable fluorescence intensity at the J-step)} = (F_j - F_o)/(F_m - F_o))$$

$$\varphi E_o \text{ (quantum yield at t = Fo for electron transport)} = [1 - (F_o/F_m)] \times \Psi_o$$

$$\varphi D_o \text{ (quantum yield at t = Fo for energy dissipation)} = 1 - F_v/F_m = 1 - (F_m - F_o)/F_m$$

$$S_m \text{ (normalized total complementary area)} = (\text{area})/(F_m - F_o)$$

$$PI_{ABS}\ (\text{performance index on absorption basis}) = RC/ABS\ [\varphi po/(1-\varphi po)]\ [\Psi_o/(1-\Psi_o)]$$

$$Dio/RC\ (\text{dissipated energy flux per RC at t = Fo}) = ABS/RC - Tro/RC$$

4.6. Determination of Chlorophyll Fluorescence Parameters

The assay was again referenced to the previous experimental procedure [64]. Determination of PSII chlorophyll fluorescence parameters and calculation of related parameters in leaves of *R. chrysanthum* were performed using the IMAGING-PAM chlorophyll fluorescence imaging system (Heinz Walz, Effeltrich, Germany). The test was carried out in a dark environment, where the temperature of the test environment was maintained at the temperature at which the test material was incubated (16 °C–18 °C).

Leaves were dark-adapted for 30 min before testing, light-induced production of Fo (minimal fluorescence) was measured, and excitation with saturating pulses of light produced maximum fluorescence Fm (maximum fluorescence). When fluorescence was reduced to Fo (the minimal fluorescence), the kinetics of fluorescence was induced by using photochemistry (1600 $\mu mol \cdot m^{-2} \cdot s^{-1}$), and saturating pulses were turned on every 20 s for the time when Fm′ (maximum fluorescence in the light) and F (actual fluorescence intensity) at any time were determined.

The final parameters measured included Fv/Fm (maximum photochemical efficiency of PSII), Y(II) (photochemical yield of PSII), Fv′/Fo′ (variable fluorescence ratio in the light), NPQ (non-photochemical quenching), and ETR (actual electron transport rate).

$$Fv'/Fo' = (Fm' - Fo')/Fo'.$$

4.7. Statistical Analysis

Orthogonal partial least squares discriminant analysis (OPLS-DA) was generated using the R package (1.0.1) MetaboAnalystR after the raw data were log2-transformed and then centered. Hierarchical cluster analysis (HCA) results for samples and metabolites are presented as heatmaps, generated by the R package ComplexHeatmap (2.9.4). The identified metabolites were annotated using the KEGG Compound Database (http://www.kegg.jp/kegg/compound/ (accessed on 6 May 2024)), and then the annotated metabolites were mapped to the KEGG pathway database. Statistical analyses were performed using IBM SPSS Statistics 26, and significant differences are indicated by different letters ($p < 0.05$). The data were analyzed using one-way analysis of variance (ANOVA). Each data set involved three biological replicates ($n = 3$). The threshold of 5% was selected to indicate substantial correlation, and the Pearson correlation test was performed.

5. Conclusions

The research clarifies the crucial function of abscisic acid (ABA) in regulating *R. chrysanthum*'s adaptive reaction to UV-B stress. Our comprehensive multi-omics study shows that exogenous ABA can have important regulatory effects on the phenylpropanoid biosynthesis pathway, aiding the plant in adapting to the negative impacts of increased UV-B radiation (Figure 8).

Exogenous ABA treatment was able to mitigate the decrease in photosynthetic efficiency due to UV-B radiation. In addition, exogenous ABA treatment activated the phenylpropanoid biosynthesis pathway in *R. chrysanthum* and altered the content of several flavonoids that play a role in the antioxidant defense mechanisms of the plant.

Taken together, the study reveals the complex regulatory relationship between *R. chrysanthum*'s ABA biosynthesis, the ABA signaling pathway, and the phenylpropanoid biosynthesis pathway in response to UV-B stress. UV-B radiation resulted in the differential expression of genes related to key enzymes in ABA biosynthesis (CYP97A3, ZEP,

and ABA2). In addition, SnRK2, a key component of the ABA signaling cascade reaction, underwent acetylation modification after UV-B radiation exposure, which had an effect on itself.

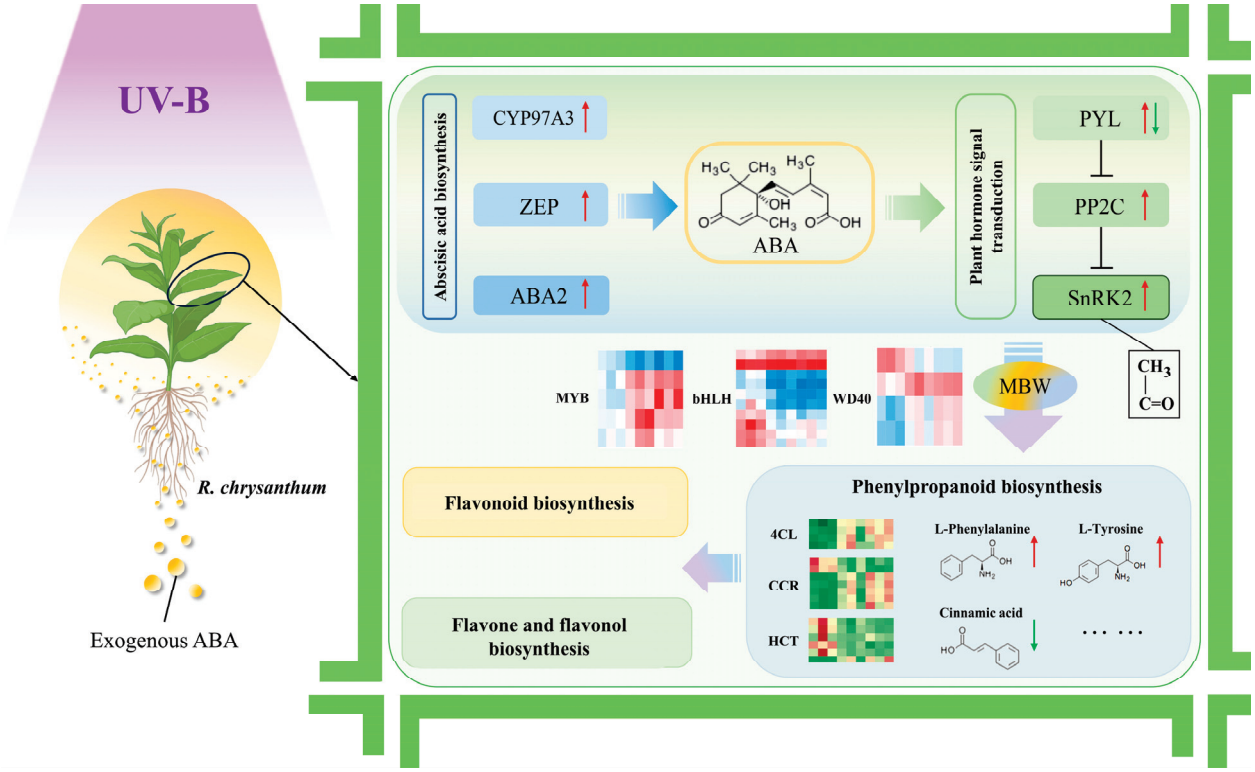


Figure 8. Molecular mechanisms of ABA regulation of the phenylpropanoid biosynthesis pathway in *R. chrysanthum* under UV-B stress.

Supplementary Materials: The supporting information can be downloaded at https://www.mdpi.com/article/10.3390/plants14010101/s1, Figure S1: Effect of UV-B radiation on OJIP curves and its parameters in leaves of *R. chrysanthum*; Figure S2: KEGG enrichment analysis of DEGs from R. chrysanthum under UV-B radiation and exogenous ABA treatment; Figure S3: Correlation analysis network diagram of MBW complex, DMs and DEGs; Figure S4: Flowchart of the culture of experimental material; Figure S5: Statistics on the number of DEPs in R. chrysanthum under UV-B stress; Table S1: Information about hydrophobic cluster of SnRK; Table S2: Quality statistics for Clean Reads; Table S3: Quality Indicators for Unigene. Reference [65] is cited in the Supplementary Materials.

Author Contributions: Writing—original draft preparation, W.Y. and X.Z. (Xiangru Zhou); writing—review and editing, W.Y.; methodology, X.Z. (Xiangru Zhou); software, W.Y.; visualization, W.Y. and J.M.; supervision, W.Y. and X.Z. (Xiangru Zhou); project administration, H.X. and X.Z. (Xiaofu Zhou). All authors have read and agreed to the published version of the manuscript.

Funding: This work was supported by the Jilin Province Science and Technology Development Plan Project (YDZJ202301ZYTS517).

Data Availability Statement: The data used in this study are available from the corresponding author upon submission of a reasonable request.

Acknowledgments: We are grateful to Jingjie PTM Biolab (Hangzhou, China) Co., Ltd., for providing mass spectrometry support.

Conflicts of Interest: The authors declare no conflicts of interest.

Abbreviations

4CL	4-Coumarate-CoA ligase
ABA	Abscisic acid
ABA2	XCanthoxin dehydrogenase
ANOVA	Analysis of variances
C12RT1	Flavanone 7-O-glucoside 2″-O-beta-L-rhamnosyltransferase
CCR	Cinnamoyl-CoA reductase
CYP97A3	Beta-ring hydroxylase
DEGs	Differentially expressed genes
DEPs	Differentially expressed proteins
DFR	Dihydroflavonol 4-reductase
DFs	Different flavonoids
DIo/RC	Dissipated energy flux per RC at t = Fo
DMS	Differential metabolites
ETR	Actual electron transport rate
FC	Fold change
Fm	Fluorescence maximum
Fm′	Maximum fluorescence in the light
Fo	Minimal fluorescence
Fo′	Minimum fluorescence in the light
FPKM	Transcript fragments per kilobase per million mapped reads
Fv′/Fo′	Variable fluorescence ratio in the light
GO	Gene Ontology
HCT	Shikimate O-hydroxycinnamoyltransferase
KEGG	Kyoto Encyclopedia of Genes and Genomes
MWDB	Metware database
NPQ	Non-photochemical quenching
OPLS-DA	Orthogonal partial least squares discriminant analysis
PAR	Photosynthetic active radiation
PI_{ABS}	Performance index on absorption basis
PP2C	Serine/threonine-protein phosphatase 2A catalytic subunit
PQ	Plastoquinone
PSII	Photosystem II
PYL	Abscisic acid receptor PYR/PYL family
QA	The primary quinone acceptor
QB	The secondary quinone acceptor
Q-value	Adjusted *p* value
R. chrysanthum	*Rhododendron chrysanthum* Pall.
S_m	Normalized total complementary area
SnRK2	Serine/threonine-protein kinase SRK2
TFs	Transcription factors
TRo	Trapped energy flux per reaction center
UPLC–MS/MS	Ultra-performance liquid chromatography tandem mass spectrometry
UV-B	Ultraviolet radiation b
VIP	Variable important in projection
ZEP	Zeaxanthin epoxidase
φD_o	Quantum yield at t = Fo for energy dissipation
φE_o	Quantum yield at t = Fo for electron transport
Ψ_o	Probability that a trapped exciton moves an electron into the electron

References

1. Vanhaelewyn, L.; Prinsen, E.; Van Der Straeten, D.; Vandenbussche, F. Hormone-controlled UV-B responses in plants. *J. Exp. Bot.* **2016**, *67*, 4469–4482. [CrossRef] [PubMed]
2. Shi, S.; Shi, R.; Li, T.; Zhou, D. UV-B Radiation Effects on the Alpine Plant Kobresia humilis in a Qinghai-Tibet Alpine Meadow. *Plants* **2022**, *11*, 3102. [CrossRef] [PubMed]
3. Eller, C.B.; Barros, F.d.V.; Bittencourt, P.R.L.; Rowland, L.; Mencuccini, M.; Oliveira, R.S. Xylem hydraulic safety and construction costs determine tropical tree growth. *Plant Cell Environ.* **2018**, *41*, 548–562. [CrossRef]
4. Parihar, P.; Singh, S.; Singh, R.; Singh, V.P.; Prasad, S.M. Changing scenario in plant UV-B research:UV-B from a generic stressor to a specific regulator. *J. Photochem. Photobiol. B* **2015**, *153*, 334–343. [CrossRef] [PubMed]
5. Falara, V.; Amarasinghe, R.; Poldy, J.; Pichersky, E.; Barrow, R.A.; Peakall, R. The production of a key floral volatile is dependent on UV light in a sexually deceptive orchid. *Ann. Bot.* **2013**, *111*, 21–30. [CrossRef] [PubMed]
6. Zhang, F.; Huang, J.; Guo, H.; Yang, C.; Li, Y.; Shen, S.; Zhan, C.; Qu, L.; Liu, X.; Wang, S.; et al. OsRLCK160 contributes to flavonoid accumulation and UV-B tolerance by regulating OsbZIP48 in rice. *Sci. China Life Sci.* **2022**, *65*, 1380–1394. [CrossRef]
7. Kottuparambil, S.; Shin, W.; Brown, M.T.; Han, T. UV-B affects photosynthesis, ROS production and motility of the freshwater flagellate, Euglena agilis Carter. *Aquat. Toxicol.* **2012**, *122–123*, 206–213. [CrossRef] [PubMed]
8. Nocchi, N.; Duarte, H.M.; Pereira, R.C.; Konno, T.U.P.; Soares, A.R. Effects of UV-B radiation on secondary metabolite production, antioxidant activity, photosynthesis and herbivory interactions in *Nymphoides humboldtiana* (Menyanthaceae). *J. Photochem. Photobiol. B* **2020**, *212*, 112021. [CrossRef] [PubMed]
9. Liu, L.-x.; Xu, S.-M.; Woo, K.C. Solar UV-B radiation on growth, photosynthesis and the xanthophyll cycle in tropical acacias and eucalyptus. *Environ. Exp. Bot.* **2005**, *54*, 121–130. [CrossRef]
10. Liu, H.; Cao, X.; Azam, M.; Wang, C.; Liu, C.; Qiao, Y.; Zhang, B. Metabolism of Carotenoids and β-Ionone Are Mediated by Carotenogenic Genes and PpCCD4 Under Ultraviolet B Irradiation and During Fruit Ripening. *Front. Plant Sci.* **2022**, *13*, 814677. [CrossRef] [PubMed]
11. Liu, Y.; Liu, J.; Abozeid, A.; Wu, K.X.; Guo, X.R.; Mu, L.Q.; Tang, Z.H. UV-B Radiation Largely Promoted the Transformation of Primary Metabolites to Phenols in Astragalus mongholicus Seedlings. *Biomolecules* **2020**, *10*, 504. [CrossRef] [PubMed]
12. Zhou, X.; Chen, S.; Wu, H.; Yang, Y.; Xu, H. Biochemical and proteomics analyses of antioxidant enzymes reveal the potential stress tolerance in *Rhododendron chrysanthum* Pall. *Biol. Direct* **2017**, *12*, 10. [CrossRef]
13. Sun, Q.; Liu, M.; Cao, K.; Xu, H.; Zhou, X. UV-B Irradiation to Amino Acids and Carbohydrate Metabolism in *Rhododendron chrysanthum* Leaves by Coupling Deep Transcriptome and Metabolome Analysis. *Plants* **2022**, *11*, 2730. [CrossRef] [PubMed]
14. Liu, M.; Sun, Q.; Cao, K.; Xu, H.; Zhou, X. Acetylated Proteomics of UV-B Stress-Responsive in Photosystem II of *Rhododendron chrysanthum*. *Cells* **2023**, *12*, 478. [CrossRef] [PubMed]
15. Pawlak-Sprada, S.; Arasimowicz-Jelonek, M.; Podgórska, M.; Deckert, J. Activation of phenylpropanoid pathway in legume plants exposed to heavy metals. Part I. Effects of cadmium and lead on phenylalanine ammonia-lyase gene expression, enzyme activity and lignin content. *Acta Biochim. Pol.* **2011**, *58*, 211–216. [CrossRef]
16. Mhiri, R.; Koubaa, I.; Chawech, R.; Auberon, F.; Allouche, N.; Michel, T. New Isoflavones with Antioxidant Activity Isolated from Cornulaca monacantha. *Chem. Biodivers.* **2020**, *17*, e2000758. [CrossRef] [PubMed]
17. Ma, L.; He, J.; Liu, H.; Zhou, h.-h. The phenylpropanoid pathway affects apple fruit resistance to *Botrytis cinerea*. *J. Phytopathol.* **2018**, *166*, 206–215. [CrossRef]
18. Treutter, D. Significance of flavonoids in plant resistance: A review. *Environ. Chem. Lett.* **2006**, *4*, 147–157. [CrossRef]
19. Shen, Y.; Sun, T.; Pan, Q.; Anupol, N.; Chen, H.; Shi, J.; Liu, F.; Deqiang, D.; Wang, C.; Zhao, J.; et al. RrMYB5- and RrMYB10-regulated flavonoid biosynthesis plays a pivotal role in feedback loop responding to wounding and oxidation in *Rosa rugosa*. *Plant Biotechnol. J.* **2019**, *17*, 2078–2095. [CrossRef]
20. Hewage, K.A.H.; Yang, J.F.; Wang, D.; Hao, G.F.; Yang, G.F.; Zhu, J.K. Chemical Manipulation of Abscisic Acid Signaling: A New Approach to Abiotic and Biotic Stress Management in Agriculture. *Adv. Sci.* **2020**, *7*, 2001265. [CrossRef]
21. Luo, M.; Liu, J.H.; Mohapatra, S.; Hill, R.D.; Mohapatra, S.S. Characterization of a gene family encoding abscisic acid- and environmental stress-inducible proteins of alfalfa. *J. Biol. Chem.* **1992**, *267*, 15367–15374. [CrossRef] [PubMed]
22. Hartung, W.; Schraut, D.; Jiang, F. Physiology of abscisic acid (ABA) in roots under stress—A review of the relationship between root ABA and radial water and ABA flows. *Crop Pasture Sci.* **2005**, *56*, 1253–1259. [CrossRef]
23. You, Y.; Wang, Y.; Zhang, S.; Sun, X.; Liu, H.; Guo, E.Y.; Du, S. Different pathways for exogenous ABA-mediated down-regulation of cadmium accumulation in plants under different iron supplies. *J. Hazard. Mater.* **2022**, *440*, 129769. [CrossRef] [PubMed]
24. Pan, W.; You, Y.; Shentu, J.L.; Weng, Y.N.; Wang, S.T.; Xu, Q.R.; Liu, H.J.; Du, S.T. Abscisic acid (ABA)-importing transporter 1 (AIT1) contributes to the inhibition of Cd accumulation via exogenous ABA application in Arabidopsis. *J. Hazard. Mater.* **2020**, *391*, 122189. [CrossRef] [PubMed]
25. Zhu, Y.; You, Y.; Zheng, S.; Li, J.; Wang, Y.; Wu, R.; Fang, Z.; Liu, H.; Du, S. ABA-importing transporter (AIT1) synergies enhances exogenous ABA minimize heavy metals accumulations in Arabidopsis. *J. Hazard. Mater.* **2024**, *473*, 134718. [CrossRef] [PubMed]

26. Zhang, C.; Ma, C.; Zhu, L.; Yao, M. Simultaneous determination of protoporphyrin IX and magnesium protoporphyrin IX in *Arabidopsis thaliana* and *Camellia sinensis* using UPLC-MS/MS. *Plant Methods* **2023**, *19*, 34. [CrossRef] [PubMed]
27. Balcke, G.U.; Handrick, V.; Bergau, N.; Fichtner, M.; Henning, A.; Stellmach, H.; Tissier, A.; Hause, B.; Frolov, A. An UPLC-MS/MS method for highly sensitive high-throughput analysis of phytohormones in plant tissues. *Plant Methods* **2012**, *8*, 47. [CrossRef] [PubMed]
28. Jiang, Z.; Zhou, X.; Li, R.; Michal, J.J.; Zhang, S.; Dodson, M.V.; Zhang, Z.; Harland, R.M. Whole transcriptome analysis with sequencing: Methods, challenges and potential solutions. *Cell Mol. Life Sci.* **2015**, *72*, 3425–3439. [CrossRef]
29. Averbeck, N.B.; Durante, M. Protein acetylation within the cellular response to radiation. *J. Cell Physiol.* **2011**, *226*, 962–967. [CrossRef]
30. Guan, K.L.; Xiong, Y. Regulation of intermediary metabolism by protein acetylation. *Trends Biochem. Sci.* **2011**, *36*, 108–116. [CrossRef]
31. Choudhary, C.; Kumar, C.; Gnad, F.; Nielsen, M.L.; Rehman, M.; Walther, T.C.; Olsen, J.V.; Mann, M. Lysine acetylation targets protein complexes and co-regulates major cellular functions. *Science* **2009**, *325*, 834–840. [CrossRef] [PubMed]
32. Takshak, S.; Agrawal, S.B. Defense potential of secondary metabolites in medicinal plants under UV-B stress. *J. Photochem. Photobiol. B* **2019**, *193*, 51–88. [CrossRef] [PubMed]
33. Suzuki, N.; Rivero, R.M.; Shulaev, V.; Blumwald, E.; Mittler, R. Abiotic and biotic stress combinations. *New Phytol.* **2014**, *203*, 32–43. [CrossRef] [PubMed]
34. Escobar-Bravo, R.; Klinkhamer, P.G.; Leiss, K.A. Interactive Effects of UV-B Light with Abiotic Factors on Plant Growth and Chemistry, and Their Consequences for Defense against Arthropod Herbivores. *Front. Plant Sci.* **2017**, *8*, 278. [CrossRef]
35. Lee, J.H.; Shibata, S.; Goto, E. Time-Course of Changes in Photosynthesis and Secondary Metabolites in Canola (*Brassica napus*) Under Different UV-B Irradiation Levels in a Plant Factory With Artificial Light. *Front. Plant Sci.* **2021**, *12*, 786555. [CrossRef] [PubMed]
36. Armbruster, U.; Correa Galvis, V.; Kunz, H.H.; Strand, D.D. The regulation of the chloroplast proton motive force plays a key role for photosynthesis in fluctuating light. *Curr. Opin. Plant Biol.* **2017**, *37*, 56–62. [CrossRef] [PubMed]
37. Laible, P.D.; Zipfel, W.; Owens, T.G. Excited state dynamics in chlorophyll-based antennae: The role of transfer equilibrium. *Biophys. J.* **1994**, *66*, 844–860. [CrossRef] [PubMed]
38. Tóth, S.Z.; Schansker, G.; Strasser, R.J. A non-invasive assay of the plastoquinone pool redox state based on the OJIP-transient. *Photosynth. Res.* **2007**, *93*, 193–203. [CrossRef] [PubMed]
39. Appenroth, K.J.; Stöckel, J.; Srivastava, A.; Strasser, R.J. Multiple effects of chromate on the photosynthetic apparatus of Spirodela polyrhiza as probed by OJIP chlorophyll a fluorescence measurements. *Environ. Pollut.* **2001**, *115*, 49–64. [CrossRef]
40. Jin, X.; Yang, G.; Tan, C.; Zhao, C. Effects of nitrogen stress on the photosynthetic CO_2 assimilation, chlorophyll fluorescence, and sugar-nitrogen ratio in corn. *Sci. Rep.* **2015**, *5*, 9311. [CrossRef]
41. Fritsche, E.; Schäfer, C.; Calles, C.; Bernsmann, T.; Bernshausen, T.; Wurm, M.; Hübenthal, U.; Cline, J.E.; Hajimiragha, H.; Schroeder, P.; et al. Lightening up the UV response by identification of the arylhydrocarbon receptor as a cytoplasmatic target for ultraviolet B radiation. *Proc. Natl. Acad. Sci. USA* **2007**, *104*, 8851–8856. [CrossRef]
42. Yu, H.; Zhang, Y.; Zhang, Z.; Zhang, J.; Wei, Y.; Jia, X.; Wang, X.; Ma, X. Towards identification of molecular mechanism in which the overexpression of wheat cytosolic and plastid glutamine synthetases in tobacco enhanced drought tolerance. *Plant Physiol. Biochem.* **2020**, *151*, 608–620. [CrossRef]
43. Gou, T.; Yang, L.; Hu, W.; Chen, X.; Zhu, Y.; Guo, J.; Gong, H. Silicon improves the growth of cucumber under excess nitrate stress by enhancing nitrogen assimilation and chlorophyll synthesis. *Plant Physiol. Biochem.* **2020**, *152*, 53–61. [CrossRef]
44. Tong, Y.; Yi, S.C.; Liu, S.Y.; Xu, L.; Qiu, Z.X.; Zeng, D.Q.; Tang, W.W. Bruceine D may affect the phenylpropanoid biosynthesis by acting on ADTs thus inhibiting *Bidens pilosa* L. seed germination. *Ecotoxicol. Environ. Saf.* **2022**, *242*, 113943. [CrossRef] [PubMed]
45. Muro-Villanueva, F.; Mao, X.; Chapple, C. Linking phenylpropanoid metabolism, lignin deposition, and plant growth inhibition. *Curr. Opin. Biotechnol.* **2019**, *56*, 202–208. [CrossRef] [PubMed]
46. Rezayian, M.; Niknam, V.; Ebrahimzadeh, H. Differential responses of phenolic compounds of *Brassica napus* under drought stress. *Plant Physiol.* **2018**, *8*, 2417–2425.
47. Yan, J.; Wang, B.; Jiang, Y.; Cheng, L.; Wu, T. GmFNSII-controlled soybean flavone metabolism responds to abiotic stresses and regulates plant salt tolerance. *Plant Cell Physiol.* **2014**, *55*, 74–86. [CrossRef] [PubMed]
48. Vogt, T. Phenylpropanoid biosynthesis. *Mol. Plant* **2010**, *3*, 2–20. [CrossRef] [PubMed]
49. Uhlmann, A.; Ebel, J. Molecular cloning and expression of 4-coumarate:coenzyme A ligase, an enzyme involved in the resistance response of soybean (*Glycine max* L.) against pathogen attack. *Plant Physiol.* **1993**, *102*, 1147–1156. [CrossRef] [PubMed]
50. Gonzalez, A.; Zhao, M.; Leavitt, J.M.; Lloyd, A.M. Regulation of the anthocyanin biosynthetic pathway by the TTG1/bHLH/Myb transcriptional complex in Arabidopsis seedlings. *Plant J.* **2008**, *53*, 814–827. [CrossRef] [PubMed]
51. Xu, F.; Ning, Y.; Zhang, W.; Liao, Y.; Li, L.; Cheng, H.; Cheng, S. An R2R3-MYB transcription factor as a negative regulator of the flavonoid biosynthesis pathway in *Ginkgo biloba*. *Funct. Integr. Genom.* **2014**, *14*, 177–189. [CrossRef] [PubMed]

52. Hichri, I.; Heppel, S.C.; Pillet, J.; Léon, C.; Czemmel, S.; Delrot, S.; Lauvergeat, V.; Bogs, J. The basic helix-loop-helix transcription factor MYC1 is involved in the regulation of the flavonoid biosynthesis pathway in grapevine. *Mol. Plant* **2010**, *3*, 509–523. [CrossRef]
53. Petridis, A.; Döll, S.; Nichelmann, L.; Bilger, W.; Mock, H.P. Arabidopsis thaliana G2-LIKE FLAVONOID REGULATOR and BRASSINOSTEROID ENHANCED EXPRESSION1 are low-temperature regulators of flavonoid accumulation. *New Phytol.* **2016**, *211*, 912–925. [CrossRef] [PubMed]
54. Luo, P.; Shen, Y.; Jin, S.; Huang, S.; Cheng, X.; Wang, Z.; Li, P.; Zhao, J.; Bao, M.; Ning, G. Overexpression of *Rosa rugosa* anthocyanidin reductase enhances tobacco tolerance to abiotic stress through increased ROS scavenging and modulation of ABA signaling. *Plant Sci.* **2016**, *245*, 35–49. [CrossRef] [PubMed]
55. Zhu, J.K. Salt and drought stress signal transduction in plants. *Annu. Rev. Plant Biol.* **2002**, *53*, 247–273. [CrossRef] [PubMed]
56. Yoshida, R.; Umezawa, T.; Mizoguchi, T.; Takahashi, S.; Takahashi, F.; Shinozaki, K. The regulatory domain of SRK2E/OST1/SnRK2.6 interacts with ABI1 and integrates abscisic acid (ABA) and osmotic stress signals controlling stomatal closure in Arabidopsis. *J. Biol. Chem.* **2006**, *281*, 5310–5318. [CrossRef] [PubMed]
57. Umezawa, T.; Nakashima, K.; Miyakawa, T.; Kuromori, T.; Tanokura, M.; Shinozaki, K.; Yamaguchi-Shinozaki, K. Molecular basis of the core regulatory network in ABA responses: Sensing, signaling and transport. *Plant Cell Physiol.* **2010**, *51*, 1821–1839. [CrossRef] [PubMed]
58. Yu, W.; Gong, F.; Xu, H.; Zhou, X. Molecular Mechanism of Exogenous ABA to Enhance UV-B Resistance in *Rhododendron chrysanthum* Pall. by Modulating Flavonoid Accumulation. *Int. J. Mol. Sci.* **2024**, *25*, 5248. [CrossRef]
59. Lyu, J.; Wang, C.; Liang, D.Y.; Liu, L.; Pandey, L.K.; Xu, H.W.; Zhou, X.F. Sensitivity of wild and domesticated *Rhododendron chrysanthum* to different light regime (UVA, UVB, and PAR). *Photosynthetica* **2019**, *57*, 841–849. [CrossRef]
60. Gong, F.; Yu, W.; Zeng, Q.; Dong, J.; Cao, K.; Xu, H.; Zhou, X. *Rhododendron chrysanthum*'s Primary Metabolites Are Converted to Phenolics More Quickly When Exposed to UV-B Radiation. *Biomolecules* **2023**, *13*, 1700. [CrossRef] [PubMed]
61. Yu, W.; Gong, F.; Zhou, X.; Xu, H.; Lyu, J.; Zhou, X. Comparative Metabolomics and Transcriptome Studies of Two Forms of *Rhododendron chrysanthum* Pall. under UV-B Stress. *Biology* **2024**, *13*, 211. [CrossRef] [PubMed]
62. Liu, M.; Lin, X.; Cao, K.; Yang, L.; Xu, H.; Zhou, X. Multi-Omic Analysis Reveals the Molecular Mechanism of UV-B Stress Resistance in Acetylated RcMYB44 in *Rhododendron chrysanthum*. *Genes* **2023**, *14*, 2022. [CrossRef] [PubMed]
63. Strasser, R.J.; Tsimilli-Michael, M.; Qiang, S.; Goltsev, V. Simultaneous in vivo recording of prompt and delayed fluorescence and 820-nm reflection changes during drying and after rehydration of the resurrection plant *Haberlea rhodopensis*. *Biochim. Biophys. Acta* **2010**, *1797*, 1313–1326. [CrossRef] [PubMed]
64. Zeng, Q.; Dong, J.; Lin, X.; Zhou, X.; Xu, H. Isolation and Identification of *Acer truncatum* Endophytic Fungus Talaromyces verruculosus and Evaluation of Its Effects on Insoluble Phosphorus Absorption Capacity and Growth of Cucumber Seedlings. *J. Fungi* **2024**, *10*, 136. [CrossRef] [PubMed]
65. Gong, F.; Yu, W.; Cao, K.; Xu, H.; Zhou, X. Rctrp5 transcription factor mediates the molecular mechanism of ligninbiosynthesis regulation in r. Chrysanthum against uv-b stress. *Int. J. Mol. Sci.* **2024**, *25*, 9205. [CrossRef]

Disclaimer/Publisher's Note: The statements, opinions and data contained in all publications are solely those of the individual author(s) and contributor(s) and not of MDPI and/or the editor(s). MDPI and/or the editor(s) disclaim responsibility for any injury to people or property resulting from any ideas, methods, instructions or products referred to in the content.

plants

MDPI

Article

WRKY Transcription Factors Modulate the Flavonoid Pathway of *Rhododendron chrysanthum* Pall. Under UV-B Stress

Wang Yu †, Xiangru Zhou †, Jinhao Meng, Hongwei Xu * and Xiaofu Zhou *

Jilin Provincial Key Laboratory of Plant Resource Science and Green Production, Jilin Normal University, Siping 136000, China

* Correspondence: xuhongwei@jlnu.edu.cn (H.X.); zhouxiaofu@jlnu.edu.cn (X.Z.)

† These authors contributed equally to this work.

Abstract: The depletion of the ozone layer has resulted in elevated ultraviolet-B (UV-B) radiation levels, posing a significant risk to terrestrial plant growth. *Rhododendron chrysanthum* Pall. (*R. chrysanthum*), adapted to high-altitude and high-irradiation environments, has developed unique adaptive mechanisms. This study exposed *R. chrysanthum* to UV-B radiation for two days, with an 8 h daily treatment, utilizing metabolomic and transcriptomic analyses to explore the role of WRKY transcription factors in the plant's UV-B stress response and their regulation of flavonoid synthesis. UV-B stress resulted in a significant decrease in rETR and Ik and a significant increase in 1-qP. These chlorophyll fluorescence parameters indicate that UV-B stress impaired photosynthesis in *R. chrysanthum*. Faced with the detrimental impact of UV-B radiation, *R. chrysanthum* is capable of mitigating its effects by modulating its flavonoid biosynthetic pathways to adapt positively to the stress. This study revealed changes in the expression of 113 flavonoid-related metabolites and 42 associated genes, with WRKY transcription factors showing significant correlation with these alterations. WRKY transcription factors can influence the expression of key enzyme genes in the flavonoid metabolic pathway, thereby affecting metabolite production. A theoretical reference for investigating plant stress physiology is provided in this work, which also offers insights into the stress responses of alpine plants under adverse conditions.

Keywords: *Rhododendron chrysanthum* Pall.; multi-omics; WRKY transcription factor; UV-B stress; metabolomics

1. Introduction

The Earth's surface is exposed to ultraviolet (UV) radiation, which originates from sunlight and has a significant impact on ecosystems [1]. Ultraviolet radiation can be categorized into three main bands, i.e., long wave (315–400 nm, UV-A), medium wave (280–315 nm, UV-B), and short wave (200–280 nm, UV-C), with UV-B having the most widespread impact on living organisms in nature [2–4]. Ultraviolet-B (UV-B) stress is a common abiotic factor that can severely limit plant growth and development [5]. UV-B radiation breaks down the structure of macromolecular DNA, alter plant morphology, reduce the plant photosynthetic rate, and affect plant productivity [6–8].

Transcriptomic studies on peach peel following UV-B stress indicate that UV RESISTANCE LOCUS 8 (*UVR8*) may be involved in phenolic biosynthesis [9]. Phosphorylated proteomic studies have shown that UV-B radiation can activate oxidative stress response, photosynthetic energy metabolism, and MAPK signal transduction and promote the accumulation of secondary metabolites [10]. Metabolomic and transcriptomic studies have

shown that amino acids and carbohydrates promote resistance to UV-B stress in *R. chrysanthum* [11]. Studies have shown that the secondary metabolites (tocopherols, polyamines, and flavonoids) of plants have different accumulation patterns under UV-B domestication [12]. *UVR8* is involved in regulating plant growth and development as a photoreceptor. Studies on *UVR8* in apple showed that *UVR8* plays an important role in regulating photomorphogenesis under UV-B light [13]. Hydrogen peroxide, as a signaling molecule, can mediate the synthesis of flavonoids under UV-B radiation [14]. It has been shown that plants are able to protect themselves against UV-B radiation damage by inducing the synthesis of UV-absorbing substances such as flavonoids [15,16]. Flavonols in Ginkgo biloba, especially isorhamnetin, increased exponentially in response to in response to UV-B stress [17]. Flavonoid synthases in maize are involved in the synthesis of flavonoids such as apigenin against UV-B stress [18]. Understanding the molecular mechanisms of plant resistance to UV-B radiation is beneficial for screening varieties with strong stress resistance [19].

As sessile organisms, plants cannot move like an animal to escape their environmental conditions. Plants adapt to harsh environments by adjusting the content of various metabolites and altering their developmental processes [20]. *R. chrysanthum* is an important plant resource. It grows at an altitude of 1300–2650 m in the Changbai Mountains in China. It is cold there all year round, and plants are exposed to strong UV radiation and strong winds. During evolution, *R. chrysanthum* was able to adapt to this extreme environment [21]. There are many studies on plant cold resistance that have found that the antioxidant system of *R. chrysanthum* is enhanced during long-term acclimatization [22]. Quantitative proteomic and phosphorylated proteomic results indicate that multiple-reactive oxygen species clearance and calcium-mediated signaling pathways are triggered to resist cold stress [23]. In a previous study, the combination of 2.3 $W \cdot m^{-2}$ and 2 days of radiation treatment was determined to have the most significant negative effect on the fluorescence characteristics of *R. chrysanthum* by varying the intensity of UV-B radiation with the duration of radiation [24].

However, less research has been performed on how alpine plants resist against UV-B stress. Metabolomic studies have shown that the accumulation of flavonoids, organic acids, amino acids, and fatty acids may protect *R. chrysanthum* from UV-B harm [21]. Proteomic studies have shown that UV-B stress starts the photosynthesis pathway in plants and photosystem II (PSII) proteins are possibly acetylated to reduce impairment [25]. The long-term acclimatization of *R. chrysanthum* helps to study its reaction to UV-B stress. Studies have confirmed that *R. chrysanthum* is sensitive to UV-B radiation and exhibits effective antagonistic mechanisms [24]. Therefore, *R. chrysanthum* is a good material for studying UV-B stress.

WRKY TFs are associated with the adjustment of plants in response to abiotic stress. Studies on *Nicotiana benthamiana* showed that *GhWRKY41* could act as a positive regulator of stomatal closure, the modulation of reactive oxygen species (ROS) scavenging, and the expression of antioxidant genes to enhance plant tolerance to salt stress and drought stress [26]. Studies on WRKY transcription factors in soybean showed that *GmWRKY21* was able to regulate tolerance to cold stress in transgenic *Arabidopsis* plants, whereas *GmWRKY54* may confer salt and drought tolerance to *Arabidopsis* by regulating DREB2A and STZ/Zat10 [27]. Investigating the alterations in WRKY TFs within the leaves of *R. chrysanthum* under UV-B stress may enhance our understanding of the molecular mechanisms underlying UV-B radiation tolerance in this species.

Widely targeted metabolomics, which can detect more metabolites, is the latest technology in metabolomic research [28]. A study was conducted to characterize phenolic compounds by using UPLC-MS/MS to study the variation in the content of polyphenols in *Spondias mombin* L. [29]. The metabolite profiles of *R. chrysanthum* in the M group (normal

light) and the N group (normal light +UV-B radiation) were analyzed and quantitatively compared based on UPLC-MS/MS. See Section 4 for specific material treatments.

In a broader application of transcriptomics, some researchers have used transcriptomics to study the role of UV-B dose in regulating L-ascorbic acid (AsA) biosynthesis in *Lactuca sativa* [30]. Examining the transcriptome of peach skins vacuum freeze-drying UV-B exposure revealed the activation of genes involved in phenolic biosynthesis, informing the use of UV-B treatments to increase the content of health-promoting compounds in peach fruit [9]. Transcriptomics was used to study the molecular mechanisms of peach trees under low-temperature stress, and it was found that soluble sugar, flavonoid, and lignin biosynthesis-related genes may play important roles in cold tolerance in peach [31]. Numerous studies have shown that transcriptomics plays an important role in the study of plant response to abiotic stresses.

Joint analysis of transcriptomics and metabolomics is an important method for omics research. One study utilized this approach to investigate the effects of short-term CO_2 treatment on the postharvest quality of chili peppers and the molecular mechanism of their regulation, which provides a reference for the study of crop preservation conditions [32]. The study of post-irradiation mouse blood using combined transcriptomic and metabolomic analyses has made a significant contribution to the field of biomedicine by finding that this approach helps to provide a deeper understanding of the crosstalk between different biomolecules [33]. Metabolomic and transcriptomic association analyses can study key pathways involving genes in differential metabolite synthesis and understand how key substances are regulated following UV-B radiation.

In order to investigate the plant response to UV-B stress, both normal light- and UV-B-irradiated *R. chrysanthum* specimens were utilized in this study. We examined the metabolites and associated genes that exhibited significant alterations in the leaves of *R. chrysanthum* under UV-B radiation conditions through metabolomic and transcriptomic analyses. Additionally, we analyzed the TFs that may be involved in flavonoid synthesis. This research study provides a valuable reference for understanding how flavonoids respond to UV-B stress and enhances our comprehension of their antagonistic effects.

2. Results

2.1. Significant Changes in Chlorophyll Fluorescence Parameters Occur Following UV-B Treatment

Following exposure to environmental stress, alterations in the photosynthetic process of plants can be reflected in the parameters of chlorophyll fluorescence. Chlorophyll fluorescence metrics that were pertinent to the UV-B-treated study subjects were established in this investigation. Following exposure to UV-B light, it became obvious that *R. chrysanthum*'s photosystem II of rETR (relative electron transfer rate) dramatically dropped (Figure 1a). The plant's capacity to withstand intense light is indicated by "I_k", while the percentage of photosystem II reaction centers in the off state is shown by "1-qP". UV-B caused a significant decrease in I_K and a significant increase in "1-qP" (Figure 1b,c). It could mean that UV-B stress severely restricted *R. chrysanthum*'s ability to carry out photosynthesis ordinarily. For the purpose of safeguarding itself from UV-B damage, *R. chrysanthum* initiates its own metabolic defense system.

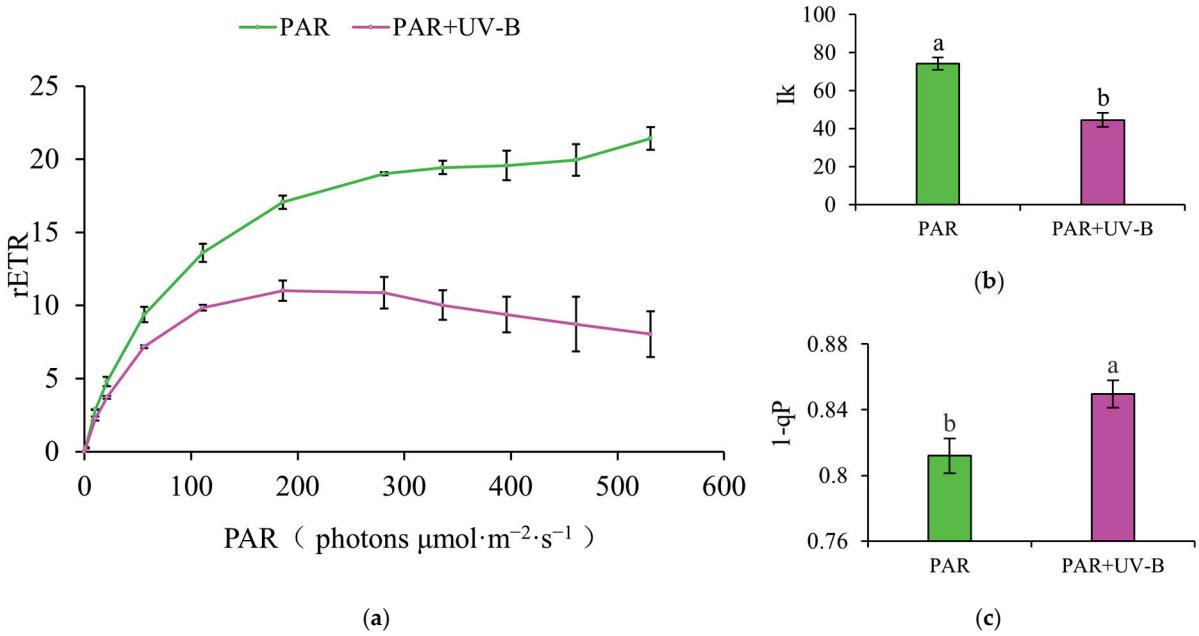


Figure 1. Changes in chlorophyll fluorescence parameters following UV-B radiation. (**a**) Line graph of rETR; (**b**) bar graph of I_K; (**c**) bar graph of "1-qP". rETR can estimate the electron transfer rate of PSII under specific light conditions, reflecting the photosynthetic potential of plants. Ik can reflect the plant's ability to tolerate strong light; the higher Ik is, the stronger the sample's tolerance to strong light is. The "1-qP" represents the reduced state of QA, which can reflect the degree of photosystem II shutdown. The bar graph illustrates the mean heights for each group, based on three biological replicates (n = 3). Error bars represent the standard deviations among these replicates. Groups marked with different letters were significantly different from each other ($p < 0.05$), indicating statistically significant variations.

2.2. UV-B Radiation Significantly Alters Flavonoid Content in Leaves of R. chrysanthum

To study the effect of UV-B radiation on the leaves of *R. chrysanthum*, we characterized the metabolites in the M and N groups. The PCA of the identified metabolites revealed that the M and N groups were clearly distinguished, and three replicates of each group were clustered together, indicating good intragroup reproducibility and significant differences between the groups (Figure S1a). To further identify the metabolites associated with leaf resistance against UV-B radiation, we used OPLS-DA analysis to explore differential metabolites between the M and N groups (Figure S1b). The first principal component explained 28.9% of the dataset, and the second principal component explained 28.3% of the dataset, giving reliable results. In this study, the screening criteria for differential metabolites were set as follows: FC (fold change) $\geq$ 1.5, FC $\leq$ 0.67, and VIP > 1. As shown in Figure S1c, the contents of 355 metabolites were increased, and 167 metabolites were decreased following UV-B radiation. These 522 differential metabolites were ranked according to FC, and the top 30 metabolites (15 metabolites with elevated levels and 15 metabolites with reduced levels) are shown in Figure S1d.

Our categorical statistics of the differential metabolites obtained from the screening revealed that the amounts of phenolic acids (115) and flavonoids (113) were the highest following UV-B stress (Figure 2a). In addition, amino acids and derivatives (51), terpenoids (46), alkaloids (36), and organic acids (30) also changed significantly following UV-B stress, which may play an influential role in the resistance of *R. chrysanthum* to UV-B stress.

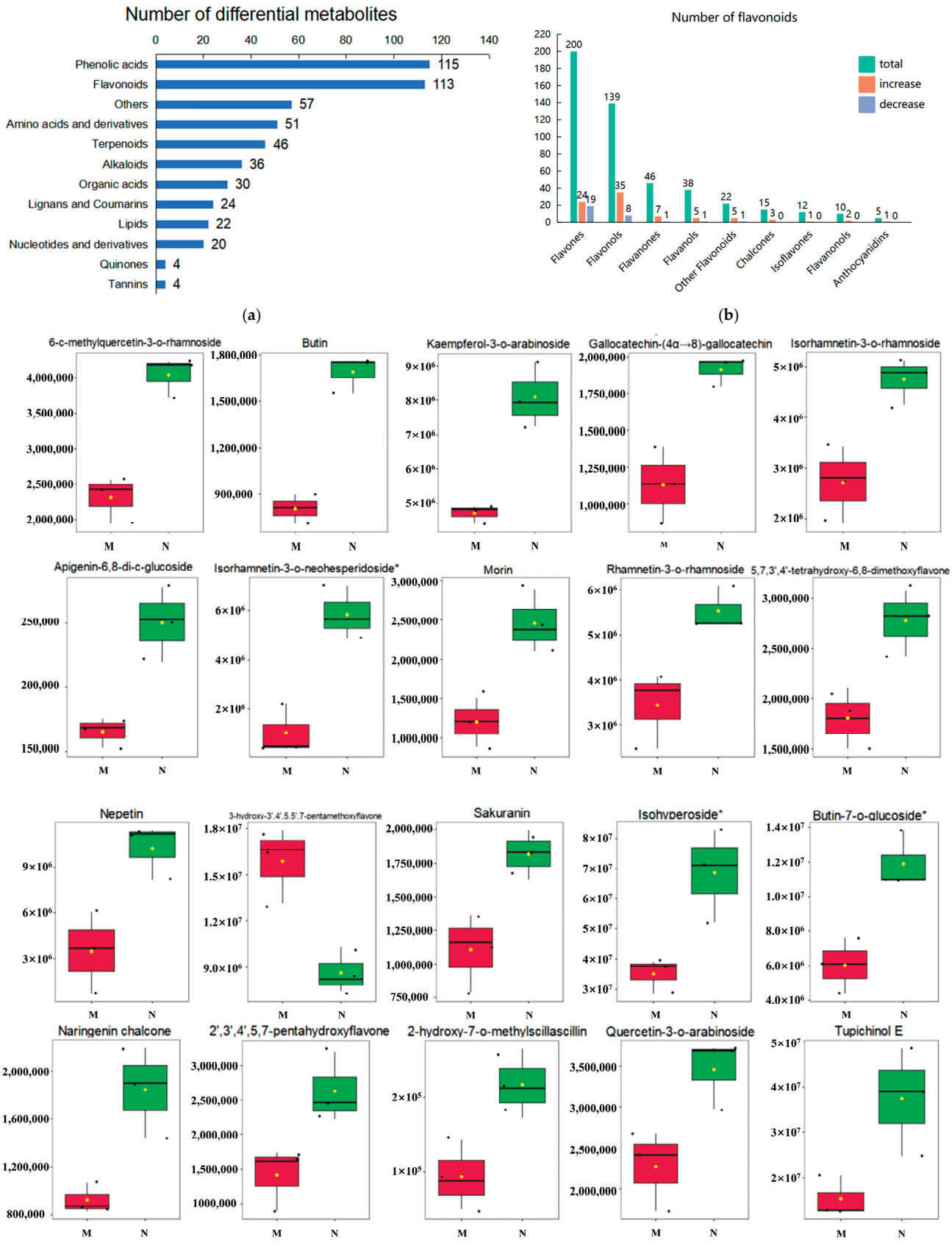


Figure 2. *Cont.*

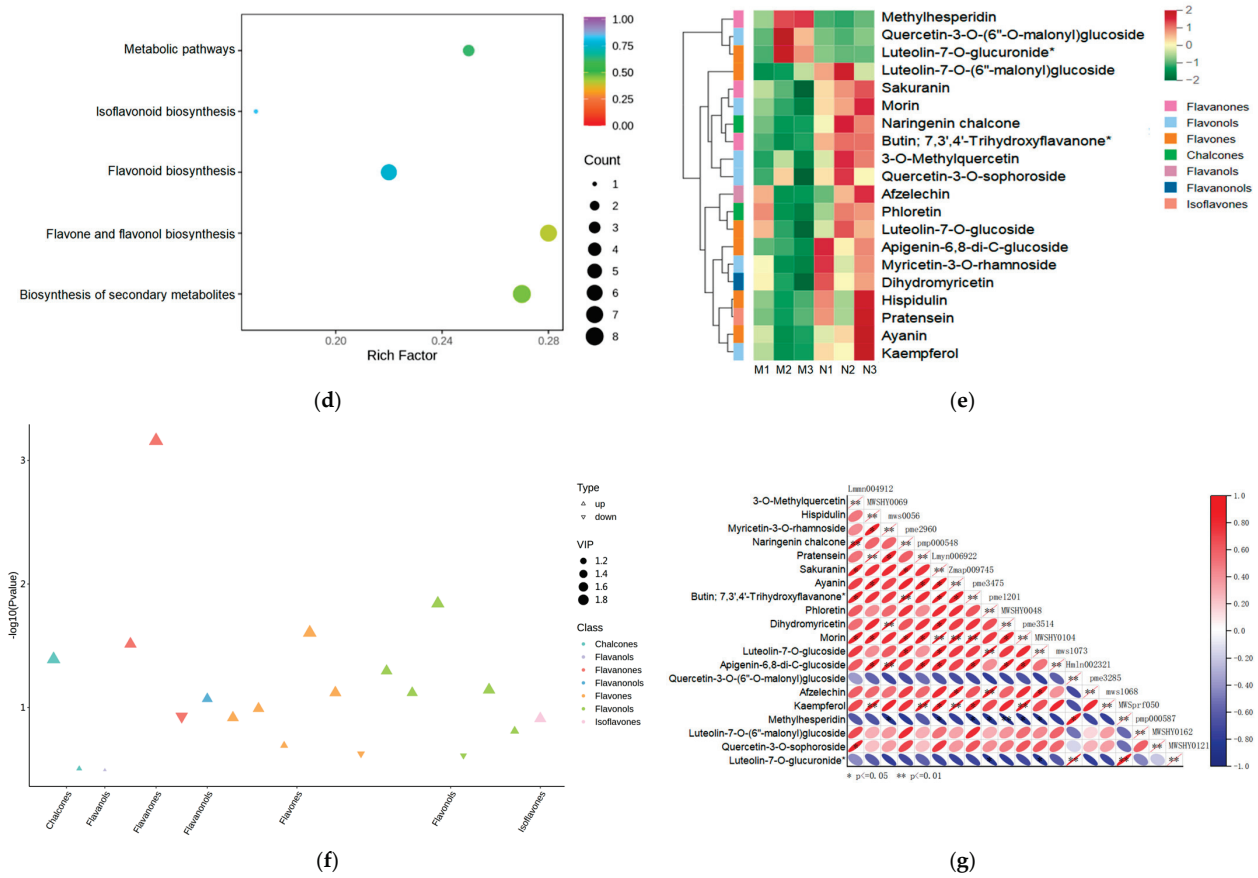


Figure 2. Significant changes in flavonoids in *R. chrysanthum* following UV-B stress. (**a**) Differential metabolite classification statistical chart; (**b**) statistical chart of secondary classification of flavonoids; (**c**) contents of top 20 metabolites of VIP value in flavonoids; (**d**) bubble map of KEGG enrichment analysis of flavonoids; (**e**) heat map of clustering of flavonoids with significant differences; (**f**) scatterplot of differential flavonoids able to be annotated to KEGG database; (**g**) correlation analysis of significantly different flavonoids. In the bubble plot, the bubble size represents the number of differential flavonoids. The bubble color represents the size of the corresponding pathway enrichment significance. In the heatmap, redder colors indicate higher metabolite content, and greener colors indicate lower content. "*" indicates that p is less than or equal to 0.05, indicating a strong correlation between the two metabolites; "**" indicates that p is less than or equal to 0.01, indicating an extremely strong correlation between the two metabolites.

We explored the response of phenolic acids in *R. chrysanthum* to UV-B stress in a previous study, so the focus of this paper is on flavonoids [34]. We performed a quantitative count of the secondary classification of flavonoids, and the results are shown in Figure 2b. There were 113 flavonoids among the screened differential metabolites, of which 83 flavonoids were increased and 30 flavonoids were decreased following UV-B radiation. These 113 flavonoids can be categorized into nine groups, with "flavones" and "flavonols" having the most, with 43 each; "flavanones" having 8; "flavanols" and "other flavonoids" having 6 each; "chalcones" having 3; "flavanonols" having 2; and "anthocyanidins" and "isoflavones" having 1 each.

The top 20 metabolites of the differential flavonoid VIP are illustrated in Figure S1e, and the box plot in Figure 2c shows the contents of these 20 flavonoids. The cumulative pattern of 3-hydroxy-3′,4′,5,5′,7-pentamethoxyflavone among these 20 metabolites was different from that of the other metabolites, suggesting that 3-hydroxy-3′,4′,5,5′,7-pentamethoxyflavone may be a negatively responsive metabolite to UV-B radiation in *R. chrysanthum*. The KEGG enrichment analysis of differential flavonoids was performed, and

the bubble plots show that these 113 metabolites were mainly enriched in five metabolic pathways: "metabolic pathways", "isoflavonoid biosynthesis", "flavonoid biosynthesis", "flavone and flavonol biosynthesis", and "biosynthesis of secondary metabolites" (Figure 2d). The number and proportion of differential metabolites annotated to these five metabolic pathways are shown in the KEGG classification diagram (Figure S1f). A total of 20 of these 113 significantly different flavonoids were annotated to the KEGG database, and the contents of these 20 metabolites were higher for 17 and lower for 3 ("methylhesperidin", "quercetin-3-o-(6″-o-malonyl) glucoside", and "luteolin-7-o-glucuronide*"), as shown in the heat map (Figure 2e). Of these 20 differential flavonoids that were able to be annotated to the KEGG database, flavones and flavonols, six of each, accounted for 30% of the total (Figure 2f).

To understand the relationships among these 20 metabolites, a correlation analysis was performed (Figure 2g). Naringenin chalcone and 3-o-methylquercetin were significantly positively correlated. Pratensein and hispidulin were significantly positively correlated. Butin and naringenin chalcone were significantly positively correlated. Dihydromyricetin was significantly positively correlated with myricetin-3-o-rhamnoside. Morin was significantly positively correlated with sakuranin, ayanin, and butin. Luteolin-7-o-glucoside was significantly positively correlated with phloretin. Apigenin-6, 8-di-c-glucoside and myricetin-3-o-rhamnoside were significantly positively correlated. Afzelechin and phloretin were significantly positively correlated. Kaempferol was positively correlated with hispidulin, pratensein, ayanin, and morin. Methylhesperidinl and dihydromyricetin were significantly negatively correlated. Luteolin-7-o-glucuronide*, and quercetin-3-o-(6″-o-malonyl) glucoside, methylhesperidin were significantly positively correlated. The metabolites identified by widely targeted metabolomics are shown in Table S1.

2.3. UV-B Radiation Significantly Alters Flavonoid-Related Genes in Leaves of R. chrysanthum

We performed transcriptomic assays on M and N group *R. chrysanthum* leaves for genes that respond to UV-B radiation. The transcriptomic data showed that 66,659 genes were expressed simultaneously in the M and N groups, 4137 genes were expressed only in the M group and 4763 genes were expressed only in the N group. Q-value < 0.05 and FC > 1 were used as the screening criteria for DEGs between the M and N groups. The results of DEG screening are shown in the volcano diagram, with a total of 2348 DEGs, of which 1157 were up-regulated and 1191 were down-regulated (Figure 3a). Of the 2348 DEGs, 42 were associated with flavonoids, with 21 being up-regulated and 21 being down-regulated (Figure 3b). The expression information of 42 genes is shown in a heat map (Figure 3c).

The KEGG enrichment analysis of the differentially expressed genes revealed enrichment in four pathways: flavonoid biosynthesis (24), anthocyanin biosynthesis (10), isoflavonoid biosynthesis (11), and flavone and flavonol biosynthesis (7) (Figure 3d). We counted the annotation of 42 DEGs in four pathways and found that 10 genes were able to be annotated in two pathways at the same time (Figure 3e). The KEGG enrichment analysis bar graph shows that these 42 genes are involved in two branches of the KEGG metabolic pathway: environmental information processing and metabolism (Figure S2a). The most enriched entry in the GO enrichment histogram is UDP-glycosyltransferase activity (9) (Figure S2b). These genes can be categorized into three main groups according to their functions: molecular function, cellular component, and biological process. Twenty-five of them had catalytic activity, nine had cellular anatomical entity, and eight had binding (Figure S2c). By performing protein–protein interaction (PPI) networks on these 42 genes, it was found that TRINITY_DN8611_c0_g2_i1-C_2 and TRINITY_DN8611_c0_g2_i3-C_2 were highly correlated and RINITY_DN21396_c0_g1_i1-C_3 and TRINITY_DN4856_c0_g5_i2-A_1 were

highly correlated (Figure 3f). Information on the 42 DEGs associated with flavonoids is shown in Table S2.

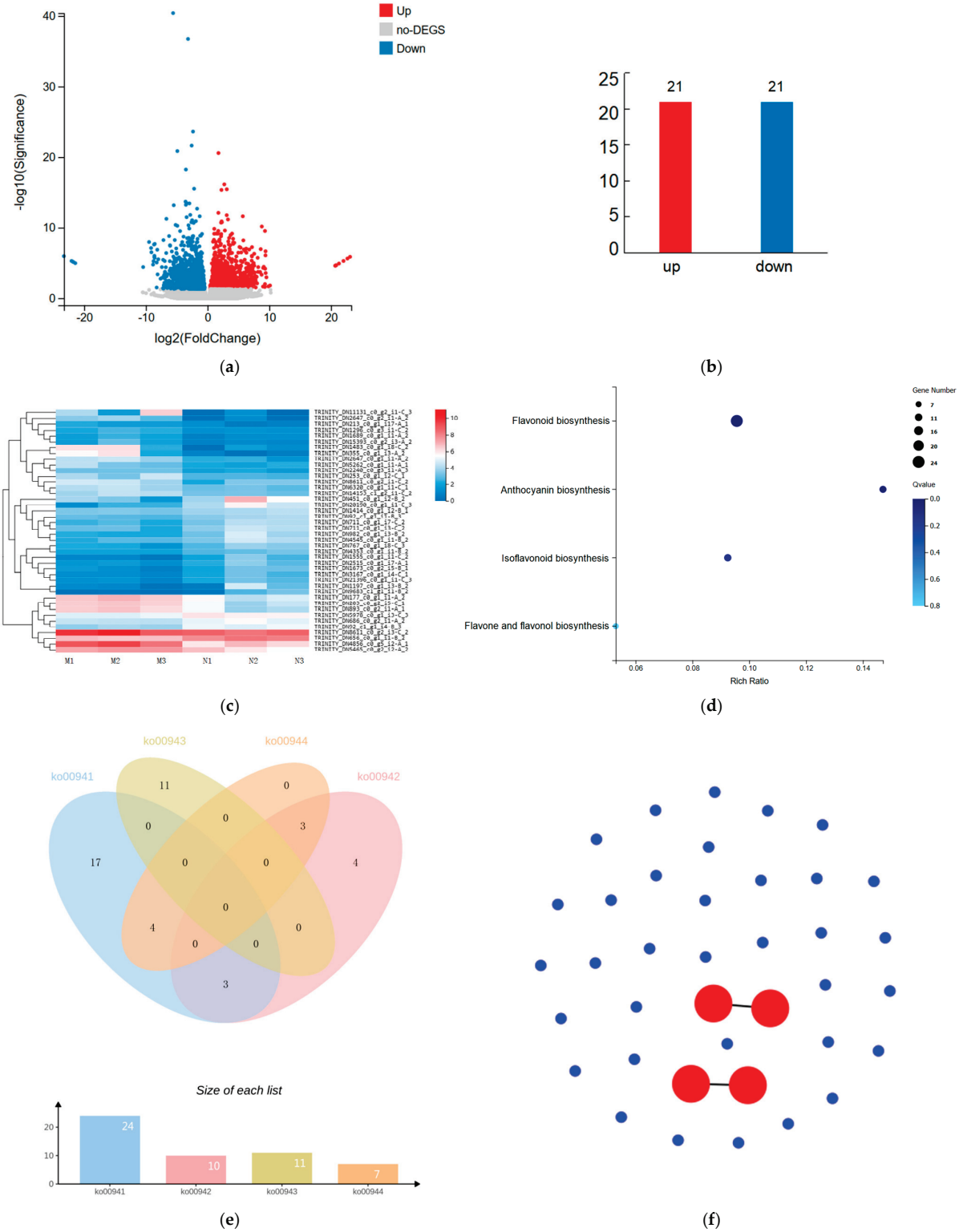


Figure 3. Transcriptomic data showed significant changes in genes related to flavonoids following UV-B radiation. (**a**) Volcano map of DEGs; (**b**) statistics on number of DEGs related to flavonoids; (**c**) heat map of DEGs related to flavonoids following UV-B stress; (**d**) KEGG bubble chart; (**e**) Venn diagram of differentially expressed genes; (**f**) protein–protein interaction network map of genes associated with flavonoid synthesis. In the bubble plot, the bubble size represents the number of DEGs. The bubble color represents the corresponding pathway enrichment significance size.

2.4. Differential Flavonoids Are Strongly Correlated with Differentially Expressed Genes

In order to understand the relationship between differentially significant flavonoids and genes, transcriptomic and metabolomic correlation analyses were performed. We constructed a correlation network graph for 113 significantly different flavonoids and genes and found that there were 363 edges in the graph, with 196 edges indicating positive correlations and 167 edges indicating negative correlations. The largest number of genes (22) were correlated with butin, with 11 positive and 11 negative correlations. There were 21 genes associated with naringenin chalcone, 14 positively and 7 negatively.

Metabolites with more than 15 edges were also gallocatechin-(4α->8)-catechin-(4α->8)-catechin (19), kaempferol-3-o-arabinoside (18), 6-c-methylquercetin-3-o-rhamnoside (18), and 3-hydroxy-3′,4′,5,5′,7-pentamethoxyflavone (18) (Figure 4a).

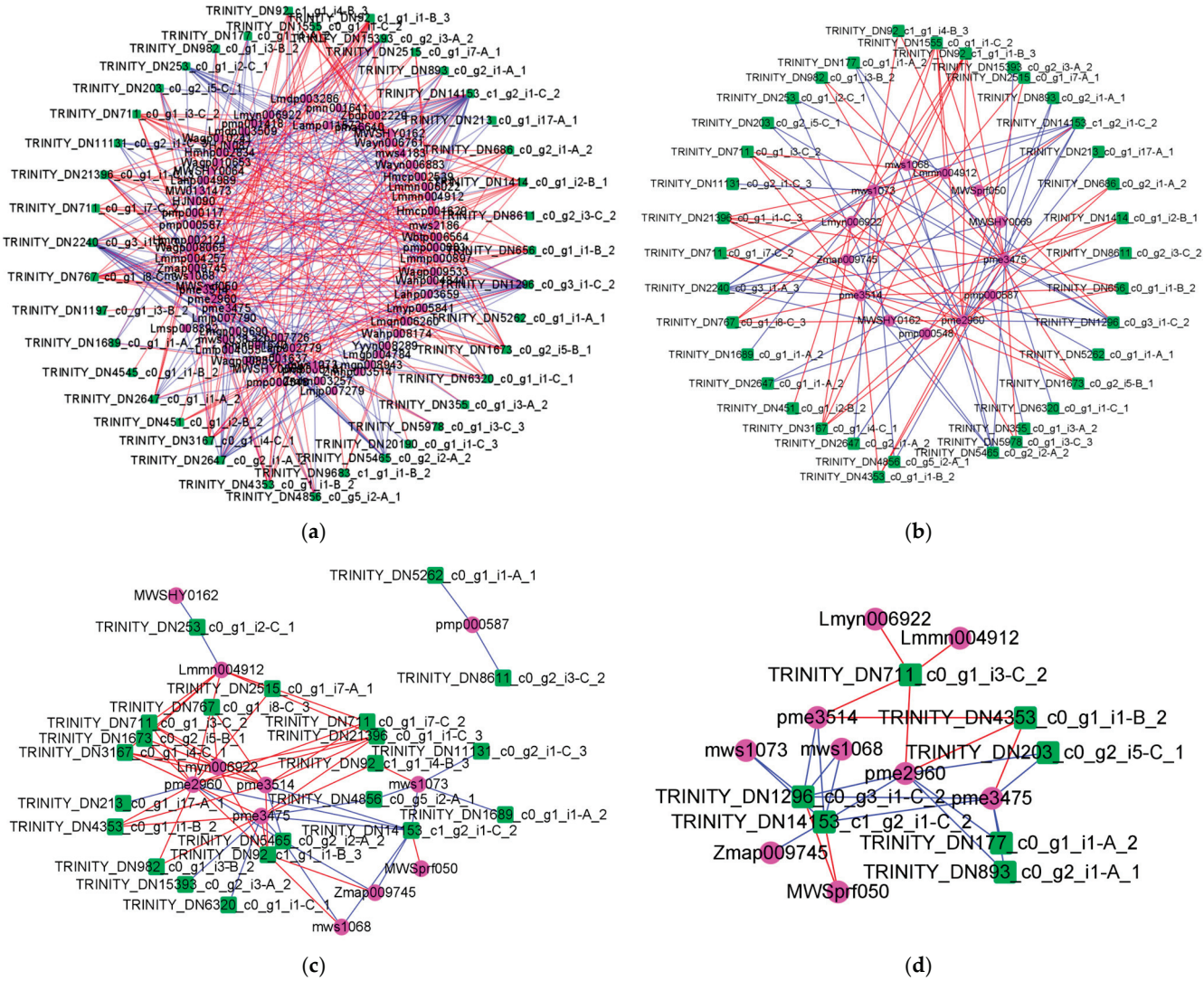


Figure 4. *Cont.*

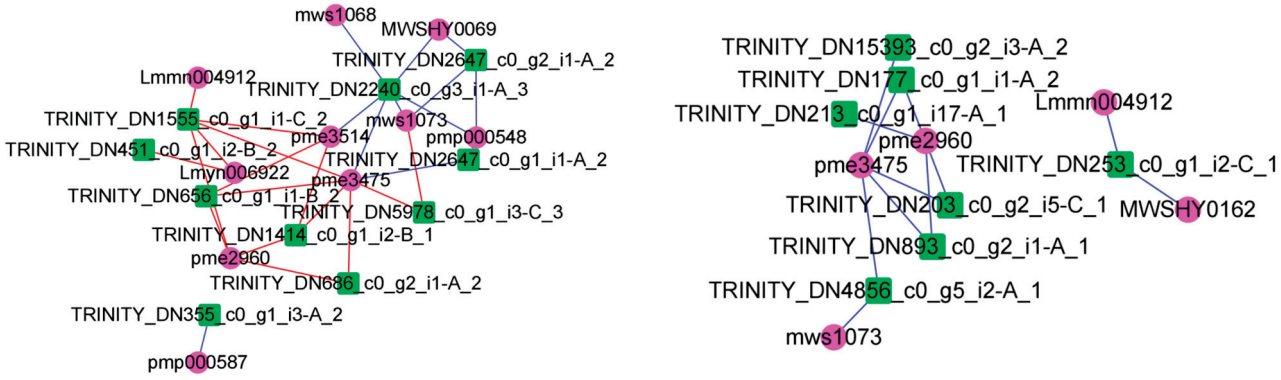


Figure 4. Transcriptomic and metabolomic analysis. (**a**) Analysis of 113 flavonoid metabolites with genetic correlation; (**b**) analysis of 20 flavonoid metabolites with genetic correlation; (**c**–**f**) correlation analysis of metabolites with ko00941 pathway-related genes, ko00942 pathway-related genes, ko00943 pathway-related genes, and ko00944 pathway-related genes, respectively. When using the Pearson correlation analysis method, the correlation analysis threshold was 0.9, $p < 0.05$. Pink nodes indicate metabolites, and green nodes indicate genes; red edges indicate positive correlations, and blue edges indicate negative correlations.

The 20 metabolites that could be annotated to the KEGG database were analyzed for correlation with the genes, and the results are shown in Figure 4b, with a total of 103 edges, with 58 indicating positive correlations and 45 indicating negative correlations. The edges linked to butin (increased content) and naringenin chalcone (increased content) were 22 and 21, respectively. Since these 20 metabolites annotated to the KEGG database were enriched in four pathways, we investigated the correlation between metabolites and genes in the four pathways. As shown in Figure 4c–f, there were 63 edges in the flavonoid biosynthesis pathway (41 positive correlations and 22 negative correlations) and 26 edges in the anthocyanin biosynthesis pathway (9 positive correlations and 17 negative correlations). There were 28 edges in the isoflavonoid biosynthesis pathway (16 positive and 12 negative) and 12 edges in the flavone and flavonol biosynthesis pathway (0 positive and 12 negative). Among these four pathways, genes related to butin, naringenin chalcone, and morin were all more abundant, suggesting that these three metabolites may be important for *R. chrysanthum* to resist against UV-B stress.

2.5. WRKY Transcription Factors Play a Crucial Role in UV-B Stress Resistance in R. chrysanthum

Gene expression is regulated by transcription factors (TFs), and in order to explore the changes in the flavonoid-related pathways of *R. chrysanthum* following UV-B stress, we counted the DEGs identified as TFs. The number of transcription factors (TFs) potentially related to flavonoids is shown in Figure 5a and involves five families of transcription factors, namely, MYB, bHLH, AP2-EREBP, NAC, and WRKY.

Two hundred and thirty-two genes were identified as members of the MYB TF family, eight of which were significantly different following UV-B stress. One hundred and eleven genes were identified as members of the bHLH TF family, twelve of which were significantly different following UV-B stress. One hundred and twenty-nine genes were identified as members of the AP2-EREBP family of TFs, ten of which were significantly different following UV-B stress. One hundred and eighteen genes were identified as members of the NAC TF family, six of which were significantly different following UV-B stress. One hundred genes were identified as members of the WRKY TF family, eleven of which were significantly different following UV-B stress.

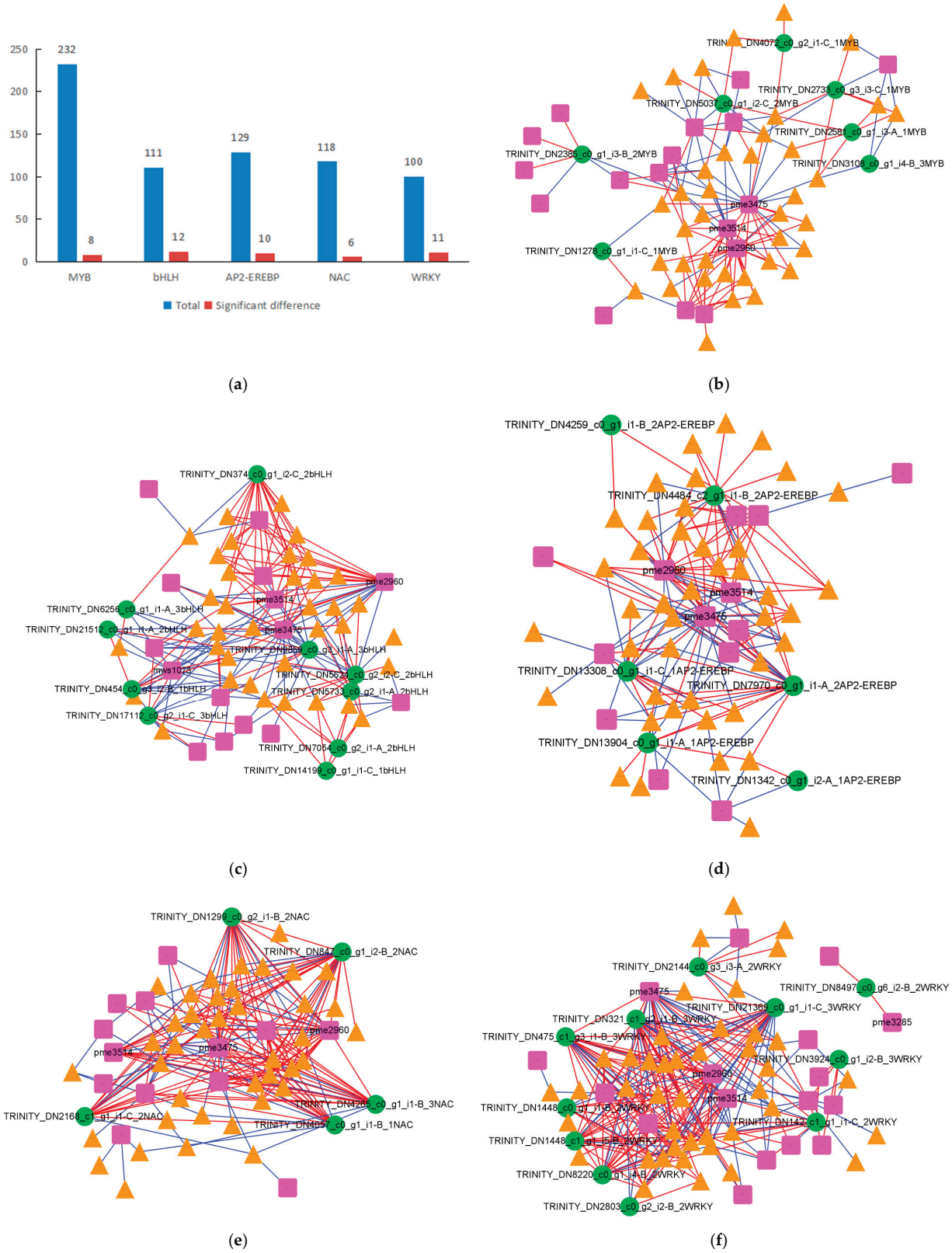


Figure 5. WRKY TFs play an important role in *R. chrysanthum*'s resistance to UV-B stress. (**a**) Number of transcription factors statistics; (**b**) correlation analysis involving MYB transcription factors; (**c**) correlation analysis involving bHLH transcription factors; (**d**) correlation analysis involving AP2-EREBP transcription factors; (**e**) correlation analysis involving NAC transcription factors; (**f**) correlation analysis involving WRKY transcription factors. In the bar chart, blue indicates the number of genes capable of encoding transcription factors detected in *R. chrysanthum*, and red indicates the number of

genes with the ability to encode transcription factors that differed significantly between the M and N groups. When using the Pearson correlation analysis method, the correlation analysis threshold was 0.9, $p < 0.05$. Pink boxes indicate metabolites, green circles indicate genes capable of encoding TFs, and orange triangles indicate DEGs. Red edges indicate positive correlations, and blue edges indicate negative correlations.

In order to systematically identify unknown TFs controlling flavonoid synthesis in the M and N groups of *R. chrysanthum* leaves following UV-B stress, correlation analyses were performed for differentially significant flavonoids, DEGs, and differentially significant TFs. The correlation of flavonoids and DEGs capable of being annotated to the KEGG pathway with these five families of TFs is illustrated (Figure 5b–f). Figure 5b–f each have 137, 198, 165, 207, and 262 edges, indicating strong correlations among the screened genes, TFs, and metabolites, which may be related to flavonoid regulation. The strong correlation of each TF family with 3-o-methylquercetin, naringenin chalcone, butin, morin, and apigenin-6,8-di-C-glucoside suggests that these five metabolites are the key metabolites regulated by TFs.

Correlation analysis involving MYB TF families revealed that 7 flavonoids and 16 DEGs were strongly correlated with 7 MYB TFs, respectively, with 7 edges being related to flavonoids and 27 edges being related to DEGs. Correlation analysis involving bHLH TF families revealed that 13 flavonoids and 35 DEGs were strongly correlated with 10 bHLH TFs, respectively, with 23 edges being related to flavonoids and 72 edges being related to DEGs. Correlation analysis involving the AP2-EREBP TF family revealed that 2 flavonoids and 35 DEGs were strongly correlated with each of the 6 AP2-EREBP TFs, with 4 edges being associated with flavonoids and 58 edges being associated with DEGs. Correlation analysis involving the NAC TF families revealed that 6 flavonoids and 33 DEGs were strongly correlated with each of the 5 NAC TFs, with 15 edges being related to flavonoids and 89 edges being related to DEGs. Correlation analysis involving WRKY TF families revealed that 13 flavonoids and 36 DEGs were strongly correlated with 11 WRKY TFs each, with 26 edges being related to flavonoids and 133 edges being related to DEGs. The correlation analyses of TFs with differentially significant flavonoids and DEGs revealed that WRKY TFs play an important role in the resistance of *R. chrysanthum* against UV-B stress (Figure 5b–f).

2.6. WRKY TFs Regulate Expression of Key Enzyme Genes in Flavonoid Synthesis Pathway

The KEGG database was utilized to localize the DEGs into flavonoid-related pathways, and it was found that the DEGs were able to encode four enzymes, namely, 3′,5′-hydroxylase, chalcone isomerase, dihydromyricetin reductase, and flavonol synthase. Information on the genes encoding the enzymes is shown in Table 1. We correlated the WRKY TFs that changed significantly following UV-B stress with the genes encoding these four enzymes (Figure 6) and found that three WRKY TFs were strongly correlated with flavonoid 3′,5′-hydroxylase (one positively and two negatively), six WRKY TFs were significantly positively correlated with chalcone isomerase, five WRKY TFs were significantly positively correlated with dihydromyricetin reductase, and three WRKY TFs were strongly correlated with flavonol synthase (one positively and two negatively).

In order to better understand the relations between differential metabolites and DEGs, we combined flavonoids annotated in the KEGG database with DEGs to construct a network to gain a clearer insight into the interrelationships between gene expression and flavonoid accumulation in *R. chrysanthum* leaves under UV-B stress.

Table 1. Information on genes encoding key enzymes in the flavonoid pathway.

Name	Enzyme	Gene ID	log2 (N/M)	Q-Value (M vs. N)
Flavonoid 3′,5′-hydroxylase	1.14.14.81	TRINITY_DN15393_c0_g2_i3-A_2	−2.051	0.002
		TRINITY_DN4856_c0_g5_i2-A_1	−2.614	0.000
Chalcone isomerase	5.5.1.6	TRINITY_DN92_c1_g1_i1-B_3	1.074	0.002
		TRINITY_DN92_c1_g1_i4-B_3	1.303	0.000
Dihydromyricetin reductase	1.1.1.219	TRINITY_DN21396_c0_g1_i1-C_3	1.967	0.001
Flavonol synthase	1.14.20.6	TRINITY_DN1689_c0_g1_i1-A_2	−1.588	0.010
		TRINITY_DN6320_c0_g1_i1-C_1	−1.258	0.000
		TRINITY_DN8611_c0_g2_i1-C_2	−1.468	0.028
		TRINITY_DN8611_c0_g2_i3-C_2	−1.155	0.022

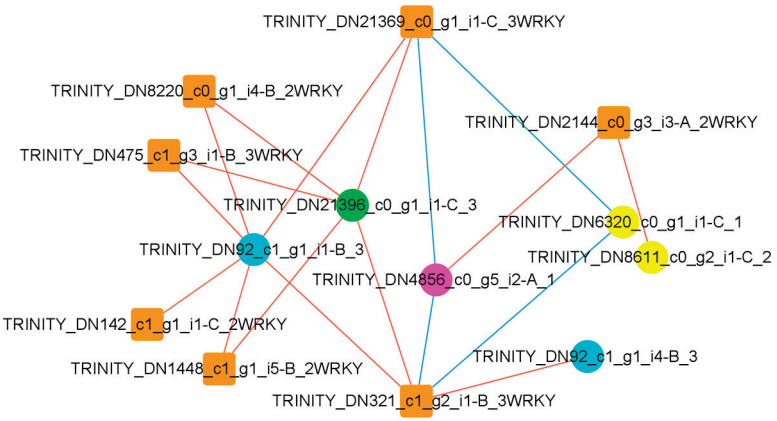


Figure 6. WRKY TFs are strongly correlated with key enzymes in the flavonoid synthesis pathway. When using the Pearson correlation analysis method, the correlation analysis threshold was 0.9, $p < 0.05$. Boxes indicate WRKY TFs, and circles indicate genes encoding 4 enzymes, where pink: flavonoid 3′,5′-hydroxylase; blue: chalcone isomerase; green: dihydromyricetin reductase; yellow: flavonol synthase. The red (blue) edges represent positive (negative) correlations.

As shown in the box-and-line diagram in Figure 7, L-phenylalanine expression was elevated following UV-B stress, leading to the accumulation of downstream flavonoids. As can be seen in Figure 7, the contents of phloretin, naringenin chalcone, butin, dihydromyricetin, kaempferol, and afzelechin, annotated to the flavonoid biosynthesis pathway, were significantly elevated in N group *R. chrysanthum*. The contents of pratensein levels annotated to the isoflavonoid biosynthesis pathway were significantly higher, and luteolin-7-o-glucoside, ayanin, 3-o- methylquercetin, quercetin-3-o-sophoroside, and kaempferol levels were significantly elevated, while luteolin-7-o-glucuronide* and quercetin-3-o-(6″-o-malonyl) glucoside levels were significantly reduced. The genes encoding the WRKY TFs in the orange box may affect the accumulation of taxifolin, luteolin, quercetin, and dihydromyricetin by affecting the genes encoding 3′,5′-hydroxylase. The genes encoding the WRKY TFs in the blue box may influence the accumulation of naringenin and butin by affecting the genes encoding chalcone isomerase. The genes encoding the WRKY TFs in the purple box may influence cis-3,4-leucopelargonidin accumulation by affecting the gene encoding dihydromyricetin reductase. The genes encoding WRKY TFs in the green box may influence kaempferol accumulation by affecting the genes encoding flavonol synthase.

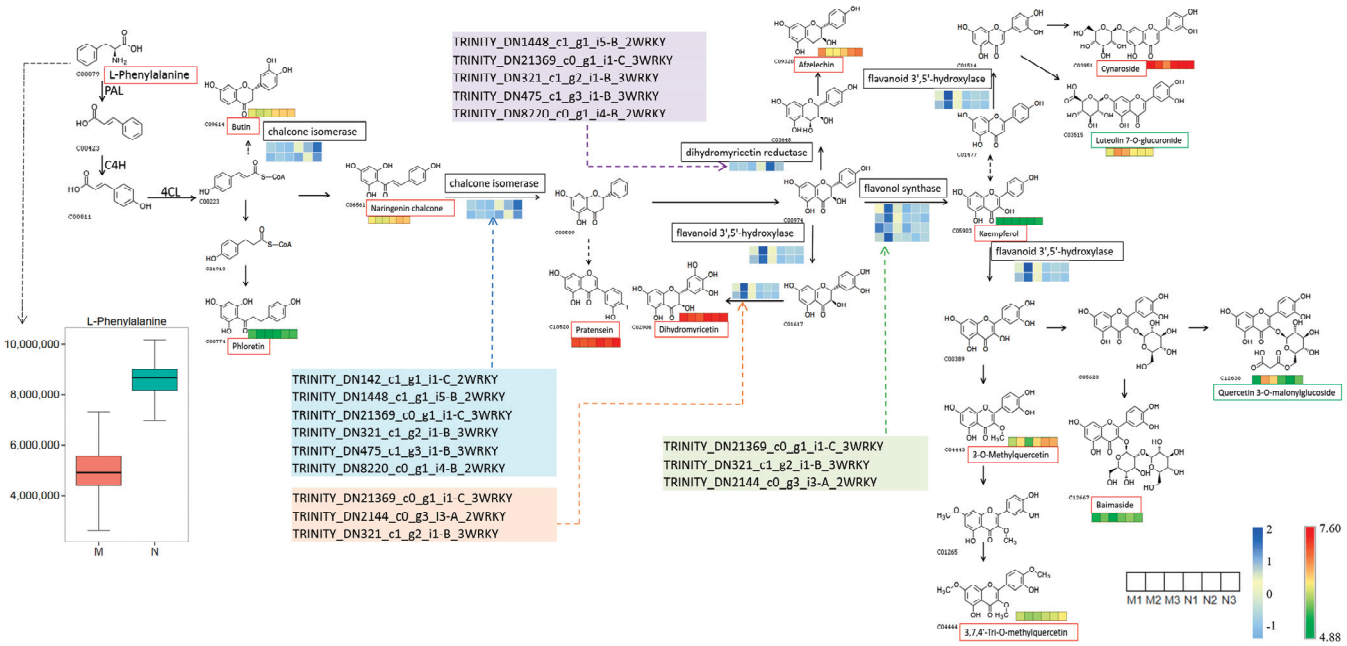


Figure 7. WRKY TFs can regulate the expression of key enzyme genes in the flavonoid synthesis pathway to improve tolerance to UV-B stress in *R. chrysanthum*. For the DEG heatmap, we used the z-score algorithm, and for the metabolite heatmap, we used substance content. A red box around a metabolite indicates that the metabolite was elevated following UV-B radiation, and a green box indicates that the level was reduced. Names in the colored boxes indicate transcription factors associated with flavonoids.

3. Discussion

UV-B radiation affects plant growth as abiotic stress due to the degradation of the ozone layer, which enhances the UV-B radiation reaching the plant surface [35]. UV-B radiation is capable of causing damage to the photosynthetic apparatus of green plants at multiple locations [36]. *R. chrysanthum* is a plant resource that grows in alpine environments and is exposed to intense UV-B radiation while growing. Previous experiments have demonstrated that the leaves of *R. chrysanthum* are able to respond to UV-B stress, mainly in photosynthesis [24]. Therefore, the present study was conducted to investigate the response to UV-B stress by using *R. chrysanthum* leaves as experimental material. Flavonoids belong to a group of phenolic compounds with antiviral activity; antioxidant, anti-inflammatory, antimutagenic, and anticancer properties; and an important role in ROS dynamic homeostasis [37–39]. Some studies have explored the relationship between the structure of flavonoids and the scavenging of hydroxyl radicals and concluded that flavonoids are potent scavengers of hydroxyl radicals and can be used as natural plant antioxidants [40]. Since *R. chrysanthum* produces a large amount of ROS after being subjected to abiotic stress, the property of flavonoids to regulate ROS homeostasis may enable *R. chrysanthum* to adapt to stressful environments [22]. In this study, we investigated the key enzyme genes affecting UV-B radiation resistance in *R. chrysanthum* and the transcription factors that may regulate the expression of these genes, using flavonoids as the main metabolic components.

The rETR is able to estimate PSII activity and photosynthetic efficiency, which reflects the rate of electron transfer driven by photosynthetically active radiation absorbed per unit of chlorophyll [41]. It can, therefore, monitor changes in the physiological state of plants under stress [42]. I_K can be used to assess the photosynthetic efficiency of plants under bright light and reflects the ability of a sample to tolerate bright light [43]. The higher its value, the more tolerant the sample is to bright light [44]. "1-qP" reflects the degree of reduction of QA (primary electron acceptor). Thus, "1-qP" measures the degree of center

closure, i.e., the proportion of reaction centers that are not involved in the photochemical reactions of photosynthesis [45]. UV-B caused a significant decrease in rETR and "1-qP" and a significant increase in I_K in the experimental material. This shows that UV-B damages the photosynthetic system and reduces the resistance to strong light in this species. *R. chrysanthum*, therefore, mobilizes its own metabolic pathways to tolerate this adverse factor.

In this study, a total of 487 flavonoids were identified, 113 of which were significantly different between the M group and the N group, indicating that UV-B radiation significantly altered the accumulation of these flavonoids. These 113 flavonoids had the highest number of flavones and flavonols, suggesting that flavones and flavonols may be conducive to the acclimatization of *R. chrysanthum* to UV-B stress. Flavone is one of the largest flavonoids present in plants and can play a role in defending the plant against pathogen attacks and unfavorable environmental conditions such as salinity and high levels of UV-B exposure. It has been shown that apigenin and lignans in flavones are able to increase the tolerance of plants exposed to UV-B. Apigenin and its glycoside derivatives are able to protect plants from oxidative damage caused by UV-B radiation by reducing ROS production [46]. Baicalein contained in *Scutellaria* can act as an H_2O_2 scavenger to protect cells from oxidative stress [47]. Elevated levels of flavones (luteolin 7-o-glycosides and luteolin) and flavonols upon UV-B exposure represent a protective mechanism in *Artemisia annua* [18]. Flavonols have been shown to protect plants from damage to the photosynthetic electron transport mechanism and to be more important for protection against PSII damage than CO_2 fixation. The induction of flavonol synthesis protects plants from UV-B stress, an effect that can be realized through their UV-absorbing properties (flavonols are capable of absorbing UV-B light at 280–320 nm) but also through the reduction of ROS once formed [48].

Some of the flavonoids detected in *R. chrysanthum* that produced significant differences under UV-B stress were not annotated in the KEGG database, suggesting that these flavonoids are not well studied in model plants and may be unique adaptive changes in *R. chrysanthum*. Isorhamnetin-3-o-neohesperidoside*, isorhamnetin-3-o-gallate, nepetin, limocitrin-3-o-arabinoside, cyanidin 3-xyloside, and other flavonoids, although not annotated in the KEGG database, were significantly elevated following UV-B radiation, suggesting that these substances can promote *R. chrysanthum*'s resistance to UV-B radiation. Twenty of the one hundred and thirteen significantly different flavonoids were able to be annotated to the KEGG database, so we focused on these twenty metabolites. RNA-seq data from the M and N groups showed 42 DEGs associated with flavonoid synthesis, significantly enriched in four pathways. Protein network interaction analysis of the DEGs revealed that TRINITY_DN8611_c0_g2_i3-C_2 has a direct interaction with TRINITY_DN8611_c0_g2_i1-C_2, both belonging to the genes encoding flavonol synthase, and the molecular functions showed that they have oxidoreductase activity. TRINITY_DN4856_c0_g5_i2-A_1 and TRINITY_DN21396_c0_g1_i1-C_3 have a direct interplay with CYP75A, capable of encoding flavonoid 3′,5′-hydroxylase with oxidoreductase activity, which acts on paired donors, and DFR, which can encode bifunctional dihydroflavonol 4-reductase/flavanone 4-reductase with dihydrokaempferol 4-reductase activity.

The correlation analyses of significantly different flavonoids with DEGs revealed that different metabolites had different correlations for the same gene and the same metabolite had different correlations for different genes. Among the four flavonoid-related pathways, the flavonoid biosynthesis pathway had the highest number of edges, with correlations between metabolites and DEGs greater than 0.9, suggesting that the screened DEGs may influence the synthesis of relevant metabolites in this pathway. This pathway had the most edges linked to naringenin chalcone, suggesting that naringenin chalcone may be an important metabolite in the response of *R. chrysanthum* to UV-B stress. One molecule of *p*-coumaroyl-CoA and three molecules of malonyl-CoA generate one molecule of naringenin chalcone,

four molecules of CoA, and three molecules of CO_2 by multi-step reaction in the presence of chalcone synthase. Naringenin chalcone as a node continues to generate flavonoids that play an important role in plant resistance, such as naringenin, dihydrokaempferol, cis-3,4-leucopelargonidin, and afzelechin. The chalcone isomerase-related genes in the transcriptomic data were TRINITY_DN92_c1_g1_i1-B_3 and TRINITY_DN92_c1_g1_i4-B_3 (expression as shown in the heat map in Figure 7), and naringenin chalcone was produced by the action of the chalcone isomerase naringenin.

In response to various abiotic stresses, the transcription of genes encoding enzymes of the flavonoid biosynthetic pathway is regulated by a combination of transcription factors [49]. It has been shown that the MYB, bHLH, WRKY, and NAC TF families are associated with flavonoid biosynthesis [50]. The MYB transcription factors influence the biosynthesis of proanthocyanidins, anthocyanidins, flavonols, and lignans in plants and play a key role in plant responses to adversity [51]. It has been shown that the MYB TFs are able to regulate the isoflavonoid biosynthesis pathway in soybean. For example, the R1-type MYB TF *GmMYB176* was able to regulate *CHS8* expression, affecting isoflavonoid synthesis [52,53]. bHLH is able to influence the composition of flavonoids in pomegranate [54]. Many bHLH genes have been detected in wheat, rice, and other crops involved in plant response to abiotic stresses [55]. bHLH plays an important role in plant adaptation to harsh environments by binding to specific sites on promoters to transcribe and regulate its target genes and direct plant metabolic processes [56]. Studies in grape have shown that the WRKY TF *VvWRKY26* is able to participate in flavonoid biosynthesis, which lays the foundation for studying the mechanism of flavonoid accumulation in grape [57]. WRKY is able to activate the transcription of antioxidant pathway genes, e.g., the overexpression of *MfWRKY70* in transgenic *Myrothamnus flabellifolia* was able to improve tolerance to drought and salt stress by regulating H_2O_2 and antioxidant levels, as well as by enhancing the transcription of genes related to stress response markers [58]. WRKY is able to regulate ROS homeostasis, thus playing a role in defense responses [59]. WRKY may affect the response of *R. chrysanthum* to UV-B radiation. NAC enhances plant survival and plant secondary growth under environmental stress conditions and plays a role in plant adaptation to stressful environments [60]. The transcriptomic data showed that more AP2-EREBP members were significantly different following UV-B stress and significantly differentiated flavonoids and DEGs were more highly correlated with AP2-EREBP, so AP2-EREBP members may be involved in the response of *R. chrysanthum* to UV-B stress by affecting gene expression.

Figure 7 demonstrates the upstream–downstream relationships of genes, TFs, and metabolites, revealing the regulatory mechanisms of flavonoid accumulation in *R. chrysanthum* under UV-B stress. This pathway involves a total of 13 significantly different flavonoids, 9 DEGs, and 7 potentially functioning WRKY TFs. These TFs are able to influence the expression of chalcone isomerase, dihydromyricetin reductase, flavonol synthase, and flavanoid 3′,5′-hydroxylase, thereby affecting downstream flavonoid synthesis. The specific regulatory mechanisms of TFs need to be further investigated.

4. Materials and Methods

4.1. Plant Materials and Treatment

Culture conditions and radiation treatments of experimental materials involved in this experiment followed previous experiments [61,62]. The experimental materials of this study were *R. chrysanthum* specimens collected from Changbai Mountain. After transferring *R. chrysanthum* from its native habitat to the laboratory, it was cultured in artificial climate chambers (daytime temperature of 18 °C, white light irradiation for 14 h, nighttime temperature of 16 °C, darkness for 10 h, and relative humidity 60%) by using 1/4

MS medium. After growing and culturing into 8-month-old seedlings, they were subjected to subsequent radiation treatments accordingly.

The light conditions required to foster the growth of *R. chrysanthum* were imposed during radiation, with additional UV-B being applied to the N group. After being exposed to PAR radiation (400–700 nm), M group samples were put on a 400 nm long-pass filter (Filter Long 2IN SQ; Edmund, Barrington, NJ, USA). The N group used a 295 nm long-pass filter with PAR + UV-B (280–315 nm) irradiation (Figure 8). The filters were able to allow for the transmission of light of the corresponding wavelength. PAR was generated by using warm-white fluorescent lamps (T5 14W; Philips, Amsterdam, The Netherlands), while UV-B radiation was emitted by UV-B fluorescent lamps (Ultraviolet-B TL 20W/01 RS; Philips, Amsterdam, The Netherlands). According to the transmission characteristics of the long-pass filter, the actual photosynthetically active radiation and UV-B intensities for the plant materials measured 50 μmol(photon)/m^2·s and 2.3 W/m^2. For two days, the experimental therapy was administered eight hours a day. Three biological replicates were performed in each group. *R. chrysanthum* leaves were stored in liquid nitrogen. Lastly, transcriptomics and metabolomics were performed on these leaves.

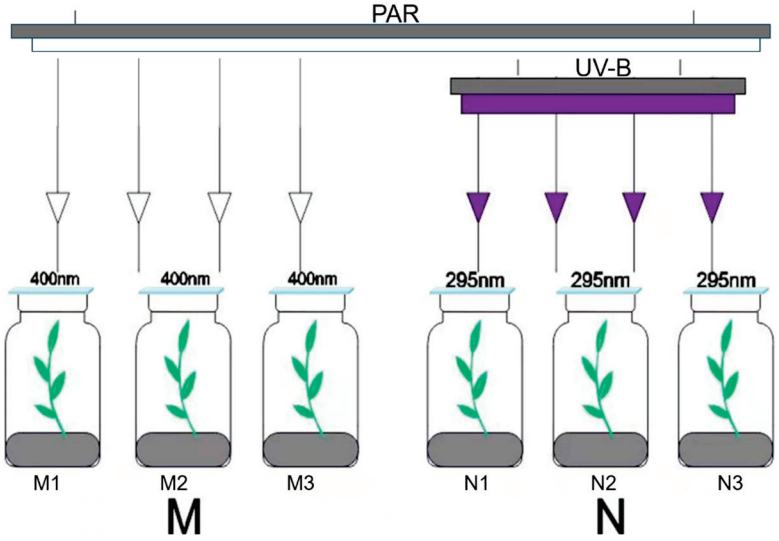


Figure 8. Schematic diagrams of the radiation treatments in the M and N groups.

4.2. Widely Targeted Metabolomics for Metabolite Identification and Quantification

Metware Biotech Inc., located in Wuhan, China, conducted a comprehensive metabolomic analysis for this study. The experimental methods and conditions adhered closely to those detailed in prior research [63].

Chromatographically pure grades of methyl alcohol, acetonitrile (Merck, Rahway, NJ, USA), and methanoic acid (Aladdin, Calhoun, GA, USA) were used for the standards. To extract metabolites from dry samples, the leaves were subjected to vacuum freeze drying and then pulverized into a fine powder by using a grinder. Subsequently, a 50 mg portion of the powdered sample was weighted and combined with 1200 μL of a pre-chilled (at −20 °C) 70% methanol aqueous solution containing an internal standard. We then performed vortexing 6 times (each lasting 30 s at 30 min intervals) and centrifuging (12,000 rpm for 3 min). A microporous filter membrane (0.22 μm) was used to filter the supernatant, which was then stored.

Metabolite separation and detection were performed by using ultraperformance liquid chromatography–tandem mass spectrometry (UPLC-MS/MS). The metabolites eluted during each interval were used to determine which set of multiple-reaction monitoring (MRM) ion pairs were monitored throughout each time. The MRM process is schematized

in Figure S3. Based on the Metware database (MWDB), substance characterization was carried out based on secondary spectral information, and isotope signals, repetitive signals containing K^+, Na^+, and $NH4^+$, were removed from the analysis. Repeated signals of fragment ions, which are themselves other substances of higher molecular weight, were removed. Triple quadrupole mass spectrometry was used for MRM analysis in order to quantify metabolites. To obtain metabolite-related data metrics, the mass spectra of the same metabolite in several samples were integrally corrected for outgoing peaks.

4.3. RNA-Seq Library Construction and Analysis

The RNA sequencing in this study was conducted by BGI Genomics Co., Ltd., Beijing, China, adhering closely to the methodologies and parameters outlined in prior research [64].

We extracted total RNA from the samples by using the CTAB procedure. Following this, single-strand circular DNA libraries were prepared and analyzed via RNA-seq.

The MGISEQ-2000 platform was employed for RNA-seq analysis. The initial step involved counting and filtering the raw sequencing data with SOAPnuke software (version 1.4.0) to eliminate sequences of poor quality. Subsequent sequence refinement was carried out by using trimmomatic to enhance data integrity. The clean reads were then mapped to the reference gene sequences by using Bowtie2 software (2.2.5), and the gene and transcript expression levels were quantified with RSEM (1.2.8). To identify changes in gene expression post-treatment, the FPKM method was applied to assess the expression levels of each transcript. The DESeq2 method, which is founded on the negative binomial distribution, was used to identify differentially expressed genes in *R. chrysanthum* following the treatments. Genes were considered differentially expressed if they had fold change (FC) > 1 and a q-value (adjusted *p*-value) < 0.05.

For the functional annotation and classification of unigenes, we utilized public databases such as KEGG, Pfam, and Swissprot. The annotation and classification process involved aligning Unigene sequences with those in the databases by using BLAST for comparison.

The transcriptome sequencing of *R. chrysanthum* was performed by the IlluminaHiSeq platform. The sequencing of the six samples yielded a total of 45.44 million raw reads each. After quality control measures, the range of clean reads obtained was between 42.21 million and 43.51 million. Additionally, the total clean bases ranged from 6.33 to 6.53 gigabases (Gb). These numbers show that the sequencing results were of a high caliber.

4.4. Measurement of Characteristics of Chlorophyll Fluorescence

The assay was based on the earlier experimental protocol [65]. The IMAGING-PAM chlorophyll fluorescence imaging system by Heinz Walz, Germany, was utilized to ascertain the PSII chlorophyll fluorescence parameters and compute associated parameters in the leaves of *R. chrysanthum*. The experiment took place in a dark setting with the ambient temperature kept consistent with the incubation temperature of the samples, ranging from 16 °C to 18 °C.

Prior to the commencement of the test, the leaves were allowed to adapt to darkness for a duration of 30 min. The minimal fluorescence level, denoted by Fo, was recorded under light-induced conditions. Subsequently, maximum fluorescence, known as Fm, was achieved through the application of saturating light pulses. Once the fluorescence intensity had returned to Fo, photochemically induced fluorescence kinetics were initiated at an intensity of 1600 $\mu mol \cdot m^{-2} \cdot s^{-1}$. Saturating pulses were applied every 20 s to ascertain both Fm′, which is the maximum fluorescence under light conditions, and the actual fluorescence intensity, F, at any given moment.

The rETR (relative electron transfer rate), 1-qP, and I_k were finally determined and calculated.

rETR = PAR·Y(II)·0.84·0.5

1-qP = 1-1-(F-Fo')/(Fm'-Fo')

$I_k = rETR_{max}/\alpha$ (α: Initial slope of the relative electron transfer rate curve).

4.5. Statistical Analysis

The experiments were conducted three times by using a completely randomized design and analyzed by using IBM SPSS Statistics 26. One-way ANOVA was employed to assess the significance of the results. When significant differences were detected, Duncan's test was applied to identify mean differences at the $p < 0.05$ level.

Figures in the metabolomics results section were plotted by using Metware Cloud (https://cloud.metware.cn). Metabolite correlation was processed by using Origin2022.

We used metaboanalyst5.0 for VIP value plots and boxplots. A variable importance in projection (VIP) plot, which is commonly used in PLS-DA, was used for ranking the metabolites based on their importance in discrimination between the M group and the N group *R. chrysanthum*. VIP score is a weighted sum of squares of the PLS loadings. The amount of explained Y-variance in each dimension influenced the weights [66].

The Orthogonal Partial Least Squares-Discriminant Analysis (OPLS-DA) model was established by utilizing the MetaboAnalystR R package, version 1.0.1, following the log2 transformation and subsequent centering of the raw data.

Transcriptomic data were analyzed by using the Dr. Tom platform. Correlations between differentially significant metabolites obtained from metabolomic analysis and DEGs obtained RNA-seq were analyzed by using Pearson correlation analysis with a correlation analysis threshold of 0.9 and $p < 0.05$. Correlation network mapping was performed by using Cytoscape 3.8.0.

5. Conclusions

In the present study, the response to UV-B radiation was investigated by using *R. chrysanthum* group seedlings grown in artificial climate chambers as the experimental material. In this study, we investigated the metabolic changes in the leaves of *R. chrysanthum* following UV-B radiation by using widely targeted metabolomics and transcriptomics. By screening, we obtained 13 significantly different flavonoids, 9 DEGs, and 7 potentially functioning WRKY TFs of the flavonoid-related synthetic pathway. The results show that WRKY TFs could affect the expression of chalcone isomerase, dihydromyricetin reductase, flavonol synthase, and flavonoid 3′,5′-hydroxylase under UV-B stress, thus affecting the flavonoid content. However, the specific mechanisms by which TFs regulate gene expression need to be further investigated. This study holds significant practical importance for understanding the dynamics of metabolite changes and the regulatory mechanisms of plant growth adaptation under UV-B stress conditions. The findings are instrumental in forecasting the future impacts of increased UV-B radiation due to ozone depletion on plant communities and ecosystems.

Supplementary Materials: The following supporting information can be downloaded at: https://www.mdpi.com/article/10.3390/plants14010133/s1, Table S1: Information on metabolites identified by widely targeted metabolomics, Table S2: Differentially expressed genes associated with flavonoid synthesis, Table S3: Correlation analysis of WRKY TFs with key enzyme genes in flavonoid synthesis pathway, Figure S1: Metabolomic changes under stress, Figure S2: DEG KEGG analysis and GO analysis, Figure S3: Schematic diagram of multiple-reaction monitoring (MRM) process.

Author Contributions: Writing—original draft preparation, X.Z. (Xiangru Zhou) and W.Y.; writing—review and editing, J.M. and W.Y.; methodology, W.Y.; software, X.Z. (Xiangru Zhou) and W.Y.; visualization, X.Z. (Xiangru Zhou) and W.Y.; supervision, J.M. and H.X.; project administration, H.X. and X.Z. (Xiaofu Zhou); All authors have read and agreed to the published version of the manuscript.

Funding: This work was supported by the Jilin Province Science and Technology Development Plan Project (YDZJ202301ZYTS517).

Data Availability Statement: The data used in this study are available from the corresponding author upon submission of a reasonable request.

Conflicts of Interest: The authors declare no conflicts of interest.

Abbreviations

Rhododendron chrysanthum Pall.	*R. chrysanthum*
differentially expressed genes	DEGs
fold change	FC
Kyoto Encyclopedia of Genes and Genomes	KEGG
Orthogonal Partial Least Squares-Discriminant Analysis	OPLS-DA
photosynthetically active radiation	PAR
photosystem II	PSII
primary electron acceptor	QA
relative electron transfer rate	rETR
transcription factor	TF
ultraviolet-B	UV-B
UV RESISTANCE LOCUS 8	UVR8
variable importance in projection	VIP

References

1. Rai, N.; Morales, L.O.; Aphalo, P.J. Perception of solar UV radiation by plants: Photoreceptors and mechanisms. *Plant Physiol.* **2021**, *186*, 1382–1396. [CrossRef] [PubMed]
2. Barlev, A.; Sen, D. DNA's Encounter with Ultraviolet Light: An Instinct for Self-Preservation? *Acc. Chem. Res.* **2018**, *51*, 526–533. [CrossRef]
3. Björn, L.O. Photoenzymes and Related Topics: An Update. *Photochem. Photobiol.* **2018**, *94*, 459–465. [CrossRef] [PubMed]
4. Bajgar, R.; Moukova, A.; Chalupnikova, N.; Kolarova, H. Differences in the Effects of Broad-Band UVA and Narrow-Band UVB on Epidermal Keratinocytes. *Int. J. Environ. Res. Public Health* **2021**, *18*, 12480. [CrossRef]
5. Piccini, C.; Cai, G.; Dias, M.C.; Araujo, M.; Parri, S.; Romi, M.; Faleri, C.; Cantini, C. Olive Varieties under UV-B Stress Show Distinct Responses in Terms of Antioxidant Machinery and Isoform/Activity of RubisCO. *Int. J. Mol. Sci.* **2021**, *22*, 11214. [CrossRef] [PubMed]
6. Strzałka, W.; Zgłobicki, P.; Kowalska, E.; Bażant, A.; Dziga, D.; Banaś, A.K. The Dark Side of UV-Induced DNA Lesion Repair. *Genes* **2020**, *11*, 1450. [CrossRef] [PubMed]
7. Ling, C.; Wang, X.; Li, Z.; He, Y.; Li, Y. Effects and Mechanism of Enhanced UV-B Radiation on the Flag Leaf Angle of Rice. *Int. J. Mol. Sci.* **2022**, *23*, 12776. [CrossRef]
8. Shi, S.; Shi, R.; Li, T.; Zhou, D. UV-B Radiation Effects on the Alpine Plant Kobresia humilis in a Qinghai-Tibet Alpine Meadow. *Plants* **2022**, *11*, 3102. [CrossRef]
9. Santin, M.; Simoni, S.; Vangelisti, A.; Giordani, T.; Cavallini, A.; Mannucci, A.; Ranieri, A.; Castagna, A. Transcriptomic Analysis on the Peel of UV-B-Exposed Peach Fruit Reveals an Upregulation of Phenolic- and UVR8-Related Pathways. *Plants* **2023**, *12*, 1818. [CrossRef]
10. Liu, A.; Liu, S.; Li, Y.; Tao, M.; Han, H.; Zhong, Z.; Zhu, W.; Tian, J. Phosphoproteomics Reveals Regulation of Secondary Metabolites in *Mahonia bealei* Exposed to Ultraviolet-B Radiation. *Front. Plant Sci.* **2021**, *12*, 794906. [CrossRef] [PubMed]
11. Sun, Q.; Liu, M.; Cao, K.; Xu, H.; Zhou, X. UV-B Irradiation to Amino Acids and Carbohydrate Metabolism in *Rhododendron chrysanthum* Leaves by Coupling Deep Transcriptome and Metabolome Analysis. *Plants* **2022**, *11*, 2730. [CrossRef] [PubMed]
12. Hectors, K.; Van Oevelen, S.; Geuns, J.; Guisez, Y.; Jansen, M.A.; Prinsen, E. Dynamic changes in plant secondary metabolites during UV acclimation in Arabidopsis thaliana. *Physiol. Plant* **2014**, *152*, 219–230. [CrossRef] [PubMed]

13. Zhao, C.; Mao, K.; You, C.X.; Zhao, X.Y.; Wang, S.H.; Li, Y.Y.; Hao, Y.J. Molecular cloning and functional analysis of a UV-B photoreceptor gene, MdUVR8 (UV Resistance Locus 8), from apple. *Plant Sci.* **2016**, *247*, 115–126. [CrossRef]
14. Ma, M.; Xu, W.; Wang, P.; Gu, Z.; Zhang, H.; Yang, R. UV-B- triggered H_2O_2 production mediates isoflavones synthesis in germinated soybean. *Food Chem. X* **2022**, *14*, 100331. [CrossRef] [PubMed]
15. Neugart, S.; Tobler, M.A.; Barnes, P.W. Different irradiances of UV and PAR in the same ratios alter the flavonoid profiles of Arabidopsis thaliana wild types and UV-signalling pathway mutants. *Photochem. Photobiol. Sci.* **2019**, *18*, 1685–1699. [CrossRef]
16. Ji, H.B.; Tang, W.; Zhou, X.; Wu, Y. Combined Effects of Blue and Ultraviolet Lights on the Accumulation of Flavonoids in Tartary Buckwheat Sprouts. *Pol. J. Food Nutr. Sci.* **2016**, *66*, 93–98. [CrossRef]
17. Zhao, B.; Wang, L.; Pang, S.; Jia, Z.; Wang, L.; Li, W.; Jin, B. UV-B promotes flavonoid synthesis in Ginkgo biloba leaves. *Ind. Crops Prod.* **2020**, *151*, 112483. [CrossRef]
18. Ferreyra, M.L.F.; Serra, P.; Casati, P. Recent advances on the roles of flavonoids as plant protective molecules after UV and high light exposure. *Physiol. Plant* **2021**, *173*, 736–749. [CrossRef] [PubMed]
19. Zhang, Q.; Li, Y.; Cao, K.; Xu, H.; Zhou, X. Transcriptome and proteome depth analysis indicate ABA, MAPK cascade and Ca^{2+} signaling co-regulate cold tolerance in *Rhododendron chrysanthum* Pall. *Front. Plant Sci.* **2023**, *14*, 1146663. [CrossRef] [PubMed]
20. Wang, Y.; Mostafa, S.; Zeng, W.; Jin, B. Function and Mechanism of Jasmonic Acid in Plant Responses to Abiotic and Biotic Stresses. *Int. J. Mol. Sci.* **2021**, *22*, 8568. [CrossRef] [PubMed]
21. Zhou, X.; Lyu, J.; Sun, L.; Dong, J.; Xu, H. Metabolic programming of *Rhododendron chrysanthum* leaves following exposure to UVB irradiation. *Funct. Plant Biol.* **2021**, *48*, 1175–1185. [CrossRef] [PubMed]
22. Zhou, X.; Chen, S.; Wu, H.; Yang, Y.; Xu, H. Biochemical and proteomics analyses of antioxidant enzymes reveal the potential stress tolerance in *Rhododendron chrysanthum* Pall. *Biol. Direct* **2017**, *12*, 10. [CrossRef] [PubMed]
23. Liu, Y.; Fan, H.; Dong, J.; Chen, J.; Xu, H.; Zhou, X. Phosphoproteomics of cold stress-responsive mechanisms in *Rhododendron chrysanthum*. *Mol. Biol. Rep.* **2022**, *49*, 303–312. [CrossRef]
24. Lyu, J.; Wang, C.; Liang, D.Y.; Liu, L.; Pandey, L.K.; Xu, H.W.; Zhou, X.F. Sensitivity of wild and domesticated *Rhododendron chrysanthum* to different light regime (UVA, UVB, and PAR). *Photosynthetica* **2019**, *57*, 841–849. [CrossRef]
25. Liu, M.; Sun, Q.; Cao, K.; Xu, H.; Zhou, X. Acetylated Proteomics of UV-B Stress-Responsive in Photosystem II of *Rhododendron chrysanthum*. *Cells* **2023**, *12*, 478. [CrossRef] [PubMed]
26. Chu, X.; Wang, C.; Chen, X.; Lu, W.; Li, H.; Wang, X.; Hao, L.; Guo, X. The Cotton WRKY Gene GhWRKY41 Positively Regulates Salt and Drought Stress Tolerance in Transgenic Nicotiana benthamiana. *PLoS ONE* **2015**, *10*, e0143022. [CrossRef] [PubMed]
27. Zhou, Q.Y.; Tian, A.G.; Zou, H.F.; Xie, Z.M.; Lei, G.; Huang, J.; Wang, C.M.; Wang, H.W.; Zhang, J.S.; Chen, S.Y. Soybean WRKY-type transcription factor genes, GmWRKY13, GmWRKY21, and GmWRKY54, confer differential tolerance to abiotic stresses in transgenic Arabidopsis plants. *Plant Biotechnol. J.* **2008**, *6*, 486–503. [CrossRef] [PubMed]
28. Zhou, J.; Hou, D.; Zou, W.; Wang, J.; Luo, R.; Wang, M.; Yu, H. Comparison of Widely Targeted Metabolomics and Untargeted Metabolomics of Wild Ophiocordyceps sinensis. *Molecules* **2022**, *27*, 3645. [CrossRef]
29. Brito, G.O.; Reis, B.C.; Ferreira, E.A.; Vilela Junqueira, N.T.; Sá-Barreto, L.C.L.; Mattivi, F.; Vrhovsek, U.; Gris, E.F. Phenolic Compound Profile by UPLC-MS/MS and Encapsulation with Chitosan of Spondias mombin L. Fruit Peel Extract from Cerrado Hotspot-Brazil. *Molecules* **2022**, *27*, 2382. [CrossRef] [PubMed]
30. Zhou, H.; Yu, L.; Liu, S.; Zhu, A.; Yang, Y.; Chen, C.; Yang, A.; Liu, L.; Yu, F. Transcriptome comparison analyses in UV-B induced AsA accumulation of *Lactuca sativa* L. *BMC Genom.* **2023**, *24*, 61. [CrossRef] [PubMed]
31. Li, Y.; Tian, Q.; Wang, Z.; Li, J.; Liu, S.; Chang, R.; Chen, H.; Liu, G. Integrated analysis of transcriptomics and metabolomics of peach under cold stress. *Front. Plant Sci.* **2023**, *14*, 1153902. [CrossRef] [PubMed]
32. Park, M.H.; Ku, K.M.; Do, K.R.; Eum, H.L.; Cho, J.H.; Park, P.H.; Malka, S.K. Carbon dioxide treatment modulates phosphatidic acid signaling and stress response to improve chilling tolerance and postharvest quality in paprika. *Front. Plant Sci.* **2023**, *14*, 1287997. [CrossRef] [PubMed]
33. Maan, K.; Baghel, R.; Dhariwal, S.; Sharma, A.; Bakhshi, R.; Rana, P. Metabolomics and transcriptomics based multi-omics integration reveals radiation-induced altered pathway networking and underlying mechanism. *NPJ Syst. Biol. Appl.* **2023**, *9*, 42. [CrossRef]
34. Zhou, X.; Gong, F.; Dong, J.; Lin, X.; Cao, K.; Xu, H.; Zhou, X. Abscisic Acid Affects Phenolic Acid Content to Increase Tolerance to UV-B Stress in *Rhododendron chrysanthum* Pall. *Int. J. Mol. Sci.* **2024**, *25*, 1234. [CrossRef] [PubMed]
35. Barnes, P.W.; Robson, T.M.; Neale, P.J.; Williamson, C.E.; Zepp, R.G.; Madronich, S.; Wilson, S.R.; Andrady, A.L.; Heikkilä, A.M.; Bernhard, G.H.; et al. Environmental effects of stratospheric ozone depletion, UV radiation, and interactions with climate change: UNEP Environmental Effects Assessment Panel, Update 2021. *Photochem. Photobiol. Sci.* **2022**, *21*, 275–301. [CrossRef]
36. Kataria, S.; Jajoo, A.; Guruprasad, K.N. Impact of increasing Ultraviolet-B (UV-B) radiation on photosynthetic processes. *J. Photochem. Photobiol. B Biol.* **2014**, *137*, 55–66. [CrossRef]
37. Badshah, S.L.; Faisal, S.; Muhammad, A.; Poulson, B.G.; Emwas, A.H.; Jaremko, M. Antiviral activities of flavonoids. *Biomed. Pharmacother.* **2021**, *140*, 111596. [CrossRef]

38. Čižmárová, B.; Hubková, B.; Tomečková, V.; Birková, A. Flavonoids as Promising Natural Compounds in the Prevention and Treatment of Selected Skin Diseases. *Int. J. Mol. Sci.* **2023**, *24*, 6324. [CrossRef]
39. Kopustinskiene, D.M.; Jakstas, V.; Savickas, A.; Bernatoniene, J. Flavonoids as Anticancer Agents. *Nutrients* **2020**, *12*, 457. [CrossRef] [PubMed]
40. Treml, J.; Šmejkal, K. Flavonoids as Potent Scavengers of Hydroxyl Radicals. *Compr. Rev. Food Sci. Food Saf.* **2016**, *15*, 720–738. [CrossRef]
41. Schreiber, U. Pulse-Amplitude-Modulation (PAM) Fluorometry and Saturation Pulse Method: An Overview. In *Chlorophyll a Fluorescence: A Signature of Photosynthesis*; Papageorgiou, G.C., Govindjee, Eds.; Springer: Dordrecht, The Netherlands, 2004; pp. 279–319.
42. Schreiber, U.; Bilger, W.; Neubauer, C. Chlorophyll Fluorescence as a Nonintrusive Indicator for Rapid Assessment of In Vivo Photosynthesis. In *Ecophysiology of Photosynthesis*; Schulze, E.-D., Caldwell, M.M., Eds.; Springer: Berlin/Heidelberg, Germany, 1995; pp. 49–70.
43. Kühl, M.; Chen, M.; Ralph, P.J.; Schreiber, U.; Larkum, A.W. Ecology: A niche for cyanobacteria containing chlorophyll d. *Nature* **2005**, *433*, 820. [CrossRef] [PubMed]
44. Ralph, P.J.; Gademann, R. Rapid light curves: A powerful tool to assess photosynthetic activity. *Aquat. Bot.* **2005**, *82*, 222–237. [CrossRef]
45. Bilger, W.; Schreiber, U. Energy-dependent quenching of dark-level chlorophyll fluorescence in intact leaves. *Photosynth. Res.* **1986**, *10*, 303–308. [CrossRef] [PubMed]
46. Righini, S.; Rodriguez, E.J.; Berosich, C.; Grotewold, E.; Casati, P.; Falcone Ferreyra, M.L. Apigenin produced by maize flavone synthase I and II protects plants against UV-B-induced damage. *Plant Cell Environ.* **2019**, *42*, 495–508. [CrossRef]
47. Morimoto, S.; Tateishi, N.; Matsuda, T.; Tanaka, H.; Taura, F.; Furuya, N.; Matsuyama, N.; Shoyama, Y. Novel hydrogen peroxide metabolism in suspension cells of Scutellaria baicalensis Georgi. *J. Biol. Chem.* **1998**, *273*, 12606–12611. [CrossRef]
48. Emiliani, J.; Grotewold, E.; Falcone Ferreyra, M.L.; Casati, P. Flavonols protect Arabidopsis plants against UV-B deleterious effects. *Mol. Plant* **2013**, *6*, 1376–1379. [CrossRef] [PubMed]
49. Matsui, K.; Oshima, Y.; Mitsuda, N.; Sakamoto, S.; Nishiba, Y.; Walker, A.R.; Ohme-Takagi, M.; Robinson, S.P.; Yasui, Y.; Mori, M.; et al. Buckwheat R2R3 MYB transcription factor FeMYBF1 regulates flavonol biosynthesis. *Plant Sci.* **2018**, *274*, 466–475. [CrossRef]
50. Qiao, Y.; Wu, L.; Yang, S.; Wang, Q.; Gu, H.; Wei, L.; Liu, G.; Zhou, S.; Wang, P.; Song, M. Metabolomic and transcriptomic analyses provide insights into variations in flavonoids contents between two Artemisia cultivars. *BMC Plant Biol.* **2023**, *23*, 288. [CrossRef] [PubMed]
51. Wang, X.; Niu, Y.; Zheng, Y. Multiple Functions of MYB Transcription Factors in Abiotic Stress Responses. *Int. J. Mol. Sci.* **2021**, *22*, 6125. [CrossRef]
52. Chu, S.; Wang, J.; Zhu, Y.; Liu, S.; Zhou, X.; Zhang, H.; Wang, C.E.; Yang, W.; Tian, Z.; Cheng, H.; et al. An R2R3-type MYB transcription factor, GmMYB29, regulates isoflavone biosynthesis in soybean. *PLoS Genet.* **2017**, *13*, e1006770. [CrossRef] [PubMed]
53. Yi, J.; Derynck, M.R.; Li, X.; Telmer, P.; Marsolais, F.; Dhaubhadel, S. A single-repeat MYB transcription factor, GmMYB176, regulates CHS8 gene expression and affects isoflavonoid biosynthesis in soybean. *Plant J.* **2010**, *62*, 1019–1034. [CrossRef]
54. Arlotta, C.; Puglia, G.D.; Genovese, C.; Toscano, V.; Karlova, R.; Beekwilder, J.; De Vos, R.C.H.; Raccuia, S.A. MYB5-like and bHLH influence flavonoid composition in pomegranate. *Plant Sci.* **2020**, *298*, 110563. [CrossRef] [PubMed]
55. Wei, K.; Chen, H. Comparative functional genomics analysis of bHLH gene family in rice, maize and wheat. *BMC Plant Biol.* **2018**, *18*, 309. [CrossRef] [PubMed]
56. Guo, J.; Sun, B.; He, H.; Zhang, Y.; Tian, H.; Wang, B. Current Understanding of bHLH Transcription Factors in Plant Abiotic Stress Tolerance. *Int. J. Mol. Sci.* **2021**, *22*, 4921. [CrossRef]
57. Amato, A.; Cavallini, E.; Zenoni, S.; Finezzo, L.; Begheldo, M.; Ruperti, B.; Tornielli, G.B. A Grapevine TTG2-Like WRKY Transcription Factor Is Involved in Regulating Vacuolar Transport and Flavonoid Biosynthesis. *Front. Plant Sci.* **2016**, *7*, 1979. [CrossRef] [PubMed]
58. Xiang, X.Y.; Chen, J.; Xu, W.X.; Qiu, J.R.; Song, L.; Wang, J.T.; Tang, R.; Chen, D.; Jiang, C.Z.; Huang, Z. Dehydration-Induced WRKY Transcriptional Factor MfWRKY70 of Myrothamnus flabellifolia Enhanced Drought and Salinity Tolerance in Arabidopsis. *Biomolecules* **2021**, *11*, 327. [CrossRef]
59. Javed, T.; Gao, S.J. WRKY transcription factors in plant defense. *Trends Genet.* **2023**, *39*, 787–801. [CrossRef]
60. Singh, S.; Grover, A.; Nasim, M. Biofuel Potential of Plants Transformed Genetically with NAC Family Genes. *Front. Plant Sci.* **2016**, *7*, 22. [CrossRef]
61. Liu, M.; Sun, L.; Cao, Y.; Xu, H.; Zhou, X. Acetylation proteomics and metabolomics analyses reveal the involvement of starch synthase undergoing acetylation modification during UV-B stress resistance in *Rhododendron chrysanthum* Pall. *Hereditas* **2024**, *161*, 15. [CrossRef]

62. Gong, F.; Zhou, X.; Cao, K.; Xu, H.; Zhou, X. Analyses of the metabolism and assessment of antioxidant activity in *Rhododendron chrysanthum* Pall. after UV-B Irradiation. *Plant Growth Regul.* **2024**, *103*, 525–537. [CrossRef]
63. Gong, F.; Yu, W.; Zeng, Q.; Dong, J.; Cao, K.; Xu, H.; Zhou, X. *Rhododendron chrysanthum*'s Primary Metabolites Are Converted to Phenolics More Quickly When Exposed to UV-B Radiation. *Biomolecules* **2023**, *13*, 1700. [CrossRef] [PubMed]
64. Yu, W.; Gong, F.; Zhou, X.; Xu, H.; Lyu, J.; Zhou, X. Comparative Metabolomics and Transcriptome Studies of Two Forms of *Rhododendron chrysanthum* Pall. under UV-B Stress. *Biology* **2024**, *13*, 211. [CrossRef] [PubMed]
65. Zeng, Q.; Dong, J.; Lin, X.; Zhou, X.; Xu, H. Isolation and Identification of Acer truncatum Endophytic Fungus Talaromyces verruculosus and Evaluation of Its Effects on Insoluble Phosphorus Absorption Capacity and Growth of Cucumber Seedlings. *J. Fungi* **2024**, *10*, 136. [CrossRef]
66. Matysiak, J.; Dereziński, P.; Klupczyńska, A.; Matysiak, J.; Kaczmarek, E.; Kokot, Z.J. Effects of a honeybee sting on the serum free amino acid profile in humans. *PLoS ONE* **2014**, *9*, e103533. [CrossRef] [PubMed]

Disclaimer/Publisher's Note: The statements, opinions and data contained in all publications are solely those of the individual author(s) and contributor(s) and not of MDPI and/or the editor(s). MDPI and/or the editor(s) disclaim responsibility for any injury to people or property resulting from any ideas, methods, instructions or products referred to in the content.

plants

MDPI

Article

Comprehensive Omics Analysis Reveals Cold-Induced Metabolic Reprogramming and Alternative Splicing in *Dendrobium officinale*

Xinqiao Zhan [1,2,*], Zhangqun Li [2], Minxia Pang [3], Guoxiang Yao [3,4] and Bizeng Mao [1,*]

[1] Institute of Biotechnology, Ministry of Agriculture Key Lab of Molecular Biology of Crop Pathogens and Insects, Zhejiang Key Laboratory of Biology and Ecological Regulation of Crop Pathogens and Insects, Zhejiang University, Hangzhou 310058, China
[2] School of Pharmaceutical Sciences, Taizhou University, Taizhou 318000, China; lizhangqun@126.com
[3] Zhejiang Jianjiuhe Group Co., Ltd., Ningbo 315000, China; pmx059@163.com (M.P.); yao.guoxiang@shunyun.cn (G.Y.)
[4] Ningbo Shunyun Electroinic Co., Ltd., Ningbo 315000, China
* Correspondence: joezhan@tzc.edu.cn (X.Z.); maobz@zju.edu.cn (B.M.)

Abstract: *Dendrobium officinale* is an economically important orchid species that is sensitive to cold stress. Understanding the molecular and metabolic mechanisms underlying its response to cold is crucial for developing strategies to improve its cold tolerance. In this study, we constructed a comprehensive cold stress response dataset for *D. officinale* and characterized its regulatory landscape in response to varying cold stress conditions. The glycine metabolism-related genes *Dca003913* and *Dca022726* play pivotal roles in both cold and drought stress adaptation, and their expression is not upregulated by hormones or fungi infection. Carbohydrate metabolism showed specific dynamic changes in freezing injury cells, which involved a variety of hormonal responses. The abundance of sphingolipids was notably higher in the freezing treatment (FT) compared to the freezing recovery (FR) plants, indicating specialized metabolic adaptations at different cold intensities. An alternative splicing (AS) analysis identified 368 DAS genes, with spliceosome pathways significantly enriched. Three key ubiquitination proteins (PKU64802, XP_020672210, and PKU75555) were found to regulate splicing factors, which showed increased abundance in cold stress. This study highlights the roles of metabolic reprogramming and RNA splicing in cold adaptation, revealing a complex molecular network activated in response to cold stress.

Keywords: *Dendrobium officinale*; alternative splicing; cold stress; ubiquitination; glycine metabolism

1. Introduction

Low and freezing temperatures pose significant challenges to crops, severely affecting their growth, metabolism, and geographical distribution [1,2]. Plants have evolved complex mechanisms to sense and respond to cold stress, including changes in gene expression, metabolic adjustments, and alterations in RNA processing [3,4]. Multi-omics has been used to study a series of physiological and biochemical changes in plants. For example, transcriptomic and lipidomic analyses found that 59 cold-tolerant genes were involved in lipid metabolism, highlighting the protective roles of increased digalactosyldiacylglycerol (DGDG) and sulfoquinovosyldiacylglycerol (SQDG) levels against photosynthetic damage and upregulated phosphatidate-phosphatase (PAP1) and phosphatidate-cytidylyltransferase (CDS1) in preventing membrane lipid peroxidation, contributing to a

comprehensive metabolic model for peanut cold tolerance [5]. Cold-acclimated seedlings of *Sonneratia apetala* exhibit enhanced cold tolerance through physiological adjustments and differential accumulation of proteins involved in ROS scavenging, photosynthesis, energy metabolism, carbohydrate metabolism, cofactor biosynthesis, and protein folding, with key regulators including translation elongation factor G, chlorophyll A-B binding protein, and ascorbate peroxidase [6]. In maize, decreasing the temperature from 20 to 16 °C alters 50% of metabolites and 18% of proteins, with specific examples including decreasing levels of photosynthesis-related proteins and increasing levels of metabolites such as trans-acetate and hydroxycinnamate derivatives, which could serve as potential markers for breeding cold-tolerant varieties [6]. Analyses of the integrated transcriptome–metabolome identified 3140 differentially expressed genes, including those involved in jasmonic acid synthesis and signaling, and found increased levels of branched-chain amino acids such as leucine, isoleucine, and valine, which together contribute to the seed browning and chilling response in *Capsicum annuum* fruit [7]. The expression of transcription factors such as C-repeat binding factors (CBFs) and the subsequent induction of downstream cold-responsive genes are well-documented [8]. However, little is known about the complex interplay between transcriptional, translational, and metabolic changes in response to cold stress.

Alternative splicing (AS) enables plants to produce diverse transcripts from a single gene, significantly enhancing the functional diversity of the transcriptome [9]. AS plays a critical role in plant responses to various environmental stresses, including cold stress [9]. The cold stress responses in plants are regulated by several transcription factors (TFs), such as the bZIP (basic leucine zipper protein), MYB (*v-myb* avian myeloblastosis viral oncogene homolog), and WRKY (conserved amino acids) families, which are associated with regulating AS to produce differences in protein function [10,11]. By generating multiple protein isoforms or non-coding RNAs, AS contributes to the complexity of the plant's response to changing environmental conditions. Thus, identification of AS events is important in transcriptional control. Currently, RNA-Seq based on next-generation sequencing technology is extensively employed in transcriptomics research in plants. It is a high-throughput method enabling the precise quantification and annotation of AS events. Studies on model plants have provided evidence that RNA-Seq technology discloses AS in 61% and 48% of multi-exon genes, in [12,13], respectively. However, the regulation of AS at the post-transcriptional level in response to both biotic and abiotic stresses still lacks study.

D. officinale is a valuable orchid species, which is mainly distributed in southern China [14,15]. *D. officinale* contains numerous bioactive extracts such as polysaccharides, alkaloids, phenols, terpenes, coumarins, and flavonoids [16,17]. Wild *D. officinale* grows on semi-shady rocks in mountainous areas at an altitude of 800–1600 m, and its quantity is scarce. At present, it has been widely cultivated artificially in southern China. The cultivars we studied were located in Zhejiang Province. In winter, the temperature can drop to around −10 °C. Although the cultivated environment is more stable and milder, extreme low temperatures in winter still cause a decrease in *D. officinale* production. At present, only two studies have reported on cold stress in *D. officinale* [18,19]. The cold stress responses of *D. officinale* are still unclear, which restricts the potential of gene engineering to attain enhanced cold tolerance. Moreover, the basic research into *D. officinale* still focuses on gene classification analysis [20,21]. The specific effects of cold stress on AS events and the regulation of splicing factors in *D. officinale* remain largely unexplored. The objective of this study is to investigate the molecular and metabolic responses of *D. officinale* to cold stress, with a focus on the dynamics of alternative splicing and the regulation of splicing factors in the treatment of cold stress. Understanding these processes will provide insights

into the mechanisms underlying cold adaptation and offer potential targets for improving cold tolerance in *Dendrobium*.

2. Results

2.1. The Core Pathway Involved in the Cold Response of D. officinale

To study the core response pathway of cold stress in *D. officinale*, we integrated two transcriptional datasets of cold treatment. The sample names for the datasets were CK1 (25 °C), CK2 (20 °C), CA (8 °C), FT1 (0 °C), FT2 (−6 °C), and FR (8 °C, recovery). A principal component analysis (PCA) indicated partial overlap between the CK and cold treatments (Figure 1a). The transcriptional data were processed through a Bayesian framework to eliminate batch effects. A PCA and hierarchical cluster analysis showed that the CK and cold treatment were obviously separated into two groups (Figure 1b,c). Furthermore, Gene Set Enrichment Analysis (GSEA) revealed the downregulation of eight core metabolic pathways during cold treatment, including nucleotide, amino acid, lipid, and secondary metabolism (Figure 1d). C5-branched dibasic acid metabolism and the glycine, serine and threonine metabolism related pathway levels were enhanced during extensive cold treatment compared to the CK group (Figure 1d). Six representative pathways were selected from the GSEA. A hierarchical cluster analysis showed these pathways related to gene levels were statistically separated into two clades based on treatment and were basically consistent under different cold treatments (Figure 1e). Random forest methods were used to identify the feature genes associated within the cold and CK groups. The top 10 genes with high accuracy were identified, among which 4 genes were abundant in cold, and 6 genes were abundant in the CK group (Figure 1f). Cold treatment induced cell dehydration and rupture, due to the formation of ice crystals in the extracellular space of the cell membrane. Thus, we detected the expression levels of three genes in leaves during the drying treatment and rewetting phase. *Dca003913* and *Dca022726* were induced by the dry treatment and were restored in expression during the rewetting phase (Figure 1g). In addition, the content of glycine increased during the dry treatment and recovered during rewetting (Figure S1). However, the expressions of *Dca003913* and *Dca022726* were not increased by hormones or fungus infection (Figure 1h). These results suggested that the gene induction of glycine degradation was a key component in cell dehydration.

The differentially expressed genes (DEGs) were identified using a fold change (FC) of >2 and an adjusted p value of <0.05 as the cutoffs. In total, 2679 genes were upregulated and 2572 were downregulated in the cold vs. CK groups (Figure S2). The top 20 genes were labeled, and they were involved in multiple pathways, including secondary metabolism, carbohydrate metabolism, and stress response (Figure S3). These genes were not only clustered under cold treatment but also varied according to their temperature changes. Thus, *D. officinale* might have a wide response mechanism to cold and a temperature-specific response mechanism.

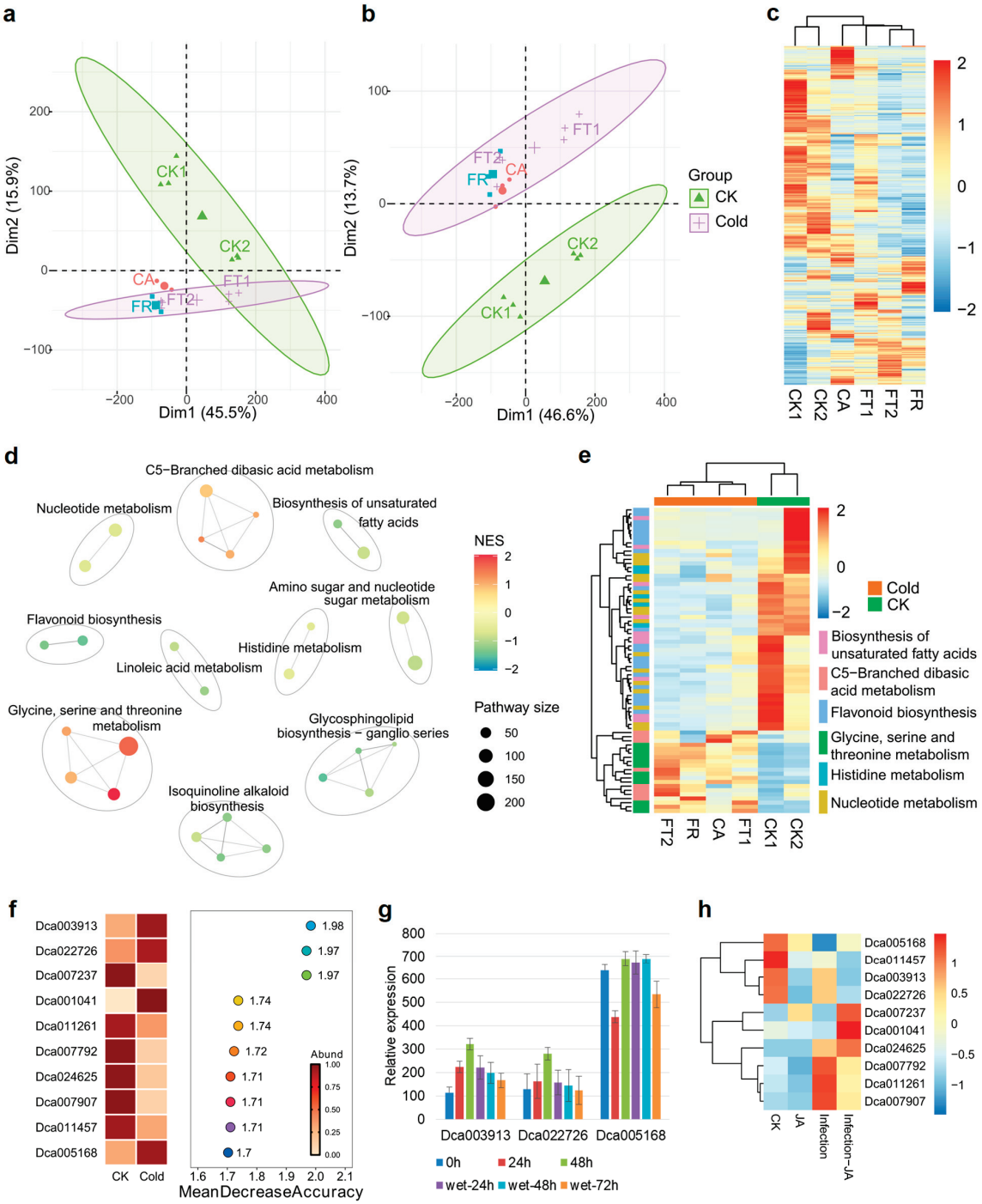


Figure 1. Glycine metabolism as a core pathway involved in cold stress. (**a**) PCA plot showing the separation between control conditions (CK1 and CK2) and cold treatments (FT1 and FT2, along with other cold treatments). (**b**) PCA plot after removing batch effects and other unwanted sources of variation. The CK and cold treatments are clearly separated. (**c**) Hierarchical clustering heatmap of transcriptional data showing the grouping of the CK and cold treatments. (**d**) GSEA results indicating pathways that are down- or up-regulated in the cold treatments compared to CK treatments. (**e**) Hierarchical clustering heatmap of selected pathways showing the expression patterns of genes related to these pathways across different treatments. (**f**) Random Forest analysis identifying the top 10 genes with a high accuracy in distinguishing between cold and CK conditions. Expression levels of genes abundant in cold versus CK conditions are indicated. (**g**) Expression profiles of selected genes during dry treatment and rewetting phases. Values are means ± S.D. (n = 3). (**h**) Expression profiles of selected genes in response to hormonal JA and fungal infection treatments.

2.2. Temperature-Specific Response in D. officinale

Transcriptome analysis suggested that *D. officinale* exhibits temperature-specific gene expression responses. To functionally characterize specific genes in cold treatment, we performed a WGCNA (Weighted Correlation Network Analysis) with transcriptomes and samples. This yielded seven distinct co-expression modules, each assigned a unique color and correlated with six treatments (Figure 2a). Four of the modules were clearly temperature-dependent, such as FT1 and FT2, exhibiting similar modules and significantly correlated ($p < 0.05$) with blue and yellow (Figure 2a). We found that the essential relationship between the modules FT2 and FR was most apparent through clustering analyses (Figure 2b). Furthermore, we merged 5251 DEGs of the cold vs. CK treatments with genes with the yellow and blue modules, and 487 overlapping genes were selected to analyze the KEGG (Kyoto Encyclopedia of Genes and Genomes) enrichment pathways (Figure 2c). KEGG terms related to carbon metabolism and photosynthesis were significantly enriched ($p < 0.05$) during freezing treatment (Figure 2d). Freezing conditions caused serious damage to the cell membrane fluidity. However, lipid metabolism did not emerge as a significant pathway in this gene set. To further analyze this consistently impacted set, we compared the carbon metabolism related gene levels in the CK1, FT2, and FR treatments. Examples include transcripts for the fructose-bisphosphate aldolase, malate dehydrogenase, and ribulose bisphosphate carboxylase, all of which were more abundant in the FT2 and FR treatments compared to the CK1 treatment (Figure 2e). The metabolic processes involved in these genes were not only involved in carbon metabolism but were also related to plastids and chloroplasts. We further identified the common genes associated with the FR-related modules and 5251 DEGs. In total, 261 overlapping genes were significantly enriched in five pathways ($p < 0.05$), including pathogen interaction, signal transduction, and sugar metabolism (Figure 2f). The five genes related to auxin, cytokinin, gibberellin, and brassinosteroid signal transduction were significantly upregulated in the FT2 and FR treatments compared to the CK1 treatment (Figure 2h). Seven genes involved in sugar metabolism had consistently increased mRNA levels in the FR treatment compared to the FT2 and CK1 treatments, including glycosyltransferase, pyruvate kinase, and trehalose-6-phosphate phosphatase (Figure 2i). These results suggested that the carbohydrate metabolism showed specific dynamic changes in freezing injury cells, which involved a variety of hormonal responses.

2.3. Metabolite-Specific Accumulation Under Cold Treatment in D. officinale

In order to identify the core metabolites specifically accumulated under cold stress, metabolomic profiling was performed. The distribution of metabolites across various treatments, based on their proportion, revealed that 60% of lipids, amino acids, and their secondary derivatives accumulations were closely associated with the FR treatment (Figure 3a). The details of these metabolites are shown in Table S1. The top 10 metabolites with respect to the mean intensity across the three treatments were selected. In comparison to the CK and FT treatments, the levels of four metabolites, namely oleamide, apigenin glucoside, rutin, and vicenin, exhibited a distinct increase in the FR treatment (Figure 3b). Under cold conditions, the unsaturated glycolipid monogalactosyldiacylglycerol (MGDG, 36:5) demonstrated an elevation relative to the CK group (Figure 3b).

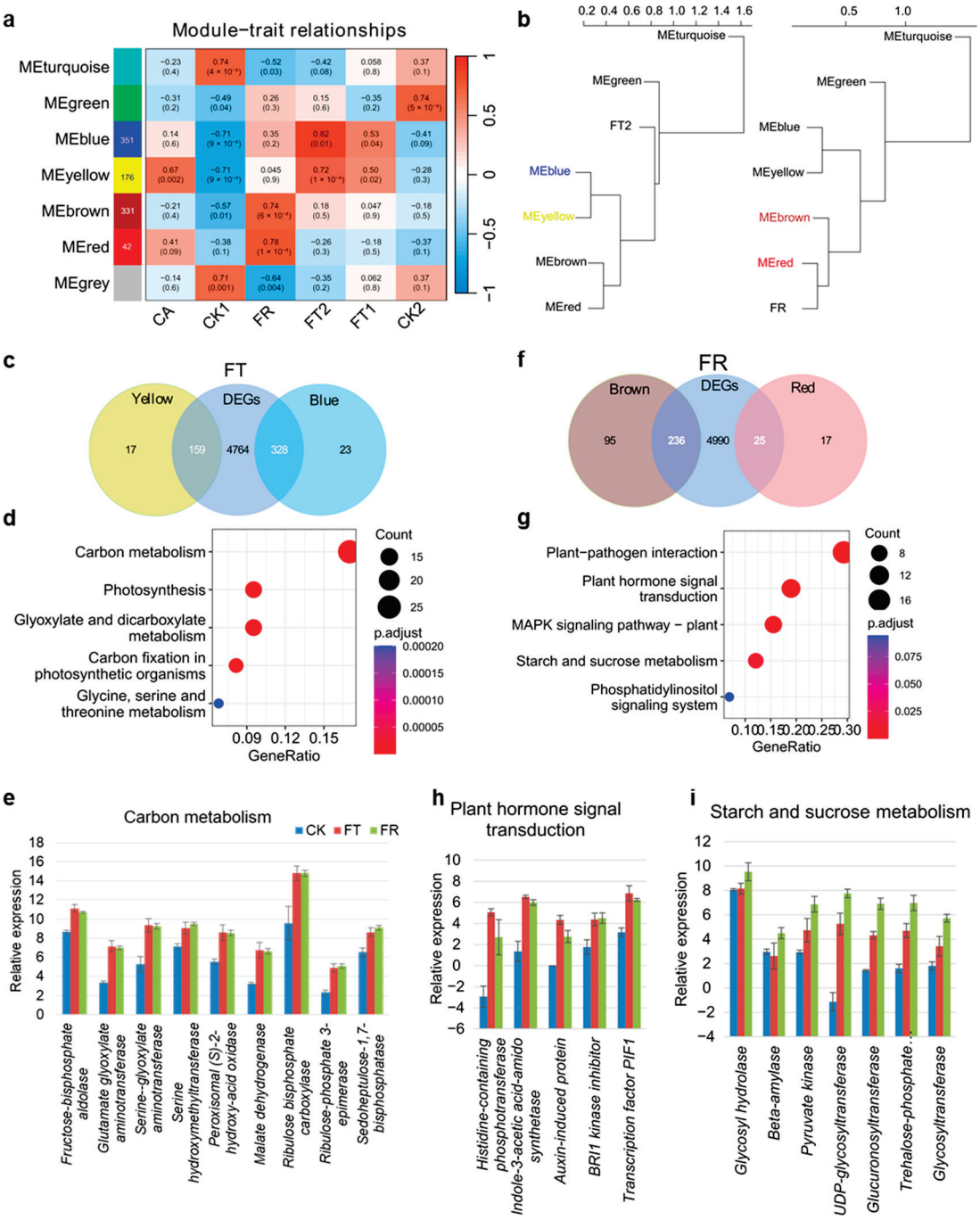


Figure 2. Temperature-specific response in *D. officinale*. (**a**) WGCNA showing seven distinct co-expression modules correlated with different treatments. (**b**) Clustering analysis highlighting the relationship between modules and specific treatments, particularly the FT2 and FR treatments. (**c**) Venn diagram showing the overlap between 5251 differentially expressed genes (DEGs) and genes within the yellow and blue modules. (**d**) KEGG pathway enrichment analysis of the overlapping genes from (**c**), indicating pathways significantly enriched during freezing treatments. (**e**) The expression levels of genes involved in carbon metabolism-related processes across the CK, FT, and FR treatments. Values are means ± S.D. (n = 3). (**f**) Venn diagram showing the overlap between genes from FR-related modules and 5251 DEGs. (**g**) KEGG pathway enrichment analysis of the overlapping genes from (**f**), indicating pathways significantly enriched during recovering treatments. (**h**) Hormone signaling-related genes that are significantly up-regulated in the FT and FR treatments compared to CK treatment. Values are means ± S.D. (n = 3). (**i**) Sugar metabolism-related genes showing consistent increases in mRNA levels in the FR treatment compared to the FT and CK treatments. Values are means ± S.D. (n = 3).

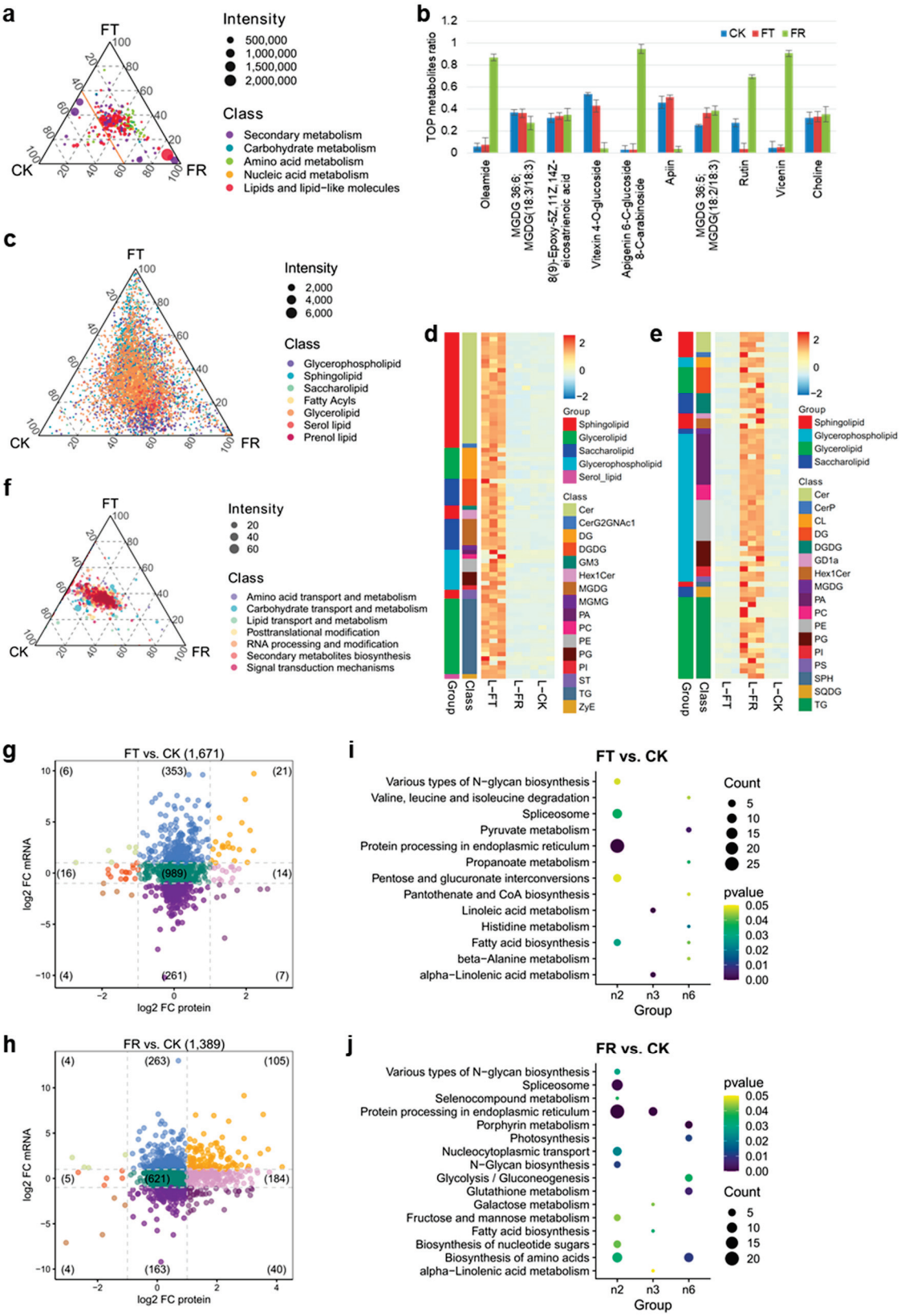


Figure 3. Metabolite-specific accumulation under cold treatment in *D. officinale*. (**a**) Distribution of metabolites according to their proportion in different treatments, highlighting the abundance of lipids, amino acids, and secondary derivatives in the FR treatment. (**b**) The top 10 metabolites with the highest intensity means across treatments. Specific metabolites that are increased in the FR treatment are highlighted. Values are means ± S.D. (n = 6). (**c**) The lipids were classified into seven

categories, illustrating the progressive increase in the FT group and FR treatment. (**d**) The top proportion of metabolites in the FT group compared to the CK group and FR treatment. (**e**) The top proportion of metabolites in the FR treatment compared to CK and FT groups. (**f**) Scatter plot showing the distribution of protein positions across treatments, with an emphasis on signal transduction and secondary metabolite biosynthesis proteins. (**g**) Scatter plot comparing $\log_2$ fold changes in mRNA and protein levels for the FT vs. CK groups. (**h**) Scatter plot comparing $\log_2$ fold changes in mRNA and protein levels for the FR vs. CK groups. (**i**) Gene enrichment analysis for the n2 sector (indigo points) showing pathways with increased mRNA levels during the FT and FR treatments. (**j**) Gene enrichment analysis for the n3 sector (orange points) and n6 sector (mauve points) showing pathways with increased protein levels, particularly amino acid biosynthesis during the FR treatment.

To comprehensively explore the lipid profile alterations under cold stress, 5981 lipids were classified into seven categories (Table S2). Most lipids were concentrated around certain regions and increased in the FT and FR treatments (Figure 3c). We further analyzed the specifically accumulated lipids in the FT and FR treatments (Figure S4 and Figure 3d,e). The species numbers of sphingolipids were 3.4-fold more extensive in the FT group compared to the FR treatment. Among them, ceramides (Cer) were the most dramatically changed sphingolipid. Glycerophospholipid and saccharolipid species were decreased 3.4-fold and 1.5-fold in the FT treatment compared to the FR treatment, respectively (Figure 3d,e). The ratio of MGDG and DGDG decreased two-fold in the FR treatment compared to the FT treatment. Another kind of saccharolipid, SQDG, was particularly increased in the FR treatment compared to the FT treatment (Figure 3d,e). These results suggest that sphingolipid and glycerophospholipid metabolism are related to enhance cold tolerance.

Transcriptome integration analysis identified several amino acid metabolites involved in cold treatment. However, further quantification and comprehensive analysis of the protein expression were important in revealing the metabolic processes during cold treatment (Table S3). Most protein positions were left of center and were close to the FT and CK groups (Figure 3f). The signal transduction and secondary metabolite biosynthesis proteins were very intensive, with a concomitant increase in the FR compartment (Figure 3f). To further analyze the consistent impact of transcription and translation during cold, we compared the $\log_2$ fold change (FC) values between the cold and CK samples in the mRNA and protein levels. Of the 1671 protein values, 41% (682 proteins) showed at least two-fold differences in mRNA and/or protein levels in the FT vs. CK groups (Figure 3g). In the FR vs. CK groups, 768 proteins showed at least two-fold differences in mRNA and/or protein levels (Figure 3h). The mauve points (n6 sector) showed significant increases only in protein abundance and not for mRNA. The protein number of the FR treatment vs. the CK group (184 proteins) was higher than that of the FT group vs. the CK group (14 proteins). These results implied that the rise in most proteins during the FR treatment was independent of transcription and/or translation. For the gene enrichment analysis of the FT group and FR treatment in the n2 sector (indigo points), n3 sector (orange points), and n6 sector (mauve points), numerous biosynthesis processes were identified whose increased mRNA and/or protein levels revealed obvious differences between the FT group and FR treatment (Figure 3i,j). For the n2 sector, the FT treatments induced the mRNA levels of pentose metabolism and fatty acid biosynthesis, and the FR treatment induced the mRNA levels of nucleotide sugar metabolism and amino acid biosynthesis. For the n3 sector, linoleic acid metabolism was especially enriched (during the FT treatments) for both protein and mRNA. For the n6 sector, amino acid biosynthesis, including glutathione metabolism, was only significantly enriched during the FR treatment at protein levels. The protein number related to thylakoids in the FT group was lower than that in the FR treatment, which was probably driven by catabolic routes in the presence of autophagy.

2.4. Identification of Key Splicing Factors in Response to Cold in D. officinale

Notably, the spliceosome pathway was significantly enriched in the individual sector during cold treatment (Figure 3i,j), which is probably driven by pre-mRNA processes. Five main types of AS events were studied in two *D. officinale* genome annotation versions in NCBI (GCA_001605985.2 and GCF_001605985.2). However, 12,569 AS events were found in the genome (GCF_001605985.2, Figure 4a). Among, them, A3SS (alternative 3′ splice sites) was the most abundant type (41%), followed by EX (exon skipping, 24%), A5SS (alternative 5′ splice sites, 22%), IR (intron retention, 11%), and MX (exclusive exons, 2%). We further identified the AS events (PSI > 0) in six temperature treatments. Low temperature exposure triggered a rapid AS response with a significantly higher number of AS events. In contrast, the FT and FR treatments significantly decreased the number of AS events compared to the CK1/2 treatment (Figure 4b). We merged the AS events for the normal and cold conditions. We discovered that the IR and MX of the cold group were the same as that of the CK group. The CA treatment induced an increase in A3SS, A5SS, and EX compared to the CK group, and all three decreased in the FT group and FR treatment. However, A3SS and EX had an increasing tendency in the FR treatment (Figure 4c). This suggests that *D. officinale* tends to induce A3SS, A5SS, and EX under low temperatures and sub-zero temperatures that seriously affect RNA splicing.

To characterize the dynamics of AS during exposure to cold treatment, we compared the differences in AS events at different temperature conditions. The results revealed that increased differential alternative splicing (DAS) events occurred in the cold compared to the controls. FT-induced AS events persisted throughout the FR period (Figure 4d). Furthermore, we merged 368 DAS genes from six comparisons that were clustered across five regions and exhibited substantial variation in the expression levels (Figure 4e). Functional annotation of the DAS genes revealed that the spliceosome was specially enriched during the CA and FR treatments (Figure 4f). Moreover, carbon metabolism and amino acid biosynthesis were specifically enriched in the FT group and FR treatment compared to the CA treatment (Figure 4f). Most of the transcripts of the DAS genes, including spliceosome, carbon, and amino acid metabolism, had higher expression in the CA treatment compared to the FT group and FR treatment (Figure S5). We selected three DAS genes to examine their transcript expression. The *malate dehydrogenase* (*LOC110113907*) and *cysteine synthase* (*LOC110093223*) transcript expression levels were especially induced in the CA treatment. The *Zinc knuckle* transcript (*LOC110095000*) expression level was suppressed by cold treatment (Figure S6). This result confirmed the accuracy of the DAS gene identification in the transcriptome.

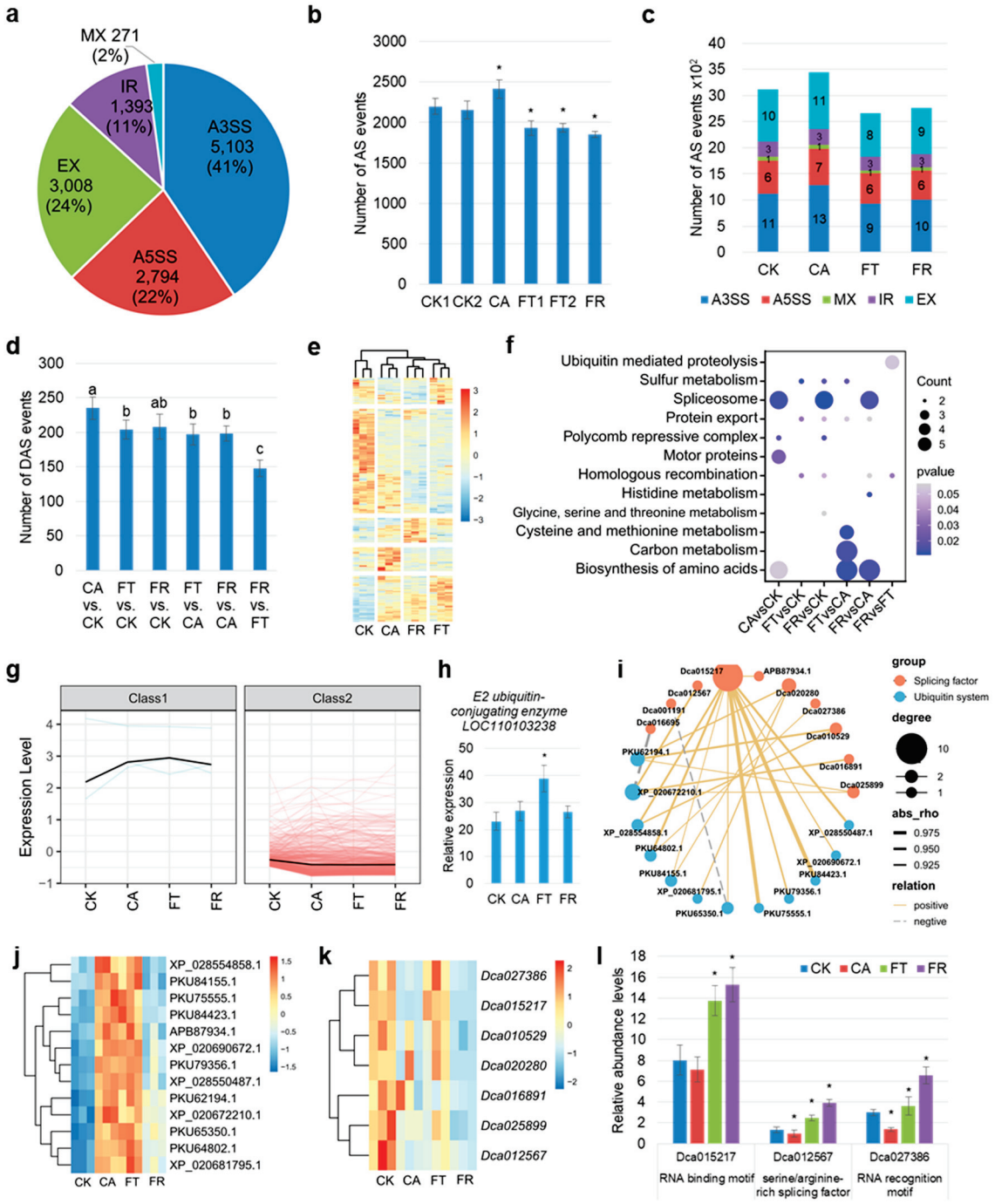


Figure 4. Identification of key splicing factors in response to cold in *D. officinale*. (**a**) The distribution of the five main types of AS events in the *D. officinale* genome (GCF_001605985.2). A3SS (alternative 3′ splice sites), EX (exon skipping), A5SS (alternative 5′ splice sites), IR (intron retention), and MX (mutually exclusive exons) are indicated. (**b**) The number of AS events across different treatments (CK1, CK2, CA, FT, and FR). Cold treatments (FT and FR) showed a significant decrease in the number of AS events compared to the control conditions (CK1/2). Values are means ± S.D. (n = 3). Student's t-test, * $p < 0.05$. (**c**) The changes in the number of AS events (A3SS, A5SS, EX, IR, and MX) across treatments. Changes in AS event numbers are indicated by numbers. (**d**) The number of DAS events between different cold treatments and the CK group. Different letters (a–c) indicate significant differences at $p < 0.05$, according to ANOVA analysis and Duncan's multiple range test. (**e**) Heatmap of the 368 DAS genes exhibiting substantial variation in expression levels across different treatments. The heatmap colors represent the relative expression levels of the genes, with warmer colors indicating higher expression and cooler colors indicating lower expression. (**f**) The functional annotation of the

DAS genes, with spliceosome, carbon metabolism, and amino acid biosynthesis pathways being specifically enriched in the CA and FR treatments. (**g**) The expression patterns of the 368 DAS genes grouped into two classes based on their expression levels across different treatments. (**h**) The expression pattern of the DAS gene (*E2 ubiquitin-conjugating enzyme*) that was specifically induced during cold treatment. Values are means ± S.D. (n = 3). Student's t-test, * $p < 0.05$. (**i**) Spearman correlation analysis between seven splicing factor genes and 13 ubiquitin proteins. Positive correlations are indicated by yellow lines, while negative correlations are indicated by grey dotted lines. (**j**) Heatmap showing the abundance levels of ubiquitin proteins across different treatments (CA, FT, and FR compared to CK). (**k**) Heatmap showing the expression levels of splicing factor genes across different treatments (CA, FT, and FR compared to CK). (**l**) The abundance levels of three key splicing factor genes encoding RNA binding motif, RNA recognition motif, and serine/arginine-rich protein across different treatments. Values are means ± S.D. (n = 3). Student's t-test, * $p < 0.05$.

To verify the key splicing factors in response to cold, we focused on the expression patterns of the 368 DAS genes. They were grouped into two classes according to expression levels, and three DAS genes were identified in class 1 (Figure 4g). Among them, *E2 ubiquitin-conjugating enzyme* was specially induced during cold treatment and *ATP binding actin* decreased during cold treatment (Figure 4h and Figure S7). Ubiquitination is an important pathway of protein modification. We speculated that ubiquitin proteins mediate the regulation of splicing factors during cold treatment. We further analyzed the abundance levels of 38 ubiquitin proteins and the expression of 324 splicing factors under cold treatment and found that the splicing factor transcript levels were strongly regulated by cold treatment. However, the expression of the vast majority of splicing factor genes was down-regulated upon exposure to cold treatment (Figure S8). Spearman correlation analysis showed seven splicing factor genes were positively correlated with 13 ubiquitin proteins (Figure 4i). Furthermore, most ubiquitin proteins increased their abundance levels in the CA treatment and FT group compared to the CK group. Most of the splicing factor genes were also significantly decreased in the CA and FR treatments compared to the CK group (Figure 4j,k). Three splicing factor genes were retrieved from the proteome in response to the FT and FR treatments, including *Dca015217*, *Dca012567*, and *Dca027386*, which respectively encoded an RNA binding motif, an RNA recognition motif, and a serine/arginine-rich protein. All of their abundance levels significantly increased in the FT group and FR treatment compared to the CK group and decreased in the CA treatment compared to the CK group (Figure 4l). Furthermore, ten ubiquitin-proteins-related genes were expressed in all tissues, and the expression levels of *PKU64802*, *XP_020672210*, and *PKU75555* were highest in leaves (Figure S9a). *PKU64802* encoded the ubiquitin carboxyl-terminal hydrolase that directly involved the intracellular protein homeostasis and signaling. *XP_020672210* and *PKU75555* belong to the E2 ubiquitin-conjugating enzyme. To verify the function of these genes in the cold response in *D. officinale*, as-ODNs were injected into mature leaves for 24 h during FT treatment. We found that these genes' expression levels were decreased by as-ODNs during FT treatment (Figure S9b). The inhibition of *PKU64802* expression resulted in a significant increase in *Dca015217* and *Dca027386* expression during FT treatment (Figure S9c). Thus, these splicing factors could be the key genes that were fine-regulated by ubiquitin systems in response to different temperature treatments, suggesting a unique role for AS in cold adaptation.

3. Discussion

This study addresses gaps in understanding the cold stress response in *D. officinale* through a multi-omics analysis of transcriptional and AS regulation. As proof-of-principle to evaluate the value of our dataset, we employ it to reveal the complex interplay between temperature, transcriptomic changes, alternative splicing dynamics, splicing factor regulation, and metabolic adjustments in *D. officinale* under cold stress (Figure 5).

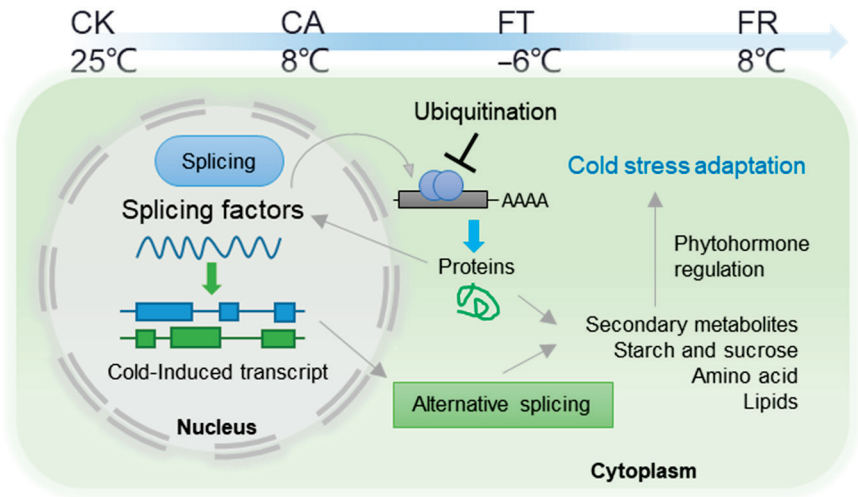


Figure 5. Molecular and metabolic adaptations in *D. officinale* under cold stress. The schematic diagram illustrates the complex interplay between temperature, transcriptomic changes, alternative splicing dynamics, splicing factor regulation, and metabolic adjustments in *D. officinale* under cold stress. It starts with different temperature treatments, including CK (normal temperature conditions), CA (mild cold stress), FT (severe cold stress), and FR (recovery after severe cold stress). These treatments trigger distinct transcriptomic and metabolic responses. Upregulation of spliceosome-related genes and metabolic pathways, such as carbon metabolism and amino acid biosynthesis, occurred primarily in freezing temperature and recovery conditions. In contrast, core metabolic pathways, including nucleotide, amino acid, lipid, and secondary metabolism, are downregulated. There is a rapid increase in AS under mild cold stress, followed by a decrease under severe cold stress. The regulation of splicing factors is depicted through the ubiquitination pathway, which involves ubiquitin proteins and specific splicing factors, such as E2 ubiquitin-conjugating enzyme, zinc knuckle factor, and others like RNA binding motif, RNA recognition motif, and serine/arginine-rich proteins. Metabolic adjustments, including the accumulation of specific metabolites such as oleamide, apigenin glucoside, rutin, and vicenin, are shown to occur in freezing conditions. Arrows and lines represent direct and indirect interactions, respectively, connecting the various components. Colored boxes and text labels provide additional information about each component, illustrating the intricate network of molecular and metabolic adaptations in *D. officinale* under cold stress.

Temperature extremes are major stressors for staple crops such as rice, spinach, and maize. Under cold stress, crops exhibit extensive differences in metabolic accumulation. A metabolomics study on rice revealed that cold stress induced the expression of *OsHPL1*, a CYP74 family member, and led to the accumulation of 12-oxo-phytodienoic acid and jasmonates [22]. Following cold stress, maize plants exhibit specific metabolomic changes, including alterations in biomass allocation, shikimate and its aromatic amino acid derivatives, and other non-polar metabolites [23]. Metabolome changes in spinach leaves were analyzed after short and long term freezing at −4.5 °C. Nineteen selected metabolites (e.g., aromatic amino acids, lactic acid) were grouped into signaling, injury, and recovery clusters, with diverse accumulations reflecting different cold stress responses and mechanisms [24]. However, the metabolic responsiveness of *D. officinale* under cold stress is still unclear. A thorough analysis of the responses of *D. officinale* to cold stress uncovers a multi-dimensional adaptive strategy encompassing both transcriptomic and metabolic modifications. At the transcriptomic scale, there is a distinct demarcation between the control and cold treatments in the plant. Key metabolic pathways, including nucleotide, amino acid, lipid, and secondary metabolism, experience downregulation (Figure 1d). This downregulation presumably indicates a reallocation of energy resources to handle the stress. In contrast, the upregulation of the C5-branched dibasic acid metabolism and the glycine, serine, and threonine metabolism pathways implies a specific adaptation mechanism for

maintaining cellular homeostasis under cold stress (Figure 1e). Glycine is one of the basic amino acids that make up proteins. It plays a role in plant stress resistance, including helping plants cope with nitrogen, drought, cold and other adverse environments [25–27]. The identification of key genes involved in glycine metabolism, such as *Dca003913* and *Dca022726* (Figure 1f–h), further supports the hypothesis that glycine metabolism plays a critical role in the plant response to dehydration caused by cold stress.

The temperature-specific response of *D. officinale* to cold stress is characterized by distinct transcriptomic and metabolic signatures. WGCNA highlights the presence of temperature-dependent co-expression modules, indicating that the plant adapts to cold stress through the activation of specific genetic programs (Figure 2). The enrichment of carbon metabolism and photosynthesis pathways in freezing conditions suggests that *D. officinale* reconfigures its metabolic processes to sustain basic functions under extreme cold (Figure 2d,g). During cold stress, plants adjust their osmotic potential by accumulating solutes such as soluble sugars within their cells [28]. Soluble sugars are generally regarded as an antioxidant to protect against anoxic injury [29]. A proteomic analysis of ABA-deficit barley and a wild type showed that ABA deficiency affected proline, soluble protein, and H_2O_2, as well as modifications in starch and sucrose biosynthesis, influencing low temperature tolerance [30]. The observed changes in carbohydrate metabolism and hormonal responses, particularly in freezing injury cells, indicate a complex interplay between metabolic and signaling pathways [31]. The plasma membrane (PM) senses cold stress and produces signaling lipids via enzymes such as phospholipases. Signaling lipids (e.g., phosphatidic acid, phosphoinositides, and sphingolipids), which account for <1% of total lipids, increase under stresses [32]. Sphingolipids in the PM, which are involved in lipid raft formation and composition within microdomains, help plants detect specific temperature ranges. [33]. Cold stress triggers a transient Ca^{2+} influx into the cytosol via PM rigidification-activated mechanosensitive or ligand-activated Ca^{2+} channels [34]. However, the direct link of sphingolipids and calcium channels is still unknown. We speculate that sphingolipids and calcium channels play crucial and complementary roles in the plant's initial perception of cold stress.

The dynamics of AS events and the regulation of splicing factors in *D. officinale* under cold stress provide novel insights into the molecular mechanisms underlying cold adaptation. AS, generating alternative 5′ and/or 3′ splice sites, is significant for plants' abiotic stress response and adaptation [35]. AS events increased during mild cold stress but decreased under freezing conditions, indicating a fine-tuned regulatory mechanism optimizing gene expression (Figure 4b). The enrichment of spliceosome-related genes and the identification of specific splicing factors that are regulated by the ubiquitination pathway highlight the role of post-translational modifications in controlling splicing events (Figure 4i). Serine/arginine-rich proteins are involved in the composition and AS of pre-mRNA in plants, and they are crucial for regulating transcriptome and proteome diversity [36]. Overexpression of the serine/arginine-rich protein SR45 reduces the sensitivity of plants to abscisic acid during the early developmental stage [37]. The observed changes in the expression and abundance of splicing factors, such as serine/arginine-rich protein *Dca012567*, indicate a complex regulatory network that is responsive to temperature changes (Figure 4l). Ubiquitination regulation is involved in numerous cellular processes. It marks proteins for degradation, thereby controlling the levels of specific proteins within the cell [38]. However, a role for the post-translational modification (PTM) of AS components has emerged in recent years, such as the ubiquitin/26S proteasome pathway in plants [39]. PTM is associated with phosphorylation, acetylation, and more and adjusts protein activity and subcellular localization in every cellular process [40]. Among them, ubiquitination or ubiquitin-like modification is a key regulator in eukaryotic cells [41]. These modify target

proteins via conjugation with small molecules, causing changes in their degradation or new interactions. Many proteins, including spliceosome-associated ones, undergo such modifications, and PTMs of spliceosome components are major regulatory factors in yeast and human cells [42,43]. The expression patterns of DAS genes provide insights into the regulation of splicing factors in response to cold stress (Figure 4). Among these, E2 ubiquitin-conjugating enzyme is specifically induced during cold treatment, while zinc knuckle factor expression decreases (Figure 4h). The abundance of ubiquitin proteins increases in the CA treatment and FT group compared to the CK group, while the expression of the majority of splicing factor genes decreases in the CA and FR treatments compared to the CK group (Figure 4j–l). These findings suggest that the regulation of splicing factors by the ubiquitin system plays a critical role in the response to different temperature treatments, affecting alternative splicing dynamics and contributing to cold adaptation in *D. officinale*.

The multi-omics analysis of *D. officinale* under cold stress provides a comprehensive view of the molecular and metabolic adaptations that enable the plant to cope with cold stress (Figure 5). The findings contribute to our understanding of the plant's temperature-specific response and offer potential targets for improving cold tolerance in this species.

4. Materials and Methods

4.1. Plant Material and Treatments

Two-year-old cultivated *D. officinale* plants were grown in soil under controlled greenhouse conditions (25 °C/23 °C day/night, 75% humidity, 12-h photoperiod, 80 μmol photons m^{-2} s^{-1}) at Zhejiang University (Hangzhou, China). Cold treatment conditions were performed according to the previous study [18,19]. In brief, plants were subjected to different temperature treatments, including control (CK1/2): maintained at 25 °C and 20 °C; cold acclimation (CA): exposed to 8 °C for 24 h; freezing treatment (FT): exposed to −6 °C for 3 h; and freezing recovery (FR): after FT, plants were allowed to recover at 8 °C for 24 h. The leaf samples were carefully collected from the above treated plants. To ensure the integrity of the samples and prevent any potential degradation of biological components, all the freshly collected leaf samples were promptly immersed in liquid nitrogen.

4.2. Multi-Omics Analysis

Transcriptome, proteome, lipidome and, metabolome data were obtained from *D. officinale* leaf samples subjected to the different temperature treatments, as described above. The methodology of the transcriptome data analysis was performed according to previous studies [44]. In brief, total RNA was extracted from leaf samples using TRIzol reagent (Thermo Scientific, Waltham, MA, USA), according to the manufacturer's instructions. Poly-A containing mRNA molecules are selectively purified from total RNA using oligo(dT) attached to magnetic beads (Invitrogen, Waltham, MA, USA). These mRNA molecules undergo reverse transcription to generate cDNA strands, which are then converted into a sequencing library through adapter ligation and PCR amplification, ensuring quality and quantity via the mRNASeq sample preparation kit (Illumina, San Diego, CA, USA), before being sequenced on a high-throughput platform to produce millions of short reads. Raw reads were filtered to remove adaptor sequences and low-quality reads. Clean reads were aligned to the *D. officinale* reference genome [15]. Differential gene expression analysis was conducted using DESeq2 (version 1.30.1) [45] with a threshold of $|\log_2(\text{fold change})| \geq 1$ and adjusted p-value < 0.05. The transcriptional data were removed for batch effects and other unwanted sources of variation based on an empirical Bayesian framework [46].

For proteome analysis, protein extraction was performed using RIPA buffer (Thermo Scientific, USA) containing protease inhibitors (Roche., Rotkreuz, Switzerland). Protein

concentration was determined using the Bradford assay (Bio-Rad, Hercules, CA, USA). Proteins were digested to peptides using trypsin (Promega, Madison, WI, USA) overnight at 37 °C. Peptides were separated via UHPLC (Bruker, Bremen, Germany) on a C18-RP column using a gradient from 2% to 80% ACN with 0.1% formic acid at 0.3 µL/min and 50 °C. The LC system was coupled to a timsTOF Pro2 mass spectrometer (Bruker, Germany) equipped with a CaptiveSpray ion source, operating under 1400 V capillary voltage and scanning m/z from 100 to 1700. Ion mobility separation was performed within the range of 0.7 to 1.4 Vs cm^{-2}, with accumulation and ramp times set to 100 ms for near 100% duty cycle. Raw data were processed using FragPipe (v17.1) for peptide and protein identification, and *Dendrobium* taxid (37818) of NCBI was performed to annotate. Differential protein expression analysis was conducted using a Wilcoxon Rank-Sum Test with a threshold of $|\log_2 FC| \geq 1$ and adjusted p-value < 0.05.

For lipidome analysis, leaf samples were homogenized in a mixture of methanol: chloroform:water (2:1:0.8, $v/v/v$) and vortexed. After centrifugation, the lower organic phase was collected, dried with nitrogen gas, and resuspended in chloroform:methanol (2:1, v/v). A 3 µL aliquot was injected into UHPLC (SHIMADZU, Kyoto, Japan) equipped with a CSH C18 column for separation using a gradient of ACN/isopropanol (1:9, v/v) with 0.1% formic acid and 0.1 mM ammonium formate at 300 µL/min. The eluent was analyzed by Q-Exactive Plus mass spectrometer (Thermo Scientific, Walham, MA, USA) with ESI parameters set to 300 °C source temperature, 350 °C capillary temperature, and 3000 V ion spray voltage, scanning m/z from 200 to 1800 with a 50% S-Lens RF level. Raw data were processed using LipidSearch (version 4.1, Thermo Fisher Scientific, Waltham, MA, USA) for lipid identification and quantification. Differential lipid analysis was conducted using PLS-DA with a threshold of VIP > 1 and p-value < 0.05.

For metabolome analysis, samples were thawed on ice and metabolites extracted by adding precooled 50% methanol, vortexing for 1 min, and incubating at 4 °C for overnight. UHPLC (Thermo Scientific, USA) was used to separate metabolites with a gradient elution of water and acetonitrile, both containing 0.1% formic acid, at a flow rate of 0.4 mL/min, and the injection volume was 4 µL. These separated products were detected using an Orbitrap Exploris 240 Mass Spectrometer (Thermo Scientific, USA) operated in positive and negative ion modes, with curtain gas set to 30 PSI, ion source gases at 60 PSI, and ion source temperature at 650 °C; ionspray voltages were 5000 V and 4500 V for positive and negative modes, respectively. Metabolites were annotated by matching m/z values to the KEGG database within a 10 ppm mass accuracy, and validated using isotopic distribution and an in-house fragment spectrum library. Differential metabolite analysis was conducted using PLS-DA with a threshold of VIP > 1 and p-value < 0.05.

4.3. Alternative Splicing Analysis

Alternative splicing (AS) events were identified from the RNA-seq data using SUPPA2 (version 1.2) [47]. Five main types of AS events were considered: alternative 3′ splice sites (A3SS), alternative 5′ splice sites (A5SS), exon skipping (EX), intron retention (IR), and mutually exclusive exons (MX). The percent spliced-in (PSI) values were calculated for each AS event, and differential AS (DAS) events were identified using a cutoff of $|\Delta PSI| > 0.1$ and FDR < 0.05. The AS events were further analyzed to understand the dynamics of splicing under cold treatment, and the DAS genes were annotated using clusterProfiler for functional enrichment analysis [48].

4.4. Real-Time Quantitative PCR

Total RNA was isolated from different tissues using the TransZol reagent (TransGen Biotech, Beijing, China). RNA extracts were treated with DNaseI (NEB, Hitchin, UK) to

eliminate DNA contamination. First-strand cDNA was produced from the RNA template by reverse transcription using the TIANscriptRTKit according to the manufacturer's instructions (TransGen Biotech, Beijing). Real-time quantitative PCR processes were performed according to the previous study [49]. In brief, processes was conducted with the subsequent cycling conditions: an initial denaturation at 95 °C for 1 min; followed by 40 cycles, each consisting of denaturation at 95 °C for 30 s, annealing at 55 °C for 30 s, and extension at 72 °C for 30 s; finally, a terminal extension step at 72 °C for 10 min to complete DNA synthesis. The primers used are listed in Table S5.

4.5. Gene Suppression Using Candidate Antisense Oligonucleotides

For gene suppression in *D. officinale* leaves, the operation was performed according to previous study [50]. In brief, candidate antisense oligonucleotides (asODN) that are complementary to a segment of the target gene were chosen via Soligo online software (version 2.2, Table S4). A total of 0.2 mL of asODN solution (20 μM) was injected into the mature leaves during in the CK and FT treatments, and leaves injected with sODN were used as control. After 24 h, leaves were harvested for real-time quantitative PCR.

4.6. Statistical Analysis

Statistical analyses were performed using R (version 4.0.2), and an ANOVA was applied to compare the differences between the two groups. Data were also treated by hierarchical clustering using the R package pheatmap and by PCA using the R package FactoMineR. Correlation analysis between splicing factors and ubiquitin proteins was performed using the Spearman rank correlation coefficient.

Supplementary Materials: The following supporting information can be downloaded at: https://www.mdpi.com/article/10.3390/plants14030412/s1, Figure S1. Quantitative analysis of glycine content in leaves of *D. officinale* during dry treatment and rewetting phases. The glycine content increases during dry treatment and recovers during the rewetting phase. Figure S2. Volcano plot depicting the distribution of DEGs between cold treatments and control conditions (CK). Genes with a fold change (FC) greater than 2 and an adjusted *p*-value less than 0.05 are considered differentially expressed. Upregulated genes are shown in red, downregulated genes in blue, and non-significantly changed genes in black. Figure S3. Heatmap showing the expression patterns of the top 20 DEGs across different treatments. These genes are involved in multiple pathways, including secondary metabolism, carbohydrate metabolism, and stress response. The heatmap colors represent the relative expression levels of the genes, with warmer colors indicating higher expression and cooler colors indicating lower expression. Figure S4. The different lipid species in CK, FT, and FR, providing a detailed view of the lipid composition changes under cold treatment. Figure S5. The expression levels of differentially alternatively spliced (DAS) genes involved in spliceosome, carbon metabolism, and amino acid metabolism across different treatments. The heatmap colors represent the relative expression levels of the genes, with warmer colors indicating higher expression and cooler colors indicating lower expression. Figure S6. The transcript expression levels of three selected DAS genes (malate dehydrogenase, cysteine synthase, and zinc knuckle) across different treatments. Figure S7. The transcript expression levels of ADP-ribosylation factor and ATP binding actin across different treatments. Figure S8. The expression levels of 324 splicing factor genes across different treatments. The heatmap colors represent the relative expression levels of the genes, with warmer colors indicating higher expression and cooler colors indicating lower expression. Figure S9. **a**, Expression profiles of three genes (*PKU64802*, XP_*020672210*, and *PKU75555*) related to ubiquitin proteins in various tissues of *D. officinale*. The expression levels are shown for different tissues, with leaves having the highest expression. **b**, Expression of three genes in mature leaves of plants treated with s-ODN (as control) and as-ODN during FT treatment. **c**, *Dca015217*, *Dca012567*, and *Dca027386* expression treated with *PKU64802* as-ODN during FT treatment. Values are means ± S.D. ($n = 3$). Student's *t*-test, * $p < 0.05$. Table S1. The classification of metabolites list. Table S2. The classification of lipidome list. Table S3.

The classification of protome list. Table S4. Primer sequence for validating ubiqutin genes expression. Table S5. qRT-PCR primer list. Table S6. The mapping statistics of RNA-seq TPM data.

Author Contributions: X.Z. conceived and designed the experiment. G.Y. and M.P. provided materials. Z.L. detected samples. X.Z. analyzed data. X.Z. and B.M. wrote and revised the manuscript. All authors have read and agreed to the published version of the manuscript.

Funding: This work was financially supported by the National Natural Science Foundation of China (32200304), the Zhejiang Province Three, the Agriculture and Nine Aspects Science and Technology Cooperation Project (2022SNJF050; 2024SNJF034), and the Contract for Cooperative Extension Plan of Major Agricultural Technologies of Ministry of Agriculture and Rural Affairs (2022XTTGZYC02).

Data Availability Statement: The original contributions presented in the study are included in the article/Supplementary Material, further inquiries can be directed to the corresponding author.

Acknowledgments: We thank Shanghai Applied Protein Technology Co., Ltd., who provided lipidome detection and Wuhan Metware Biotechnology Co., Ltd., who provided proteome detection.

Conflicts of Interest: Authors Minxia Pang and Guoxiang Yao are employed by the company Zhejiang Jianjiuhe Group Co., Ltd. Author Guoxiang Yao is also employed by the company Ningbo Shunyun Electroinic Co., Ltd. The remaining authors declare that the research was conducted in the absence of any commercial or financial relationships that could be construed as a potential conflict of interest.

References

1. Steponkus, P.L. Role of the Plasma Membrane in Freezing Injury and Cold Acclimation. *Annu. Rev. Plant Physiol.* **1984**, *35*, 543–584. [CrossRef]
2. Pearce, R.S. Plant Freezing and Damage. *Ann. Bot.* **2001**, *87*, 417–424. [CrossRef]
3. Miura, K.; Furumoto, T. Cold signaling and cold response in plants. *Int. J. Mol. Sci.* **2013**, *14*, 5312–5337. [CrossRef] [PubMed]
4. Porto, D.D.; Bruneau, M.; Perini, P.; Anzanello, R.; Renou, J.P.; dos Santos, H.P.; Fialho, F.B.; Revers, L.F. Transcription profiling of the chilling requirement for bud break in apples: A putative role for FLC-like genes. *J. Exp. Bot.* **2015**, *66*, 2659–2672. [CrossRef]
5. Zhang, H.; Jiang, C.; Ren, J.; Dong, J.; Shi, X.; Zhao, X.; Wang, X.; Wang, J.; Zhong, C.; Zhao, S.; et al. An Advanced Lipid Metabolism System Revealed by Transcriptomic and Lipidomic Analyses Plays a Central Role in Peanut Cold Tolerance. *Front. Plant Sci.* **2020**, *11*, 1110. [CrossRef]
6. Shen, Z.J.; Qin, Y.Y.; Luo, M.R.; Li, Z.; Ma, D.N.; Wang, W.H.; Zheng, H.L. Proteome analysis reveals a systematic response of cold-acclimated seedlings of an exotic mangrove plant Sonneratia apetala to chilling stress. *J. Proteom.* **2021**, *248*, 104349. [CrossRef]
7. Lee, J.G.; Yi, G.; Seo, J.; Kang, B.C.; Choi, J.H.; Lee, E.J. Jasmonic acid and ERF family genes are involved in chilling sensitivity and seed browning of pepper fruit after harvest. *Sci. Rep.* **2020**, *10*, 17949. [CrossRef] [PubMed]
8. Xie, Y.; Chen, P.; Yan, Y.; Bao, C.; Li, X.; Wang, L.; Shen, X.; Li, H.; Liu, X.; Niu, C.; et al. An atypical R2R3 MYB transcription factor increases cold hardiness by CBF-dependent and CBF-independent pathways in apple. *New Phytol.* **2018**, *218*, 201–218. [CrossRef] [PubMed]
9. Dikaya, V.; El Arbi, N.; Rojas-Murcia, N.; Nardeli, S.M.; Goretti, D.; Schmid, M. Insights into the role of alternative splicing in plant temperature response. *J. Exp. Bot.* **2021**, *72*, 7384–7403. [CrossRef] [PubMed]
10. Li, W.; Zhong, J.; Zhang, L.; Wang, Y.; Song, P.; Liu, W.; Li, X.; Han, D. Overexpression of a Fragaria vesca MYB Transcription Factor Gene (FvMYB82) Increases Salt and Cold Tolerance in Arabidopsis thaliana. *Int. J. Mol. Sci.* **2022**, *23*, 10538. [CrossRef] [PubMed]
11. Liu, W.; Liang, X.; Cai, W.; Wang, H.; Liu, X.; Cheng, L.; Song, P.; Luo, G.; Han, D. Isolation and Functional Analysis of VvWRKY28, a Vitis vinifera WRKY Transcription Factor Gene, with Functions in Tolerance to Cold and Salt Stress in Transgenic Arabidopsis thaliana. *Int. J. Mol. Sci.* **2022**, *23*, 13418. [CrossRef] [PubMed]
12. Marquez, Y.; Brown, J.W.S.; Simpson, C.; Barta, A.; Kalyna, M. Transcriptome survey reveals increased complexity of the alternative splicing landscape in Arabidopsis. *Genome Res.* **2012**, *22*, 1184–1195. [CrossRef] [PubMed]
13. Zhong, Y.; Luo, Y.; Sun, J.; Qin, X.; Gan, P.; Zhou, Z.; Qian, Y.; Zhao, R.; Zhao, Z.; Cai, W.; et al. Pan-transcriptomic analysis reveals alternative splicing control of cold tolerance in rice. *Plant Cell* **2024**, *36*, 2117–2139. [CrossRef] [PubMed]
14. Liang, Y.; Xiao, W.; Hui, L.; Yang, T.; Lian, J.; Yang, R.; Hao, S.; Wang, X.; Yang, S.; Li, Q. The Genome of Dendrobium officinale Illuminates the Biology of the Important Traditional Chinese Orchid Herb. *Mol. Plant* **2015**, *8*, 922–934.

15. Zhang, G.Q.; Xu, Q.; Bian, C.; Tsai, W.C.; Yeh, C.M.; Liu, K.W.; Yoshida, K.; Zhang, L.S.; Chang, S.B.; Chen, F.; et al. The Dendrobium catenatum Lindl. genome sequence provides insights into polysaccharide synthase, floral development and adaptive evolution. *Sci. Rep.* **2016**, *6*, 19029. [CrossRef]
16. Zhan, X.; Qian, Y.; Mao, B. Metabolic Profiling of Terpene Diversity and the Response of Prenylsynthase-Terpene Synthase Genes during Biotic and Abiotic Stresses in Dendrobium catenatum. *Int. J. Mol. Sci.* **2022**, *23*, 6398. [CrossRef] [PubMed]
17. Zhan, X.; Qi, J.; Zhou, B.; Mao, B. Metabolomic and transcriptomic analyses reveal the regulation of pigmentation in the purple variety of Dendrobium officinale. *Sci. Rep.* **2020**, *10*, 17700. [CrossRef]
18. Zhan, X.; Qi, J.; Shen, Q.; He, B.; Mao, B. Regulation of phenylpropanoid metabolism during moderate freezing and post-freezing recovery in Dendrobium officinale. *J. Plant Interact.* **2022**, *17*, 290–300. [CrossRef]
19. Wu, Z.G.; Jiang, W.; Chen, S.L.; Mantri, N.; Tao, Z.M.; Jiang, C.X. Insights from the Cold Transcriptome and Metabolome of Dendrobium officinale: Global Reprogramming of Metabolic and Gene Regulation Networks during Cold Acclimation. *Front. Plant Sci.* **2016**, *7*, 1653. [CrossRef]
20. Zhan, X.; Qian, Y.; Mao, B. Identification of Two GDSL-Type Esterase/Lipase Genes Related to Tissue-Specific Lipolysis in Dendrobium catenatum by Multi-Omics Analysis. *Life* **2022**, *12*, 1563. [CrossRef] [PubMed]
21. Chen, D.H.; Qiu, H.L.; Huang, Y.; Zhang, L.; Si, J.P. Genome-wide identification and expression profiling of SET DOMAIN GROUP family in Dendrobium catenatum. *BMC Plant Biol.* **2020**, *20*, 40. [CrossRef]
22. Wu, Z.; Guo, Z.; Wang, K.; Wang, R.; Fang, C. Comparative Metabolomic Analysis Reveals the Role of OsHPL1 in the Cold-Induced Metabolic Changes in Rice. *Plants* **2023**, *12*, 2032. [CrossRef]
23. Sun, C.X.; Gao, X.X.; Li, M.Q.; Fu, J.Q.; Zhang, Y.L. Plastic responses in the metabolome and functional traits of maize plants to temperature variations. *Plant Biol.* **2016**, *18*, 249–261. [CrossRef] [PubMed]
24. Min, K.; Chen, K.; Arora, R. Short versus prolonged freezing differentially impacts freeze—Thaw injury in spinach leaves: Mechanistic insights through metabolite profiling. *Physiol. Plant.* **2020**, *168*, 777–789. [CrossRef]
25. Ma, L.; Cheng, K.; Li, J.; Deng, Z.; Zhang, C.; Zhu, H. Roles of Plant Glycine-Rich RNA-Binding Proteins in Development and Stress Responses. *Int. J. Mol. Sci.* **2021**, *22*, 5849. [CrossRef]
26. Xiaochuang, C.; Chu, Z.; Lianfeng, Z.; Junhua, Z.; Hussain, S.; Lianghuan, W.; Qianyu, J. Glycine increases cold tolerance in rice via the regulation of N uptake, physiological characteristics, and photosynthesis. *Plant Physiol. Bioch* **2017**, *112*, 251–260. [CrossRef]
27. Obata, T.; Witt, S.; Lisec, J.; Palacios-Rojas, N.; Florez-Sarasa, I.; Yousfi, S.; Araus, J.L.; Cairns, J.E.; Fernie, A.R. Metabolite Profiles of Maize Leaves in Drought, Heat, and Combined Stress Field Trials Reveal the Relationship between Metabolism and Grain Yield. *Plant Physiol.* **2015**, *169*, 2665–2683. [CrossRef]
28. Vyse, K.; Penzlin, J.; Sergeant, K.; Hincha, D.K.; Arora, R.; Zuther, E. Repair of sub-lethal freezing damage in leaves of Arabidopsis thaliana. *BMC Plant Biol.* **2020**, *20*, 35. [CrossRef] [PubMed]
29. Couée, I.; Sulmon, C.; Gouesbet, G.; El Amrani, A. Involvement of soluble sugars in reactive oxygen species balance and responses to oxidative stress in plants. *J. Exp. Bot.* **2006**, *57*, 449–459. [CrossRef]
30. Guo, J.; Beemster, G.T.S.; Liu, F.; Wang, Z.; Li, X. Abscisic Acid Regulates Carbohydrate Metabolism, Redox Homeostasis and Hormonal Regulation to Enhance Cold Tolerance in Spring Barley. *Int. J. Mol. Sci.* **2023**, *24*, 11348. [CrossRef]
31. Cai, P.; Lan, Y.; Gong, F.; Li, C.; Xia, F.; Li, Y.; Fang, C. Comparative physiology and transcriptome response patterns in cold-tolerant and cold-sensitive varieties of Solanum melongena. *BMC Plant Biol.* **2024**, *24*, 256. [CrossRef] [PubMed]
32. Bargmann, B.O.; Laxalt, A.M.; ter Riet, B.; van Schooten, B.; Merquiol, E.; Testerink, C.; Haring, M.A.; Bartels, D.; Munnik, T. Multiple PLDs required for high salinity and water deficit tolerance in plants. *Plant Cell Physiol.* **2009**, *50*, 78–89. [CrossRef]
33. Jan, S.; Rustgi, S.; Barmukh, R.; Shikari, A.B.; Leske, B.; Bekuma, A.; Sharma, D.; Ma, W.; Kumar, U.; Kumar, U.; et al. Advances and opportunities in unraveling cold-tolerance mechanisms in the world's primary staple food crops. *Plant Genome* **2024**, *17*, e20402. [CrossRef]
34. Chen, X.; Ding, Y.; Yang, Y.; Song, C.; Wang, B.; Yang, S.; Guo, Y.; Gong, Z. Protein kinases in plant responses to drought, salt, and cold stress. *J. Integr. Plant Biol.* **2021**, *63*, 53–78. [CrossRef] [PubMed]
35. Ule, J.; Blencowe, B.J. Alternative Splicing Regulatory Networks: Functions, Mechanisms, and Evolution. *Mol. Cell* **2019**, *76*, 329–345. [CrossRef]
36. Zhao, X.; Tan, L.; Wang, S.; Shen, Y.; Guo, L.; Ye, X.; Liu, S.; Feng, Y.; Wu, W. The SR Splicing Factors: Providing Perspectives on Their Evolution, Expression, Alternative Splicing, and Function in Populus trichocarpa. *Int. J. Mol. Sci.* **2021**, *22*, 11369. [CrossRef]
37. Albuquerque-Martins, R.; Szakonyi, D.; Rowe, J.; Jones, A.M.; Duque, P. ABA signaling prevents phosphodegradation of the SR45 splicing factor to alleviate inhibition of early seedling development in Arabidopsis. *Plant Commun.* **2023**, *4*, 100495. [CrossRef]
38. Gao, C.; Tang, D.; Wang, W. The Role of Ubiquitination in Plant Immunity: Fine-Tuning Immune Signaling and Beyond. *Plant Cell Physiol.* **2022**, *63*, 1405–1413. [CrossRef]
39. Lan, W.; Qiu, Y.; Xu, Y.; Liu, Y.; Miao, Y. Ubiquitination and Ubiquitin-Like Modifications as Mediators of Alternative Pre-mRNA Splicing in Arabidopsis thaliana. *Front. Plant Sci.* **2022**, *13*, 869870. [CrossRef]

40. McKay, S.L.; Johnson, T.L. A bird's-eye view of post-translational modifications in the spliceosome and their roles in spliceosome dynamics. *Mol. Biosyst.* **2010**, *6*, 2093–2102. [CrossRef]
41. Smalle, J.; Vierstra, R.D. The ubiquitin 26S proteasome proteolytic pathway. *Annu. Rev. Plant Biol.* **2004**, *55*, 555–590. [CrossRef] [PubMed]
42. Mulvaney, K.M.; Blomquist, C.; Acharya, N.; Li, R.; Ranaghan, M.J.; O'Keefe, M.; Rodriguez, D.J.; Young, M.J.; Kesar, D.; Pal, D.; et al. Molecular basis for substrate recruitment to the PRMT5 methylosome. *Mol. Cell* **2021**, *81*, 3481–3495.e3487. [CrossRef]
43. Wilkinson, C.R.; Dittmar, G.A.; Ohi, M.D.; Uetz, P.; Jones, N.; Finley, D. Ubiquitin-like protein Hub1 is required for pre-mRNA splicing and localization of an essential splicing factor in fission yeast. *Curr. Biol.* **2004**, *14*, 2283–2288. [CrossRef]
44. Zhan, X.; Qian, Y.; Mao, B. Dendrobium Multi-Omics Reveal Lipid Remodeling in Response to Freezing. *Metabolites* **2022**, *12*, 1216. [CrossRef]
45. Love, M.I.; Huber, W.; Anders, S. Moderated estimation of fold change and dispersion for RNA-seq data with DESeq2. *Genome Biol.* **2014**, *15*, 550. [CrossRef]
46. Leek, J.T.; Johnson, W.E.; Parker, H.S.; Jaffe, A.E.; Storey, J.D. The sva package for removing batch effects and other unwanted variation in high-throughput experiments. *Bioinformatics* **2012**, *28*, 882–883. [CrossRef]
47. Trincado, J.L.; Entizne, J.C.; Hysenaj, G.; Singh, B.; Skalic, M.; Elliott, D.J.; Eyras, E. SUPPA2: Fast, accurate, and uncertainty-aware differential splicing analysis across multiple conditions. *Genome Biol.* **2018**, *19*, 40. [CrossRef] [PubMed]
48. Yu, G.; Wang, L.G.; Han, Y.; He, Q.Y. clusterProfiler: An R package for comparing biological themes among gene clusters. *Omics A J. Integr. Biol.* **2012**, *16*, 284–287. [CrossRef]
49. Zhan, X.; Shen, Q.; Wang, X.; Hong, Y. The sulfoquinovosyltransferase-like enzyme SQD2.2 is involved in flavonoid glycosylation, regulating sugar metabolism and seed setting in rice. *Sci. Rep.* **2017**, *7*, 4685. [CrossRef]
50. Zhao, M.; Jin, J.; Gao, T.; Zhang, N.; Jing, T.; Wang, J.; Ban, Q.; Schwab, W.; Song, C. Glucosyltransferase CsUGT78A14 Regulates Flavonols Accumulation and Reactive Oxygen Species Scavenging in Response to Cold Stress in Camellia sinensis. *Front. Plant Sci.* **2019**, *10*, 1675. [CrossRef]

Disclaimer/Publisher's Note: The statements, opinions and data contained in all publications are solely those of the individual author(s) and contributor(s) and not of MDPI and/or the editor(s). MDPI and/or the editor(s) disclaim responsibility for any injury to people or property resulting from any ideas, methods, instructions or products referred to in the content.

plants

MDPI

Article

Genome-Wide Identification, Characterization, and Expression Analysis of *BES1* Family Genes in '*Tieguanyin*' Tea Under Abiotic Stress

Yanzi Zhang [1], Yanlin Zhang [2], Zhicheng Yang [3], Qingyan Li [2], Weixiang Chen [3], Xinyan Wen [4], Hao Chen [5,*] and Shijiang Cao [6,*]

[1] Metabolomics Center, Haixia Institute of Science and Technology, Fujian Agriculture and Forestry University, Fuzhou 350002, China; zhangyanzi163@163.com
[2] College of Jun Cao Science and Ecology (College of Carbon Neutrality), Fujian Agriculture and Forestry University, Fuzhou 350002, China; 17770899282@163.com (Y.Z.); 15255665669@163.com (Q.L.)
[3] College of Future Technologies, Fujian Agriculture and Forestry University, Fuzhou 350002, China; 18359797810@163.com (Z.Y.); 19896657097@163.com (W.C.)
[4] College of Food Science, Fujian Agriculture and Forestry University, Fuzhou 350002, China; dalethandalef@outlook.com
[5] College of Computer and Information Sciences, Fujian Agriculture and Forestry University, Fuzhou 350002, China
[6] College of Forestry, Fujian Agriculture and Forestry University, Fuzhou 350002, China
* Correspondence: chenhaox@outlook.com (H.C.); 000q813040@fafu.edu.cn (S.C.)

Abstract: The *BRI1-EMS-SUPPRESSOR 1* (*BES1*) family comprises plant-specific transcription factors, which are distinguished by atypical bHLH domains. Over the past two decades, genetic and biochemical studies have established that members of the *BRI1-EMS-SUPPRESSOR 1* (*BES1*) family are crucial for regulating the expression of genes involved in brassinosteroid (BR) response in rapeseed. Due to the significance of the *BES1* gene family, extensive research has been conducted to investigate its functional properties. This study presents a comprehensive identification and computational analysis of *BES1* genes in '*Tieguanyin*' (*TGY*) tea (*Camellia sinensis*). A total of 10 *BES1* genes were initially identified in the *TGY* genome. Through phylogenetic tree analysis, this study uniquely revealed that *CsBES1.2* and *CsBES1.5* cluster with *SlBES1.8* from *Solanum lycopersicum*, indicating their critical roles in fruit growth and development. Synteny analysis identified 20 syntenic genes, suggesting the conservation of their evolutionary functions. Analysis of the promoter regions revealed two types of light-responsive cis-elements, with *CsBES1.4* exhibiting the highest number of light-related cis-elements (13), followed by *CsBES1.9* and *CsBES1.10*. Additional validation via qRT-PCR experiments showed that *CsBES1.9* and *CsBES1.10* were significantly upregulated under light exposure, with *CsBES1.10* reaching approximately six times the expression level of the control after 4 h. These results suggest that *CsBES1.9* and *CsBES1.4* could play crucial roles in responding to abiotic stress. This study offers novel insights into the functional roles of the *BES1* gene family in '*Tieguanyin*' tea and establishes a significant foundation for future research, especially in exploring the roles of these genes in response to abiotic stresses, such as light exposure.

Keywords: *Tieguanyin*; *BES1*; gene family; abiotic stress; expression analysis

1. Introduction

Brassinosteroids (BRs), a group of steroidal plant hormones, play a crucial role in regulating plant growth and numerous physiological functions. Maintaining appropriate BR

levels is essential for proper root development and the overall growth of plants [1–7]. Brassinosteroids (BRs) were the sixth class of plant hormones to be discovered, following auxins, gibberellins, cytokinins, abscisic acid, and ethylene [8,9]. They promote cell elongation by stimulating hormone accumulation in meristematic tissues, thereby transitioning cells into elongation zones. In *Arabidopsis thaliana*, mutants deficient in brassinosteroids (BRs) exhibit traits such as dwarfism, impaired cell expansion, reduced apical dominance, delayed flowering and senescence, and male sterility [10,11]. Moreover, the BR signaling pathway interacts with various response networks to coordinate plant growth, development, and adaptation to abiotic stresses [8]. For details, please refer to Figure 1.

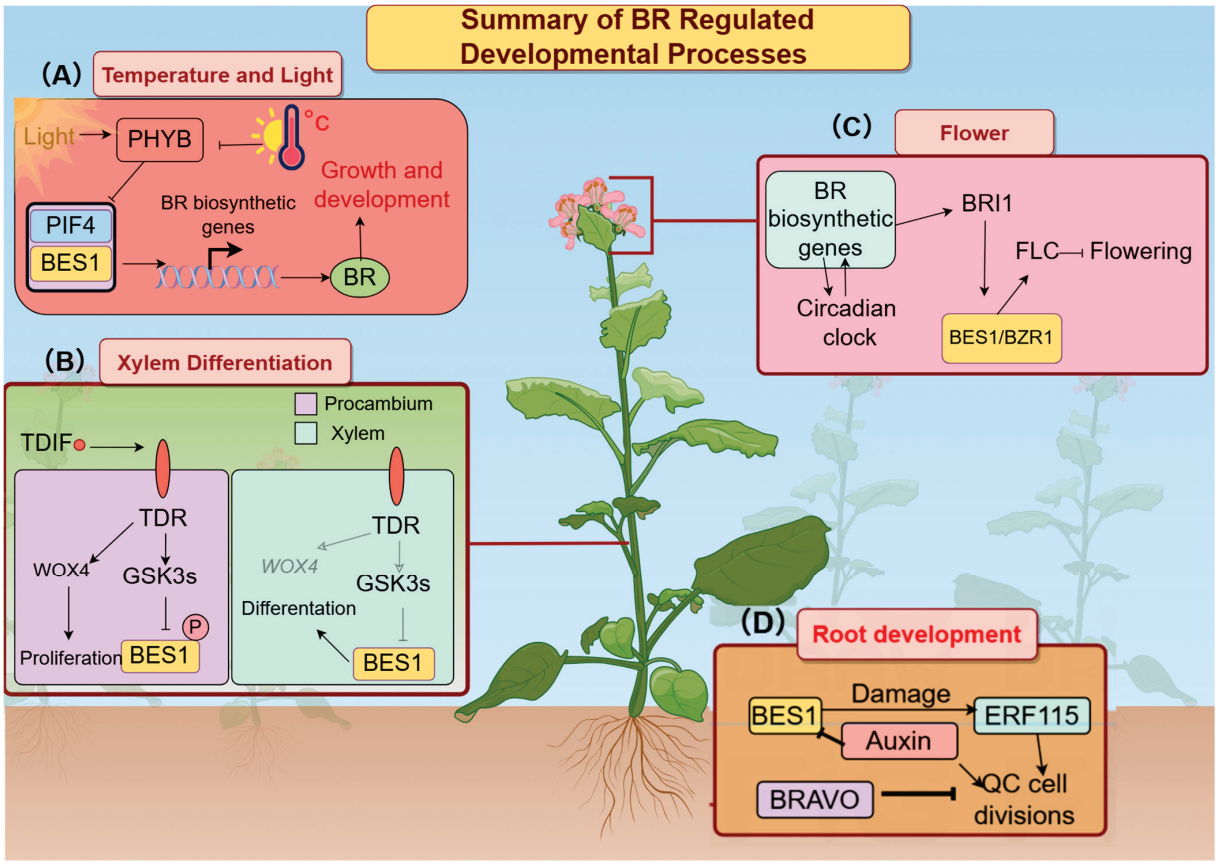


Figure 1. Summary of BR regulating developmental processes in *A. thaliana*. (**A**) High temperature inhibits thTFs, determines their gene targets, and leads to different cellular responses. (**B**) Xylem differentiation is controlled by the TRACHEARY ELEMENT DIFFERENTIATION INHIBITORY FACTOR (TDIF) signaling pathway (the red dots represent the TDIF signal). GSK3 is a key component in this pathway. It acts as a negative regulator of xylem differentiation and crosstalks with the brassinosteroid (BR) signaling pathway. The TDIF signal acts on the TDR receptor on cambium cells, resulting in the inhibition of *BRS1* activity by GSK3s. In the xylem where it is not inhibited by the activity of PHYB, light promotes the activity of PHYB. PHYB inhibits the production of PIF4 and indirectly determines the level of PIF4-BES1 heterodimerization. The interactions among these transcription factors (DIF and *BES1*) functions to promote cell elongation (the gray arrows indicate that no has reaction occurred). (**C**) Brassinosteroids (BRs) inhibit flowering by promoting the expression of the flowering inhibitor FLC. (**D**) In the root apical meristem, BRs control the size of the stem cell niche by balancing the expression of BRAVO, which negatively regulates cell division in the quiescent center. BR signaling levels increase along the longitudinal axis, with higher levels present in cells closer to the differentiation/elongation zone. Arrows indicate activation and blunt-ended lines indicate inhibition.

For instance, BRs negatively regulate the plant drought stress response via RESPONSIVE TO DESICCATION 26 (RD26) and interact with light, abscisic acid (ABA), and gibberellic acid (GA) signaling pathways through *BES1* [2,12–14].

Transcription factors (TFs) regulate the expression of specific target genes in response to biotic and abiotic stresses, playing key roles in plant growth, development, and stress resistance. Through the activation of various defense mechanisms, they influence yield and quality [15,16]. *BRI1-EMS-SUPPRESSOR 1* (*BES1*) and *BRASSINAZOLE RESISTANT 1* (*BZR1*) are key transcription factors that directly mediate BR signaling [2,17–20]. *BES1* and *BZR1* exhibit significant sequence similarity and serve as crucial regulators in plant responses to stress [3,17,21–25]. Both function as activators of the BR signaling pathway [26]. Studies have shown that a conserved DNA-binding motif at the N-terminus of *BES1*-type proteins binds to E-box or BR response elements, thereby regulating the transcription of target genes [2,3,19,21]. In plant cells, when a brassinosteroid (BR) binds to the extracellular domain of the BR receptor BRI1, it activates the intracellular kinase activity of the receptor.

This activation triggers the release of BKI1 from the cell membrane and facilitates the interaction between BRI1 and BAK1, thereby transmitting BR signals into the cell [27,28]. In the cytoplasm, *BR SIGNAL KINASE 1* (*BSK1*) activates *BRI1 SUPPRESSOR 1* (*BSU1*) via a phosphorylation-dephosphorylation cascade. This process leads to the dephosphorylation and degradation of *BR-INSENSITIVE 2* (*BIN2*), thus alleviating the inhibition of *BES1* [29–31]. Additionally, *BES1* undergoes dephosphorylation by *PROTEIN PHOSPHATASE 2A* (*PP2A*), which facilitates its accumulation in the nucleus and regulates downstream target genes [32,33]. In addition to mediating BR signaling, *BES1/BZR1* integrates multiple plant hormone pathways, controlling tapetum development and various stress responses [34–41]. *BES1* interacts with TFs such as phytochrome interacting factor 4 (PIF4), WRKY46, WRKY54, and WRKY70 to regulate cell expansion and enhance stress resistance [42,43].

A. thaliana contains eight members of the *BES1* family, whereas other species, such as rapeseed (*Brassica napus*), cotton (*Gossypium hirsutum*), maize (*Zea mays*), tomato (*Solanum lycopersicum*), cabbage (*Brassica oleracea*), and cucumber (*Cucumis sativus*), possess varying numbers of *BES1* homologs: 28, 22, 11, 9, 15, and 6, respectively [34,44–49]. *BES1*s are involved in cell growth [50], pollen development [51], plant immunity [52], and stress responses. For example, in cotton, the *GhBES1* gene displays functional variability, influencing fiber development, plant morphology, and stress resistance [46]. The cotton variety '*Xinluzao 17*' shows a rapid response to drought stress, which is regulated by *BES1*. In tomatoes, *BES1* expression is significantly upregulated following salt stress at 6 and 24 h [47,53].

The tea plant, *Camellia sinensis* (L.) O. Kuntze, is native to southwestern China, where it has been grown and used for thousands of years [54]. Tea, the second most consumed beverage globally, is rich in amino acids, vitamins, minerals, tea polyphenols, and alkaloids [55]. It is renowned for its health benefits, including its antioxidant, anti-tumor, and cardiovascular properties [56–58]. Environmental conditions significantly affect the growth of tea plants, with factors such as extreme temperatures, drought, and light stress playing critical roles in their natural habitats [59]. Among these factors, light is a crucial environmental factor influencing various economic traits, including leaf size, shoot weight, harvest duration, and the synthesis of health-promoting compounds [60–62]. Previous research has demonstrated that *BES1/BZR1* is essential for regulating light signaling in plant development [63].

Its phosphorylation status and stability are regulated by light signals, with dephosphorylation enhancing activity in the dark and phosphorylation by BIN2 keeping it in an inactive state under light [64]. The increasing frequency of extreme weather events, including high temperatures and droughts, exacerbated by global climate change, has

caused significant damage to tea production. To improve both the yield and quality of tea, understanding the mechanisms underlying plants' tolerance to environmental stress is essential. Therefore, investigating the molecular mechanisms by which *BES1* responds to light and dark stress is vital for optimizing the growth and development of tea plants.

Among oolong teas, '*Tieguanyin*' (*TGY*) is notable for its high concentration of nutritional and medicinal compounds. However, research on the *BES1* gene family in *TGY* is still limited. Few studies have investigated changes in *BES1* expression under light stress, despite its growing significance in the context of environmental challenges. This study systematically identified the *BES1* gene family in *TGY* through bioinformatics, analyzing its physicochemical properties, evolutionary relationships, gene architecture, conserved domains, and intraspecies/interspecies variation. The expression profile of the *CsBES1* gene was analyzed to provide insights into its role in adapting *TGY* tea to environmental stresses, improving quality, increasing yield, and developing stress-resistant crops in the face of global climate change.

2. Results

2.1. Identification and Characterization of CsBES1 Genes

The amino acid sequences of ten members of the *CsBES1* family were predicted and labeled as *CsBES1.1* to *CsBES1.10* (details provided in Table 1). The size of the protein is generally positively correlated with the length of the amino acid sequence. Within the *CsBES1* family, the number of amino acids varies significantly, ranging from 315 in *CsBES1.5* to 699 in *CsBES1.6*. The molecular weight of these proteins ranges from 34,258.36 kDa (*CsBES1.9*) to 78,007.57 kDa (*CsBES1.6*), while their theoretical isoelectric points (pI) range from 5.37 (*CsBES1.6*) to 10.02 (*CsBES1.1*), with an average of 8.17. Variations in pI suggest that *CsBES1* proteins function in diverse microenvironments.

Table 1. Physical and chemical characteristics of the '*Tieguanyin*' *BES1*s including Gene Name, Gene ID, Size/aa (Size in Amino Acids), Molecular Weight/kDa (Molecular Weight in Kilodaltons), Theoretical PI (Theoretical Isoelectric Point), Grand Average of Hydropathicity, Instability Index, and Subcellular Localization.

Gene Name	Gene ID	Size/aa (Size in Amino Acids)	Molecular Weight/kDa (Molecular Weight in Kilodaltons)	Theoretical PI (Theoretical Isoelectric Point)	Grand Average of Hydropathicity	Instability Index	Subcellular Localization
CsBES1.1	*CsTGY03G0001903*	495	55,357.08	10.02	−0.765	72.8	Nucleus
CsBES1.2	*CsTGY15G0001195*	395	44,896.92	9.05	−0.391	43.17	Nucleus
CsBES1.3	*CsTGY04G0000351*	377	40,575.01	8.92	−0.654	81.82	Nucleus
CsBES1.4	*CsTGY02G0000736*	322	34,442.06	8.6	−0.608	70.99	Nucleus
CsBES1.5	*CsTGY12G0000463*	315	35,172.59	8.13	−0.604	37.02	Chloroplast
CsBES1.6	*CsTGY03G0002935*	699	78,007.57	5.37	−0.454	37.34	Nucleus
CsBES1.7	*CsTGY08G0002091*	323	34,725.64	7.61	−0.603	58.53	nucleus
CsBES1.8	*CsTGY08G0000981*	326	34,687.46	8.81	−0.609	59.21	nucleus
CsBES1.9	*CsTGY09G0002593*	316	34,258.36	9.25	−0.708	76.49	nucleus
CsBES1.10	*CsTGY14G0000640*	683	77,043.46	5.96	−0.511	40.49	nucleus

All ten *CsBES1* proteins exhibited negative hydrophilicity, classifying them as hydrophilic proteins. The lipid solubility indices of these proteins ranged from 37.02 (*CsBES1.5*) to 81.82 (*CsBES1.3*), with four proteins exhibiting indices above 70, suggesting heat stability. Proteins with instability coefficients below 40 are typically considered stable, whereas those with coefficients above 40 are classified as unstable. Among the ten *CsBES1* family members, only *CsBES1.5* and *CsBES1.6* had instability coefficients below 40, indicating that they are stable proteins. The remaining members were predicted to be unstable.

Subcellular localization analysis also revealed that approximately nine *CsBES1* proteins are localized in the nucleus. Notably, *CsBES1.5* was the only member predicted to be localized in the chloroplast, emphasizing potential functional diversity within the family.

2.2. The Motif, Domain, and Gene Structure of CsBES1 Family

Gene structure is a key characteristic of gene families, offering valuable insights into their evolutionary history [65]. Conserved protein domains, characterized by high sequence similarity, provide essential insights into evolutionary relationships [66]. To explore the evolutionary relationships within the *BES1* family, 10 conserved protein motifs and their structures were analyzed. Using MEME, 10 conserved motifs were identified among the 10 *BES1* proteins (Figure 2). Most family members cluster within the same branch and share similar motif and domain structures, although notable diversity exists among *CsBES1* proteins. Nearly all *CsBES1* proteins contain motif 1, the most highly conserved motif across the family, emphasizing its potential functional significance. The widespread presence of motif 1 suggests a critical role in fundamental biological activities, possibly involving DNA binding or protein–protein interactions.

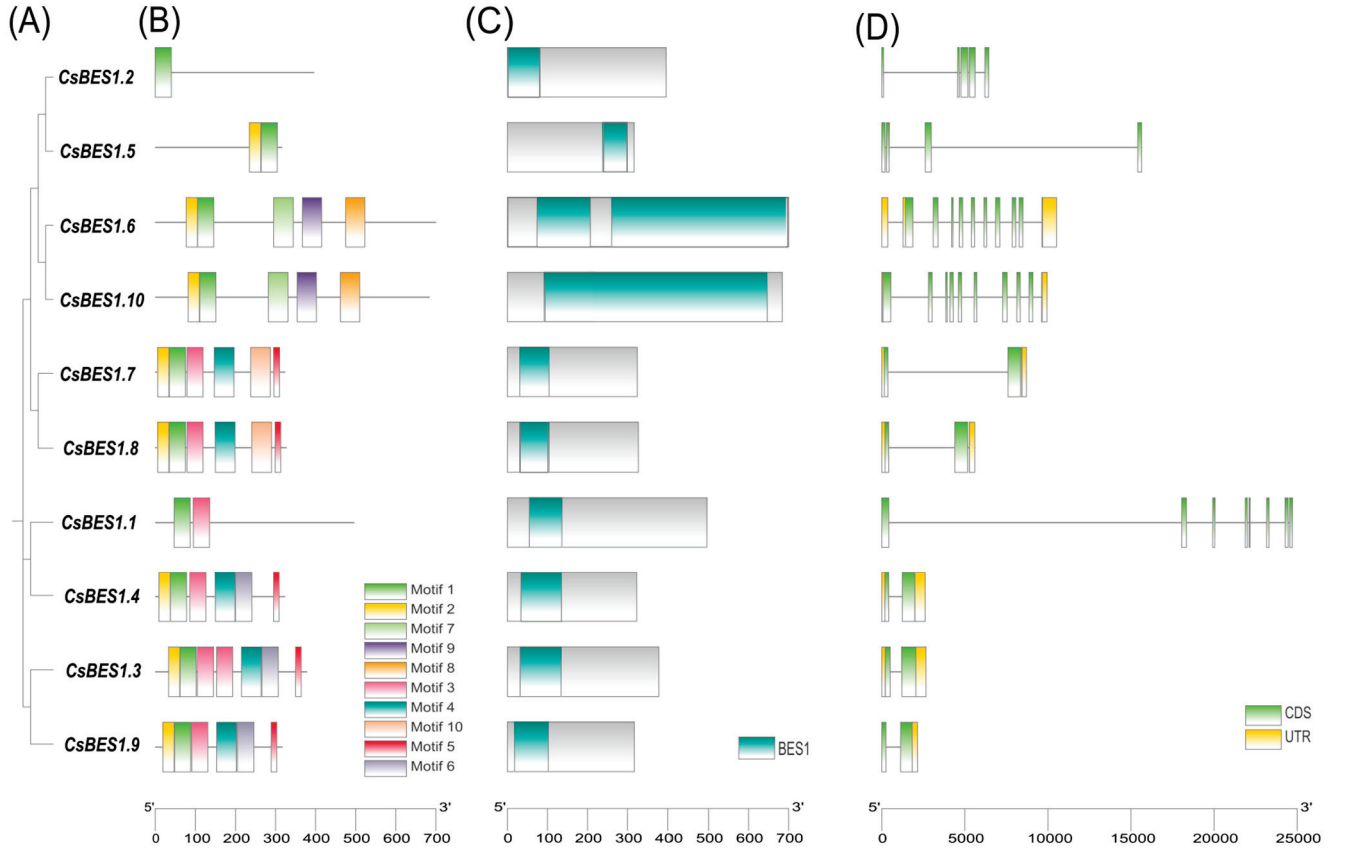


Figure 2. Protein motifs, domains, and structures of the *BES1* gene family in '*Tieguanyin*'. (**A**) A phylogenetic tree of *CsBES1* proteins was constructed using MEGAX 12.0 software. The tree was generated with the maximum likelihood method and validated through 1000 bootstrap replications, ensuring consistency and reliability. (**B**) Protein motifs in *CsBES1* members are represented by colorful boxes, each denoting a distinct motif. (**C**) Conserved domains are depicted, illustrating the shared structural features of the *BES1* proteins. (**D**) The gene structures of the *CsBES1* gene family are shown. Coding sequence (CDS) regions are represented by green rectangles, untranslated regions (UTRs) are represented by yellow rectangles, and introns are represented by black lines.

With the exception of *CsBES1.2* and *CsBES1.1*, all proteins contain motif 2, indicating its relatively conserved nature. Notably, *CsBES1.6* and *CsBES1.10* both possess motifs 1, 2, 7,

9, and 8, while *CsBES1.7* and *CsBES1.8* share motifs 1, 2, 3, 4, 10, and 5, suggesting potential functional similarities. These proteins may regulate similar sets of genes or biological processes. Additionally, conserved domains were identified across all *CsBES1* proteins, further supporting a high degree of conservation. This finding highlights the need for further exploration of their diverse biological functions.

Exon–intron structure analysis revealed a total of 10 genes. Notably, *CsBES1.2* and *CsBES1.5* lack non-coding regions, which are crucial for regulating mRNA stability and gene expression. Interestingly, *CsBES1* members within the same group exhibit minimal variation in exon and intron number and length, reinforcing the functional conservation of BES1 genes within these groups.

2.3. Phylogenetic Analysis of CsBES1s

The phylogenetic tree illustrates the evolutionary relationships among members of the *CsBES1* gene family and their counterparts in other species. To further explore these relationships, a multiple sequence alignment and a maximum likelihood phylogenetic tree were constructed, with *Arabidopsis* and *Solanum lycopersicum* as reference species. The *CsBES1* family in *TGY* comprises 10 members, while *A. thaliana* and *S. lycopersicum* have 14 and 9 members, respectively, yielding a total of 33 members, which are classified into four groups (I–IIIB) based on the grouping in *A. thaliana* (Figure 3). The distribution of *CsBES1* genes among these groups is uneven. Group IIIB contains the majority of *CsBES1* members (*CsBES1.1*, *CsBES1.2*, *CsBES1.5*, *CsBES1.6*, *CsBES1.7*, *CsBES1.8*, and *CsBES1.10*), whereas Group IIIA includes three members (*CsBES1.3*, *CsBES1.4*, and *CsBES1.9*). Groups I and II consist only of *BES1* genes from *A. thaliana*, suggesting that *BES1* in *TGY* underwent expansion after the divergence of monocots and retains conserved features.

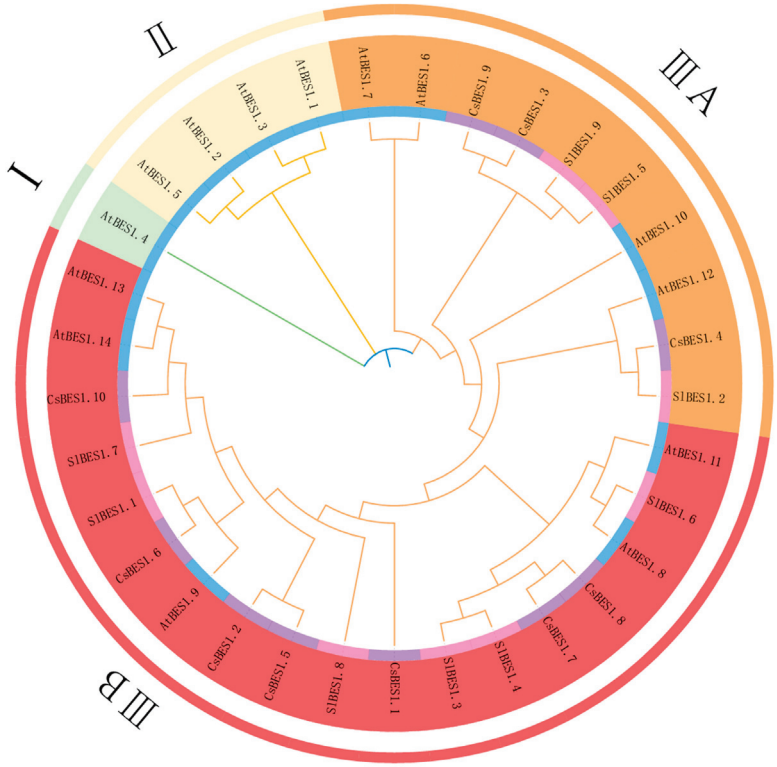


Figure 3. A phylogenetic analysis of *BES1* proteins from *Tieguanyin* (Cs), *A. thaliana* (At), and *Solanum lycopersicum* (Sl) was conducted using the neighbor-joining method with the maximum likelihood approach and 1000 bootstrap replicates. Different colors in the inner circle represent the three species, while the four subgroups of *BES1* proteins (Groups I–IIIB) are distinguished by varying colors in the outer circle.

Martin's analysis suggests that *BES1* genes originated during the bryophyte stage of biological evolution and further evolved after the phytoplankton stage [67]. Within Group IIIB, *SlBES1.1* and *CsBES1.6*, as well as *SlBES1.7* and *CsBES1.10*, form direct homologous relationships. Similarly, *CsBES1.2* and *CsBES1.5* cluster with *SlBES1.8*. Notably, *SlBES1.8* plays a critical role in fruit setting and development in *S. lycopersicum*, with its activity being induced by auxin and gibberellin [19]. Since *CsBES1.1* is a direct homolog of *SlBES1.8*, it is plausible to hypothesize that *CsBES1.1* may play a similar role in *TGY* tea development. Further analysis revealed that *CsBES1.10* clusters with *AtBES1.13* and *AtBES1.14*, while *CsBES1.6* and *AtBES1.9* are orthologous pairs, potentially involved in similar regulatory pathways.

2.4. Chromosome Distribution of CsBES1s and Genomic Amplification in TGY

TGY tea has a total of 12 chromosomes, with 10 *CsBES1* genes distributed across 8 of them. Chromosomes 8 and 3 contain the highest number of *CsBES1* members, as shown in Figure 4. Specifically, *CsBES1.7* and *CsBES1.8* are located on chromosome 8, while *CsBES1.1* and *CsBES1.6* are found on chromosome 3. The remaining *CsBES1* genes are distributed singly across chromosomes 9 (*CsBES1.9*), 12 (*CsBES1.5*), 14 (*CsBES1.10*), 15 (*CsBES1.2*), 2 (*CsBES1.4*), and 4 (*CsBES1.3*). This uneven distribution pattern likely reflects genetic variations that occurred during evolution. The collinear model provides valuable insights into the evolutionary history of the genome and facilitates subsequent correlation analyses [68]. Notably, three pairs of collinear genes were identified: one tandem duplication (*CsBES1.7* and *CsBES1.8*) and two segmental duplications (*CsBES1.9* and *CsBES1.3*, *CsBES1.4* and *CsBES1.3*).

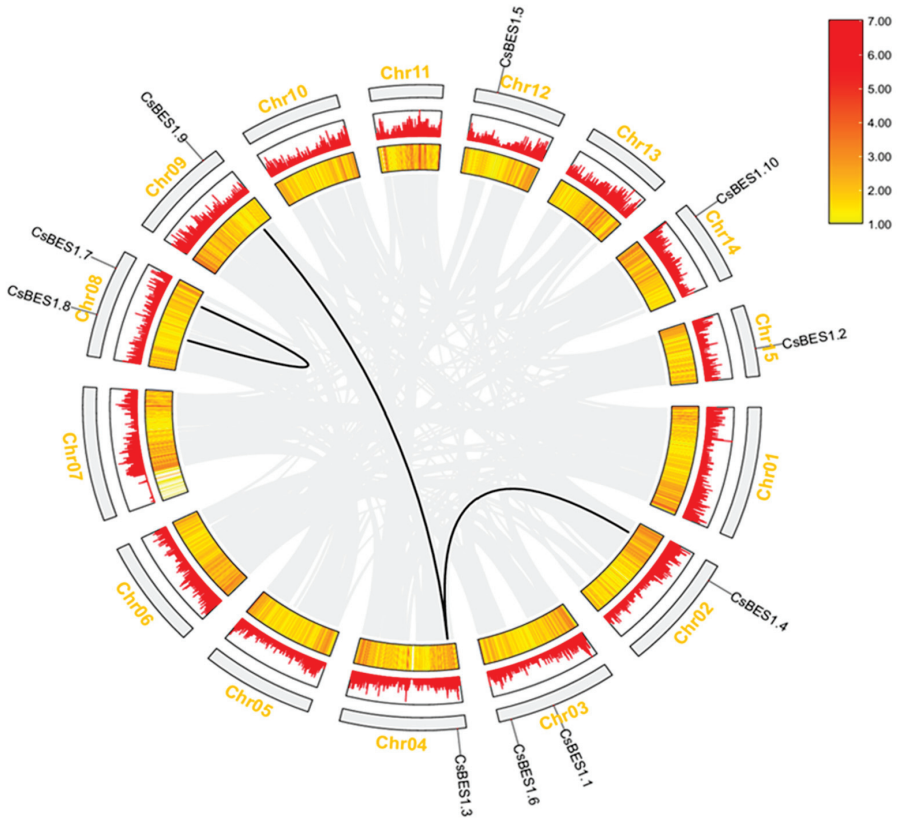


Figure 4. The distribution of *CsBES1* genes across 15 chromosomes, along with evidence of genomic amplification. A line plot and heatmap display the density of *CsBES1* genes along each chromosome. Black lines indicate gene pairs originating from *CsBES1*.

Gene duplications, whether tandem (within a 200 kb region) or segmental (between different chromosomes), are crucial drivers of evolutionary innovation and functional diversification [41,69,70]. To gain deeper insights into the evolution of the *BES1* gene family, interspecific and intraspecific collinearity analyses were conducted (Figure 5). For interspecific analysis, *A. thaliana*, *S. lycopersicum*, and *TGY* were selected as study subjects to examine the consistency of their gene sequences. The results revealed 10 collinear gene pairs between *TGY* and each of the other two species, with chromosome 8 in *TGY* exhibiting the highest number of collinear pairs. Specifically, *TGY* shares 4 collinear pairs with *S. lycopersicum* and 2 pairs with *A. thaliana*. Across the three species, a total of 20 collinear genes were identified, suggesting conserved evolutionary roles.

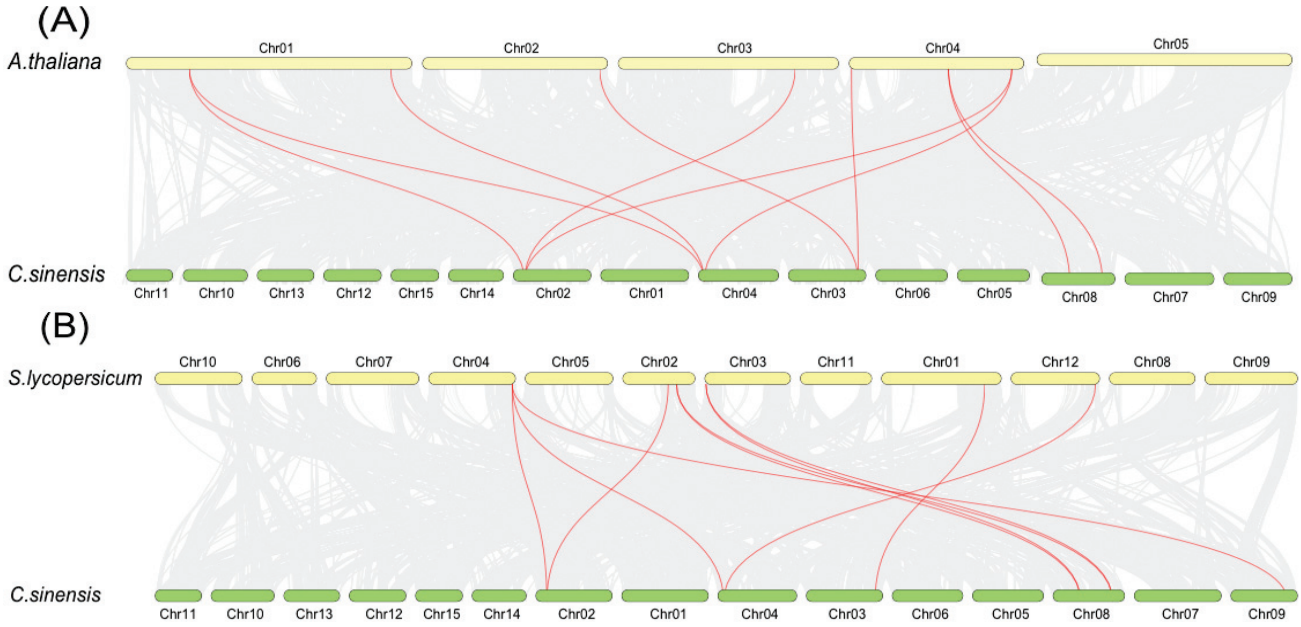


Figure 5. Comparative synteny analysis of *BES1* genes across *TGY*, *A. thaliana* (**A**), and *S. lycopersicum* (**B**). Grey lines in the background highlight syntenic *BES1* gene pairs, while red lines indicate collinearity between *CsBES1* and genes from other species. Chromosome numbers are displayed at the top or bottom of their respective diagrams.

2.5. Cis-Regulatory Element Prediction of Promoters in 10 CsBES1 Genes

Transcription factors (TFs) mainly exert their regulatory function by binding to specific cis-acting elements found in the promoter regions of target genes. This interaction regulates gene expression and influences the expression patterns of downstream genes [71]. In this study, the 2.0 kb promoter sequences of *CsBES1* genes were analyzed using the PlantCARE online software, which identified several cis-acting elements [72]. Based on their functional characteristics, these elements were categorized into four groups (Figure 6): hormonal response, stress signaling, light signaling, and growth and development.

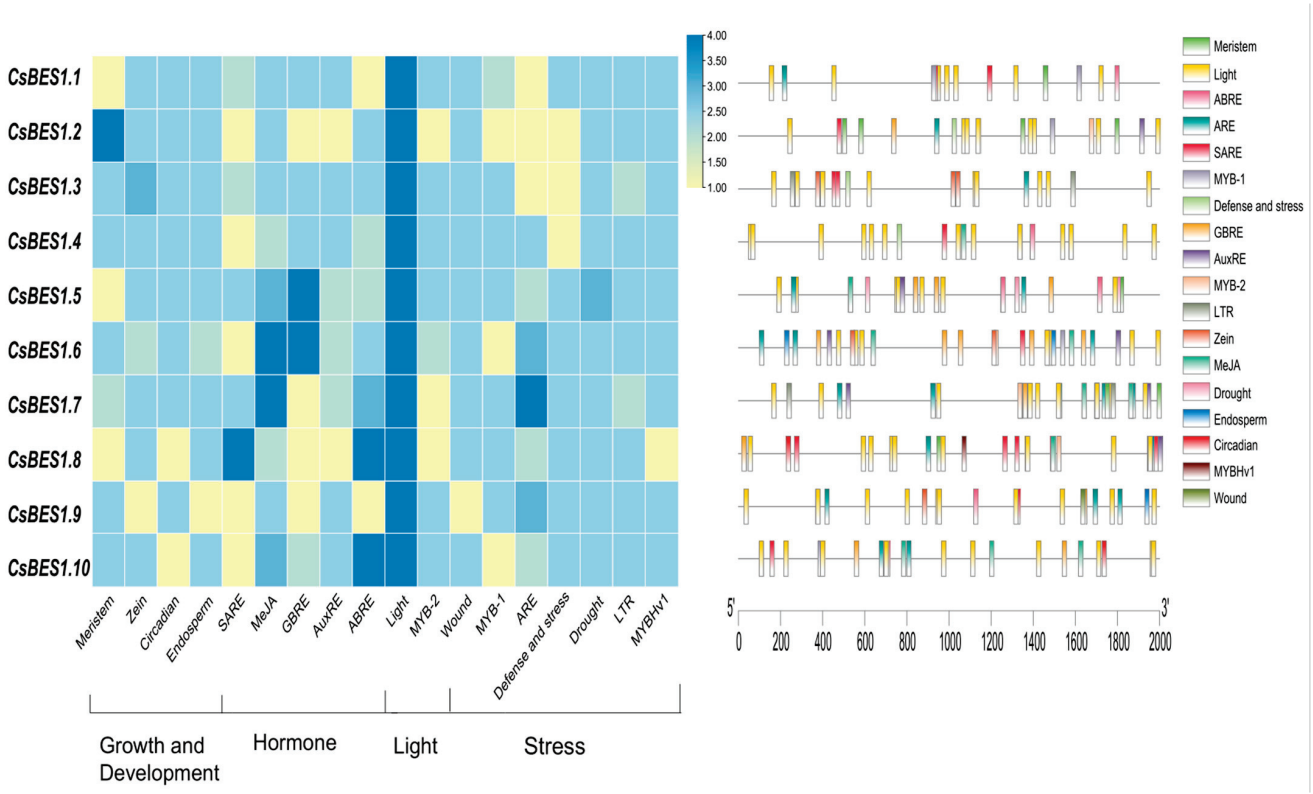


Figure 6. Schematic representation and visualization of the localization of cis-acting elements in each *CsBES1* gene.

The *CsBES1* genes showed significant correlations with hormone response elements, particularly ABA response elements (ABRE), salicylic acid response elements (SARE), methyl jasmonate (MeJA) response elements, gibberellin response elements (GBRE), and auxin response elements (AuxRE). This indicates a possible link between the *CsBES1* gene family and the signaling pathways of ABA and growth hormones, which is consistent with prior studies [14,73]. Additionally, these genes respond to various external stressors, including drought (e.g., MYB-1, MYBHv1, and other drought-related factors), low temperature (LTR), wounding and defense (WUN), and hypoxia (ARE). Nearly all *CsBES1* genes contain MYB-like transcription factor binding sites, which are strongly associated with drought response. MYB-like TFs are critical for regulating abiotic stress responses, especially drought stress [74]. These findings underscore the significant role of the *CsBES1* gene family in enhancing plant resistance to drought stress.

Notably, two types of light-responsive cis-elements were detected, making them the most common cis-elements in the *CsBES1* promoter regions. *CsBES1.4* was found to contain 13 light-related cis-elements, the highest among all family members. *CsBES1.9* and *CsBES1.10* were found to contain 12 light-related cis-elements. In addition, *CsBES1.2*, *CsBES1.7*, and *CsBES1.8* have only one photo-responsive homeostatic element. Several *CsBES1* genes contain cis-elements that are associated with various aspects of plant growth and development. These include elements linked to mesophyll expression (MREs), components involved in zein metabolism, regulatory elements for circadian rhythm (Circadian), and those specific to endosperm expression. Genes such as *CsBES1.3*, *CsBES1.4*, *CsBES1.5*, *CsBES1.6*, and *CsBES1.7*, which contain diverse regulatory elements, are likely to play critical roles in responding to abiotic stresses. These family members merit further investigation.

2.6. Gene Ontology (GO) and KEGG Analysis in CsBES1

In order to gain deeper insights into the functions of *CsBES1* genes, a Gene Ontology (GO) enrichment analysis was performed (Figure 7A). This analysis covered three main categories: molecular function, cellular components, and biological processes. This analysis provides valuable insights and a foundation for future exploration of the functions and mechanisms of *CsBES1* genes. Notably, *CsBES1* genes may interact with DNA-binding TF activity and transcription regulator activity. Furthermore, these genes are predominantly localized in the nucleus, aligning with subcellular localization predictions. Additionally, *CsBES1* genes collectively contribute to the biosynthesis of various secondary metabolites and participate in plant hormone signaling pathways (Figure 7B).

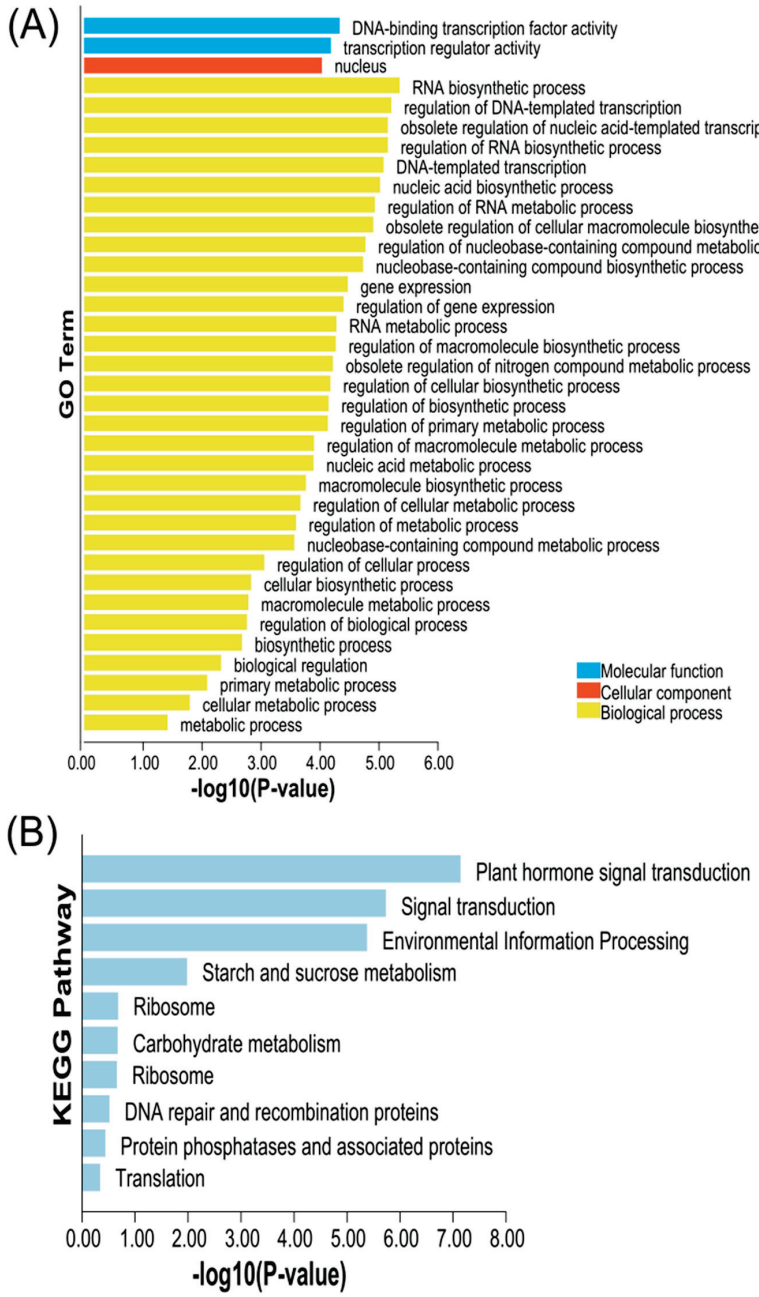


Figure 7. GO enrichment (**A**) and KEGG pathway and (**B**) analysis of *BES1* genes.

2.7. Protein–Protein Interaction Network of CsBES1 Proteins

Alignment of *CsBES1* genes with *AtBES1* genes identified ten homologous genes, offering insights into potential functional interactions between *CsBES1*-encoded proteins

and other key regulatory proteins. This understanding establishes a foundation for future functional validation and mechanistic studies. The interaction network of *CsBES1* proteins was constructed using STRING and refined in Cytoscape (Figure 8). *BES1*, a plant-specific TF, is a critical regulator of plant embryonic development. Homologous proteins BEH1, BEH2, BEH3, and BEH4 function alongside *BES1* to regulate plant growth and development by modulating downstream gene expression [75]. In the interaction network, *BES1* serves as a central node, linking with other proteins to form a complex signal transduction network. It acts as a downstream TF in the TPD1-SERK1 signaling pathway, which regulates tapetum development and plays a vital role in plant reproduction [17].

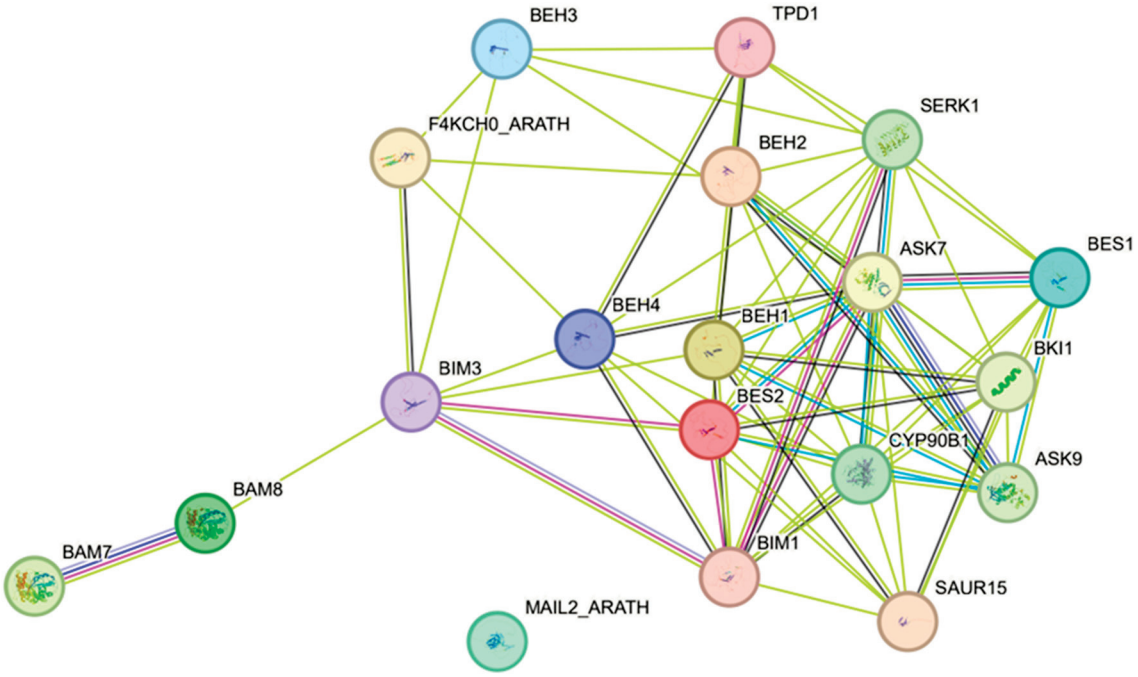


Figure 8. Protein–protein interaction network generated using STRING. The size of each protein's circle corresponds to its number of interactions, with larger circles and deeper colors indicating higher correlation.

BES1 is also predicted to interact with additional signaling components, including CYP90B1, SAUR15, ASK7, and BKI1; this process plays a crucial role in controlling and influencing the growth and development of plants. Furthermore, the probable interactions of *BES1* with SAUR15, ASK7, BKI1, and SCRM suggest a role for CsBES1 in helping plants cope with abiotic stress [76,77]. CYP90B1, indirectly associated with *BES1*, is an enzyme from the cytochrome P450 family involved in diverse metabolic processes, highlighting its potential role in growth and development [78]. A deep understanding of the functional interactions between *CsBES1* proteins and essential regulatory proteins establishes a solid basis for subsequent investigations into their roles and mechanisms.

2.8. Expression Patterns of CsBES1 Genes in Response to Dark and Light Treatments

Earlier research has thoroughly investigated the fundamental roles of the *BES1* gene family in response to abiotic stress. In the present study, we examined the expression profiles of eight *CsBES1* genes, categorized into four subgroups (I–IIIB), under two different abiotic stress conditions using quantitative real-time PCR (qRT-PCR). Stress treatments included light exposure (continuous 1200 $\mu mol \cdot m^{-2} \cdot s^{-1}$) and darkness. And the TmThe expression patterns of *CsBES1* genes exhibited similar responses to abiotic stresses, with some genes showing significant upregulation or downregulation under specific conditions (Figure 9).

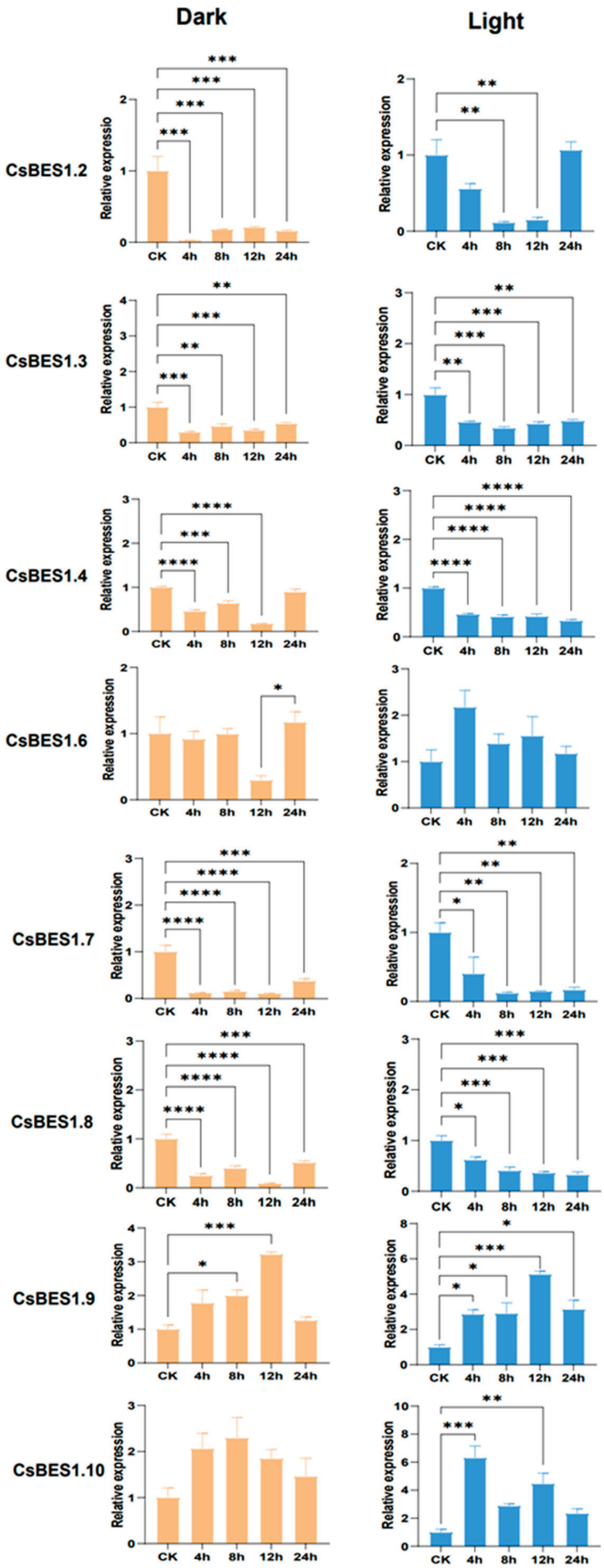


Figure 9. Expression profiles of *CsBES1* genes under various stress conditions. Error bars represent the standard deviation (SD). Statistical significance was assessed using one-way ANOVA, with the number of asterisks (*) indicating the level of significance ($p < 0.05$). Significant differences relative to the control group are indicated as follows: * $p < 0.05$, ** $p < 0.01$, *** $p < 0.0005$, and **** $p < 0.0001$.

Under dark treatment, *CsBES1.2*, *CsBES1.3*, *CsBES1.4*, *CsBES1.7*, and *CsBES1.8* displayed significant downregulation after four hours of treatment. Notably, *CsBES1.4*, *CsBES1.7*, and *CsBES1.8* showed pronounced downregulation ($p < 0.0001$), reaching their lowest expression levels after 12 h. Subsequently, their expression levels began to increase as the duration of dark treatment was prolonged. In contrast, *CsBES1.9* and *CsBES1.10* exhibited upregulation after 12 h, with *CsBES1.9* demonstrating a three-fold increase compared to the control group, suggesting that *CsBES1.9* may be particularly sensitive to light reduction. However, the underlying regulatory mechanism remains unclear and requires further investigation.

Under light exposure, *CsBES1.9* and *CsBES1.10* showed significant upregulation, with *CsBES1.10* reaching approximately six-fold the control expression level after four hours. After eight hours, the expression of all genes was inhibited except for *CsBES1.9*, which continued to upregulate and peaked at 12 h. Conversely, the expression of *CsBES1.2* and *CsBES1.7* became nearly undetectable. Notably, *CsBES1.9* exhibited significant upregulation after 12 h of both darkness and light exposure ($p < 0.0005$), while *CsBES1.4* showed significant downregulation under both conditions after 12 h ($p < 0.0001$). These findings suggest that *CsBES1.9* and *CsBES1.4* may have critical roles in responding to abiotic stress. Furthermore, it is speculated that responses to light and dark stress in ferroptosis are primarily regulated by a few specific *CsBES1* genes.

3. Discussion

Tea, as a perennial woody plant, is widely distributed and exhibits significant resource diversity. Over its evolutionary history, the tea plant has developed specialized mechanisms to adapt to environmental changes. One critical area requiring further investigation is the molecular mechanism by which *CsBES1* regulates the tea plant's resistance to light stress. *BES1* family members are widely distributed across plants and are essential for regulating BR signaling pathways. These proteins are involved in various processes, including responses to abiotic stress, cell proliferation and differentiation, seed germination, trichome cell degradation, and pollen development. This study identified 10 *BES1* genes using bioinformatics methods, fewer than the 14 identified in *Populus tomentosa* [41], but more than the 6 identified in rice [79], and comparable to the counts in grape (8) [80] and *Machilus nanmu* (9) [81].

Analysis of the physicochemical properties of *CsBES1* revealed that it is an unstable, hydrophilic protein capable of functioning in mildly acidic and alkaline environments. Consistent with these findings, the subcellular localization of *AtBES1* has been observed in both the nucleus and cytoplasm [26,34]. Similarly, in our investigation, we found that the 10 genes are distributed across the nucleus and cytoplasm (Table 1), suggesting that *TGY BES1* proteins participate in phosphorylation-regulated processes.

To explore the evolutionary relationships among *Arabidopsis thaliana*, *Solanum lycopersicum*, and *TGY*, we constructed a phylogenetic tree for the *CsBES1* protein family. This analysis revealed that the 33 *BES1* proteins are classified into four subgroups, with the majority of *CsBES1* genes residing in subgroup IIIB (Figure 3). Previous studies have shown that changes in gene family size can lead to beneficial, harmful, or neutral outcomes and that variations in gene family numbers significantly influence species specificity [79]. Our findings align with this, demonstrating that the phylogenetic relationships of *BES1* genes differ among species.

Additionally, *SlBES1.8*, a key regulator of fruit setting and development in *S. lycopersicum* is induced by auxin and gibberellin [19]. Since *CsBES1.1* is a direct homolog of *SlBES1.8* in subgroup IIIB, it is plausible that *CsBES1.1* also contributes to *TGY* development. Interestingly, motif analysis (Figure 2) reveals that *CsBES1.1* is approximately 25 kb

in length, making it the longest gene in this family. Given the established relationship between gene structure and function [80], further investigation into *CsBES1.1* is of significant scientific interest. Furthermore, *CsBES1.2* and *CsBES1.5* cluster with *SlBES1.8*, suggesting their potential involvement in related regulatory processes. It is also noteworthy that *BES1* genes in Class I and II groups are exclusively found in *Arabidopsis thaliana*, indicating that *BES1* genes in *TGY* may have undergone expansion following the divergence of monocots.

Martin's analysis suggests that *BES1* first appeared in bryophytes and evolved further after phytoplankton [67]. Previous studies have shown that *AtBZR1* plays a redundant role in plant growth and development by facilitating BR-induced growth while providing feedback inhibition on BR biosynthesis [81,82]. In contrast, *AtBES1* is involved in glucosinolate biosynthesis via BR signaling [26]. Our study identified that *CsBES1.10* clusters with *AtBES1.13-14*, while *CsBES1.6* forms an orthologous gene pair with *AtBES1.9*, both potentially involved in related regulatory processes.

To further investigate the evolution of the *BES1* gene family, we performed both inter- and intra-species synteny analyses, which revealed 20 pairs of syntenic genes across the three species, underscoring their conserved evolutionary significance.

Gene families mainly arise through six distinct mechanisms: whole-genome duplication, tandem duplication, segmental duplication, insertion of retrotransposons, exon duplication, and reshuffling [69]. The expansion of the *CsBES1* gene family primarily occurs through fragment replication events, which represent its primary evolutionary mechanism. Similarly, the *BES1* gene family in wheat expands through segmental duplication [83]. In species such as *A. thaliana*, cabbage, rice, and apple, segmental duplications are predominantly observed among homologous *BES1* paralogous genes, aligning with our findings in *TGY* [84,85]. These results underscore the importance of segmental duplication in the amplification of *CsBES1* genes and highlight the gene family's critical role in understanding *TGY*'s biological evolution.

Introns are crucial in plant evolution [86]. Exon-intron structure analysis further revealed that *CsBES1.2* and *CsBES1.5* lack non-coding regions, which are crucial for regulating mRNA stability and gene expression. A phylogenetic tree constructed for the *BES1* gene family indicated a clear evolutionary relationship between *CsBES1* genes in '*Tieguanyin*' tea, *Arabidopsis thaliana*, and *Solanum lycopersicum*. Specifically, *CsBES1.2* and *CsBES1.5* clustered with *SlBES1.8* from tomato, which is known to play a key role in fruit set and development in tomato and is induced by auxin and gibberellin. This suggests that *CsBES1.1*, as a direct homolog of *SlBES1.8*, may play a similar role in the development of '*Tieguanyin*' tea. Furthermore, *CsBES1.10* clustered with *AtBES1.13* and *AtBES1.14* from *Arabidopsis*, while *CsBES1.6* is homologous to *AtBES1.9*, possibly participating in similar regulatory pathways.

Exon–intron analysis identified 10 *CsBES1* genes, with *CsBES1.6*, *CsBES1.10*, *CsBES1.7*, and *CsBES1.8* showing conserved motifs and similar structures. Phylogenetic analysis supports these findings. *CsBES1.2* and *CsBES1.5* lack non-coding regions, unlike the grape *BES1* family [87], which includes regulatory non-coding regions affecting mRNA stability and gene expression. Most *CsBES1* proteins contain motif 1, the most conserved. These results highlight the importance of motifs 1 and 2 in the *CsBES1* gene family.

To further investigate the potential role of the *BES1* gene family in environmental responses, we analyzed the light-responsive cis-acting elements in the promoter regions of *CsBES1* genes. Cis-acting elements, which play a crucial role in the initiation of genes and the regulation of transcription, are found within the promoters [88]. The *BES1* gene family plays a critical role in various stress responses [13,42,89,90]. The results showed that *CsBES1.4* contains the highest number of light-related cis-acting elements (13), followed by *CsBES1.9* and *CsBES1.10*. QRT-PCR analysis revealed that under light conditions, the

expression of *CsBES1.9* and *CsBES1.10* was significantly upregulated, with *CsBES1.10* reaching six times the control group's expression level after 4 h. After 8 h, all genes except *CsBES1.9* showed suppressed expression, while *CsBES1.9* continued to increase and peaked at 12 h. In contrast, the expression of *CsBES1.2* and *CsBES1.7* was nearly undetectable. Notably, *CsBES1.9* exhibited significant upregulation after 12 h of both dark and light exposure ($p < 0.0005$), while *CsBES1.4* showed significant downregulation under both conditions ($p < 0.0001$). These results suggest that *CsBES1.9* and *CsBES1.4* may play key roles in responding to abiotic stress.

Using *A. thaliana* as a model, we predicted a protein–protein interaction network. As a key downstream TF in the TPD1-SERK1 signaling pathway, *BES1* plays an essential role in regulating tapetum layer development, thereby influencing plant reproduction. Building on previous findings, we identified eight *CsBES1* homologous genes and analyzed their expression patterns under different light conditions. Quantitative real-time polymerase chain reaction (qRT-PCR) analysis revealed that the upregulation of *CsBES1.9* and *CsBES1.10* under light exposure, along with the downregulation of *CsBES1.4*, *CsBES1.7*, and *CsBES1.8* under dark conditions, highlights the differential regulation of these genes in response to light and dark stress. It is speculated that the genes containing the most light-responsive cis-elements (*CsBES1.4*, *CsBES1.9*, and *CsBES1.10*) play critical roles in regulating light stress responses and ferroptosis processes in plants. These results suggest that these genes may play pivotal roles in responding to light variations and adapting to environmental stress.

BES1/BZR1 plays a central role in regulating light signaling during plant morphogenesis, with its phosphorylation status and stability modulated by light signals [63]. Previous studies have shown that under dark stress, the protein levels of SINATs decrease, leading to the activation of COP1 [91]. Simultaneously, inactive CRY1 fails to interact with dephosphorylated *BES1*, resulting in elevated levels of dephosphorylated *BES1*. This dephosphorylated form can form homodimers (*BES1-BES1* and *BZR1-BZR1*) and heterodimers (*BES1-PIF4* and *BZR1-PIF4*) to regulate downstream gene expression, promoting hypocotyl elongation (Figure 10A) [92]. It is important to note that Constitutive Photomorphogenic 1 (COP1), an E3 ubiquitin ligase, is responsible for the dark-induced degradation of the inactive, phosphorylated version of *BZR1* [64].

In the presence of light, SINAT levels rise, facilitating the degradation of dephosphorylated *BES1/BZR1*. At the same time, COP1 activity is inhibited, leading to a decrease in the ratio of *BES1/BZR1* to p*BES1*/p*BZR1* [91]. Additionally, activated CRY1 interacts with dephosphorylated *BES1* through its N-terminal (CNT1), inhibiting its DNA-binding activity and suppressing hypocotyl growth (Figure 10B) [93]. UV-B light, an integral component of sunlight, significantly affects plant development via the UVR8 photoreceptor [94–97]. Under UV-B exposure, UVR8 interacts with COP1 and accumulates in the nucleus, where it binds to dephosphorylated *BES1*. This interaction inhibits *BES1*'s DNA-binding activity, reducing the transcription of growth-promoting genes and thereby suppressing hypocotyl elongation [97–99].

When UV-B radiation is not present, UVR8 remains mainly in the cytoplasm, whereas BIM1 and active *BES1* are localized in the nucleus, where they facilitate the transcription of genes induced by brassinosteroids (BR). This activity enhances cell elongation under low-temperature conditions. Our analysis of cis-acting elements and protein–protein interactions (Figures 5 and 7) suggests a potential link between key response proteins and *CsBES1*, indicating that *CsBES1* may play a crucial role in environmental stress resistance by interacting with or regulating these proteins (Figure 10). While these findings align with our research on *CsBES1* and previous studies on plant stress responses, further experiments are necessary to confirm its precise contributions to plant resilience.

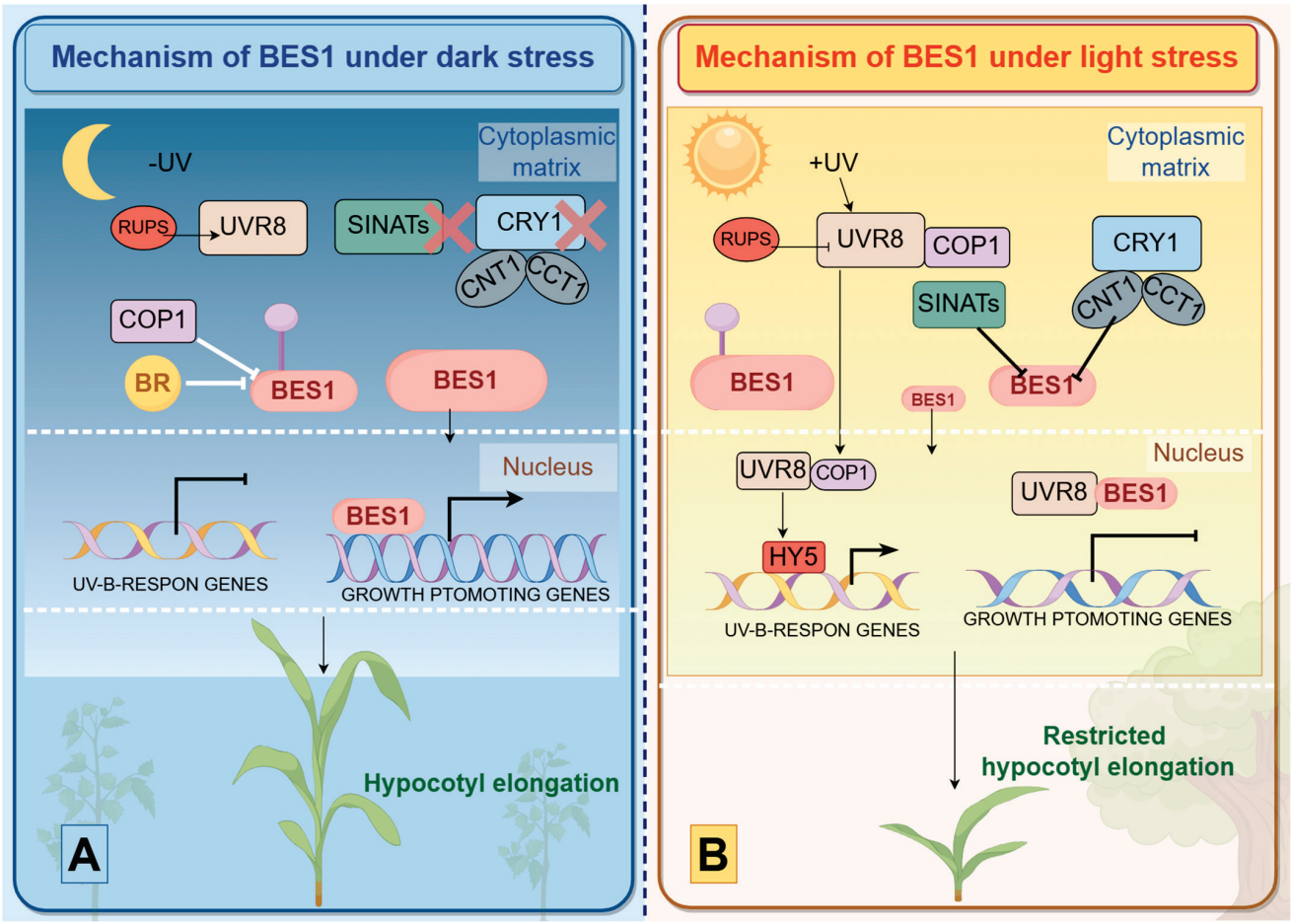


Figure 10. In darkness (**A**), CRY1 remains in its inactive form and is unable to suppress BR signaling because it does not interact with dephosphorylated *BES1*. SINATs undergo self-degradation, leading to a rise in the levels of dephosphorylated *BES1*, while phosphorylated *BES1* (*pBES1*) is degraded via the COP1 pathway. As a result, the ratio of dephosphorylated *BES1* to *pBES1* increases. The active dephosphorylated *BES1* then regulates gene expression to promote hypocotyl elongation. During this phase, UVR8 predominantly resides in the cytoplasm, whereas BIM1 and functional BES1 are localized in the nucleus, where they facilitate the transcription of BR-induced genes to enhance hypocotyl growth. The meaning of 'X' is not to express it in this situation. In light conditions (**B**), CRY1 becomes activated and binds to dephosphorylated *BES1*, inhibiting its ability to bind DNA. The accumulation of SINATs promotes the degradation of *BES1*, resulting in a decrease in dephosphorylated *BES1*/*BZR1* levels and reducing the ratio of dephosphorylated *BES1*/*BZR1* to phosphorylated *BES1*/*BZR1* (*pBES1*/*pBZR1*). This reduction in the ratio leads to the suppression of hypocotyl elongation. Under UV-B light, UVR8 accumulates in the nucleus, where it interacts with nuclear BIM1 and dephosphorylated *BES1*, blocking their DNA-binding activity and thereby repressing the transcription of BR-responsive genes and hypocotyl elongation. The varying font sizes for *BES1* indicate different levels of dephosphorylated and phosphorylated *BES1*.

4. Materials and Methods

4.1. Identification and Analysis of BES1 Gene Families in TGY

TGY was acquired from the China National GeneBank genome sequence database sequence file (https://db.cngb.org/search/project/CNP0002030/ (accessed on 1 October 2024)) [100]. Meanwhile, amino acid sequence information of *A. thaliana BES1* was obtained from the TAIR database (https://www.arabidopsis.org (accessed on 1 October 2024)). The protein sequence of *TGY* was compared with *AtBES1*s using the BLASTp 2.12.0 program of the National Center for Biotechnology Information (NCBI). Combining the results obtained using these two methods, *CsBES1*s was accurately located. Then, we used the NCBI

CDD search tool (https://www.ncbi.nlm.nih.gov/Structure/bwrpsb/bwrpsb.cgi (accessed on 2 October 2024)) and SMART network database (http://smart.Embl-heidelberg.de/ (accessed on 3 October 2024)) to carry out in-depth analysis and verification of *CsBES1*s.

Finally, Tie Guanyin's *BES1* gene family was successfully identified as having 10 gene family members, and it was renamed *CsBES11-10*. ExPASy online (https://web.expasy.org/protparam (accessed on 15 July 2024)) [101] was utilized to predict and calculate the molecular weight, number of amino acids, theoretical PI (isoelectric point), number of positive (negative) residues, instability coefficient, lipolysis coefficient, and total average hydrophilicity of each *BES1* protein in *TGY*.

4.2. Physical and Chemical Properties of TGY

HMMER 3.3 software was used to conduct comprehensive screening of the *TGY* genome and accurately locate *the BES1* homologous sequence. The preliminary screening of the proceeds of the gene sequences was uploaded to the SMART database (https://smart.embl-Heidelberg.DE/ (accessed on 4 October 2024)) and the National Center for Biotechnology Information (NCBI) website (https://www.ncbi.nlm.nih.gov/ (accessed on 8 October 2024)). In this way, its domain can be accurately confirmed. In this process, the redundant sequences were effectively eliminated through meticulous manual comparison and screening, so as to successfully obtain *CsBES1* gene members. Subsequently, the physicochemical properties of *CsBES1* gene members were further investigated using the Protparam database (https://www.expasy.org/ (accessed on 9 October 2024)).

The ProtParam tool available on the ExPasy website was used to perform an in-depth analysis of essential protein characteristics, including the number of amino acids, molecular weight, and isoelectric point for each member. This analysis provided valuable data and a theoretical foundation for a deeper understanding of the properties and functions of the *CsBES1* gene family. Furthermore, the CDD function of the NCBI website (https://www.ncbi.nlm.nih.gov/cdd (accessed on 10 October 2024)) and SMART online (https://smart.embl.de/ (accessed on 11 October 2024)) [31] were employed to analyze and integrate the obtained protein sequences.

4.3. Phylogenetic Analysis of CsBES1s and BES1s from Other Species

In this study, the *BES1* protein sequence of *TGY* was successfully obtained by accessing the Ensemble Plant database. For *Arabidopsis* and *S. lycopersicum*, the genome and annotated data were downloaded from the specific ftp (https://www.etc.site/ftp/genomes/Nicotiana_tabacum/edwards_et_al_2017/ (accessed on 13 October 2024)). In order to deeply explore the evolutionary relationship between different species, the phylogenetic tree was constructed by adopting the neighbor-joining method (NJ) and setting 1000 repeats (the bootstrap value was 1000). Firstly, the online tool ITOL (https://itol.embl.de/ (accessed on 14 October 2024)) was used to construct preliminary phylogenetic trees for *Arabidopsis* and *S. lycopersicum* and *TGY* species, and MEGA 7.0.26 software was applied to construct the phylogenetic trees.

4.4. Collinearity Analysis and Replication Event Analysis of BES1

We used MCScanX (https://github.com/wyp1125/MCScanX/ (accessed on 15 October 2024)) software to study *Arabidopsis* and rice and maize *CsBES1* and *BES1* gene synthesis relationship in depth [68]. With the help of this software, the segmentation and tandem replication events occurring in the *CsBES1* gene were identified, providing key genetic structural variation information. At the same time, TBtools-v2.10 [102], a software tool, was utilized to conduct a comprehensive analysis of the visual distribution and collinearity of *CsBES1* genes.

4.5. GO and KEGG Analysis

In this study, the egg NOG-MAPPER platform was used to implement GO and KEGG analysis processes for the *BES1* protein (https://www.kegg.jp/ (accessed on 20 October 2024)) [103]. In the framework of this analysis, the number of *CsBES1* proteins was subdivided into three categories [104]. Then, Tbtools v2.10 software was used to visualize and analyze the annotation results.

4.6. Protein–Protein Interaction Network of CsBES1s

Complete and in-depth analysis is performed by uploading the *BES1* protein sequence to the STRING database (https://cn.string-db.org/ (accessed on 25 October 2024)). Based on the observations of protein interactions in Arabidopsis, the association patterns among key proteins were prospectively predicted. Finally, Cytoscape (V3.10.2) software is used to visualize and optimize the acquired network [105].

4.7. Abiotic Stress Therapy

In this experiment, *TGY* seedlings were selected from *TGY* specimens. The soil for planting seedlings was prepared using a mixture of peat, humus, sandy soil, and perlite in a ratio of 5:2:2:1, resulting in soil organic content ranging from 2.57% to 6.07%. The average annual temperature was 16–20 °C, the annual precipitation was 900–2100 mm, and the annual relative humidity was about 77%. There were three experimental groups, drought, heat stress, and light treatment, and each experimental group included several groups. The drought and heat stress groups were divided into 4 groups, and the light stress groups were divided into 3 groups. Each group was treated with customized experimental conditions. In the sampling time setting, the sampling time of the drought and heat treatment groups was 0, 4, 8, 12, and 24 h.

The Nt group was sampled at 0, 24, 48, and 72 h, and seedlings collected at 0 h were used as the control group. During stress treatment, the parameters of the artificial climate chamber were set as follows: photocycle was 12 h/day, LED lighting was used, photosynthetic activity E radiation was set at 1200 μmol·mol^{-1}·s^{-1}, and the temperature was constant at 25 °C. Drought stress simulation was carried out with a specific scheme. The seedlings were incubated at 40 °C during temperature treatment. For light treatment, the corresponding treatment group was exposed to a light intensity of 1200 μmol·mol^{-1}·s^{-1} for 24, 48, and 72 h, while the control group was exposed to 12 h of dark treatment and sampled at the half photocycle time. After processing, leaf specimens were quickly collected and stored in liquid nitrogen at −80 °C for subsequent RNA extraction.

Real-time PCR analysis was performed with 1 μL cDNA template, 10 μL SYBR Premix-Ex TaqTM II, 2 μL specific primers, and 7 μL ddH_2O. The reaction conditions were as follows: 95 °C for 30 s; 95 °C for 5 s; 60 °C for 30 s; 95 °C for 5 s; 60 °C for 60 s; and 50 °C for 30 s, for a total of 40 cycles. The internal reference gene was *GAPDH* (GenBank No. KX682032) [106]. The expression level of the target gene was calculated using the 2-AACt method, and the quantitative data were analyzed with the *t*-test in SPSS26. Statistical significance was determined when $p < 0.05$. GraphPad Prism8.0 was applied for data visualization. Table 2 lists the primer sequences used, with *GAPDH* serving as the reference gene.

Table 2. Primer sequences used for qRT-PCR analysis of each *CsBES1* genes.

Gene Name	Forward Primer (5′-3′)	Reverse Primer (5′-3′)
CsBES1.2	GGGTTAAGCAGATGGGTGGT	GTTCCGGTGAGGTCGGAATG
CsBES1.3	GGAGGAGGGAGGAGGAAGCC	GTGCCATCGGGTTCGACTGT
CsBES1.4	CAAACACTGCGACAACAACG	CGATAAGTGGTGCCATCGTC
CsBES1.6	TGTGGAGGCAACGTTGGTGA	ATTCAGGGTTGCGCCTTCCC
CsBES1.7	TGGACTCCTGGGCAAAGTGG	TCCCATGCCTTCACCAACCC
CsBES1.8	GGGTCAGCTTCAGCAAGTCC	TGGCAGCGTAACGTGATGAG
CsBES1.9	CGCCAACTATGGTCCCAACC	GCTTCACTGGGACGCTTTCA
CsBES1.10	GTCAGGGCTGGTTCCGTGTC	ATCCTCGATCCCAGGCCGAA
GAPDH	TTGGCATCGTTGAGGGTCT	CAGTGGGAACACGGAAAGC

4.8. RNA Extraction and Statistical Analysis

For the RNA extraction and cDNA synthesis experiment, we used Omega Bio-Tek's RNA extraction (Norcross, GA, USA) kit to extract total RNA from the sample. RNA extracted from Transgen was used as a template to synthesize cDNA for subsequent experiments. For the qRT-PCR experiment, the materials required are 1 μL cDNA, 2 μL specific primers (concentration 0.5 μM), 10 μL SYBR Premix Ex TaqTM II, and 7 μL ddH_2O. The reaction process is denaturation annealing and extension. Finally, the relative expression of the *CsBES1* gene was calculated using $2^{-\Delta\Delta CT}$ method, and one-way variance analysis and Duncan multiple comparison tests were performed using GraphPad Prism 9.0 software (software web site: https://www.graphpad.com/ (accessed on 1 November 2024)) [107]. All quantitative PCR experiments were repeated three times.

5. Conclusions

In this study, a total of 10 *CsBES1* genes were identified in *TGY*, and their properties, structural features, functional roles, relationships, and expression profiles were thoroughly analyzed. Among them, *CsBES1.3*, *CsBES1.4*, *CsBES1.5*, *CsBES1.6*, and *CsBES1.7*, which contain promoter regions, are more likely to play critical roles in responding to various abiotic stresses. The *BES1* proteins may interact with other signal transduction components, such as CYP90B1, SAUR15, ASK7, and BKI1, to regulate plant growth and development. Further analysis revealed that *CsBES1.9* and *CsBES1.4* exhibit the most significant expression changes under different stress conditions.

Specifically, the expression of *CsBES1.9* was most strongly upregulated under light stress, suggesting its potential role in light stress resistance. Nevertheless, the exact mechanisms by which *CsBES1* genes control the growth and development of *TGY* remain unclear and warrant further exploration. This study offers a comprehensive analysis of the expression patterns of *CsBES1* genes across various tissues and their responses to abiotic stress, shedding light on their potential roles in plant stress tolerance.

Author Contributions: Conceptualization, Y.Z. (Yanlin Zhang); Methodology, Y.Z. (Yanzi Zhang), W.C. and H.C.; Software, Z.Y. and S.C.; Validation, Y.Z. (Yanlin Zhang); Formal analysis, Y.Z. (Yanlin Zhang) and Q.L.; Investigation, X.W. All authors have read and agreed to the published version of the manuscript.

Funding: Fuiian Aariculture and Forestry Wniversity Forestry Peak Discipline Construction project. This research received no external funding.

Data Availability Statement: Data are contained within the article.

Conflicts of Interest: The authors declare no conflict of interest.

References

1. Li, L.; Deng, X.W. It runs in the family: Regulation of brassinosteroid signaling by the *BZR1-BES1* class of transcription factors. *Trends Plant Sci.* **2005**, *10*, 266–268. [CrossRef] [PubMed]
2. Wang, Z.Y.; Bai, M.Y.; Oh, E.; Zhu, J.Y. Brassinosteroid signaling network and regulation of photomorphogenesis. *Annu. Rev. Genet.* **2012**, *46*, 701–724. [CrossRef] [PubMed]
3. Anwar, A.; Liu, Y.; Dong, R.; Bai, L.; Yu, X.; Li, Y. The physiological and molecular mechanism of brassinosteroid in response to stress: A review. *Biol. Res.* **2018**, *51*, 46. [CrossRef] [PubMed]
4. Feng, Z.; Shi, H.; Lv, M.; Ma, Y.; Li, J. Protein farnesylation negatively regulates brassinosteroid signaling via reducing *BES1* stability in Arabidopsis thaliana. *J. Integr. Plant Biol.* **2021**, *63*, 1353–1366. [CrossRef] [PubMed]
5. Li, Q.; Xu, F.; Chen, Z.; Teng, Z.; Sun, K.; Li, X.; Yu, J.; Zhang, G.; Liang, Y.; Huang, X.; et al. Synergistic interplay of ABA and BR signal in regulating plant growth and adaptation. *Nat. Plants* **2021**, *7*, 1108–1118. [CrossRef]
6. González-García, M.P.; Vilarrasa-Blasi, J.; Zhiponova, M.; Divol, F.; Mora-García, S.; Russinova, E.; Caño-Delgado, A.I. Brassinosteroids control meristem size by promoting cell cycle progression in Arabidopsis roots. *Development* **2011**, *138*, 849–859. [CrossRef]
7. Planas-Riverola, A.; Gupta, A.; Betegón-Putze, I.; Bosch, N.; Ibañes, M.; Caño-Delgado, A.I. Brassinosteroid signaling in plant development and adaptation to stress. *Development* **2019**, *146*, dev151894. [CrossRef]
8. Mitchell, J.W.; Mandava, N.; Worley, J.F.; Plimmer, J.R.; Smith, M.V. Brassins--a new family of plant hormones from rape pollen. *Nature* **1970**, *225*, 1065–1066. [CrossRef]
9. Peres, A.; Soares, J.S.; Tavares, R.G.; Righetto, G.; Zullo, M.A.T.; Mandava, N.B.; Menossi, M. Brassinosteroids, the Sixth Class of Phytohormones: A Molecular View from the Discovery to Hormonal Interactions in Plant Development and Stress Adaptation. *Int. J. Mol. Sci.* **2019**, *20*, 331. [CrossRef]
10. Nolan, T.M.; Vukašinović, N.; Hsu, C.W.; Zhang, J.; Vanhoutte, I.; Shahan, R.; Taylor, I.W.; Greenstreet, L.; Heitz, M.; Afanassiev, A.; et al. Brassinosteroid gene regulatory networks at cellular resolution in the Arabidopsis root. *Science* **2023**, *379*, eadf4721. [CrossRef]
11. Kim, E.J.; Russinova, E. Brassinosteroid signalling. *Curr. Biol.* **2020**, *30*, R294–R298. [CrossRef] [PubMed]
12. Jiang, H.; Tang, B.; Xie, Z.; Nolan, T.; Ye, H.; Song, G.Y.; Walley, J.; Yin, Y. GSK3-like kinase BIN2 phosphorylates RD26 to potentiate drought signaling in Arabidopsis. *Plant J.* **2019**, *100*, 923–937. [CrossRef] [PubMed]
13. Ye, H.; Liu, S.; Tang, B.; Chen, J.; Xie, Z.; Nolan, T.M.; Jiang, H.; Guo, H.; Lin, H.-Y.; Li, L.; et al. RD26 mediates crosstalk between drought and brassinosteroid signalling pathways. *Nat. Commun.* **2017**, *8*, 14573. [CrossRef]
14. Bulgakov, V.P.; Avramenko, T.V. Linking Brassinosteroid and ABA Signaling in the Context of Stress Acclimation. *Int. J. Mol. Sci.* **2020**, *21*, 5108. [CrossRef]
15. Liu, Z.; Guo, J.T.; Li, T.; Xu, Y. Structure-based prediction of transcription factor binding sites using a protein-DNA docking approach. *Proteins Struct. Funct. Genet.* **2008**, *72*, 1114–1124. [CrossRef]
16. Century, K.; Reuber, T.L.; Ratcliffe, O.J. Regulating the regulators: The future prospects for transcription-factor-based agricultural biotechnology products. *Plant Physiol.* **2008**, *147*, 20–29. [CrossRef]
17. Chen, W.; Lv, M.; Wang, Y.; Wang, P.A.; Cui, Y.; Li, M.; Wang, R.; Gou, X.; Li, J. *BES1* is activated by EMS1-TPD1-SERK1/2-mediated signaling to control tapetum development in Arabidopsis thaliana. *Nat. Commun.* **2019**, *10*, 4164. [CrossRef]
18. Cui, X.Y.; Gao, Y.; Guo, J.; Yu, T.F.; Zheng, W.J.; Liu, Y.W.; Chen, J.; Xu, Z.S.; Ma, Y.Z. BES/BZR Transcription Factor TaBZR2 Positively Regulates Drought Responses by Activation of TaGST1. *Plant Physiol.* **2019**, *180*, 605–620. [CrossRef]
19. Su, D.; Xiang, W.; Wen, L.; Lu, W.; Shi, Y.; Liu, Y.; Li, Z. Genome-wide identification, characterization and expression analysis of *BES1* gene family in tomato. *BMC Plant Biol.* **2021**, *21*, 161. [CrossRef]
20. Kono, A.; Yin, Y. Updates on BES1/BZR1 Regulatory Networks Coordinating Plant Growth and Stress Responses. *Front. Plant Sci.* **2020**, *11*, 617162. [CrossRef]
21. Yin, Y.; Vafeados, D.; Tao, Y.; Yoshida, S.; Asami, T.; Chory, J. A new class of transcription factors mediates brassinosteroid-regulated gene expression in Arabidopsis. *Cell* **2005**, *120*, 249–259. [CrossRef] [PubMed]
22. Guo, H.; Ye, H.; Li, L.; Yin, Y. A family of receptor-like kinases are regulated by *BES1* and involved in plant growth in Arabidopsis thaliana. *Plant Signal Behav.* **2009**, *4*, 784–786. [CrossRef] [PubMed]
23. Reinhold, H.; Soyk, S.; Simková, K.; Hostettler, C.; Marafino, J.; Mainiero, S.; Vaughan, C.K.; Monroe, J.D.; Zeeman, S.C. β-amylase-like proteins function as transcription factors in Arabidopsis, controlling shoot growth and development. *Plant Cell* **2011**, *23*, 1391–1403. [CrossRef]
24. Lachowiec, J.; Mason, G.A.; Schultz, K.; Queitsch, C. Redundancy, Feedback, and Robustness in the Arabidopsis thaliana BZR/BEH Gene Family. *Front. Genet.* **2018**, *9*, 523. [CrossRef]
25. Otani, Y.; Tomonaga, Y.; Tokushige, K.; Kamimura, M.; Sasaki, A.; Nakamura, Y.; Nakamura, T.; Matsuo, T.; Okamoto, S. Expression profiles of four *BES1/BZR1* homologous genes encoding bHLH transcription factors in Arabidopsis. *J. Pestic. Sci.* **2020**, *45*, 95–104. [CrossRef]

26. Yin, Y.; Wang, Z.Y.; Mora-Garcia, S.; Li, J.; Yoshida, S.; Asami, T.; Chory, J. *BES1* accumulates in the nucleus in response to brassinosteroids to regulate gene expression and promote stem elongation. *Cell* **2002**, *109*, 181–191. [CrossRef]
27. Mueller, A.K.; Labaied, M.; Kappe, S.H.; Matuschewski, K. Genetically modified Plasmodium parasites as a protective experimental malaria vaccine. *Nature* **2005**, *433*, 164–167. [CrossRef]
28. Li, J.; Wen, J.; Lease, K.A.; Doke, J.T.; Tax, F.E.; Walker, J.C. BAK1, an Arabidopsis LRR receptor-like protein kinase, interacts with BRI1 and modulates brassinosteroid signaling. *Cell* **2002**, *110*, 213–222. [CrossRef]
29. Kim, T.W.; Guan, S.; Burlingame, A.L.; Wang, Z.Y. The CDG1 kinase mediates brassinosteroid signal transduction from BRI1 receptor kinase to *BSU1* phosphatase and GSK3-like kinase BIN2. *Mol. Cell* **2011**, *43*, 561–571. [CrossRef]
30. He, J.-X.; Gendron, J.M.; Yang, Y.; Li, J.; Wang, Z.-Y. The GSK3-like kinase BIN2 phosphorylates and destabilizes *BZR1*, a positive regulator of the brassinosteroid signaling pathway in Arabidopsis. *Proc. Natl. Acad. Sci. USA* **2002**, *99*, 10185–10190. [CrossRef]
31. Li, J.; Nam, K.H. Regulation of brassinosteroid signaling by a GSK3/SHAGGY-like kinase. *Science* **2002**, *295*, 1299–1301. [CrossRef] [PubMed]
32. Toledo-Ortiz, G.; Huq, E.; Quail, P.H. The Arabidopsis basic/helix-loop-helix transcription factor family. *Plant Cell* **2003**, *15*, 1749–1770. [CrossRef] [PubMed]
33. Wang, R.; Wang, R.; Liu, M.; Yuan, W.; Zhao, Z.; Liu, X.; Peng, Y.; Yang, X.; Sun, Y.; Tang, W. Nucleocytoplasmic trafficking and turnover mechanisms of BRASSINAZOLE RESISTANT1 in Arabidopsis thaliana. *Proc. Natl. Acad. Sci. USA* **2021**, *118*, e2101838118. [CrossRef]
34. Jiang, J.; Zhang, C.; Wang, X. A recently evolved isoform of the transcription factor *BES1* promotes brassinosteroid signaling and development in Arabidopsis thaliana. *Plant Cell* **2015**, *27*, 361–374. [CrossRef]
35. Saha, G.; Park, J.I.; Jung, H.J.; Ahmed, N.U.; Kayum, M.A.; Kang, J.G.; Nou, I.S. Molecular characterization of BZR transcription factor family and abiotic stress induced expression profiling in Brassica rapa. *Plant Physiol. Biochem.* **2015**, *92*, 92–104. [CrossRef]
36. Setsungnern, A.; Muñoz, P.; Pérez-Llorca, M.; Müller, M.; Thiravetyan, P.; Munné-Bosch, S. A defect in *BRI1-EMS-SUPPRESSOR 1* (*bes1*)-mediated brassinosteroid signaling increases photoinhibition and photo-oxidative stress during heat stress in Arabidopsis. *Plant Sci.* **2020**, *296*, 110470. [CrossRef]
37. Yan, M.Y.; Xie, D.L.; Cao, J.J.; Xia, X.J.; Shi, K.; Zhou, Y.H.; Zhou, J.; Foyer, C.H.; Yu, J.Q. Brassinosteroid-mediated reactive oxygen species are essential for tapetum degradation and pollen fertility in tomato. *Plant J.* **2020**, *102*, 931–947. [CrossRef]
38. Mecchia, M.A.; García-Hourquet, M.; Lozano-Elena, F.; Planas-Riverola, A.; Blasco-Escamez, D.; Marquès-Bueno, M.; Mora-García, S.; Caño-Delgado, A.I. The *BES1/BZR1*-family transcription factor M*pBES1* regulates cell division and differentiation in Marchantia polymorpha. *Curr. Biol.* **2021**, *31*, 4860–4869.e4868. [CrossRef]
39. Korwin Krukowski, P.; Visentin, I.; Russo, G.; Minerdi, D.; Bendahmane, A.; Schubert, A.; Cardinale, F. Transcriptome Analysis Points to *BES1* as a Transducer of Strigolactone Effects on Drought Memory in Arabidopsis thaliana. *Plant Cell Physiol.* **2022**, *63*, 1873–1889. [CrossRef]
40. Sun, Z.; Liu, X.; Zhu, W.; Lin, H.; Chen, X.; Li, Y.; Ye, W.; Yin, Z. Molecular Traits and Functional Exploration of *BES1* Gene Family in Plants. *Int. J. Mol. Sci.* **2022**, *23*, 4242. [CrossRef]
41. Yang, J.; Wu, Y.; Li, L.; Li, C. Comprehensive analysis of the *BES1* gene family and its expression under abiotic stress and hormone treatment in Populus trichocarpa. *Plant Physiol. Biochem.* **2022**, *173*, 1–13. [CrossRef] [PubMed]
42. Chen, J.; Nolan, T.M.; Ye, H.; Zhang, M.; Tong, H.; Xin, P.; Chu, J.; Chu, C.; Li, Z.; Yin, Y. Arabidopsis WRKY46, WRKY54, and WRKY70 Transcription Factors Are Involved in Brassinosteroid-Regulated Plant Growth and Drought Responses. *Plant Cell* **2017**, *29*, 1425–1439. [CrossRef] [PubMed]
43. Franklin, K.A.; Lee, S.H.; Patel, D.; Kumar, S.V.; Spartz, A.K.; Gu, C.; Ye, S.; Yu, P.; Breen, G.; Cohen, J.D.; et al. PHYTOCHROME-INTERACTING FACTOR 4 (PIF4) regulates auxin biosynthesis at high temperature. *Proc. Natl. Acad. Sci. USA* **2011**, *108*, 20231–20235. [CrossRef] [PubMed]
44. Song, X.; Ma, X.; Li, C.; Hu, J.; Yang, Q.; Wang, T.; Wang, L.; Wang, J.; Guo, D.; Ge, W.; et al. Comprehensive analyses of the *BES1* gene family in Brassica napus and examination of their evolutionary pattern in representative species. *BMC Genom.* **2018**, *19*, 346. [CrossRef]
45. Liu, Z.; Qanmber, G.; Lu, L.; Qin, W.; Liu, J.; Li, J.; Ma, S.; Yang, Z.; Yang, Z. Genome-wide analysis of *BES1* genes in Gossypium revealed their evolutionary conserved roles in brassinosteroid signaling. *Sci. China Life Sci.* **2018**, *61*, 1566–1582. [CrossRef]
46. Feng, W.; Zhang, H.; Cao, Y.; Liu, Y.; Zhao, Y.; Sun, F.; Yang, Q.; Zhang, X.; Zhang, Y.; Wang, Y.; et al. Maize Zm*BES1/BZR1*-1 transcription factor negatively regulates drought tolerance. *Plant Physiol. Biochem.* **2023**, *205*, 108188. [CrossRef]
47. Gao, Y.; Hu, J.; Zhao, T.; Xu, X.; Jiang, J.; Li, J. Genome-wide Identification and Expression Pattern Analysis of BRI1-EMS–suppressor Transcription Factors in Tomato under Abiotic Stresses. *J. Am. Soc. Hortic. Sci.* **2018**, *143*, 84–90. [CrossRef]
48. Song, X.; Li, Y.; Hou, X. Genome-wide analysis of the AP2/ERF transcription factor superfamily in Chinese cabbage (*Brassica rapa* ssp. *pekinensis*). *BMC Genom.* **2013**, *14*, 573. [CrossRef]
49. Ma, S.; Ji, T.; Liang, M.; Li, S.; Tian, Y.; Gao, L. Genome-Wide Identification, Structural, and Gene Expression Analysis of *BRI1-EMS-Suppressor 1* Transcription Factor Family in Cucumis sativus. *Front. Genet.* **2020**, *11*, 583996. [CrossRef]

50. Xie, L.; Yang, C.; Wang, X. Brassinosteroids can regulate cellulose biosynthesis by controlling the expression of CESA genes in Arabidopsis. *J. Exp. Bot.* **2011**, *62*, 4495–4506. [CrossRef]
51. Ye, Q.; Zhu, W.; Li, L.; Zhang, S.; Yin, Y.; Ma, H.; Wang, X. Brassinosteroids control male fertility by regulating the expression of key genes involved in Arabidopsis anther and pollen development. *Proc. Natl. Acad. Sci. USA* **2010**, *107*, 6100–6105. [CrossRef] [PubMed]
52. Lozano-Durán, R.; Macho, A.P.; Boutrot, F.; Segonzac, C.; Somssich, I.E.; Zipfel, C. The transcriptional regulator *BZR1* mediates trade-off between plant innate immunity and growth. *Elife* **2013**, *2*, e00983. [CrossRef] [PubMed]
53. Li, X.; Liu, L.; Sun, S.; Li, Y.; Jia, L.; Ye, S.; Yu, Y.; Dossa, K.; Luan, Y. Leaf-transcriptome profiles of phoebe bournei provide insights into temporal drought stress responses. *Front. Plant Sci.* **2022**, *13*, 1010314. [CrossRef]
54. Reygaert, W.C. The antimicrobial possibilities of green tea. *Front. Microbiol.* **2014**, *5*, 434. [CrossRef]
55. Huang, Z.; Sanaeifar, A.; Tian, Y.; Liu, L.; Zhang, D.; Wang, H.; Ye, D.; Li, X. Improved generalization of spectral models associated with Vis-NIR spectroscopy for determining the moisture content of different tea leaves. *J. Food Eng.* **2021**, *293*, 110374. [CrossRef]
56. Zeng, L.; Zhou, Y.; Fu, X.; Mei, X.; Cheng, S.; Gui, J.; Dong, F.; Tang, J.; Ma, S.; Yang, Z. Does oolong tea (*Camellia sinensis*) made from a combination of leaf and stem smell more aromatic than leaf-only tea? Contribution of the stem to oolong tea aroma. *Food Chem.* **2017**, *237*, 488–498. [CrossRef]
57. Hara, Y. Elucidation of Physiological Functions of Tea Catechins and Their Practical Applications. *J. Food Drug Anal.* **2012**, *20*, 296–300. [CrossRef]
58. Zhang, S.; Takano, J.; Murayama, N.; Tominaga, M.; Abe, T.; Park, I.; Seol, J.; Ishihara, A.; Tanaka, Y.; Yajima, K.; et al. Subacute Ingestion of Caffeine and Oolong Tea Increases Fat Oxidation without Affecting Energy Expenditure and Sleep Architecture: A Randomized, Placebo-Controlled, Double-Blinded Cross-Over Trial. *Nutrients* **2020**, *12*, 3671. [CrossRef]
59. Wang, W.; Xin, H.; Wang, M.; Ma, Q.; Wang, L.; Kaleri, N.A.; Wang, Y.; Li, X. Transcriptomic Analysis Reveals the Molecular Mechanisms of Drought-Stress-Induced Decreases in Camellia sinensis Leaf Quality. *Front. Plant Sci.* **2016**, *7*, 385. [CrossRef]
60. Yu, S.; Li, P.; Zhao, X.; Tan, M.; Ahmad, M.Z.; Xu, Y.; Tadege, M.; Zhao, J. CsTCPs regulate shoot tip development and catechin biosynthesis in tea plant (*Camellia sinensis*). *Hortic. Res.* **2021**, *8*, 104. [CrossRef]
61. Zhang, Q.; Shi, Y.; Ma, L.; Yi, X.; Ruan, J. Metabolomic analysis using ultra-performance liquid chromatography-quadrupole-time of flight mass spectrometry (UPLC-Q-TOF MS) uncovers the effects of light intensity and temperature under shading treatments on the metabolites in tea. *PLoS ONE* **2014**, *9*, e112572. [CrossRef] [PubMed]
62. Zheng, C.; Ma, J.Q.; Ma, C.L.; Shen, S.Y.; Liu, Y.F.; Chen, L. Regulation of Growth and Flavonoid Formation of Tea Plants (*Camellia sinensis*) by Blue and Green Light. *J. Agric. Food Chem.* **2019**, *67*, 2408–2419. [CrossRef] [PubMed]
63. Li, Q.F.; Huang, L.C.; Wei, K.; Yu, J.W.; Zhang, C.Q.; Liu, Q.Q. Light involved regulation of *BZR1* stability and phosphorylation status to coordinate plant growth in Arabidopsis. *Biosci. Rep.* **2017**, *37*, BSR20170069. [CrossRef] [PubMed]
64. Kim, B.; Jeong, Y.J.; Corvalán, C.; Fujioka, S.; Cho, S.; Park, T.; Choe, S. Darkness and gulliver2/phyB mutation decrease the abundance of phosphorylated *BZR1* to activate brassinosteroid signaling in Arabidopsis. *Plant J.* **2014**, *77*, 737–747. [CrossRef]
65. Roy, S.W.; Penny, D. A very high fraction of unique intron positions in the intron-rich diatom Thalassiosira pseudonana indicates widespread intron gain. *Mol. Biol. Evol.* **2007**, *24*, 1447–1457. [CrossRef]
66. Kolodny, R. Searching protein space for ancient sub-domain segments. *Curr. Opin. Struct. Biol.* **2021**, *68*, 105–112. [CrossRef]
67. Zhou, Q.; Zhao, M.; Xing, F.; Mao, G.; Wang, Y.; Dai, Y.; Niu, M.; Yuan, H. Identification and Expression Analysis of CAMTA Genes in Tea Plant Reveal Their Complex Regulatory Role in Stress Responses. *Front. Plant Sci.* **2022**, *13*, 910768. [CrossRef]
68. Wang, Y.; Tang, H.; Debarry, J.D.; Tan, X.; Li, J.; Wang, X.; Lee, T.H.; Jin, H.; Marler, B.; Guo, H.; et al. MCScanX: A toolkit for detection and evolutionary analysis of gene synteny and collinearity. *Nucleic Acids Res.* **2012**, *40*, e49. [CrossRef]
69. Panchy, N.; Lehti-Shiu, M.; Shiu, S.H. Evolution of Gene Duplication in Plants. *Plant Physiol.* **2016**, *171*, 2294–2316. [CrossRef]
70. Holub, E.B. The arms race is ancient history in Arabidopsis, the wildflower. *Nat. Rev. Genet.* **2001**, *2*, 516–527. [CrossRef]
71. Xiong, M.; Yu, J.; Wang, J.; Gao, Q.; Huang, L.; Chen, C.; Zhang, C.; Fan, X.; Zhao, D.; Liu, Q.-Q.; et al. Brassinosteroids regulate rice seed germination through the *BZR1*-RAmy3D transcriptional module. *Plant Physiol.* **2022**, *189*, 402–418. [CrossRef] [PubMed]
72. Lescot, M.; Déhais, P.; Thijs, G.; Marchal, K.; Moreau, Y.; Van de Peer, Y.; Rouzé, P.; Rombauts, S. PlantCARE, a database of plant cis-acting regulatory elements and a portal to tools for in silico analysis of promoter sequences. *Nucleic Acids Res.* **2002**, *30*, 325–327. [CrossRef] [PubMed]
73. Gendron, J.M.; Wang, Z.Y. Multiple mechanisms modulate brassinosteroid signaling. *Curr. Opin. Plant Biol.* **2007**, *10*, 436–441. [CrossRef]
74. Wang, X.; Niu, Y.; Zheng, Y. Multiple Functions of MYB Transcription Factors in Abiotic Stress Responses. *Int. J. Mol. Sci.* **2021**, *22*, 6125. [CrossRef]
75. Kim, S.H.; Lee, S.H.; Park, T.K.; Tian, Y.; Yu, K.; Lee, B.H.; Bai, M.Y.; Cho, S.J.; Kim, T.W. Comparative analysis of *BZR1/BES1* family transcription factors in Arabidopsis. *Plant J.* **2024**, *117*, 747–765. [CrossRef]
76. Li, M.; Liu, C.; Hepworth, S.R.; Ma, C.; Li, H.; Li, J.; Wang, S.M.; Yin, H. SAUR15 interaction with BRI1 activates plasma membrane H+-ATPase to promote organ development of Arabidopsis. *Plant Physiol.* **2022**, *189*, 2454–2466. [CrossRef]

77. Kojima, K.; Ichijo, H.; Naguro, I. Molecular functions of ASK family in diseases caused by stress-induced inflammation and apoptosis. *J. Biochem.* **2021**, *169*, 395–407. [CrossRef]
78. Ohnishi, T.; Godza, B.; Watanabe, B.; Fujioka, S.; Hategan, L.; Ide, K.; Shibata, K.; Yokota, T.; Szekeres, M.; Mizutani, M. CYP90A1/CPD, a brassinosteroid biosynthetic cytochrome P450 of Arabidopsis, catalyzes C-3 oxidation. *J. Biol. Chem.* **2012**, *287*, 31551–31560. [CrossRef]
79. Demuth, J.P.; Hahn, M.W. The life and death of gene families. *Bioessays* **2009**, *31*, 29–39. [CrossRef]
80. Oudelaar, A.M.; Higgs, D.R. The relationship between genome structure and function. *Nat. Rev. Genet.* **2021**, *22*, 154–168. [CrossRef]
81. Li, L.; Yu, X.; Thompson, A.; Guo, M.; Yoshida, S.; Asami, T.; Chory, J.; Yin, Y. Arabidopsis MYB30 is a direct target of *BES1* and cooperates with *BES1* to regulate brassinosteroid-induced gene expression. *Plant J.* **2009**, *58*, 275–286. [CrossRef] [PubMed]
82. Saito, M.; Kondo, Y.; Fukuda, H. *BES1* and *BZR1* Redundantly Promote Phloem and Xylem Differentiation. *Plant Cell Physiol.* **2018**, *59*, 590–600. [CrossRef] [PubMed]
83. Roy, S.W.; Gilbert, W. The evolution of spliceosomal introns: Patterns, puzzles and progress. *Nat. Rev. Genet.* **2006**, *7*, 211–221. [CrossRef] [PubMed]
84. Song, X.M.; Huang, Z.N.; Duan, W.K.; Ren, J.; Liu, T.K.; Li, Y.; Hou, X.L. Genome-wide analysis of the bHLH transcription factor family in Chinese cabbage (*Brassica rapa* ssp. *pekinensis*). *Mol. Genet. Genom.* **2014**, *289*, 77–91. [CrossRef]
85. Cao, X.; Khaliq, A.; Lu, S.; Xie, M.; Ma, Z.; Mao, J.; Chen, B. Genome-wide identification and characterization of the *BES1* gene family in apple (*Malus domestica*). *Plant Biol.* **2020**, *22*, 723–733. [CrossRef]
86. Cheng, M.; Yuan, H.; Wang, R.; Wang, W.; Zhang, L.; Fan, F.; Li, S. Identification and characterization of *BES1* genes involved in grain size development of *Oryza sativa* L. *Int. J. Biol. Macromol.* **2023**, *253*, 127327. [CrossRef]
87. Cao, X.; Ma, W.; Zeng, F.; Cheng, Y.; Ma, Z.; Mao, J.; Chen, B. Grape *BES1* transcription factor gene Vv*BES1*-3 confers salt tolerance in transgenic Arabidopsis. *Gene* **2023**, *854*, 147059. [CrossRef]
88. Cartharius, K.; Frech, K.; Grote, K.; Klocke, B.; Haltmeier, M.; Klingenhoff, A.; Frisch, M.; Bayerlein, M.; Werner, T. MatInspector and beyond: Promoter analysis based on transcription factor binding sites. *Bioinformatics* **2005**, *21*, 2933–2942. [CrossRef]
89. Yang, C.J.; Zhang, C.; Lu, Y.N.; Jin, J.Q.; Wang, X.L. The mechanisms of brassinosteroids' action: From signal transduction to plant development. *Mol. Plant* **2011**, *4*, 588–600. [CrossRef]
90. Ibañez, C.; Delker, C.; Martinez, C.; Bürstenbinder, K.; Janitza, P.; Lippmann, R.; Ludwig, W.; Sun, H.; James, G.V.; Klecker, M.; et al. Brassinosteroids Dominate Hormonal Regulation of Plant Thermomorphogenesis via *BZR1*. *Curr. Biol.* **2018**, *28*, 303–310.e303. [CrossRef]
91. Yang, M.; Li, C.; Cai, Z.; Hu, Y.; Nolan, T.; Yu, F.; Yin, Y.; Xie, Q.; Tang, G.; Wang, X. SINAT E3 Ligases Control the Light-Mediated Stability of the Brassinosteroid-Activated Transcription Factor *BES1* in Arabidopsis. *Dev. Cell* **2017**, *41*, 47–58.e44. [CrossRef] [PubMed]
92. Oh, E.; Zhu, J.Y.; Wang, Z.Y. Interaction between *BZR1* and PIF4 integrates brassinosteroid and environmental responses. *Nat. Cell Biol.* **2012**, *14*, 802–809. [CrossRef]
93. Wang, W.; Lu, X.; Li, L.; Lian, H.; Mao, Z.; Xu, P.; Guo, T.; Xu, F.; Du, S.; Cao, X.; et al. Photoexcited CRYPTOCHROME1 Interacts with Dephosphorylated *BES1* to Regulate Brassinosteroid Signaling and Photomorphogenesis in Arabidopsis. *Plant Cell* **2018**, *30*, 1989–2005. [CrossRef] [PubMed]
94. Heijde, M.; Ulm, R. UV-B photoreceptor-mediated signalling in plants. *Trends Plant Sci.* **2012**, *17*, 230–237. [CrossRef] [PubMed]
95. Jenkins, G.I. Structure and function of the UV-B photoreceptor UVR8. *Curr. Opin. Struct. Biol.* **2014**, *29*, 52–57. [CrossRef] [PubMed]
96. Tilbrook, K.; Arongaus, A.B.; Binkert, M.; Heijde, M.; Yin, R.; Ulm, R. The UVR8 UV-B Photoreceptor: Perception, Signaling and Response. *Arab. Book* **2013**, *11*, e0164. [CrossRef]
97. Rizzini, L.; Favory, J.J.; Cloix, C.; Faggionato, D.; O'Hara, A.; Kaiserli, E.; Baumeister, R.; Schäfer, E.; Nagy, F.; Jenkins, G.I.; et al. Perception of UV-B by the Arabidopsis UVR8 protein. *Science* **2011**, *332*, 103–106. [CrossRef]
98. Huang, X.; Yang, P.; Ouyang, X.; Chen, L.; Deng, X.W. Photoactivated UVR8-COP1 module determines photomorphogenic UV-B signaling output in Arabidopsis. *PLoS Genet.* **2014**, *10*, e1004218. [CrossRef]
99. Liang, T.; Mei, S.; Shi, C.; Yang, Y.; Peng, Y.; Ma, L.; Wang, F.; Li, X.; Huang, X.; Yin, Y.; et al. UVR8 Interacts with *BES1* and BIM1 to Regulate Transcription and Photomorphogenesis in Arabidopsis. *Dev. Cell* **2018**, *44*, 512–523.e515. [CrossRef]
100. Han, X.; Zhang, J.; Han, S.; Chong, S.L.; Meng, G.; Song, M.; Wang, Y.; Zhou, S.; Liu, C.; Lou, L.; et al. The chromosome-scale genome of Phoebe bournei reveals contrasting fates of terpene synthase (TPS)-a and TPS-b subfamilies. *Plant Commun.* **2022**, *3*, 100410. [CrossRef]
101. Gasteiger, E.; Gattiker, A.; Hoogland, C.; Ivanyi, I.; Appel, R.D.; Bairoch, A. ExPASy: The proteomics server for in-depth protein knowledge and analysis. *Nucleic Acids Res.* **2003**, *31*, 3784–3788. [CrossRef]
102. Chen, C.; Wu, Y.; Li, J.; Wang, X.; Zeng, Z.; Xu, J.; Liu, Y.; Feng, J.; Chen, H.; He, Y.; et al. TBtools-II: A "one for all, all for one" bioinformatics platform for biological big-data mining. *Molecular Plant* **2023**, *16*, 1733–1742. [CrossRef]

103. Cantalapiedra, C.P.; Hernández-Plaza, A.; Letunic, I.; Bork, P.; Huerta-Cepas, J. eggNOG-mapper v2: Functional Annotation, Orthology Assignments, and Domain Prediction at the Metagenomic Scale. *Mol. Biol. Evol.* **2021**, *38*, 5825–5829. [CrossRef] [PubMed]
104. Kanehisa, M.; Furumichi, M.; Tanabe, M.; Sato, Y.; Morishima, K. KEGG: New perspectives on genomes, pathways, diseases and drugs. *Nucleic Acids Res.* **2017**, *45*, D353–D361. [CrossRef] [PubMed]
105. Otasek, D.; Morris, J.H.; Bouças, J.; Pico, A.R.; Demchak, B. Cytoscape Automation: Empowering workflow-based network analysis. *Genome Biol.* **2019**, *20*, 185. [CrossRef] [PubMed]
106. Winters, M.; Eskes, M.; Weir, A.; Moen, M.H.; Backx, F.J.; Bakker, E.W. Treatment of medial tibial stress syndrome: A systematic review. *Sports Med.* **2013**, *43*, 1315–1333. [CrossRef] [PubMed]
107. Day, R.W.; Quinn, G.P. Comparisons of Treatments After an Analysis of Variance in Ecology. *Ecol. Monogr.* **1989**, *59*, 433–463. [CrossRef]

Disclaimer/Publisher's Note: The statements, opinions and data contained in all publications are solely those of the individual author(s) and contributor(s) and not of MDPI and/or the editor(s). MDPI and/or the editor(s) disclaim responsibility for any injury to people or property resulting from any ideas, methods, instructions or products referred to in the content.

plants

MDPI

Article

Nitrogen Fertilization Coupled with Zinc Foliar Applications Modulate the Production, Quality, and Stress Response of *Sideritis cypria* Plants Grown Hydroponically Under Excess Copper Concentrations

Nikolaos Tzortzakis *, Giannis Neofytou and Antonios Chrysargyris

Department of Agricultural Sciences, Biotechnology and Food Science, Cyprus University of Technology, 3603 Limassol, Cyprus; gp.neofytou@edu.cut.ac.cy (G.N.); a.chrysargyris@cut.ac.cy (A.C.)
* Correspondence: nikolaos.tzortzakis@cut.ac.cy

Abstract: The demand for medicinal and aromatic plants (MAPs) has grown significantly in recent years, due to their therapeutic value. Among these, *Sideritis cypria* Post is a promising yet under-evaluated species. Existing research assessing the effects of nitrogen (N) fertilization, zinc (Zn) foliar applications, and toxic copper (Cu) concentrations often overlooks MAPs such as *S. cypria*. Additionally, the interactions among these parameters, as well as their combined roles in MAPs plant physiology and secondary metabolite biosynthesis, have yet to be fully elucidated. In this study, hydroponically grown *S. cypria* plants were cultivated using nutrient solutions (NSs) with different N (75, 150, and 300 mg L^{-1}) and Cu (5 and 100 μM) levels, combined with foliar spraying (0 and 1.74 mM Zn), to evaluate the growth, mineral uptake, secondary metabolites production and stress response. N levels at 75 and 150 mg L^{-1} resulted in increased dry matter content, whereas fresh biomass production was preserved. Foliar Zn applications enhanced chlorophylls and antioxidants, contingent upon N and Cu in the NS. Increased N accumulation was observed via the increase in N in the NS, while foliar Zn enhanced its uptake at moderate N levels. Excess Cu stimulated its accumulation, while a reduction was observed with foliar Zn at low and high N levels. Excess Cu increased lipid peroxidation (MDA) at low and moderate N in the NS, while foliar Zn decreased both MDA and hydrogen peroxide, contingent upon Cu and N levels. Low-to-moderate N in the NS can be applied under excess Cu without compromising the yield, quality, and safety of *S. cypria* plants, while foliar Zn can modulate the stress response of plants under excess Cu and the production of secondary metabolites. These results may be utilized for optimizing nutrient management strategies for the cultivation of MAPs, contributing to conservation efforts by supporting the cultivation of endemic species like *S. cypria*, considering the potential benefits of Zn foliar applications under Cu-contaminated conditions.

Keywords: copper stress; soilless culture; micronutrients; antioxidant capacity; mineral uptake

1. Introduction

Consumer demand for medicinal and aromatic plants (MAPs) has increased over the years due to the awareness of their potential benefits. To meet the growing demand, the agro-industrial and pharmaceutical sector require consistent yield and quality [1,2]. However, various factors, such as climatic conditions, seasonal changes, pathogen levels,

pests, and the status of soils, affect the amount of secondary metabolites produced by MAPs, complicating the standardization of their cultivation [3]. To address this, protected cultivation and soilless culture systems (SCSs) offer effective strategies for ensuring stable MAP production [4]. In SCS, a crucial parameter is the optimization of the nutrient solution composition, which can have a substantial impact on MAPs' growth. Furthermore, tailor-made fertilization strategies can be critical for the synthesis of components with medicinal attributes [5].

The genus *Sideritis*, belonging to the Lamiaceae family, encompasses 150 species commonly known as "ironwort" or "mountain tea" [6,7]. These species are primarily found in the Mediterranean region, and they are recognized for their medicinal properties due to the presence of chemical components such terpenes, flavonoids, and coumarins [8]. Among these species, *Sideritis cypria* Post, a perennial herb endemic to Cyprus, is traditionally used against stomach disorders, headaches, and the common cold, as infusions; however, it largely remains underexplored both commercially and scientifically [9,10]. The lack of comprehensive scientific research presents an obstacle to unlocking the full potential of various MAPs [4], including *S. cypria*, as a limited number of studies have been conducted to investigate its cultivation [10,11].

Nitrogen (N) fertilization is often associated with increased yields and is widely employed in the cultivation of various MAPs [12]. In addition, N is critical in the chemical and medicinal composition of MAPs [13]. As a fundamental constituent of proteins, chlorophyll, amino acids, and alkaloids, N directly influences key bioactive compounds [14]. Amino acids, in particular, serve in the biosynthesis of numerous essential oil (EO) constituents, which contribute to the medicinal properties of MAPs [15]. However, excess N application often leads to N losses (e.g., nitrate leaching), increased nitrous oxide emissions, and soil degradation [16,17]. In addition, increased and unbalanced N fertilization may negatively affect the plant's metabolism and medicinal status, as evidenced in *Ocimum basilicum* L. [18] and *Salvia miltiorrhiza* Bunge [19]. Nonetheless, N deprivation exerts a detrimental effect on plant physiology, restricting photosynthesis, transpiration, and stomatal conductance, while N-starved plants may also exhibit increased synthesis of secondary metabolites [3].

Soil pollution by heavy metals has become a significant environmental concern, particularly due to the heavy industrialization and agrochemicals use [20]. This has led to the accumulation of heavy metals such as copper (Cu). Copper is an essential plant micronutrient, constituting a redox-active transition element and influencing photosynthesis, C and N metabolism, respiration, and oxidative stress protection [21]. Although essential, in excess, Cu can become hazardous to plants, leading to phytotoxicity [22,23]. Elevated Cu can disrupt plant growth by interfering with metabolic processes due to the increased production of reactive oxygen species (ROS), influencing membrane function and permeability [24]. Damage occurs due to redox cycles between Cu^{2+} and Cu^{+}, inducing the production of hydroxyl radicals. Additionally, oxidative damage occurs as copper binds to proteins, disrupting cellular processes [25]. Interestingly, Cu is also involved in the nitrogen metabolism, where optimal concentrations enhance the plants' utilization of N in soils [26]. However, increased levels of Cu may also undermine the uptake of ammonium (NH_4^+) and nitrate (NO_3^-) through the inhibition of N assimilation-related enzymatic activities [27].

Zinc (Zn) is another essential micronutrient that has roles in the structure and regulation of various enzymes and proteins via its influence in the carbohydrate metabolism, photosynthesis, protein metabolism, auxin metabolism, and the integrity of biological membranes [28,29]. Zinc can alleviate the harmful effects of environmental stressors, as it increases active oxygen scavenging substances and reduces lipid peroxidation [30,31]. Interestingly, Zn also exhibits antagonistic interactions with Cu, which significantly influences their uptake, bioavailability, and quantitative status [29]. For this reason, the interaction be-

tween Zn and Cu may reduce the effects of Cu toxicity [25]. Moreover, the co-supply of Zn and N can prompt increased root-to-shoot translocation and distribution of both nutrients, significantly influencing plant growth [32]. In addition, agronomic Zn biofortification has become more prevalent, as a means of overcoming human health concerns related to Zn deficiency [33].

While N is essential for biomass production and enzymatic functions, in the presence of excessive Cu, its uptake is disrupted, and oxidative stress is induced. Zinc may alleviate this response, and although excess N levels may enhance its mobility, they could also exacerbate Cu toxicity under certain conditions. Despite their importance, the interactions between these micronutrients and their collective effect on plant growth, in conjunction with variable N fertilization, remain relatively overlooked, particularly in under-researched species such as *S. cypria*. The objective of this study was to investigate the impact of various N levels in the nutrient solution on the growth and physiology of *S. cypria* plants grown in soilless cultivation systems, while simultaneously investigating the impact of elevated Cu concentrations and foliar Zn applications. As this examination explores these effects, it is hypothesized that excess Cu in the hydroponic NSs may negatively affect the growth and physiological performance of *S. cypria*, while combined foliar Zn applications are expected to mitigate Cu-induced stress. In addition, varying N levels are expected to modulate the effects of both Cu and Zn, potentially influencing the overall plant growth, nutrient status, and secondary metabolite production.

2. Results

Table 1 presents an overview of the effect of the different N levels (N), Zn foliar applications (Zn), and Cu applications (Cu); their first-order interactions (N × Cu, N × Zn, Cu × Zn); and their second-order interaction (N × Cu × Zn) on *S. cypria* plant growth and physiology. N levels affected Chl a, Total Chl, Total Car, leaf Zn, and root Cu at $p < 0.05$. Also, N levels affected SPAD; DM; Fv Fm^{-1}; leaf N, K, Na, and Fe; root N, P, K, Na, and Zn; phenols; flavonoids; and H_2O_2 at $p < 0.001$. Cu impacted flavonoids at $p < 0.01$. And it impacted DM; Fv Fm^{-1}; leaf Na and Cu; and root N, K, Na, and Cu at $p < 0.001$. Zn impacted root Fe at $p < 0.05$; and DM, leaf N, and root Zn at $p < 0.01$. It also impacted leaf P and Na; root P, K, and Na; phenols; DPPH; FRAP; ABTS; flavonoids; and MDA at $p < 0.001$. The N × Cu interaction affected Total Chl, leaf Fe, FRAP, and H_2O_2 at $p < 0.05$; Chl a and root K, Na, Cu, and Zn at $p < 0.01$; and Total Car, leaf N and Na, root N and P, phenols, DPPH, ABTS, flavonoids, and MDA at $p < 0.001$. The N × Zn interaction affected leaf Cu and Zn, and root Cu and Fe at $p < 0.05$; Fv Fm^{-1}, Chl b, and leaf N at $p < 0.01$; and Chl a, Total Chl, Total Car, leaf P and Na, root macronutrients and Zn, phenols, DPPH, FRAP, ABTS, flavonoids, and H_2O_2 at $p < 0.001$. The Cu × Zn interaction affected Chl a, Total Chl, Total Car, leaf Cu, FRAP, and MDA at $p < 0.05$; and root N and K, phenols, DPPH, and ABTS at $p < 0.001$. The N × Cu × Zn interaction affected Chl b, root P, and Cu at $p < 0.05$; Total Chl, root Zn, and ABTS at $p < 0.01$; and Chl a, Total Car, leaf Cu, root K and Na, phenols, DPPH, FRAP, flavonoids, and H_2O_2 at $p < 0.001$.

The effects of the examined parameters on *S. cypria* upper biomass production (fresh weight, FW) and dry matter content (DM) are presented in Figure 1. Plant FW remained unaffected by the examined parameters. However, DM was significantly influenced by the examined parameters. The lowest values were attained under the application of N300 and foliar Zn (1.74 mM). However, these values did not differ significantly with no foliar Zn (0 mM) and Cu at 100 μM. Plants grown using the N75 NS and 100 μM Cu exhibited decreased DM with the application of foliar Zn, compared to foliar spraying with pure water. Finally, plants grown using the N150 exhibited decreased DM with the combined application of Cu at 100 μM and foliar Zn, compared to plants treated with Cu at 5 μM.

Table 1. The effect of N levels (N), Cu application (Cu), and Zn foliar application (Zn); their first-order interactions (N × Cu, N × Zn, and Cu × Zn); and their second-order interaction (N × Cu × Zn).

	N	Cu	Zn	N × Cu	N × Zn	Cu × Zn	N × Cu × Zn
FW (g)	ns	ns	ns	ns	ns	ns	ns
DM (%)	***	***	**	ns	ns	ns	ns
SPAD	ns	ns	ns	ns	ns	ns	ns
Fv Fm^{-1}	***	***	ns	ns	**	ns	ns
Chl a (mg g^{-1})	*	ns	ns	**	***	*	***
Chl b (mg g^{-1})	ns	ns	ns	ns	**	ns	*
Total Chl (mg g^{-1})	*	ns	ns	*	***	*	**
Total Car (mg g^{-1})	*	ns	ns	***	***	*	***
Leaf N (g kg^{-1})	***	ns	**	***	**	ns	ns
Leaf P (g kg^{-1})	ns	ns	***	ns	***	ns	ns
Leaf K (g kg^{-1})	***	ns	ns	ns	ns	ns	ns
Leaf Na (g kg^{-1})	***	***	***	***	***	ns	ns
Leaf Fe (mg kg^{-1})	***	ns	ns	*	ns	ns	ns
Leaf Cu (mg kg^{-1})	ns	***	ns	ns	*	*	***
Leaf Zn (mg kg^{-1})	*	ns	ns	ns	*	ns	ns
Root N (g kg^{-1})	***	***	ns	***	***	***	ns
Root P (g kg^{-1})	***	ns	***	***	***	ns	*
Root K (g kg^{-1})	***	***	***	**	***	***	***
Root Na (g kg^{-1})	***	***	***	**	***	ns	***
Root Fe (mg kg^{-1})	ns	ns	*	ns	*	ns	ns
Root Cu (mg kg^{-1})	*	***	ns	**	*	ns	*
Root Zn (mg kg^{-1})	***	ns	**	**	***	ns	**
Phenols (mg GAE g^{-1})	***	ns	***	***	***	***	***
DPPH (mg Trolox g^{-1})	ns	ns	***	***	***	***	***
FRAP (mg Trolox g^{-1})	ns	ns	***	*	***	*	***
ABTS (mg Trolox g^{-1})	ns	ns	***	***	***	***	**
Flavonoids (mg Rutin g^{-1})	***	**	***	***	***	ns	***
H_2O_2 (μmol g^{-1})	***	ns	ns	*	***	ns	***
MDA (nmol g^{-1})	ns	Ns	***	***	ns	*	ns

*** Significant at $p < 0.001$; ** significant at $p < 0.01$; * significant at $p < 0.05$; ns, not significant, according to three-way ANOVA. Fresh weight (FW); dry matter (DM); chlorophyll fluorescence (Fv Fm^{-1}) chlorophyll a (Chl a); Chlorophyll b (Chl b); total chlorophylls (Total Chl); total chlorophylls (Total Chl); total carotenoids (Total Car); 2,2-diphenyl-1-picrylhydrazyl (DPPH); ferric reducing antioxidant power (FRAP); 2,20-azino-bis (3-ethylbenzothiazoline-6-sulphonic acid) (ABTS); hydrogen peroxide (H_2O_2); malondialdehyde (MDA).

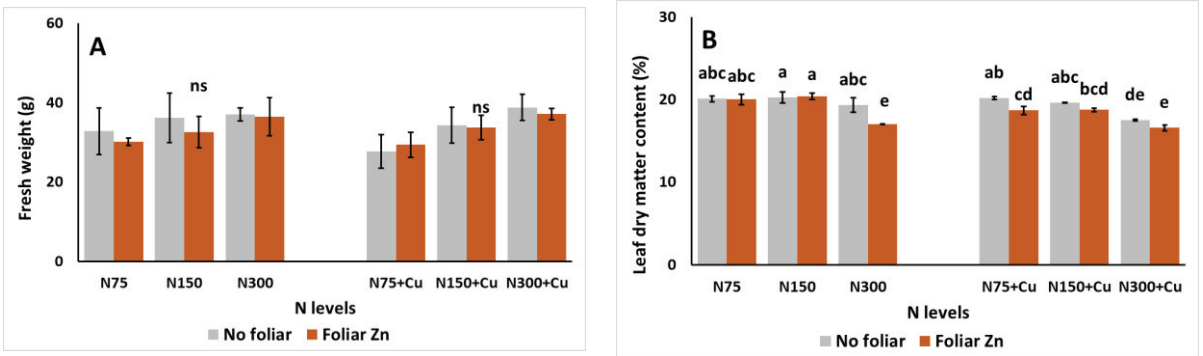


Figure 1. The effect of N levels (N75, 75 mg L^{-1}; N150, 150 mg L^{-1}; and N300, 300 mg L^{-1}), Zn foliar application (0 and 1.74 mM Zn), and Cu application (no additional, 5 μM Cu; and with additional Cu, 100 μM Cu) on the fresh weight (FW; g) (**A**) and dry matter (DM; %) (**B**) of *Sideritis cypria* plants grown in soilless cultivation. Significant differences ($p < 0.05$) among the different applications are indicated by different letters. ns: not significant.

Leaf phytochemistry features, as affected by the examined parameters, are presented in Figure 2. SPAD (Figure 2A) was decreased with the applications of N75 with 100 μM Cu and foliar spraying with Zn (1.74 mM), and N300 with 5 μM Cu and foliar spraying without Zn (0 mM). For chlorophyll fluorescence (Fv Fm^{-1}) (Figure 2B), the highest value was recorded for plants that were subjected to the co-application of N75, 5 μM Cu, and foliar spraying with Zn, which was significantly higher than the rest of the treatments, excluding intermediate values, such as those attained with the co-application of N75, foliar spraying without Zn, and with 5 or 100 μM Cu. In contrast, the lowest Fv Fm^{-1} was presented with the co-application of N150, 100 μM Cu, and foliar spraying with Zn. For Chl a (Figure 2C), the highest value was recorded with the co-application of N150, 100 μM Cu, and foliar spraying with Zn, which was significantly greater than the lowest value attained with the co-application of N75, 100 μM Cu, and foliar spraying with Zn. A similar finding is observed in both Chl b (Figure 2D) and Total Chl (Figure 2E), while Total Car (Figure 2F) was mostly negatively affected with lower N levels in the NS.

The impacts of the examined parameters on the leaf and root mineral content are examined in Figure 3. In leaves, the N content was increased at the highest N concentration in the NS (N300), while this increase was amplified with the co-application of N300 and Cu at 100 μM (Figure 3A1). Similarly, in roots, N was accumulated with the application of N300, while the highest N content was observed with the co-application of N300, 100 μM Cu, and the foliar application of Zn (Figure 3A2). In both leaves and roots, the lowest accumulation of N was observed with the co-application of N75 and 100 μM Cu. P content in leaves was the lowest with the application of N300 without foliar Zn, while the application of Zn in foliar spraying led to a marginal increase in P with the use of the same NS (Figure 3B1). In the case of root P content, it was generally decreased by the increase in N in the NS (Figure 3B2), while no significant influences were observed for Cu and Cu × Zn applications (Table 1). Leaf K remained unaffected by the examined treatments (Figure 3C1), while root K was the lowest and highest with the application of N300 and N75, respectively, under 5 μM Cu and without foliar Zn (Figure 3C2). In the case of Na in leaves, it was generally increased with the highest N in the NS (N300), while the highest values were observed with the application N300, 100 μM Cu, and no foliar Zn. Interestingly, for the N150 treatments, Na was decreased with the foliar application of Zn (Figure 3D1). A similar trend was observed in the accumulation of Na in roots, as it decreased with the foliar application of Zn in all treatments, excluding the case of N150 and 100 μM Cu, as no significant differences were observed (Figure 3D2).

In terms of micronutrients, the Fe content of leaves was significantly decreased with the application of 100 μM Cu, under the N300 NS, compared to the application of lower Cu levels (5 μM) (Figure 3E1). In addition, foliar Zn caused a decrease in root Fe in the N300 NS with 5 μM Cu (Figure 3E2). The Cu content of leaves was significantly increased by the application of 100 μM Cu, compared to the application of normal Cu levels (5 μM) in the NS (Figure 3F1). Foliar Zn applications led to the decrease in Zn content of leaves using the N75 NS, while a significant increase was evident using the N150 NS with 5 μM Cu. A decrease was also observed when excess Cu was applied, using the N75 NS with foliar Zn (Figure 3G1). The highest root Zn was recorded for plants treated with N150, 100 μM Cu, and no foliar Zn. Finally, root Zn was decreased with the application of foliar Zn, using the N75 NS and 5 μM Cu, while the opposite occurred using the N300 NS and 5 μM Cu (Figure 3G2).

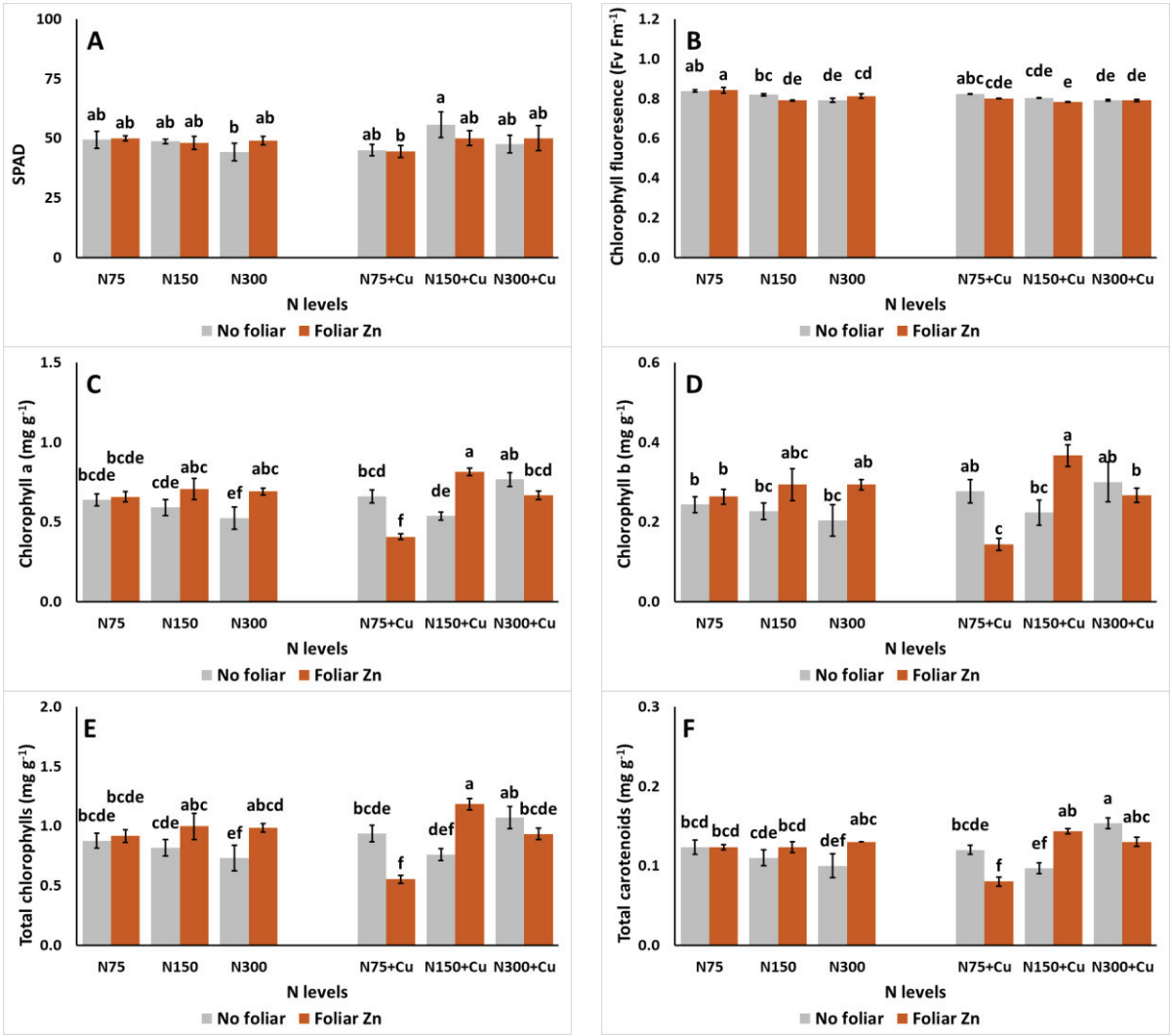


Figure 2. The effect of N levels (N75, 75 mg L^{-1}; N150, 150 mg L^{-1}; and N300, 300 mg L^{-1}), Zn foliar application (0 and 1.74 mM Zn), and Cu application (no additional, 5 μM Cu; and with additional Cu, 100 μM Cu) on leaf SPAD (**A**), chlorophyll fluorescence (Fv Fm^{-1}) (**B**), chlorophyll a (Chl a; mg g^{-1}) (**C**), chlorophyll b (Chl b; mg g^{-1}) (**D**), total chlorophylls (Total Chl; mg g^{-1}) (**E**), and total carotenoids (Total Car; mg g^{-1}) (**F**) of *Sideritis cypria* plants grown in soilless cultivation. Significant differences ($p < 0.05$) among the different applications are indicated by different letters.

The effects of the N-modified nutrient solutions, different Cu levels, and foliar Zn on total phenols content, antioxidant capacity, and flavonoids of *S. cypria* plants are presented in Figure 4. The lowest phenolics (Figure 4A) were recorded in plants cultivated with N150, 5 μM Cu, and no foliar Zn. The application of foliar Zn, however, in the same treatment, resulted in a significant increase in phenolics. The same was observed with the applications of N75 with 5 μM Cu, and N150 with 100 μM Cu. In the case of N75 and N150, the application of increased Cu led to an increase in total phenolics when no foliar Zn was applied. Similar observations can be viewed in terms of antioxidant capacity, assayed by DPPH (Figure 4B), FRAP (Figure 4C), and ABTS (Figure 4D). Interestingly, DPPH and FRAP were increased with the application of foliar Zn in the treatment with N300 and 100 μM Cu, whereas the inverse occurred with the lower Cu dose (5 μM). For ABTS, the highest values were observed with the application of N300 with 5 μM Cu and foliar Zn, compared to the rest of the treatments, whereas the lowest was observed with the application of N75 with 5 μM Cu and no foliar Zn. Finally, the highest flavonoids (Figure 4E)

were observed with the application of N150 with 5 µM Cu and foliar Zn compared to the rest of the treatments, whereas the lowest were observed with the equivalent treatment with no foliar Zn application.

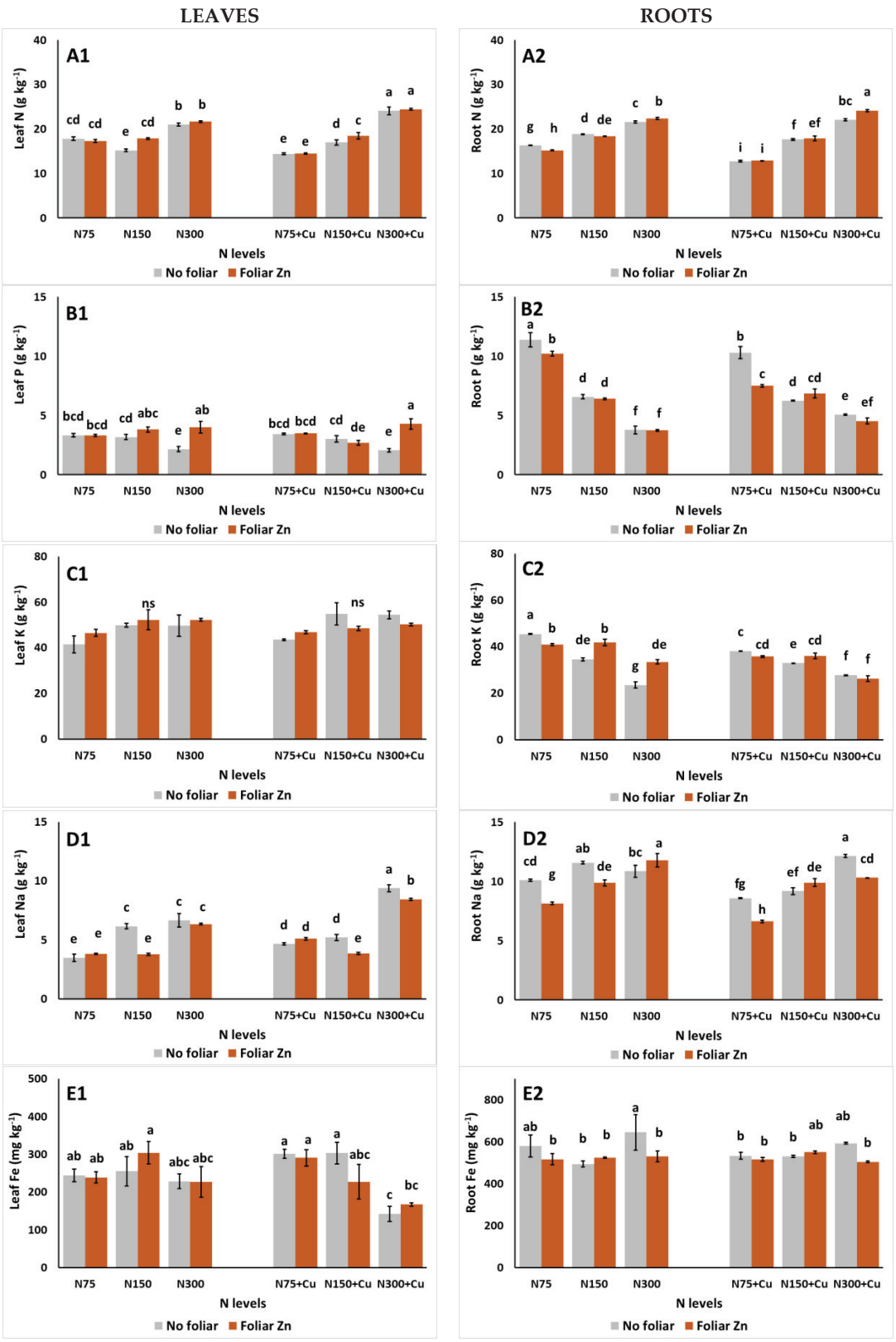


Figure 3. *Cont.*

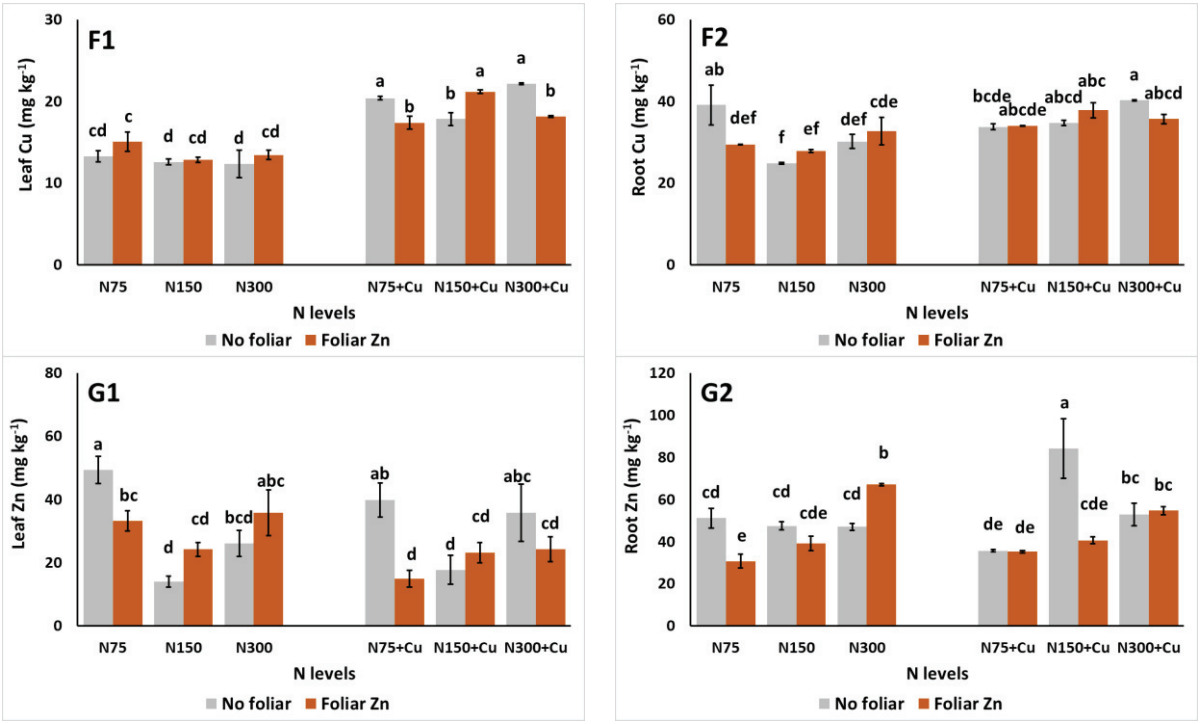


Figure 3. The effect of N levels (N75, 75 mg L^{-1}; N150, 150 mg L^{-1}; and N300, 300 mg L^{-1}), Zn foliar application (no foliar, 0 mM Zn; and foliar Zn, 1.74 mM Zn), and Cu application (no additional, 5 μM Cu; and with additional Cu, 100 μM Cu) on leaf and root N (**A1**,**A2**), P (**B1**,**B2**), K (**C1**,**C2**), Na (**D1**,**D2**), Fe (**E1**,**E2**), Cu (**F1**,**F2**), and Zn (**G1**,**G2**), respectively, of *Sideritis cypria* plants grown in soilless cultivation. Significant differences ($p < 0.05$) among the different applications are indicated by different letters. ns: not significant.

The effects on hydrogen peroxide (H_2O_2) and lipid peroxidation in terms of MDA are presented in Figure 4. In the case of H_2O_2 (Figure 4F), a significant increase was observed with the application of N150, 100 μM Cu, and foliar Zn, compared to the rest of the treatments, excluding N75, 5 μM Cu, and foliar Zn. In addition, the lowest H_2O_2 levels were observed in plants treated with the co-application of N300 with 5 or 100 μM Cu and foliar Zn, and N150 with 100 μM Cu and no foliar Zn. In the case of MDA (Figure 4G), decreased values were observed with the application of foliar Zn; in N75, N150, and N300 combined with 5 μM Cu; and N300 with 100 μM Cu.

Linear correlation coefficients were calculated to demonstrate the contribution of the N (Supplementary Table S2), Cu (Supplementary Table S3), and Zn (Supplementary Table S4) concentrations for each individual factor. Regarding N levels in the NS, there was a positive correlation with N (75–150–300 mg L^{-1}) concentrations and leaf minerals (N, Na, and Zn), and root N; and a negative correlation with leaf Fe, root P, root K, dry matter content, and H_2O_2 content (Supplementary Table S2). Regarding Cu levels in the NS, there was a positive correlation with Cu (5 and 100 μM) concentrations and leaf Cu and root Cu, and a negative correlation with chlorophyll fluorescence and dry matter content (Supplementary Table S3). Regarding Zn foliar applications, there was a positive correlation with Zn (0 and 1.74 mM) concentrations and leaf P, phenols, and antioxidant (FRAP and ABTS) content, and a negative correlation with MDA (Supplementary Table S4).

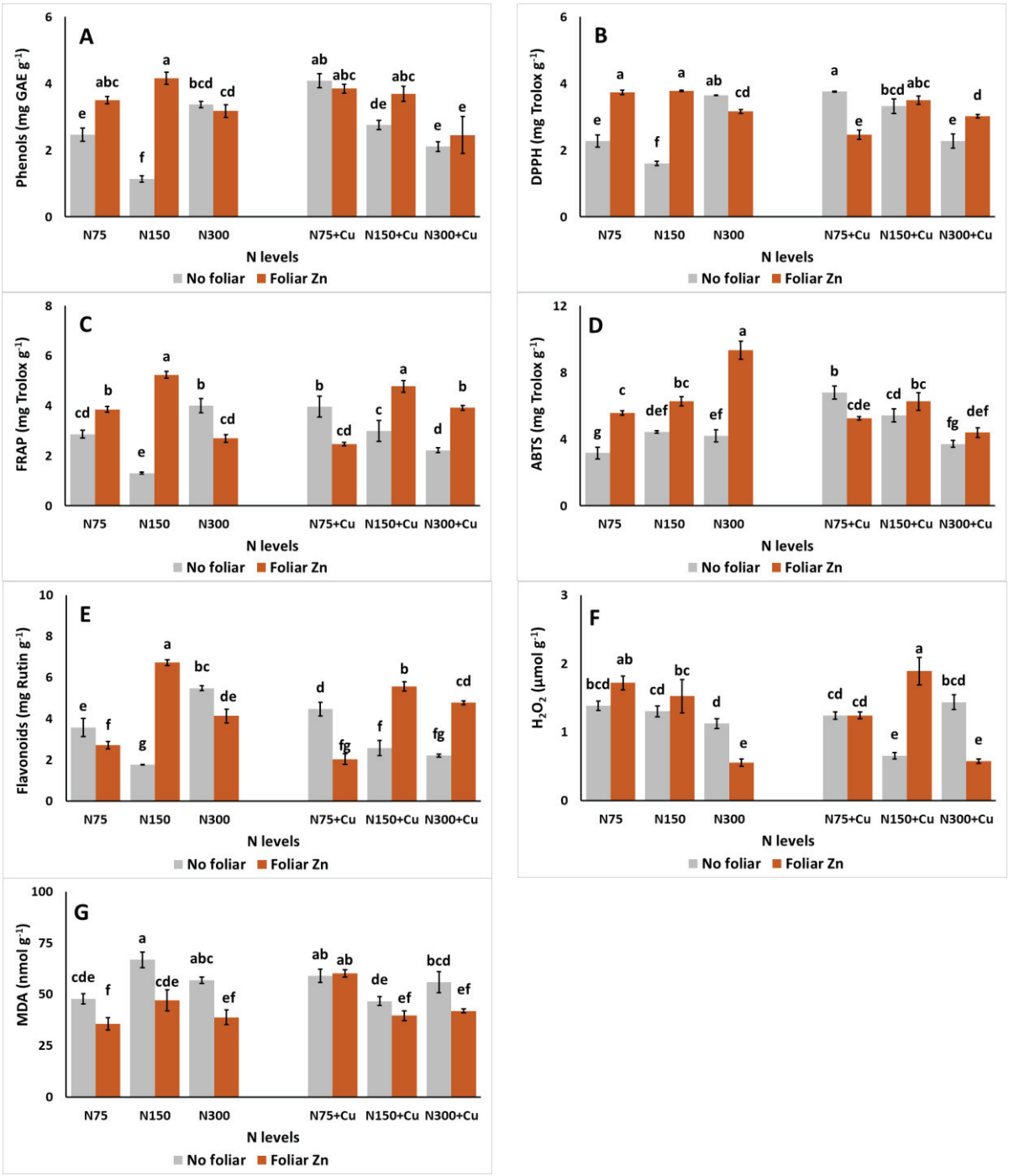


Figure 4. The effect of N levels (N75, 75 mg L^{-1}; N150, 150 mg L^{-1}; and N300, 300 mg L^{-1}), Zn foliar application (no foliar, 0 mM Zn; and foliar Zn, 1.74 mM Zn), and Cu application (no additional, 5 µM Cu; and with additional Cu, 100 µM Cu) on phenols (**A**), DPPH (**B**), FRAP (**C**), ABTS (**D**), flavonoids (**E**), H_2O_2 (**F**), and MDA (**G**) of *Sideritis cypria* plants grown in soilless cultivation. Significant differences ($p < 0.05$) among the different applications are indicated by different letters.

3. Discussion

Soilless cultivation provides control over nutrient management, allowing for the optimization of plant growth. This is particularly important for specialty crops, including MAPs, where consistent yield and quality are of utmost importance [4]. Nitrogen fertilization remains an important parameter for the growth of MAPs, as it can directly affect the yield and quality of the final product [12]. However, in the case of *S. cypria*, knowledge

regarding this topic is scarce [10]. Moreover, nutrient interactions represent an intricate aspect of plant nutrition, as the dynamics of a nutrient can influence the uptake, transport, and utilization of another. Knowledge of such interactions could promote the improvement of nutritional disorders, as well as the biofortification of elements such as Zn [34]. In addition, excessive accumulation of heavy metals such as Cu presents a critical parameter, as it may affect yield an quality, and it may also interact with nutrients such as N and Zn [26].

The present research examined different N levels in the NS of *S. cypria* grown in soilless cultivation, due to the importance of this essential element. In terms of plant growth and biomass production, previous findings indicate that *S. cypria* plants exhibit increased biomass production at moderate and elevated N levels (150–300 mg N L^{-1}), compared to lower N levels (75 mg N L^{-1}) [10]. In the present study, however, the application of various N levels did not affect the FW of *S. cypria* plants. This may be due to the seeds used to grow the experimental plants which originated from wild ecotypes, lacking breeding and selection for improved growth rates under high N availability. Stamnagathi (*Cichorium spinosum* L.) plants grown in an open hydroponic system, consisting of perlite as a growing media, exhibited a similar response, as increasing N levels from 4 to 16 mmol L^{-1} did not influence plant yield [35]. Nevertheless, the plants exhibited improved dry matter content under low and moderate N levels, in accordance with the findings of Chrysargyris and Tzortzakis [10]. Although fresh biomass production was unaffected, high N availability generally promotes increased cell expansion and subsequent leaf growth, as well as water uptake, negatively influencing DM [36]. This is a significant observation, as *S. cypria* is primarily purchased as dried material. Interestingly, excess Cu and Zn foliar applications did not have a significant effect on the plant growth of *S. cypria*. However, the combined application of increased Cu and foliar Zn led to a general decline in dry matter content. Similarly, in the study of Balamurugan et al. [37], a gradual increase in Cu applications resulted in a corresponding decrease in the dry matter content produced by green-gram (*Vigna radiata* (L.) Wilczek) plants. In addition, the application of excessive concentrations of Cu (60 μM), combined with beneficial or excessive concentrations of Zn (50 μM), significantly reduced the dry weight of *Arabidopsis thaliana* (L.) Heynh. plants. This was primarily attributed to the reduction in the activity of the photosynthetic apparatus, accompanied by a decrease in the relative total chlorophyll contents and chlorophyll fluorescence, caused by the excessive concentrations of Cu and Zn, applied individually or simultaneously [38]. Likewise, in the current study, low N levels (75 mg L^{-1}) with excess Cu and foliar Zn caused a reduction in phytochemistry features such as SPAD, chlorophyll fluorescence, and chlorophyll content. However, under moderate N levels (150 mg L^{-1}), the application of foliar Zn led to an increase in chlorophylls (a, b, and total). Likewise, Irmes et al. [39] observed a positive effect of foliar Zn application in the chlorophyll content of winter wheat (*Triticum aestivum* L.), contingent on the macronutrient levels utilized during fertilization, including N. This effect can be attributed to the essential role of Zn in chlorophyll biosynthesis and N metabolism, as well as its crucial function in facilitating N absorption, which indirectly contributes to enhanced chlorophyll content [29].

The different N levels applied in the current study, in conjunction with Cu and foliar Zn applications, impacted the nutrient content of *S. cypria* leaves and roots. The main finding indicates that, while the interaction between the three parameters did not significantly affect the nutrient content *S. cypria* leaves, it exerted a significant influence on root nutrient content and, specifically, the content of P, K, Na, Cu, and Zn. This is mainly attributed to the influence of N levels on uptake and mobility of macronutrients (P, K, and Na) and micronutrients (Cu and Zn) within the plants [40]. In addition, Cu may disrupt root cell membrane integrity, altering ionic homeostasis and disrupting ion selectivity

mechanisms [41]. Supplementation of Zn also influences the uptake and translocation of macronutrients such as P and K, while it also competes with Cu for its utilization [42]. The N content in leaves and roots was positively influenced by the increased levels of N in the NS. Likewise, Chrysargyris and Tzortzakis [10] reported high N accumulation in *S. cypria* leaves, with the application of elevated N (300 mg L^{-1}) in the NS. Similarly, in previous studies of MAPs, the N content of leaves and stems was enhanced by the increasing N supply in *Portulaca oleracea* L. and *Panax notoginseng* (Burkill) F. H. Chen [43,44]. Nitrogen contents in leaves and under moderate N fertilization (N150) were also marginally enhanced with the foliar application of Zn, as previously observed by Alinejad Elahshah et al. [45] in hydroponically grown strawberry (*Fragaria* × *ananassa* Duch.). The extent of the influence of Zn on shoot and root N uptake is directly related to the N availability during growth [46], with Zn improving the absorption capacity of N under recommended rates of N in maize (*Zea mays* L.) [47]. Owing to the mutual interaction between N and P nutrition in plants, an adequate supply of N has a positive effect in the uptake of P [48], while an excessive supply of N can reduce the uptake of P [49]. In the current study, increased N levels in the NS were linked to decreased accumulation of P in leaves and roots. This might be attributed to the plants' ability to adjust their nutrient-allocation strategy in response to N addition [50]. Similarly, Li et al. [51] observed that N addition increased P limitation and demand for upper plant growth, affecting its concentrations in roots. In addition, K in roots was negatively influenced by the excessive Cu concentration in the NS, highlighting the influence of Cu toxicity in the uptake and accumulation of other nutrients. Similarly, the K content in roots of *Z. mays* L. was significantly reduced with the gradual increase in Cu to up to 78.7 μM in the NS [52]. Cu uptake generally depends on the plant species, organ, concentrations of Cu, and exposure duration. Saleem et al. [53] reported that flax (*Linum usitatissimum* L.) exposed to high Cu (up to 600 mg kg^{-1} soil) had initially accumulated Cu mainly in roots; meanwhile, following 140 DAS, Cu was mostly accumulated in leaf tissues. Similarly, in the current study, the application of 100 μM Cu in the NS increased its accumulation in *S. cypria* leaf tissues, compared to the application of 5 μM Cu, whereas its content in roots was relatively unaffected. This may be attributed to the duration of exposure, which allowed for the transportation to shoots, in line with the results obtained in earlier studies [53,54]. In addition, foliar Zn applications were able to reduce the accumulation of Cu in plant leaf tissues, at low and high N levels in the NS. This aligns with the findings of Shahriaripour and Tajabadipour [55], as the application of Zn adversely affected the uptake and leaf content of Cu in pistachio (*Pistacia vera* L.) seedlings. Nonetheless, the accumulation of Cu in leaves of *S. cypria* exposed to excess Cu in the NS aligns closely with previously reported findings under typical hydroponic cultivation [10], ranging from 17.3 to 22.2 mg Cu kg^{-1} DW under Cu excess. Moreover, these levels remain below the maximum residue levels of 100 mg kg^{-1} for Cu compounds in leaves and herbs for infusions, as outlined by EFSA [56]. Transition metals such as Cu, Zn, and Fe compete for their uptake, transport, and chemical reaction within the plant [57]. For instance, Cu above optimal concentrations may also influence Fe contents in plants due the rapid synthesis of Cu proteins that replace Fe proteins, reducing the demand for Fe [58]. In fact, in the current study, Fe was reduced in leaf tissues with the application of excess Cu; however, this was mostly evident with the combined application of high N (300 mg L^{-1}) in the NS. For Zn, its foliar applications were anticipated to result in its accumulation in *S. cypria* plant tissues, as evidenced by Fatemi et al. [59] in pak choi (*Brassica rapa* L.) treated with foliar Zn at low (25 μM) and high (500 μM) concentrations. However, in the current study, a variable effect was observed, with Zn accumulation being contingent on N and Cu concentrations in the NS. This may be attributed to various factors such as Zn dosing, application frequency, and crop life cycle [60]. In addition, Zn optimization for

its biofortification requires the optimization of N fertilization to ensure optimal synergy effects among the two nutrients [61]. Furthermore, proper N fertilization influences Zn cellular mobility and availability by its effects on Zn-chelating compounds such as amino acids and peptides. However, increased N supply may cause increased biomass production and decreased dry matter content, leading to a decrease in Zn concentration [47].

The biosynthesis of secondary metabolites, including phenolics, flavonoids, and antioxidants, is substantial in stress tolerance and protection from oxidative stress, inhibiting lipid peroxidation and neutralizing ROS [62,63]. It is generally accepted that the plant stress occurring from the excess of heavy metals prompts the antioxidant response of plants, with high levels of Cu prompting the increase in total phenolics in plants such as basil (*Ocimum basilicum* L.), common nettle (*Urtica dioica* L.), and *Acer platanoides* L. [25,62]. In addition, Zn can prompt the synthesis of phenolic compounds [25]. For instance, foliar applications of zinc oxide (ZnO) nanoparticles increased phenols, flavonoids, and antioxidant capacity according to ABTS, DPPH, and FRAP in habanero pepper plants (*Capsicum chinense* Jack.) [64]. Similarly, the foliar application of $ZnSO_4$ increased total phenolics in *Lavandula stoechas* L. plants [65]. However, these responses, as observed by the researchers, were concentration-dependent. Interestingly, while discerning the main effects on the antioxidant status of *S. cypria* plants, Cu did not influence the content of phenolics and antioxidants (DPPH, FRAP, and ABTS). However, these indices were affected by the first- and second-order interactions of the examined parameters, suggesting that N, Cu, and Zn determine the antioxidant response of *S. cypria*. These coincides with the variation in total phenolics and antioxidant activity observed in the current study, which depended on the treatment applied. Particularly, foliar Zn applications increased total phenolics under moderate N levels (150 mg L^{-1}), with similar response being observed for the antioxidant status of *S. cypria* plants, in terms of DPPH, FRAP, and ABTS. The response to Zn application is linked to the protective role of Zn, as an antioxidant cofactor, improving the synthesis of enzymatic and non-enzymatic antioxidants [66]. In addition, N levels may also exert influence on the antioxidant status of plants, especially under low or high concentrations [67]. However, differences were reported with the presence of increased Cu in the NS, possibly due to the influence of excess Cu on the synthesis and accumulation of antioxidant molecules.

A substantial effect of excess Cu is oxidative stress, attributed to the increased ROS production [63]. Rehman et al. [68] reported that the presence of excess Cu significantly increased leaf MDA contents of *Boehmeria nivea* L. plants, resulting in Cu-induced oxidative damage. However, the researchers also observed that this response was contingent on the level of N fertilization applied. Similarly, in the current study, MDA was relatively increased with the application of excess Cu concentrations when combined with 75 and 150 mg N L^{-1}, corroborating with the notion that N fertilization modulates oxidative stress. In addition, Zn foliar application generally reduced the MDA content of *S. cypria*; however, this effect was subdued with the application of excess Cu in the NS. This can be attributed to the role of Zn in the maintenance of cell membrane integrity, and the activation of enzymes such as superoxide dismutase (SOD) and catalase (CAT) [66]. Similarly, in the current study, the application of foliar Zn decreased the content of H_2O_2, although this effect was limited to the application of the highest N concentration in the NS, as appropriate combined applications of N and Zn have a significant impact on the antioxidant enzyme activities to scavenge ROS as H_2O_2 [69].

4. Materials and Methods

4.1. Plant Materials and Experimental Site

The current study was conducted in a plastic multi-span greenhouse, located at the experimental farm of the Cyprus University of Technology, located in Kato Polemidia,

Limassol, Cyprus, at a latitude of 34.700120 and a longitude of 32.984276. The experiment took place during the autumn–winter season. *S. cypria* seedlings were acquired from the Department of Aromatic Plants, Ministry of Agriculture, Cyprus. The seedlings were transplanted in 2.3 L pots in a 4:1 (*v*/*v*) mixture of coco soil and perlite, at the 7–10 leaf stage, on 25 November 2022. Each pot was accompanied by a plastic tray to collect runoff.

Plants were kept for 28 days after transplanting (DAT) in the same basic NS (sNS). Following this period, three different NS compositions were applied, consisting of the following N levels: (i) lower N, N75 (75 mg N L^{-1}); (ii) intermediate (control) N, N150 (150 mg N L^{-1}); and (iii) higher N, N300 (300 mg N L^{-1}). These levels were determined based on previously reported data on the experimental evaluation of *S. cypria* [10,70]. Total N is the sum of NO_3^--N and NH_4^+-N. All the other minerals were kept constant. The fertilizers used were calcium nitrate, potassium nitrate, ammonium nitrate, magnesium sulphate, magnesium nitrate, potassium sulphate, phosphoric acid, nitric acid, sulfuric acid, iron-chelate, manganese sulphate, zinc sulphate, copper sulphate, boric acid, and ammonium heptamolybdate. The electrical conductivity (EC) of the NS was maintained at 2.57 dS m^{-1}, and the pH at 5.9 by adding HNO_3. The composition of the different NS applied, including the sNS, is presented in Supplementary Table S1. Fertigation applications were determined based on real-time monitoring of weather conditions and substrate humidity. NSs were applied at a volume of 50–100 mL pot^{-1}, with a frequency of one or two applications per week. Treatments were further diversified, considering the application of foliar spraying with pure dH_2O (no foliar Zn) or dH_2O with Zn (0.5 mg L^{-1} $ZnSO_4 \cdot 7H_2O$ or 1.74 mM Zn) (foliar Zn). Foliar was chosen, as it can more effectively be absorbed by and incorporated into plant tissues, resulting in rapidly improved micronutrient status, especially in the context of biofortification. In addition, short-term cultivation periods and successive harvesting of MAPs like *S. cypria* prompt swift and efficient supplementation methods. Foliar applications were conducted at three intervals, commencing at 58 DAT. The concentration, as well as the spraying interval, was based on preliminary findings [71]. At 58 DAT, plants were subjected to different Cu levels in the three NSs (N75, N150, and N300), namely (i) 5 μM Cu (control) and (ii) 100 μM Cu, with the addition of $CuSO_4$. Plants were grown under these different Cu levels, with periodical fertigation applications every 2–3 days for an additional 42 days, resulting in a total growth duration of 100 DAT. During cultivation, common agricultural practices were followed. The average day and night temperatures were 19.5 °C and 13.6 °C, respectively, while the average day and night humidity values were 60.4% and 71.5%, respectively.

4.2. Agronomic Parameters

A total of 120 plants were used. Following 58 DAT of growth in the three different NS with 40 plants each, subsets of 20 plants were allocated to two different treatment groups: one group received the application of 5 μM Cu, while the other received 100 μM Cu in each NS. In addition, each subset was further partitioned to accommodate foliar applications as no foliar Zn applications, while the other was subjected to foliar Zn. Therefore, 12 treatments were used (3 N levels × 2 Cu levels × 2 Zn foliar applications), and each treatment accommodated 10 plants (replicates). Following cultivation, six plants for each treatment were considered for agronomic evaluation, and plant growth-related parameters were evaluated, including plant fresh (g) and dry weight (g), and dry matter content (%).

4.3. Leaf Phytochemistry Features

Prior to plant sampling, the relative chlorophyll content in terms of SPAD (Soil Plant Analysis Development) was assessed using an optical chlorophyll meter (SPAD-502, Minolta, Osaka, Japan). Leaf chlorophyll fluorescence (Fv Fm^{-1}) was measured using

OptiSci OS-30p Chlorophyll Fluorometer (Opti-Sciences, Hertfordshire, UK), while photosynthesis pigments (chlorophyll a, b, and total; and carotenoid content) were determined as previously described [72,73]. The ratios of Chla:Chlb and carotenoids/Total Chls were also calculated.

4.4. Plant-Tissue Ion Concentration Analysis

At the completion of the study, three leaf tissue samples were collected from a pool of plants per treatment and were dried at 42 °C. Dried leaf tissues were then ash-burned at 550 °C for four and a half hours and then acid-digested (2 M HCl). Potassium (K) and sodium (Na) were determined by flame photometry (Lasany Model 1832, Lasany International, Panchkula, India). Phosphorus (P) was determined using the molybdate/vanadate method (yellow method) by spectrophotometry (Multiskan GO, Thermo Fischer Scientific, Waltham, MA, USA). N was determined using the Kjeldahl method (BUCHI, Digest automat K-439 and Distillation Kjelflex K-360, Flawil, Switzerland), as described by Chrysargyris et al. [74]. Finally, iron (Fe), Zn, and Cu were determined by an atomic absorption spectrophotometer (PG Instruments AA500FG, Leicestershire, UK).

4.5. Total Phenols, Total Flavonoids, Antioxidants, and Stress Indicators

Methanolic extracts of leaf tissue (three replicates per treatment) were used for the determination of total phenols and flavonoids content. Total phenols content was determined by the Folin–Ciocâlteu assay at 755 nm. Results were expressed in gallic acid equivalents (mg GAE g^{-1} FW).

The antioxidant activity of the extracts was determined by the assays of 2,2-diphenyl-1-picrylhydrazyl (DPPH), ferric-reducing antioxidant power (FRAP), and the 2,2′-azino-bis (3-ethylbenzothiazoline-6-sulphonic acid) (ABTS) assay, as previously described [67]. DPPH radical scavenging activity was measured by bleaching with 0.3 M DPPH solution, where
1 mL of the solution was mixed with 15 μL leaf tissue extract and 1985 μL methanol (50%). Following incubation in the dark, the absorbance was measured at 517 nm (Multiskan GO, Thermo Fischer Scientific, Waltham, MA, USA). To measure FRAP, a FRAP solution was prepared with 2.5 mL $CH_3COONa{\cdot}3H_2O$ (0.3 mol L^{-1}, pH 3.6), 0.25 mL TPTZ (Tripyridyl-s-triazine, 10 mmol L^{-1}), $FeCl_3{\cdot}10H_2O$ (40 mmol L^{-1}), and 15 μL leaf tissue extract. The absorbance was measured at 593 nm (Multiskan GO, Thermo Fischer Scientific, Waltham, MA, USA). Finally, for ABTS, 3 mL ABTS solution was added with 50 μL leaf tissue extract. Absorbance was measured at 734 nm. Results were expressed as Trolox (6-hydroxy-2,5,7,8-tetramethylchromane-2-carboxylic acid) equivalents (mg of Trolox g^{-1} FW).

Total flavonoids were determined by aluminum chloride colorimetric assay at 510 nm [67], and results were expressed in rutin equivalents (mg rutin g^{-1} FW).

Hydrogen peroxide (H_2O_2) and lipid peroxidation in terms of malondialdehyde (MDA) content were evaluated as described by Chrysargyris et al. [75]. Briefly, H_2O_2 was determined by measuring the absorbance at 390 nm, and results are expressed as μmol of H_2O_2 per gram of fresh weight (μmol H_2O_2 g^{-1} FW). MDA was determined by measuring the absorbance of reaction mixtures at 532 nm (corrected at 600 nm). MDA was calculated using the extinction coefficient of 155 mM^{-1} cm^{-1}, and results are expressed as nmol of MDA per gram of fresh weight (nmol MDA g^{-1} FW).

4.6. Statistical Methods

Experimental data were analyzed by applying three-way analysis of variance (ANOVA) using SPSS v.21 (IBM, New York, NY, USA) to assess the main effects (N levels (N), Cu application (Cu), and Zn foliar application (Zn)), three first-order interactions

(N × Cu, N × Zn, Cu × Zn), and a second-order interaction (N × Cu × Zn). Results are expressed as mean ± standard error (SE). Duncan's multiple range tests were performed when ANOVA rendered a significant treatment impact at $p < 0.05$. The correlation coefficients between N levels in the NS, Cu levels in the NS, and foliar Zn application with individual parameters were tested by Pearson's correlation test.

5. Conclusions

This study investigated the effects of different N levels (75, 150, and 300 mg L^{-1}) in the NSs of *S. cypria* plants grown in soilless cultivation, in conjunction with normal (5 μM) and elevated (100 μM) Cu levels, with the aim of assessing the potential adverse effects of Cu toxicity. Moreover, foliar Zn was employed to examine their influence on plant nutritional status under varying NS regimes and their potential role in mitigating Cu-induced toxicity. Although the different N levels in the NSs did not affect the fresh biomass production of *S. cypria* plants, low (75 mg L^{-1}) and moderate (150 mg L^{-1}) N levels resulted in increased dry matter content. However, a general decline in dry mater content was observed with the combined application of foliar Zn and increased Cu, mainly due to the reduction in the activity of the photosynthetic apparatus. In addition, at moderate N (150 mg L^{-1}), foliar Zn applications led to the increase in chlorophylls (a, b, and total). Increased concentrations of N in the NS facilitated the increase in the N content in leaves and roots, while foliar Zn enhanced the uptake of N under moderate N levels (150 mg L^{-1}) in the NS. Excess Cu in the NS stimulated the accumulation of Cu in leaf tissues, while foliar Zn applications were able to reduce this accumulation at low (75 mg L^{-1}) and high (150 mg L^{-1}) N levels in the NS. At moderate N (150 mg L^{-1}), foliar Zn applications enhanced total phenolics and antioxidants (DPPH, FRAP, and ABTS), with variations being observed depending on the N and Cu concentrations of the NS. In terms of stress response, MDA was increased with excess Cu at moderate-to-low N concentrations, while foliar Zn decreased both MDA and H_2O_2, contingent on Cu and N levels in the NS. The main outcome of this study is that exposure of *S. cypria* to excess Cu can impact the antioxidant activity and Cu content of *S. cypria* plants, with Zn alleviating potentially phytotoxic effects. N has a pivotal role in modulating these responses, while appropriate combined applications of N and Zn have a significant impact on the antioxidant response of plants and on the alleviation of Cu toxicity. Ultimately, low-to-moderate N levels in the NS can be applied under excess Cu conditions without impairing the growth, yield, and quality of *S. cypria* plants, and without compromising safety for consumption. In addition, Zn foliar applications can be applied as a means of modulating the response of plants under excess Cu, while also improving the quality of the final product.

Supplementary Materials: The following supporting information can be downloaded at https://www.mdpi.com/article/10.3390/plants14050691/s1, Table S1: Electrical conductivity (EC) and nutrient concentrations in the nutrient solution (NS) supplied to *S. cypria* plants grown in soilless cultivation under three levels in nitrogen; Table S2: Correlation coefficients and (*p*-values) between the N concentrations in the NS and the *Sideritis cypria* plant mineral content, growth, and physiology attributes; Table S3: Correlations coefficients and (*p*-values) between the Cu concentrations in the NS and the *Sideritis cypria* plant mineral content, growth, and physiology attributes; Table S4: Correlations coefficients and (*p*-values) between the Zn foliar application and the *Sideritis cypria* plant mineral content, growth, and physiology attributes.

Author Contributions: Conceptualization, A.C. and N.T.; methodology, A.C.; software, G.N. and A.C.; validation, G.N., A.C. and N.T.; formal analysis, G.N., A.C. and N.T.; investigation, G.N., A.C. and N.T.; resources, N.T.; data curation, A.C.; writing—original draft preparation, G.N. and A.C.; writing—review and editing, A.C. and N.T.; visualization, N.T.; supervision, A.C. and N.T.; project

administration, N.T.; funding acquisition, N.T. All authors have read and agreed to the published version of the manuscript.

Funding: This research was funded by the Project "Opti-AromaQ" EXCELLENCE/0421/0299, which is co-financed by the European Union and the Republic of Cyprus through the Research and Innovation Foundation.

Data Availability Statement: The original contributions presented in this study are included in the article/Supplementary Material. Further inquiries can be directed to the corresponding author.

Conflicts of Interest: The authors declare no conflicts of interest.

References

1. Neocleous, D.; Ntatsi, G. Seasonal Variations of Antioxidants and Other Agronomic Features in Soilless Production of Selected Fresh Aromatic Herbs. *Sci. Hortic.* **2018**, *234*, 290–299. [CrossRef]
2. Maggini, R.; Kiferle, C.; Guidi, L.; Pardossi, A.; Raffaelli, A. Growing Medicinal Plants in Hydroponic Culture. *Acta Hortic.* **2012**, *952*, 697–704. [CrossRef]
3. Nchu, F.; Matanzima, Y.; Laubscher, C.P. Prospects of N Fertilization in Medicinal Plants Cultivation. In *Nitrogen in Agriculture—Updates*; InTech: London, UK, 2018.
4. Maggini, R.; Tzortzakis, N.; Currey, C.J. Editorial: Soilless Culture for Vegetative Biomass Production and Specialized Metabolites: Medicinal, Aromatic, and Edible Plants. *Front. Plant Sci.* **2022**, *13*, 887487. [CrossRef] [PubMed]
5. Chrysargyris, A.; Tzortzakis, N. Tailor-Made Hydroponic Recipes for the Production of High Quality Medicinal and Aromatic Plants. *Acta Hortic.* **2021**, *1321*, 87–94. [CrossRef]
6. Aneva, I.; Zhelev, P.; Kozuharova, E.; Danova, K.; Nabavi, S.F.; Behzad, S. Genus *Sideritis*, Section Empedoclia in Southeastern Europe and Turkey—Studies in Ethnopharmacology and Recent Progress of Biological Activities. *DARU J. Pharm. Sci.* **2019**, *27*, 407–421. [CrossRef] [PubMed]
7. Sarikurkcu, C.; Locatelli, M.; Mocan, A.; Zengin, G.; Kirkan, B. Phenolic Profile and Bioactivities of *Sideritis perfoliata* L.: The Plant, Its Most Active Extract, and Its Broad Biological Properties. *Front. Pharmacol.* **2020**, *10*, 1642. [CrossRef] [PubMed]
8. González-Burgos, E.; Carretero, M.E.; Gómez-Serranillos, M.P. *Sideritis* spp.: Uses, Chemical Composition and Pharmacological Activities—A Review. *J. Ethnopharmacol.* **2011**, *135*, 209–225. [CrossRef] [PubMed]
9. Lytra, K.; Tomou, E.-M.; Chrysargyris, A.; Drouza, C.; Skaltsa, H.; Tzortzakis, N. Traditionally Used *Sideritis cypria* Post.: Phytochemistry, Nutritional Content, Bioactive Compounds of Cultivated Populations. *Front. Pharmacol.* **2020**, *11*, 650. [CrossRef]
10. Chrysargyris, A.; Tzortzakis, N. Nitrogen, Phosphorus, and Potassium Requirements to Improve *Sideritis cypria* Growth, Nutrient and Water Use Efficiency in Hydroponic Cultivation. *Heliyon* **2025**, *11*, e40755. [CrossRef] [PubMed]
11. Chrysargyris, A.; Kloukina, C.; Vassiliou, R.; Tomou, E.-M.E.-M.; Skaltsa, H.; Tzortzakis, N. Cultivation Strategy to Improve Chemical Profile and Anti-Oxidant Activity of *Sideritis perfoliata* L. subsp. *perfoliata*. *Ind. Crops Prod.* **2019**, *140*, 111694. [CrossRef]
12. Hao, D.; Luan, Y.; Wang, Y.; Xiao, P. Unveiling Nitrogen Fertilizer in Medicinal Plant Cultivation. *Agronomy* **2024**, *14*, 1647. [CrossRef]
13. Ahmadi, F.; Samadi, A.; Rahimi, A. Improving Growth Properties and Phytochemical Compounds of *Echinacea purpurea* (L.) Medicinal Plant Using Novel Nitrogen Slow Release Fertilizer under Greenhouse Conditions. *Sci. Rep.* **2020**, *10*, 13842. [CrossRef] [PubMed]
14. Sun, J.; Li, W.; Zhang, Y.; Guo, Y.; Duan, Z.; Tang, Z.; Abozeid, A. Metabolomics Analysis Reveals Potential Mechanisms in *Bupleurum* L. (Apiaceae) Induced by Three Levels of Nitrogen Fertilization. *Agronomy* **2021**, *11*, 2291. [CrossRef]
15. Khammar, A.A.; Moghaddam, M.; Asgharzade, A.; Sourestani, M.M. Nutritive Composition, Growth, Biochemical Traits, Essential Oil Content and Compositions of *Salvia officinalis* L. Grown in Different Nitrogen Levels in Soilless Culture. *J. Soil Sci. Plant Nutr.* **2021**, *21*, 3320–3332. [CrossRef]
16. Zhao, H.; Li, X.; Jiang, Y. Response of Nitrogen Losses to Excessive Nitrogen Fertilizer Application in Intensive Greenhouse Vegetable Production. *Sustainability* **2019**, *11*, 1513. [CrossRef]
17. Li, B.-B.; Roley, S.S.; Duncan, D.S.; Guo, J.; Quensen, J.F.; Yu, H.-Q.; Tiedje, J.M. Long-Term Excess Nitrogen Fertilizer Increases Sensitivity of Soil Microbial Community to Seasonal Change Revealed by Ecological Network and Metagenome Analyses. *Soil Biol. Biochem.* **2021**, *160*, 108349. [CrossRef]
18. Sabah Alhasan, A.; Kadhem Abbas, M.; Al-Ameri, M.; Tareq Al-Ameri, D. Growth and Yield Response of Basil (*Ocimum basilicum* L.) to Different Rates of Urea Fertilizer Under Field Conditions. *IOP Conf. Ser. Earth Environ. Sci.* **2020**, *553*, 012044. [CrossRef]
19. He, C.E.; Lu, L.L.; Jin, Y.; Wei, J.H.; Christie, P. Effects of Nitrogen on Root Development and Contents of Bioactive Compounds in *Salvia miltiorrhiza* Bunge. *Crop Sci.* **2013**, *53*, 2028–2039. [CrossRef]

20. Amin, H.; Arain, B.A.; Jahangir, T.M.; Abbasi, A.R.; Mangi, J.; Abbasi, M.S.; Amin, F. Copper (Cu) Tolerance and Accumulation Potential in Four Native Plant Species: A Comparative Study for Effective Phytoextraction Technique. *Geol. Ecol. Landsc.* **2021**, *5*, 53–64. [CrossRef]
21. Hawkesford, M.J.; Cakmak, I.; Coskun, D.; De Kok, L.J.; Lambers, H.; Schjoerring, J.K.; White, P.J. Functions of Macronutrients. In *Marschner's Mineral Nutrition of Plants*; Elsevier: Amsterdam, The Netherlands, 2023; pp. 201–281.
22. Asle-Mohammadi, Z.; Kharazmi, M.; Sheikhi, H.; Mohammadkhani, N.; Nicola, S. Foliar Application of Fe, Zn, and Mn as a Practical Strategy to Alleviate the Soil Cu Toxicity and Stimulate the Physiological and Biochemical Properties of Peppermint (*Mentha piperita* L.). *J. Soil Sci. Plant Nutr.* **2024**, *24*, 371–388. [CrossRef]
23. Keller, A.A.; Adeleye, A.S.; Conway, J.R.; Garner, K.L.; Zhao, L.; Cherr, G.N.; Hong, J.; Gardea-Torresdey, J.L.; Godwin, H.A.; Hanna, S.; et al. Comparative Environmental Fate and Toxicity of Copper Nanomaterials. *NanoImpact* **2017**, *7*, 28–40. [CrossRef]
24. Ibrahim, M.; Chee Kong, Y.; Mohd Zain, N. Effect of Cadmium and Copper Exposure on Growth, Secondary Metabolites and Antioxidant Activity in the Medicinal Plant Sambung Nyawa (*Gynura procumbens* (Lour.) Merr). *Molecules* **2017**, *22*, 1623. [CrossRef] [PubMed]
25. Adamczyk-Szabela, D.; Wolf, W.M. The Influence of Copper and Zinc on Photosynthesis and Phenolic Levels in Basil (*Ocimum basilicum* L.), Borage (*Borago officinalis* L.), Common Nettle (*Urtica dioica* L.) and Peppermint (*Mentha piperita* L.). *Int. J. Mol. Sci.* **2024**, *25*, 3612. [CrossRef] [PubMed]
26. Kuziemska, B.; Trębicka, J.; Wysokinski, A. Uptake and Utilization of Nitrogen from Organic Fertilizers Influenced by Different Doses of Copper. *Agronomy* **2021**, *11*, 1219. [CrossRef]
27. Huo, K.; Shangguan, X.; Xia, Y.; Shen, Z.; Chen, C. Excess Copper Inhibits the Growth of Rice Seedlings by Decreasing Uptake of Nitrate. *Ecotoxicol. Environ. Saf.* **2019**, *190*, 110105. [CrossRef]
28. Suganya, A.; Saravanan, A.; Manivannan, N. Role of Zinc Nutrition for Increasing Zinc Availability, Uptake, Yield, and Quality of Maize (*Zea mays* L.) Grains: An Overview. *Commun. Soil Sci. Plant Anal.* **2020**, *51*, 2001–2021. [CrossRef]
29. Behtash, F.; Abedini, F.; Ahmadi, H.; Mosavi, S.B.; Aghaee, A.; Morshedloo, M.R.; Lorenzo, J.M. Zinc Application Mitigates Copper Toxicity by Regulating Cu Uptake, Activity of Antioxidant Enzymes, and Improving Physiological Characteristics in Summer Squash. *Antioxidants* **2022**, *11*, 1688. [CrossRef] [PubMed]
30. Jahani, F.; Tohidi-Moghadam, H.R.; Larijani, H.R.; Ghooshchi, F.; Oveysi, M. Influence of Zinc and Salicylic Acid Foliar Application on Total Chlorophyll, Phenolic Components, Yield and Essential Oil Composition of Peppermint (*Mentha piperita* L.) under Drought Stress Condition. *Arab. J. Geosci.* **2021**, *14*, 691. [CrossRef]
31. Balandrán-Valladares, M.I.; Cruz-Alvarez, O.; Jacobo-Cuellar, J.L.; Hernández-Rodríguez, O.A.; Flores-Córdova, M.A.; Parra-Quezada, R.Á.; Sánchez-Chávez, E.; Ojeda-Barrios, D.L. Changes in Nutrient Concentration and Oxidative Metabolism in Pecan Leaflets at Different Doses of Zinc. *Plant Soil Environ.* **2021**, *67*, 33–39. [CrossRef]
32. Cui, X.; He, H.; Hu, S.; Zhang, B.; Cai, H. Synergistic Interaction between Copper and Nitrogen-Uptake, Translocation, and Distribution in Rice Plant. *Plants* **2022**, *11*, 2612. [CrossRef] [PubMed]
33. Maqbool, M.A.; Beshir, A. Zinc Biofortification of Maize (*Zea mays* L.): Status and Challenges. *Plant Breed.* **2019**, *138*, 1–28. [CrossRef]
34. Romera, F.J.; Lan, P.; Rodríguez-Celma, J.; Pérez-Vicente, R. Editorial: Nutrient Interactions in Plants. *Front. Plant Sci.* **2021**, *12*, 782505. [CrossRef] [PubMed]
35. Chatzigianni, M.; Alkhaled, B.; Livieratos, I.; Stamatakis, A.; Ntatsi, G.; Savvas, D. Impact of Nitrogen Source and Supply Level on Growth, Yield and Nutritional Value of Two Contrasting Ecotypes of *Cichorium spinosum* L. Grown Hydroponically. *J. Sci. Food Agric.* **2017**, *98*, 1615–1624. [CrossRef] [PubMed]
36. Marschner, P. *Marschner's Mineral Nutrition of Higher Plants*, 3rd ed.; Academic Press: Cambridge, MA, USA, 2011; pp. 1–651. [CrossRef]
37. Balamurugan, S.; Thiyagarajan, G.; Manivasagaperumal, R.; Vijayarengan, P. Effect of Copper on Growth, Dry Matter Yield and Nutrient Content of *Vigna radiata* (L.) Wilczek. *J. Phytol.* **2011**, *3*, 53–62.
38. Moeen-ud-din, M.; Wang, S.; Yang, S.; Wang, J. The Combined Effects of Copper and Zinc on *Arabidopsis* Involve Differential Regulation of Chlorophyll Synthesis and Photosystem Function. *Plant Physiol. Biochem.* **2024**, *216*, 109160. [CrossRef] [PubMed]
39. Irmes, K.; Kristó, I.; Szentpéteri, L.; Rácz, A.; Vályi-Nagy, M.; Kassai, M.K.; Valentinyi, K.V.; Tar, M. The Effect of Foliar Zinc Application on the Leaf Chlorophyll Concentrations and Grain Yields of the Winter Wheat (*Triticum aestivum* L.) in the Field Experiments of Two Seasons. *Agronomy* **2023**, *13*, 1640. [CrossRef]
40. Hawkesford, M.; Horst, W.; Kichey, T.; Lambers, H.; Schjoerring, J.; Møller, I.S.; White, P.J. Functions of Macronutrients. In *Marschner's Mineral Nutrition of Higher Plants*, 3rd ed.; Elsevier: Amsterdam, The Netherlands, 2012; pp. 135–189. [CrossRef]
41. Yruela, I. Copper in Plants: Acquisition, Transport and Interactions. *Funct. Plant Biol.* **2009**, *36*, 409. [CrossRef] [PubMed]
42. White, P.J.; Broadley, M.R. Physiological Limits to Zinc Biofortification of Edible Crops. *Front. Plant Sci.* **2011**, *2*, 80. [CrossRef] [PubMed]

43. El-Sherbeny, S.E.; El-Saadany, S.S.; Youssef, A.A.; El-Massry, R.A.; El-Newary, S.A. Response of *Portulaca oleracea* L. Plants to Various Fertilizers Ratios on Growth, Yield and Chemical Composition under Egyption Conditions. *World J. Pharm. Sci.* **2015**, *3*, 2297–2307.
44. Cun, Z.; Wu, H.M.; Zhang, J.Y.; Shuang, S.P.; Hong, J.; An, T.X.; Chen, J.W. High Nitrogen Inhibits Biomass and Saponins Accumulation in a Medicinal Plant Panax Notoginseng. *PeerJ* **2023**, *11*, e14933. [CrossRef]
45. Alinejad Elahshah, A.; Moradi, H.; Sadeghi, H. Boron and Zinc Foliar Application Enhanced the Morphophysiological Responses and Mineral Absorption in the Hydroponically Grown 'Aromas' Strawberry. *J. Plant Nutr.* **2023**, *46*, 3487–3498. [CrossRef]
46. Kutman, U.B.; Yildiz, B.; Cakmak, I. Improved Nitrogen Status Enhances Zinc and Iron Concentrations Both in the Whole Grain and the Endosperm Fraction of Wheat. *J. Cereal Sci.* **2011**, *53*, 118–125. [CrossRef]
47. Xue, Y.; Yan, W.; Gao, Y.; Zhang, H.; Jiang, L.; Qian, X.; Cui, Z.; Zhang, C.; Liu, S.; Wang, H.; et al. Interaction Effects of Nitrogen Rates and Forms Combined With and Without Zinc Supply on Plant Growth and Nutrient Uptake in Maize Seedlings. *Front. Plant Sci.* **2021**, *12*, 722752. [CrossRef] [PubMed]
48. Kumar, S.; Kumar, S.; Mohapatra, T. Interaction Between Macro- and Micro-Nutrients in Plants. *Front. Plant Sci.* **2021**, *12*, 665583. [CrossRef]
49. Ranade-Malvi, U. Interaction of Micronutrients with Major Nutrients with Special Reference to Potassium. *Karnataka J. Agric. Sci.* **2011**, *24*, 106–109.
50. Yan, G.; Luo, X.; Huang, B.; Wang, H.; Xing, Y.; Wang, Q. Imbalance in Nitrogen and Phosphorus Allocation between Tree Roots and Leaves Induced by Nitrogen Addition. *Sci. Total Environ.* **2025**, *958*, 177925. [CrossRef] [PubMed]
51. Li, L.; Liu, B.; Gao, X.; Li, X.; Li, C. Nitrogen and Phosphorus Addition Differentially Affect Plant Ecological Stoichiometry in Desert Grassland. *Sci. Rep.* **2019**, *9*, 18673. [CrossRef] [PubMed]
52. Ait Ali, N.; Bernal, M.P.; Ater, M. Tolerance and Bioaccumulation of Copper in *Phragmites australis* and *Zea mays*. *Plant Soil* **2002**, *239*, 103–111. [CrossRef]
53. Saleem, M.H.; Kamran, M.; Zhou, Y.; Parveen, A.; Rehman, M.; Ahmar, S.; Malik, Z.; Mustafa, A.; Ahmad Anjum, R.M.; Wang, B.; et al. Appraising Growth, Oxidative Stress and Copper Phytoextraction Potential of Flax (*Linum usitatissimum* L.) Grown in Soil Differentially Spiked with Copper. *J. Environ. Manag.* **2020**, *257*, 109994. [CrossRef] [PubMed]
54. Chrysargyris, A.; Maggini, R.; Incrocci, L.; Pardossi, A.; Tzortzakis, N. Copper Tolerance and Accumulation on *Pelargonium graveolens* L'Hér. Grown in Hydroponic Culture. *Plants* **2021**, *10*, 1663. [CrossRef]
55. Shahriaripour, R.; Tajabadipour, A. Zinc Nutrition of Pistachio: Interaction of Zinc with Other Trace Elements. *Commun. Soil Sci. Plant Anal.* **2010**, *41*, 1885–1888. [CrossRef]
56. European Food Safety Authority (EFSA) Review of the Existing Maximum Residue Levels for Copper Compounds According to Article 12 of Regulation (EC) No 396/2005. *EFSA J.* **2018**, *16*, e05212. [CrossRef]
57. Rai, S.; Singh, P.K.; Mankotia, S.; Swain, J.; Satbhai, S.B. Iron Homeostasis in Plants and Its Crosstalk with Copper, Zinc, and Manganese. *Plant Stress* **2021**, *1*, 100008. [CrossRef]
58. Waters, B.M.; Armbrust, L.C. Optimal Copper Supply Is Required for Normal Plant Iron Deficiency Responses. *Plant Signal. Behav.* **2013**, *8*, e26611. [CrossRef] [PubMed]
59. Fatemi, H.; Zaghdoud, C.; Nortes, P.A.; Carvajal, M.; Martínez-Ballesta, M.D.C. Differential Aquaporin Response to Distinct Effects of Two Zn Concentrations after Foliar Application in Pak Choi (*Brassica rapa* L.) Plants. *Agronomy* **2020**, *10*, 450. [CrossRef]
60. Guardiola-Márquez, C.E.; Martínez-Ballesta, M.d.C.; García-Sánchez, C.V.; Bojorquez-Rodríguez, E.M.; Jacobo-Velázquez, D.A.; Martínez-Hernández, G.B. Effects of Foliar and Root Application of Zn and Fe Bio-Nanofertilizers on the Glucosinolate, Zn and Fe Contents of Pak Choi (*Brassica rapa* subsp. Chinensis) Grown under Hydroponic and Pot Cultivation. *Sci. Hortic.* **2024**, *338*, 113654. [CrossRef]
61. Montoya, M.; Vallejo, A.; Recio, J.; Guardia, G.; Alvarez, J.M. Zinc–Nitrogen Interaction Effect on Wheat Biofortification and Nutrient Use Efficiency. *J. Plant Nutr. Soil Sci.* **2020**, *183*, 169–179. [CrossRef]
62. Mleczek, M.; Budka, A.; Gąsecka, M.; Budzyńska, S.; Drzewiecka, K.; Magdziak, Z.; Rutkowski, P.; Goliński, P.; Niedzielski, P. Copper, Lead and Zinc Interactions during Phytoextraction Using *Acer platanoides* L.—A Pot Trial. *Environ. Sci. Pollut. Res.* **2023**, *30*, 27191–27207. [CrossRef] [PubMed]
63. Adrees, M.; Ali, S.; Rizwan, M.; Ibrahim, M.; Abbas, F.; Farid, M.; Zia-ur-Rehman, M.; Irshad, M.K.; Bharwana, S.A. The Effect of Excess Copper on Growth and Physiology of Important Food Crops: A Review. *Environ. Sci. Pollut. Res.* **2015**, *22*, 8148–8162. [CrossRef]
64. García-López, J.I.; Niño-Medina, G.; Olivares-Sáenz, E.; Lira-Saldivar, R.H.; Barriga-Castro, E.D.; Vázquez-Alvarado, R.; Rodríguez-Salinas, P.A.; Zavala-García, F. Foliar Application of Zinc Oxide Nanoparticles and Zinc Sulfate Boosts the Content of Bioactive Compounds in Habanero Peppers. *Plants* **2019**, *8*, 254. [CrossRef]
65. Vojodi Mehrabani, L.; Kamran, R.V.; Hassanpouraghdam, M.B.; Pessarakli, M. Zinc Sulfate Foliar Application Effects on Some Physiological Characteristics and Phenolic and Essential Oil Contents of *Lavandula stoechas* L. Under Sodium Chloride (NaCl) Salinity Conditions. *Commun. Soil Sci. Plant Anal.* **2017**, *48*, 1860–1867. [CrossRef]

66. Umair Hassan, M.; Aamer, M.; Umer Chattha, M.; Haiying, T.; Shahzad, B.; Barbanti, L.; Nawaz, M.; Rasheed, A.; Afzal, A.; Liu, Y.; et al. The Critical Role of Zinc in Plants Facing the Drought Stress. *Agriculture* **2020**, *10*, 396. [CrossRef]
67. Chrysargyris, A.; Panayiotou, C.; Tzortzakis, N. Nitrogen and Phosphorus Levels Affected Plant Growth, Essential Oil Composition and Antioxidant Status of Lavender Plant (*Lavandula angustifolia* Mill.). *Ind. Crops Prod.* **2016**, *83*, 577–586. [CrossRef]
68. Rehman, M.; Saleem, M.H.; Fahad, S.; Maqbool, Z.; Peng, D.; Deng, G.; Liu, L. Medium Nitrogen Optimized *Boehmeria nivea* L. Growth in Copper Contaminated Soil. *Chemosphere* **2021**, *266*, 128972. [CrossRef]
69. Shehzadi, N.; Mahmood, A.; Kaleem, M.; Chishti, M.S.; Bashir, H.; Hashem, A.; Abd-Allah, E.F.; Shahid, H.; Ishtiaq, A. Zinc and Nitrogen Mediate the Regulation of Growth, Leading to the Upregulation of Antioxidant Aptitude, Physio-Biochemical Traits, and Yield in Wheat Plants. *Sci. Rep.* **2024**, *14*, 12897. [CrossRef]
70. Chrysargyris, A.; Tzortzakis, N. Optimising Fertigation of Hydroponically Grown Sowthistle (*Sonchus oleraceus* L.): The Impact of the Nitrogen Source and Supply Concentration. *Agric. Water Manag.* **2023**, *289*, 108528. [CrossRef]
71. Chrysargyris, A.; Michailidi, E.; Tzortzakis, N. Physiological and Biochemical Responses of *Lavandula angustifolia* to Salinity Under Mineral Foliar Application. *Front. Plant Sci.* **2018**, *9*, 489. [CrossRef]
72. Richardson, A.D.; Duigan, S.P.; Berlyn, G.P. An Evaluation of Noninvasive Methods to Estimate Foliar Chlorophyll Content. *New Phytol.* **2002**, *153*, 185–194. [CrossRef]
73. Wellburn, A.R.A.R. The Spectral Determination of Chlorophylls a and b, as Well as Total Carotenoids, Using Various Solvents with Spectrophotometers of Different Resolution. *J. Plant Physiol.* **1994**, *144*, 307–313. [CrossRef]
74. Chrysargyris, A.; Papakyriakou, E.; Petropoulos, S.; Tzortzakis, N. The Combined and Single Effect of Salinity and Copper Stress on Growth and Quality of *Mentha spicata* Plants. *J. Hazard. Mater.* **2019**, *368*, 584–593. [CrossRef]
75. Chrysargyris, A.; Charalambous, S.; Xylia, P.; Litskas, V.; Stavrinides, M.; Tzortzakis, N. Assessing the Biostimulant Effects of a Novel Plant-Based Formulation on Tomato Crop. *Sustainability* **2020**, *12*, 8432. [CrossRef]

Disclaimer/Publisher's Note: The statements, opinions and data contained in all publications are solely those of the individual author(s) and contributor(s) and not of MDPI and/or the editor(s). MDPI and/or the editor(s) disclaim responsibility for any injury to people or property resulting from any ideas, methods, instructions or products referred to in the content.

plants

MDPI

Article

Genome-Wide Identification and Expression Analysis of Heat Shock Transcription Factors in *Camellia sinensis* Under Abiotic Stress

Guimin Li [1], Xinying Shi [2], Qinmin Lin [2], Mengmeng Lv [3], Jing Chen [1], Yingxin Wen [3], Zhiyi Feng [4], Syed Muhammad Azam [4], Yan Cheng [5], Shucai Wang [1,*] and Shijiang Cao [3,*]

[1] Laboratory of Plant Molecular Genetics & Crop Gene Editing, School of Life Sciences, Linyi University, Linyi 276000, China; liguimin@lyu.edu.cn (G.L.); chenjing2488@outlook.com (J.C.)
[2] College of Life Sciences, Fujian Agriculture and Forestry University, Fuzhou 350002, China; 13163835793@163.com (X.S.); 18760030926@163.com (Q.L.)
[3] College of Forestry, Fujian Agriculture and Forestry University, Fuzhou 350002, China; youyosihq@163.com (M.L.); 18050409132@139.com (Y.W.)
[4] College of Resources and Environment, Fujian Agriculture and Forestry University, Fuzhou 350002, China; savannah11210802@163.com (Z.F.); syedazamfafu@gmail.com (S.M.A.)
[5] College of Plant Protection, Fujian Agriculture and Forestry University, Fuzhou 350002, China; chengyan1220@hotmail.com
* Correspondence: wangshucai@lyu.edu.cn (S.W.); 000q813040@fafu.edu.cn (S.C.)

Abstract: The tea plant (*Camellia sinensis*) is an economically important crop that plays an important role not only in the beverage industry but also in the pharmaceutical industry. The environment has a great influence on the quality of the tea plant. Heat shock factors (Hsfs) are transcriptional regulators that control the plant response to adversity. However, only a limited number of studies have reported the *Hsf* gene in *Camellia sinensis*, and most of these reports involve high-temperature, drought, and salt stress. Research on light, dark, and cold stress is limited. In this study, 22 *CsHsf* genes were obtained by whole genome sequencing and found to be located on 11 chromosomes. In addition, the gene structure, protein motif, and phylogeny were studied. We classified the genes into three major subfamilies: CsHsfA, CsHsfB, and CsHsfC. Interestingly, we found that there was more alignment between *CsHsf* and *Hsf* genes in dicotyledons, including *Arabidopsis thaliana* and *Solanum lycopersicum*, than in the monocotyledon *Oryza sativa*. The expression of many *CsHsf* genes was affected by low-temperature, light, and dark abiotic stresses. Notably, *CsHsf15* and *CsHsf16* showed high induction rates under both light and cold stress, and both genes carried *cis*-acting elements associated with light and low-temperature responses. These results lay a solid groundwork for further investigations into the involvement of *CsHsf* genes in the response of *Camellia sinensis* to abiotic stresses.

Keywords: tea; Hsf; gene family; abiotic stress

1. Introduction

The tea plant (*Camellia sinensis*) is native to Southeast Asia, East Asia, and the Indian subcontinent, but it is now widely grown in tropical and subtropical regions around the world [1]. As one of the world's most significant beverage crops, the tea plant (*Camellia sinensis*) has substantial economic and health benefits, making it an essential cash crop globally [2]. However, tea plants are susceptible to a variety of environmental stresses throughout their life cycle. On the one hand, low temperatures under abiotic stress can

change the indole formation of tea plants [3], salt stress can cause the accumulation of reactive oxygen species (ROS) [4], and drought stress can significantly affect the biosynthesis of abscisic acid, ethylene, and jasmonic acid and the expression levels of genes related to signal transduction [5]. On the other hand, when herbivores eat tea under biological stress, it affects the yield of tea [6,7].

To cope with these environmental challenges, plants have evolved sophisticated defense mechanisms, with transcription factors playing a critical role in activating or inhibiting the expression of stress-responsive genes. Transcription factors are DNA-binding proteins that can activate or inhibit the transcription of multiple target genes by binding to certain gene promoter regions [4,8,9]. Plants can regulate the expression of related stress-resistance genes at the mRNA level and then cause a series of physiological and biochemical reactions in plants to adapt to the environment [2,10].

Among the various defense mechanisms, heat shock proteins (HSPs) are highly conserved molecular chaperones crucial for the plant defense against heat stress and other abiotic stresses [11,12]. HSPs aid in maintaining cellular structure and function, which is essential for plant survival in stressful environments. At present, the functional mechanisms of HSP90, HSP70, and sHSP in plant stress responses have been widely reported. For instance, the expression of Arabidopsis *HSP90* genes is strongly induced under heat, cold, salinity, and heavy metal stress. The overexpression of alfalfa's *MsHSP70* and horse gram's *MuHSP70* can improve the resistance of plants to cold, heat, drought, salinity, and oxidation stress [13] Heat shock factors (*Hsfs*), which are a group of transcription factors, regulate the expression of HSP genes in response to stress. The regulatory capacity of *Hsfs* is largely due to their ability to preserve protein stability under stressful conditions [14,15].

Hsfs have a highly conserved protein structure with five key domains: the nuclear localization signal (NLS), nuclear export signal (NES), DNA-binding domain (DBD), oligomerization domain (OD), and a short C-terminal activator peptide motif (AHA motif) [16–18]. The NLS allows Hsf proteins to be transported from the cytoplasm to the nucleus, where they can bind to the heat shock elements in the promoter regions of HSP genes, triggering their transcription [19–21]. Hsfs are classified into A, B, and C groups based on the structure of their HR-A/B region, with A-group Hsfs having a more complex structure than the simplified B- and C-group Hsfs [22].

The function of the Hsf gene family has also been reported in previous work. *ZoHSF16* and *ZoHSF25* are believed to play a role in ginger's response to high-temperature and strong light stress [23]. *AeHSFA2b* significantly enhances the tolerance of *Actinidia eriantha* to salt stress by increasing the expression of *AtRS5*, *AtGolS1*, and *AtGolS2* [24]. In peanuts (*Arachis hypogaea* L.), the overexpression of *AhHsf20* enhances salt tolerance. In rice (*Oryza sativa* L.) [25], *Os03g53340* is essential for the early activation of heat shock protein genes under heat stress [26]. These results suggest that plants have evolved subclass specificity and multiple functions in some members of the Hsf family. In addition, a large number of studies have shown that the *HSF* family plays an important regulatory role in various physiological aspects of growth and development in other plants. For example, the overexpression of *TaHSFB4*-2B inhibits the seed germination and growth of *Arabidopsis thaliana* under salinity and mannitol treatment [26]. The whole genome sequencing of plants like rye (*Secale cereale* L.), the common bean (*Phaseolus vulgaris*), *Arabidopsis*, rice, and alfalfa (*Medicago sativa*) has further deepened our understanding of these gene families [27–32].

Despite extensive research on Hsf genes in various plants, studies on Hsf genes in tea plants remain limited, and most of the existing research has primarily focused on their response to high-temperature, salinity, and drought stress. Previous studies have shown that *CsHsfs* are differentially regulated by drought, salt, and heat stress, and the heterologous expression of *CsHsfA2* in yeast has been found to improve thermotolerance,

suggesting its potential role in regulating heat stress responses [33]. Our study, which explores the response of tea trees to light, low-temperature, and dark stress, fills a gap in current knowledge by addressing these less-explored stress factors. Given that abiotic stresses significantly reduce tea plant yield and considering the crucial role of *Hsfs* in helping plants cope with adverse environments, a deeper understanding of *CsHsf* genes in tea trees is essential for advancing future research. In this study, we identified 22 *CsHsf* genes in tea plants and examined their chromosomal locations, *cis*-regulatory elements, phylogenetic relationships, conserved regions, and gene structures. We also explored the intrinsic mechanisms of *CsHsf* genes in the tea plant's adaptation to stress. The findings of this research provide a valuable theoretical foundation for further investigation into the functions of *Hsf* genes in tea trees and other species as well as for advancing plant genetic improvement.

2. Results

2.1. Identification of the CsHsf Genes in Camellia sinensis

In this study, we successfully identified 22 *CsHsf* genes from the genome of *Camellia sinensis* 'Tieguanyin'. These genes were named *CsHsf1* to *CsHsf22* based on phylogenetic relationships (Table 1 and Figure 1). A variety of gene characteristics were identified, including locus name, amino acid sequence length, protein molecular weight, isoelectric points, instability index, aliphatic index, and predicted location (Table 1). In particular, the length of these genomic sequences is variable, with *CsHsf12* containing only 79 amino acids (aa), the shortest of the 22 *Hsf* genes. In contrast, the longest, *CsHsf13*, has 536 amino acids (aa). These 22 genes vary in protein molecular weight from 9.030 kDa (*CsHsf12*) to 60.823 kDa (*CsHsf13*), ranging from 4.75 (*CsHsf15*) to 8.97 (*CsHsf18*) in isoelectric points. The instability index varies between 36.81 (*CsHsf12*) and 80.56 (*CsHsf17*). All 22 members of this family have an instability index higher than 40 and are therefore considered unstable. Of particular note, subcellular localization shows that all members of the *CsHsf* family are localized to the nucleus.

Table 1. List of the 22 CsHsf genes identified in this study.

Gene Name	Number of Amino Acids/aa	Molecular Weight/Da	Theoretical PI	Grand Average of Hydropathicity	Instability Index	Aliphatic Index	Subcellular Localization
CsHsf1	423	48.81	5.28	−0.852	56.04	64.23	Nucleus.
CsHsf2	375	41.89	5.88	−0.562	62.11	74.16	Nucleus.
CsHsf3	299	34.05	6.47	−0.873	60.21	64.25	Nucleus.
CsHsf4	508	56.45	5.13	−0.553	57.85	71.14	Nucleus.
CsHsf5	290	32.14	5.38	−0.821	38.90	59.21	Nucleus.
CsHsf6	326	36.48	7.71	−0.500	54.80	70.58	Nucleus.
CsHsf7	407	46.42	4.98	−0.774	55.45	71.35	Nucleus.
CsHsf8	211	24.52	8.97	−0.877	68.00	63.36	Nucleus.
CsHsf9	321	36.304	5.75	−0.533	66.85	68.35	Nucleus.
CsHsf10	416	46.937	4.95	−0.647	54.37	75.22	Nucleus.
CsHsf11	479	53.663	5.76	−0.772	56.17	64.36	Nucleus.
CsHsf12	79	9.030	5.07	−0.397	36.81	71.52	Nucleus.
CsHsf13	546	60.823	4.95	−0.563	58.24	75.31	Nucleus.
CsHsf14	240	27.854	8.20	−0.715	53.05	64.17	Nucleus.
CsHsf15	388	44.338	4.75	−0.633	54.97	79.33	Nucleus.
CsHsf16	495	54.879	4.89	−0.600	62.72	70.69	Nucleus.
CsHsf17	240	27.825	5.60	−0.851	80.56	62.12	Nucleus.
CsHsf18	513	56.783	4.78	−0.620	55.54	68.07	Nucleus.
CsHsf19	314	35.057	5.37	−0.680	55.13	71.46	Nucleus.
CsHsf20	499	55.592	5.15	−0.567	54.76	81.66	Nucleus.
CsHsf21	310	35.134	6.46	−0.332	37.59	88.03	Nucleus.
CsHsf22	282	32.796	6.39	−0.720	62.81	65.32	Nucleus.

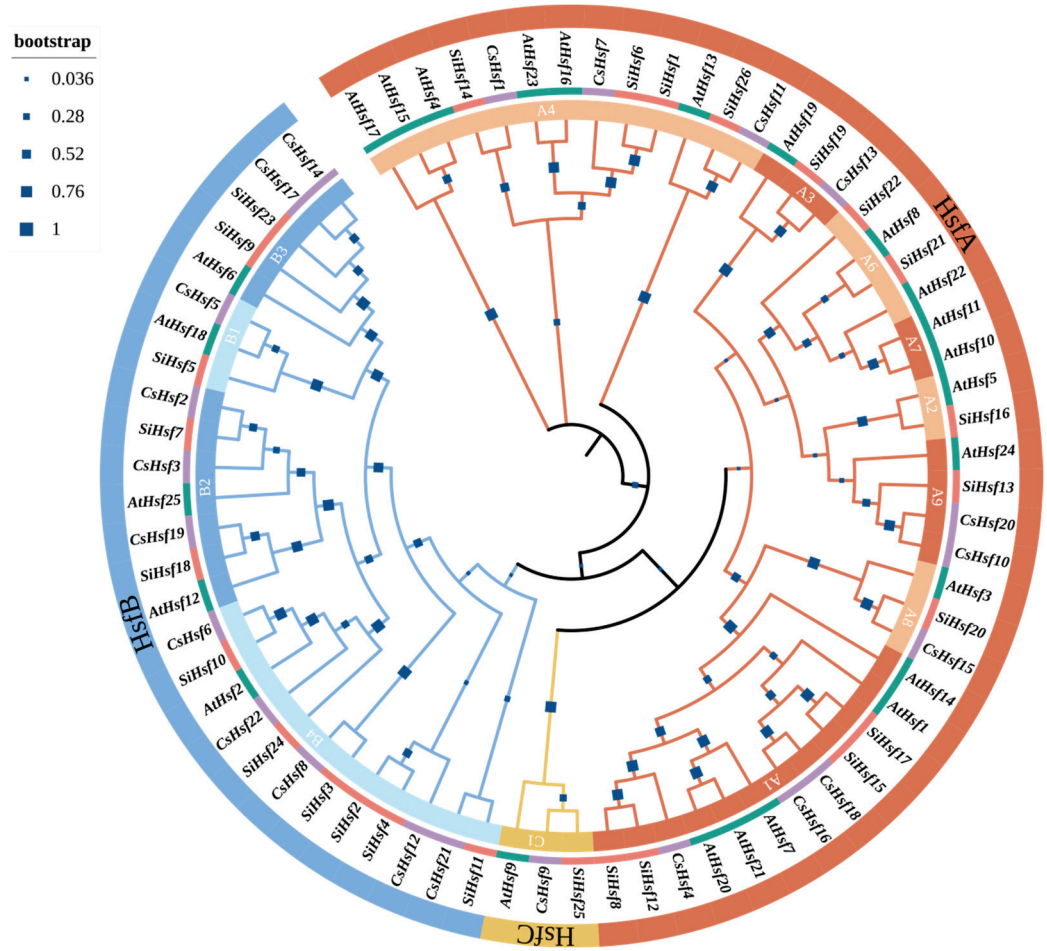


Figure 1. Phylogenetic tree of the *Camellia sinensis*, *Solanum lycopersicum*, and *Arabidopsis thaliana* Hsf family. A phylogenetic tree was generated based on maximum likelihood (ML) analysis, utilizing 1000 bootstrap replicates for accuracy.

2.2. Phylogenetic Analysis and Classification of CsHsfs

We used 22 Hsf proteins to construct a phylogenetic tree with 25 and 26 Hsf proteins from Arabidopsis thaliana and Solanum lycopersicum. The results show that members of the CsHsf family are found in all three groups. According to the results, we divided Hsf into three groups: HsfA, HsfB, and HsfC. The largest of these is CsHsf A, consisting of 10 proteins (CsHsf11 CsHsf12, CsHsf1, CsHsf7, CsHsf21, CsHsf4, CsHsf16, CsHsf18, CsHsf13, CsHsf9), accounting for 45.5% of the total CsHsfs. It was followed by CsHsf B, accounting for 40.1%. CsHsf C had the least protein members, with only three proteins, namely CsHsf15, CsHsf10, and CsHsf20. Phylogenetic tree studies show that the tea plant is closely related to Arabidopsis thaliana and Solanum lycopersicum.

2.3. Distribution of CsHsf Genes Across Chromosomes

We identified 22 *CsHsf* genes in the tea plant genome, and the 22 identified sequences were more uniformly localized on 11 chromosomes of the tea plant (Figure 2). To avoid confusion, we named these sequences *CsHsf01* to *CsHsf22*. The *CsHsf* genes were distributed across all the chromosomes, with the highest number of *CsHsf* genes distributed on chromosomes 1 and 14. The lowest number of *CsHsf* genes were distributed on chromosomes 4 and 13, all of which had one *CsHsf* gene.

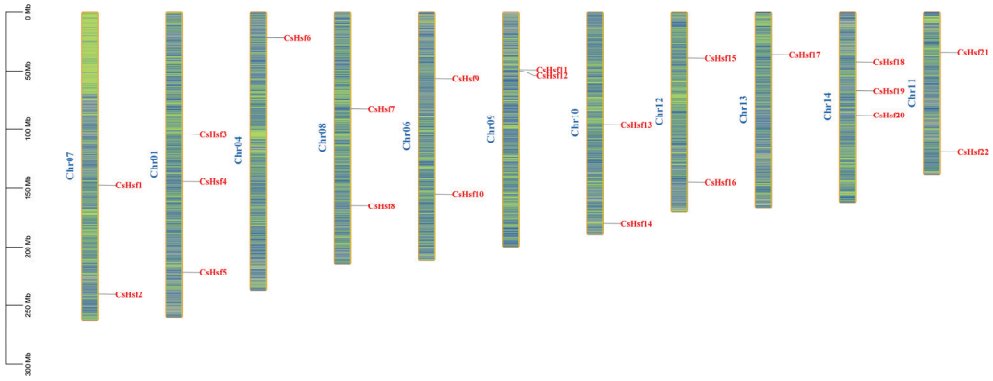


Figure 2. The distribution of *Hsf* genes across the chromosomes in *Camellia sinensis* shows areas of higher gene density marked in blue, while regions with lower gene density are represented in green.The blue letters identify the different chromosomes.

2.4. Gene Structure and Conserved Motif Composition

To further elucidate the structural features of the 22 Hsf transcription factor families, we thoroughly analyzed its exons and introns, focusing on their quantity and distribution (Figure 3D). The gene structure analysis revealed that the number of exons in different CsHsf genes varied from two to five. Most of the CsHsf genes had two exons. There were five CsHsf genes (CsHsf12, CsHsf21, CsHsf10, CsHsf20, and CsHsf22), and only CsHsf2 contained one exon. Moreover, members of genes from the same family show similar exon and intron structures.

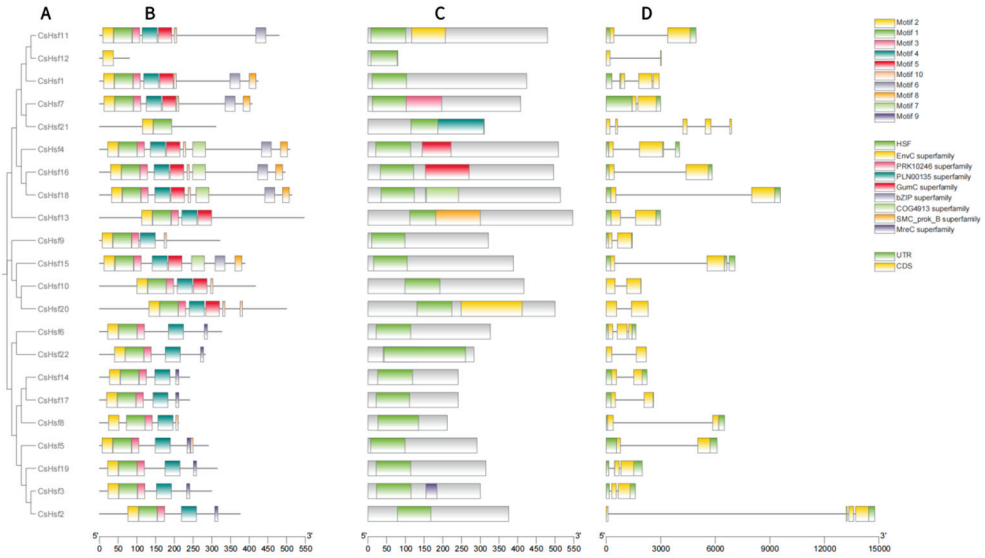


Figure 3. The phylogenetic relationships, conserved protein motif structures, *cis*-acting elements, and gene structure analysis of the CsHsfs are shown. (**A**) A phylogenetic tree was generated in MEGA with the maximum likelihood method, using 1000 bootstrap replicates. (**B**) The distribution of conserved motifs in CsHsf proteins is illustrated, with each of the 10 motifs represented by distinct colored boxes. (**C**) Different color blocks represent different domains. (**D**) The exon–intron structure of the *Camellia sinensis Hsf* gene; exons are indicated by yellow boxes, untranslated regions are indicated by green boxes, and black lines indicate introns.

Using the online MEME tool, we conducted a further analysis of conserved motifs within the Hsf protein family members. The results showed that motifs 1, 2, and 3 were present in all the members except CsHsf12 and CsHsf21, although CsHsf12 contained only motif 2 and CsHsf21 only motifs 1 and 2 (Figure 3B). Notably, motif 8 and motif 6 were found only in group A Hsfs, and motif 9 was found only in group B Hsfs. Overall, each

group of CsHsf members shared similar motifs, yet notable differences were observed between the various groups (Figure 3B).

2.5. Analysis of cis-Acting Elements

In order to deeply investigate the response of *CsHsf* genes to abiotic stresses, we used preliminary experimental validation and data analysis (Figure 4). We found that *CsHsfs* contain a series of cis-regulatory elements, stress-related elements (anaerobic induction, low-temperature responsiveness, anoxic specific inducibility, and defense and street responsiveness), hormone-related elements (salicylic acid response, abscisic acid response, MeJA response), and development-related components (light responsiveness, meristem expression, control of circadian rhythms). The results showed that there were 18 genes with *cis*-acting elements related to light response, 8 genes with *cis*-acting elements related to low-temperature response, and 12 genes with *cis*-acting elements related to the abscisic acid reaction.

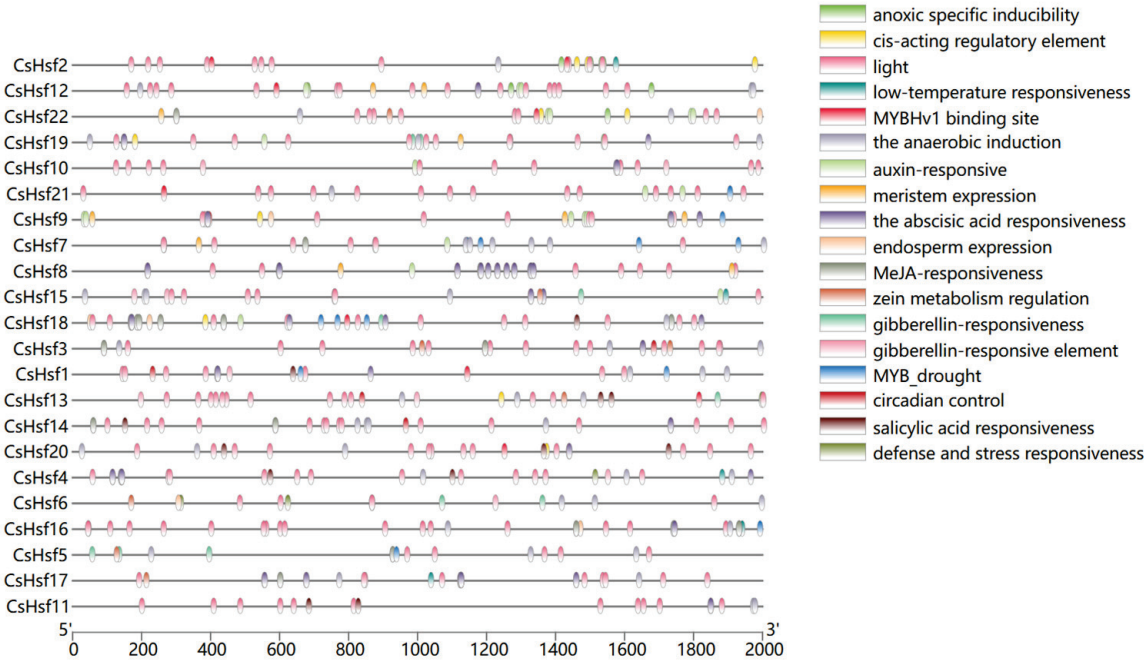


Figure 4. Different colored squares indicate different *cis*-acting elements of the CsHsf promoter region.

2.6. Intraspecific Collinearity Analysis of CsHsf Genes

The main causes of gene function changes are the loss and gain of genes [8]. To investigate the replication events of *Hsfs*, we conducted a collinear analysis within the species (Figure 5). The analysis results indicate that 10 genes out of the 22 *CsHsfs* have collinear relationships, with a total of 7 gene pairs. We also found that some *CsHsf* genes were linearly related to multiple genes, such as *CsHsfs16* being collinear with both *CsHsfs18* and *CsHsfs4*. Combined with the evolutionary analysis, all three genes belonging to taxon A. *CsHsfs19* were collinear with *CsHsfs2* and *CsHsfs3*, all of which exist in the B taxon. This indicates the tendency of genes with collinearity to be clustered in the same taxon. These genes may arise through genome replication events and are structurally and functionally similar. In addition, 10 *CsHsfs* were involved in segmental duplication, and the gene duplication events all took place between different chromosomes, which suggests that segmental duplication is the main driving force in the evolution of *CsHsfs*.

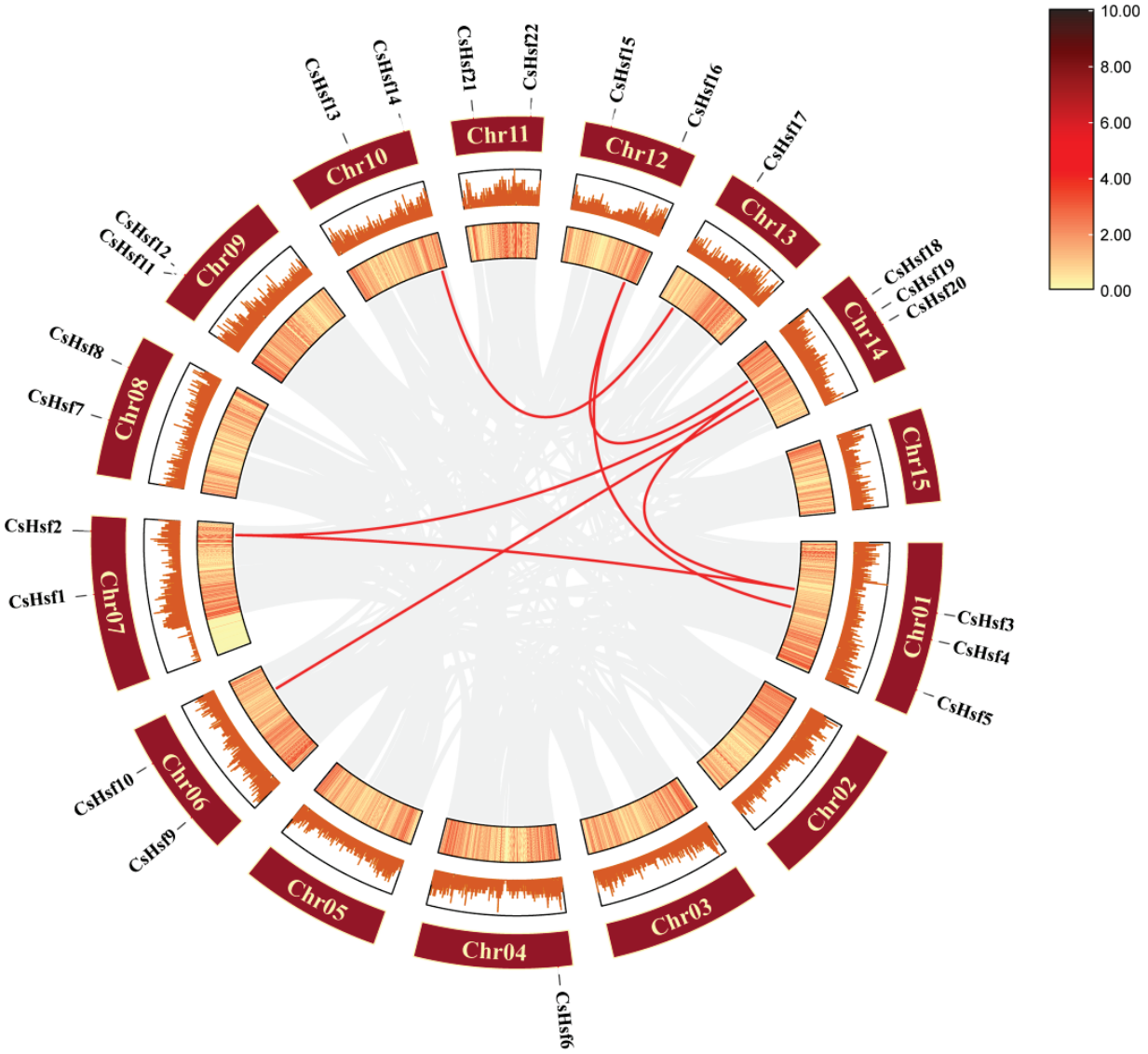


Figure 5. Collinearity among *CsHsf* members in *Camellia sinensis*. Red lines represent collinear relationships among *CsHsf* members, and the gray line indicates all duplicate gene pairs.

2.7. Synteny Analysis Among CsHsf Genes

In order to explore the underlying evolutionary mechanisms driving the development of tea plants, we conducted a comparative analysis of collinearity among *CsHsf* gene pairs in the genomes of *Arabidopsis thaliana*, *Solanum lycopersicum*, and *Oryza sativa* (Figure 6). We found that 16 homologous gene pairs were identified between *CsHsf* and *AtHsf* genes, 10 homologous gene pairs were found between *CsHsf* and *OsHsf* genes, and 29 homologous gene pairs were found between *CsHsf* and *SiHsf* genes. We found more collocated genes between *CsHsf* and *Hsf* genes in the dicotyledonous plants *Arabidopsis thaliana* and *Solanum lycopersicum* than in the monocotyledonous plant *Oryza sativa*. In addition, three *CsHsf* genes, *CsHsf5*, *CsHsf2*, and *CsHsf19*, showed collinearity with the *Arabidopsis thaliana*, *Oryza sativa*, and *Solanum lycopersicum* genes. Based on the collinearity analysis, it can be inferred that these three *CsHsf* genes likely existed prior to the divergence of these species.

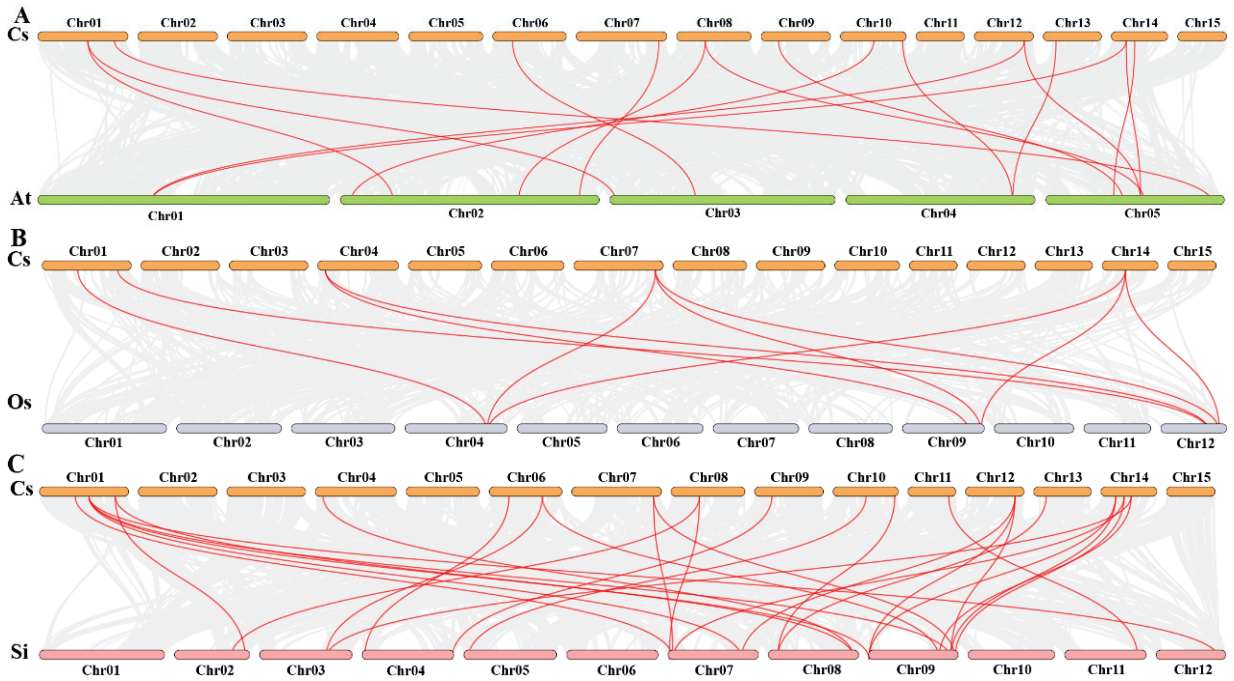


Figure 6. Collinearity analysis plot of *Camellia sinensis* with *Arabidopsis thaliana*, *Oryza sativa*, and *Solanum lycopersicum*. Subfigure (**A**) shows *Camellia sinensis* and *Arabidopsis thaliana*. Subfigure (**B**) is *Camellia sinensis* and *Oryza sativa*, and Subfigure (**C**) is *Camellia sinensis* and *Solanum lycopersicum*. Collinear blocks are marked with gray lines, while collinear gene pairs with *Hsf* genes are highlighted with red lines.

2.8. Expression Patterns of CsHsfs Under Light, Shade, and Cold Stress

We used quantitative real-time PCR (qRT-PCR) to confirm how the *CsHsf* gene responds to different abiotic stresses, including light, shade, and cold. The results showed that the expression levels of all *CsHsf* genes increased and decreased significantly under different stress treatments (Figure 7). Under light stress, *CsHsf* gene expression showed a trend of first increasing, then decreasing, and then increasing, increasing at 4 h, downregulating at 8 h, and upregulating again at 12 h and 24 h. *CsHsf16* had the most significant upregulation, followed by *CsHsf22*, *CsHsf8*, and *CsHsf15*. Most *CsHsfs* peaked at 4 h and decreased significantly at 8 h, indicating that the hsf family has a certain response to light stress. Under shade stress, the expression of *CsHsf* genes was suppressed to varying degrees. All *CsHsfs* showed a downward trend at 4 h and then upregulated under shade stress, reaching a peak at 24 h. This trend may reflect the potential role of these genes in plant adaptation to low-light conditions. Under cold stress, *CsHsf* gene expression decreased at 4 h and 12 h and increased at 8 h and 24 h. It is worth noting that the expression level of *CsHsf15* increased the most significantly, and the expression level increased by about six times compared with the initial stage of treatment. This was followed by *CsHsf8*, *CsHsf16*, and *CsHsf17*. This may indicate that *CsHsf* family members have a potential ability to withstand cold stress.

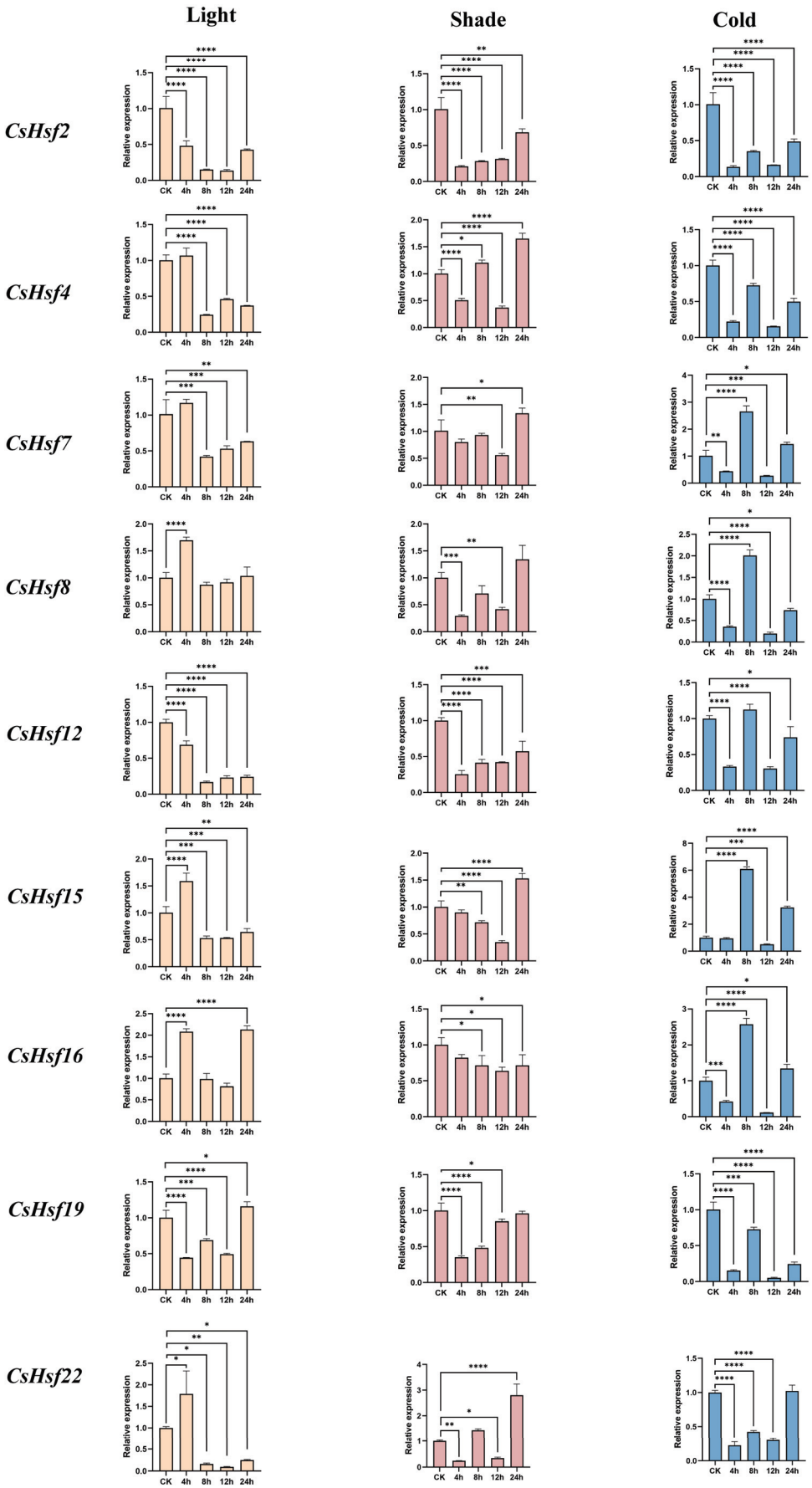


Figure 7. qRT-PCR analysis of *CsHsf* genes under abiotic stress. Light, shade, and cold stress conditions were used for 4 h, 8 h, 12 h, and 24 h, respectively. The data were means ± SD of three biological repeats.* $p \leq 0.05$; ** $p \leq 0.005$; *** $p \leq 0.0005$; **** $p \leq 0.0001$.

3. Discussion

Changes in global temperatures have caused severe abiotic stress, and a growing body of research supports the critical role of the Hsf gene in plants coping with harsh conditions [25]. Verifying the function of plant genes can be accomplished effectively by plant genome analysis [34]. The *Hsf* gene has been studied in a variety of plants in *Hsf* gene family members. These include garlic [35], alfalfa [30], soybean [36], wheat [37], *A. thaliana* [38], *Vitis vinifera* (grapes), and *Beta vulgaris* (sugar beet). However, until now, only a limited number of studies have been conducted on the *Hsf* gene in tea plants. In the limited number of studies, most have involved the response of tea *Hsfs* to high-temperature, drought, and salt stress. In order to improve the comprehensive understanding of the tea Hsf gene family, Liu et al. [39] first identified the *Hsf* gene family in *Camellia sinensis* using RNA-seq data. However, limited by the lack of reference genome sequencing, only 16 *CsHsf* genes were identified. Here, we used *Camellia sinensis* as the research object to identify the *CsHsf* family using high-quality tea tree reference genomes. In our study, the *Hsf* gene family of tea trees was studied in depth, and 22 *CsHsf* gene family member encoding transcription factors were identified. There were less *Hsf* genes in tea plants than in rice (25) [40], populus (28), and soybeans (26) but more than in algae. Previous studies have shown that there are certain differences in the content of Hsf transcription factors in different species, and the content of Hsf in land plants is significantly higher than that in algae, which is consistent with our research results.

Subsequently, the basic physicochemical properties of CsHsfs were analyzed, as shown in Table 1. Nineteen of the 22 members of the CsHsf protein are unstable in vitro, which is consistent with most studies showing that most members of the Hsf gene family are behaviorally unstable proteins [30]. From a biological significance perspective, unstable proteins may be more easily recognized and regulated by intracellular regulatory mechanisms. When plants respond to environmental stresses, this instability may help cells rapidly adjust the content of Hsf proteins. The isoelectric points of the Hsf gene family exhibited similarities. The theoretical isoelectric points of CsHsfs range from 4.75 to 8.97, which is very similar to those of *Pisum sativum* [41]. All CsHsfs are distributed in the nucleus, which may be an activator that induces the expression of other genes.

To elucidate the evolutionary links between *Arabidopsis thaliana*, *Solanum lycopersicum* L., and *Camellia sinensis*, we constructed a phylogenetic tree of Hsfs. Phylogenetic analyses showed that CsHsfs could be classified into three major groups, corresponding to the Hsfs of *Arabidopsis thaliana* and *Solanum lycopersicum* L. This result is in agreement with previously reported results [33]. Subfamily Hsf A had the most members, and subfamily Hsf C had the least members. The results showed that *Camellia sinensis* had three fewer Hsf members than *Arabidopsis thaliana* and four fewer than *Solanum lycopersicum* L. *Camellia sinensis* has fewer Hsf members than other plant species, which may reflect the insufficient expansion of the CsHsf family. Interestingly, the Hsf family members of these three species were not isolated but showed a cross-distribution pattern (Figure 1). This suggests that the evolution of the Hsf family is more conserved in dicot plants. Since genes clustered in the same subpopulation may handle similar functions, we can infer the function of our gene family by clustering nearby *Hsfs*. Notably, *CsHsfs* frequently congregate with *Arabidopsis thaliana*. The *Hsf* gene of *Arabidopsis thaliana* can increase cold resistance by activating the expression of the Hsp20 family of proteins when induced by cold stress. The aggregation of *CsHsfs* with *AtHsfs* may indicate a similar function for *CsHsfs* [42].

In order to fully understand the *Hsf* gene family, we further studied the motif, domain structure, and gene structure of the CsHsf protein. Short sequences that are important for biological processes are made into motifs. During evolution, members within the same genus and species have similar genetic structures and closely related motifs [43]. In this

experiment, in terms of protein motifs, most CsHsfs have one to four motifs, which may indicate that they have a general role in biology. Motif 6 was identified only in group CsHsf A, and motif 9 was found only in group CsHsf B, which may indicate that these two sets of Hsf genes have unique functions. In addition, in terms of gene structure, we found that the same group of *CsHsf* genes had the same intron–exon structure (Figure 3). In the present study, there were two to five exons in the *CsHsf* genes. Previous research has revealed that *Medicago sativa* L. *Hsf* genes contain two to three exons [44]. In the maize Hsf gene family, the number of exons ranges from one to three [45], and this, to a certain extent, reflects the evolutionary differences between dicotyledonous plants and monocotyledonous plants from the perspective of gene structure.

Unlike animals, plants are constantly exposed to environmental stress, which leads them to evolve a range of molecular mechanisms to adapt to environmental changes. The *cis*-element of the promoter plays a key role in initiating gene expression [46]. Through the analysis of promoters, a large number of core promoter elements and binding sites related to hormone response and stress are distributed in the 22 Hsf promoter regions of *Camellia sinensis*. Notably, most of the *CsHsf* members have abscisic acid reaction-associated elements, suggesting that *CsHsfs* may be involved in communication between signaling pathways in abscisic acid reactions. These signaling pathways also include a wide range of calcium ion-related signaling pathways.

Based on our results, we selected nine *CsHsf* genes from different subfamilies and analyzed their expression patterns. The expression of *CsHsf* genes under light stress, shade stress, and cold stress was analyzed by qRT-PCR. The results showed that the expression of most *CsHsf* genes was downregulated, and some genes were upregulated under cold stress. This expression pattern was consistent with those of *Dianthus caryophyllu* and *Verbena bonariensis* [46,47]. Notably, *CsHsf15* and *CsHsf16* showed high induction rates under light and cold stress, and both genes carried *cis*-acting elements associated with light and low-temperature responses. This may indicate that these genes play a role in stress resistance during the development of *Camellia sinensis*. However, due to the lack of functional verification experiments, the specific regulatory mechanisms cannot be determined at present. Interestingly, in a previous study, the *CsHsfB1* gene was highly upregulated under cold treatment, and its expression was increased 3.3- and 4.3-fold in 'Yingshuang' and 'Anjibaicha' at 24 h and 4.7-fold in 'Yunnanshilixiang' [39]. In contrast, in our study, the expression of *CsHsf15* and *CsHsf16* increased threefold and onefold at 8 h, respectively. The time-specificity of the increase in expression under cold treatment in different varieties of *Camellia sinensis* may reflect the variability in the response of different genes. However, *CsHsf15* and *CsHsf16* can be induced by light, showing a trend of first increasing and then decreasing, which is consistent with the expression patterns of *ZoHSF05*, *ZoHSF12*, *ZoHSF16*, and *ZoHSF25* in ginger [23]. Our study has played a role in mutual validation with the *ZoHSF* gene family in ginger.

Hsf plays an important role in the plant response to abiotic stress [48]. Plants can mitigate the effects of abiotic stress by modulating the expression of various *Hsf* genes. Upon sensing environmental stress signals, such as low temperature, light changes, or darkness, plants activate downstream signaling pathways via Ca^{2+} receptors to regulate their adaptation to adversity. When Ca^{2+} binds to calmodulin (CaM) [49], it induces the expression of key genes like CDPK, initiating multiple stress tolerance pathways [50]. Previous studies have shown that specific types of transcription factors of HSF not only regulate the expression of HSP genes but are also involved in interactions between HSP proteins [51,52]. All of us hypothesized that *HSF* first expresses HSP proteins before initiating the regulation of the expression of core enzymes in the lipid metabolic pathway (e.g., *GPAT*, *SAD*, *KCS*), followed by the promotion of the synthesis of key lipids, such as

phosphatidic acid (PA), phosphatidylethanolamine (PE), and digalactosyldiacylglycerol (DGDG), thereby enhancing cell membrane stability and increasing cold resistance [53]. Under stress, the expression of genes related to jasmonate (MeJA) synthesis is suppressed, leading to reduced MeJA pathway activity, accompanied by malondialdehyde (MDA) accumulation and electrolyte leakage, indicating cellular damage [54]. Our study found that some genes involved in the stress response contain MeJA response elements, and the presence of these elements is closely related to the sensitivity of genes to stress signals. The expression of the *CsHsf* gene promotes the accumulation of ABA, which in turn promotes the synthesis of MeJA, thereby increasing the activity of antioxidant enzymes. The accumulation of MeJA also increases the production of jasmonic acid (JA), and all these series of changes significantly improve the plant's stress tolerance [55]. In our study of cis-elements (Figure 4), we found a potential relationship between *CsHsfs* and these key response proteins, suggesting that *CsHsfs* may be resistant to environmental stress through the interaction of these proteins. Plants produce toxic reactive oxygen species (ROS) in response to different types of stresses, and the excessive accumulation of ROS is harmful to cells. Therefore, the timely removal of ROS becomes crucial for plants to enhance their stress tolerance. With the rising MeJA content, the antioxidant system of plants is activated and the ROS scavenging rate improves [56]. Plants demonstrate their multi-level adaptive capacity and physiological regulation potential by maintaining stable growth under complex environmental stresses through multiple defense mechanisms in vivo, such as signal transduction, metabolic regulation, and gene expression regulation (Figure 8). This mechanism is derived from our research on *CsHsfs* and other hypotheses about plant responses to stress. More experiments are needed to confirm whether *CsHsfs* help plants cope with stress challenges by regulating the expression of related proteins.

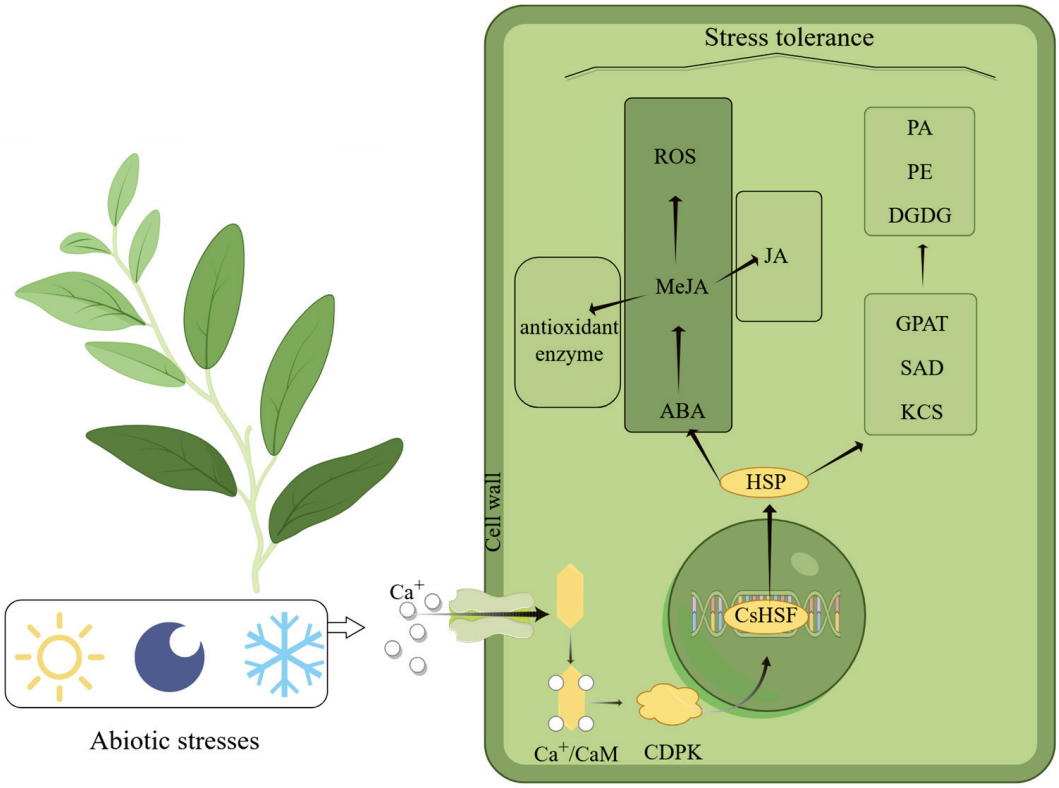


Figure 8. Diagram of the predicted mechanism by which the Hsf gene enables plants to cope with severe environmental stress, produced by Figdraw.

4. Materials and Methods

4.1. Identification and Characterization of the Hsf Gene Family in Camellia sinensis

The genome sequence and corresponding annotation data for *Camellia sinensis*, sourced from the Tea Research Institute of the Fujian Academy of Agricultural Sciences, were obtained through PacBio sequencing technology, followed by a de novo assembly process. Leaf samples were collected from a solitary tea plant (*Camellia sinensis*), cultivated in Anxi County, Fujian Province, China, located at coordinates 119.576708° E, 27.215297° N. To identify *Hsf* genes, we conducted a hidden Markov model (HMM) analysis against the conserved domains (PF00447) using the Pfam protein family database (http://pfam.xfam.org/, accessed on 2 June 2024). The Hummer search tool (version 3.0) was utilized to pinpoint genes containing these domains. Further validation of the CsHsf gene family was achieved by aligning the amino acid sequences of Hsfs from Arabidopsis thaliana, which were retrieved from the PlantTFDB database (https://planttfdb.gao-lab.org/, accessed on 2 July 2024) by utilizing the BLASTp tool available at NCBI. The structural domains were analyzed utilizing the NCBI-CDD search tool (found at https://www.ncbi.nlm.nih.gov/Structure/bwrpsb/bwrpsb.cgi, accessed on 2 July 2024) and the Pfam network database (available at https://pfam-legacy.xfam.org/, accessed on 2 July 2024). A total of 22 genes were ultimately identified and designated as CsHsf1-22.

4.2. Evolutionary Analysis and Gene Structure of the CsHsfs

To identify conserved motifs within the CsHsfs, the MEME website (https://meme-suite.org/meme/tools/meme, accessed on 3 July 2024) was employed, configured to search for 10 patterns while maintaining the default settings. The protein sequences were analyzed using the NCBI Batch Web CD-Search tool (accessible at https://www.ncbi.nlm.nih.gov/, accessed on 3 July 2024) to predict their conserved domains. The gene structure, including its introns and exons, was depicted through the Gene Structure Display Server (GSDS2.0; https://gsds.gao-lab.org/, accessed on 6 January 2025).

4.3. Physicochemical Characteristics and Subcellular Localization

The physicochemical characteristics of members of the CsHsf family were assessed utilizing the ProParam tool available on the Expasy online software platform (https://www.expasy.org/; accessed on 2 July 2024). The subcellular localization of these proteins was forecasted using Plant-mPLoc (https://www.csbio.sjtu.edu.cn/bioinf/plant-multi/; accessed on 2 July 2024).

4.4. Phylogenetic Analysis

The protein sequences for Hsfs derived from Arabidopsis thaliana and tomato were procured from PlantTFDB (https://planttfdb.gao-lab.org/, accessed on 2 July 2024). The phylogenetic tree was built utilizing MEGA software (version 11) by aligning sequences via ClustalW and applying the neighbor-joining method with the JTT + G model, including 1000 bootstrap repetitions. The visual depiction of the tree was enhanced utilizing the iTOL web-based tool (https://itol.embl.de/, accessed on 3 July 2024).

4.5. Collinearity and Repetition Analysis

The homologous relationships between CsHsf genes and Hsf genes in Arabidopsis, tomato, and rice were analyzed using MCScanX. The study identified segmental and tandem duplication events in the CsHsf genes. These results were subsequently visualized with the aid of TBtools-II v2.136.

4.6. Abiotic Stress Treatments

Tea plant (*Camellia sinensis*) seedlings of uniform size were segregated into two groups: a control group and a stress treatment group. The control group consisted of 30 seedlings, while the stress group contained 3. The stressor conditions included exposure to simulated high-intensity light, total darkness, and a low-temperature environment of 4 °C, all maintained at a relative humidity of 75%. Sample collections occurred at 0, 4, 8, 12, and 24 h post-treatment. Each sample was immediately submerged in liquid nitrogen and stored at −80 °C prior to RNA extraction.

4.7. RNA Extraction and Quantitative Analysis

RNA was isolated from both the control and stressed samples using an RNA extraction kit manufactured by Omega Bio-Tek, located in Shanghai, China. Following this, cDNA was produced through the EasyScript one-step process for gDNA removal and cDNA synthesis, utilizing SuperMix provided by Transgen, Beijing, China. A quantitative real-time polymerase chain reaction (qRT-PCR) was carried out with TransStart Top Green qPCR SuperMix from Transgen, Beijing, China, strictly adhering to the manufacturer's instructions. The reaction mixture was composed of 1 μL of cDNA, 2 μL of primers designed for the specific target, 10 μL of SYBR Premix Ex TaqTM II, and 7 μL of ddH_2O, which is nuclease-free. The internal reference gene was selected as CsGAPDH (accession no. GE651107). The qRT-PCR thermal protocol involved an initial denaturation step at 95 °C for 30 s, followed by 40 cycles of denaturation at 95 °C for 5 s, annealing at 60 °C for 30 s, and a melt curve analysis comprising 95 °C for 5 s, 60 °C for 60 s, and 50 °C for 30 s. The $2^{-\Delta\Delta CT}$ method was applied to calculate relative gene expression levels, and statistical analysis was performed utilizing GraphPad Prism version 9.0, accessible at https://www.graphpad.com/, accessed on 20 August 2024. To ensure the reproducibility of the qRT-PCR results, each experiment was conducted using three biological replicates and three technical replicates.

5. Conclusions

In this study, the *Hsf* gene family of *Camellia sinensis* was comprehensively and systematically analyzed. A total of 22 members of the *Hsf* gene family were identified, and the analysis covered the physical and chemical characteristics of the proteins, conserved structural motifs, evolutionary relationships, chromosomal distribution, cis-acting element distribution, and synteny. The response of *CsHsf* genes in *Camellia sinensis* to abiotic stresses was investigated. Hsf transcription factors may interact with other signal transduction molecules, such as the HSP protein family, to participate in the resistance response. Further studies showed that *CsHsf15* and *CsHsf16* had high induction rates under both light and cold stress, and both genes carried *cis*-acting elements related to light and low-temperature responses, suggesting that they may play a potential role in light and low-temperature stress resistance. Our results lay the foundation for exploring the function of the *CsHsf* gene family in tea plant growth and development and in stress response. Additionally, they offer valuable insights for enhancing the adaptability of tea plants to extreme climatic conditions.

Author Contributions: Conceptualization, S.C. and G.L.; methodology, X.S.; software, Q.L.; validation, X.S.; investigation, M.L. and Y.W.; resources, S.C. and S.W.; data curation, X.S.; writing—original draft preparation, X.S.; writing—review and editing, X.S. and J.C.; visualization, Q.L.; supervision, Z.F., S.M.A. and Y.C.; funding acquisition, G.L. All authors have read and agreed to the published version of the manuscript.

Funding: This research was jointly funded by Fujian Agriculture and Forestry University Forestry peak discipline construction project (71201800739 to Shijiang Cao).

Data Availability Statement: The data utilized in this study are readily accessible, housed in a publicly available repository. Specifically, the original datasets can be located within the National Center for Biotechnology Information, under accession number JAFLEL000000000, and within the GWH (https://bigd.big.ac.cn/gwh/, accessed on 15 February 2025), where they are assigned the accession numbers GWHASIV00000000.

Conflicts of Interest: The authors declare no conflict of interest.

References

1. Paul, A.; Chatterjee, A.; Subrahmanya, S.; Shen, G.; Mishra, N. NHX Gene Family in Camellia sinensis: In-silico Genome-Wide Identification, Expression Profiles, and Regulatory Network Analysis. *Front. Plant Sci.* **2021**, *12*, 777884. [CrossRef]
2. Shen, C.; Li, X. Genome-wide analysis of the P450 gene family in tea plant (*Camellia sinensis*) reveals functional diversity in abiotic stress. *BMC Genom.* **2023**, *24*, 535. [CrossRef] [PubMed]
3. Zhou, Y.; Zeng, L.; Hou, X.; Liao, Y.; Yang, Z. Low temperature synergistically promotes wounding-induced indole accumulation by INDUCER OF CBF EXPRESSION-mediated alterations of jasmonic acid signaling in *Camellia sinensis*. *J. Exp. Bot.* **2020**, *71*, 2172–2185. [CrossRef]
4. Chen, Z.; Lin, S.; Li, J.; Chen, T.; Gu, Q.; Yang, T.; Zhang, Z. Theanine Improves Salt Stress Tolerance via Modulating Redox Homeostasis in Tea Plants (*Camellia sinensis* L.). *Front. Plant Sci.* **2021**, *12*, 770398. [CrossRef]
5. Xu, X.; Ye, X.; Xing, A.; Wu, Z.; Li, X.; Shu, Z.; Wang, Y. *Camellia sinensis* small GTPase gene (CsRAC1) involves in response to salt stress, drought stress and ABA signaling pathway. *Gene* **2022**, *821*, 146318. [CrossRef]
6. Waadt, R.; Seller, C.A.; Hsu, P.K.; Takahashi, Y.; Munemasa, S.; Schroeder, J.I. Plant hormone regulation of abiotic stress responses. *Nat. Rev. Mol. Cell Biol.* **2022**, *23*, 516. [CrossRef] [PubMed]
7. Wang, Y.; Mostafa, S.; Zeng, W.; Jin, B. Function and Mechanism of Jasmonic Acid in Plant Responses to Abiotic and Biotic Stresses. *Int. J. Mol. Sci.* **2021**, *22*, 8568. [CrossRef] [PubMed]
8. Murre, C.; McCaw, P.S.; Baltimore, D. A new DNA binding and dimerization motif in immunoglobulin enhancer binding, daughterless, MyoD, and myc proteins. *Cell* **1989**, *56*, 777–783. [CrossRef]
9. Riechmann, J.L.; Heard, J.; Martin, G.; Reuber, L.; Jiang, C.; Keddie, J.; Adam, L.; Pineda, O.; Ratcliffe, O.J.; Samaha, R.R.; et al. *Arabidopsis* transcription factors: Genome-wide comparative analysis among eukaryotes. *Science* **2000**, *290*, 2105–2110. [CrossRef] [PubMed]
10. Baillo, E.H.; Kimotho, R.N.; Zhang, Z.; Xu, P. Transcription Factors Associated with Abiotic and Biotic Stress Tolerance and Their Potential for Crops Improvement. *Genes* **2019**, *10*, 771. [CrossRef] [PubMed]
11. Matsuura, H.; Ishibashi, Y.; Shinmyo, A.; Kanaya, S.; Kato, K. Genome-wide analyses of early translational responses to elevated temperature and high salinity in *Arabidopsis thaliana*. *Plant Cell Physiol.* **2010**, *51*, 448–462. [CrossRef]
12. Shigeta, T.; Zaizen, Y.; Asami, T.; Yoshida, S.; Nakamura, Y.; Okamoto, S.; Matsuo, T.; Sugimoto, Y. Molecular evidence of the involvement of heat shock protein 90 in brassinosteroid signaling in *Arabidopsis* T87 cultured cells. *Plant Cell Rep.* **2014**, *33*, 499–510. [CrossRef]
13. Chen, J.; Gao, T.; Wan, S.; Zhang, Y.; Yang, J.; Yu, Y.; Wang, W. Genome-Wide Identification, Classification and Expression Analysis of the HSP Gene Superfamily in Tea Plant (*Camellia sinensis*). *Int. J. Mol. Sci.* **2018**, *19*, 2633. [CrossRef]
14. Arrigo, A.P. Human small heat shock proteins: Protein interactomes of homo- and hetero-oligomeric complexes: An update. *FEBS Lett.* **2013**, *587*, 1959–1969. [CrossRef]
15. Scarpeci, T.E.; Zanor, M.I.; Valle, E.M. Investigating the role of plant heat shock proteins during oxidative stress. *Plant Signal. Behav.* **2008**, *3*, 856–857. [CrossRef]
16. Guo, M.; Liu, J.H.; Ma, X.; Luo, D.X.; Gong, Z.H.; Lu, M.H. The Plant Heat Stress Transcription Factors (HSFs): Structure, Regulation, and Function in Response to Abiotic Stresses. *Front. Plant Sci.* **2016**, *7*, 114. [CrossRef] [PubMed]
17. Li, P.S.; Yu, T.F.; He, G.H.; Chen, M.; Zhou, Y.B.; Chai, S.C.; Xu, Z.S.; Ma, Y.Z. Genome-wide analysis of the Hsf family in soybean and functional identification of GmHsf-34 involvement in drought and heat stresses. *BMC Genom.* **2014**, *15*, 1009. [CrossRef]
18. Mittal, D.; Chakrabarti, S.; Sarkar, A.; Singh, A.; Grover, A. Heat shock factor gene family in rice: Genomic organization and transcript expression profiling in response to high temperature, low temperature and oxidative stresses. *Plant Physiol. Biochem. PPB* **2009**, *47*, 785–795. [CrossRef]
19. Feng, N.; Feng, H.; Wang, S.; Punekar, A.S.; Ladenstein, R.; Wang, D.C.; Zhang, Q.; Ding, J.; Liu, W. Structures of heat shock factor trimers bound to DNA. *iScience* **2021**, *24*, 102951. [CrossRef]
20. Heerklotz, D.; Döring, P.; Bonzelius, F.; Winkelhaus, S.; Nover, L. The balance of nuclear import and export determines the intracellular distribution and function of tomato heat stress transcription factor HsfA2. *Mol. Cell. Biol.* **2001**, *21*, 1759–1768. [CrossRef] [PubMed]

21. Lyck, R.; Harmening, U.; Höhfeld, I.; Treuter, E.; Scharf, K.D.; Nover, L. Intracellular distribution and identification of the nuclear localization signals of two plant heat-stress transcription factors. *Planta* **1997**, *202*, 117–125. [CrossRef]
22. Liu, X.; Meng, P.; Yang, G.; Zhang, M.; Peng, S.; Zhai, M.Z. Genome-wide identification and transcript profiles of walnut heat stress transcription factor involved in abiotic stress. *BMC Genom.* **2020**, *21*, 474. [CrossRef] [PubMed]
23. Jiang, D.; Xia, M.; Xing, H.; Gong, M.; Jiang, Y.; Liu, H.; Li, H.L. Exploring the Heat Shock Transcription Factor (HSF) Gene Family in Ginger: A Genome-Wide Investigation on Evolution, Expression Profiling, and Response to Developmental and Abiotic Stresses. *Plants* **2023**, *12*, 2999. [CrossRef]
24. Ling, C.; Liu, Y.; Yang, Z.; Xu, J.; Ouyang, Z.; Yang, J.; Wang, S. Genome-Wide Identification of HSF Gene Family in Kiwifruit and the Function of AeHSFA2b in Salt Tolerance. *Int. J. Mol. Sci.* **2023**, *24*, 15638. [CrossRef] [PubMed]
25. Wang, Q.; Zhang, Z.; Guo, C.; Zhao, X.; Li, Z.; Mou, Y.; Sun, Q.; Wang, J.; Yuan, C.; Li, C.; et al. Hsf transcription factor gene family in peanut (*Arachis hypogaea* L.): Genome-wide characterization and expression analysis under drought and salt stresses. *Front. Plant Sci.* **2023**, *14*, 1214732. [CrossRef] [PubMed]
26. Yun, L.; Zhang, Y.; Li, S.; Yang, J.; Wang, C.; Zheng, L.; Ji, L.; Yang, J.; Song, L.; Shi, Y.; et al. Phylogenetic and expression analyses of HSF gene families in wheat (*Triticum aestivum* L.) and characterization of TaHSFB4-2B under abiotic stress. *Front. Plant Sci.* **2022**, *13*, 1047400. [CrossRef] [PubMed]
27. Ren, Y.; Ma, R.; Xie, M.; Fan, Y.; Feng, L.; Chen, L.; Yang, H.; Wei, X.; Wang, X.; Liu, K.; et al. Genome-wide identification, phylogenetic and expression pattern analysis of HSF family genes in the Rye (*Secale cereale* L.). *BMC Plant Biol.* **2023**, *23*, 441. [CrossRef]
28. Shamshad, A.; Rashid, M.; Zaman, Q.U. In-silico analysis of heat shock transcription factor (OsHSF) gene family in rice (*Oryza sativa* L.). *BMC Plant Biol.* **2023**, *23*, 395. [CrossRef]
29. Zhang, Q.; Geng, J.; Du, Y.; Zhao, Q.; Zhang, W.; Fang, Q.; Yin, Z.; Li, J.; Yuan, X.; Fan, Y.; et al. Heat shock transcription factor (Hsf) gene family in common bean (*Phaseolus vulgaris*): Genome-wide identification, phylogeny, evolutionary expansion and expression analyses at the sprout stage under abiotic stress. *BMC Plant Biol.* **2022**, *22*, 33. [CrossRef] [PubMed]
30. Ma, J.; Zhang, G.; Ye, Y.; Shang, L.; Hong, S.; Ma, Q.; Zhao, Y.; Gu, C. Genome-Wide Identification and Expression Analysis of HSF Transcription Factors in Alfalfa (*Medicago sativa*) under Abiotic Stress. *Plants* **2022**, *11*, 2763. [CrossRef]
31. Thirumalaikumar, V.P.; Gorka, M.; Schulz, K.; Masclaux-Daubresse, C.; Sampathkumar, A.; Skirycz, A.; Vierstra, R.D.; Balazadeh, S. Selective autophagy regulates heat stress memory in Arabidopsis by NBR1-mediated targeting of HSP90.1 and ROF1. *Autophagy* **2021**, *17*, 2184–2199. [CrossRef] [PubMed]
32. Yin, X.; Fan, H.; Chen, Y.; Li, L.Z.; Song, W.; Fan, Y.; Zhou, W.; Ma, G.; Alolga, R.N.; Li, W.; et al. Integrative omic and transgenic analyses reveal the positive effect of ultraviolet-B irradiation on salvianolic acid biosynthesis through upregulation of SmNAC1. *Plant J. Cell Mol. Biol.* **2020**, *104*, 781–799. [CrossRef]
33. Zhang, X.; Xu, W.; Ni, D.; Wang, M.; Guo, G. Genome-wide characterization of tea plant (*Camellia sinensis*) Hsf transcription factor family and role of CsHsfA2 in heat tolerance. *BMC Plant Biol.* **2020**, *20*, 244. [CrossRef] [PubMed]
34. Zhang, K.; Dearing, J.A.; Dawson, T.P.; Dong, X.; Yang, X.; Zhang, W. Poverty alleviation strategies in eastern China lead to critical ecological dynamics. *Sci. Total Environ.* **2015**, *506–507*, 164–181. [CrossRef] [PubMed]
35. Hao, X.; He, S. Genome-wide identification, classification and expression analysis of the heat shock transcription factor family in Garlic (*Allium sativum* L.). *BMC Plant Biol.* **2024**, *24*, 421. [CrossRef] [PubMed]
36. Chung, E.; Kim, K.M.; Lee, J.H. Genome-wide analysis and molecular characterization of heat shock transcription factor family in Glycine max. *J. Genet. Genom.* **2013**, *40*, 127–135. [CrossRef] [PubMed]
37. Duan, S.; Liu, B.; Zhang, Y.; Li, G.; Guo, X. Genome-wide identification and abiotic stress-responsive pattern of heat shock transcription factor family in *Triticum aestivum* L. *BMC Genom.* **2019**, *20*, 257. [CrossRef] [PubMed]
38. Yang, X.; Wang, S.; Cai, J.; Zhang, T.; Yuan, D.; Li, Y. Genome-wide identification, phylogeny and expression analysis of Hsf gene family in Verbena bonariensis under low-temperature stress. *BMC Genom.* **2024**, *25*, 729. [CrossRef]
39. Liu, Z.W.; Wu, Z.J.; Li, X.H.; Huang, Y.; Li, H.; Wang, Y.X.; Zhuang, J. Identification, classification, and expression profiles of heat shock transcription factors in tea plant (*Camellia sinensis*) under temperature stress. *Gene* **2016**, *576 Pt 1*, 52–59. [CrossRef] [PubMed]
40. Agarwal, G.; Garg, V.; Kudapa, H.; Doddamani, D.; Pazhamala, L.T.; Khan, A.W.; Thudi, M.; Lee, S.H.; Varshney, R.K. Genome-wide dissection of AP2/ERF and HSP90 gene families in five legumes and expression profiles in chickpea and pigeonpea. *Plant Biotechnol. J.* **2016**, *14*, 1563–1577. [CrossRef] [PubMed]
41. Kanwar, M.; Chaudhary, C.; Anand, K.A.; Singh, S.; Garg, M.; Mishra, S.K.; Sirohi, P.; Chauhan, H. An insight into *Pisum sativum* HSF gene family-Genome-wide identification, phylogenetic, expression, and analysis of transactivation potential of pea heat shock transcription factor. *Plant Physiol. Biochem. PPB* **2023**, *202*, 107971. [CrossRef] [PubMed]
42. Swindell, W.R.; Huebner, M.; Weber, A.P. Transcriptional profiling of Arabidopsis heat shock proteins and transcription factors reveals extensive overlap between heat and non-heat stress response pathways. *BMC Genom.* **2007**, *8*, 125. [CrossRef] [PubMed]

43. Sun, W.; Ma, Z.; Chen, H.; Liu, M. MYB Gene Family in Potato (*Solanum tuberosum* L.): Genome-Wide Identification of Hormone-Responsive Reveals Their Potential Functions in Growth and Development. *Int. J. Mol. Sci.* **2019**, *20*, 4847. [CrossRef] [PubMed]
44. Liu, H.; Li, X.; Zi, Y.; Zhao, G.; Zhu, L.; Hong, L.; Li, M.; Wang, S.; Long, R.; Kang, J.; et al. Characterization of the Heat Shock Transcription Factor Family in *Medicago sativa* L. and Its Potential Roles in Response to Abiotic Stresses. *Int. J. Mol. Sci.* **2023**, *24*, 12683. [CrossRef] [PubMed]
45. Jiang, L.; Hu, W.; Qian, Y.; Ren, Q.; Zhang, J. Genome-wide identification, classification and expression analysis of the Hsf and Hsp70 gene families in maize. *Gene* **2021**, *770*, 145348. [CrossRef] [PubMed]
46. Yang, J.; Zhang, B.; Gu, G.; Yuan, J.; Shen, S.; Jin, L.; Lin, Z.; Lin, J.; Xie, X. Genome-wide identification and expression analysis of the R2R3-MYB gene family in tobacco (*Nicotiana tabacum* L.). *BMC Genom.* **2022**, *23*, 432. [CrossRef]
47. Li, W.; Wan, X.L.; Yu, J.Y.; Wang, K.L.; Zhang, J. Genome-Wide Identification, Classification, and Expression Analysis of the Hsf Gene Family in Carnation (*Dianthus caryophyllus*). *Int. J. Mol. Sci.* **2019**, *20*, 5223. [CrossRef] [PubMed]
48. Wang, C.; Zhou, Y.; Yang, X.; Zhang, B.; Xu, F.; Wang, Y.; Song, C.; Yi, M.; Ma, N.; Zhou, X.; et al. The Heat Stress Transcription Factor LlHsfA4 Enhanced Basic Thermotolerance through Regulating ROS Metabolism in Lilies (*Lilium longiflorum*). *Int. J. Mol. Sci.* **2022**, *23*, 572. [CrossRef]
49. Li, M.; Guo, S.; Xu, Y.; Meng, Q.; Li, G.; Yang, X. Glycine betaine-mediated potentiation of HSP gene expression involves calcium signaling pathways in tobacco exposed to NaCl stress. *Physiol. Plant.* **2014**, *150*, 63–75. [CrossRef] [PubMed]
50. Cui, Y.; Lu, S.; Li, Z.; Cheng, J.; Hu, P.; Zhu, T.; Wang, X.; Jin, M.; Wang, X.; Li, L.; et al. CYCLIC NUCLEOTIDE-GATED ION CHANNELs 14 and 16 Promote Tolerance to Heat and Chilling in Rice. *Plant Physiol.* **2020**, *183*, 1794–1808. [CrossRef]
51. Zhu, Y.X.; Yan, H.W.; Wang, Y.Y.; Feng, L.; Chen, Z.; Xiang, Y. Genome Duplication and Evolution of Heat Shock Transcription Factor (HSF) Gene Family in Four Model Angiosperms. *J. Plant Growth Regul.* **2016**, *35*, 903–920. [CrossRef]
52. Jacob, P.; Hirt, H.; Bendahmane, A. The heat-shock protein/chaperone network and multiple stress resistance. *Plant Biotechnol. J.* **2017**, *15*, 405–414. [CrossRef] [PubMed]
53. Gao, L.; Pan, L.; Shi, Y.; Zeng, R.; Li, M.; Li, Z.; Zhang, X.; Zhao, X.; Gong, X.; Huang, W.; et al. Genetic variation in a heat shock transcription factor modulates cold tolerance in maize. *Mol. Plant* **2024**, *17*, 1423–1438. [CrossRef] [PubMed]
54. Islam, F.; Khan, M.S.S.; Ahmed, S.; Abdullah, M.; Hannan, F.; Chen, J. OsLPXC negatively regulates tolerance to cold stress via modulating oxidative stress, antioxidant defense and JA accumulation in rice. *Free Radic. Biol. Med.* **2023**, *199*, 2–16. [CrossRef] [PubMed]
55. Gong, Q.; Wang, Y.; He, L.; Huang, F.; Zhang, D.; Wang, Y.; Wei, X.; Han, M.; Deng, H.; Luo, L.; et al. Molecular basis of methyl-salicylate-mediated plant airborne defence. *Nature* **2023**, *622*, 139–148. [CrossRef]
56. Han, Z.; Zhang, C.; Zhang, H.; Duan, Y.; Zou, Z.; Zhou, L.; Zhu, X.; Fang, W.; Ma, Y. CsMYB Transcription Factors Participate in Jasmonic Acid Signal Transduction in Response to Cold Stress in Tea Plant (*Camellia sinensis*). *Plants* **2022**, *11*, 2869. [CrossRef]

Disclaimer/Publisher's Note: The statements, opinions and data contained in all publications are solely those of the individual author(s) and contributor(s) and not of MDPI and/or the editor(s). MDPI and/or the editor(s) disclaim responsibility for any injury to people or property resulting from any ideas, methods, instructions or products referred to in the content.

plants

MDPI

Article

Heat Priming and Heat Stress Enhance Transgenerational Heat Tolerance in the Early Growth Stages of *Oryza sativa* L. Progeny

Younghwan Ju [1], Juyoung Choi [1], Sungho Yun [2] and Jun Ichi Sakagami [1,3,*]

[1] The United Graduate School of Agricultural Sciences, Kagoshima University, Korimoto 1-21-24, Kagoshima 890-0065, Japan; joh7598@naver.com (Y.J.); jychoi8519@gmail.com (J.C.)
[2] Digitalomics Research Center, Korea Basic Science Institute (KSBI) Ochang Center, 161, Yeongudanji-ro, Ochang-eup, Cheongwon-gu, Cheongju-si 28119, Chungcheongbuk-do, Republic of Korea; sungho@kbsi.re.kr
[3] Faculty of Agriculture, Kagoshima University, Kagoshima 890-0065, Japan
* Correspondence: sakagami@agri.kagoshima-u.ac.jp; Tel./Fax: +81-99-285-8543

Abstract: Rice (*Oryza sativa* L.) is a staple crop that provides essential nutrients and energy; however, it is sensitive to heat stress, posing a threat to sustainable productivity. Heat stress can cause delayed germination in progeny, increased oxidative stress, reduced biomass accumulation, and excessive water loss. Notably, heat stress memory induced through heat priming can be inherited, potentially strengthening heat tolerance in subsequent generations. This study examined the effects of heat priming and heat stress on delayed germination, shoot length, and shoot fresh and dry weight under elevated-temperature conditions. The results showed that while heat stress delayed germination in progeny, heat priming significantly accelerated germination rates. Furthermore, heat stress elevated oxidative stress levels, thereby hindering biomass synthesis. In contrast, heat priming helped maintain low levels of reactive oxygen species (ROS) and malondialdehyde (MDA), contributing to greater biomass accumulation. These findings suggest that heat priming enhances transgenerational heat tolerance in rice, leading to faster germination, higher biomass accumulation, and improved ROS homeostasis in progeny.

Keywords: heat priming; transgenerational heat tolerance; oxidative stress; biomass accumulation

1. Introduction

Rice (*Oryza sativa* L.) is a major staple crop, feeding more than half of the global population and supplying essential nutrients, including antioxidants, vitamins, carbohydrates, proteins, and fats [1]. However, rising global temperatures [2] present significant threats to rice productivity [3–5]. For instance, a 1 °C rise in global mean temperature is projected to reduce rice yields by approximately 3.2% [6].

Germination, the transition from a heterotrophic seed to an autotrophic seedling, is a critical phase for seedling growth and organ development [7,8]. Germination is regulated by energy metabolism using storage compounds, such as starch, which is a major source of energy for germination by glycolysis, the pentose phosphate pathway, and the tricarboxylic acid cycle (TCA) [8]. Starch synthesis can be limited by temperature stress, which may lead to a decline in grain quality [9]. Also, heat stress during this stage can lead to excessive water loss, oxidative damage, stunted shoot and root growth, and even seedling mortality. Additionally, the number of viable seedlings may decline under heat stress, potentially reducing the final rice yield [10]. Therefore, understanding the physiological responses of rice to heat stress is imperative for ensuring stable crop production.

Under heat stress conditions, impaired electron transport chains in chloroplasts and mitochondria result in the excessive generation of reactive oxygen species (ROS) due to disrupted cellular redox homeostasis. This ROS overproduction can cause oxidative stress, resulting in lipid peroxidation, protein denaturation, and DNA damage. To mitigate this, plants activate antioxidant defense pathways that include enzymes such as ascorbate peroxidase (APX), catalase (CAT), and superoxide dismutase (SOD). While ROS play essential roles in stress signaling and tolerance, their excessive accumulation is detrimental, emphasizing the importance of maintaining ROS homeostasis for heat stress tolerance [11–13].

Plants have the ability to "remember" previous stress events, thereby enabling more rapid and effective responses to subsequent stresses. This phenomenon, known as priming, alters the plant's response to future stress exposures [14–16]. Heat priming contributes to improved tolerance by limiting excessive ROS accumulation [11–13]. Previous studies have shown that stress priming involves histone methylation, modifications in regulatory proteins, and other epigenetic mechanisms, and that the resulting heat tolerance can be inherited by the next generation [14–17].

In this study, we hypothesized that heat priming induces transgenerational heat tolerance, thereby enhancing rice germination and early seedling growth under heat stress conditions. To test this hypothesis, we examined the germination rate, shoot length, biomass accumulation, ROS production, and lipid peroxidation in the progeny of two rice varieties, N22 and IR64, that were heat-primed during the flowering stage. These traits were selected as they represent key physiological indicators of early-stage heat stress response and seedling vigor. Our aim was to evaluate whether priming-induced stress memory could be inherited and functionally expressed in the next generation. By integrating physiological and biochemical measurements, this study provides a mechanistic understanding of how parental exposure to heat stress may enhance stress tolerance in progeny. Our findings provide insights into the epigenetic effects of heat priming on transgenerational heat tolerance and offer promising avenues for mitigating heat stress, particularly in the context of global climate change.

2. Results

2.1. Experimental Design Overview

To investigate the transgenerational effects of heat priming under different developmental stages, we established four experimental progeny groups derived from plants subjected to different heat priming and stress conditions (Figure 1).

2.2. Changes in Germination Parameters

Table 1 presents germination parameters at 28 °C, including germination percentage (GP), time for 50% germination (T50), and mean germination time (MGT), for progenies of heat-primed N22 and IR64 with heat stress during flowering. GP was recorded every 12 h, with the first germination observed 36 h after imbibition. In both varieties, germination of the CH (no heat priming with heat stress at flowering for seven days) treatment began at 48 h after imbibition (hai), whereas germination in heat-primed treatments and the CC (no heat priming with no heat stress) group started earlier, at 36 hai. Compared to CC, CH showed the greatest GP reduction at 48 hai in N22 and 60 hai in IR64. In N22, PTH (heat priming at the tillering stage for five days with heat stress at flowering for seven days) had a higher GP compared to PBH (heat priming at the booting stage for five days with heat stress at flowering for seven days) at 48 hai, whereas in IR64, PBH had a higher GP relative to PTH at 60 hai. T50 and MGT were significantly higher in CH than in CC for both varieties, but they decreased in PTH and PBH compared to CH. In N22, T50, and MGT were lower in PTH than in PBH, whereas in IR64, PBH had lower values compared with

PTH. Heat priming significantly influenced GP, T50, and MGT across all time points, as confirmed via a three-way ANOVA. At 60 hai, a significant interaction between variety and treatment was observed, indicating differential responses to heat priming.

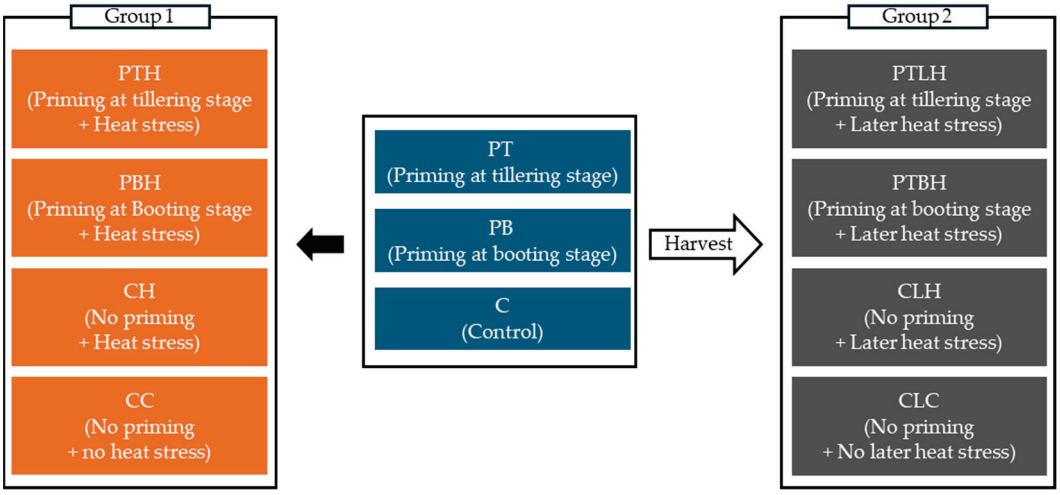


Figure 1. Schematic diagram of seed preparation and treatments. The blue boxes represent the heat-priming treatments applied before any heat stress. Heat priming was applied for five days either at the tillering stage (PT) or the booting stage (PB), while the control group (C) received no priming. After priming, rice plants were divided into two major groups. Group 1 was subjected to heat stress before harvest to examine the effects of heat priming on the same generation. This group included four treatments: PTH (tillering-stage priming with heat stress), PBH (booting-stage priming with heat stress), CH (no priming with heat stress), and CC (no priming without heat stress). Group 2 was maintained without heat stress after priming and used to investigate the heat stress response in the progeny. This group consisted of four treatments: PTLH (progeny from tillering-stage heat priming for five days, exposed to later heat stress for three days), PBLH (progeny from booting-stage heat priming for five days, exposed to later heat stress for three days), CLH (progeny from non-primed parents, exposed to later heat stress for three days), and CLC (progeny from non-primed parents, not exposed to heat stress). Solid black arrows indicate heat stress applied within the same generation, and white-center hollow arrows indicate postharvest progression to the next generation for stress evaluation.

Table 1. Germination parameters at 28 °C including germination percentage, time for 50% germination (T50), and mean germination time (MGT) of progenies of heat-primed N22 and IR64 at the tillering or booting stages for five days with heat stress applied for seven days during the flowering stage. Germination percentage was measured every 12 h using 15 seeds with three replicates per group.

Variety	Treatment	Germination Percentage (%)				T50	MGT
		36 hai	48 hai	60 hai	72 hai		
N22	CC	6.67 a	73.33 a	84.44 a	91.11 a	43.7 b	50.3 b
	PTH	8.89 a	46.67 ab	75.56 ab	88.89 a	48.7 ab	54.1 ab
	PBH	11.11 a	28.89 ab	60.00 b	84.44 a	53.0 ab	57.7 ab
	CH	0.00 a	26.67 b	42.22 c	77.78 a	54.6 a	61.3 a
IR64	CC	11.11 a	55.56 a	91.11 a	91.11 a	46.4 b	51.2 b
	PTH	4.44 a	42.22 ab	66.67 b	82.22 a	48.6a b	55.3 a
	PBH	8.89 a	44.44 ab	80.00 ab	82.22 a	46.8 b	52.5 b
	CH	0.00 a	31.11 b	62.22 b	71.11 a	50.8 a	56.3 a

Table 1. *Cont.*

Variety	Treatment	Germination Percentage (%)				T50	MGT
		36 hai	48 hai	60 hai	72 hai		
Variety		ns	ns	*	ns	ns	ns
Treatment		*	**	***	*	**	**
Variety × Treatment		ns	ns	*	ns	ns	ns

* $p < 0.05$, ** $p < 0.01$, and *** $p < 0.001$ indicate the interactions between variety and stress calculated using two-way ANOVA. The letter ns indicates no interaction. Tukey's Honest Significant Difference (HSD) test was conducted to divide treatments of each variety at the level of $p < 0.05$. The same lowercase letter indicates no significant difference. Abbreviation; CC: no heat priming with no heat stress, PTH: heat priming at the tillering stage for five days with heat stress at flowering for seven days, PBH: heat priming at the booting stage for five days with heat stress at flowering for seven days, CH: no heat priming with heat stress at flowering for seven days, hai: hours after imbibition, and MGT: mean germination time.

2.3. Biomass Parameters

Biomass parameters, including shoot length (SL), fresh weight (FW), and dry weight (DW), were measured after three days of heat stress (Figure 2). In both varieties, SL, FW, and DW decreased significantly under heat stress compared to CLC (progeny from non-primed parents, exposed to later heat stress for three days), but the negative effects were significantly alleviated by transgenerational heat priming. The most pronounced alleviation was observed in N22 under the PTLH treatment (progeny from tillering-stage heat priming for five days, exposed to later heat stress for three days) across all three parameters. In contrast, IR64 showed the greatest mitigation under PBLH (progeny from booting-stage heat priming for five days, exposed to later heat stress for three days). According to two-way ANOVA revealed that SL, FW, and DW were strongly influenced by variety, treatment, and their interaction.

2.4. H_2O_2 and MDA Content

ROS were quantified by measuring hydrogen peroxide (H_2O_2) content, and lipid peroxidation was measured according to malondialdehyde (MDA) content (Figure 3). Three days of heat stress significantly elevated the H_2O_2 and MDA content in both varieties across all treatments compared to CLC. In the CLH (progeny from non-primed parents, exposed to later heat stress for three days) treatment, H_2O_2 levels increased by 314% in N22 and 361% in IR64. In contrast, the PTLH treatment resulted in smaller increases of 153% and 248% in N22 and IR64, respectively, while the PBLH treatment led to increases of 241% in N22 and 144% in IR64. Similarly, the MDA content in CLH increased by 203% and 219% in N22 and IR64, respectively, compared with CLC. However, in PTLH, the MDA levels increased by only 103% and 176% in N22 and IR64, respectively, and in PBLH, the increases were limited to 159% and 131% in N22 and IR64, respectively.

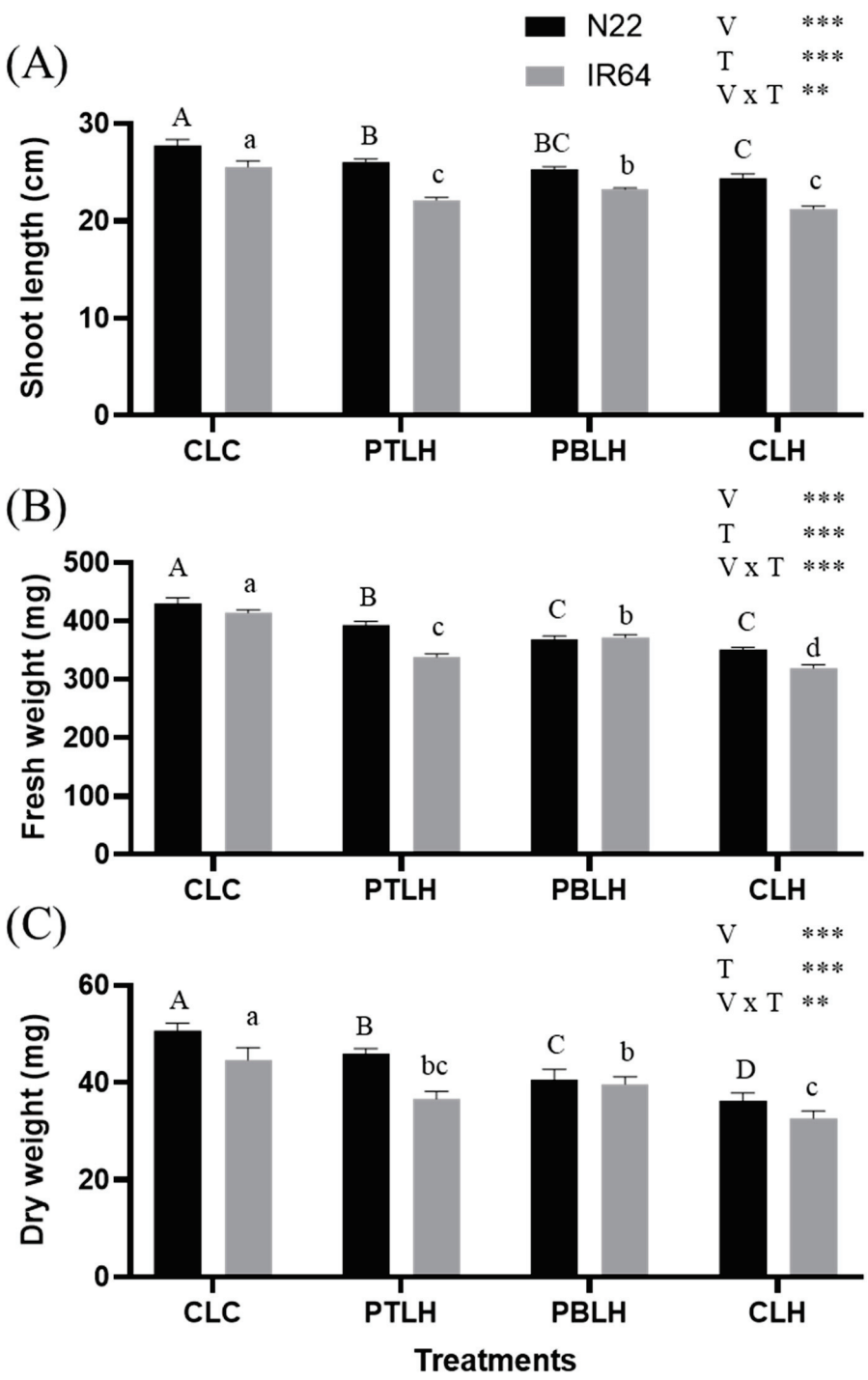


Figure 2. Biomass parameters, including shoot length (**A**), shoot fresh weight (**B**), and shoot dry weight (**C**), of the progenies of heat-primed rice (cv. N22 and IR64) under heat stress. Heat stress was applied at the 14-day seedling stage with 16 h of light (38 °C) and 8 h of darkness (28 °C) for three days. Asterisks, ** $p < 0.01$, and *** $p < 0.001$) indicate significant interaction effects between variety (V) and treatment (T), as determined by two-way ANOVA. Tukey's HSD test ($p < 0.05$) was performed to compare treatment means within each variety. Identical uppercase letters (A, B, C, D) indicate no significant difference among treatments in N22, and identical lowercase letters (a, b, c, d) indicate no significant difference among treatments in IR64. Abbreviations: CLC: progeny from non-primed parents, not exposed to heat stress; PTLH: progeny from tillering-stage heat priming for five days, exposed to later heat stress for three days; PBLH: progeny from booting-stage heat priming for five days, exposed to later heat stress for three days; CLH: progeny from non-primed parents, exposed to later heat stress for three days.

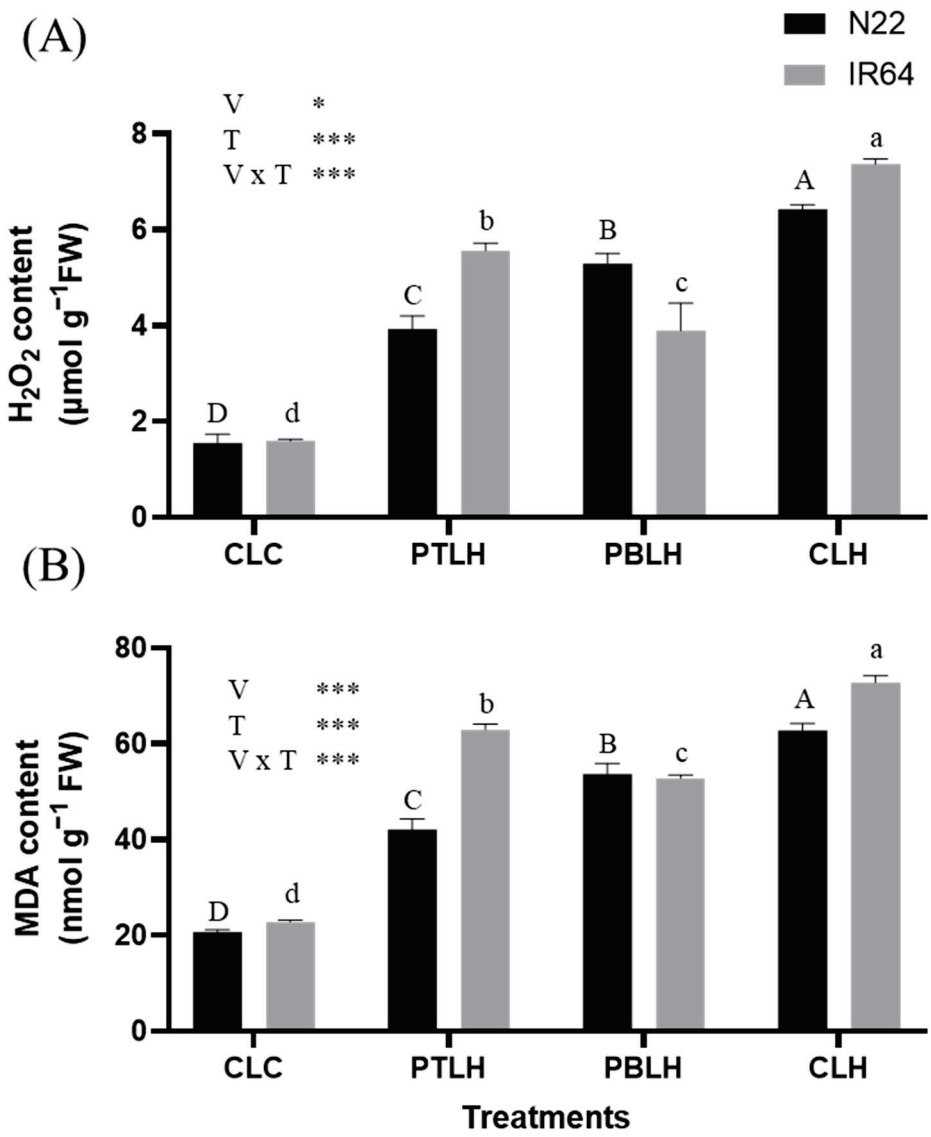


Figure 3. Hydrogen peroxide (H_2O_2) (**A**) and malondialdehyde (MDA) (**B**) contents in the progenies of heat-primed rice (cv. N22 and IR64) under heat stress. Heat stress was applied at the 14-day seedling stage with 16 h of light (38 °C) and 8 h of darkness (28 °C) for three days. Asterisks (* $p < 0.05$ and *** $p < 0.001$) indicate significant interaction effects between variety (V) and treatment (T), as determined by two-way ANOVA. Tukey's HSD test ($p < 0.05$) was performed to compare treatment means within each variety. Identical uppercase letters (A, B, C, D) indicate no significant difference among treatments in N22, and identical lowercase letters (a, b, c, d) indicate no significant difference among treatments in IR64. Abbreviations: CLC: progeny from non-primed parents, not exposed to heat stress; PTLH: progeny from tillering-stage heat priming for five days, exposed to later heat stress for three days; PBLH: progeny from booting-stage heat priming for five days, exposed to later heat stress for three days; CLH: progeny from non-primed parents, exposed to later heat stress for three days.

3. Discussion

To assess heat priming's impact on mitigating heat stress effects on progeny germination, parameters such as GP, T50, and MGT were measured (Table 1). Transgenerational heat stress delayed germination at 48 and 60 hai in N22 and IR64, respectively. Notably, all germination parameters were influenced by treatment, indicating that both rice varieties experienced transgenerational effects from heat priming and heat stress.

During germination, marking the initial stage in a plant's life cycle, essential processes occur, including mRNA translation and DNA repair, and germination is followed by seedling growth and organ development [7,8,18]. Heat stress during grain filling can lead to spikelet sterility and delayed germination, without affecting progeny seed vigor [19,20]. In the present study, T50 and MGT increased in both varieties, although no significant differences were observed among the treatments, supporting the notion that heat stress delays germination without reducing seed vigor.

Epigenetic modifications, such as histone modifications, DNA methylation, chromatin remodeling, and RNA production, are involved in germination [21,22]. These modifications may mitigate heat stress effects on progeny germination by regulating the expression of genes involved in hormonal signaling, dormancy release, and ROS homeostasis, all of which play critical roles in seed germination under stress conditions, suggesting an association with the observed germination parameters (Table 1). While this interpretation remains hypothetical, further investigation into the epigenetic regulation of transgenerational germination responses would be both valuable and scientifically intriguing.

Abiotic stresses, including heat, drought, and salt, markedly impact crop productivity [23]. Heat stress can irreversibly damage growth, photosynthesis, respiration, water relations, and membrane stability. It may also trigger ROS hyperaccumulation, leading to oxidative damage, cell death, growth inhibition, and potential seedling death [10,24,25]. Although antioxidant enzymes, such as superoxide dismutase, catalase, and glutathione reductase, typically regulate ROS, heat stress can damage these scavengers, resulting in ROS accumulation [26]. Low ROS concentrations can serve as secondary messengers, whereas high concentrations cause oxidative stress. Among ROS, H_2O_2 is notably stable and diffusive, with higher cell membrane permeability [25]. Excessive ROS levels also elevate MDA content, causing protein and nucleic acid damage. Thus, low ROS and MDA levels under heat stress indicate heat tolerance [27,28]. Heat priming induces numerous heat stress responses, including changes in histone protein, heat shock protein, and heat shock factor expression. Studies have shown that heat tolerance acquired through priming can be inherited, enabling the progeny of heat-primed rice plants to exhibit enhanced tolerance [12,16,29].

Under heat stress conditions, heat-primed progeny displayed reduced SL, FW, and DW compared to CLC (Figure 2). Notably, the SL, FW, and DW of heat-primed N22 and IR64 rice plants were higher compared to CLH, highlighting the heat-stress-mitigating effect of priming. This suggests that heat-primed progeny can produce more biomass under heat stress. Heat stress elevated the H_2O_2 and MDA levels (Figure 3), but these levels were reduced in PTLH and PBLH compared to CLH, reflecting heat priming's alleviative effect. ROS accumulation from heat stress can lead to lipid peroxidation [30,31]; therefore, the relative increases in SL, FW, DW, H_2O_2, and MDA in PTLH and PBLH compared to CLH likely indicate increased heat tolerance due to transgenerational priming effects (Figures 2 and 3).

Although heat stress reduced biomass and increased oxidative damage parameters, the responses varied between the rice varieties, as confirmed via a two-way ANOVA. In CLH, the H_2O_2 and MDA increases were smaller in N22 than in IR64. Two-way ANOVA also revealed the differing mitigating effects of heat priming between the cultivars: in N22, PBLH had a stronger alleviative effect compared to PTLH, whereas in IR64, PTLH's effects surpassed those of PBLH. These observations may reflect the innate differences in heat tolerance between N22 and IR64, which show tolerance and susceptibility, respectively. Additionally, the high responsiveness of N22 during the tillering stage may represent an avoidance strategy to cope with early-stage stress, while the strong response of IR64 during the reproductive stage could be associated with its greater vulnerability and stress memory

formation at that phase. These observations suggest that the optimal timing of priming treatments may need to be tailored based on cultivar-specific characteristics.

The results of the present study demonstrated that heat tolerance acquired through heat priming in rice can be inherited, helping maintain heat stress memory across generations. Heat priming effectively reduced the delay in germination observed in the progeny of heat-stressed rice. Additionally, heat-primed rice maintained lower ROS and MDA levels under heat stress, contributing to increased SL, fresh weight, and DW. These results highlight the transgenerational relief of oxidative stress achieved through heat priming, which enables rice plants to accumulate more biomass. Although our study demonstrates the inheritance of heat priming effects in the immediate progeny, it remains unclear whether these effects persist beyond a single generation. Several studies in model and crop species have reported partial transmission of stress-induced epigenetic changes to subsequent generations (e.g., F2), though these effects are often attenuated or reversible [15,32,33]. Further studies are required to determine the stability and functional significance of such transgenerational memory in rice.

4. Materials and Methods

4.1. Seed Preparation

Seeds of *Oryza sativa* L. varieties N22 and IR64 were surface-sterilized using 1% (*v*/*v*) sodium hypochlorite (NaClO) for 20 min and then rinsed thoroughly ten times with distilled water until NaClO was completely removed. The sterilized seeds were transferred to sterile glass Petri dishes (90 mm diameter) containing 25 seeds (n = 10) and wet filter paper as a moisture source and incubated in the dark at 25 °C for 24 h in a growth chamber (INCUBATOR SIB-35, SANSYO, Hamamatsu, Japan) to induce germination. Uniformly germinated seeds were then transplanted into nursery trays and maintained in a glasshouse located outdoors. During this 1-week nursery period, temperature, humidity, and light were not artificially controlled and followed the natural environmental cycle. Seedlings were watered daily to ensure adequate soil moisture. After one week, seedlings with uniform growth were selected and transplanted into plastic pots (256 × 234 × 297 mm) filled with commercial bed soil (Ryoto Fertilizer Co., Ltd., Oita, Japan) containing NKP (0.6:1.5:1.0) per pot. The experiment was conducted at an outdoor laboratory of Kagoshima University (31°34′23.5″ N, 130°32′35.0″ E). At 45 days after transplanting, an additional 10 g of NPK (1:1:1) fertilizer was applied to each pot. Each pot contained five rice seedlings, and five replicate pots were used per treatment in a completely randomized block design (CRBD).

Heat priming was conducted for five days in a greenhouse where the average temperature was approximately 2–3 °C higher than the ambient temperature. Heat-priming treatment was applied at either at the tillering stage (PT) or booting stage (PB). After priming, the plants were divided into two major experimental groups (Figure 3). The first group was used to study the effect of heat priming and heat stress on progeny seed germination. These plants were subjected to 7 days of heat stress at the flowering stage under conditions that were 4–5 °C higher on average than the ambient temperature by transferring them back to the glasshouse. After stress application, the plants were returned to the outdoor environment for seed maturation. The second group was maintained under outdoor conditions until harvest without exposure to additional heat stress. All harvested seeds were dehydrated in a shaded greenhouse at 30–35 °C and 40–60% relative humidity for two weeks and then stored in sealed bags at 4 °C in the dark prior to use in progeny experiments. The first group consisted of four treatments based on heat priming and heat stress conditions: PTH: heat priming at the tillering stage for five days with heat stress at flowering for seven days, PBH: heat priming at the booting stage for five days with

heat stress at flowering for seven days, CC: no heat priming with no heat stress. Temperature and humidity were continuously monitored during the entire experiment using remote sensors (Long-Range Wireless Connection Logger, Telemoni, Tokyo, AXEL, Japan) (Table S1).

4.2. Germination Parameters

Seeds from the first group were sterilized with 1% NaClO for 20 min and then washed. Subsequently, 15 sterilized seeds (n = 3) were germinated for 72 h on wet filter paper in darkness at 28 °C (Yamato Scientific Co., Tokyo, Japan), with germination measured every 12 h thereafter. Germination percentage (GP), germination speed (T50), and mean germination time (MGT) were calculated as follows:

$$GP = {}^{Germinated\ seeds}/_{Total\ number\ of\ seeds}$$

$$T50 = ti + \left[\frac{\left(\frac{n+1}{2-ni} \right)}{(nj - ni)} \right] \times (tj - ti),$$

where N is the final germinated seed count, and ni and nj are cumulative germinated seed counts at times when $ni < N/2 < nj$ [33].

$$MGT = \sum(n \times t) / \sum N,$$

where n is the number of seeds germinated each time, t is the number of times from the beginning of the experiment, and N is the total number of seeds germinated at the termination of the experiment [34].

4.3. Later Heat Stress Application

Seeds from the second group (Group 2), which were derived from plants that had undergone different priming treatments had not been subjected to flowering-stage heat stress, were sterilized and germinated as previously described. After germination, uniformly germinated seedlings were transplanted into plastic containers (50 mm wide × 200 mm long × 50 mm deep), with 10 seedlings per container. Three biological replicates were used per treatment. The seedlings were grown in a controlled growth chamber under a 16 h light/8 h dark photoperiod, with light intensity maintained at 500 μmol m^{-2} s^{-1}. Day and night temperatures were set at 32 °C and 28 °C, respectively.

After 14 days of growth under these conditions, the seedlings were transferred to a plant growth chamber (LPH-241-S, Biotron NK System, Nippon Medical and Chemical Instruments Co., Ltd., Osaka, Japan) for heat stress treatment. Heat stress was applied by exposing the seedlings to 38 °C during the 16 h light period and 28 °C during the 8 h dark period for three consecutive days.

The purpose of this experiment was to evaluate transgenerational heat stress tolerance in the progeny of heat-primed and non-primed parental plants. Accordingly, seedlings were divided into the following four treatment groups (Figure 1):

(1) PTLH: progeny from tillering-stage heat priming for five days, exposed to later heat stress for three days.
(2) PBLH: progeny from booting-stage heat priming for five days, exposed to later heat stress for three days.
(3) CLH: progeny from non-primed parents, exposed to later heat stress for three days.
(4) CLC: progeny from non-primed parents, not exposed to heat stress.

All containers were placed in the chamber in a completely randomized manner to eliminate positional effects. After the heat stress treatment, the plants were used for further analysis of morphological and physiological responses.

4.4. Shoot Length and Shoot Biomass

Shoot length (SL) was measured in centimeters using a ruler and shoot fresh weight (FW) was recorded using an electronic scale (HR-100AZ, A&D Company, Tokyo, Japan) before samples were dried at 70 °C for 72 h to determine shoot dry weight (DW) [35]. All measurements were conducted with three biological replicates.

4.5. H_2O_2 and MDA Analyses

To measure the ROS, H_2O_2, 100 mg of leaves was immediately frozen in liquid nitrogen and then homogenized with 5 mL of 0.1% trichloroacetic acid (TCA; w/v) using a mortar and pestle. The samples were then centrifuged at 12,000× g for 15 min (GR-15R, BECKMAN COULTER, Indianapolis, IN, USA). The supernatant was mixed with 0.5 mL of 10 mM potassium phosphate (pH 7) and 1 mL of 1 M potassium iodide, and absorbance was measured immediately at 390 nm using a Spectronic 200 UV-Vis spectrophotometer using an H_2O_2 standard curve [36,37].

MDA was measured as a marker of lipid peroxidation using the thiobarbituric acid (TBA) method [38,39]. Leaves (100 mg) were ground with 1 mL of 0.5% (w/v) TBA containing 20% (w/v) TCA using a pre-chilled mortar and pestle. The mixture was then incubated at 95 °C for 30 min. To stop the reaction, the mixture was placed in an ice bath, followed by centrifugation at 10,000× g for 10 min. Absorbance was measured at 532 and 600 nm, with MDA equivalents calculated as follows:

$$MDA\ equivalents\left(\text{nmol g}^{-1}\right) = \left[(A_{532} - A_{600})/155,000\right]10^6$$

All biochemical measurements were performed with three biological replicates. H_2O_2 and MDA were extracted immediately after the three-day heat stress treatment, which was applied after 14 days of seedling growth.

4.6. Statistical Analysis

Using RStudio (version 4.2.1), Tukey's honestly substantial difference test was conducted to separate means, with statistical significance set at $p < 0.05$. Three-way ANOVA was performed using the obtained data. Graphical representations were generated via GraphPad Prism (version 10.3.1).

5. Conclusions

In the present study, we demonstrated that heat stress during the reproductive stage in rice induces transgenerational effects that delay germination and reduce seedling vigor, as evidenced by increased ROS and MDA levels and reduced biomass in the progeny. In contrast, heat priming at the tillering and booting stages significantly alleviated these negative effects, resulting in improved germination, reduced oxidative damage, and increased metabolite levels in the progeny. These beneficial effects may be attributed to (1) better membrane integrity, (2) enhanced synthesis of protective metabolites, and (3) more effective antioxidant activity. Our findings highlight the potential of heat priming as a strategy to induce transgenerational stress tolerance, especially in susceptible cultivars such as IR64, and suggest that the timing of priming may need to be optimized depending on genotype. This study also offers practical insights for breeding programs aimed at enhancing heat tolerance in rice. However, the mechanisms underlying these effects remain speculative, as the current study did not directly assess epigenetic modifications. In addition, further

research across multiple generations and growth stages, as well as yield-related evaluations under field conditions, will be essential to fully validate the transgenerational benefits of heat priming.

Supplementary Materials: The following supporting information can be downloaded at: https://www.mdpi.com/article/10.3390/plants14111593/s1, Table S1: Temperature during heat priming and heat stress.

Author Contributions: Conceptualization, Y.J. and J.I.S.; methodology, Y.J. and J.I.S.; validation, J.I.S. and S.Y.; investigation, Y.J. and J.C.; writing—original draft preparation, Y.J.; writing—review and editing, Y.J. and J.I.S.; visualization, Y.J.; supervision, J.I.S. All authors have read and agreed to the published version of the manuscript.

Funding: This research received no external funding.

Data Availability Statement: The raw data supporting the conclusions of this article will be made available by the authors on request.

Conflicts of Interest: The authors declare no conflicts of interest.

Abbreviations

The following abbreviations are used in this manuscript:

PT	Heat priming at the tillering stage
PB	Heat priming at the booting stage
CC	No heat priming with no heat stress
PTH	Heat priming at the tillering stage with heat stress at the flowering stage for seven days
PBH	Heat priming at the booting stage with heat stress at the flowering stage for seven days
CH	No heat priming with heat stress at the flowering stage for seven days
CLC	Progeny from non-primed parents, not exposed to heat stress
CLH	Progeny from non-primed parents, exposed to later heat stress for three days
PTLH	Progeny from tillering-stage heat priming for five days, exposed to later heat stress for three days
PBLH	Progeny from booting-stage heat priming for five days, exposed to later heat stress for three days

References

1. Sen, S.; Chakraborty, R.; Kalita, P. Rice-not just a staple food: A comprehensive review on its phytochemicals and therapeutic potential. *Trends Food Sci. Technol.* **2020**, *97*, 265–285. [CrossRef]
2. Masson-Delmotte, V.; Zhai, P.; Pirani, A.; Connors, S.L.; Péan, C.; Berger, S.; Zhou, B. Climate Change 2021: The Physical Science Basis. In *Contribution of Working Group I to the Sixth Assessment Report of the Intergovernmental Panel on Climate Change*; IPCC: Geneva, Switzerland, 2021; Volume 2, p. 2391.
3. Wu, C.; Cui, K.; Fahad, S. Heat stress decreases rice grain weight: Evidence and physiological mechanisms of heat effects prior to flowering. *Int. J. Mol. Sci.* **2022**, *23*, 10922. [CrossRef] [PubMed]
4. Begcy, K.; Sandhu, J.; Walia, H. Transient heat stress during early seed development primes germination and seedling establishment in rice. *Front. Plant Sci.* **2018**, *9*, 1768. [CrossRef] [PubMed]
5. Kilasi, N.L.; Singh, J.; Vallejos, C.E.; Ye, C.; Jagadish, S.K.; Kusolwa, P.; Rathinasabapathi, B. Heat stress tolerance in rice (*Oryza sativa* L.): Identification of quantitative trait loci and candidate genes for seedling growth under heat stress. *Front. Plant Sci.* **2018**, *9*, 1578. [CrossRef] [PubMed]
6. Zhao, C.; Liu, B.; Piao, S.; Wang, X.; Lobell, D.B.; Huang, Y.; Huang, M.T.; Yao, Y.T.; Bassu, S.; Ciais, P.; et al. Temperature increase reduces global yields of major crops in four independent estimates. *Proc. Natl. Acad. Sci. USA* **2017**, *114*, 9326–9331. [CrossRef]
7. Wolny, E.; Betekhtin, A.; Rojek, M.; Braszewska-Zalewska, A.; Lusinska, J.; Hasterok, R. Germination and the early stages of seedling development in *Brachypodium distachyon*. *Int. J. Mol. Sci.* **2018**, *19*, 2916. [CrossRef]
8. Tarnawa, Á.; Kende, Z.; Sghaier, A.H.; Kovács, G.P.; Gyuricza, C.; Khaeim, H. Effect of abiotic stresses from drought, temperature, and density on germination and seedling growth of barley (*Hordeum vulgare* L.). *Plants* **2023**, *12*, 1792. [CrossRef]

9. Tian, B.; Talukder, S.K.; Fu, J.; Fritz, A.K.; Trick, H.N. Expression of a rice soluble starch synthase gene in transgenic wheat improves the grain yield under heat stress conditions. *In Vitro Cell. Dev. Biol. Plant* **2018**, *54*, 216–227. [CrossRef]
10. Xu, Y.; Chu, C.; Yao, S. The impact of high-temperature stress on rice: Challenges and solutions. *Crop J.* **2021**, *9*, 963–976. [CrossRef]
11. Devireddy, A.R.; Tschaplinski, T.J.; Tuskan, G.A.; Muchero, W.; Chen, J.G. Role of reactive oxygen species and hormones in plant responses to temperature changes. *Int. J. Mol. Sci.* **2021**, *22*, 8843. [CrossRef]
12. Wang, X.; Cai, J.; Liu, F.; Dai, T.; Cao, W.; Wollenweber, B.; Jiang, D. Multiple heat priming enhances thermo-tolerance to a later high temperature stress via improving subcellular antioxidant activities in wheat seedlings. *Plant Physiol. Biochem.* **2014**, *74*, 185–192. [CrossRef] [PubMed]
13. Xu, W.; Miao, Y.; Kong, J.; Lindsey, K.; Zhang, X.; Min, L. ROS signaling and its involvement in abiotic stress with emphasis on heat stress-driven anther sterility in plants. *Crop Environ.* **2024**, *3*, 65–74. [CrossRef]
14. Kinoshita, T.; Seki, M. Epigenetic memory for stress response and adaptation in plants. *Plant Cell Physiol.* **2014**, *55*, 1859–1863. [CrossRef]
15. Lämke, J.; Bäurle, I. Epigenetic and chromatin-based mechanisms in environmental stress adaptation and stress memory in plants. *Genome Biol.* **2017**, *18*, 124. [CrossRef]
16. Fan, Y.; Ma, C.; Huang, Z.; Abid, M.; Jiang, S.; Dai, T.; Zhang, W.; Ma, S.; Jiang, D.; Han, X. Heat priming during early reproductive stages enhances thermo-tolerance to post-anthesis heat stress via improving photosynthesis and plant productivity in winter wheat (*Triticum aestivum* L.). *Front. Plant Sci.* **2018**, *9*, 805. [CrossRef]
17. Hilker, M.; Schmülling, T. Stress priming, memory, and signalling in plants. *Plant Cell Environ.* **2019**, *42*, 753–761. [CrossRef]
18. Zhang, X.; Zhou, Q.; Wang, X.; Cai, J.; Dai, T.; Cao, W.; Jiang, D. Physiological and transcriptional analyses of induced post-anthesis thermo-tolerance by heat-shock pretreatment on germinating seeds of winter wheat. *Environ. Exp. Bot.* **2016**, *131*, 181–189. [CrossRef]
19. Balla, K.; Karsai, I.; Bencze, S.; Veisz, O. Germination ability and seedling vigour in the progeny of heat-stressed wheat plants. *Acta Agron. Hung.* **2012**, *60*, 299–308. [CrossRef]
20. Suriyasak, C.; Oyama, Y.; Ishida, T.; Mashiguchi, K.; Yamaguchi, S.; Hamaoka, N.; Iwaya-Inoue, M.; Ishibashi, Y. Mechanism of delayed seed germination caused by high temperature during grain filling in rice (*Oryza sativa* L.). *Sci. Rep.* **2020**, *10*, 17378. [CrossRef]
21. Wang, Y.; Sun, X.; Peng, J.; Li, F.; Ali, F.; Wang, Z. Regulation of seed germination: ROS, epigenetic, and hormonal aspects. *J. Adv. Res.* **2024**, *10*, 17378. [CrossRef]
22. Suriyasak, C.; Kawaguchi, R.; Matsumoto, R.; Sawada, Y.; Nong, H.T.; Hamaoka, N.; Ishibashi, Y. Adaptive memory induced by heat stress during grain filling enhances subsequent thermotolerance in rice (*Oryza sativa* L.). *Sci. Rep.* **2025**, *15*, 14135. [CrossRef] [PubMed]
23. Shah, K.; Chaturvedi, V.; Gupta, S. Climate Change and Abiotic Stress-Induced Oxidative Burst in Rice. In *Advances in Rice Research for Abiotic Stress Tolerance*; Woodhead Publishing: Sawston, UK, 2019; pp. 505–535.
24. Liu, J.; Zhang, C.; Wei, C.; Liu, X.; Wang, M.; Yu, F.; Xie, Q.; Tu, J. The RING finger ubiquitin E3 ligase OsHTAS enhances heat tolerance by promoting H_2O_2-induced stomatal closure in rice. *Plant Physiol.* **2016**, *170*, 429–443. [CrossRef] [PubMed]
25. Liu, J.; Sun, X.; Xu, F.; Zhang, Y.; Zhang, Q.; Miao, R.; Zhang, Z.J.; Liang, L.J.; Xu, W. Suppression of OsMDHAR4 enhances heat tolerance by mediating H_2O_2-induced stomatal closure in rice plants. *Rice* **2018**, *11*, 38. [CrossRef]
26. Sailaja, B.; Subrahmanyam, D.; Neelamraju, S.; Vishnukiran, T.; Rao, Y.V.; Vijayalakshmi, P.; Voleti, S.R.; Bhadana, V.P.; Mangrauthia, S.K. Integrated physiological, biochemical, and molecular analysis identifies important traits and mechanisms associated with differential response of rice genotypes to elevated temperature. *Front. Plant Sci.* **2015**, *6*, 1044. [CrossRef]
27. Bahuguna, R.N.; Jha, J.; Pal, M.; Shah, D.; Lawas, L.M.; Khetarpal, S.; Jagadish, K.S. Physiological and biochemical characterization of NERICA-L-44: A novel source of heat tolerance at the vegetative and reproductive stages in rice. *Physiol. Plant.* **2015**, *154*, 543–559. [CrossRef]
28. Niu, Y.; Xiang, Y. An overview of biomembrane functions in plant responses to high-temperature stress. *Front. Plant Sci.* **2018**, *9*, 915. [CrossRef]
29. Bäurle, I. Plant heat adaptation: Priming in response to heat stress. *F1000Research* **2016**, *5*, 664. [CrossRef]
30. Szymańska, R.; Ślesak, I.; Orzechowska, A.; Kruk, J. Physiological and biochemical responses to high light and temperature stress in plants. *Environ. Exp. Bot.* **2017**, *139*, 165–177. [CrossRef]
31. Karwa, S.; Bahuguna, R.N.; Chaturvedi, A.K.; Maurya, S.; Arya, S.S.; Chinnusamy, V.; Pal, M. Phenotyping and characterization of heat stress tolerance at reproductive stage in rice (*Oryza sativa* L.). *Acta Physiol. Plant.* **2020**, *42*, 29. [CrossRef]
32. Choi, Y.; Gehring, M.; Johnson, L.; Hannon, M.; Harada, J.J.; Goldberg, R.B.; Jacobsen, S.E.; Fischer, R.L. DEMETER, a DNA glycosylase domain protein, is required for endosperm gene imprinting and seed viability in Arabidopsis. *Cell* **2002**, *110*, 33–42. [CrossRef]

33. Wibowo, A.; Becker, C.; Marconi, G.; Durr, J.; Price, J.; Hagmann, J.; Papareddy, R.; Putra, H.; Kageyama, J.; Becker, J.; et al. Hyperosmotic stress memory in Arabidopsis is mediated by distinct epigenetically labile sites in the genome and is restricted in the male germline by DNA glycosylase activity. *Elife* **2016**, *5*, e13546. [CrossRef] [PubMed]
34. Nakao, Y.; Sone, C.; Sakagami, J.I. Genetic diversity of hydro priming effects on rice seed emergence and subsequent growth under different moisture conditions. *Genes* **2020**, *11*, 994. [CrossRef] [PubMed]
35. Kulkarni, M.G.; Street, R.A.; Van Staden, J. Germination and seedling growth requirements for propagation of *Dioscorea dregeana* (Kunth) Dur. and Schinz—A tuberous medicinal plant. *S. Afr. J. Bot.* **2007**, *73*, 131–137. [CrossRef]
36. Shahidullah, S.M.; Hanafi, M.M.; Ashrafuzzaman, M.; Ismail, M.R.; Salam, M.A.; Khair, A. Biomass accumulation and energy conversion efficiency in aromatic rice genotypes. *Comptes Rendus. Biol.* **2010**, *333*, 61–67. [CrossRef]
37. Libron, J.A.M.A.; Putri, H.H.; Bore, E.K.; Chepkoech, R.; Akagi, I.; Odama, E.; Goto, K.; Tamaru, S.; Yabuta, S.; Sakagami, J.I. Halopriming in the submergence-tolerant rice variety improved the resilience to salinity and combined salinity-submergence at the seedling stage. *Plant Physiol. Biochem.* **2024**, *208*, 108494. [CrossRef]
38. Nakao, Y.; Tamaru, S.; Yabuta, S.; Sakagami, J.I. Vitality of primed rice seeds sown under prolonged dry soil conditions in an upland field. *Crop Sci.* **2022**, *62*, 1277–1287. [CrossRef]
39. Bore, E.K.; Ishikawa, E.; Libron, J.A.M.A.; Goto, K.; Odama, E.; Nakao, Y.; Yabuta, S.; Sakagami, J.I. Primed Seeds of NERICA 4 Stored for Long Periods under High Temperature and Humidity Conditions Maintain Germination Rates. *Appl. Sci.* **2023**, *13*, 2869. [CrossRef]

Disclaimer/Publisher's Note: The statements, opinions and data contained in all publications are solely those of the individual author(s) and contributor(s) and not of MDPI and/or the editor(s). MDPI and/or the editor(s) disclaim responsibility for any injury to people or property resulting from any ideas, methods, instructions or products referred to in the content.

MDPI AG
Grosspeteranlage 5
4052 Basel
Switzerland
Tel.: +41 61 683 77 34

Plants Editorial Office
E-mail: plants@mdpi.com
www.mdpi.com/journal/plants



Disclaimer/Publisher's Note: The title and front matter of this reprint are at the discretion of the Guest Editors. The publisher is not responsible for their content or any associated concerns. The statements, opinions and data contained in all individual articles are solely those of the individual Editors and contributors and not of MDPI. MDPI disclaims responsibility for any injury to people or property resulting from any ideas, methods, instructions or products referred to in the content.





Academic Open
Access Publishing

mdpi.com

ISBN 978-3-7258-9292-1